AD-A092 953 ADVISORY GROUP FOR AEROSPACE RESEARCH AND DEVELOPMENT--ETC F/G 21/2
TESTING AND MEASUREMENT TECHNIQUES IN HEAT TRANSFER AND COMBUST--ETC(U)
SEP 80
UNCLASSIFIED AGARD-CP-281

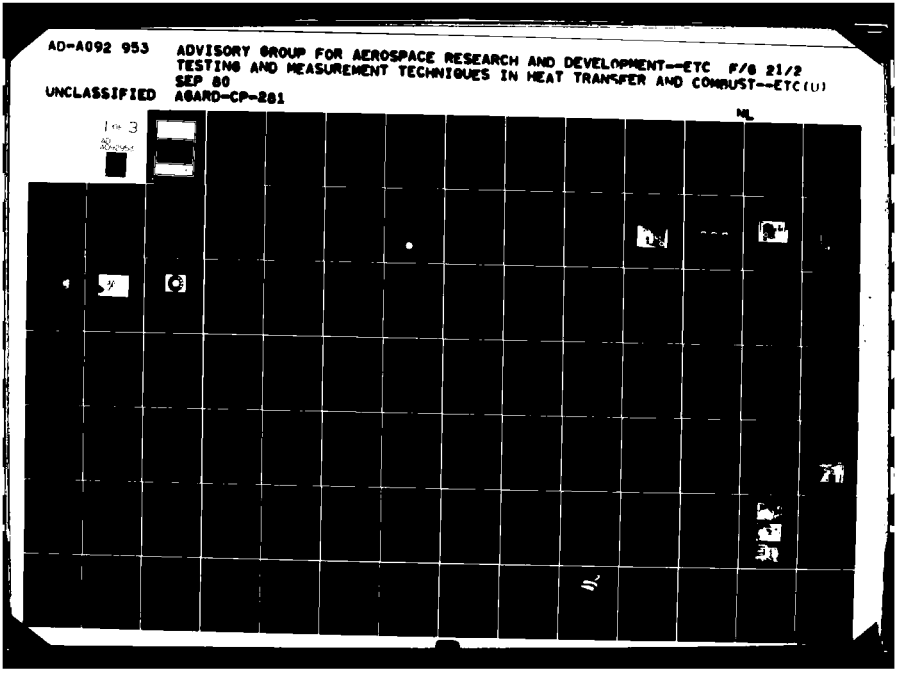

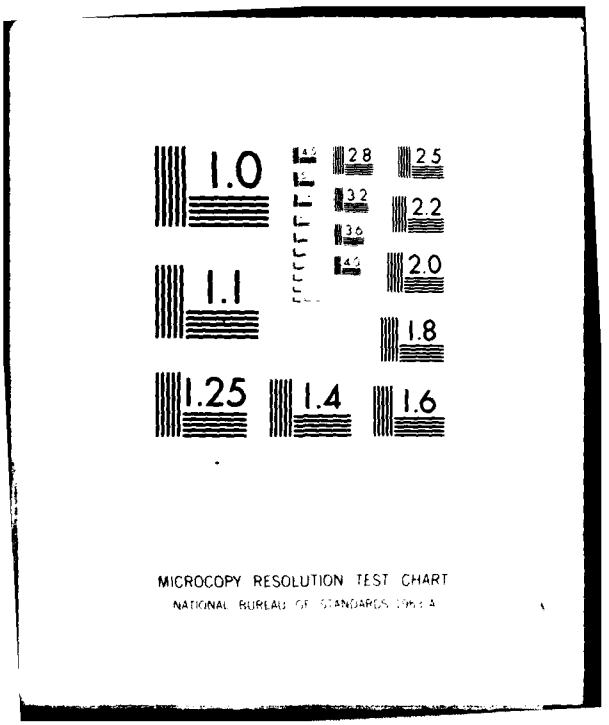
1.0
1.1
1.25
1.4
1.6
1.8
2.0
2.2
2.5
2.8
3.2
3.6
4.0
MICROCOPY RESOLUTION TEST CHART
NATIONAL BUREAU OF STANDARDS 1963-A

AGARD-CP-281

AGARD

ADVISORY GROUP FOR AEROSPACE RESEARCH & DEVELOPMENT

7 RUE ANCELLE 92200 NEUILLY SUR SEINE FRANCE

AGARD CONFERENCE PROCEEDINGS No.281

Testing and Measurement Techniques in Heat Transfer and Combustion

NORTH ATLANTIC TREATY ORGANIZATION

DISTRIBUTION AND AVAILABILITY
ON BACK COVER

(14) AGARD-CP-281

NORTH ATLANTIC TREATY ORGANIZATION

ADVISORY GROUP FOR AEROSPACE RESEARCH AND DEVELOPMENT

(ORGANISATION DU TRAITE DE L'ATLANTIQUE NORD)

(11) Sep 80

(9) AGARD Conference Proceedings No. 281

(6) # TESTING AND MEASUREMENT TECHNIQUES IN HEAT TRANSFER AND COMBUSTION

(12) 1284

Papers presented at the 55th(A) Specialists' Meeting of the AGARD Propulsion and Energetics Panel, held at the Royal Library, Brussels, Belgium, on 5–7 May 1980.

THE MISSION OF AGARD

The mission of AGARD is to bring together the leading personalities of the NATO nations in the fields of science and technology relating to aerospace for the following purposes:

Exchanging of scientific and technical information;

Continuously stimulating advances in the aerospace sciences relevant to strengthening the common defence posture;

Improving the co-operation among member nations in aerospace research and development;

Providing scientific and technical advice and assistance to the North Atlantic Military Committee in the field of aerospace research and development;

Rendering scientific and technical assistance, as requested, to other NATO bodies and to member nations in connection with research and development problems in the aerospace field;

Providing assistance to member nations for the purpose of increasing their scientific and technical potential;

Recommending effective ways for the member nations to use their research and development capabilities for the common benefit of the NATO community.

The highest authority within AGARD is the National Delegates Board consisting of officially appointed senior representatives from each member nation. The mission of AGARD is carried out through the Panels which are composed of experts appointed by the National Delegates, the Consultant and Exchange Programme and the Aerospace Applications Studies Programme. The results of AGARD work are reported to the member nations and the NATO Authorities through the AGARD series of publications of which this is one.

Participation in AGARD activities is by invitation only and is normally limited to citizens of the NATO nations.

Published September 1980

ISBN 92-835-0272-8

Printed by Technical Editing and Reproduction Ltd
Harford House, 7–9 Charlotte St, London, W1P 1HD

PROPULSION AND ENERGETICS PANEL

CHAIRMAN: Dr J.Dunham
National Gas Turbine Establishment
Pyestock
Farnborough
Hants GU14 OLS
UK

DEPUTY CHAIRMAN: Professor E.E.Covert
Dept. of Aeronautics and Astronautics
Massachusetts Institute of Technology
Cambridge, Mass 02139
US

PROGRAM COMMITTEE

Professor F.J.Bayley (Chairman)
Dean of the School of Engineering and Applied Sciences
The University of Sussex
Falmer, Brighton BN1 9QT
UK

Professor C.Casci
Politecnico di Milano
Istituto di Macchine
Piazza L. da Vinci 32
20133 Milano
Italy

Professor F.E.C.Culick
Professor of Engineering and Applied Physics
California Institute of Technology
Pasadena, California 91125
US

M. le Professeur R.Jacques
Ecole Royale Militaire
30 Avenue de la Renaissance
1040 Bruxelles
Belgique

M. l'Ingénieur Principal D.Mouranche
Service Technique Aéronautique
Section Moteurs
4 Avenue de la Porte d'Issy
75996 Paris Armées
France

Professor Dr-Ing. G.Winterfeld
DFVLR
Institut für Antriebstechnik
Postfach 90 60 58
5000 Köln 90
Germany

HOST NATION COORDINATOR

M. le Professeur Ch. Hirsch
Vrije Universiteit Brussel
Dienst Stromingsmechanica
Pleinlaan 2
1050 Brussel
Belgie

LOCAL COORDINATOR

Major d'Aviation A.Cuffez
Etat Major Force Aérienne
Quartier Reine Elisabeth
1040 Bruxelles
Belgique

PANEL EXECUTIVE

Dr-Ing E.Riester
AGARD-NATO
7 rue Ancelle
92200 Neuilly sur Seine
France

ACKNOWLEDGEMENT

The Propulsion and Energetics Panel wishes to express its thanks to the Belgian National Delegates to AGARD for the invitation to hold its 55th Meeting in Brussels, and for the personnel and facilities made available for this meeting.

CONTENTS

TECHNICAL EVALUATION REPORT

by

Dr. L. C. Daniels

Department of Engineering Science
University of Oxford
Parks Road
Oxford

INTRODUCTION

The present economic climate of ever increasing energy costs has dictated that the major design target of all aircraft engine manufacturers is the reduction of the specific fuel consumption (S.F.C.). Present design studies are aiming at a 15 - 20% reduction on present figures. The thermodynamics of the engine cycle dictate that this will in part be achieved by raising the maximum cycle temperature and pressure ratio. Coupled with the need to reduce the S.F.C. is the desire to achieve adequate life cycles of the hot components, and the necessity of meeting E.P.A. and F.A.A. regulations on smoke and pollutant emissions. To help meet these design objectives engine manufacturers are using increasingly advanced design methods for the prediction of the temperatures of the hot section components and the performance of the combustion system. The development of the design methods requires a detailed, accurate knowledge of the engine environment together with an understanding of the physical processes taking place in it.

The Ankara P.E.P. meeting considered some of the problems associated with the hot components of the gas turbine, whilst last year's meeting* considered the problems of modeling the combustion process. Both meetings emphasised the need of engine designers and model developers for data of a high accuracy. Blade metal temperatures are required to within 10K, and gas stream temperatures to within 20K such requirements impose severe constraints upon the measurements techniques. The purpose of the present meeting was to review techniques currently available and their possible development.

The hostility of the engine, or combusting environment to probes and the possible influence of probes upon the flowfield within the various components favours the use of techniques of a non-intrusive nature. The larger percentage of papers presented at the meeting were concerned with the development of non-intrusive instrumentation. Regrettably relatively few of the papers were concerned with making measurements in the engine or a simulated engine evnironment, and whilst many of the techniques described in papers presented at the meeting show considerable potential their capability for use as diagnostic tools in real engine or combustion systems is yet to be adequately demonstrated. Furthermore many of the techniques are incapable of, even in well controlled laboratory experiments of making measurements to the tolerances demanded by the engine designers and model developers. New instrumentation techniques inevitably take longer to develop than theoretical models and the present technology credibility gap will inevitably get wider unless efforts are made to close it.

Table I gives a breakdown of the papers presented to the conference on the basis of intrusive vs non-intrusive instrumentation and a further subdivision at the basis of the experimental environment i.e. engine measurements vs laboratory tests.

	ENGINE MEASUREMENTS	LAB TESTS
INTRUSIVE	1, 2, 3, 4	4, 5, 6, 8, 9 10, 13, 14
NON-INTRUSIVE	18, 17	10, 11, 12, 13, 14 15, 18, 17, 16, 19 22, 23, 21

The number refers to the number of the paper in the proceedings. (Appendix 1). The content and context of the various papers in relation to each other and the needs outlined above are discussed in the

* P.E.P. Meeting on combustor modeling conference preprint no. 275.

summary, from which various conclusions are drawn and recommendations are made.

SUMMARY OF THE MEETING

The papers presented at the meeting broadly represent the two options open to any developer of diagnostic techniques for the measurement of various parameters in combustion systems and turbines. The first is to try to measure directly the quantities of interest by placing some sort of probe connected to appropriate instrumentation in the flowfield. The second option is to infer the required information from the light scattering properties of particles or molecules in the flow. In instrumentation terms the second option is the more complicated of the two; however the pursuit of the first option requires the probe to have a reasonable life expectancy, not to perturb the flowfield and to have good resolution. In the hostile combusting flows in the hot end of a gas turbine the problems of using probes have encouraged the persuit of the non-intrusive option. This interst is reflected in the number of papers presented at this Conference which dealt with the development and application of such techniques.

INTRUSIVE TECHNIQUES

(a) Pressure Measurements

In theory one of the easier measurements to obtain is of course a knowledge of the pressures (total and static) within the flowfield, pitot static and five hole probes are routinely used for this purpose. In practice difficulties may be caused be the probe interacting with the flowfield, particularly if measurements are taken in zones of recirculation, and furthermore the response of the probe to the highly unsteady nature of the flowfield will bias the measurements.

The interaction of the probe with the flowfield cannot be addressed within any generality being highly dependent on the type of flow and probe. The effect of the unsteady flow environment upon pitot static and 5 hole probes is dealt with by Gouldin [4]. His analysis shows that the turbulent fluctuations could have a significant effect on the time mean measurements. In particular when density fluctuations are significant i.e. in a combusting flow large errors can occur. Gouldin's [4] analysis considered the response of the probe to the turbulent fluctuations. Possible effects due to the remoteness of the pressure transducer from the measuring port, which in some cases could be quite considerable are not considered. Are such effects as frequency dependent attenuation and phase distortion going to introduce further errors and what is the likely magnitude of such errors?

Modern electronic manufacturing techniques have made it possible to fabricate pressure transducers with a very wide frequency response, the coupling of such a transducer with a suitable probe design enable Charpenel et al [13] to obtain information about the fluctuating flow field as well as the mean flow. The use of such probes to obtain a turbulence spectrum as Charpenel and his co-workers have done [13] has many advantages when the likely life of a hot wire type probe is considered.

(b) Temperature Measurements

With the possible exceptions of C.A.R.S., see below, and the optical pyrometry method of Charpenel et al [13], the measurement of the hot gas stream temperatures are usually made with a noble metal thermocouple. They can also be used to measure the temperatures of various metal components although in such applications they may cause a disturbance in the surface heat flux optical pyrometry is thus frequently used in such applications.

Alwang [1] discussed a variety of techniques used by industry and then possible development, including the use of new couple materials which would extend the range of temperatures which could be measured. Where details of the spectra of the temperature fluctuations is required the thermocouple will have to be frequency compensated. Wittmer et al [10] describe the used of such a technique to measure the temperatuee fluctations in a turbulent free jet diffusion of flame.

Wittmer et al [10] used a fine wire thermocouple, as did Whitelaw and Taylor [4]. In their experiments Whitelaw and Taylor [14] found considerable difficulty in maintaining the thermocouple integrity in an environment more typical of a gas turbine combustor.

(c) Concentration Measurements

The study of the chemical processes in the combustion chambers and after burners requires a knowledge of the chemical composition of the combustion products. This is usually obtained by withdrawing a sample from the flow and determining its chemical composition. Optical methods e.g. C.A.R.S. have only recently become feasible, and their use is not yet a routine matter. Sampling techniques are thus likely to be used for the immediate future. Gastebois et al [3] presented a survey of the exhaust gases of an Olympus 593 engine, using a sonic orifice quenching probe. Apart from problems concerning the freezing of the chemistry, and preventing water condensation on the sampling lines, a major concern is the effect of the fluctuating flowfield upon the sampling process. Gouldin [4] presents an analysis of the effects of velocity, density and concentration fluctuations on the sample. He concludes that accurate samples of mean mass fractures will require corrections for the effect the large density fluctuations found in a combusting flow. He further recommends that sonic orifice sampling probes should be used in preference to 'slow speed' sampling, since the former are easier to correct.

(d) Heat Flux Measurements

Heat Flux measurements rely on the measurement of temperature together with a conduction analysis of a time dependent or steady nature. Hence heat flux measurements in engines and practical combustors are limited by present thermocouple technology and as such the determination of the heat flux in practical engine situations is not possible Alwang [1]. The limitations in thermocouple technology results in all heat flux measurements being made in test rigs which operate at reduced temperatures.

The scaling laws that are necessary for maintaining similarity at reduced temperatures and pressures are discussed by von Schwerdtner and Hosenfeld [5]. Maintaining strict similarity is difficult particularly in the areas of blade surface finish and turbulence. Bayley and Priddy [9] use a high speed rotating 'squirrel cage' upstream of their test cascade to simulate the high turbulence level and spectral content thought to be found in an engine. Strict similarity cannot be maintained if air is used as a test gas, there will be differences in the Prandtl number and the value of γ, the ratio of specific heats. The variation of Prandtl number was considered by von Schwerdtner and Hosenfeld [5], the difference in γ, the ratio of specific heats, was not.

Testing at reduced temperatures and pressures results in considerable savings in the power required to operate the test facility. Further gains can be made by the use of the transient techniques developed by Schultz et al [8] and adopted by Richards [7]. Transient techniques also simplify the analysis required in the determination of the surface heat flux, and test rigs running in a transient mode do not require the use of exotic high temperature materials or cooled instrumentation.

NON INTRUSIVE-OPTICAL TECHNIQUES

The hostile environment present in gas turbines and combustion systems favour the use of non-intrusive instrumentation. Provided optical access can be arranged, metal temperatures can be obtained by pyrometry, velocities by Laser Optical Anemometry, and with the recent progress in the application on non-linear optical processes, temperature and concentration measurements by techniques such as Raman Scattering and Coherent Anti-Stokes Raman Spectrosocopy (C.A.R.S.)

Optical Pyrometry

The use of rapid response optical pyrometry to measure blade temperatures is described by Alwang [1]. The effects of radiation from the flame in the combustion can are corrected for, by high speed analogue circuitry which yields a continuous record of turbine blade or vane temperature.

Charpenel et al [13] have developed a pyrometer capable of measuring the mean and variance of the fluctuation temperatures in a hot gas stream.

Laser-Optical-Velocimetry

The use of Laser Doppler Velocimetry in isothermal, non-reacting flows, is a well established technique and is a powerful diagnostic tool particularly if it is coupled with flow visualisation as shown by Owen and Pincombe [15]. The provision of optical access and suitable light scattering particles in a combusting flow are some of the practical problems associated with the application of L.D.V. to such flows. Furthermore the analysis of the possible sources of error in the measurements is not straightforward.

Whitelaw and Taylor [14] describe measurements made in the premixed flame in an axisymmetric combustor, together with a discussion of the possible sources and magnitudes of the errors in the measurements. Whitelaw and Taylor [14] used a real fringe, forward scatter optical system. This type of arrangement was also used by Wittmer and Gunther [10] to measure the turbulence characteristics of a diffusion flame. Forward scatter optics required 'dual port' access which is clearly a disadvantage in gas turbine application, but forward scattering has the advantage that the signal strength is at least 2 orders of magnitude higher than in back scatter.

Back scattering measurements in combusting systems are probably better made with the 2 spot or L2F system, which has a higher intrinsic signal to noise ratio than the more conventional LDV, it is a useful technique in photon limited situations e.g. high speed flows with low concentrations of small particles. It does however require special data processing and handling equipment usually correlstor or multichannel digital analysis to produce a 2 dimensional probability distribution function for velocity and flow angle. The production of this P.D.F. for the velocity in a turbulent flow requires a large number of measurements and the L2F technique thus has a low data rate. Eickhoff and Schodl [11] describe the use of the L2F technique to study the turbulence characteristics of hydrogen air and propane air diffusion flames. It is significant that the qualitative interpretation of their data is greatly helped by the use of flow visualisation.

Particle Size and Concentration Measurements

Coghe et al [22] and Bornego and Olivari [23] have adopted LDV techniques to provide information about particle size and concentration in flows based in the scattering propoerties of large particles in the flow. The difference in the scattering properties of the 'large' and 'small' particles in a typical LDV sample volume is the basis of a technique described by Riethmuller and Buchlin [12] for measuring velocities gas-liquid sprays.

Temperature and Composition Measurements

The need to obtain temperatures and species concentrations in combusting flows has prompted the application of conventional spectroscopic techniques and the more recent developments of spatially and temporally precise laser spectroscopic techniques.

Duran and Bellet [16] used U.V. Absorbtion Spectroscopy to determine the concentration of NO in two types of burner. They compared the results obtained from the spectrosopic technique with those obtained using sampling probes.

An accurate spatial distribution of temperature in a combusting system is of course a very important and desirable piece of information. As a results there is considerable interest in the development of optical techniques capable of giving such information. These techniques are based on the inelastic

scattering of light by atoms or molecules in the flow. The scattered light is shifted in frequency away from the source frequency. The frequency spectrum of the scattered light depends upon the population temperature and concentration of the scattering molecular species. To obtain adequate signal strength from the light scattering processes requires either atoms or molecules with a high scattering cross section to be present in the flow or the use of high power sources i.e. lasers. Unfortunately all the species generally found in a combusting system have a low scattering cross section.

Zizak et al [20] obtained temperature profiles in hydrogen and acetylene laboratory flames, using the Two-Line Atomic Fluorescence Method (T.L.A.F.). The spectral properties of light produced by fluorescing indium or thallium atoms added in small concentrations to the combusting gases enable the electronic 'temperature' of the fluorescing atoms to be determined, thus by assuming thermal equilibrium between the seeding atoms and the combusting gases the electronic temperature can be taken as the gas temperature. Unfortunately the scattered signal has a poor signal to noise ratio, and photon correlation techniques have to be used to extract it from the background noise. Such correlation techniques have poor data rates and as a result the T.L.A.F. technique is only suitable for use in highly stable laboratory flames.

The need for temporally as well as spatially accurate spectroscopic information so that practical turbulent combustion can be studied has led to the development of techniques using high power short duration pulsed lasers, the high powers are necessary to obtain sufficient output signal since the involved phenomena have low scattering cross sections.

Two different techniques using inelastic scattering from high power pulsed laser sources were described by speakders at the Conference, Raman Scattering Lapp and So [19], and C.A.R.S. Pealat et al [17] and Eckbreth [18].

Raman Scattering is the older technique. It has been widely developed, is well understood, and is used as a diagnostic tool in certain branches of chemistry. Its use in gas phase and combustion diagnostics is limited by the weakness of the scattered signal, which can be masked by laser induced interference i.e. fluorescence and incandescence generated by the high power probe laser interacting with particles of unburnt fuel or soot in the flame. Lapp and So [19] discuss in detail the needs of advanced combustion models and the measurement implications of the model needs. They describe the use of Raman Scattering in detailed study of a hydrogen air diffusion flame, carried out by Lapp and co-workers (see [19] for reference). They also describe a conditional sampling technique enabling LDV and Raman Scattering measurements to be used in conjunction with each other and hence obtain temperature velocity correlation data.

C.A.R.S. does not suffer from the limitations of signal strength inherent in Raman Scattering. The signal conversion efficiency of C.A.R.S. is several orders of magnitude higher, the scattered light is coherent in character and as such can be collected over such small solid angles that interferances can be reduced to a minimum. These advantates are such that C.A.R.S. is capable of probing practical combustion processes and providing the temperature and species concentration. Eckbreth [18] and Pealat et al [17], both describe the development of C.A.R.S. diagnostics and demonstrate the use of C.A.R.S. in practical combustion environments.

Temperature and concentration measurements (down to about 1%) can be obtained from the shape of the C.A.R.S. spectra. The measured spectra are compared with theoretical spectra generated by a computer code, and the temperature is inferred from a best fit. Species concentrations can also be inferred from the shape of the spectrum provided the susceptibility of the non-resonant background is known or can be approximated, Eckbreth [18]. In the highly turbulent environments typical of combustion system a temperature P.D.F. has to be built up from a number of measurements. The turbulent environments also dictate the use of broadband laser sources and detection, to produce the C.A.R.S. spectra in one single shot of the pulsed laser system; this is because C.A.R.S. spectra are highly non-linear with temperature and density and generating a spectrum piecewise by using a tunable narrow band laser is inappropriate. Eckbreth [18] and Pealat et al [17] suggest that temperatures inferred from spectra obtained in this way are accurate to within ± 40K in 2000 K.

CONCLUSIONS

Advances in measurement technology particularly in the use of non-intrusive instrumentation have been made since the Ankara meeting. Although measurements technology still lags behind engine developments.

Conventional intrusive techniques for the measurement of temperature pressure, and compositions are very difficult to make in the hostile environment of the hot section of a modern gas turbine. Adequate probe lives are difficult if not impossible to obtain and the interpretation of measurements from pressure, and sampling probes may be complicated by the effects of the highly turbulent flow field. Pyrometry is an attractive practical alternative to the use of thermocouples for the measurements of metal temperatures and can be used for gas temperature measurements.

L.D.V. techniques have developed to the point where measurements in the flames of laboratory burners can be made can be made successfully. The techniques have not been demonstrated in practical combustion, where the problems of optical access, control of the light scattering particles will be much more difficult.

C.A.R.S. has developed into a practical tool for combustion diagnostics. The technology is still undergoing rapid development, but already it has demonstrated its capabilities, in realistic combustion situations, where no other means of extracting gas temperatures and species concentrations appears to be possible. It is not a simple technique to use, it requires considerable capital investment and expertise on the part of the user particularly in setting up the system and in the interpretation of the data. It also requires the use of high power pulsed lasers. These factors may limit its use.

RECOMMENDATIONS

It is clear that L.D.V. and C.A.R.S. have developed to the point where they appear to be capable of being used as practical diagnostic tools in combustion systems and turbines. Efforts must be made to realisetheir potential in more realistic or practical situations. Clearly a great deal of work will have to be done in designing, building and developing the equipment and test rigs so that the technique can be transported from the laboratory situation to an engine test stand for example. Nevertheless it is clear that since the techniques are past the stage of proving the physical principles involved, efforts must concentrate on application of the existing technology rather than on increasing the sophistication and refinement of the physics.

Since it is unlikely that the development of C.A.R.S. and L.D.V. in the immediate future is going to reach the stage where their use is going to be a matter of routine, and furthermore the high capital cost of the equipment will restrict its availability. It therefore may be very useful to encourage the development and application of less sophisticated new methods and to reconsider some of the older techniques with a view to possibly extending their application.

A strong interaction between combustion modelers and experimentalists must be maintained if the continued development of the understanding of the combustion processes is to take place. Unfortunately, there appears to be a 'technology gap', mentioned in the introduction, between the current combustion models and our ability to make measurements. The rapid growth of computer power and numerical techniques exploiting the new computers has resulted in extremely sophisticated calculation procedures which have the potential of high numerical and physical accuracy. However, these methods still require empirical input particularly in the modelling of the fluctuation quantities and such input is the factor which controls the accuracy of the computation. The development and validation of a combustion model to a certain standard of accuracy will require the availablity of data to the required accuracy. At present numerical techniques are developing faster than experimental techniques and the technology or credibility gap is in danger of growing wider, unless steps are taken to close it. The closing of the technology gap will be aided by the holding of joint meetings of technologists and modelers at suitable intervals of time.

Appendix I PAPERS PRESENTED AT CONFERENCE

1. Problems in the Measurement of Metal Temperature, Gas Temperature, Heat Flux and Strain in Combustors and Turbines,
W. G. ALWANG, Pratt and Whitney, US.

2. Technical Suppositions Developed for Smoke Emission Measurements during High Pressure Full Annular Combustor Tests and Engine Trials,
G. KAPPLER, J. SEYBOTH and G. HUSTER, MTU, Germany.

3. Etude dex Gaz d'Echappement d'un Moteur en Réchauffe,
Ph. GASTEBOIS, SNECMA, et S. ROPARS, CEPr, France.

4. Probe Measurements in Multi-Dimensional Reacting Flows,
F. C. GOULDIN, Cornell University, US.

5. Application of Model Laws when Determining the Heat Transfer Coefficients by Experiments on Cooled Turbine Blades,
O. A. von SCHWERDTNER and H. G. HOSENFELD, Kraftwerk Union, Germany.

6. Heat Transfer Measurements in Relation to Turbine Blade Cooling,
B. RICHARDS, VKI, Belgium (NO WRITTEN PAPER AVAILABLE).

7. Heat Transfer and Friction in High Aspect Ratio Rectangular Channels with Repeated-Rib Roughness,
C. CASCI, G. Giglioli and P. FERRARI, Istituto Politecnico di Milano, Italy.
NOT PRESENTED AT CONFERENCE

8. Heat Transfer Rate and Film Cooling Effectiveness Measurements in Transient Cascades Related to External and Internal Flows,
D. L. SCHULTZ, T. V. JONES and M. L. G. OLDFIELD, University of Oxford, U.K.

9. Studies of Turbulence Characteristics and their Effects upon the Distribution of Heat Transfer to Turbine Blading,
P. J. BAYLEY and W. J. PRIDDY, University of Sussex, U.K.

10. Correlation Measurement of Velocity and Temperature Fluctuations in a Free Jet Diffusion Flame,
V. WITTMER and R. GUNTHER, Universitat Karlsruhe, Germany.

11. Velocity and Turbulence Measurements in Turbulent Flames Using the L2F Techniques,
H. EICKHOFF and R. SCHODL, DFVLR, Germany.

12. Velocity Measurement Techniques in Gas Liquid Sprays using Laser-Doppler Velocimetry,
M. RIETHMULLER and J. M. BUCHLIN, VKI, Belgium.

13. Méthodes de Mesure à Court Temps de Response pour la Determination des Fluctuations de Vitesse, Température et Pression dans un Ecoulement à Température Elevée,
M. CHARPENEL, Y. LEBOT, P. MOREAU, P. MAGRE et J. LABBE, ONERA, France.

14. Velocity and Temperature Measurements in the Premixed Flame within an Axisymmetric Combustor,
J. H. WHITELAW and A. M. K. TAYLOR, Imperial College of Science and Technology, UK.

15. The Use of Optical Techniques in the Interpretation of Heat Transfer Measurements,
J. M. OWEN and J. R. PINCOMBE, University of Sussex, UK.

16. Application de la Spectroscopie U.V. au Dosage de l'Oxyde Nitrique,
J. C. BELLET, ENSMA et J.Ph. DURAND, SNIAS, France.

17. Etat Actual des Mesures par DRASC à l'ONERA dans les Milieux en Réaction,
M. PEALAT, B. ATTAL, S. DRUET et J. P. TARAN, ONERA, France.

18. Investigations of Coherent Anit-Stokes Raman Spectroscopy (CARS) for Practical Combustion Diagnostics,
A. C. ECKBRETH, United Technologies Research Center, US.

19. Measurements of Flame Properties by Raman Scattering: Experimental Capabilities and Modelling Needs,
M. LAPP and R.M.C. SO, General Electric RandD Center, U.S.

20. Flame Temperature Profiles Obtained by the Two-line Atomic Fluorescence Method,
G. ZIZAK, F. CIGNOLI and S. BENECCHI, CNPM, Italy.

21. Applications of Optical Diagnostic Techniques in Combustion Research,
D. L. HARTLEY and M. A. GUSINOW, Sandia Laboratories, US.
(NO WRITTEN PAPER AVAILABLE)

22. Droplet Size Measurements in Combustion by the Visibility Method,
A. COGHE, U. GHEZZI and C. BRIOXCHI, CNPM, Italy.

23. A Method for the Measurement of Mixing Properties in a Turbulent Jet Flow,
C. BORREGO and D. OLIVARI, VKI, Belgium.

PROBLEMS IN THE MEASUREMENT OF METAL TEMPERATURE, GAS TEMPERATURE, HEAT FLUX AND STRAIN IN COMBUSTORS AND TURBINES

W. G. Alwang
Pratt & Whitney Aircraft Group
Commercial Products Division
United Technologies Corporation
400 Main Street
East Hartford, Connecticut, USA 06108

Summary

The verification of a gas turbine engine design requires that all critical design parameters be measured as directly and accurately as possible during development testing. The hot section of the engine poses some particularly difficult measurement problems. In this paper the limitations of current instrumentation used in the combustor and turbine will be described and work in progress to overcome these limitations will be reviewed.

Among the topics to be covered are: limitations on the use of advanced dual spectral range optical pyrometers for metal surface temperature measurement, use of sputtered thin film thermocouples, problems in measuring gas temperature distributions and burner pattern factor, particularly above 3000°F (1925K), problems in measuring static strain and strain range in hot section hardware, and finally problems in the measurement of radiative and total heat flux.

INTRODUCTION

The trend in advanced gas turbine engines, both commercial and military, is toward higher compression ratios and higher maximum cycle temperatures. This is a consequence of the desire to improve the performance and efficiency of engines and is especially significant in the present climate of rapidly escalating fuel costs. The increased pressures and gas temperatures in the engine hot section must be achieved while maintaining very high reliability and durability of the combustor and turbine hardware. In addition, stringent limitations with respect to emissions of smoke, NO_x and hydrocarbons must be met. This combination of requirements is a major technical challenge and has lead to intensive activity in combustor research, heat transfer, materials and structural design. It also presents a major challenge to the testing and measurements techniques needed for developing gas turbine engines.

Engine development testing requires careful planning in the use of instrumentation to insure a successful final product. Measurements are used extensively throughout and for a variety of different purposes. First, they serve to provide the raw material necessary for the continued evolution of theoretical and empirical foundations in structures, aerodynamics, and heat transfer, which make up the analytical systems used to generate the engine design. In this stage, great ingenuity is applied to obtain representative data in model experiments which are in most cases simplifications or idealizations of real engine components.

As an engine design progresses, engine components and finally experimental versions of the engine are built and tested, and the emphasis in the use of measurements then shifts to the problem of confirming design objectives. For those planning instrumentation, this is a very fundamental change, since the freedom to choose test conditions for which reliable and accurate sensors are easily available nc longer exists. The measurements should be made in the actual engine environment.

In using measurements to confirm design objectives' the following rules should be adhered to as closely as is permitted by the current state-of-the-art.

1. Identify all critical parameters in the design.

2. Measure these parameters directly and in a realistic environment.

As we will see, these rules are simple and obvious but very difficult to accomplish. They point the way to those areas in which improved measurement methods need to be developed.

There is a further measurement principle which seems obvious but is often neglected in practice. It applies to all measurements, not only to those intended to confirm design objectives. The principle is, no measurement is complete without an estimate of its accuracy. A turbine blade temperature measurement with an accuracy of $\pm 10°F$ (5.6K), might be completely adequate while one whose accuracy is 100°F (56K), is almost worthless.

In this paper I will concentrate on some problems in the use of measurements to confirm design objectives in the hot section of the engine, that is, in the combustor and turbine.

CRITICAL MEASUREMENTS IN THE HOT SECTION OF THE ENGINE

In Figure 1, an example of the temperature distribution through a film cooled wall with a thermal barrier is shown. The principle quantities potentially accessible to measurement are the gas temperature T_g, the coolant temperature Tc, thermal barrier surface temperature Tb, as well as metal temperatures Tmi and Tmo.

The convective heat flux Qc cannot be measured directly, however, the total heat flux and the radiative heat flux can, in principal at least, be obtained and from this the film cooling effectiveness η_f can be obtained.

The stress in combustor and turbine structures is also a critical ingredient in predicting lifetime of hardware.

In order to determine how these parameters must be combined to predict component lifetimes, it is necessary to identify the failure mode which limits the life of each component. (See Ref. 1 for example) Typically in high temperature turbines failure is dominated by creep rupture, low cycle fatigue, creep fatigue interaction or corrosion and erosion. Prediction of failure in creep requires knowledge of the steady state distribution of temperature and stress. Corrosion and erosion are strongly temperature dependent and are also sensitive to trace quantities of impurities in the air, particularly salt and hard particulates. Low cycle fatigue on the other hand is determined by transient temperature and stress distributions generated by the accelerations and decelerations accompanying landing' take-off and flight maneuvers.

The turbine designer beginning with a statistical prediction of gas temperature and cooling air temperature produces a blade cooling design which yields a satisfactory blade lifetime. To verify this design prediction, it is necessary to run cyclic endurance tests and to measure the following quantities:

1. Metal Temperature - Steady state and transient metal temperature distributions.

2. Gas Temperature - Maximum temperatures and distributions under a variety of steady state and transient operating conditions and engine service hours.

3. Radiant and total heat flux.

4. Steady and transient stresses.

In addition to these more obvious characteristics of the design problem in the hot section of an engine, a number of more subtle characteristics are very important. These include the flame distribution in the combustor, the flow field including turbulence and the tendency of the combustor to produce hard carbon and cause erosion.

In the following sections I will try to summarize the state-of-the-art in making these measurements in a turbine engine environment.

BLADE AND VANE METAL TEMPERATURE

Cooled turbine blades and vanes are characterized by high temperatures, large temperature gradients both in and perpendicular to solid surfaces and, frequently, considerable blade-to-blade variability. Figure 1 shows a typical temperature distribution perpendicular to the blade surface. Measurements, to be useful must sample many points on the surface. In addition, at the maximum temperature conditions, a change of +25°F (14K) in metal temperature can cause as much as a factor of two reduction in fatigue lifetime, therefore, the accuracy of the temperature measurement should be about ±10°F (5.6K). (At P&WA we employ measurement accuracy definition in Reference 2. Error estimates are given as $\pm 2\sigma$, the 95% confidence level)

The most frequently used instrument for mapping rotor blade temperatures is the optical pyrometer (Reference 3). With careful attention to calibration and given a system designed to compensate for or eliminate such things as temperature dependence of the detector sensitivity, measurements of the required accuracy can be made. The primary sources of bias are first, accumulation of dirt on the optics and second, radiation from the flame in the combustor which is usually immediately upstream of the turbine.

At P&WA a dual spectral area pyrometer has been developed which permits flame radiation to be effectively corrected. Dirty optics are avoided by a properly designed purge system.

This pyrometer measures the radiant energy, in two broad spectral ranges, which issue from a small area on the surface to be measured. One spectral range is much more sensitive to short wavelength radiation characteristic of the flame, and the other is more sensitive to the longer wavelength radiation emitted by the cooler turbine hardware. A theoretical description of the means for correcting for the reflected radiation is described in Reference 4. The computations can be carried out in real time using high speed analog circuitry yielding a continuous record of turbine blade or vane temperature. A typical installation is shown in Figure 2. The pyrometer is focused at a fixed location in space and yields a record of the blade temperatures appearing in its field of view. A typical example for one rotation of a rotor is shown in Figure 3. This trace is corrected for flame radiation and shows an exceptionally hot blade, a consequence in this case of an unanticipated obstruction in the blade cooling passage.

The point of observation can be scanned from the root to the tip of the rotor blades and, from this, blade by blade mapping of surface temperature distribution can be made.

Some limited data has been obtained which validates these pyrometer measurements through direct observation of a rotor blade which suffered localized melting. The indicated pyrometer temperatures at the time of melting agreed with the characteristic liquidus temperature for the alloy to within about 36°F (20K). Direct comparisons with thermocouples have also been done in some cases Reference 5, but again data is very limited especially when flame is present. In order to validate the pyrometer results, it is very desirable to occasionally make redundant measurements with metal thermocouples installed on the blade or vane surfaces at surfaces where installation of the thermocouple produces negligible perturbation of heat flow.

Pyrometry is frequently limited by lack of optical accessibility, or particularly at the turbine inlet, excessive interference from direct or reflected flame radiation. In such cases use of thermocouples may be essential although installation of wire thermocouples on cooled blades without modification of local heat transfer can be very difficult (Reference 6). For this reason sputtered thin film thermocouples, as

shown in Figure 4, are being developed (Reference 7)*. These thermocouples are in the form of very thin films of platinum and platinum rhodium deposited on the blade surface over an oxide coating. Total thickness of oxide and metal is less than 0.001 inches (.0025cm).

GAS TEMPERATURE

The gas temperature exiting a combustor has a very complex distribution in space and time. The measured spatial distribution of gas temperature is used by the turbine designer to calculate burner pattern factors which are used as inputs to the turbine cooling design analysis. In order to determine pattern factors, arrays of point measurements are required. A typical means for obtaining such data is through the use of shielded thermocouples installed on the leading edges of turbine inlet guide vanes which are located immediately downstream of the combustor exit (Figure 5).

The number of point measurements required to characterize the combustor exit temperature is large. The potential range of temperatures of the gases entering the combustor extend from the compressor discharge temperature, about 1000°F (810K), to stoichimetric burning temperatures for common jet fuels, 3800°F (2370K).

In an efficient combustor the highest gas temperature must be prevented from direct contact with metal surfaces or local burnout will occur: Complete combustion of the fuel must occur with minimal formation of NO_x and finally turbulent mixing of the combustion and cooling gases must produce as isothermal a temperature distribution at the combustor exit as possible to minimize the occurrence of local hot spots.

Some idea of the number of point measurements needed can be obtained by reference to the accuracy required of the turbine blade metal temperature measurements which, as stated above, is about $\pm$10°F (5.6K). In a typical cooled blade, a $\pm$10°F (5.6K) error in prediction of metal temperature is equivalent to about $\pm$30°F (17K) in gas temperature. If we assume that we are sampling from a distribution of gas temperature ranging from the compressor discharge temperature to the stoichiometric burning temperature, a range of over 2000°F (1375K), between 100 and 1000 point measurements are required depending on the precision of the individual point measurements and the complexity of the distribution.

Many efforts have been made to measure the mean and extreme properties of the gas stream (Reference 8) These have included ultrasonic, radiation, optical and acoustic techniques, but none have been very successful so far.

A typical approach to the measurement of temperature of a point in a high temperature gas stream is by the use of a shielded thermocouple. The shielded thermocouple is designed to operate near the gas stream temperature with minimal correction for radiation and conduction error. To obtain reasonable operating lifetime, it is necessary to maintain the most commonly used couples (Type B Pt PT6Rh) below about 3000°F (1925K). This temperature is less than the hot spot temperatures in many advanced engines and in fact during engine development when the combustor design is still evolving, it is not unusual to expect local hot spots at stoichiometric burning temperatures. A new thermocouple pairing (Pt40Rh Ir40Rh) devised by Glawe at NASA (Reference 9) promises to extend the limit for noble metal couples by about 200°F (110K). These thermocouple limitations often make it necessary to obtain pattern factor data with the engine running at less than full power in order not to destroy the thermocouples.

A number of approaches are in progress for overcoming this problem as follows:

Refractory Metal Thermcouples - Metals like tungsten and rhenium make good thermocouples but oxidize rapidly particularly in the high pressure environment of a gas turbine engine. Efforts to avoid rapid failure by providing protective coatings or sheaths have so far been unsuccessful.

Cooled Thermocouples - Thermocouples can be run at well below the gas temperature either by deliberately designing for enhanced radiation and/or conduction cooling or by providing a colder gas for convection cooling. When using such designs, it is essential to have well proven procedures for correcting to the actual gas temperature from the measured thermocouple temperature. A very interesting thermocouple of this type has been under development at NASA (Reference 10) which they call a pulsed thermocouple. However, none of these have been used in large arrays for pattern factor measurements.

Another form of cooled probe usable at gas temperatures exceeding the limits of currently available thermocouples is the calorimetric probe shown in Figure 6. In this probe the hot gas is aspirated through a small jacketed heat exchanger or calorimeter. The amount of heat given up to the calorimeter is determined by the flow rate and temperature rise of the liquid coolant. Measurement of the flow rate and temperature of the gas at the calorimeter exit then allows the initial gas temperature to be deduced as shown.

Optical Methods for Temperature Measurement - In the future it may be possible to probe hot flows with laser beams and measure local temperature and density using techniques such as CARS (Coherent Antistokes Raman Scattering). These techniques are under active development (Reference 11), but they have not yet been applied in high pressure liquid fuel combustors.

Gas Analysis - A frequently used technique for calculating gas temperature uses a traversible cooled probe to extract gas samples and then by chemical analysis of the constituents and given the combustor inlet temperature, calculating the enthalpy rise and temperature of the gas, Reference 12. The method is complex and requires great care to achieve reasonable accuracy, nevertheless it does work.

* Development work is currently in progress under NASA contract NAS3-22002.

OPTICAL METHODS FOR FLOW MEASUREMENTS IN COMBUSTORS

BURNER VISUALIZATION

Information on the gross properties of the flow in a combustor may be obtained by direct visualization using an optical system capable of operation at high temperatures. The feasibility of direct visualization has improved significantly in recent years with the availability of low loss high resolution fiber optics that can be run at relatively high temperatures.

An example of an installation with a 100° field of view is shown in Figure 7. Systems of this type are currently under development and are intended to yield information on spray angles, location and dynamics of flame, flame impingement on liner walls and location of carbon deposits.

LASER VELOCIMETRY

The introduction of laser velocimetry has made possible the measurement of gas velocity and turbulence at locations which were previously difficult or impossible to achieve with conventional probes. Because of the nonintrusive nature of the technique it is especially useful in and near rotating blades in small passages, and in very high temperature gases. Thus, it is now possible to measure the velocity field in combustors and turbines provided that suitable optical access can be obtained.

At P&WA in addition to extensive applications in fans, we have applied the technique to the measurement of velocity fields at the exit of a duct burning fan (concentric high temperature jets). and at the exit plane of experimental combustors. Measurements in high pressure combustors have also been demonstrated.

There are two basically different forms of the technique currently in use, the laser fringe velocimeter as in References 13 and the laser transit or two focus velocimeter, as in Reference 14. Each has its relative advantages and disadvantages. The principle difficulties in the use of laser velocimetry, aside from the relative complexity of the apparatus, includes the selection of the most appropriate form of velocimeter and involves the following issues:

1. Optical access to the point of measurement must be provided.

2. Since the technique is based on the scattering of light from small particles either natural or artificially entrained in the flow, the particles must be small enough to accurately follow local flow accelerations. Generally, particles smaller than one micron in diameter are required. Our experience has been that there usually are sufficient particulates in the flow downstream of liquid fueled combustors to provide quite adequate data rates. When insufficient particulates are naturally available, we seed high temperature flows with finely divided aluminum oxide, using a fluidized bed with inertial separations to insure dispersal of only small particles.

3. Because of light scattering from solid surfaces, measurements close to walls can be difficult. Seeding with fluorescent particles can improve the situation in low temperature flows but since the fluorescent dye is dispersed in droplets of organic solvent, it cannot be used at high temperatures.

The laser transit velocimeter because of its higher intrinsic signal-to-noise ratio may give the best results near walls in hot flows although at present no comparative data on the two systems has been published.

4. If information is required on such things as the turbulence power spectrum or spatial correlation of velocity fluctuations, it is necessary to use the fringe type velocimeter since, in the present state of development of these instruments, only the fringe velocimeter preserves the velocity-time relationships in the flow.

Verification of turbulence power spectrum by comparison between a laser fringe velocimeter and a hot wire is shown in Figure 8. The technique used in this measurement is unique in that the spectrum is the Fourier transform of the cross correlation function between two separate laser velocimeter channels measuring the same velocity component at the same point in space.

Velocity correlations at different points in space, as well as correlations between velocity and temperature fluctuations, have also been demonstrated in our laboratory.

RADIANT AND TOTAL HEAT FLUX

Although extensive measurements of heat flux have been made at low temperature, data taken in the hot sections of actual gas turbines varies from very limited to nonexistent.

The conventional methods for making total heat flux measurements, Reference 15, involve the use of thermocouples to measure temperature differences in sections of material of known geometry and conductivity. A typical configuration is shown in Figure 9. The principle problems with the application of these heat transfer measurement techniques in real combustors and turbines where very high temperatures and temperature gradients are present is to devise an installation which is rugged enough to survive the environment without significantly modifying the local heat flux and thus producing intolerably large measurement uncertainty.

Some work has been done on cooled turbine vanes by implanting large numbers of thermocouples, overcooling the vane, and then abruptly restoring normal cooling. Extensive analysis of the distribution of transient temperature rise then allows heat flux to be deduced.

Sensors for the measurement of total heat flux employing carefully designed fine wire thermocouples and/or sputtered thermocouples are currently under development but are not yet generally available.

In a high pressure combustor it is necessary to distinguish between convective and radiative heat flux. The temperature gradient sensors described above respond to total heat flux. The radiant component of the total heat flux can, in principle at least, be measured with a radiometer. A very interesting instrument of this type was reported by Professor Moffat of Stanford, Reference 16. In this device the heat transfer to a porous plug, Figure 10, is measured while blowing a cooling fluid through the plug. When sufficient coolant is flowing, the convective heat flux is reduced to zero and only the radiative component is measured.

STATIC AND DYNAMIC STRAIN

Extensive measurements of strain distribution on engine hardware are normally carried out as part of the engine development cycle; however, these measurements become increasingly difficult and unreliable as metal temperature increases. Capacitive type strain gages (Reference 17), which are best for use at high temperature, are currently much too large to resolve the strain field in typical hot section components. Resistive wire gages have the desired spatial resolution but exhibit the properties illustrated in Figure 11. Temperature and drift effects shift the gage zero point while leaving the slope approximately constant. Therefore, dynamic or vibratory strain is much more easily measured than static strain.

In engine development it would be very desirable to measure the strain range in turbine blade roots, burner liners, etc. during typical take-off and landing engine power settings in order to confirm predictions related to the low cycle fatigue lifetime of the engine components. This is currently beyond the state-of-the-art for parts which run above about 900°F (775K).

A technique which has proven very useful in the examination of hot section hardware under actual operating conditions is engine radiography, Reference 18. Although the method does not allow direct measurement of strain, it can very vividly show internal clearances, distortion and dimensional changes of combustor liners, cooling louvers and the like under both steady state and transient operating conditions. The system in use at Pratt & Whitney Aircraft employs an 8 Mev linear accelerator X-ray source in a shielded engine test stand, Figure 12. Images are recorded with either film or through a video fluoroscope. The accuracy of dimensional measurements from radiographs is limited by the characteristic blur in X-ray images and is typically ±.003" (.008cm) to ±.008" (.020cm) on well defined edges. To get better accuracy especially with thin sections and components with poor edge definition, it is necessary to use digital image analysis techniques such as described in Reference 19.

CONCLUSIONS

Combustor and turbine development is hampered at present by significant limitations in measurement technology. Many of the most critical parameters required for confirming the lifetime of hot section hardware cannot be measured directly. This complicates the interpretation of endurance tests and increases the time and cost of engine development.

Measurement of blade, vane and combustor liner metal temperatures can be accomplished using pyrometry and/or thermocouples provided the precautions mentioned in the text are taken. The development of sputtered thin film sensors should significantly improve our ability to install thermocouples in cooled components without modifying local heat transfer.

Gas temperature distributions using vane leading edge sensors in the range above 3200°F (2050K) present a difficult problem because of the rapid failure of standard noble metal thermocouples. Traversible cooled probes using thermocouples or gas analysis can be used, but it is difficult to get complete coverage of the entire gas path with a traversing probe. Optical techniques such as CARS have not yet been demonstrated in gas turbine combustors.

Direct measurement in engines of radiant and total heat flux distributions on combustor liners or turbine vanes and blades is currently beyond the state-of-the-art.

Spatially resolved static strain and measurement of strain range during engine acceleration and deceleration cycles is also currently beyond the state-of-the-art for hardware operating above about 900°F (775K).

REFERENCES

1. Loferski, M. T , "Turbine Airfoil Life Prediction by Mission Analysis", Journal of Aircraft, Vol. 12, No. 4, pp 400-402, April, 1975

2. Abernethy, R.B., Thompson, J.W. Jr., "Handbook, Uncertainty in Gas Turbine Measurements", Arnold Engineering Development Center, AEDC-TR-73-5

3. Rohy, D.A., Duffy, T.E., Compton, W.A., "Radiation Pyrometer for Gas Turbine Blades"' SAE Paper 720159, Automotive Engineering Congress, Detroit, Michigan, January 1972

4. Atkinson, W.H., Strange, R.R., "Pyrometer Temperature Measurements in the Presence of Reflected Radiation", ASME Paper 76-HT-74, Heat Transfer Conference, St. Louis, Missouri, August, 1976

5. Uguccini, O.W., Pollock, F.G., "High-Resolution Surface Temperature Measurements on Rotating Turbine Blades with an Infrared Pyrometer", NASA TN D-8213, May 1976

6. Moffat, R.J., "Temperature Measurement in Solids", Paper No. 68-514, Transactions of the Instrument Society of America Annual Meeting, New York, October 1968

7. Dils, R.R., Follansbee, P.S., "High Temperature Sputtered Surface Sensors", Proceedings of the 21st International Instrumentation Symposium, Philadelphia, PA., May 1975, p. 127-132

8. Duffy, T.E., et al, "Research Analysis of Advanced Sensors for Turbine Inlet Gas Temperature", Final Report, NASC Contract N00019-69-C-0574

9. Glawe, G.E., "New High Temperature Noble Metal Thermocouple Pairing", Review of Scientific Instruments' Vol. 46, No. 8, August 1975

10. Glawe, G.E., Krause, L.N., "A New Approach to the Pulsed Thermocouple for High Gas Temperature Measurements"' NASA TM-X 71883.

11. Eckbreth, A.C., Hall, R.J., Shirley, J.A., "Investigations of Coherent Anti-Stokes Raman Spectroscopy (CARS) for Combustion Diagnostics", AIAA Paper No. 79-0083, 17th Aerospace Sciences Meeting, New Orleans, LA., January 1979

12. Williamson, R.C., Stanforth, C.M., 'Measurement of Jet Engine Combustion Temperature by the Use of Thermocouples and Gas Analysis", SAE National Air Transport Meeting, New York, April 1969, Paper No. 690433

13. Brayton, D.B., Kalb, H.T., Crosswy, F.L., "Two-Component Dual Scatter Laser-Doppler Velocimeter with Frequency Burst Signal Readout", Applied Optics, Vol. 12, pp 1145-1155, June 1973

14. Schodl, R., "A Laser-Dual Beam Method for Flow Measurement in Turbomachines", ASME Paper No. 74 GT-157(1974)

15. Baines, D.J., "Selecting Unsteady Heat Flux Sensors", Instrument and Control Systems, pp 80-83, May 1972

16. Moffat, R.J., Hunn, B.D., Ayers, J.F., "Development of Transpiration Radiometer", ISA Paper No. 71-613.

17. NASA Tech Brief B75-10069 "High Temperature Capacitive Strain Measurement System" May 1975.

18. Alwang, W.G., Kinchen, B.E., "Internal Running Clearance Measurements in Gas Turbines Using High Energy X-Radiography", ISA Aerospace Instrumentation Symposium 1975, Paper No. 75260, p. 339-348.

19. Davies, D.L., Kinchen, B.E., "Radiographic Clearance Measurement of Turbine Engines Using Digital Image Analysis Techniques", American Society of Non-Destructive Testing Spring Conference, San Diego, California, April 1979.

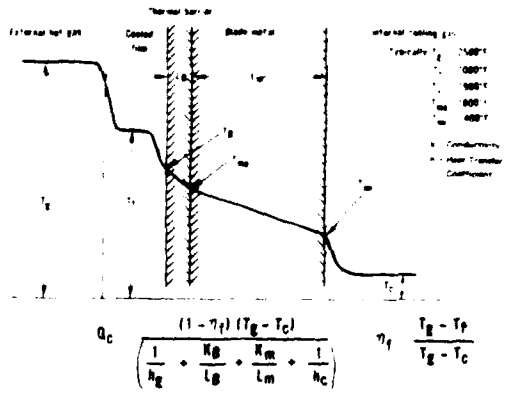

$$Q_c = \frac{(1-\eta_f)(T_g - T_c)}{\left(\frac{1}{h_g} + \frac{K_B}{L_B} + \frac{K_m}{L_m} + \frac{1}{h_c}\right)} \qquad \eta_f = \frac{T_g - T_p}{T_g - T_c}$$

Figure 1 Heat Flux in a Cooled Airfoil

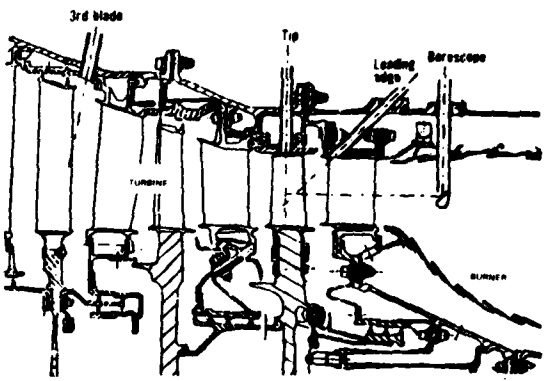

Figure 2 Pyrometer Engine Installations

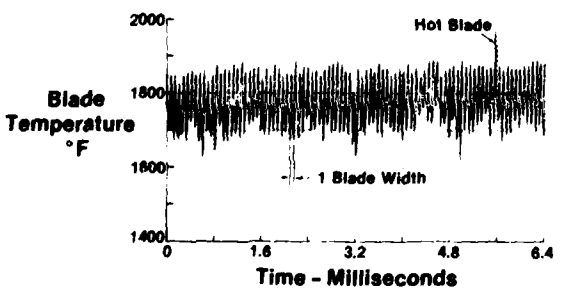

Figure 3 Pyrometer Signal For One Rotation

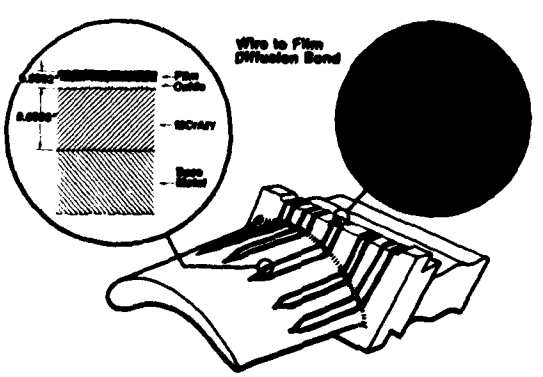

Figure 4 Sputtered Thin Film Thermocouples

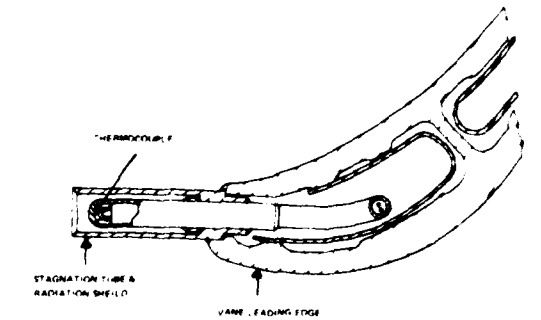

Figure 5 Vane Leading Edge Thermocouple

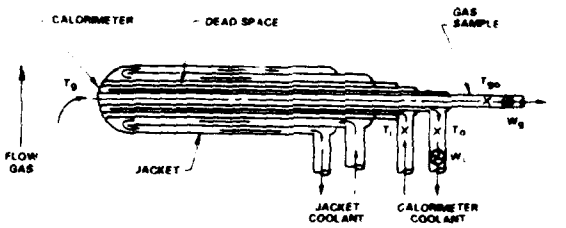

$$T_g = T_{go} + \frac{W_L C_L (T_o - T_i) - Q}{W_g C_g}$$

where

W_L, W_g = Mass flow of liquid and gas

C_L, C_g = Specific heats of liquid and gas

Q = Calibration constant

Figure 6 Calorimetric Probe

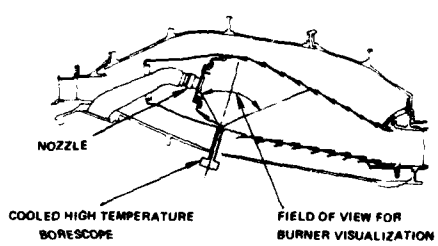

Figure 7 Burner Visualization

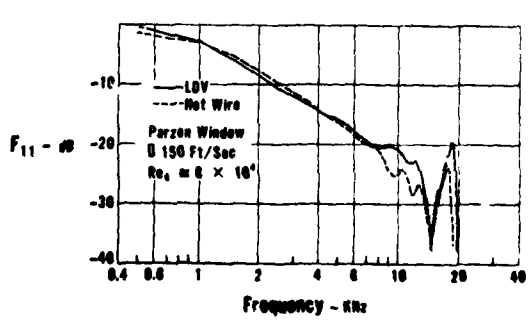

Figure 8 Spectrum of Axial Velocity Component in a Turbulent Jet

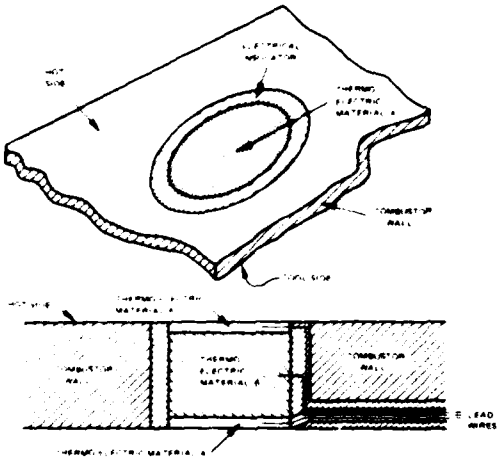

Figure 9 Typical Heat Flux Sensor Installation Schematic

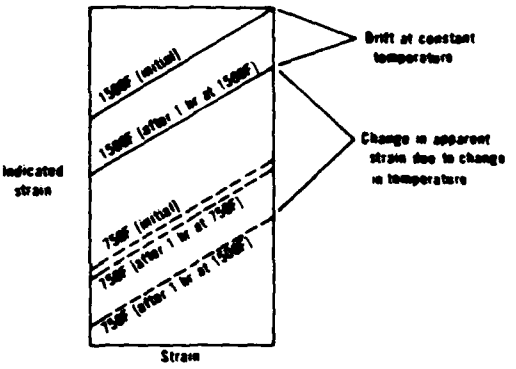

Figure 11 Typical Effects of Time and Temperature on the Calibration of a Resistive Strain Gage

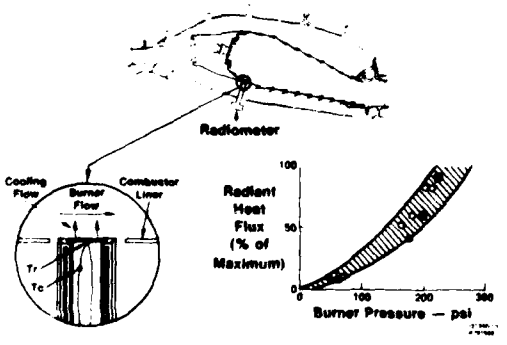

Figure 10 Porous Plug Radiometer

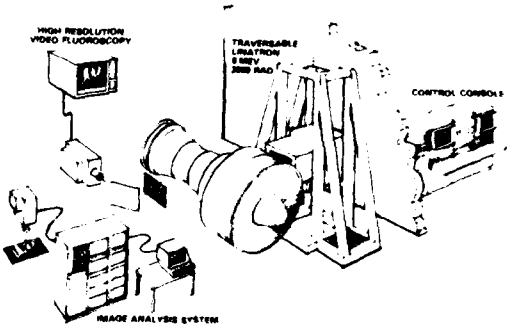

Figure 12 Engine Radiography

DISCUSSION

K Kohse-Hoinghaus, Ge

In the first part of your lecture you have shown a slide where you compared the "true" metal temperature with pyrometer measurements. How did you get this "true" temperature?

Author's Reply

The slide showed two temperature signals from the pyrometers with filtered inputs and the third trace was the "corrected" temperature with the correction being accomplished by the "dual spectral" technique described in Reference 4 of this paper, i.e. Atkinson, W.H. and Strange, R.R., "Pyrometer Temperature Measurements in the Presence of Reflected Radiation". How well this "corrected" temperature agrees with the "true" temperature needs to be determined by comparison with metal temperature measurements made by other means.

J.M.Owen, UK

With respect to the instrumentation of turbine discs, are sputtered thermocouples used and how are the reference air temperatures measured? Do the sputtered thermocouples need individual calibration or can standard calibrations be applied?

Author's Reply

We normally use wire thermocouples on turbine discs although when the development of sputtered thermocouples is complete, they could also be used in situations where conventional wire thermocouples are considered to be unsatisfactory.

The intention of the sputtered thermocouple development programme is to produce a thermocouple with a calibration very close to that of the bulk thermocouple material, so that no separate calibration is required.

Reference air temperature in disc cavities is normally measured with appropriately placed air thermocouples. The data on air temperature are frequently not as complete as one would like because of the difficulties in placing such thermocouples.

TECHNICAL SUPPOSITIONS DEVELOPED FOR SMOKE MEASUREMENTS DURING HIGH-PRESSURE FULL ANNULAR COMBUSTOR TESTS AND ENGINE TRIALS

G. Kappler, J. Seyboth, G. Huster
MTU Motoren- und Turbinen-Union GmbH
Dachauer Str. 665, 8000 München 50
West-Germany

1. Summary

The knowledge of smoke emissions from jet engines is of interest for civil as well as for military engine applications. Smoke emission measurements have become a necessary and reliable tool for low-emission combustor development. At MTU-München two measuring techniques were designed: one for reliable cross-correlations and basic calibrations using stained filter paper, and another for fast continuous measurements based on an optical extinction method. The measuring systems are described in the paper and cross-correlation data with a sucked Hartridge smoke meter is presented. The paper also covers the sampling technique and the sampling probes developed at MTU-München. Analysis of results of smoke-emission measurements from three combustors with different smoke suppression methods showed good accuracy and reproducibility of the incorporated measuring systems.

2. Introduction

The design of low smoke-emission combustors initiated by environmental regulations[1] and military requirements[2] has prompted the development of exhaust smoke measurement techniques. The test procedure for sampling and measuring exhaust smoke emissions for aircraft gas-turbine engines compliance was specified by the U.S. Environmental Protection Agency[3]. The procedure involves the divertion of a smal fraction of the engine exhaust stream which is passed through a standardized filter at known sample volume, and the loss in reflectivity of the filter is measured. Since this method was specially conceived for engine compliance tests it has some drawbacks regarding combustor development work. The main disadvantages are its inability to carry out continuous smoke emission measurements and the time-consuming data acquisition which makes full annular combustor traversing practically impossible. Other smoke measurement methods, where the transmission of light through an exhaust gas sample is measured, exhibit unacceptable high errors at low smoke concentrations. Furthermore, the accuracy of the measuring systems displays a marked drift because of smoke particles which collect at the optical windows changing the light transmission. The in situ smoke measurement methods, which are based on the light-scattering properties of aerosols[4], are still too sophisticated for engine development work.

Relying on the method that involves withdrawal of a sample flow, an improved optical smoke meter was designed at MTU-München which permits continuous smoke-emission measurements with sufficient accuracy at low smoke concentrations.

3. Description of smoke meters

The improved optical smoke meter designed at MTU-München is shown schematically in Fig. 1. The exhaust gas sample is ducted through a circumferential slit into the measuring tube. The sample flow which was greatly calmed and homogenized in the circumferential channel splits uniformly towards the tube ends. The homogeneous introduction of the sample flow was necessary to avoid the formation of local density concentrations. The measuring tube was uniformly heated by electrical coils wrapped tightly around the outer surface. The inner surface of the tube was fitted with aluminum rings having their surface stained to disperse light.

Purge air was introduced radially on both sides of the tube. The mass flow was balanced in such a way as to keep the optical lens and the refelctor clean and to divert the exhaust gas sample towards the outer collecting channel. The mixture of air and exhaust gas sample was finally vented from the collecting channel. The length of the tube relevant for smoke measurements was optimized as described later to 0.5 meters. A photograph of the instrument is shown in Fig. 2. The measuring tube is placed behind the panel which displays the control instruments for pressure, temperature and mass flow of the gas sample and the purge air. The optical instrument is featured to the left of the smoke meter.

The optical instrument, which was provided by the E. Sick[5] company, employs a chopped, dual beam optical system. The light from the source is divided into two parts by a beam splitter. The measuring beam is transmitted through a semipermeable mirror and an optical lens across the entire width of the measuring tube to a corner - cube reflector on the opposite side. The beam is reflected back to a photocell receiver in the optical instrument. The reference light beam is projected directly to the receiver. The rotating disk modulates the two light beams at two different frequencies (1.5 kHz) so that both beams can be measured by the single photocell in conjunction with an electronic amplifier and a readout unit. The reference beam provides automatic gain control and therefore compensates for any change in light output or change in photocell response as a result of temperature changes, voltage fluctuations or aging of these components. Therefore, the optical system is free of inherent drift errors. The reflector aperture size was adapted

to the tube width to maintain a large ratio of beam cross sectional area to reflector area. Since the beam is uniform, the reflector returns a constant amount of light, regardless of what portion of the beam hits the reflector.

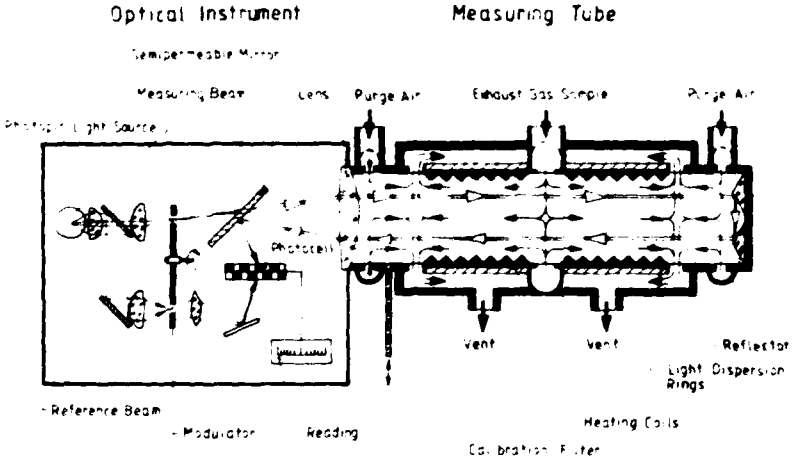

Fig. 1 Scheme of Optical Smoke Meter

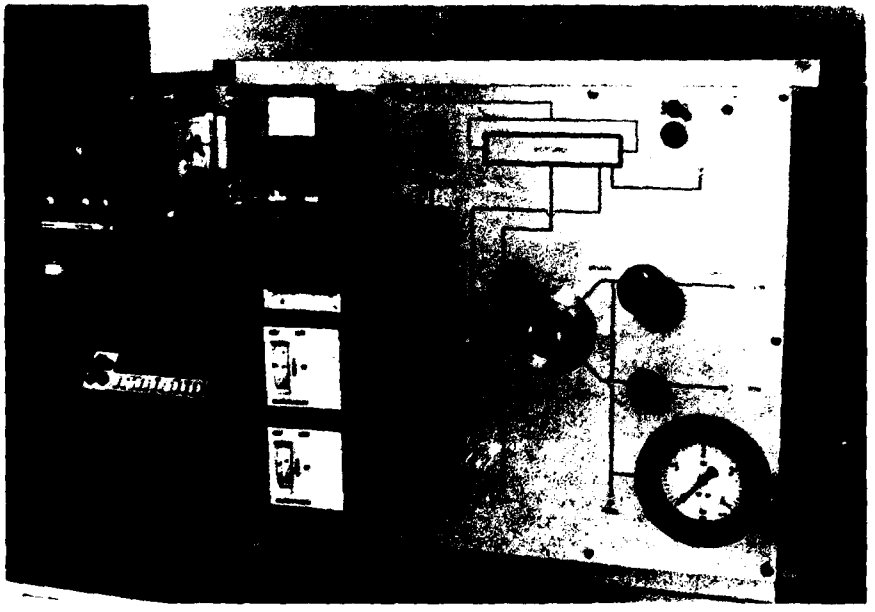

Fig. 2 Optical Smoke Meter

The optical instrument utilizes a photocell-filter combination to achieve a photopic spectral sensitivity. The maximum light intensity is at 0.55 micron wavelength. The instrument avoids therefore large errors caused by water absorption bands in the near infrared region of the light spectrum. Furthermore it has a low response to submicron particulate matter which results in low errors implied by aerosols.

The milliamp current output of the instrument is direct proportional to the optical density (D) across the light path (1). The optical density is defined as the logarithm to the base 10 of one over the transmittance (T):

$$D = \log 1/T \qquad (1)$$

The light transmission through a measuring volume is expressed by the ratio of the attenuated light intensity (I) to the initial intensity (I_o).

$$T = \frac{I}{Io} \qquad (2)$$

It can be related to the more practical scale of opacity (Op) used in Hartridge smoke meters as:

$$Op = 1-T \qquad (3)$$

Equation (1) can be rewritten in the form of Bouguer's Law:

$$T = 10^{-D} \qquad (4)$$

By employing the well known Lambert-Beer's Law to a unit volume of gas and assuming that the light attenuation is caused by carbon particles alone, one can show that the optical density is proportional to the pathlength and the concentration (C) of carbon particles:

$$D = k \quad C \quad l \qquad (5)$$

where k is the coefficient of extinction.

This relationship can be readable used to optimize the smoke tube width. Since for the two folded light beam the light path is twice the smoke tube width the latter was designed to yield high density sensitivities for the range of smoke emissions encountered from aircraft engines.

The design features of the SICK optical instrument assure an operational accuracy of $\pm$ 2.5% of the full scale span. The absolute accuracy of the scale of optical density can be calibrated by density filters of known optical density. The calibration filters used are shown in Fig. 3. Since the smoke emission of gas-turbine engines is low and falls into a range where the optical density is nearly linear to the opacity only the filter with an optical density of 0.073 was used for continuous calibrations. For the specific light path optimized for the smoke meter its optical density corresponds to on opacity of 15.75%. The filter can be easily swept by hand or by a time monitor into the light path.

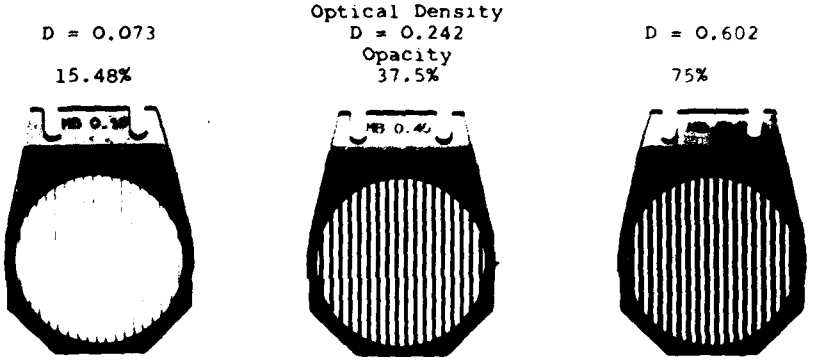

Fig. 3 Calibration Filters of the Optical Smoke Meter

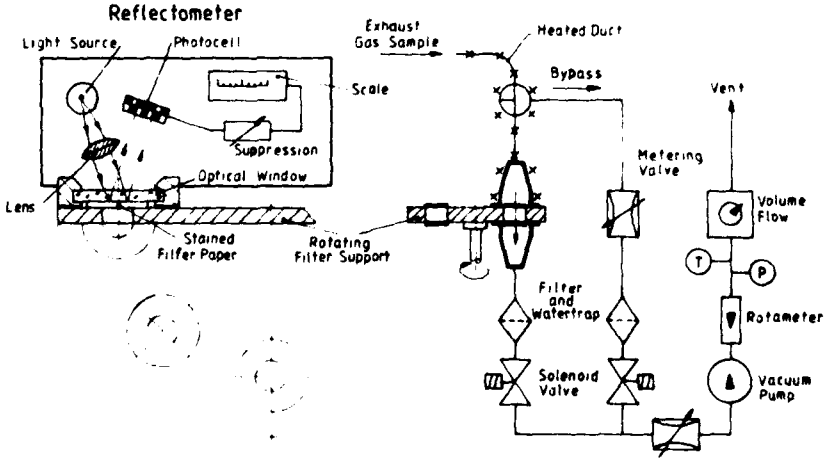

Fig. 4 Scheme of MTU-ARP1179 Smoke Meter

The second smoke meter employed at MTU Munchen was assembled according to the Aerospace Recommended Practice ARP-1179. It is the system put forward by the EPA in their rules. A schematic of the system is shown in Fig. 4. The exhaust gas sample which was diluted in heated lines was divided by the first valve into a sample and bypass mode of operation. During the sample mode the gas was passed across the filter paper which was fixed in a rotatable support.

The filter holder was also heated and clamped firmly the filter paper avoiding any small leaks. Its internal geometry corresponded to the EPA requirements and it was made of corrosion-resistant material. The filter paper area 'A' was 7.52 cm^2.

The downstream metering valves were used to establish the system flow rates. The gas sample was drawn by a vacuum pump which was bypassed when drawing from high-pressure sources such as the combustor rig and the engine exhaust. The flow rate, once established, was held constant and measured by the rotameter. The sample size 'W' was determined with a positive displacement volume meter, with pressure and temperature measurements taken immediately upstream. Its reading was generally close to the standard volume value, since the associated pressure and temperature values were near atmospheric.

A photograph of the MTU ARP-1179 smoke meter is shown in Fig. 5. The flow rate adjustment valves and the rotameter are on the right of the panel. One can see the rotatable filter support in the middle of the apparatus.

Fig. 5 ARP-1179 Smoke meter

The filter paper inserted into the filter support was the required Whatman No. 4 paper. The smoke spots accumulated on the filter paper during the sample operation and were evaluated with a reflectometer which was incorporated in the apparatus shown in Fig. 5. The measuring principle of the reflectometer is shown in Fig. 4. The light beam of the source was directed onto the filter paper and the diffuse reflectance was measured by a photocell. The smoke number (SN) was calculated from the reflectance reading of each spot by:

$$SN = 100 \ (1 - R_s/R_w) \qquad (6)$$

where R_s and R_w are the diffuse reflectance of the sample spot and clean filter, respectively. The smoke number of four sample sizes was determined according to the specifications and plotted on semilog coordinates, with the sample size per unit filter medium area (W/A) as the logarithmic abscissa. The reported smoke number was read from the straight line joining the four points for the specified sample size W/A = 0.0162 gm/mm^2.

The reflectometer was calibrated for total reflectance with a standard having a white chalk coloured surface and for total diffusion with a black standard. Calibration was made regularly throughout the measurements.

4. Sampling technique and probe design

The sampling system used for smoke measurements during combustor rig and engine compliance tests is shown schematically in Fig. 6. The sampling lines, their geometry, overall length and bending radius correspond to the EPA requirements. The lines were

heated and the gas sample temperature kept at 150°C up to the measuring instruments. An isokinetic mass flow reducer was installed in the sampling line in order to ensure that the mass flow directed to the instruments contained the respresentative smoke concentration. Dry purge air was used for operation of the optical smoke meter and for cleaning the ARP 1179 instrument. The continuously measured smoke emission and some characteristic data of test conditions were traced by a multi-channel chart recorder.

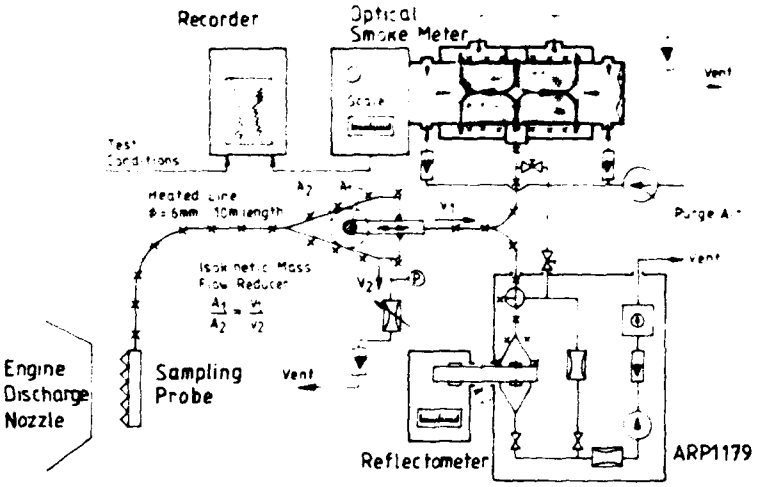

Fig. 6 Sampling System Schematic Diagram

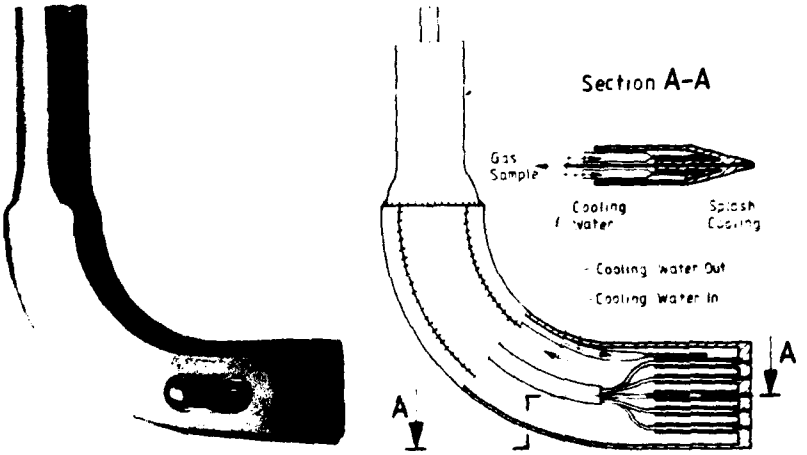

Fig. 7 Sampling Probe for Combustor Tests

For sampling smoke emissions from combustor rig tests a five-point water cooled pitot-like probe was designed, and is depicted in Fig. 7. The width of the probe corresponds to the annular combustor exit plane height. The cooling water impinges on the hot leading surface of the probe and is drained along the inner structure. It is kept under pressure above a temperature of 100°C. The five gas sampling lines are joined in a main duct as shown in the photograph. The sample gas temperature inside the duct is monitored by a thermocouple.

Three gas sampling probes were installed in the combustor chamber outlet plane as shown in Fig. 8. In order to obtain a full outlet traverse during a complete traverse gear sweep they were placed 120° apart. During the same sweeps, temperature traverses of the combustor chamber outlet were also recorded and it was possible to select a single probe smoke emission traverse as well. The photograph shows the probe set-up for high-pressure combustor tests. One can see the combustor exit liner and the pressure nozzle.

A multipoint sampling probe for smoke measurements was designed at MTU Munchen based on the specification for engine compliance tests laid down by EPA. A schematic of the probe and some special design features are shown in Fig. 9. The 28 sampling holes were of equal diameter and covered the exhaust gas jet. The sampling probe was placed immediately behind the engine exit plane. The cooling system was designed to protect the probe even during engine reheat operation. The cooling water was injected into the forward plenum of the probe. From the plenum the largest part of the water was passed through thin holes in the wall and impinged on a cooling jacket. It was then directed along the slit between the jacket and the outer structure surface to the rear and vented into the exhaust gas stream. The other part of the water passed through holes in the strut from the plenum into the afterbody of the probe, from where it was also vented into the gas stream.

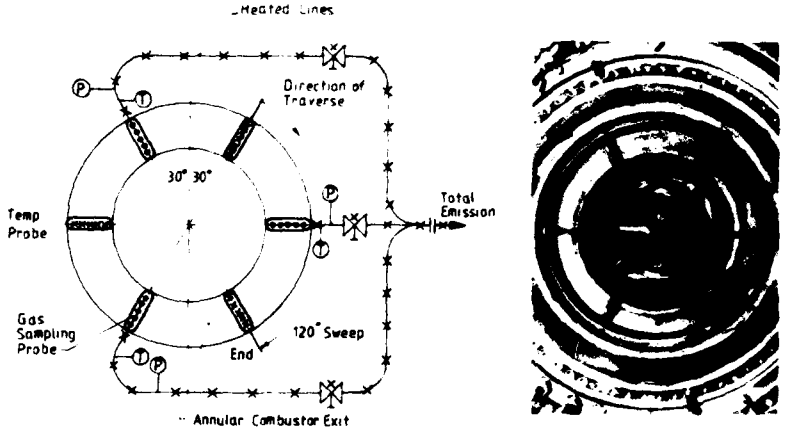

Fig. 8 Probe Installation for High Pressure Combustor Full Annular Traverse

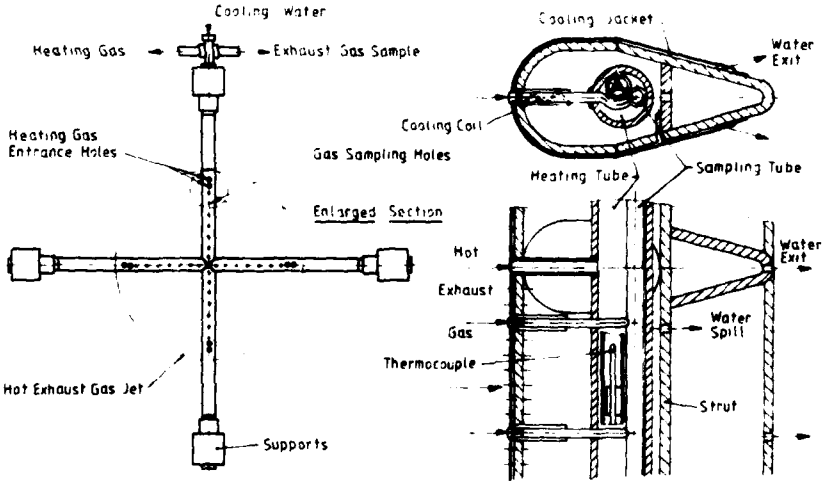

Fig. 9 Sampling Probe for Engine Tests

The principal pressure drop of the exhaust gas sample occurred at the entrance orifices. The samples were mixed in a main sampling tube installed in a heating tube, thus avoiding the precipitation of water. The heating medium was hot exhaust gas entering the tube through pipes arranged at the outer region of the gas jet. The flow rate of the hot gas was monitored by thermocouples to keep the temperature in the tube around 150°C. The installed probe during engine reheat operation is shown in Fig. 10. The probe was used for smoke and gas component emission measurements as well.

5. Correlation of smoke emission data

The two smoke meters connected to the same sampling probe as shown in Fig. 6 were calibrated to each other during high pressure combustor rig tests. This method of cross-calibration was chosen because no specified absolute smoke concentration caliber exists and techniques basing on the formation of well defined aerosol mists were not reliable. A typical example of such a cross-calibration is shown on the graph in Fig. 11. The direct reading of the ARP 1179 instrument, i.e. SN, acquired from four samples, is plotted against the optical density indicated by the optical smoke meter for the same combustor operating conditions. The scale on the right represents the smoke density of the sample. It was obtained by measuring the mass of each smoke spot on the filter paper and relating it to the unit sample size. The calibration results plotted on the graph were obtained from tests with various combustors.

Fig. 10 Smoke Sampling Probe During Engine Test

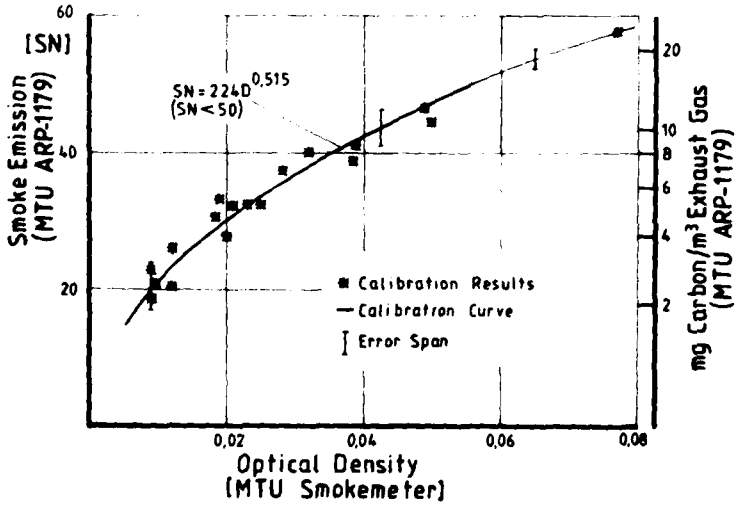

Fig. 11 Calibration of MTU Smoke Emission Instruments

The range of data scatter depicted on the graph can thus be explained by the error in the instruments themselves which becomes larger for low smoke numbers and by the difference of carbon particle size distribution for low and high smoke emission combustors. Viewed through a microscope the nature of carbon particles deposited on the filter paper appeared somewhat different for low smoke and high smoke-emission combustors. An example of smoke spots sampled from various combustors is shown in Fig. 12. The filter papers were placed on the rotating disc in such a way as to show a clockwise reduction of SN. Although no detailed investigation was included in this program for determining the

composition and the particle size distribution of the smoke spots, it was qualitatively observed that low-smoke combustors deposited small (0.1 μm) and soft carbon particles whereas high-smoke combustors emitted larger (0.2 μm) and more brittle material. The soft carbon particles tended to agglomerate very irregularly on the filter paper surface which made the smoke spot become more or less diffuse to light reflection. The optical diffusion coefficient (K) of the smoke spot can be expressed by the number of particles per unit volume (n), the average projected area of each particle (A) and the specific absorbance (q):

$$K = n\ A\ q \tag{7}$$

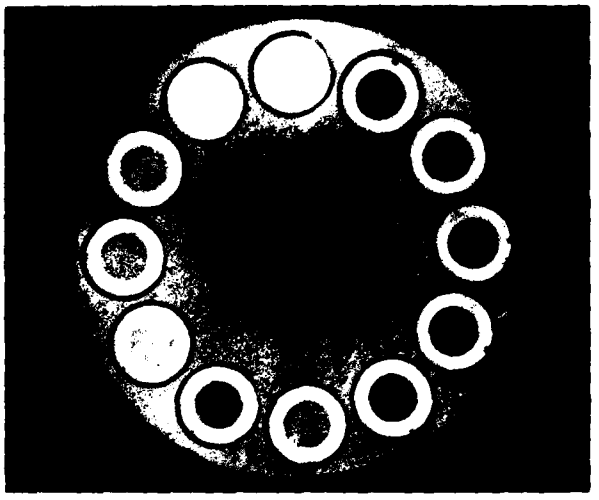

Fig. 12 Smoked Stained Filter Paper

Stochastic agglomeration of particles on the filter surface can obscure the average projected area and since the intensity of the reflected light is a function of the optical diffusion coefficient, different reflectivities where measured for the same true smoke density.

It should be noted therefore that the optical diffusion coefficient (eq. 7) can be set equal to the extinction coefficient (eq. 5) only if the smoke spot is uniformly covered by particles. This result restricts the characterization of smoke emitted by turbomachines made by Pianko[6] to such cases of uniform particle distribution on the smoke spot.

The correlation between the smoke number SN and the smoke density agrees well with a similar relationship reported by Champagne[6].

As can be seen from Fig. 11, the optical density was affected to a lesser degree by the constitution of the smoke plume. Since the smoke particles moved homogeneously through the smoke tube, no local agglomeration was possible and, as has already been described, the photopic light system prevented the light attenuation by small particulate matter. Furthermore, low smoke-emission combustors had a steady smoke emission characteristic as is shown in Fig. 15.

The correlation between the smoke number and the optical density for SN 50 can be expressed as

$$SN = 224\ D^{0.515} \tag{8}$$

This relationship was used to compare engine smoke emission measurements with compliance regulations. The MTU optical smoke meter was calibrated against a Hartridge smoke meter by using the same sampling line connections shown in Fig. 6 only substituting the ARP 1179 instrument. The calibration results are shown in Fig. 13 where the Hartridge Smoke Units (HSU) are plotted against the measured optical density for the same combustor operating point. The relationship between HSU, wich is identical to the opacity of the gas sample, and the optical density is linear for the low smoke emission. Since the exhaust gas sample under investigation was the same for both instruments the coefficient of extinction and the smoke concentration were identical. The optical density of the Hartridge smoke meter can be deduced therefore, from equation 5 as:

$$D_{HSU} = D_{MTU}\ \frac{l_{HSU}}{l_{MTU}} \tag{9}$$

The broken line in Fig. 13 represents this relationship. Since the length of the optical path of the MTU smoke meter was chosen to be approximately twice that used for the Hartridge meter, the sensitivity of the MTU measuring instrument was greatly improved. As illustrated in the graph by the shaded portions, the sensitivity of the optical density of the MTU smoke meter has doubled in the range of smoke visibility. A further increase in the path length, which would have resulted in still higher sensitivities, was

discarded because the transient response of the instrument would have been worsened owing to the longer filling time of the smoke tube.

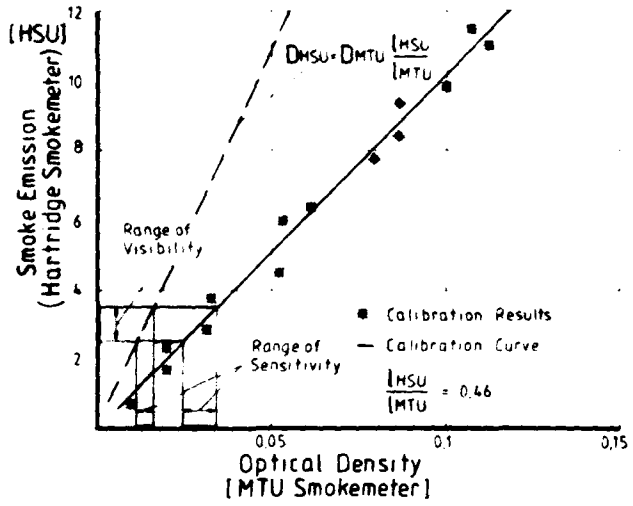

Fig. 13 Calibration between MTU-Smoke Meter and Hartridge-Smoke Meter

The calibration results were compared with correlation formulas deduced from previous measurements. They are plotted in Fig. 14 as HSU versus SN together with correlations given by Pianko[6] and Shaffernocker[8]. The improved sensitivity of the MTU smoke meter made it possible to obtain reproducible results for low smoke emissions, which allows for a reliable correlation at SN<20.

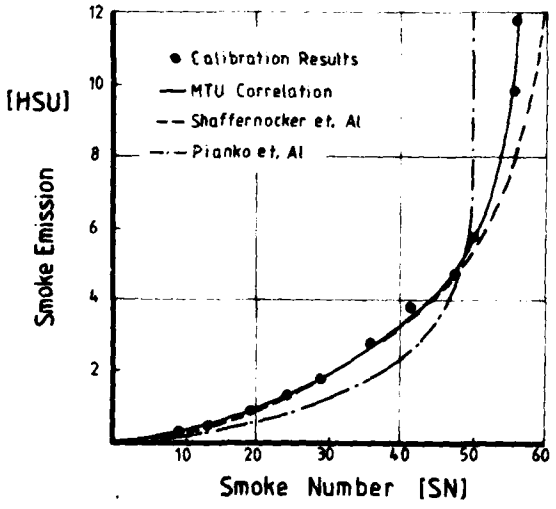

Fig. 14 Comparison of Smoke Emission Data

The MTU correlation curve and the relationship given by Shaffernocker agree well for SN<50. Both curves were determined experimentally. The theoretical curve by Pianko for an assumed coefficient of extinction k = 0.5 deviates from the measured values even for SN<50. The reason of this deviation has already been described and stems from the assumption that the coefficient of absorbtion is equal to that of extinction. Shaffernocker has obtained a good correlation of his experimental data by using a value of k = 0.913 for the extinction coefficient.

6. Combustion chamber and engine smoke measurements

The optical smoke meter has been extensively used for combustor development work and engine compliance tests. Its ability to monitor continuously the optical density of exhaust gas samples made it possible to determine locally sources of high smoke production in combustors during high pressure operating conditions.

Some typical traces of smoke emissions from combustor development tests are shown in Fig. 15. The variation in smoke emission expressed in HSU sampled by a single sampling

rake (see Fig. 7) during a stepwise traverse of 120° is plotted for a combustor at three development stages. The traverse gear, which was rotated by an increment of 5 degrees, was held in the same position for 0.5 minute to allow stabilization of the measuring conditions. The combustor operating conditions were the same for all three traces: inlet pressure and temperature 15 bar and 830 K respectively, and air fuel ratio 42.

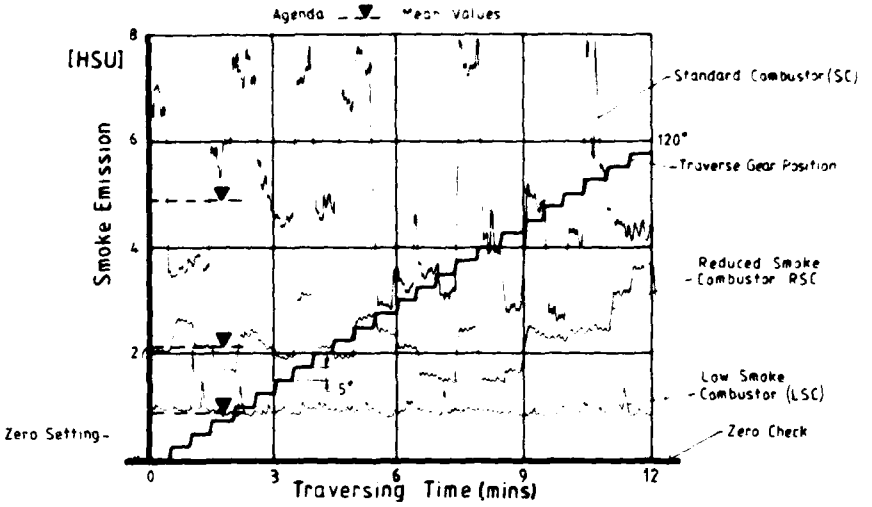

Fig. 15 Smoke Emission Traverse from HP Combustor Tests

The standard combustor, which incorporated vaporizers for fuel injection, exhibited large variations in smoke emission levels. From the pattern of smoke variation it was possible to locate sources of smoke formation in the primary zone and hence design modifications to avoid them, which were incorporated in a reduced-smoke combustor. This combustor showed a more uniform annular smoke distribution at a lower level. Aerodynamic rebalancing of the primary zone resulted in a low-smoke combustor which had a uniform smoke emission at a mean level below 1 HSU. The mean values shown on the graph were calculated off-line by an automatic data acquisition system. The knowledge of full annular smoke emission distribution has proved to be a necessary prerequisite for developing successful smoke reduction modifications for combustors.

Results of smoke emission measurements from engine tests using the according sampling probe (see Fig. 9) are represented in Fig. 16. The measured HSU values are plotted against the high pressure shaft rotation. The result of combustor development work becomes very obvious, the engine fitted with the low smoke combustor has a smoke emission level below the visibility threshold over the full operation range. The results of combustor rig tests at engine conditions compare well with the engine results. Since they are not corrected by the amount of HPT cooling flow which mixes with the main gas stream and causes a reduction in the smoke concentration and thus in the HSU value, they lie above the curves linking the engine smoke measurements.

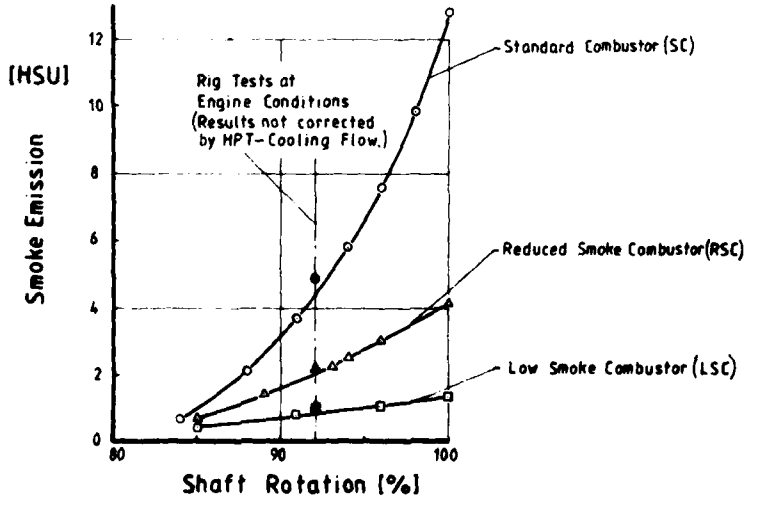

Fig. 16 Smoke Emission Measurements from Engines

7. Conclusions

By using an optical densitometer with high accuracy and incorporating it in a newly-designed smoke tube an indirect optical system has been developed with sufficient sensitivity to evaluate low smoke emissions from gas turbine engines. Because of the optimization of the optical path length of the system with regard to high sensitivity and transient response, continuous monitoring of smoke emission from combustors and aircraft engines was possible. Calibration of the optical system with an ARP 1179 smoke meter, using the stained filter paper technique, for smoke measurement, and a Hartridge instrument showed reliable data, which were reproducible at low smoke concentrations. Since the system is compatible with automatic data acquisition, fast evaluation of test data was possible.

The sampling probes designed for high-pressure combustor and engine compliance tests permitted the extraction of representative exhaust smoke samples. The measurement of full annular smoke distributions at combustor outlets has proved to be an indispensable information for low-smoke combustor design.

8. References

1. Environmental Protection Agency: "Control of Air Pollution from Aircraft and Aircraft Engines; Emissions Standards and Test Procedures for Aircraft". Federal Register 38 (136) Part II: 190 76 (July 17, 1973)

2. W.S. Blazowski, R.E. Henderson "Aircraft Exhaust Pollution and its Effect on the U.S. Air Force". Technical Report AFAPL-TR-74-64 (August 1974)

3. Environmental Protection Agency "Control of Air Pollution from Aircraft and Aircraft Engines". Federal Register 43 (58) Part III (March 24, 1978)

4. B.T. Zinn "Experimental Diagnostics in Gas Phase Combustion Systems". Progress in Astronautics and Aeronautics Vol.53 (1977)

5. E. Sick "Measurement of Opacity and Particulate Emissions with the Erwin Sick Smoke Density Meter". Optic Electronic, Munich (1975)

6. M. Pianko, C. Verdier "Characterization of Smoke Emitted by Turbomachines". L'Aéronautique et L'Astronautique No. 67 (1977)

7. D.L. Champagne "Standard Measurement of Aircraft Gas Turbine Engine Exhaust Smoke". ASME Paper No. 71-GT-88 (April 1971)

8. W.M. Shaffernocker, C.M. Stanforth "Smoke Measurement Techniques". SAE Paper No. 680346 (April 1968)

DISCUSSION

K.Kohse-Hoinghaus, Ge

How do you define smoke so that it is not dependent on the type of mixture and so that you have no need to correct for absorption of Hydrocarbons, SO_2, H_2O, etc

Author's Reply

Smoke in our terminology is black, grey or even white particles, including aerosols, suspended in the gaseous exhaust stream which obscure, reflect and refract light. Therefore any particles or chemical substances like hydrocarbons or SO_2 that attenuate light are smoke and we do not have to correct for their absorption. For the gas turbine producer smoke is, if you wish, a definition and not a specific substance.

E.Covert, U S

Would you please discuss the problem of selecting the velocity of flow in the sampling tube and the cell to keep particles suspended over a wide range of particle size?

Author's Reply

The velocity of the flow in the sampling tube was selected to keep smoke particles afloat. To achieve this, a series of tests was necessary and the results from those tests are in fact the actual operational know-how. The way the exhaust gas sample is introduced into the smoke measuring tube and the purge air mass flow is adjusted, required a good deal of experimental work. Although I don't want to quote exact figures, I can give you an indication of the range of velocities by telling you that the sample mass flow is four to five litres per minute and the approximate inner diameter of the tube is 50 cm.

V.Wittmer, Ge

In the paper a smoke number (SN) is described. Does a correlation exist between this SN and the soot number of the Bacharach scale?

Author's Reply

The correlation between the smoke number, SN and the Bacharach soot number is described in the literature. You can find a correlation curve in the paper by Shaffernocker which I have listed in the references. We have not calibrated our optical smoke meter against an instrument recording soot numbers because the latter is much too insensitive at low smoke concentrations. The Bacharach soot number is therefore also not being applied in combustor or engine development work.

D.H.Lister, UK

One of your slides showed the calibration curve of the MTU optical smoke meter against an ARP-1179 filter system. The minimum values were about SN = 20 where the errors were becoming significant. Would it be feasible to use the optical method for making satisfactory measurements below SN = 20, (e.g. at SN = 10) since this is the region for many civil engines?

Author's Reply

The graph in Figure 11 you are referring to was limited to SN = 20 because the ARP-1179 instrument was not accurate enough for lower values. It was difficult to get a decent grey spot on the filter paper even for large sample sizes like 500 litres. We omitted, therefore, for calibration purposes, smoke concentrations below SN = 20. The optical instrument, however, is well suited to measure values of SN = 10 (i.e. D = 0.01) with the accuracy described in the paper. In fact Figure 13 shows a measuring point at D = 0.012. If one concentrates measurements of smoke emissions below SN = 20 one can calibrate the full-scale span of the optical instrument accordingly to D = 0.025 and use such a calibration filter for continuous checks. Let me stress especially for civil applications the advantage of the optical smoke meter, which needs a sample flow of only about five litres per minute for accurate readings, as compared to up to one hundred litres per minute for the ARP-1179. The saving in measuring time and costs becomes thus obvious.

J.S.Lewis, UK

Are you surprised at the good correlation that you obtain between rig and engine tests particularly when you consider the different conditions that exist; for example,

(i) on the bypass engine in question the turbine exhaust gases partially mix with the clear air from the fan at the nozzle exit plane which makes obtaining a representative sample difficult?

(ii) does any burn-out of carbon particles occur between the combustor exit plane (on the rig) and the engine nozzle exhaust plane?

Author's Reply

I was surprised, and obviously pleased, by the good correlation between engine and rig results, but a detailed look at the correlation, which will also answer your two questions, makes it not so surprising but obvious. First, the exhaust gas sample holes in our engine rake cover only the outlet area of the core jet. We avoid therefore the mixing effect of the bypass air and do measure in fact the smoke emission from the combustor. Second, the already small smoke concentration measured during combustor tests makes after burning of smoke particles improbable and this is proved in fact by the good correlation. If one bears in mind that the combustor tests are performed under true engine conditions (pressure, entry temperature and AFR) the good correlation is, as I have mentioned, not really surprising anymore.

W.G.Alwang, US

Is it a problem to keep the optics free of dirt and soot? Does the calibration drift due to this effect?

Author's Reply

Since the purge air on both ends of the tube diverts the exhaust gas sample completely, no dirt or soot reaches the optics and hence we do not have problems of keeping them clean. In fact, as you can see from the sketch in Figure 1, the advantage of our design is that we can even skip the application of windows which are the source of problems in conventional apparatus. As a consequence we do not have a calibration drift caused by sooting of glass windows. We use, if you wish, aerodynamic curtains.

ETUDE DES GAZ D'ECHAPPEMENT D'UN TURBOREACTEUR EN RECHAUFFE

Ph. GASTEBOIS
SNECMA
Centre d'Essais de Villaroche
77550 Moissy Cramayel, France

S. ROPARS
Centre d'Essais des Propulseurs
Saclay
91406 Orsay, France

RESUME

La connaissance des températures locales et des concentrations en espèces polluantes dans le jet d'un turboréacteur en rechauffe est utile au motoriste à deux titres :

- d'une part, pour optimiser le rendement de la réchauffe,
- d'autre part, pour évaluer l'importance de la pollution de l'air créée par le moteur.

Un dispositif d'analyse des gaz prélevés par peignage à la sortie de la tuyère d'un moteur OLYMPUS au sol et en altitude simulée est présenté.

Les résultats obtenus montrent la difficulté de figer la composition des gaz prélevés avant l'analyse et la nécessité d'améliorer les techniques de mesure dans les gaz d'échappement à haute température.

1 - INTRODUCTION

La connaissance des températures locales et des concentrations en espèces polluantes dans le jet d'un turboréacteur en rechauffe est utile au motoriste à plus d'un titre. Elle lui permet d'une part de calculer le rendement de profil et le rendement enthalpique de la rechauffe et de disposer des données de base pour optimiser la répartition du carburant dans le système de rechauffe. Elle lui permet d'autre part de rechercher les solutions susceptibles de diminuer la pollution due à la rechauffe en partant des données recueillies expérimentalement.

Rappelons en effet qu'en rechauffe une combustion résiduelle importante se produit dans le jet issu de la tuyère permettant l'oxydation d'une fraction du Co et des hydrocarbures imbrûlés présents à la sortie de la tuyère. La mesure de la pollution d'un moteur doit donc en principe se faire dans un plan situé suffisamment loin dans le jet pour que par suite du mélange avec l'air ambiant, les évolutions chimiques soient terminées. Ceci a été effectué pour connaître la pollution au régime de décollage au sol mais ne peut se faire si l'on veut mesurer la pollution d'un moteur en rechauffe dans les conditions d'altitude. En effet on ne peut en général pas réaliser la mesure au caisson d'altitude très loin de la tuyère et en outre la simulation de l'écoulement externe n'est pas correctement simulée, les évolutions chimiques n'étant alors pas semblables à ce qu'elles sont dans la réalité ; on est donc contraint d'effectuer la mesure dans le plan de sortie de la tuyère et d'utiliser une modélisation de l'évolution des espèces polluantes dans le jet pour calculer la pollution résiduelle effective.

Toutefois la mesure de ces températures locales très élevées, dans un environnement très sévère, ainsi que le figeage des échantillons gazeux prélevés posent des problèmes difficiles que nous avons tenté de résoudre par l'utilisation de sondes à détente supersoniques.

Une campagne d'essais sur moteur OLYMPUS au caisson d'altitude R5 du CEPr a permis d'exploiter ces techniques sur un système de rechauffe simple ; les résultats de ces essais sont présentés dans ce qui suit.

2 - MATERIEL EN ESSAI - EQUIPEMENT DE MESURE

2.1 - Le moteur en essai

Le moteur en essai est un turboréacteur simple flux avec rechauffe OLYMPUS 593 Mark 610 de conception ROLLS-ROYCE/SNECMA présenté en coupe Figure 1.

Le taux de compression est de 16 au décollage et 11,3 en croisière. Les compresseurs basse et haute pressions ont tous deux sept étages de compression et chacun est entraîné par une turbine mono-étage. Le moteur est équipé d'une tuyère primaire à section variable qui permet en ajustant des vitesses de rotation des corps haute pression (HP) et basse pression (BP) d'obtenir simultanément les vitesses de rotation et la température d'entrée turbine optimales dans toute la plage de variation de la température de l'air à l'entrée du moteur.

La rechauffe permet avec un taux de rechauffe de 20 % de réaliser au décollage une poussée très élevée par rapport à la poussée utilisée en croisière (5 fois plus). Elle est utilisée pendant l'accélération transsonique et la phase de montée à l'altitude de croisière. Le système de rechauffe est de conception SNECMA ainsi que l'ensemble des tuyères primaires et secondaires. Le système de rechauffe comprend un stabilisateur torique à profil en V de 570 mm de diamètre et une rampe d'injection de carburant à contre-courant à enclume située en amont du stabilisateur. L'ensemble est fixé sur le cône d'échappement.

2.2 - Equipements de mesures et d'essais

2.2.1 - Caisson de vol simulé

Le caisson en vol simulé peut être utilisé pour des essais aérodynamiques et des essais de moteurs complets en veine forcée ou en jet libre. Un schéma du caisson est présenté figure n° 2. Il est représentatif d'un essai en veine forcé du moteur OLYMPUS. Le caisson est divisé en deux compartiments.

- un compartiment de tranquillisation relié aux circuits d'air d'alimentation et qui assure par ses dimensions une faible vitesse favorable à la mesure de la pression génératrice et au fonctionnement du pavillon d'aspiration. Ce pavillon, qui n'est pas lié mécaniquement au moteur permet, après un étalonnage préalable, le calcul du débit d'air.
- un compartiment aval, relié aux circuits d'extraction, dans lequel est disposé le moteur en essai. Ce dernier est fixé sur une bascule reposant sur des lames élastiques et solidaire d'un dynamomètre à jauges de contrainte permettant la mesure de la poussée.

Les dispositifs de mesure sont reliés à un ordinateur capable d'acquisitions et de calculs en temps réel. Le système d'acquisition automatique permet de relever en 6 secondes plus de 300 paramètres. L'ordinateur assure également un contrôle du bon fonctionnement de la chaîne de mesures et le calcul en temps réel des paramètres utiles à la conduite de l'essai. Les calculs plus élaborés sont effectués en temps différé à partir des valeurs enregistrées pendant l'essai.

2.2.2 - Le dispositif mobile de prélèvement

Le dispositif mobile d'analyse de gaz comprend :

- un peigne de prélèvement des gaz,
- un support motorisé assurant le déplacement du peigne.

a) - Peigne de prélèvement

Le peigne de prélèvement de gaz a été conçu et réalisé par la SNECMA. Il est du type dit "à fixage rapide". Ce peigne est représenté sur la planche n° 3. L'ensemble du peigne est en acier inoxydable Z 10 CNT 18.

Il se compose de huit sondes identiques équidistantes. Dans chaque sonde, comme l'indique le dessin de la figure n° 4, les gaz sont détendus dans un divergent dont le col a un diamètre de 1 mm, puis circulent dans un premier tube à section constante suivi d'un second tube d'un diamètre supérieur.

Les gaz brûlés sont acheminés dans huit tubes disposés axialement et collectés à une extrémité sur un support thermiquement isolé. Les tubes passent dans une gaine alimentée par de l'air chaud obtenu par le chauffage électrique de l'air industriel et maintenu à 150° C afin d'éviter toute condensation d'eau et d'hydrocarbures.

Les efforts aérodynamiques sont supportés par un tube interne épais et repris aux extrémités par deux brides liées au dispositif de déplacement.

Un circuit d'eau assure le refroidissement de l'envelope externe et des huit sondes de prélèvement de manière que la température du métal n'excède pas 200° C et ce afin d'assurer une bonne tenue mécanique du peigne dans le jet du réacteur. Ce circuit est alimenté par une pompe à eau dont le débit est de 12 m3/h sous une pression de 2 bars par l'intermédiaire d'une arrivée unique ; l'évacuation se fait par deux orifices calibrés permettant de régler la répartition des débits servant au refroidissement de l'enveloppe externe d'une part et des huit sondes de prélèvement d'autre part. La température de sortie de l'eau a été maintenue au-dessous de 80° C par le réglage du débit d'eau.

Le peigne de prélèvement a été disposé à une distance de 0,25 m du plan de sortie de la tuyère.

b) - Support motorisé

Le support motorisé assurant le déplacement du peigne de prélèvement est représenté schématiquement sur la figure n° 5.

Le peigne est fixé :

- à sa partie inférieure à une bride solidaire d'un tube mobile autour d'un palier fixé sur la partie basse du caisson,
- à sa partie supérieure à une bride solidaire d'un écrou sur coulisseau se déplaçant sur une tige filetée dont la rotation est assurée par un moteur électrique refroidi à l'air comprimé.

Le déplacement du peigne est donc angulaire. Son déplacement permet d'assurer les mesures dans toute la section de la tuyère.

A l'autre extrémité de la tige filetée sont fixés deux potentiomètres refroidis par de l'air atmosphérique, qui déterminent la position angulaire du peigne par des tensions variables enregistrées sur voltmètres numériques. Une courbe d'étalonnage transforme ces tensions en valeurs angulaires qui sont enregistrées sur l'ordinateur.

Des butées limitent le déplacement angulaire du peigne et déterminent une position de référence peigne vertical.

La commande de la motorisation est effectuée à partir du local d'analyses, mais une commande de sécurité permet de figer le peigne en dehors du jet à partir de la cabine d'essais

2.2.3 - Le circuit de transfert

A la sortie du peigne, les gaz sont acheminés jusqu'au local d'analyse par huit tuyauteries. Ce circuit se compose de 2 parties :

- un tronçon de 1 m en tuyauteries souples (Téflon) de diamètre 8 mm à la sortie du peigne de prélèvement,

- un tronçon d'une longueur de 7,5 m en tuyauteries inoxydables de diamètre 8 mm reliées par des raccords inoxydables.

Chaque tronçon forme un faisceau de 8 tubes entourant une âme d'amiante et sur lequel est enroulé un cordon chauffant calorifugé (figure n° 6). Le maintien de la température des tubes à 150° C est assuré par des thermocouples de masse qui commandent la marche ou l'arrêt du chauffage.

2.2.4 - Le circuit d'analyse de gaz

Le circuit d'analyse de gaz est situé dans le local d'analyse et est constitué par (figure n° 6).

a) L'ensemble de commutation chauffé,

b) L'ensemble pompe à vide et circuit de refoulement,

c) Le circuit de purge,

d) Les analyseurs,

e) Les circuits de mesures.

a) L'ensemble de commutation

Cet ensemble a pour but de sélectionner une des 8 lignes de prélèvement à l'aide d'un jeu d'électrovannes. Il permet donc d'effectuer successivement l'échantillonnage des 8 lignes de mesures et la mesure de la pression de chaque ligne. Cet ensemble est chauffé à 150° C.

b) L'ensemble pompe à vide

Son rôle est d'extraire le prélèvement de gaz échantillonné en créant une très forte dépression dans la sonde (sonde à figeage supersonique).

La pompe est chauffée, elle a un débit de 400 l/h à 20 kPa.

A la sortie de la pompe un circuit en dérivation permet de décharger la pompe vers l'atmosphère afin de maintenir constant une pression de 105 kPa vers les analyseurs pour un débit de 250 l/h environ.

En dehors des périodes d'analyse, le gaz prélevé est refoulé vers l'atmosphère. Un clapet anti-retour interdit l'entrée d'air atmosphérique vers les analyseurs dans le cas où la pression de refoulement devient inférieure à la pression atmosphérique.

c) Le circuit de purge

Son rôle est de purger à contre-courant à partir de l'ensemble de commutation jusqu'au peigne de prélèvement les huit lignes avec un gaz neutre (azote) pour éviter un encrassement de celles-ci lors de l'allumage du moteur ou de la post-combustion.

Ce circuit comprend :

- une bouteille d'azote. Cet azote est détendu à 5 bars,
- des électrovannes qui isolent le circuit vers la pompe pendant la phase de purge.

d) Les analyseurs

A la sortie de la pompe les gaz prélevés entrent dans quatre analyseurs :

- un analyseur de CO
- un analyseur de CO_2
- un analyseur de CH_4
- un analyseur de NO_X

Chaque analyseur prélève un débit de 60 l/h que l'on peut régler individuellement. La pression et la température sontmesurées à l'entrée des analyseurs.

Analyseurs CO - CO_2

Les analyseurs fonctionnent sur le principe de l'absorption de rayonnement infrarouge (NDIR) par le monoxyde et le dioxyde de carbone.

Le circuit de prélèvement est commun aux 2 analyseurs. A l'entrée des analyseurs, dès la fin de la partie de ligne chauffée sont montés en série un vase de condensation maintenu à 0° C, un dessicateur chimique et un filtre afin d'éliminer toute trace d'eau et de particule.

Chaque analyseur a son propre circuit d'étalonnage comprenant des bouteilles de gaz de titres différents et un rack d'étalonnage qui permet de sélectionner la teneur désirée et de régler le débit à l'entrée de l'analyseur.

Analyseur de NO_X

Cet analyseur fonctionne sur le principe de la chimiluminescence. Il possède une pompe de circulation à la sortie, le réglage du débit se fait par un robinet de laminage à l'entrée. Il n'y a pas d'élimination d'eau préalable, un dispositif spécial permet d'éviter les condensations dans l'appareil.

Cet analyseur possède également son circuit d'étalonnage partiellement chauffé.

Analyseur de CH_4

Cet analyseur fonctionne sur le principe de l'ionisation d'une flamme d'hydrogène. Il possède une pompe de circulation chauffée à 150° C et possède également un circuit d'étalonnage.

e) Les circuits de mesures

Les températures des gaz dans les tuyauteries de prélèvement, les températures de masse de ces tuyauteries, les températures des gaz à l'entrée des analyseurs sont enregistrées dans la cabine d'essais.

Les mesures effectuées par les analyseurs sont enregistrées et envoyées sur l'ordinateur.

3 - EXPLOITATION DES RESULTATS D'ESSAIS

3.1 - Paramètres intervenant dans le dépouillement

L'ensemble des dispositifs de mesure présentés ci-dessus, ainsi que les paramètres aérothermodynamiques du moteur permettent de connaître les variables suivantes qui serviront directement au dépouillement des essais :

- pression totale sortie moteur PTJ : valeur thermodynamique calculée,
- pression totale au nez de chaque sonde : valeur mesurée en chaque point de mesure P'i,
- pression statique externe du jet : pression caisson PC mesurée,
- débits de carburants dans la chambre principale et dans le foyer de rechauffe mesurés au banc d'essai,
- débit d'air moteur : valeur calculée,
- paramètres aérothermodynamiques à l'entrée du moteur,
- concentration en polluants gazeux : valeurs mesurées en chaque point de mesure par analyse de gaz et corrigées pour tenir compte des dérives éventuelles des analyseurs contrôlés périodiquement pendant l'essai.

3.2 - Calcul de la valeur moyenne de l'indice d'émission

Les analyses des gaz prélevés au travers du jet fournissent les valeurs des concentrations ponctuelles en CO_2, CO, CH_X, NO et NO_X.

Nous avons porté les valeurs mesurées en fonction du rayon relatif de mesure $r_{mesure}/r_{tuyère}$ et tracé le profil moyen de chaque polluant obtenu sur l'ensemble du jet.

Ce profil doit être intégré pour obtenir la valeur moyenne de l'indice d'émission de chaque polluant :

$$IE_{(x)} = \frac{\int_{R_0}^{R_1} 2\pi \; R \; IE_{(x)} \; dR}{\int_{R_0}^{R_1} 2\pi \; R \; dR}$$

Pour cela il faut calculer en tout point la masse volumique et la vitesse à partir des mesures de pression d'arrêt en aval du choc situé au nez de la sonde P'i et des concentrations en CO, CO_2, etc ...

Un programme de calcul fournit les températures d'arrêt et la richesse en chaque point de mesure à partir de la température à l'entrée du moteur et les valeurs des concentrations mesurées.

On suppose que la pression totale à la sortie du jet est uniforme et égale à la valeur thermodynamique calculée PTJ. Le rapport P'i/PTJ permet de calculer le nombre de Mach local et la pression statique locale.

Si la pression statique ainsi calculée est inférieure à la pression caisson, ce qui se produit sur les bords du jet en raison du gradient de pression totale, on fait l'hypothèse que la pression statique est égale à la pression caisson, (hypothèse réaliste compte-tenu de l'étude des profils de pression et du nombre de Mach par la méthode des caractéristiques), et on recalcule à partir de P'i mesuré la valeur du nombre de Mach.

Ceci permet de calculer en tout point la valeur du produit ρV et d'intégrer l'indice d'émission des polluants pourvu que la limite géométrique du domaine du jet soit connue. Il est parfois difficile, compte-tenu des dimensions de la barre de mesure et du petit nombre de points de mesure de délimiter le jet avec précision, dans ce cas nous avons choisi la limite de jet de telle sorte que les écarts entre les valeurs recalculées par intégration et les valeurs mesurées du débit de carburant et du débit d'air moteur soient minimales.

En fait c'est là que réside la plus grande incertitude dans le dépouillement en ce qui concerne le rendement dynalpique de rechauffe, car celui-ci est très sensible au choix de la limite d'intégration. Par contre l'influence de la limite d'intégration est moins sensible sur la mesure des polluants gazeux compte-tenu des valeurs très faibles rencontrées sur les bords du jet.

4 - RESULTATS DES ESSAIS

Nous présentons ici les résultats obtenus dans les conditions simulées d'accélération transsonique ainsi que ceux mesurés dans les conditions plein gaz au sol.

Les résultats figurent dans le tableau 1.

Les figures 7 à 15 montrent :

La carte de température en rechauffe dans les conditions transsoniques à M = 1,2 - Z = 38000 ft, les profils de température et concentrations en polluants mesurées au plein gaz sec et au plein gaz rechauffe dans les conditions sol.

La connaissance de ces profils est indispensable si l'on veut modéliser l'évolution des espèces polluantes dans le jet, on notera particulièrement les profils de CO très plats en moteur sec alors qu'en rechauffe la présence d'une zone réactive est révélée par le pic de CO.

C'est d'ailleurs sur le profil de température et la position de ce pic de CO que l'ingénieur pourra jouer pour diminuer la pollution résultante à quelques dizaines de mètres en aval de la tuyère.

La figure 16 montre les rapports $\frac{NO_2}{NOX}$ tels qu'ils ont été mesurés en sec et en rechauffe montrant la proportion non négligeable de NO_2 présente en rechauffe au décollage.

Nous avons cherché à comparer le rendement enthalpique mesuré par analyse de gaz et le rendement enthalpique déduit des calculs de cycle aérothermodynamique.

Il apparaît un écart d'environ 6 points qui peut être dû à plusieurs causes d'erreurs, d'une part une mauvaise estimation du rendement de profil résultant du profil de température à la sortie de la tuyère et dont la valeur absolue varie beaucoup avec la limite d'intégration, d'autre part les hétérogénéités de température et vitesse dont la figure 1 donne une idée et qui rendent l'intégration imprécise en faisant l'hypothèse d'une symétrie de révolution, enfin il n'est pas impossible que les réactions chimiques se poursuivent en aval de l'onde de choc détachée présente au nez de la sonde. Des mesures optiques effectuées dans des conditions aussi sévères que celles-ci permettraient de lever le doute en ce qui concerne l'efficacité du figeage réalisé par l'ensemble de prélèvement.

5 - CONCLUSION

Une technique de prélèvements d'échantillons gazeux dans le jet d'un moteur en rechauffe a été développée et mise en oeuvre par la SNECMA et le CEPr pour caractériser le fonctionnement de la rechauffe dans les conditions d'accélérations transsoniques et au régime de décollage au sol du moteur OLYMPUS 593. Une telle technique permet de disposer des profils de température et des polluants gazeux à la sortie de la tuyère et permet de connaître le rendement enthalpique et le rendement de profil de la rechauffe ainsi que les valeurs initiales nécessaires à un calcul d'évolution des espèces polluantes dans le jet supersonique.

Une telle technique peut être appliquée également avec succès à un moteur double flux et apporter des renseignements précieux pour améliorer le fonctionnement de la rechauffe ou réduire les émissions polluantes.

TABLEAU 1

Conditions simulées		Conditions entrée moteur		Conditions amont rechauffe		Taux de rechauffe	Indices d'émissions de polluants		
M	Z ft	P_1 kPa	T_1 °C	P kPa	T °K	$\Delta F/F$	CO	HC	NO_X
0,9	33000	44,7	- 8	145	990	0 14,5 %	8,36 80,05	0,32 27	10,92 7,73
1,2	38000	50,4	12,6	149	977	0 13,2 %	7,35 58,72	0,582 33,19	11,45 6,55
1,7	43000	80	78	180	966	0 13 %	5 63,5	0,875 33,34	17,6 11,8
0	0	95,7	12	302	1040	0 17,5 %	3,75 154	0,27 17,9	17,8 10,9

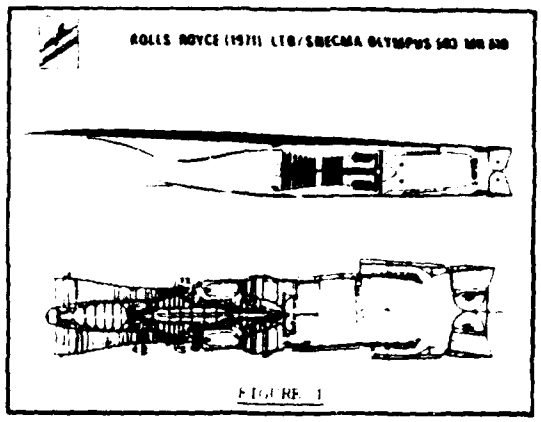

FIGURE 1

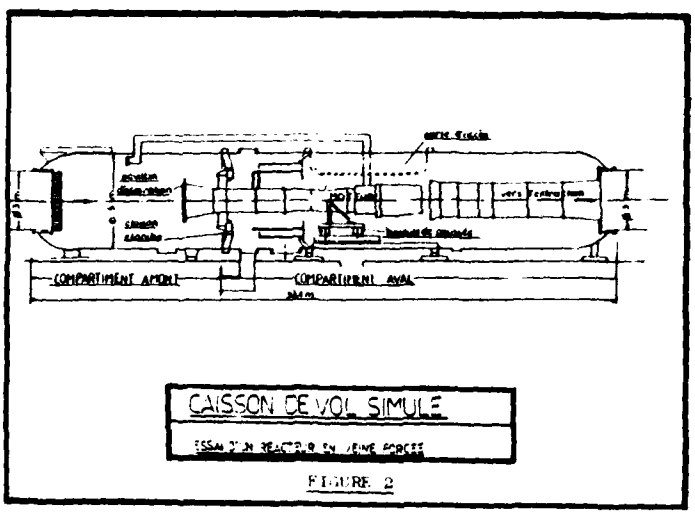

FIGURE 2

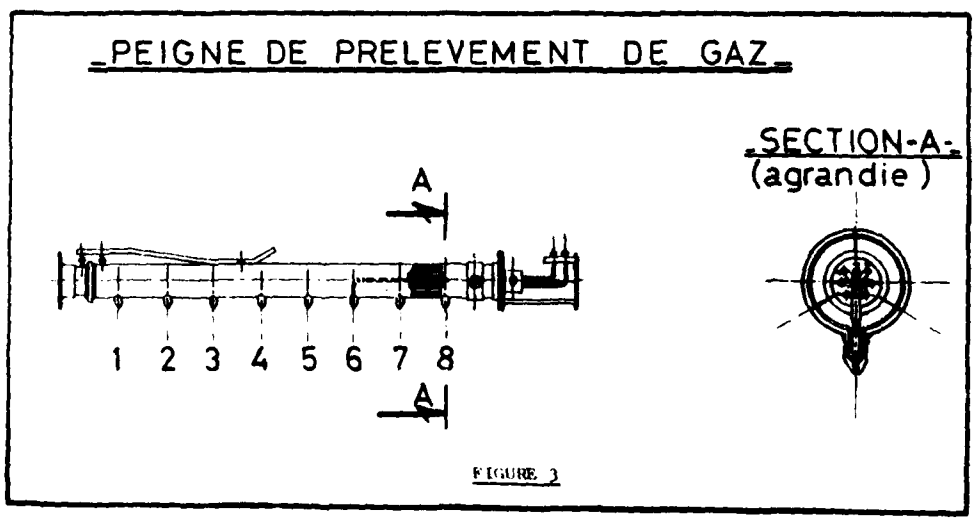

FIGURE 3

COUPE D'UNE
SONDE DE PRELEVEMENT

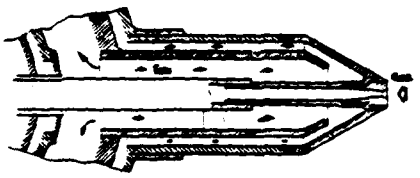

FIGURE 4

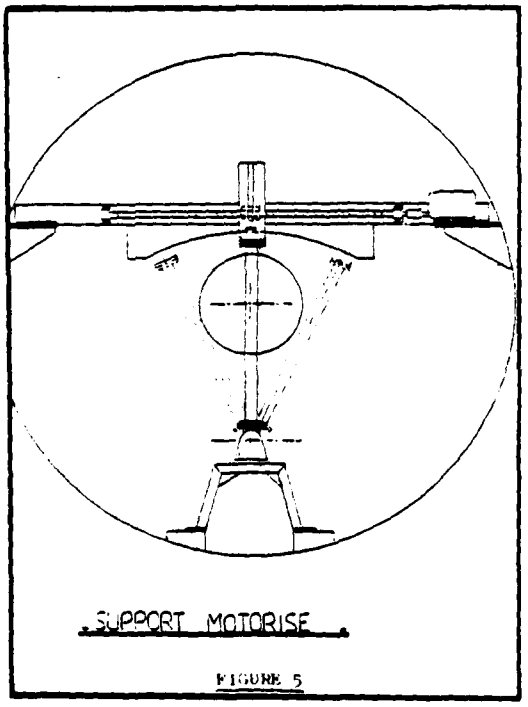

SUPPORT MOTORISE

FIGURE 5

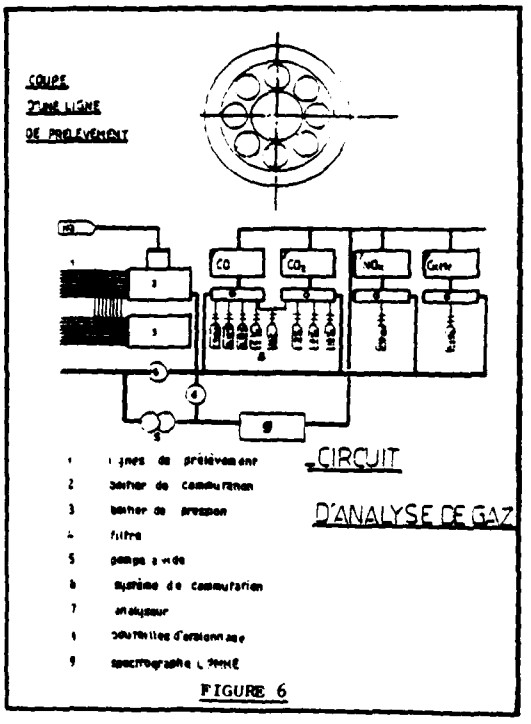

CIRCUIT
D'ANALYSE DE GAZ

FIGURE 6

FIGURE 7 - REPARTITION DES TEMPERATURES DANS LE JET EN TRANSSONIQUE AVEC RECHAUFFE à M = 1,2 Z = 38000 ft

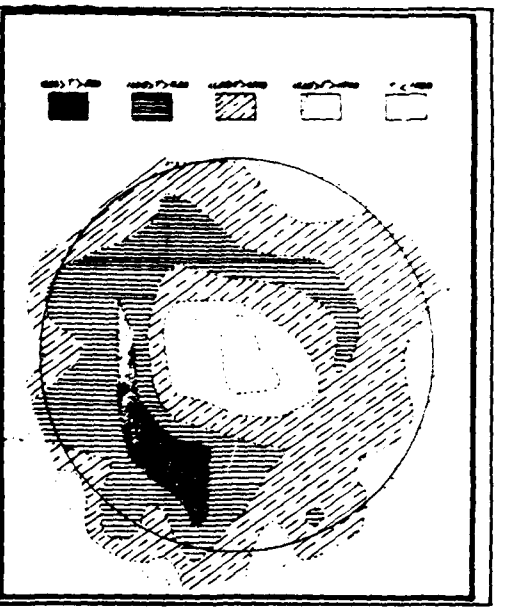

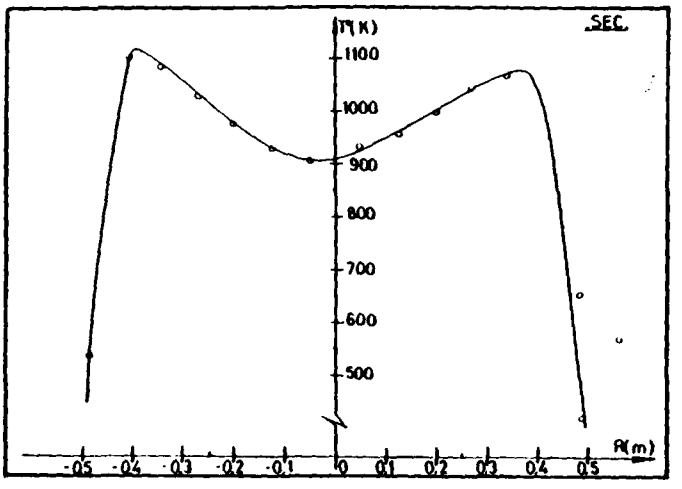

FIGURE 8 - PROFIL DE TEMPERATURE AU PLEIN GAZ SEC

FIGURE 9 - PROFIL DE CO AU PLEIN GAZ SEC

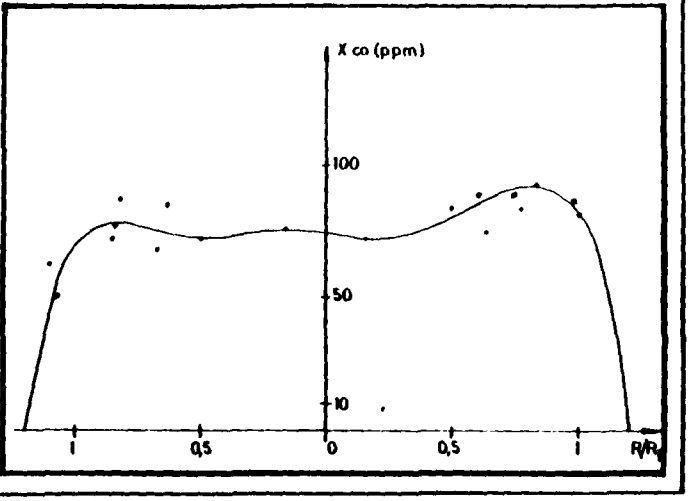

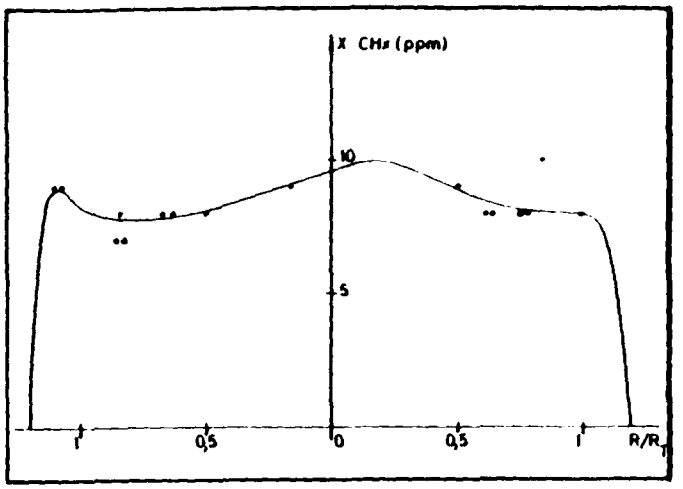

FIGURE 10 - PROFIL DES HYDROCARBURES AU PLEIN GAZ SEC

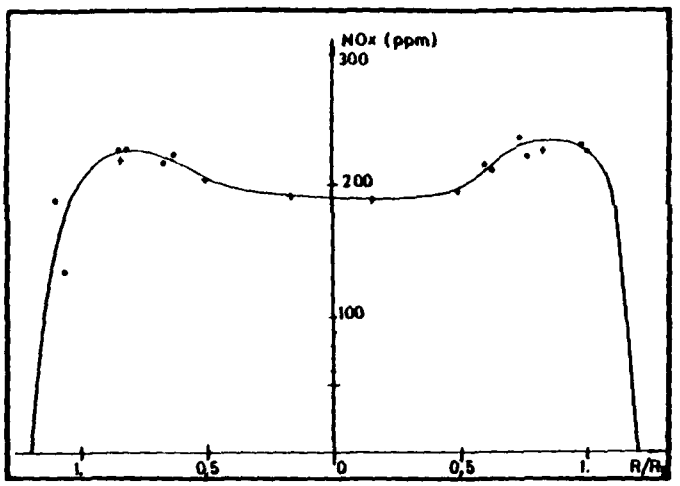

FIGURE 11 - PROFIL DE NOx AU PLEIN GAZ SEC

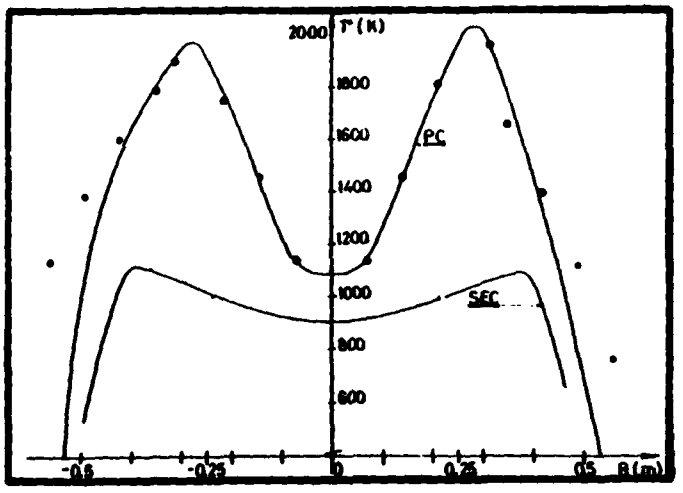

FIGURE 12 -
PROFIL DE TEMPERATURE A LA SORTIE DE LA TUYERE AU PLEIN GAZ PC ET AU PLEIN GAZ SEC

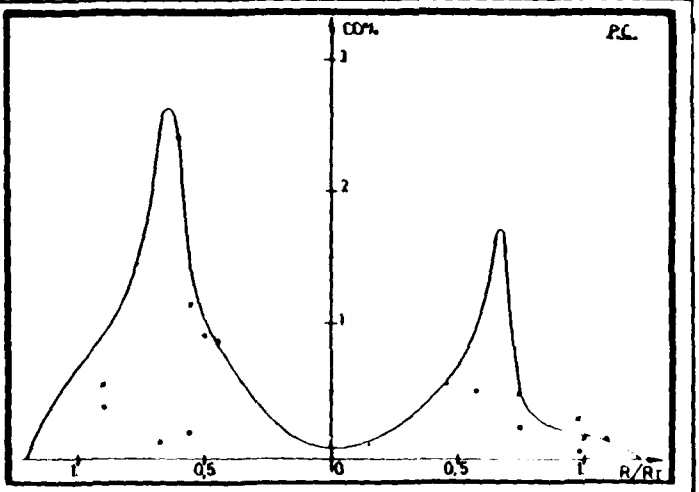

FIGURE 13 - PROFIL DE CO EN RECHAUFFE

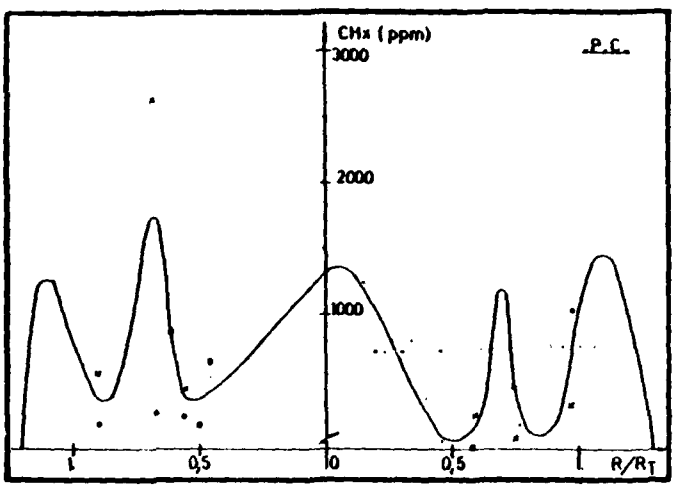

FIGURE 14 - PROFIL DES HYDROCARBURES EN RECHAUFFE

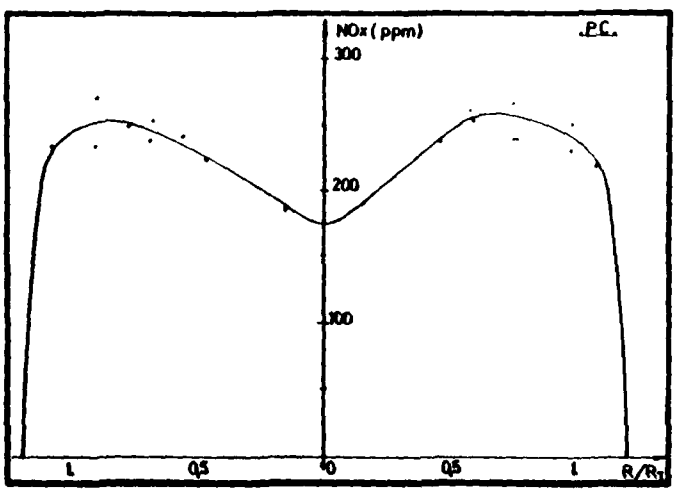

FIGURE 15 - PROFIL DES NOx EN RECHAUFFE

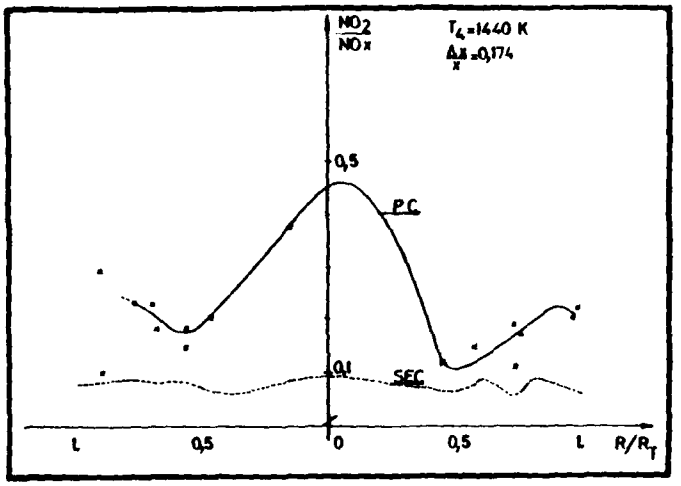

FIGURE 16 - EVOLUTION DU RAPPORT $\frac{NO_2}{NOx}$ AU PLEIN GAZ SEC ET EN RECHAUFFE

DISCUSSION

G.Kappler, Ge

(1) Are your sampling lines heated and, if so, what was your gas sample temperature?

(2) You did present results of emission measurements only for one engine operation point Since we have done similar measurements, I would be particularly interested if you can comment on the variation of unburned Hydrocarbon when accelerating the engine from minimum reheat to full reheat.

(3) How well does the air-fuel ratio measured from gas sampling compare to the ratio calculated from engine data?

Réponses des auteurs

S.Ropars

(1) Les lignes de prelevement sont chauffers a 150°C, il en est demins pour la pompe.

P.Gastebois

(2) Les essais n'ont été faits qu'aux reglapes nominaux de la réchauffe en accélération transsonique et au sol.

(3) Le recoupement de la richesse est utilise pour calculer le rayon limite d'integration, en minimisant les ecants entre débit d'au calcule et mesure ainsi que débit carburant calcule et injecte.

N.I.Hay, UK

What is the position of the reheat stabiliser in relation to the non-dimensionalised radial profiles given in the figures?

Réponse d'auteur

P.Gastebois

Le stabilisateur et situe environ au 1/7e diamètre de la tuyere.

PROBE MEASUREMENTS IN MULTI-DIMENSIONAL REACTING FLOWS

F. C. Gouldin
Associate Professor
Sibley School of Mechanical
and Aerospace Engineering
Cornell University
Ithaca, New York 14853
U.S.A.

SUMMARY

The time-mean response of pressure and sampling probes to pressure, density and velocity fluctuations in turbulent reacting flows is examined by averaging over the instantaneous probe response. Corrections for fluctuation effects are found to be necessary if data obtained by these probes are to be used to find mean velocity and concentration information. Correction terms for pressure probe readings are well founded and of general applicability, while sampling probe correction terms are well founded only if the sample flow is choked at the probe inlet, a state which may be difficult to achieve in practice. Also, probe induced flow field perturbations are discussed for measurements in swirling flow. It is recommended that to avoid perturbations the smallest possible probes be used and that combustion conditions be monitored, e.g. with wall pressure taps, during probe insertion in order to detect perturbations should they occur.

INTRODUCTION

Sophisticated new diagnostic techniques such as Raman scattering (RS) and laser doppler velocimetry (LV) are expected to provide new and important information for velocity, temperature and composition in flames, model combustors and practical hardware. However, it is highly unlikely that these and other new measurement techniques will evolve to a point where their use is routine in combustor design and development procedures. Instead, because of complexity and expense, their use will be restricted to situations where no other satisfactory technique is available and the information to be obtained is essential for progress. It is clear that probe techniques will continue to find application and, consequently, there is incentive to refine these techniques and expand their range of applicability.

The use of advanced diagnostic techniques for conventional probe development has been suggested, and the advantages of such an approach are obvious. In anticipation of research and development work on probes, it seems appropriate to review what is known presently about probe measurements and to suggest important experiments to verify probe performance and guide improvements. In this paper, such a task is undertaken for gas sampling probes and pressure probes. Attention is focused on measurements in turbulent reacting flows such as would be encountered in model combustors and practical hardware as opposed to laboratory flames. Primary interest is focused on effects of turbulent fluctuations in pressure, density, temperature and composition on probe performance.

To be effective a sampling probe must be accurately located in the flow field, extract a sample characteristic of the local gas composition in the absence of the probe and convey that sample to the analysis equipment without chemical change (by quenching the chemical reactions). These requirements have been discussed to varying depths in the literature. Quenching requirements have received the most attention and excellent papers are available [e.g., 1,2]. Pressure probes face similar requirements. Namely, pressure(s) related to local static or stagnation pressure(s) must be attained at the probe pressure tap(s) and then faithfully transmitted to the pressure transducers used in the measurement procedure. For both types of probes there should be no disturbances created in the flow by the probe. In turbulent, reacting combustor flows these goals are never fully realized, and it is therefore necessary to determine the extent of departure from ideal behavior and to assess the errors incurred thereby.

PRESSURE PROBES

In turbulent flow a probe is subject to varying yaw and pitch angles, varying velocity magnitude and varying static pressure. Generally, the dynamic response of the pressure probe and transducer system is too slow to allow for instantaneous pressure measurements. Therefore, in the present discussion attention is focused on the measurement of time mean properties, and it is assumed that the probe and transducer system are designed to give an accurate measurement of the mean static pressure occurring at the probe's pressure tap(s) [3]. Under this assumption, probe performance in turbulent flow is determined by the relationship of the static pressure at the probe's pressure tap(s) to the local undisturbed values of pressure and velocity.

There are a large number of pressure probe configurations available for various applications; see the review by Bryer and Pankhurst [4]. For steady laminar flow, probes are available for measuring total pressure, local static pressure and flow direction. When the local flow direction is known and the pressure probe aligned with respect to that flow, static and total pressure may be measured to good accuracy with relatively simple

and reliable pitot-static probes. Pressure and velocity gradients, flow confinement and the proximity of solid boundaries are well known sources of error in such pressure measurements for which, in most laminar flow cases, correction schemes are available [4]

The measurement problem is considerably more complex when the flow direction is either unknown or is to be determined. Total pressure and to a lesser extent static pressure probes are available which are insensitive to flow direction up to relatively large yaw and pitch angles. However, multi-hole probes are required if both velocity direction and magnitude are to be measured. Multi-hole probes are employed in two distinct ways 1) Pressure differences in appropriate pairs of pressure taps are used to find yaw and pitch angles relative to the probe axis via calibration curves, or 2) the probe may be aligned with the flow as indicated by equal pressures in appropriate pairs of pressure taps, the null mode. The latter mode is considered more accurate but requires a complex apparatus for manipulating the probe and relatively free access to the flow of interest to allow for this manipulation. Bryer and Pankhurst [4] discuss a number of these probes and probe support systems; references 5 and 24 contains an example of such an access problem and one possible solution. In either mode of operation, probe calibration is required, and the density must be known (or measured) if the velocity magnitude is to be found along with the flow direction and static and dynamic pressures.

In general, multi-hole probes are larger and less accurate than standard total head and static pressure probes. They are also susceptable to errors induced by velocity and pressure gradients, and the magnitude of these errors has not been fully assessed. If sufficient data for the pressure and velocity fields are available some correction for these errors seems possible, but no guidance for correction procedures is readily available in the literature.

The maximum yaw and pitch angles to which these probes will operate are limited (60° is near maximum for the best three- and five-hole designs), and consequently experimental problems arise when the flow direction is highly variable over the measurement volume and null model operation is not feasible, e.g. in practical combustors. Macfarlane [6] has proposed a seven-hole probe especially for gas turbine combustors which mitigates these problems. The probe (Figure 1) is designed to rotate around the probe support axis upon which the probe tip lies. This probe configuration allows one to align the probe tip in yaw. Five pressure tapes are located on the spherical surface of the probe tip in the plane of the probe support axis. Using appropriate combinations of these five taps very large ($\lesssim \pm 90°$) pitch angles can be measured.

For these probes, calibration in steady laminar flow is required to develop the required relationships between pressure readings and dynamic head and flow direction. In principle, the flow to be measured must be steady or slowly varying laminar flow and locally, near the probe tip, the decelerating flow must be adiabatic, quasi-steady, and inviscid. The latter two requirements are considered satisfied provided $|1/U\ \partial U/\partial t| \ll |U/D|$ and $Re = UD/\nu \gtrsim 100$ [4,7] where U is the undisturbed local flow velocity and D is a characteristic dimension of the probe tip. If the decelerating flow is constant density, Bernoulli's equation may be used to relate static and total pressure, which further requires $|1/\rho\ \partial\rho/\partial t| \ll |U/D|$ and $M = U/c \lesssim 0.2$ (c is the sound speed and M the Mach number).

For applications in laminar flow the multi-hole pressure probe may be considered to be well developed, and, provided errors introduced by probe interference, large pressure gradients, etc. are either avoided or accounted for, accurate measurements of total pressure and flow direction can be made. Compared to standard static and total pressure probes, when applied to flows of known direction, the multi-hole probe is not as accurate [4].

In practice, multi-hole probes are frequently employed for turbulent flow measurements, and although turbulence is known to influence the probe response, the effect is frequently ignored. Laminar flow calibrations are used to interpret the raw, time-mean pressure data, and the results are reported as mean velocity, mean static pressure, etc. Hinze [8] suggests that the influence of turbulence on pressure probe readings may be analyzed by considering appropriate averages of the time varying probe response as determined from laminar flow calibrations. Becker and Brown [3] pursue this line of reasoning for a simple impact probe, while Bennett [9] follows a similar path for a five-hole probe.

Hinze proposed that the directional response of a total pressure probe in a steady laminar incompressible and inviscid flow may be represented by

$$P_s - P = 1/2\rho U^2[1 - B(1 - \cos\theta)],$$

where P_s is the measured pressure; P the local static pressure; U the speed; θ the angle between the probe axis and velocity vector; and B is a constant. Becker and Brown [3] suggest an alternate form based on extensive measurements and a literature review,

$$P_s - P = 1/2\rho\ U^2(1 - K(\sin^2\theta)^m), \qquad (1)$$

which is good up to flow angles of 40° to 45°. K and m are constants which depend on probe design and are best found by calibration. m generally falls between 1 and 3, while K varies from 2 to about 5.

In turbulent flow with proper internal design, the measured pressure from a pressure probe will be the time-mean of the static pressure at the probe pressure tap. Furthermore if the decelerating flow associated with the probe is quasi-steady, incompressible, etc. Equation 1 is valid for any time, and the measured time mean is simply the mean of P_s

$$\bar{P}_s = \bar{P} + 1/2\,\rho\langle u'^2\rangle - 1/2K\rho\langle U^{2(1-m)}U_n^{2m}\rangle. \qquad (2)$$

Angle brackets and overbars are used to denote time-averaged quantities. Becker and Brown define U_n as the velocity component perpendicular to the probe axis. $U_n^2 = U_y^2 + U_z^2$ with the probe axis parallel to the x axis. It is assumed that the probe is aligned with the mean flow, and therefore, $U_n^2 = u_y'^2 + u_z'^2$, since $\bar{U}_y = \bar{U}_z = 0$, with lower case, primed letters denoting fluctuations about the mean value. The assumptions made in establishing Eq. (2) imply a turbulence length scale much larger than D.

In order to evaluate $\langle U^{2(1-m)}U_n^{2m}\rangle$ Becker and Brown assume the velocity fluctuations are uncorrelated and normally distributed with $\langle u_y'^2\rangle = \langle u_z'^2\rangle$ and $\langle u_x'^2\rangle = \beta\langle u_n'^2\rangle$, where β is a constant equal to 1/2 in isotropic turbulence and to approximately one in shear flow.

With the probe response and turbulence characteristics established, Becker and Brown propose and evaluate procedures for measuring $1/2\rho\langle U^2\rangle$ and $1/2\rho\bar{U}_x^2$. Errors in the measured quantities due to turbulence are calculated and reported as a function of turbulence level for different probe parameters. The results indicate that certain probe tip designs are more desireable than others due to differences in response to yaw and pitch, and they allow one to judge the error in his measurements based on his estimates of turbulence intensity. Furthermore, if the intensity is known corrections can be applied.

The need for an independent measurement of the mean static pressure is recognized by the authors as a fundamental problem with their approach, but they make no attempt to analyze the response of a static pressure probe in turbulent flow. There has been speculation regarding the effect of turbulence on static pressure measured with a standard static pressure probe [e.g. 4,7 and 10], but little systematic research. Bradshaw and Goodman [10] have shown for jet flows and probes of reasonable size that measured static pressure readings are very close to the actual static pressure (less than approximately $(0.02)1/2\rho\bar{U}^2$ difference). Extension of these results to other turbulent flows and to flows of high turbulent intensity appears unwarranted. A systematic evaluation of static probe directional response in steady laminar flow should be of value, but the assumption of quasi-steady probe flow needed to apply the results of such a study to turbulent flows will be difficult to justify since it requires $|L/\bar{U}| \ll |\ell/\langle u'^2\rangle^{1/2}|$ where L is the distance from the probe tip to the static pressure holes and ℓ is the scale of energy containing eddies. The preferred approach to measure $\bar{P}$, where possible, is to measure $\bar{P}$ at a wall and to determine $\bar{P}$ in the free stream by solution of the appropriate momentum equation [e.g. see References 3 and 4].

Becker and Brown [3] recognize in the pressure probe response to turbulent fluctuations an opportunity to measure root-mean-square fluctuation levels. They propose that two physically different impact probes with different K and m values be used to measure $\bar{P}_s$ at dynamically equivalent locations in a flow and show how the results may be analyzed to estimate $\langle u'^2\rangle^{1/2}$. This approach is obviously a method of last resort and its significance has diminished with the continued refinement of hot-wire and pulsed-wire techniques and the introduction of laser doppler anemometry.

Bennett [9] considers the response of a five-hole probe in a general, reacting turbulent flow. Under similar assumptions for probe response as those of Becker and Brown the pressure at tap i on the hemispherical probe of Figure 2 may be written as

$$P_{si} = P_o - A_i(\theta,\phi)\rho U^2, \qquad (3)$$

where P_{si} is the static pressure at the i^{th} tap, P_o is the local total pressure, A_i accounts for the probe response in yaw and pitch, and U is the local spee The $A_i(\theta,\phi)$ for a probe are found by calibration in a steady, laminar incompressible flow. To further analyze the probe response, Bennett expands A_i in a Taylor's series about $\bar{\phi}$ and $\bar{\theta}$, the mean yaw and pitch angles, and calculates the mean of P_{si}. Neglecting terms of third order and higher in fluctuation quantities, he finds that

$$\begin{aligned}\bar{P}_{si} = \bar{P}_o &- A_{io}[\bar{\rho}\,\bar{U}^2 - \bar{\rho}\langle u'^2\rangle + 2\bar{U}\langle\rho'u'\rangle] \\ &- A_{i,\theta}[\bar{U}^2\langle\rho'\theta'\rangle + 2\bar{U}\,\bar{\rho}\langle\theta'u'\rangle] \\ &- A_{i,\phi}[\bar{U}^2\langle\rho'\phi'\rangle + 2\bar{U}\,\bar{\rho}\langle\phi'u'\rangle] \\ &- \bar{\rho}\,\bar{U}^2[1/2A_{i,\phi\phi}\langle\phi'^2\rangle + A_{i,\phi\theta}\langle\phi'\theta'\rangle + 1/2A_{i,\theta\theta}\langle\theta'^2\rangle] \\ &+ \text{higher order terms.} \qquad (4)\end{aligned}$$

Subscripts preceded by a comma denote partial differentiation with respect to that variable e.g., $A_{i,\theta\theta} = \partial^2 A_i / \partial\theta^2$. All derivatives are evaluated at $\bar{\theta}$ and $\bar{\phi}$, and A_{i_o} is the value of A_i at $\bar{\theta}$ and $\bar{\phi}$.

Typically, all correlation terms are neglected and the measured $\bar{P}_{si}$ from the five pressure taps are analyzed to obtain $\bar{\theta}$, $\bar{\phi}$ and $\frac{1}{2}\bar{\rho}\bar{U}^2$. If turbulent fluctuations are significant the error in this approach can be estimated from Eq. 4. For example, Bennett presents error estimates for measurements in the flow behind an array of rotating compressor blades. The flow is constant density and hence Eq. 4 may be simplified

$$\bar{P}_{si} = \bar{P}_o - A_{i_o}[\tfrac{1}{2}\bar{\rho}\bar{U}^2 - \tfrac{1}{2}\langle u'^2\rangle]$$
$$- A_{i,\theta}\, 2\bar{U}_o \langle\theta' u'\rangle - A_{i,\phi}\, 2\bar{U}_o \langle\phi' u'\rangle$$
$$- \tfrac{1}{2}\bar{U}^2[1/2A_{i,\phi\phi}\langle\phi'^2\rangle + A_{i,\theta\phi}\langle\theta'\phi'\rangle + 1/2A_{i,\theta\theta}\langle\theta'^2\rangle] \qquad (5)$$

Hot-film anemometry is used to obtain information on turbulent fluctuations $\langle u'^2\rangle/\bar{U}^2 = 0.06$, $\langle\phi'^2\rangle = 10^{-4}(\text{rad}^2)$ and $\langle\theta'^2\rangle = 10^{-2}(\text{rad}^2)$. The resulting errors are estimated to be -2.0° in yaw, -0.2° in pitch, 1% increase in dynamic head, and a 3.5% decrease in total pressure divided by dynamic pressure. For high intensity combustors which are characterized by more intense turbulence and by density fluctuations, larger errors are expected if fluctuations are ignored.

Bennett sees the influence of turbulent fluctuations on pressure probes primarily as a complication. On the other hand, one may view the appearance of fluctuation terms in Equation 4 as an opportunity. Including $\bar{\theta}$ and $\bar{\phi}$, Equation 4 contains fourteen unknowns. With a five-hole probe used at three different orientations and/or with a probe with more holes, it is possible to obtain sufficient pressure readings allowing one to solve for all the unknowns. Alternatively, in the spirit of Becker and Brown, one might consider the use of more than one probe configuration to obtain the necessary data. These pressure measurements lead to a set of 14 algebraic equations for the unknowns. In general the solution of these equations would be by an iteration technique since the A_i and their derivatives are functions of $\bar{\theta}$ and $\bar{\phi}$ and these functions must be determined by probe calibration. According to Bennett [9] calibration can be performed with sufficient accuracy to obtain accurate values of both the A_i and their derivatives. Clearly, error accumulation in this procedure can be significant, and therefore, the pressure readings must be made with precision and the choice of probe configuration and orientation must be made with care.

In certain flows, Equation 4 may be simplified usually by taking advantage of symmetry characteristics. For instance, in a two-dimensional shear layer with the probe axis in the plane of the mean flow, the mean yaw angle, $\bar{\phi}$, is zero and $\langle\phi'\theta'\rangle = 0$, $\langle\rho'\phi'\rangle = 0$ and $\langle\phi' u'\rangle = 0$. Furthermore, the assumption that $\langle\phi'^2\rangle \approx \langle\theta'^2\rangle \approx \alpha\langle u'^2\rangle/\bar{U}^2$ would appear consistent with the foregoing development. α is estimated from independent considerations of the flow field, e.g., it is 3 in isothermal, isotropic turbulence and approximately 4 in isothermal shear flows. Also, density can be inferred with sufficient accuracy from temperature measurements. One now if faced with seven unknown including $\bar{\theta}$, rather than fourteen, and seven independent pressure readings must be obtained from pressure taps in the plane of the mean flow either with a seven-hole probe, with multiple probe orientations or with different probe configurations placed at dynamically equivalent positions in the flow.

Of the turbulence quantities to be measured by this approach $\langle\rho' u'\rangle$ is perhaps the most significant. In principle, all the other quantities can be measured, provided there is access for LV; $\langle\rho' u'\rangle$ cannot be measured with confidence. Furthermore, interpretation of LV results is clouded by a number of singal analysis and seeding bias problems; seed bias introduced by density fluctuations in reacting flows is one of the more significant ones. Thus, the measurement of $\langle\rho' u'\rangle$ and an independent measurement of $\bar{U}$ and $\langle u'^2\rangle$ for comparison with LV results would be very helpful in furthering the development of laser velocimetry for combustion applications. Also, a measurement of $\langle\rho' u'\rangle$ along with $\bar{U}$ and $\bar{\rho}$ will allow for a direct determination of the Favre mean velocity, $\tilde{U} = \langle\rho U\rangle/\bar{\rho} = \bar{U} + \langle\rho' u'\rangle/\bar{\rho}$, a quantity about which there has been much spectulation [11]. Also this procedure of making multiple pressure measurements will give improved results for the mean velocity and flow direction over those obtained by ignoring fluctuations effects and will provide an estimate of the errors introduced by neglecting fluctuations without having to make auxiliary turbulence measurements.

To the author's knowledge there has been no attempt to employ multi-hole pressure probes in the manner suggested here. In view of the ease of pressure probe measurements and the nature of the information which can be obtained, this approach deserves careful evaluation. For example, the results of multi-hole probe experiments conducted in laboratory turbulent flames, e.g., jet diffusion flames, according to the foregoing suggestions could be compared to velocities obtained by laser velocimetry. Furthermore, density measurements by laser scattering, either Raman [12] or Rayleigh [13,14], could be coordinated with velocity measurements to determine correlations such as $\langle\rho' u'\rangle$ and $\langle\rho'\theta'\rangle$ thus allowing for a complete evaluation of the probe technique. More complex flow conditions could also be considered.

In the above analysis as noted, the assumption is made that the decelerating flow in front of the probe is adiabatic, incompressible and inviscid. If there is significant heat transfer to the probe tip, the adiabatic assumption is no longer valid. Therefore, highly cooled probes should be avoided if possible.

PROBE DISTURBANCES

A major difficulty associated with probe measurements of any kind is the possibility of probe induced perturbations of the flow field. Well known examples of such perturbations are probe blockage in confined flows and flow distortion when measuring in boundary layers. This problem can be especially severe in combustors which are characterized by complex flow patterns and a high degree of confinement. Furthermore, in combustors and other flow systems with limited access, perturbations may not be readily apparent during the experiment or in the experimental results. For instance, apparent flow asymmetries observed in data obtained with a probe inserted transverse to the flow may be the result of probe blockage which increases as the probe traverses the flow field. Also, in combustion systems there is more opportunity for interferences, for example, the probe may act as a flame holder. Most experimentalists are aware of the potential for probe induced perturbation, but, unfortunately, there is little information either in the form of theory or empirical rules to help one anticipate and avoid these problems [1].

The following types of interferences appear to be of major concern: probe blockage, generation of secondary flows, tripping of flow instability and local flow changes due to the presence of the probe. For combustion systems we must add to the list possible interactions between the probe and chemical reactions, e.g. flame holding and catalytic reactions. The occurrence of any of these effects is dependent on the probe geometry and location in the flow field and on the apparatus configuration and flow conditions. Therefore, generalizations concerning the potential for interference are difficult to make and are of limited usefulness. It seems obvious that an important consideration is to keep the probe dimensions small compared to local characteristic flow dimensions. If probe cooling is necessary, small probes such as may be required to probe regions with large gradients will be difficult to manufacture.

Swirl flow is known to be particularly sensitive to distortion by probes [1,15] and is a flow characteristic common to many gas turbine combustors. Bilger [1] notes for swirling flow the potential for secondary flow along the probe support towards the vortex core when a probe is introduced perpendicular to the vortex axis. In laminar flow for intermediate swirl levels when vortex breakdown is either present or incipient, the occurrence of significant probe induced perturbations is well documented [13,14], while at higher Reynolds number with turbulence present, evidence in the literature, [15,18,24,25] though not conclusive, indicates that perturbations may or may not occur depending on specific flow conditions and probe design. For very high levels of swirl, extremely long recirculation zones are observed and the flow field may be quite complex. Such high swirl levels are not typical of gas turbine combustors. Of concern in the present context is the potential for perturbation in turbulent flow for all but the highest swirl levels, especially when reverse flow is present. Thus, the laminar flow experience is primarily of interest for what it implies about turbulent flows. As an example of the nature of probe interference problems and because of the significance of swirling flow to gas turbine combustors, the present discussion will be limited to this type of flow.

Hot-wire anemonetery and multi-hole pitot probes have been used widely in the past to investigate turbulent, swirling flow [5,18,19,20,24]. The shortcomings of these methods in three-dimensional highly turbulent flow have been recognized, but in the absence of more satisfactory techniques they were accepted and the experimental results treated accordingly. More recently, laser doppler velocimetry techniques have been employed to make non-intrusive velocity measurements in swirling flow. These new data provide an opportunity to make, at least indirect, comparisons between data obtained by intrusive and non-intrusive methods.

With all the probe measurements made in turbulent swirling flow there have been very few references to significant disturbances induced by the probe. Both Chigier [15] and Oven, et al. [27] report perturbations when a probe is introduced into or near the swirl generated recirculation zone for intermediate levels of swirls in combusting flows where the probe acts as a flame holder. Comparison between velocity measurements made with probes and laser velocimetry [5,19,17,18] show differences as would be expected due to the large number of possible errors associated with probe techniques and, to a lesser degree, to errors in LV measurements, but the differences do not suggest probe perturbations. Also, comparisons between hot-wire and pressure probe data for mean velocity magnitude [5,24] in swirl flow with and without recirculation are favorable indicating no probe interference since one would expect different disturbances from the different probes. Cassidy and Falvey [25] note the disappearance of hot-wire probe interferences in their data as the flow Reynolds number is increased and turbulence is observed, which supports the hypothesis that interference is much less likely in turbulent flow than in laminar flow.

Chigier [26] suggests that interference in these flows can be avoided if the probe dimension is much less than the thickness of the vortex core. The laminar swirling flows in which probe perturbations are observed are of sufficiently large Reynolds number to be predominately inviscid, and the vortex core in such flow is a small confined cylindrical region. In turbulent flow, at least in the mean, the vortex core is much larger. Therefore, if Chigier is correct, a perturbing probe in laminar flow may be small enough to be non-perturbing in turbulent flow. Alternatively, these differences might be explained

in terms of probe interactions with the axial vortex filaments which compose the vortex core. In cylindrical laminar flow, those filaments are undisturbed upstream of the vortex breakdown, but with the insertion of a probe, filaments are locally disturbed and disturbances may propagate along them causing a significant change in the flow far away from the probe. If the flow is turbulent, these vortex filaments are highly distorted by the turbulence and the insertion of the probe adds no significant new distortion. In either case the evidence indicates that turbulent flows with low or moderate swirl levels appear much less susceptable to probe perturbations than are laminar flows, provided the probes are small.

With combustion present, flame holding by the probe is always a potential problem and in swirling flows has been reported by Chigier [15] and by Oven, et al [27]. Furthermore, Oven, et al. report apparent inconsistencies between measured mean temperature and mean fuel concentration at various points in the recirculation zone of thier model combustor. Large mean temperatures are observed at points where on a time-mean basis substantial amounts of fuel are unreacted. For these measurement points, no probe distortion is apparent visually. This inconsistency may be due to the influence of turbulent fluctuations on the sampling and measurement process--which seems unlikely to the author. Alternatively, it may be due to radial in-flow along the probe body--a cylindrical probe, transverse to the flow was employed--as predicted by Bilger (see above and Reference 1). Other subtle probe effects may be a frequent but as yet unobserved occurrence in these flows. More research on these problems is required for their resolution, and until such time as they are resolved, we must proceed with caution.

These swirling flow, probe interaction problems are an example, perhaps the best example, of problems stemming from probe aerodynamic effects which will occur to varying degrees for any type of probe be it thermocouple, gas sampling or pressure probe. Interference can be expected in any flow especially recirculating flows and in other elliptic flows. In conducting experiments, probes should be small and steps should be taken to monitor one or more critical combustor parameter(s), e.g. wall static pressure, flame appearance, combustor exit temperature, or flame luminosity, during probe insertion for indications of probe induced disturbances.

Systematic studies of probe interferences are needed to resolve these questions and to guide probe designs and application. Probe performance in flows such as bluff body wakes, behind steps and in swirl generated recirculation zones should be evaluated for different probe configurations. Non-intrusive flow measurement techniques such as schlieren and laser velocimetry can be used to monitor flow conditions with and without the probe present. Pitot probe performance in such flows could also be checked by comparison with laser velocemetry results. The influence of flow confinement in promoting or suppressing interferences should also be studied. Optical techniques such as Raman scattering and coherent anti-Stokes Raman scattering also can be used to measure composition and temperature for comparison with probe results.

SAMPLING PROBES

In this section, our discussion will focus on the influence of external aerodynamic effects and not address probe quenching questions. The importance of rapidly quenching reactions in the gas sample to preserve sample composition is broadly recognized [1,2,28,29,30]. Recently this subject has been studied intensively especially in regard to the conversion of NO to NO_2 in conventional sampling probes [26,27]. With reasonable care it appears possible to freeze major species concentrations in the sample via rapid quenching with water or low pressure steam cooled probes. With regard to aerodynamic quenching, a technique frequently used in low pressure flames, theoretical analysis [2] indicates that it is difficult to obtain sonic velocity at the sampling orifice due to viscous effects and therefore in many cases "aerodynamic" quench probes actually depend on conduction for quenching. In low pressure flames conduction along the probe body and support may be sufficient to keep a cool tip on an aerodynamic probe. However, in high intensity combustors, cooled probes should be used to insure quenching.

Quenching in conventional (thermal or aerodynamic quench) probes is not sufficiently rapid to preserve reactive species concentrations in the sample. If these components are to be measured through gas sampling, molecular beam sampling systems are required [31]; it is doubtful that these cumbersome sampling devices will ever be suitable for sampling from model combustors or actual hardware. They will not be considered here.

In this paper, attention is focused on the the aerodynamic aspect of the problems of bringing an accurate gas sample to the mouth of the sampling probe in turbulent reacting flows. These problems include 1) turbulence effects on sampling, 2) aerodynamic perturbations by the probe and 3) thermal and chemical perturbations induced by the probe. Probe perturbations are discussed in the previous section; in this section the emphasis is on the first item.

The possibility of sample distortion due to turbulent fluctuations in density, composition and velocity has been noted by a number of investigators. Drawing an analogy with the problem of sampling small particles from a two phase flow it has been suggested that isokinetic sampling (presumably relative to the mean flow velocity) is necessary to avoid bias due to density fluctuations [1,32]. However, to the author's knowledge, there has been no systematic study of this problem. In light of the preceeding discussion of pressure probe measurements it seems appropriate to approach this question by considering the response to yaw and pitch, velocity and density of a sample probe in steady laminar flow and then average over the turbulent fluctuations.

For reacting flows this approach is complicated by the possibility of large density fluctuations. In addition, unless the probe has a sonic orifice, fluctuations in ambient conditions may drive flow oscillations in the sampling system - the probe, sample transfer line and conditioning system, and gas analysis equipment. For the purposes of illustration it will be sufficient to examine the sampling problem under two limiting cases, a small mass flow rate probe and a sonic orifice probe.

For low sampling rate, assume that the sampling orifice is small compared to the probe diameter ($(d/D) \ll 1$) and consider the limit of extremely low sampling rate. In this case, the flow field around the standard impact-type sample probe is very nearly that observed for an equivalent total pressure pitot probe where there is no sample flow. Thus, the pressure driving the sample flow is P_s from Equation 1. Let $P/P_s - P_p$ be the pressure drop across the sampling orifice at the probe tip. Then the sample mass flow is given by the following:

$$\dot{m} = C A_p \sqrt{2\rho_p (P - P_p)} = C A_p \sqrt{\rho_p (P - P_p) 2 + \rho_p^2 U^2 (1 - K(\sin^2\theta)^m)}. \tag{5}$$

A_p is the flow area in the probe where the pressure P_p occurs. C is the discharge coefficient which is assumed constant. The sample mass flow for the species i is given by (Y_i is the mass fraction of i)

$$\dot{m}_i = Y_i \dot{m} = C A_p Y_i \sqrt{2\rho_p (P - P_p) + \rho_p^2 U^2 (1 - K(\sin^2\theta)^m)}. \tag{6}$$

For low flow rates, including the condition of isokinetic sampling, $2\rho_p(P - P_p) \ll O(\rho_p^2 U^2 (1 - K(\sin^2\theta)^m))$ which means that $\dot{m}_i$ will respond to changes in Y_i, P, ρ_p and U and that when the instantaneous probe response is averaged over time a complex relationship between the mean and fluctuating components of mass fraction, density, pressure and velocity is obtained.

$$\bar{\dot{m}}_i = C A_p \left\langle Y_i \sqrt{2\rho_p (P - P_p) + \rho_p^2 U^2 (1 - K(\sin^2\theta)^m)} \right\rangle \tag{7}$$

As before, the flow approaching the probe tip is assumed to be quasi-laminar and quasi-steady, inviscid and constant density. Furthermore, the orifice flow into the probe is assumed to be quasi-steady. These assumptions imply that fluctuations in the sample system are small. If, further, they may be neglected then P_p is constant. Otherwise, $\dot{m}_i$ will depend on the dynamical response characteristics of the sample system as well as the turbulent fluctuations in the flow field. In either case, a reasonable interpretation of such a gas sample appears virtually impossible, and therefore, one should avoid sampling at low velocities. This comment applies equally to the condition of isokinetic sampling; it may appear attractive intuitively, but this simplified analysis clearly shows that it is a bad idea. In this development, the length scale of the turbulent eddies (ℓ) is assumed to be larger than the probe scale (see above), while the analogy with particulate sampling procedures drawn to support the use of isokinetic sampling conditions requires that the eddies be small compared to d. Therefore, the conflicting conclusion drawn here is not surprising. The condition that $d \gg \ell$ required for isokinetic sampling will be very difficult to realize in practice and conflicts with the recommendations of the previous section.

The basic problem with low speed sampling is that the instantaneous mass flow depends on the local density, static pressure and dynamic pressure. As these quantities vary, the sample mass flow rate varies, and the mean mass flow rate will be contaminated with correlations between fluctuations in all of these quantities. It does not seem feasible to take advantage of the presence of correlation terms in the probe response to measure them since the present analysis is rather artificial and a more realistic one will lead to much more complex results. Thus, it is concluded that low velocity sampling probes should not be employed for sampling when large density, pressure and velocity fluctuations are present. In combustion systems, the main difficulties arise in the reaction zone where density fluctuations can be extremely large.

Support for the above conclusions can be found in the experimental results of Kennedy and Kent [33] who report significant differences between values of fuel atom fraction obtained in a turbulent H_2-air diffusion flame with an isokinetic sampling probe and similar data obtained with a light scattering technique, Figure 3. The mixture fraction, ξ, is the mass fraction of fuel atoms present in a sample regardless of the molecules in which the atoms are found. Figure 3a shows centerline variations; for smaller x/D there are no significant differences between normal ($\bar{\xi}$) and Favre ($\tilde{\xi}$) averaged values of ξ obtained by light scattering which implies that density fluctuations are not large enough to influence the averages. Discrepencies between probe and scattering data occur only at larger x/D where density fluctuations are more significant as noted by differences between $\bar{\xi}$ and $\tilde{\xi}$. The half-radii data, Figure 3b, show much larger discrepencies, and density fluctuations are much significant. Clark, et al. [34] report measurements of CO, NO_x and unburned hydrocarbons in a continuous combustor using different probe configurations. There is considerable scatter in their data which possibly obscures small changes due to probe variations. Marked changes in measured concentrations are observed with a change in probe tip geometry, indicative of possible aerodynamic effects stemming from turbulence.

As ΔP is increased, the sensitivity to fluctuations in static pressure and dynamic head is reduced. Furthermore, if the sampling orifice is choked, oscillations in the sample system do not influence the flow rate. Thus, one expects a sonic orifice probe to have significant advantages for turbulent flow measurements.

For a choked orifice assuming isentropic, quasi-steady flow with constant gas properties (R and k)

$$\dot{m} = C A_t f(R,k) P_o / \sqrt{T_o} \tag{8}$$

C is the discharge coefficient, A_t the throat area, f a known function of the specific gas constant (R) and the ratio of specific heats (k), and P_o and T_o are the stagnation pressure and temperature. If the combustor flow is low Mach number and the combustor pressure is approximately uniform, $P_o = P$ and may be assumed constant and $T_o = T$ (i.e., the local static values). Therefore, by introducing the density, one may write

$$\dot{m} = C A_t f(R,k)(RP)^{1/2} \rho^{1/2}.$$

Neglecting small variations in C, R and k due to reaction and to temperature fluctuations, one finds that $\dot{m}$ is proportional to $\rho^{1/2}$ and $\dot{m}_i$ to $Y_i \rho^{1/2}$.

$$\dot{m} = K_m \rho^{1/2} \tag{9}$$

$$\dot{m}_i = K_m Y_i \rho^{1/2} \tag{10}$$

Thus, the response of the sonic probe is greatly simplified compared with the first probe, while the assumptions leading to these expressions are more reasonable.

The analysis of time averaged samples from such a probe may be used to obtain the ratio $\bar{\dot{m}}_i/\bar{\dot{m}}$. Expanding $\rho^{1/2}$ in a Taylors series about $\bar{\rho}$ and averaging $\dot{m}$ and $\dot{m}_i$ one obtains:

$$\bar{\dot{m}}_i/\bar{\dot{m}} = \bar{Y}_i\left(1 + \frac{1}{2}\frac{\langle Y_i' \rho' \rangle}{\bar{Y}_i \bar{\rho}} - \frac{1}{8}\frac{\langle \rho'^2 \rangle}{\bar{\rho}^2} - \frac{1}{8}\frac{\langle Y_i' \rho'^2 \rangle}{\bar{Y}_i \bar{\rho}^2} + \ldots\right)/\left(1 - \frac{1}{8}\frac{\langle \rho'^2 \rangle}{\bar{\rho}^2} + \ldots\right). \tag{11}$$

If density fluctuations are not too large, e.g. outside the reaction zone, this type of probe may be used to obtain an accurate measure of sample composition. However, in the reaction zone, large fluctuations in density are expected, and for major reactant and product species $\langle Y_i' \rho' \rangle$ will be large. Note that the half power dependency of mass flow rate on density means that there is no simple interpretation of results in terms of Favre averaged quantities either.

Thus, one concludes that accurate sampling measurements for mean mass fractions in regions of large density fluctuations will require corrections for the influence of these fluctuations on measurement quantities. Furthermore, it is obvious that the corrections for a sonic orifice probe are much less complicated than for other probes, and therefore this sample flow condition is preferred. Corrections will require estimates of density fluctuations and correlations between density and species mass fraction fluctuations. It may be satisfactory to infer density fluctuation characteristics from instantaneous temperature measurements by compensated thermocouples or some other technique, while a relatively crude combustion model might be satisfactory for estimating the $\langle Y_i' \rho' \rangle$ term. For instance, under the assumptions of fast chemistry, equal diffusivities and unit Lewis number, the temperature (or density) and species concentrations are related unambiguously for premixed combustion, and $\langle Y_i' \rho' \rangle$ for major species may be estimated from instantaneous temperature (density) data. Advanced diagnostic techniques can provide necessary data to support the development of sonic flow probe techniques in general and correction methods in particular.

As noted previously, a one dimensional compressible flow analysis for the probe and sampling lines [2] indicates that in many situations for small orifice area there may not be enough pressure drop available between the combustor volume and the sample pump to choke the sample orifice and drive the required mass flow against wall friction through the sample system. This inability is the inevitable consequence of wall friction effects and a more refined analysis is not expected to alter the conclusion. Thus, for sonic orifice sampling, there is a minimum allowed orifice area which depends on combustor pressure and sample system configuration. Care should be exercised to insure that the sonic condition is obtained.

The consequences of an unchoked sample flow are not entirely clear. The pressure drop across the probe and sample line is large, and it is doubtful that fluctuations in static and dynamic pressure in the combustor will significantly alter the overall pressure drop across the sampling system. Furthermore, if the flow in the sample system is assumed to be quasi-steady and one-dimensional, expressions for the instantaneous flow accounting for friction and heat transfer may be obtained. Mass flow rate will be dependent on P, ρ and ΔP but not on the dynamic head (since $M \lesssim 0.2$). As for choked flow, turbulent fluctuations will be important especially if the density fluctuations are large. The utility of this approach seems doubtful because the quasi-steady sample

flow assumption is poor since the time scales for sample flow are large. Also, the dynamical response of flow in the probe and sample line needs to be analyzed to determine if instabilities are present under such conditions. Research may make it possible to design a sampling probe and system which ameliorates these unsteady flow effects. However, at this time, the possibility of such a design seems remote and the sonic sample flow condition should be be employed if at all possible.

In the previous discussion it is assumed implicitly that the sample probe exterior configuration is similar to standard impact probe designs and that the probe is aligned to at least face into the flow. In a recirculating flow such alignment may be difficult to achieve. Even so, in high velocity streams, some alignment appears to be essential for obtaining an interpretable sample. On the other hand, if the flow velocity is low enough such that the sink flow of sample into the probe is not significantly influenced by the combustor flow, no alignment seems necessary.

The errors introduced in probe samples by turbulent fluctuations in density, pressure and velocity have been demonstrated by two examples. Under special circumstances, sonic orifice sampling, these errors may be estimated and corrections made if auxiliary measurements are made. When density fluctuations are significant these errors are large and if corrections are not possible, the results are of limited quantitative value.

SUMMARY

The performance of pressure and sampling probes in turbulent reacting flows has been discussed with regard to the influence of turbulent fluctuations on the quantities measured and with respect to possible perturbations of the flow field by the probe. Analyses of probe response to turbulent fluctuations under various assumptions indicate that turbulent fluctuations can have a significant effect on results and that the large density fluctuations present in reaction zones introduce correspondingly large errors in the results if corrections are not made.

The analyses of multi-hole pressure probes are general and corrections seem feasible if auxiliary measurements are performed. Furthermore, if multiple probes or probe orientations are employed, these interferences provide an opportunity to measure significant turbulence parameters such as $\langle \rho' u' \rangle$. For sampling probes, the analyses are much less general, while the effects of fluctuations are both significant and complex. In the case of unchoked sampling probes, correction for turbulence effects appears infeasible. If the probe flow can be choked at its inlet, corrections are necessary only when density fluctuations are large, and under certain conditions corrections appear feasible. Recent studies indicate that choking the sample flow is not possible if the sampling orifice is too small. For conditions where choking is not possible, there is little hope that corrections can be made, and considerable error in probe data must be accepted.

The possibilities for probe induced flow perturbation are discussed in the paper, and the case of swirling flow is reviewed in some depth. As a general rule, probes should be as small as possible; thus uncooled or partially cooled probes as that of Macfarlane [6] are preferred. To guard against undetected probe perturbations, the combustor should be monitored during probe insertion and no measurement should be considered valid if changes are observed. Asided from these general rules, there is little other advice that can be given. These perturbations are a significant problem and they deserve more attention.

REFERENCES

1. R. W. Bilger, Probe measurements in turbulent combustion, pp 333-356 in Combustion Measurements, R. Goulard, edt., Academic Press, New York, 1976.

2. M. B. Colket, III., L. J. Chiappetta, M. F. Zabielskii, D. J. Seery, R. N. Guile, and L. G. Dodge, Internal aerodynamics of gas sampling probes, submitted to the Eighteenth Symposium (International) on Combustion, Combustion Institute by United Technologies Research Center, East Hartford, CT, Jan. 1980.

3. H. A. Becker and A. P. G. Brown, Response of pitot probes in turbulent streams, J. Fluid Mech. 62, 85-114, 1974.

4. D. W. Bryer and R. C. Pankhurst, Pressure - probe methods for determining wind speed and flow direction, HMSO, London, 1971.

5. B. T. Vu and F. C. Gouldin, Flow measurements in a model swirl combustor, AIAA Paper 80-0076, AIAA, New York, 1980.

6. J. J. Macfarlane, An omni-directional velocity vector probe suitable for use in gas turbine combustors; design development and preliminary tests in a model combustor, Aeronautical Research Council C.P. No. 1254, HMSO, London, 1973.

7. P. Bradshaw, An Introduction to Turbulence and Its Measurement, Pergament Press, Oxford, 1971.

8. J. O. Hinze, Turbulence, McGraw-Hill, New York, 1959, p 136.

9. J. C. Bennett, Use of five-hole pneumatic probe in unsteady flows, pp 71-80 in Experimental Diagnostics in Gas Phase Combustion Systems, B. T. Zinn, edt., Vol. 53, Progress in Astronautics and Aeronautics, AIAA, New York, 1977.

10. P. Bradshaw and D. G. Goodman, The effect of turbulence on static-pressure tubes Aeronautical Research Council R&M No. 3527, HMSO, London, 1968

11. R. W. Bilger, A note on Favre averaging in variable density flows, Combustion Science and Technology 11, 215-217, 1975.

12. M. Lapp and R. M. C. So, Measurements of flame properties by Raman scattering experimental capabilities and modeling needs, presented at the AGARD Propulsion and Energetics Panel 55th (A) Specialists' Meeting on Testing and Measurement Techniques in Heat Transfer and Combustion, Brussels, May 1980

13. F. Roehen, Comparison of density and temperature measurements using Raman and Rayleigh scattering, pp 180-196 in Combustion Measurements, R. Goulard, edt., Academic Press, New York, 1976.

14. G. D. Rambach, R. W. Dibble, and R. E. Hollenbach, Velocity and temperature measurements in turbulent diffusion flames, Paper No. WSS 79-51 presented at the 1979 Fall Meeting of the Western States Section of the Combustion Institute, Lawrence Berkeley Laboratory, Berkeley, CA, October 1979.

15. N. A. Chigier, p 349 in Combustion Measurements, R. Goulard, edt., Academic Press, New York, 1976.

16. S. Leibovich, The structure of vortex breakdown, Ann. Rev. Fluid Mech. 12, 221-246, Annual Reviews, Palo Alto, 1978.

17. J. K. Harvey, Some observations of vortex breakdown phenomena, J. Fluid Mech. 14, 585-592 (2 plates), 1962.

18. N. Syred and J. M. Beér, Combustion in swirling flows: A review, Comb. Flame 23, 143-201, 1974.

19. N. A. Chigier and A. Chervinsky, Aerodynamic study of turbulent burning free jets with swirl, pp 489-497 in the Eleventh Symposium (International) on Combustion, Combustion Institute, Pittsburgh 1967.

20. N. Syred, N. A. Chigier and J. M. Beér, Flame Stabilization in recirculation zones of jets with swirl, pp 617-624, Thirteenth Symposium (International) on Combustion, Combustion Institute, Pittsburgh, 1971.

21. N. A. Chigier and K. Dvorak, Laser aneorometer measurements in flames with swirl, pp 573-582 in the Fifteenth Symposium (International) on Combustion, Combustion Institute, Pittsburgh, 1975.

22. H. A. Habib and J. A. Whitelaw, Velocity characteristics of combined coaxial jets with and without swirl, to appear in the J. of Fluids Engineering.

23. S.-L. Lee, "Laser doppler velocity measurements in a swirl-stabilized combustor," M. S. Thesis, Cornell University, Ithaca, New York, January 1980.

24. B. T. Vu, "Experiments on Turbulent Co-axial Swirling Flows," Ph.D. Thesis, Cornell University, Ithaca, New York (in preparation).

25. J. J. Cassidy and H. T. Falvey, Observations of unsteady flow arising after vortex breakdown, J. Fluid Mech. 41, 727-736, 1970.

26. N. A. Chigier, Velocity measurements in vortex flows, pp 399-408 in Flow, Its Measurement and Control in Science and Industry, Part I, Vol. I, H. W. Stoll, edt., Instru. Society of America, Pittsburgh, 1974.

27. M. J. Oven, F. C. Gouldin and W. J. McLean, Temperature and species concentration measurements in a swirl-stabilized combustor, pp 363-374 in the Seventeenth Symposium (International) on Combustion, Combustion Institute, Pittsburch, 1979.

28. R. M. Fristrom and A. A. Westenberg, Flame Structure, McGraw-Hill, New York, 1965.

29. J. C. Kramlich and P. C. Malte, Modeling and measurements of sample probe effects on pollutant gases drawn from flame zones, Comb. Sci. Tech. 18, 91-104, 1978.

30. J. D. Allen, Probe sampling of oxides of nitrogen from flames, Comb. Flame 24, 133, 1975.

31. J. C. Biordi, Investigating the fundamental chemistry of flames with molecular beam mass spectrometry, pp 125-152 in Experimental Diagnostics in Gas Phase Combustion Systems, Vol. 53 Progress in Astronautics and Aeronautics, B. T. Zinn, edt., AIAA New York, 1977.

32. G. Tine', Gas Sampling and Chemical Analysis in Combustion Processes, AGARDograph 47, Pergaman Press, New York, 1961.

33. I. B. Kennedy and J. H. Kent, Laser scattering measurements in turbulent diffusion flames AIAA Paper 80-0206, AIAA, New York, 1980.

34. J. A. Clark, J. E. Peters and A. M. Mellor, Probe effects in gas turbine combustor emissions measurements, AFAPL-TR-79-2041, Air Force Aero Propulsion Laboratory, Wright-Patterson Air Force Base, Ohio, June 1979 (work performed at Purdue University, West Lafayette, IN).

ACKNOWLEDGEMENTS

This work was partially supported by a grant from the Lewis Research Center of the National Aeronautics and Space Administration (Grant No. NSG-3019); C. J. Marek was the technical monitor.

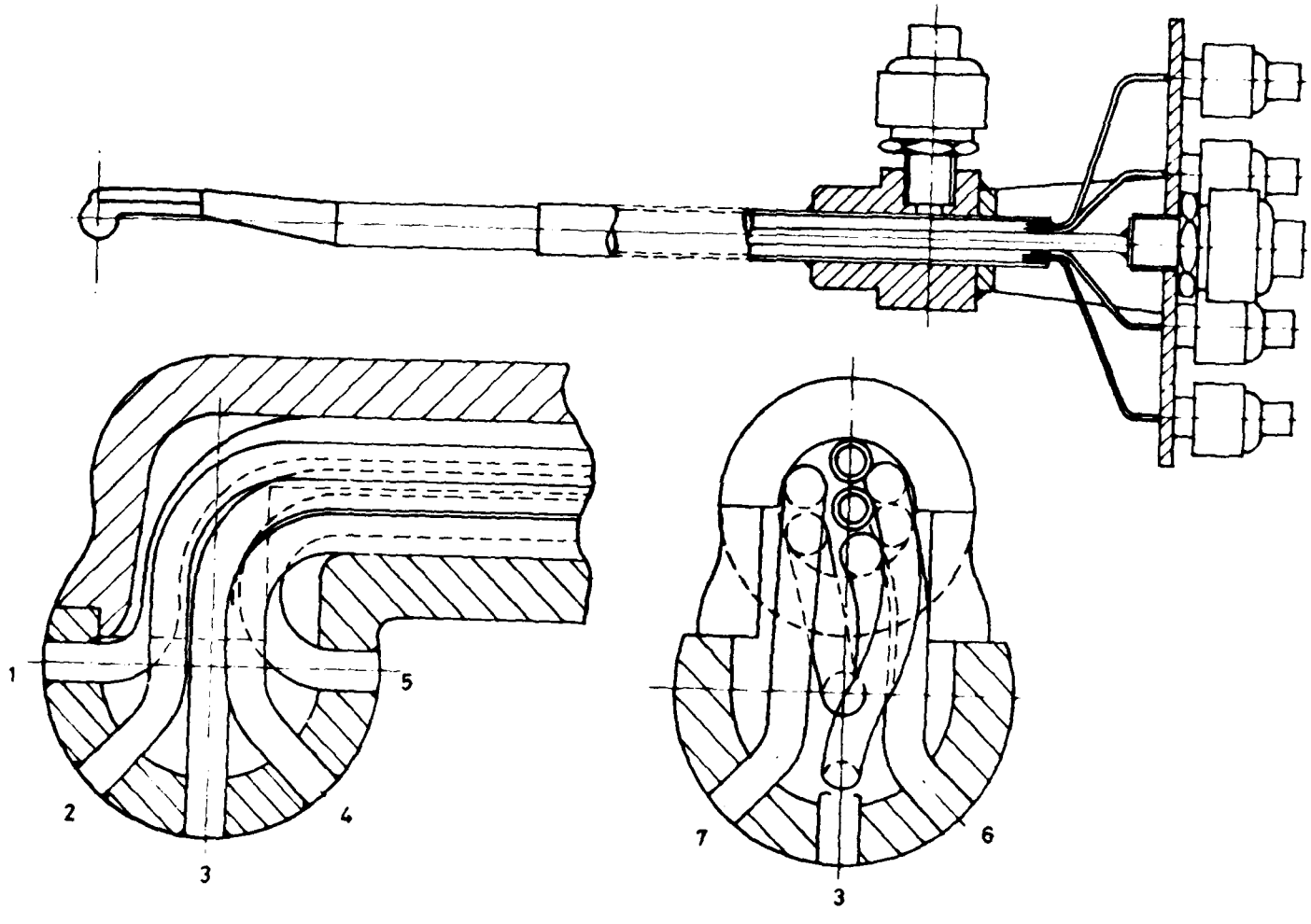

Figure 1. Seven-hole pressure probe from Reference 6. The spherical probe tip has a diameter of 6 mm, is made from platinum/20% rhodium, and is uncooled. Rotation around the axis of the probe support allows for alignment in yaw.

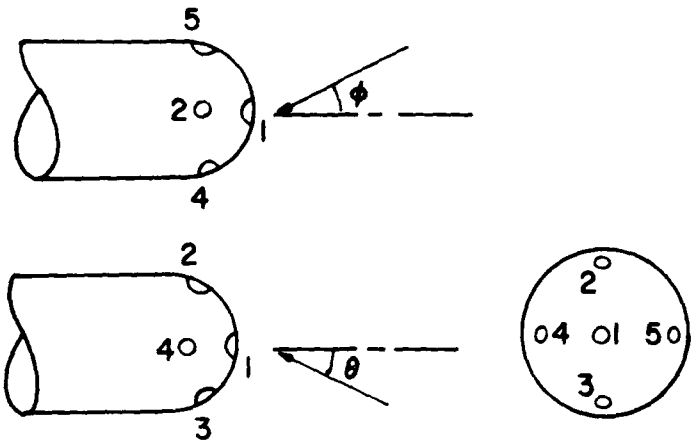

Figure 2. Standard configuration for five-hole hemispherical pressure probe from Reference 9. : is the yaw angle and the pitch angle

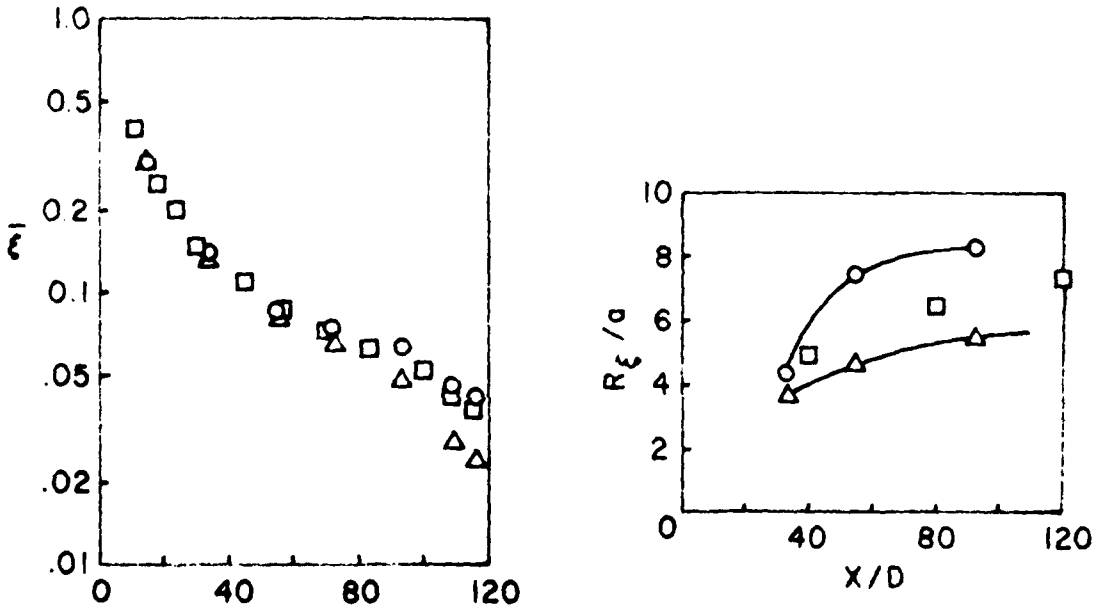

Figure 3. Comparison of mixture mass fraction (ξ) data obtained from a H_2-air diffusion flame with a conventional probe (□) and by light scattering (○,△) from Reference 33: a) centerline variation of mean mixture fraction by probe (□) and conventional (○) and Favre (△) mean values from light scattering and b) axial development of mean mixture fraction half-radii (R_ξ/a) from probe measurements (□) and from conventional (○) and Favre (△) mean data (a is the jet nozzle radius).

DISCUSSION

W.G. Alwang, US

What are the magnitudes of the expected errors in P_t and $\dot{m}$ for typical situations?

Author's Reply

In the Becker and Brown paper error data for impact probes in incompressible shear flow are presented, and Bennett gives error estimates for a five-hole probe in a compressor discharge flow (the estimates are reported in my paper). For reacting flows I have no estimates for specific combustion situations. I expect that considerable error occurs when probing reaction zones where density fluctuates by hundreds of percent and density and velocity fluctuations may be correlated. The sampling probe data of Kent and Bilger and the particle scattering results of Kennedy and Kent are compared in the paper to provide some indication of the errors incurred with isokinetic sampling. The comparison indicates that significant errors can occur in regions of large density fluctuations.

APPLICATION OF MODEL LAWS WHEN DETERMINING THE HEAT TRANSFER COEFFICIENTS BY EXPERIMENTS ON COOLED TURBINE BLADES

O. A. von Schwerdtner and H.-G. Hosenfeld

Kraftwerk Union, Mülheim/Ruhr, F.R.Germany

Summary

Fulfilling model laws for geometry, aerodynamics and heat transfer by reducing temperature and pressure of the operational and cooling fluids as opposed to the conditions in the turbine. With these requirements: Conception of a cascade wind tunnel with closed circuit; enables the independent variation of influence values e.g. Mach No., Reynolds No., degree of turbulence, temperature ratio operating fluid/cooling fluid. Two measuring methods : 1. Determining the local heat transfer coefficients by calorimetric means when cooling the blade surface with water in sections; 2. Distribution of the cooling efficiency on the profile contour with the original cooling process. Examples of results.

LIST OF SYMBOLS

c	velocity
c_p	specific heat at constant pressure
c_p^*	critical pressure coefficient per (20)
d	blade wall thickness
H_{ad}	cooling degree per (21)
K_d	factor per (17)
l	length
$\dot{m}$	mass flow rate
Ma	Mach number
Nu	Nusselt number
p	pressure
p^*	critical pressure
Pr	Prandtl number
q	heat flow
R	gas constant
Re	Reynolds number
s	distance
$\vec{s}$	vector of distance
T	temperature
Tu	degree of turbulence
$\vec{w}$	vector of local velocity
α	heat transfer coefficient
η	dynamic viscosity
Θ	characteristic quantity of temperature field per (15)
$\varkappa$	isentropic exponent
λ	thermal conductivity
ν	kinematic viscosity

Subscripts

a	external
ad	adiabatic
D	pressure side
F	water
G	air or flue gas
i	internal
k	outline
K	cooling air
M	experiment
P	profile
S	suction side
T	turbine
W	wall
x	coordinate of distance
1	inlet
2	outlet
∞	free stream condition

1. INTRODUCTION

The increase in turbine inlet temperatures of gas turbines results in higher stresses at all machine components coming into contact with the hot gas flow. On the one hand it requires the utilization of temperature resistant materials and on the other the cooling of extremely stressed areas. This primarily applies to the blades of the first turbine stages. An efficient cooling system must first restrict the blade temperatures to an allowable level and second keep temperature differences small; third as the relevant cooling air results in a certain loss of output, it has to be minimized. Even in case of simple cooling systems as it is the case with stationary gas turbines, contrary to those for aircraft propulsion, any optimum design can't be achieved based on theoretical findings only. At Kraftwerk Union the required experimental investigations are primarily performed at operating conditions on gas turbines. Above all there is a gas turbine test field at Berlin, the water friction brake of which can brake ratings up to 120 MW. Thus, rating and speed may be varied separately [1,2]. Such experiments require much time and financial expenditure, it therefore should be investigated if and to what a degree they may be supplemented or replaced by laboratory investigations.

2. CONCEPT OF LABORATORY INVESTIGATIONS

Laboratory investigations must be favourable with respect to time and costs without simplifying the problem

too much. The disadvantage being unavoidable in most cases, i.e. the fact that some factors are partially or completely neglected, is generally connected with the definite advantage of having the possibility to study the effects of especially interesting and important factors to an better extend than in the turbine test field. Regarding the test set up, the investigations at original components applying pressures and temperatures as in the turbine, result in only slight advantages compared to turbine test field measurements. Accordingly, we planned the test according to the following concept:

a) investigation of the cooling system at one blade cross-section, i.e., investigations in a cascade,
b) measurements at pressures and temperatures being reduced compared to the turbine.

To a): The cascade represents a simplification compared to the turbine. Thus, e.g. it isn't fan-shaped, the rotational influences and the three dimensional effects are lacking. The investigations are reduced to one blade section, causing in case of severe radial profile modifications that probably several sections must be investigated to assess the blade cooling phenomena to a sufficient extend. Cooling systems including, as in the case of the rotor blades, radial flow paths may be investigated, too, - they require, however, enlarged expenditures. I.e., the question if a problem may be researched and moreover, to what an extend, must be decided from case to case, regarding the limiting boundary conditions of such a test facility.

To b): The lowering of pressure and temperature is possible, if the relevant laws of similitude are adhered to. The following section deals with this question.

3. CONSIDERATIONS OF SIMILITUDE

The considerations apply to the similitude of geometrical arrangement, flow and heat transfer.

3.1 Similitude with respect to geometrical arrangement

In case of a cascade, geometrical similitude refers to the selected profile section of the original blade. The formation of the wall boundary layer depends on the roughness of the blade surface while the known model laws of wall roughness, e.g. [3], must be fulfilled. Applying a model scale of about 1:1, the surface finish can be adequately adapted. In general, we perform model tests with hydraulically smooth surfaces corresponding to gas turbine blades which are free of dirt and flaws due to high temperature corrosion.

3.2 Similitude with respect to flow and heat transfer

It is important that the effects of surface and gas radiation may be neglected in the following. As estimates show, the surface radiation will participate in heat transfer to only a small percentage in case of the temperatures existing with stationary gas turbines; in the test bed this percentage value will again be less than one tenth. The emitting gases carbon dioxid and water vapour contained in air contribute to heat transfer to an even far less extend than surface radiation.

In the cooling systems discussed in the following, heat transfer takes primarily place by forced convection. Provided the Navier-Stoke's equation, the energy equation, the equation of state for gases and the continuity equation are non-dimensionalised, the following relations result for velocity and temperature field as well as for heat transfer [3, 4, 5]

$$\frac{\vec{w}}{c_\infty} = f_c\ (\vec{s},\ Re,\ Pr,\ Ma,\ Tu,\ T_\infty/T_W) \tag{1a}$$

$$\vartheta_W = \frac{T - T_\infty}{T_\infty - T_W} = f_T\ (\vec{s},\ Re,\ Pr,\ Ma,\ Tu,\ T_\infty/T_W) \tag{1b}$$

$$Nu = f_{Nu}\ (\vec{s},\ Re,\ Pr,\ Ma,\ Tu,\ T_\infty/T_W) \tag{1c}$$

Where $\vec{s}$ is a vector of distance, the coordinates of which are non-dimensionalised by reference to a characteristic length. The definitions for Reynolds number Re, Prandtl number Pr, Mach number Ma and the degree of turbulence Tu are:

$$Re = \frac{c \cdot l_p}{\nu} = \frac{c \cdot l_p \cdot p}{\eta \cdot R \cdot T} \tag{2}$$

$$Pr = c_p \frac{\eta}{\lambda} \tag{3}$$

$$Ma = c\ /\ (\varkappa \cdot R \cdot T)^{0.5} \tag{4}$$

and

$$Tu = \left(\overline{c_x'^2} \right)^{0.5} / c_\infty \tag{5}$$

Equation (5) applies to the socalled isotropic turbulence, the mean fluctuation velocities in the 3 coordinate directions are equal, while the mean longitudinal fluctuation $c_x'^2$ may be considered the only determining factor for the degree of turbulence.

The dependencies of (1), however, are only partially explicit, i.e. there are e.g. several formulars for the influence of $\vec{s}$, Re, Pr and T_∞/T_W on Nu, being mostly, however, restricted to a certain area of validity. The knowledge of the relevant mathematical dependency may be regarded unnecessary, however, if each parameter is going to be set up in the test bed as in the turbine. In case of $\vec{s}$ this requirement is fulfilled

per section 3.1, and there are no principal difficulties regarding Ma, Re and T_∞/T_w. The Prandtl number in its function of exclusive fluid properties exhibits slight deviations in the test bed and the turbine which can be considered by calculations. The degree of flow turbulence has a telling influence on the transition point from laminar to turbulent boundary layer or the position and extension of such a transition zone. It is unknown in the turbine flow; estimates amount to Tu = 20 % at the combustion chamber outlet with a decrease down to below 10 % at the turbine inlet [6]. It must be variable in the test.

3.3 Temperature dependency of fluid properties

The equation (1) applies to constant values of η, c_p and λ within the temperature regions to be considered. If the temperature level is essentially lowered in the test bed compared to reality, the similitude of the temperature influence on the properties has to be checked.
This may be established as follows:

$$\eta/\eta_{K1} = \exp\,(\gamma_\eta \cdot \Delta T \cdot \vartheta_K) \tag{6a}$$

$$c_p/c_{p_{K1}} = \exp\,(\gamma_{c_p} \cdot \Delta T \cdot \vartheta_K) \tag{6b}$$

$$\lambda/\lambda_{K1} = \exp\,(\gamma_\lambda \cdot \Delta T \cdot \vartheta_K) \tag{6c}$$

The subscript K1 applies to the cooling air inlet condition having the lowest temperature within the relevant system; the reference units for the temperature are:

$$\Delta T = T_\infty - T_{K1} \tag{7}$$

and

$$\vartheta_K = \frac{T - T_{K1}}{T_\infty - T_{K1}} \tag{8}$$

where

$$0 \leq \vartheta \leq 1 \tag{9}$$

The products $\gamma_\eta \cdot \Delta T$, $\gamma_{c_p} \cdot \Delta T$ and $\gamma_\lambda \cdot \Delta T$ are the model numbers to be noted. The smaller they are, the smaller the temperature dependency of the properties will be; if they become zero, there is no temperature influence left.

Equal model numbers correspond to a similar temperature variation of the properties in the relevant temperature ranges. The temperature ranges within the stationary gas turbine and in the test bed are about:

	T_∞ [K]	T_{K1} [K]	T [K]
turbine	1200	600	$600 \leq T \leq 1200$
model	600	300	$300 \leq T \leq 600$

Provided equation (6) is solved for this area applying the values per (7), the result will be:

model number	$\gamma_\eta \cdot \Delta T$	$\gamma_{c_p} \cdot \Delta T$	$\gamma_\lambda \cdot \Delta T$
turbine	0.405	0.111	0.557
model	0.458	0.052	0.438

Accordingly, the model numbers of turbine and model are small and quite similar to one another, thus the requirement of similitude in the temperature variations of the properties may be regarded as adequately fulfilled.

3.4 Similitude of cooling systems

The a.m. considerations can be directly applied to in the case of test facilities set up to determine separately the external heat transfer coefficient (refer to para. 6). Moreover, in case of investigations regarding the entire cooling system, the external heat transfer, the heat conduction via the blade wall and the internal heat transfer must relate to one another as in the turbine. The equations for the external heat flow, through the wall, and internally say:

$$q = \alpha_a\,(T_\infty - T_{W_a}) = \frac{\lambda_a}{l}\,Nu_a\,(T_\infty - T_{W_a}) \tag{10a}$$

$$q = \frac{\lambda_W}{d} (T_{W_a} - T_{W_i}) \tag{10b}$$

$$q = \alpha_i (T_{W_i} - T_K) = \frac{\lambda_i}{l} Nu_i (T_{W_i} - T_K) \tag{10c}$$

or summarized $$q \left(\frac{l}{\lambda_a Nu_a} + \frac{l}{\lambda_i Nu_i} + \frac{d}{\lambda_W}\right) = T_\infty - T_K \tag{11}$$

Dividing (11) by (10a) amounts to:

$$1 + \frac{\lambda_a Nu_a}{\lambda_i Nu_i} + \frac{d}{l} \frac{\lambda_a}{\lambda_W} Nu_a = \frac{T_\infty - T_K}{T_\infty - T_{W_a}} \tag{12}$$

and by (10c): $$1 + \frac{\lambda_i Nu_i}{\lambda_a Nu_a} + \frac{d}{l} \frac{\lambda_i}{\lambda_W} Nu_i = \frac{T_\infty - T_K}{T_{W_i} - T_K} \tag{13}$$

In order to fulfill the a.m. requirements with respect to the ratios of heat conductions and transfers, the relevant left sides of (12) and (13) must coincide in turbine and experiment. The separate consideration of the individual units or quotients is intended to show to what an extend this will apply. If the required agreement applies, (13) may be neglected, as there are no other units on the left than with (12). Thus, the model condition may be formulated:

$$\left(\frac{\lambda_a}{\lambda_i}\right)_M \frac{(Nu_a)_M}{(Nu_i)_M} + \left(\frac{d}{l}\right)_M \left(\frac{\lambda_a}{\lambda_W}\right)_M (Nu_a)_M = \left(\frac{\lambda_a}{\lambda_i}\right)_T \frac{(Nu_a)_T}{(Nu_i)_T} + \left(\frac{d}{l}\right)_T \left(\frac{\lambda_a}{\lambda_W}\right)_T (Nu_a)_T \tag{14}$$

The similitude of Nu_a will be well fulfilled according to the considerations per para. 3.2. If this consideration is also applied to Nu_i, the result will be satisfactory, as well. - The agreement of ratio d/l results from the provision of geometrical similitude. - The ratio of the thermal conductivities of air i.e. λ_{aM} and λ_{iM}, are established due to the fact that the temperatures are given by the setting of Nu_a and Nu_i. Now the deviation from linear temperature variation won't be high, and the thermal conductivity variation of the original blade material will be similar. Thus, the requirement of similitude for λ_a/λ_i and λ_a/λ_W has been fulfilled quite well; it may, however, be improved by an adequate selection of a model blade material.

Those considerations have shown that the relevant similitude characteristics of complete cooling systems may be gained quite well within a model test. Thus, satisfactory statements on the distribution of temperatures at all points, vertical and parallel to the blade surface are to be expected. If radial flow conditions appear additionally, the achievable model similitude must be considered from case to case.

4. CONCLUSIONS REGARDING TEST BED OPERATION

Prerequisite of the test bed setting values will be the selection of the air inlet temperature $(T_{GI})_M$. It'll be set at 600 K with regard to the temperature compatibility of the test bed. According to the conditions of similitude

$$\left(\frac{T_{GI}}{T_{KI}}\right)_M = \left(\frac{T_{GI}}{T_{KI}}\right)_T \tag{15}$$

the inlet temperature of the cooling air will be achieved at 300 K. Compressed air of this temperature is at hand due to laboratory facilities. The inlet air pressure results from the condition of Mach number and Reynolds number equivalent to reality. With respect to this pressure the equations (2) and (4) result in:

$$(p_{GI})_M = K_d (p_{GI})_T \left[(T_{GI})_M / (T_{GI})_T \right]^{0.5} \tag{16}$$

with the factor $$K_d = \frac{(\eta_{GI})_T}{(\eta_{GI})_M} \frac{R_T}{R_M} \left(\frac{\varkappa_M}{\varkappa_T}\right)^{0.5} \tag{17}$$

The inlet pressure may be calculated to 4 bar by (16) and (17). The condition of equal Mach number leads to the pressure ratio at the cascade and this, assuming identical profiles, results in the actual pressure distribution and thus temperature distribution in the air flow. By means of (15) as well as the relevant Reynolds number, Mach number and Prandtl number for the cooling air, the blade wall will be confronted with the actual temperature distribution.

2. DESCRIPTION OF TEST BED

Fig. 2 shows the test bed which has been designed for the investigations mentioned above. The air is circulated in a closed circuit by a blower via a settling chamber to the test section. The pressure in front of it here will be gained back to quite an extend by an adjacent diffuser. The air will be heated via heat exchangers; a cooler is required to control the temperatures, it is connected between diffuser and blower (Fig. 2 doesn't show the compressor unit supplying the test bed as well as the cooling air). Fig. 3 shows the part measuring range for the stator and blade investigations. The lateral duct walls of the inlet and outlet are adjustable even in operation in order to allow for an adjustment of the required pressure distribution around the model blade. The boundary layer at the end of the inlet duct walls may be extracted. Pressure distribution measurements in planes parallel to the blade before and behind the blade as well as in the center section of the blade itself allow for a continuous checking of the flow conditions.

The production of various degrees of turbulence by means of the insertion of grids is known, e.g. [9]. In the case at hand these installations have been mounted at the end of the settling chamber. The measuring of the degree of turbulence Tu in accordance with the hot wire method as it is usual at DFVLR as well, is not without some trouble in case of higher temperatures and minim. pressures, as detailed in the ball method [8], [7]. All the measuring points of the test bed and the model blades were connected to a computer controlled data logging system. This computer is responsible for the analysis immediately after the test and will print out the results via printer or typewriter printer.

3. DETERMINATION OF NUSSELT NUMBER Nu_a

The basic principle of this test program part has been to test the blade section by section with the individual cooling segments insulated towards one another. Fig. 3 illustrates a model blade of such a kind. The individual cooling segments are perpendicular to the air flow direction and are made out of copper. The cooling medium will be water flowing perpendicular to the air flow. The temperature of the cooling water and thus of the element's surface doesn't increase exactly linearly along the cooling water path, but in an exponential way. Calculations, however, and measurements at some cooling elements do prove that in the range of usual measuring accuracy the surface temperature established in the blade center may be considered the medium temperature of the whole element surface. The insulating material between the cooling elements exhibits only 1 % of the copper thermal conductivity.
Thus, the heat exchange between the elements will be extraordinary small; it nevertheless will be considered in a corrective calculation. The cooling water mass flow has an influence on the surface temperature; it'll be adjusted in order to adapt this temperature to a required distribution. The tests showed, however, that even a definitely deviating temperature distribution will be without any significant influence on the heat transfer, thus the dependency $Nu_a = f\ (T_x/T_W)$ per (1c) will be neglectably small within the range to be investigated. The amount of heat for each element which will be transmitted from the air to the cooling element and then removed by the water, can now be set up:

$$\alpha_a F_a (T_G - T_W) = \dot{m}_F \; c_{pF} (T_{F2} - T_{F1}) \tag{18}$$

The cooling water mass flow $\dot{m}_F$ and all temperatures will be measured or calculated from measured values, so that the external heat transfer coefficient α_a and per

$$Nu_a = \frac{\alpha_a \; l_p}{\lambda_a} \tag{19}$$

Nu_a as well may be determined. Experiments with this concept have been performed for the stator and rotor blade profile, as fig. 4 and 5 show. There, at the top the critical pressure coefficient

$$c_p^* = \frac{p_k - p^*}{p^*} \tag{20}$$

and at the bottom Nu_a have been plotted versus the dimensionless blade outline length. When assessing the diagrams it has to be noted that trip edges in the area of the profile leading edge reduce the lengths of laminar boundary layers. Fig. 4 shows the results of a Reynolds number and degree of turbulence variation for the same stator blade profile as in fig. 3. The distribution of the critical pressure coefficients will be uninfluenced by Re and Tu; values smaller than zero are equivalent to supersonic velocities.

The variation of the Nusselt number downstream of the profile leading edge shall first be treated for the lowest inflow Reynolds number (curve 1): The stagnation point at the leading edge is shown by a maximum which has been slightly offset towards the suction side. The drop to the right and left is indicating laminar boundary layers at the suction and pressure side with the boundary layer staying in a laminar condition (about horizontally). The significant upward tendency of the curves at the suction side with $s/l_{k_3} \approx 0.5$ illustrates the conversion to turbulent boundary layers. - The laminar lengths will consequently be reduced with higher inlet Reynolds numbers (curve 2 and 3); at the suction side of curve 3 the boundary layer will be turbulent practically from the stagnation point onwards. The two drops in the further course of the curve at the suction side can on the one hand be caused by a relaminarisation process [10] and on the other by a socalled separation bubble of the boundary layer. The latter is also indicated by the c_p^* - distribution dropping to a horizontal section at this point of the curve. - Smaller degrees of turbulence (dotted curves) result in smaller Nusselt numbers nearly everywhere.

Fig. 5 shows the critical pressure coefficient and Nusselt number for 2 Reynolds numbers and constant degree of turbulence in case of a rotor blade profile. The high Nusselt number in the area of the blade leading edge is remarkable, dropping severely to the pressure and suction side. On the pressure side it is followed by a continuous increase and on the suction side this is reversed into a decreasing Nusselt number after about half-way the contour length.

7. DETERMINATION OF TEMPERATURE DISTRIBUTION

This requires a model stator blade being realistically cooled as it is shown in fig. 5. The cooling air is entering a cooling insert at its centre and leaving it via a row of holes at the nose as well as a series of holes ("shower") at the pressure and suction side; i.e., the cooling of especially hot blade portions takes place by impingement cooling. It has to be noted that the cooling air isn't flowing perpendicular to the direction of the outer air flow. The blade temperature is the decisive result of a cooling system, its assessment, however, will require the relating of this temperature to the important temperatures of the fluids involved. If the blade weren't cooled in any way and produced out of a material exhibiting indefinite high thermal resistance, the blade surface would adopt the adiabatic gas temperature $T_{G,ad}$. With given total temperature, it is a function of static pressure and recovery factor. Thus, the degree of cooling may be defined as follows:

$$H_{ad} = \frac{T_W - T_{K1}}{T_{G,ad} - T_{K1}} \cdot 100\ [\%] \qquad (1)$$

It can be adapted to the turbine and constitutes an analysis of the cooling system characteristics: The lower the blade temperature T_W, and the higher $T_{G,ad}$ and T_{K1}, the smaller will be H_{ad} and the better the final cooling efficiency. Thus, H_{ad} = 100 % means uncooled and H_{ad} = 0 % cooled to cooling air inlet temperature blades.

Fig. 7 shows the degree of cooling for two degrees of turbulence spread over the relative length and with respect to an early state of development of the cooling insert (type A), allowing an uneven distribution of the cooling air at pressure and suction side as well as high temperature differences within the blade material. The cooling air mass flow increases starting from zero in two steps whereas the degree of cooling decreases accordingly. With missing cooling air, H_{ad} won't be continuously 100 % but due to the temperature equalization within the blade and the thermal losses to the blade internal it will be somewhat smaller. The influence of the degree of turbulence becomes clearer than in case of the determination of Nu_a (fig. 4), i.e., especially on the pressure side where the laminar boundary layer is approaching the blade center in case of small Tu.

Fig. 8 cites examples of further developed stages: the suction side gap between blade and cooling insert has been sealed near the leading edge. The type B doesn't include holes in the front edge of the insert but only showers by various hole arrangements at the pressure and suction side. The positions of sealing and showers have been identified in the fig. Type C, D and E illustrate the cooling inserts with stepwisely enlarged holes in the front edge. The variation of the cooling degree leads to the conclusion that the blade gets cooled increasingly more uniform.

8. COMPARISON OF MEASURED AND THEORETICAL HEAT TRANSFER COEFFICIENTS

In case of a simple flow of cooling air in the gap between blade and cooling insert and known cooling mass flows, the calculation of the internal heat transfer coefficient will be quite safe. From this, the measured wall temperature distribution and the known thermal conductivity in the blade, the external heat transfer coefficient α_a will be calculated. Fig. 9 shows its variation across the contour length for two degrees of turbulence. In case of small Tu there is a definite laminar boundary layer at the pressure side similar to fig. 7. Assuming a fully turbulent and laminar boundary layer, the relations of heat transfer at a flat plate may be applied to the blade profile velocity distribution. The heat transfer coefficients gained in such a way, have been included in fig. 9, too. It is to be recognized that at nearly all points the turbine flow exhibits a higher heat transfer, even in case of a very small degree of turbulence, Tu = .1 %, than the laminar flow according to the mentioned theoretical set up and that the theoretical values of a fully turbulent flow can't be achieved in case of the not too high degree of turbulence Tu = 3 %.

9. COMPARISON OF TEMPERATURES MEASURED IN TEST AND AT TURBINE

Finally there'll be a comparison between a temperature distribution calculated from experiments and applied to the turbine and those blade temperatures measured in the turbine. For this purpose, 2 blades equipped with thermocouples were installed in a unit. As expected those tests applying Tu = 3 % represent the actual temperature distribution to a better extend than those with Tu = .1 % which have been analyzed also for reasons of comparison. The temperature level is comparably low though the share of cooling air at the mass flow as a whole amounts to about 1 % only; these are reserves for further increases in the turbine inlet temperature. The positive forecast of the blade temperature based on the experimental results has been a confirmation of our philosophy and gives sense to future investigations - within the mentioned limits.

REFERENCES

[1] Den[illegible], B.: [illegible] Load Tests [illegible] the [illegible]-MW Gas Turbine [illegible] Using a Water Brake. ASME [illegible]-68.

[2] Be[illegible]ker, B.: Erprobung einer neuen Leistungs[illegible] für Gasturbinen [illegible] Last über 100 MW. Motortechnische Zeitschrift [illegible]

[3] Schlichting, H.: Grenzschichttheorie, [illegible] Aufl. Karlsruhe, [illegible] Braun [illegible]

[4] Pawlowski, J.: Die Ähnlichkeitstheorie in der physikalisch[illegible] Berlin, Springer-Verlag 197[illegible].

[5] Zierep, J.: Ähnlichkeitsgesetze und Modellregeln der Strömungslehre. Karlsruhe, G. Braun 1972.

[6] Zysina, L.M.; Roost, E.G.: Influence of Turbulence of the Approach Flow on [illegible] Heat Transfer in Turbine Nozzle Cascades. Thermal Engineering [illegible] 1979 (Translated from: Teploenergetika).

[7] VDI-Wärmeatlas. Düsseldorf, VDI-Verlag 196[illegible]

[8] Meier, H.U.: The Response of Turbulent Boundary Layers to Small Turbulence Levels in the External Free Stream. ICAS Paper 76-[illegible].

[9] Pankhurst, R.C.; Holder, D.W.: Wind-Tunnel Technique. London, Sir J. Pitmann & Sons, Ltd. 19[illegible].

[10] Dejc, M.E.; Trojanovskij, B.M.: Untersuchung und Berechnung axialer Turbinenstufen. Berlin, VEB Verlag Technik o.J.

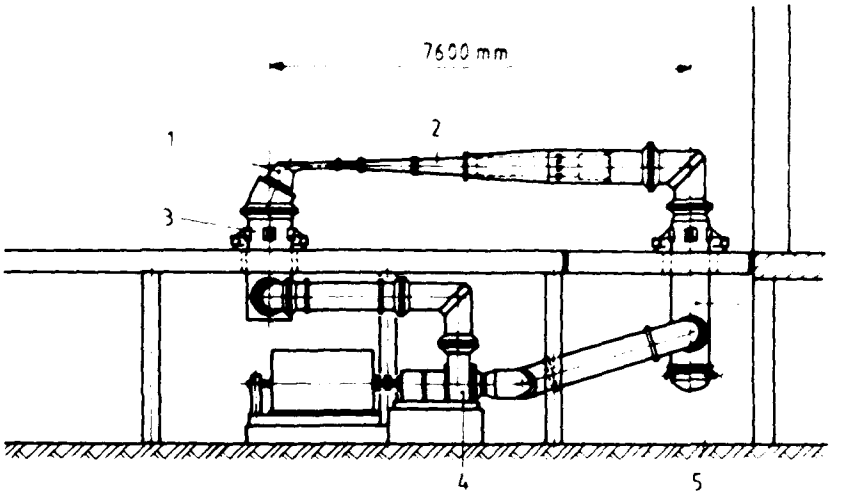

Figure 1. Blade cooling test bed.
1 - Test section, 2 - Diffuser, 3 - Settling chamber, 4 - Blower, 5 - Cooler.
N = 500 kW, p_{max} = 5 bar, T_{max} = 630 K

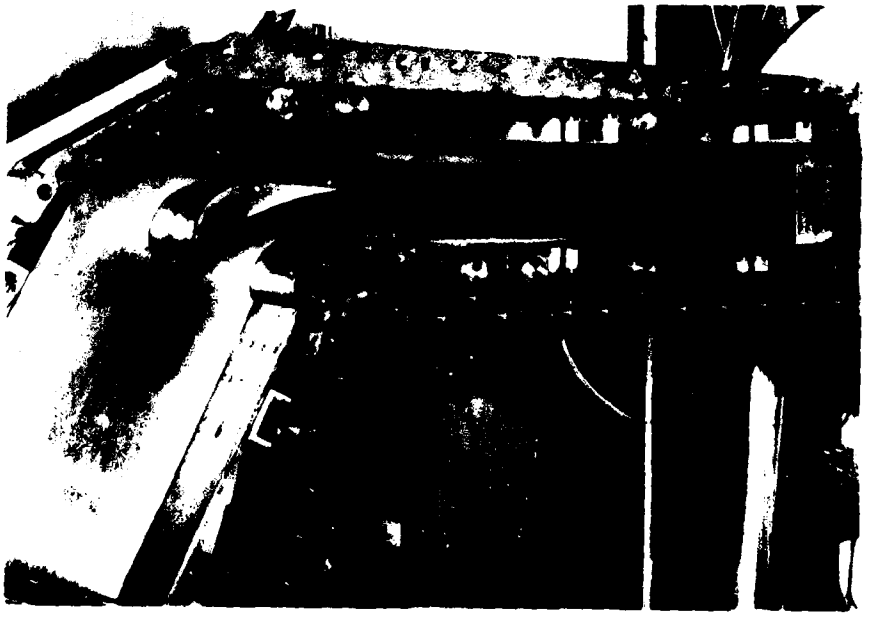

Figure 2. Stator blade measuring range, opened.

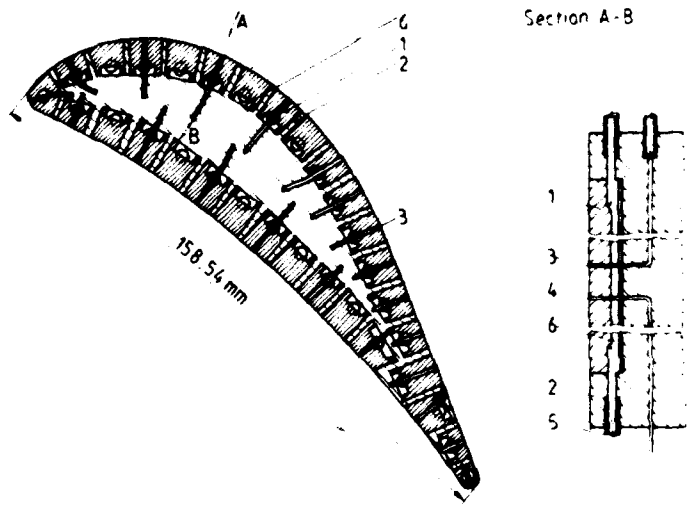

Figure 3. Model blade to determine the external heat transfer coefficient. 1 - Cooled section (Cu), 2 - Insulation material, 3 - Pressure measuring point, 4 - Temperature measuring point, 5 - Cooling water supply, 6 - Cooling duct

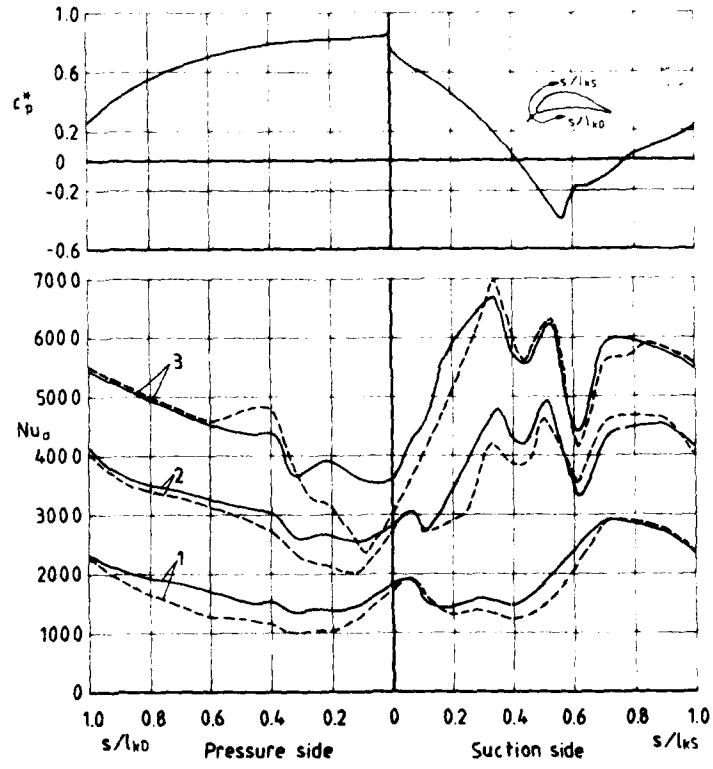

Figure 4. Distribution of critical pressure coefficient c_p^* and Nusselt number Nu_a around a guide blade.

$Ma_1 = 0.246$

- - - $Tu_1 = 0.1\ \%$ —— $Tu_1 = 3\ \%$

1 - $Re_1 = 0.65 \cdot 10^6$, 2 - $Re_1 = 1.38 \cdot 10^6$, 3 - $Re_1 = 2.1 \cdot 10^6$

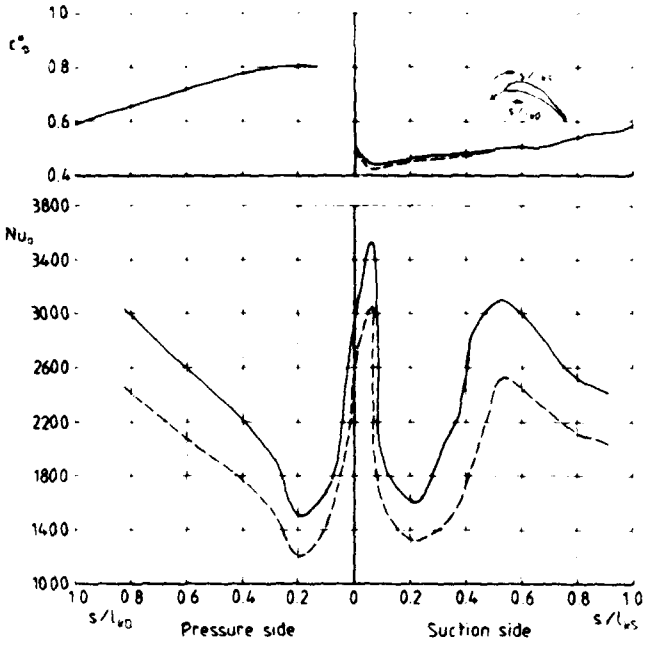

Figure 5. Distribution of critical pressure coefficient c_p^* and Nusselt number Nu_a around a rotor blade.

$Ma_1 = 0.38$, - - - $Re_1 = 0.92 \cdot 10^6$, —— $Re_1 = 1.18 \cdot 10^6$

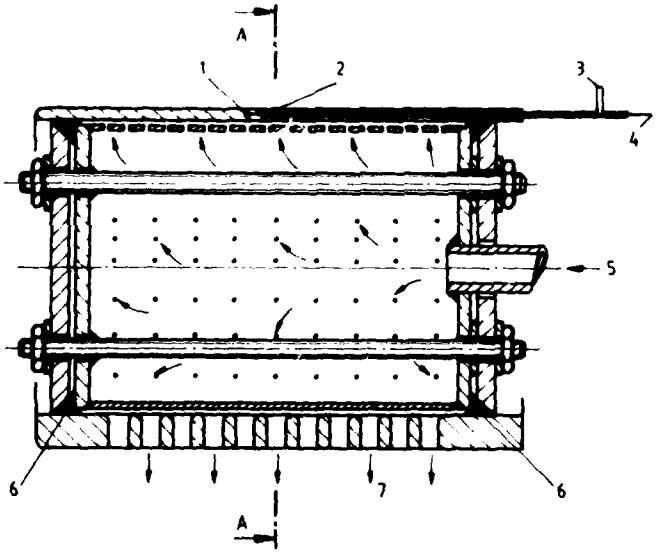

Section A-A

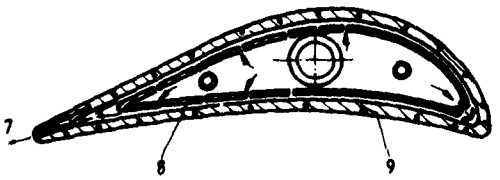

Figure 6. Model blade cooled as in reality.

1 - Thermocouple, 2 - Pressure measuring bore, 3 - Pressure measurement, 4 - Temperature measurement, 5 - Cooling air inlet, 6 - Packing, 7 - Cooling air outlet, 8 - Sheet metal insert, 9 - Measuring point

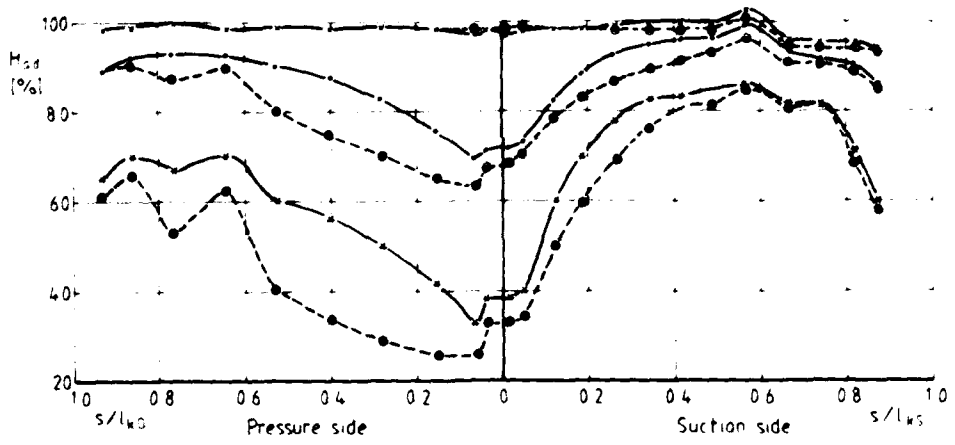

Figure 7. Cooling degree H_{ad} at different degrees of turbulence Tu and cooling air mass flows $\dot{m}_K$.
$Ma_1 = 0.246$, $Re_1 = 1.37 \cdot 10^6$
x - $\dot{m}_K = 0$ %, o - $\dot{m}_K = 14$ %, * - $\dot{m}_K = 100$ %
- - - $Tu_1 = 0.1$ %, —— $Tu_1 = 3$ %

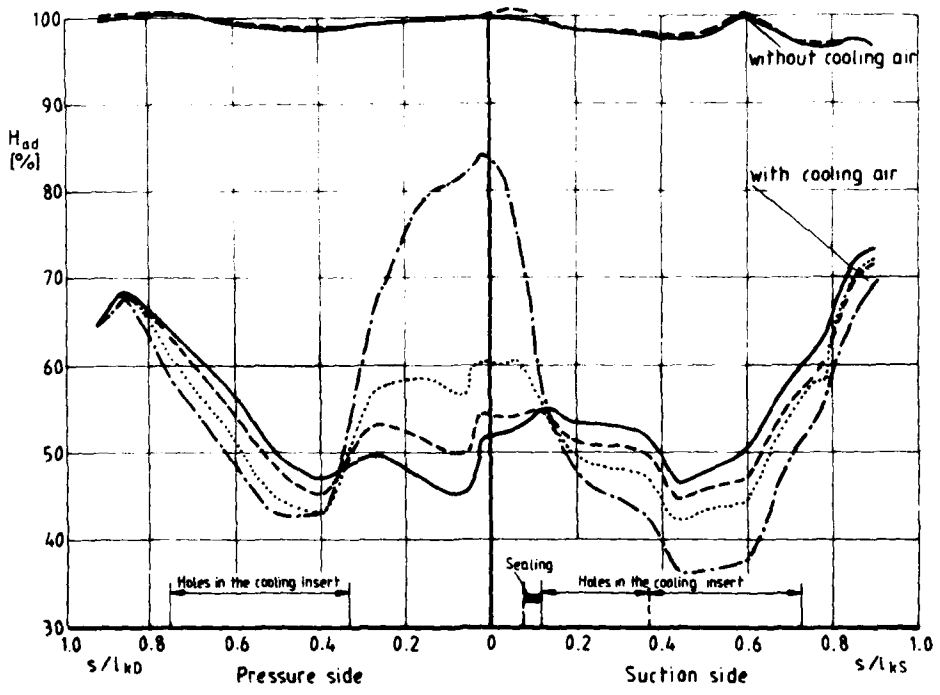

Figure 8. Cooling degree H_{ad} with several cooling insert types.
$Ma_1 = 0.242$, $Re_1 = 1.35 \cdot 10^6$, $Tu_1 = 0.1$ %
—— —— insert B: no holes in the leading edge of the insert
..... insert C:
- - - - insert D:
——— insert E:
} step-by-step enlargement of the leading edge holes

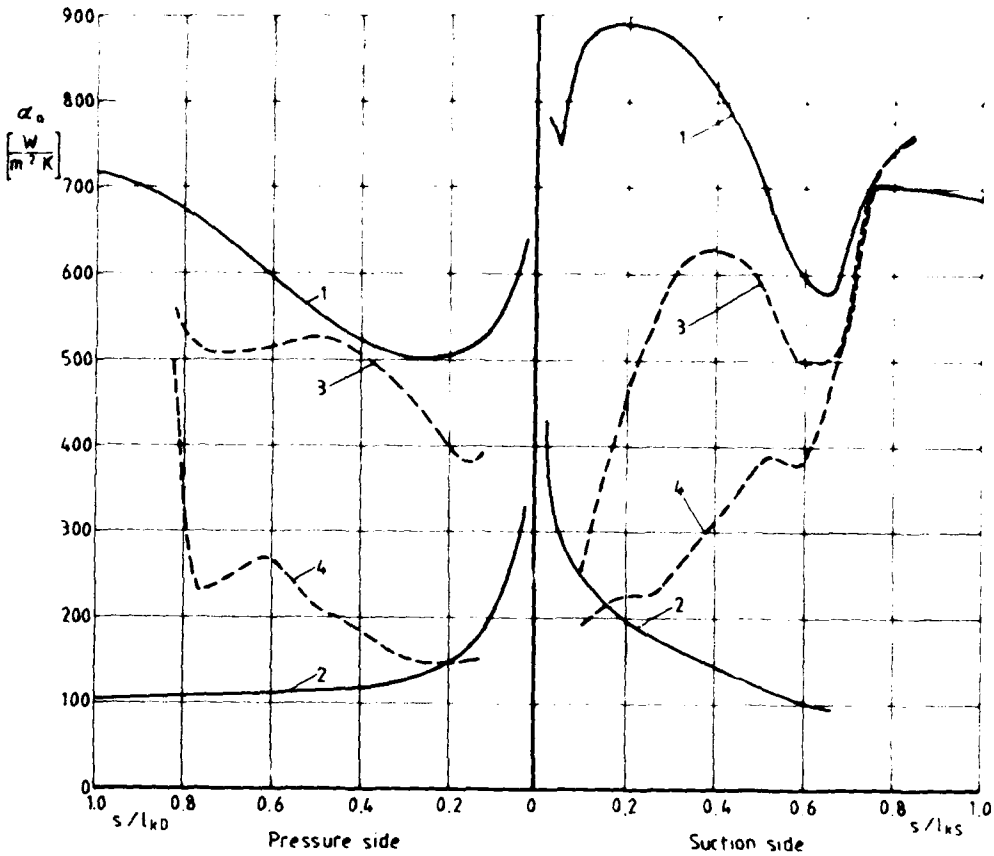

Figure 9. Measured and theoretical heat transfer coefficients.

1 ——— Theory for turbulent flow (flat plate)

2 ——— Theory for laminar flow (flat plate)

3 - - - - Measurement for Tu_1 = 3 % (profile as in fig. 6)

4 - - - - Measurement for Tu_1 = 0.1 % (profile as in fig. 6)

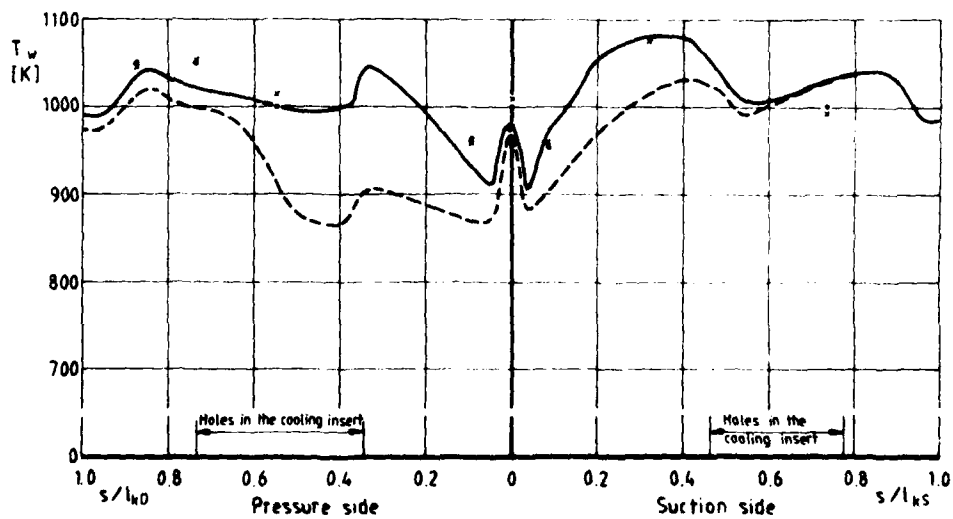

Figure 10. Blade temperatures from model tests and full scale engine tests.
Temperature distribution calculated from model tests:
- - - Tu_1 = 0.1 %, ——— Tu_1 = 3 %
x, o: results from full scale engine tests

DISCUSSION

D.K.Hennecke, Ge

In your Figure 4 the leading edge Nusselt numbers are relatively low compared to the rest of the blade surface. Is this a peculiarity of your particular blade or is your measuring technique not fine enough to resolve the leading edge region? Have you compared the measured Nusselt numbers at the leading edge to theoretical ones for an equivalent cylinder in cross-flow?

Author's Reply

We think the low measuremement of Nusselt number at the leading edge arises because the stagnation region covers only a small portion of the leading edge element. The integral value of heat transfer over the element is therefore low compared to the peaked stagnation level. (In the case of the rotor blade with its greater inlet radius we found a higher Nusselt number at the leading edge, Figure 5.) Were it necessary to obtain the Nusselt number distribution in more detail one would have to use smaller cooled elements.

The comparison between our measured values and the theoretical ones for a cylinder is of doubtful validity because of the different velocity distributions for the two cases.

G.Kappler, Ge

You presented results of heat transfer measurements at low and high levels of turbulence, the highest degree of turbulence being 3%. The degree of turbulence in an engine is however above 10%. Latest tests at MTU at Tu = 11% have shown a dramatic change of heat transfer conditions, especially on the suction side of the blade, when compared to our results at Tu = 4%. Do you have test experience at degrees of turbulence above 3%, or do your model predictions encompass true engine conditions, that is, highly turbulent flow?

Author's Reply

In our gas turbines with a relatively long distance between combustion chamber and turbine inlet, we think the degree of turbulence isn't as high as you measured in your turbine. Nevertheless, it is foreseen to raise the turbulence level in our tests in order to see the further dependence of the heat transfer coefficient on the degree of turbulence.

E.Covert, US

(1) Is the turbulence isotropic or anisotropic?

(2) Have you considered the problem of modelling anisotropic turbulence of the kind encountered in real flows?

Author's Reply

(1) The given values of the degree of turbulence refer to the isotropic turbulence.

(2) Yes, we considered this problem. However, up to now we have hardly any information about structure and degree of turbulence at the turbine inlet in our turbines. Therefore we decided to start our tests with this simple kind of turbulence. At the same time, we are trying to get further information about the turbulence by means of measurements in our turbines.

HEAT TRANSFER MEASUREMENTS RELATED TO HOT TURBINE COMPONENTS IN THE VON KARMAN INSTITUTE HOT CASCADE TUNNEL

B.E. Richards*
Professor, von Karman Institute for Fluid Dynamics
Chaussée de Waterloo, 72
B-1640 Rhode Saint Genèse, Belgium

SUMMARY

The paper describes the new hot cascade tunnel developed to extend turbine research at VKI to heat transfer studies. It is based on a free piston compressor of 1 m in diameter and 5 meters in length with a test section of 100 mm×250 mm compatible with an existing ambient temperature blowdown cascade tunnel at VKI. Some typical results on heat transfer and film cooling from the first 1200 tests are described.

1. INTRODUCTION

Historically, the one gas turbine engine component which has presented few problems and anxieties has been the turbine. However, requirements for higher specific power, higher efficiency, longer blade and disc life and reduced weight dictated turbines with higher turbine inlet temperatures, minimization of the losses and improved prediction methods. The high temperatures made necessary the introduction of optimized cooling concepts which in turn introduced the need for a good prediction method for the temperature and flow fields. Furthermore, the high temperatures cause the operational life of the blades and discs to be shortened drastically and, hence, the need for an accurate stress analysis that could lead to the prediction of this life, has arisen. A thermal stress analysis, however, requires a good knowledge of the thermal field and the heat transfer rates across the blade passage walls.

It is with these requirements and expectations of support of future research in mind that the von Karman Institute embarked upon the construction of a heated flow facility which would enable fundamental and configurational measurements of heat transfer on models of various turbine components to be generated. The measurements then would be used to test developing prediction methods or to provide data for designers on specific configurations. It was decided to use the short duration slow piston compression concept as conceived by Oxford University to generate the heated flow. After gaining experience in this type of piston facility with a small converted calibration shock tube (designated tunnel CT1), a large heated flow cascade tunnel, CT2, was designed and built. This facility as described in this paper is similar in many respects to the Oxford University cascade tunnel described fully in reference 1 and indeed the design benefited from discussions with the authors of this latter publication.

The particular area of heat transfer measurements which was aimed at studying in building the tunnel was the effect of the three dimensional secondary flows on heat transfer on blades and end-walls, with and without film cooling. In order to build up the measurement techniques and to test computer codes then simpler two dimensional channel flows were also examined. The paper contains a review of the work carried out to date.

2. THE VKI CT2 HOT CASCADE TUNNEL AND INSTRUMENTATION

2.1 General

The short duration cascade tunnel uses the isentropic light piston tunnel concept developed by Jones et al. (Ref. 2). It is based on isentropic compression heating of the test gas in a tube to moderate temperatures by a light weight piston, whose path during the running time is controlled by "marching" volume flow rates into and out of the tube. This feature, which had not been previously explored, has been shown to provide during this time relatively constant conditions with superimposition of only small fluctuations due to interaction of the finite weight piston and unsteady flow effects. Fast operating valves can be used instead of diaphragms to initiate a test thus eliminating the time-consuming operation of opening the tube between tests. The most useful feature of such a tunnel other than its simplicity of construction and operation is its producing long running times (0.1-1 sec) enabling wider scope for testing techniques than in shock tunnels. Another useful feature is that by suitably alternating driver, barrel, "matching" and dump tank pressures any pressure and temperature condition within the available range of conditions could be achieved in the test section.

A number of factors controlled the design of the VKI tunnel. The main feature was that the test section would enable a straight cascade of turbine blades to be tested and that this should have similar dimensions and fitments to an existing ambient temperature compressible flow cascade tunnel (designated C3) of dimensions 250 mm×100 m such that one model could be used for both heat transfer and aerodynamic studies. The total pressure contained by the test section would be 7 bars which with a nominal maximum flow temperature of 600 K and the size of model at room temperatures which could be fitted in the tunnel, would be sufficient to simulate Mach numbers, Reynolds numbers and wall-to-recovery temperature ratios typical of projected advanced turbine concepts. The running time should not be less than 0.1 sec over the range of conditions and model sizes available. The tunnel should use the copious compressed air supply available at 7 bar, 40 bar and 250 bar levels and be contained in an available room of 10 m length. Instrumentation costs, which for short duration tunnels are high (one disadvantage of such facilities), would be kept to a minimum by using equipment available to the VKI Longshot heavy piston

* Now Mechan Professor in Department of Aeronautics and Fluid Mechanics, U. of Glasgow.

hypersonic tunnel and assuming future equipment acquisitions would be shared by these two facilities. The tunnel and its ancillary equipment would be designed such that the minimum time would be needed to 'turn round' the tunnel between tests, and that it would be safe and easy to use by postgraduate students with the minimum of support personnel. The design incorporated features used in the Oxford University hot cascade tunnel (Ref. 1) which was starting up operation at the time of design of the VKI tunnel.

2.2 Tunnel details

The result of such design constraints produced a compression tube of 5 meters in length with a machined and polished bore of 1 meter diameter which was designed to withstand pressures of 40 bars (Fig. 1). This high pressure was selected to leave an option open to use the compression heater at a later date for kinetic heating studies of aircraft and missile configurations at high speeds with a suitably different test section. The tube was driven directly from the Institute's main 250 bar air supply of 20 m³ volume by means of a 3 inch diameter 90 m length pipe fitted with two appropriately placed isolating ball-valves, a pneumatically controlled starting ball-valve and after a five-branch manifold by five 1 inch ball valves one of which is in parallel with a specially constructed "carrot" regulating valve. The latter system allowed adjustment of the throttled area of compressed air into the compression tube to control the "matching" of the tunnel during the running time. The ball-valves were fitted with special high temperature resistant seats to counter deterioration due to gas heating caused by the rapid opening of upstream valves during the pre-test and test phases. The pneumatically controlled ball-valve was fitted such that in the event of a compressed air failure, the valve would stay in a closed position.

The specially constructed gate valve (Fig. 2) which was used to start and stop the heated flow from the compression tube to the test section was initiated with precise tuning at a threshold point of the rising pressure in the tube using a pressure transducer timing unit and a perspex tube, propping a piston acted on by compressed air, which is disintegrated by a detonator in the same way as described in reference 2. The gate-valve itself was slightly wedge shaped to allow good setting when the valve was closed but small friction during the valve opening. Despite the high accelerations imposed upon the valve and its mechanisms during the opening time of around 40 milliseconds, it has withstood over a thousand tests without damage.

The piston is designed to a minimum weight consistent with its structural integrity to withstand the striking of the downstream wall of the tube at the end of the test and the rigidity to slide freely down the tube. The piston skirt is constructed of rolled aluminium sheet with aluminium stiffening annula at both ends which also acts as guides for impregnated nylon bands used as piston ring seals. To the front annulus is attached an aluminium honeycomb sheet. The final weight was 27 kg. Because of the finite weight of the piston, low frequency fluctuations in pressure are created due to the oscillation of the piston after its rapid acceleration on gate valve opening. So far no compensator mechanism, as has been described in reference 2, has been fitted to alleviate the effects of piston oscillation, since it has been found in practice that their presence, although making data reduction difficult, for the tests carried out so far, have been of such low oscillation and amplitude that the flow can be considered quasi steady. Furthermore, the instrumentation has closely followed their variations. The problem becomes more evident at low pressure operating conditions.

Cascades of blades with a vertical height of 250 mm and a span of 100 mm can be fitted into the test section (Fig. 3) which itself is capable of withstanding pressures up to 7 bars. The upper and lower walls can be adjusted vertically through screw jacks to allow simple fitting of cascade models with smaller vertical height. To allow simple model installation and easy model access, the whole of one side of the test section acts as a door held on vertical hinges. Instrumentation and the leads from the instrumentation are usually fixed in or taken out of the opposite fixed wall. On each side of the test section two large circular ports are positioned encompassing the region of the cascade models. For channel flow studies, a special insert can be placed within these ports and is designed in such a way that access can be obtained to horizontal test surfaces. The flow downstream of the test section is dumped in a tank of approximately 5 m³ located below the test section.

For film cooling tests, four independent coolant injection systems are available which can deliver gas at constant chosen plenum chamber pressures. Two of the systems can deliver gas at temperatures approximately 40° above and below ambient temperature. Standard gas bottles, filled from the 40 bar compressed air supply, are used to provide a constant pressure supply at typical flow rates over a period of 1 second. Solenoid valves, operated to open at a pre-set time before a test, are used to initiate the coolant flow. Flow rate is calculated using appropriate critical flow formulae from the pressure and temperature measured upstream of a round edged orifice of known effective area which is ensured to be choked during the test period and placed as close as possible to the coolant plenum chamber. Coolant flow temperature is changed by passing the gas through regenerative heat exchangers constructed of 25 mm pipe of 250 mm length filled with discs of fine brass gauze, which have initially been heated or cooled by passing air through copper spiral coils immersed in a bath of heated oil or alcohol and solid carbon dioxide. More details of the system are given in reference 3.

Because of the dangers of handling large air flow rates at high pressures in limited volume pressure vessels of different structural integrity,a number of safety systems were built into the system, the ultimate of which were safety diaphragms on each pressure vessel. Before these would operate (breaking of these diaphragms could cause the loss of the complete Institute compressed air supply, thus interrupting the operation of other wind tunnels and services) other safety features were incorporated including pressostats which would closed down the main valve and the gate valve on achieving a preset pressure, and time delays which would likewise act after a selected period. Operation of the tunnel was only possible if all the valves were set in their correct positions and a panel light indicated when the tunnel was in this correct firing mode. The tunnel was operated by

means of a push button, however, another button sited distantly had to be pressed to arm the detonator, to prevent accidental firings. The tunnel operation would immediately stop and pressurized parts of the tunnel bled to atmosphere if the fire buttons were released. Furthermore, the tube pressure was visually monitored by a bourdon gauge to keep track of progress of the compression cycle.

The tunnel control system was designed at the outset to synchronise events including operation of the tunnel, the safety devices mentioned above, coolant flow injection, recording instrumentation, etc. On pressing the fire button the main valve opens and timers are started to operate appropriately a U.V. recorder and the automatic shutting down of the main valve after the test if this safety feature needed bringing into action. The output from a pressure transducer (processed so as to not exceed 1 volt) is connected to the control system and three triggers were operated when the voltage achieves respectively three threshold valves which can be pre-set by means of potentiometers. These triggers themselves operated the detonator and coolant injection but also delayed triggers operating oscilloscopes, a data acquisition system, schlieren spark, main valve shutdown and tube and tunnel venting, compensator for coolant system and compensator to reduce piston oscillation.

2.3 Instrumentation

The tube pressure is measured with a Validyne type DP15TL variable reluctance differential transducer, which gave the stability and accuracy to provide a reliable input into the control system of the tunnel. These and inexpensive National Semiconductor differential transducers with built-in integrated circuit amplifiers were used to measure model, coolant plenum chamber and flow measurement pressures. A resistance linear transducer of 100 mm travel was used to monitor the opening motion of the gate valve.

Heat transfer rates are measured using standard thin film platinum resistance thermometers brush painted on pyrex, quartz or Macor mashinable ceramic. These thermometers are used in conjunction with appropriately designed analogue circuits to give outputs directly proportional to heat transfer rate.

Main stream flow temperatures are measured using fine tungsten wires (5-10 μm) as equilibrium temperature probes. The temperature is assessed from the change in resistivity of the wire during the test, and this value is corrected for conduction end losses to the wire supports, and radiation losses (Ref. 4). Response times of less than 1 msec are achieved and because of this the technique has a great advantage over others in that any subtle disturbances away from that expected can easily be detected.

Coolant flow temperatures in the plenum chamber and before the calibrated orifices were measured using 20 μm chromel-alumel thermocouples with cold junctions immersed in a bath of melting ice.

External turbulence could be generated by a grid of parallel horizontal bars in the test section (Fig. 3). The bars have a diameter of 3 mm and are 9 mm apart giving a solidity of 0.33, these values had been chosen using classical correlations available in the literature. With such a grid, different turbulent intensities may be generated by placing it at different streamwise positions upstream of the test section. The turbulence intensity was measured using a VKI manufactured constant temperature anemometer with a frequency response up to 15 kHz and recorded on the VKI fast on-line data acquisition system. The probe consisted of a 9 μm diameter tungsten wire with an active length of 1 mm. At a Mach number of 0.2 and total temperature of 430 K, which enabled satisfactory overheat ratios to be obtained, the signals were analyzed using 2500 data points over a test period of 100 msecs (i.e., sampling rate of 25 kHz). Temperature fluctuations, evaluated by varying the overheat ratio, were found to be of the order of 0.2%. Analysis of the velocity fluctuations showed that without the grid, the turbulence level was found to be between 0.9% and 1.2%. Depending in the position of the grid, turbulence levels from 2% to 5.9% were measured at the normal model leading edge position.

Early in the use of the tunnel signals were recorded using 12 channels on oscilloscopes singly triggered with the trace recorded on polaroid film, and 12 channels on UV oscillographs with speeds up to 256 cm/sec. Galvanometers with response times up to 5 kHz are available and sufficient for most purposes. The initiation of the operation of these instruments is carried out by the control system as described earlier.

More recently, the recording capability has been enhanced through the use of the Institute's 16 channel 50 kHz on-line data acquisition system. The system, developed within the Institute's electronics department is based around a Datel a-to-d converter with a 16 channel multiplexer. Signals are conditioned to have values between ±2.5 V and filtered to a frequency less than a third of the sampling rate. Sample-and-hold devices are used to synchronize the signals. The output from the converter, a 12 bit parallel word is serialized to allow transmission through a single cable to a centralized PDP11/34 computer. Here the signal is de-serialized and the signal passed to the main computer core memory through a direct memory access module. The system was built to be adaptable to a number of different facilities. For tunnel CT2, software was developed to cope with the particular data reduction problems required for this system. Generally, the extra sixteen channels provided by the data acquisition system were used to record the signal from the tube pressure, the linear transducer fixed to the gate valve (used for synchronization) and fourteen heat transfer measurements, although in some experiments, pressures were monitored at the expense of heat transfer measurements.

The data analysis procedure allowed initially a quick look at the raw data on a graphical display (particular traces could be recorded on a digital X-Y plotter). If the data was found to be acceptable then the raw data was transferred to a floppy disc. Before each run, a run data sheet was entered into the disc. This was achieved by firstly displaying a previous run sheet on a visual display unit, and updating appropriate quantities. Calibration information, of which the Heat transfer analogues and amplifiers is carried out on the data acquisition system itself, such as voltage across a gauge, transducer calibration, etc., are entered on a calibration sheet. Appropriate data reduction programs were then developed to analyze the data, and presented it in a printed or plotted form.

Recently developed and ready for entering service is a data acquisition system designed specifically for industrially oriented work involving 48 channels at higher data rates and parallel transmission of data (providing a simplification to the serialized system). Signal conditioning involves a completely new system of 24 amplifiers, bridges and analogues to process thin film platinum heat transfer signals and further amplifiers enabling signals from pressure transducers, thermocouples, cold wire temperature sensors, hot wire equipment, etc., thus enabling a fully on-line data acquisition system to be available to cope with the complicated tests from requests from industrial organizations.

3. REVIEW OF SOME EXPERIMENTS

A variety of experiments have been carried out in the short duration hot cascade tunnel, covering over 1200 tests to date, initially of a fundamental nature on channel flows to build up a picture of the separate parameters affecting the heat transfer to turbine blades, and to developing the most suitable method for generating film cooling effectiveness data in short duration facilities. The work has proceeded on to measurement of heat transfer rate on high flow turning rotor blades, and on end walls of inlet guide vanes. This work has provided the background experience necessary to tackle the extensive project work of a configurational, hence proprietary, nature of film cooling of end walls with strong secondary flows carried out but not reported in this paper. Three areas of research have been selected for further description as follows.

3.1 Flat plate heat transfer

This study was initiated to provide experimental heat transfer data obtained under well controlled and measured conditions simulating parameters encountered in a real machine (Reynolds number, wall-to-recovery temperature ratio, turbulence intensity). The effects of strong favourable pressure gradient and different external turbulence intensities were studied; consequently, a simple flat plate model was used (Fig. 5). Results of various prediction methods could then be compared with the experimental data. The results in full are given in reference 5.

For M = 0.20 and 0.28, laminar heat transfer measurements in zero pressure gradient agreed well with the reference temperature of Eckert. Transition was found to advance from Re = 250,000 at 1% turbulence level to 100,000 at 3.6% turbulence in agreement with usual correlations. At $Re_x = 5 \cdot 10^5$, a change in turbulence level from 1% to 6% caused an increase of 60% in heat transfer which could not be ascribed to transition. After transition it is found that free stream turbulence has little effect on heat transfer rate and that good agreement was found with the semi-empirical theory of Spalding and Chi.

To create a pressure gradient, the upper uninstrumented wall was contoured to provide a strongly accelerated boundary layer typical of the aft part of the pressure surface of a turbine blade. Heat transfer in laminar flow achieved by operating at low tunnel pressures was found to be increased by turbulence up to 3.6%, without any evidence of transition, which was assumed to be held off by the pressure gradient (Fig. 6). Agreement with a numerical solution developed using the Spalding-Patankar scheme gave good agreement with the experimental results. At 6% turbulence, transition was however caused, but the trends indicated that laminarization set in when the pressure gradient parameter $K = \frac{\nu}{\rho u^2} \frac{du}{dx}$ achieves a value of 2×10^{-6}.

For the turbulent boundary layer in a favourable pressure gradient, it was again found that free stream turbulence had little effect on the heat transfer rate (Fig. 7). Fortuitiously, it is found that Spalding & Chi (a zero pressure gradient theory) provides good agreement with the measurements if applied segmentally. Integral solutions by Gauntner and Sucec (Ref. 6) and finite difference methods such as the one equation Bradshaw et al. method (Ref. 7) and a mixing length program based on the Spalding-Patankar (Ref. 8) numerical procedure failed to give good agreement with the experiments. It is evident that more sophisticated modeling, for example the k-ε model, should be used.

3.2 Heat transfer on the end wall of a cascade

The cascade used in this study (described in more detail in reference 9) was based on the hub section of a blade designed by NASA (Ref. 10) for a high temperature design. The cascade geometry was as follows : 60 mm chord; 43.5 mm pitch; -42.5° stagger angle; 100 and 90 mm blade height; and 0° inlet air angle. There were 6 blades giving 5 passages (Fig. 3). Heat transfer measurements were taken on one end wall with the help of thin film platinum resistance sensors. To provide densely spaced measurements, gauges (on the polished ends of 3.2 mm in diameter quartz rods) were fixed on circular discs of perspex which were inserted in the end wall and could be rotated. Pressure measurements were made on the sidewall upstream and downstream of the cascade. A turbulence grid, similar to that described in the previous study was available to alter the level of turbulence at the cascade inlet. The boundary layer at the inlet of the cascade could be changed by the use of a boundary layer suction slot located 100mm upstream of the blade leading edge. In both configurations the state of the boundary layer at the entry to the blades is turbulent.

The flow total pressure and the temperature during the test was 1.83 bars, and 390 K. The static pressure at the inlet of the cascade was 1.76 bars giving a local Mach number of 0.24. The downstream static pressure was 1.14 bars corresponding to an exit Mach number equal to 0.85. The corresponding Reynolds number, based on the chord, upstream and downstream of the blade row, were 0.40×10^6 and 1.08×10^6 respectively. The test time was 850 msecs, shutter opening time 20 msecs and the flow was completely established after 40 msecs.

The results of oil flow visualization, created by placing oil dots on the surface of the end wall illustrated that flow periodicity was achieved and demonstrated the extent of the cross flow of the surface streamlines caused by the transverse pressure gradient between the walls.

More than 120 heat transfer measurements were recorded during each of the test series. From these measurements, constant heat transfer lines were drawn. An example of the heat transfer distribution is shown in figure 8. It is found that a low region of heat trans-

fer is found upstream and between the blades, reflecting the region in which the lowest speed flow is found combined with the thickest, relatively undisturbed side wall boundary layer. Low heat transfer rates are also encompassed at around 15% chord directly upstream of the leading edge corresponding with the separation points of the upstream boundary layer, which is the origin of the leading edge vortex. The high heating downstream of the leading edge on the suction side can be attributed to the rapid increase in Mach number in this region.

In the passage the heat transfer rate increased as expected due to the increasing Mach number. At about 1/3 of the chord, there commence large pitchwise heat transfer rates which can be attributed to secondary flows. The primary effect of the secondary flow behaviour is for the low energy and low temperature flow adjacent to the surface to be swept away exposing the surface to the higher energy flow resulting in enhanced rates near the pressure surface.

The region of low heating rate adjacent to the downstream suction surface coincides with the accumulation and subsequent separation due to the presence of the blade, of this low energy fluid.

The changes in heat transfer rate due to decreasing the size of the inlet boundary layer is to provide an approximately uniform increase of the heat transfer rate without altering the shape of the distribution of the iso-heat-transfer lines. The effect of turbulence seems to be minimal, as may have been expected from the flat plate tests, since the incoming boundary layer was fully turbulent. Only a small region (about 3-4 measurement points) near the pressure side was affected in that the heat transfer was decreased by 20-30% by the introduction of turbulence.

Attempts to develop prediction methods based on one or two dimensional approaches provided only ±50% agreement with the experiments, indications that three dimensional Navier-Stokes solutions should be sought.

3.3 Film cooling of flat plates

Film cooling has been used and is increasingly being applied for cooling various critical components, such as the combustion chamber walls, inlet guide vanes and first row rotor blades to the core turbine. Short duration techniques have the ability to provide useful heat transfer data inexpensively and under well controlled conditions. Nevertheless, the type of data obtained has been criticized when it is presented simply in the form called the isothermal effectiveness

$$\eta_q = 1 - \frac{q_f}{q_0} \qquad (1)$$

where q_f and q_0 are the heat transfer rates with and without the film.
This presentation gives no information related to the distortion of the boundary layer by the film, usually created by injection through inclined holes, which would tend to decrease the effectiveness compared to the hypothetical case of a perfectly applied film which would cause no modification to the boundary layer. From more traditional experimental methods used in the past, designers have used the adiabatic wall effectiveness

$$\eta_{ad} = \frac{T_{rm}-T_{aw}}{T_{rm}-T_{rc}} \qquad (2)$$

where T_{rm} and T_{rc} are the main stream and coolant recovery temperature and T_{aw} is the adiabatic wall temperature of the cooled layer, i.e., the temperature the wall would achieve if the flow was continued for an infinite time. This information would provide the adiabatic wall temperature which could provide the heat transfer through the equation

$$q_f = h_f (T_{aw}-T_w) \qquad (3)$$

where h_f is the film heat transfer coefficient and T_w the wall temperature. In the past frequently h_f has erroneously been equated to the heat transfer coefficient h_0 from the equation

$$q_0 = h_0 (T_{rm}-T_w) \qquad (4)$$

which gives the heat transfer, q_0, without film cooling, whereas in reality, due to the distortion of the boundary layer, especially close to the film injection, $h_0 \neq h_f$. The criticism of the adiabatic wall approach is that since internal convection of blades is used, the blade wall temperature more closely resembles isothermal than adiabatic conditions in practice.

By changing wall conditions or coolant conditions in sequential tests, short duration tunnels can provide in theory data which can resolve this dilemna by presenting the heat transfer data as a heat transfer coefficient, h, defined as

$$q_f = h (T_{rm}-T_w) \qquad (5)$$

which has been obtained at different values of wall or coolant temperatures defined by the non dimensional coolant temperature parameter :

$$\theta = \frac{T_{rm}-T_{rc}}{T_{rm}-T_w} \qquad (6)$$

From plots of the h/h_f vs θ data, the use of the relation developed from equations 2, 3, 5 and 6 suggests a linear variation of h with θ :

$\eta = \eta_f (1 - \tau_{ad})$

which experimentally can provide assessments of η_f and τ_{ad} by suitable extrapolation of the data to $m = 0$ and $m = \infty$ respectively illustrated in figure 9.

Careful experiments (described in reference 3) were carried out to ascertain the linearity and uniqueness of equation 6 by changing both the coolant and wall temperatures also determining the degree of difference between η_f and η_{ad}, valuable in assessing the distortion of the boundary layer by the film and hence its effect on the heat transfer rate.

The experiments were carried out at a total pressure of 3.0 bars, a total temperature of 387 K and a Mach number of 0.64 giving a unit Reynolds number of $2.75 \cdot 10^{7}$ per meter. The coolant temperature was varied from 250-365 K and the wall temperature from 2[illegible]-386 K. Three relative coolant mass flow rate, m, used was 0.63, 0.95 and 1.45%.

The coolant was injected through two rows of holes of 0.5 mm diameter, 1.5 mm apart with a spanwise spacing of 1.0 mm at an injection angle of 30°. The injection hole was 4 mm in length and the total number of holes was 150.

By plotting values of η/η_∞ against m for tests performed at 4 wall and 4 coolant temperatures, various mass injection rates, various selected positions downstream of injection (even for "lift off" conditions at large m and for gauges close to the coolant injection) the reliability of equation 7 in representing film cooling was demonstrated (Fig. 10). A straight line can be drawn through points and extrapolated to $m = 0$ to give h_f/h_∞ and interpolated or extrapolated to obtain $\eta_\infty = 1/\tau_{ad}$. Most of the results generated lay on straight lines within the small normal experimental error. This confirms the reliability of equation 7 and proves that there is no significant influence of the wall or coolant temperature on the final values of h_f and τ_{ad} assessed by this method. Both methods involving a variation of coolant temperature or of wall temperature lead to the same results so that any of these can be used.

Figures 11 and 12 present the variations of τ_{ad} and h_f/h_∞ thus calculated as a function of distance from injection in hole diameters. Effectiveness is shown generally to decrease with decreasing and increasing distance from injection, except for the highest injection case near the slot when the relatively low injection rate demonstrates lift off. The departure of a film cooled layer from the undisturbed boundary layer is assessed from the deviation of h_f/h_∞ from unity. It can be seen that close to the slot h_f/h_∞ can rise considerably above 1 near the slot indicating the high mixing characteristic of the boundary layer in this region. At large distances from the slot h_f/h_∞ asymptotes to values below unity, indicating that the flow is reverting to a boundary layer behaviour, but in a thickened state. It is interesting to note that the highest value of h_f/h_∞ achieved was 2.6, a very large deviation from the assumption often used and mentioned earlier that $h_f = h_\infty$ in a film cooled layer.

These latter experiments thus provide results of fundamental usefulness, and justify the use of short duration tunnels in providing useful film cooling data for the more complicated configurations required by designers.

4. CONCLUSIONS

A short duration hot cascade tunnel using the isentropic light piston tunnel has been designed and built to supplement the ambient temperature compressible cascade tunnels at VKI, to extend work on turbine flows to heat transfer studies. The design contraints, construction and features of the tunnel, its operation and instrumentation, are described Examples of experimental work to date, including heat transfer caused by two and three dimensional flows and results of film cooling measurements have demonstrated its ability to generate accurate and useful data at representative turbine conditions. The tunnel provides, and has provided, a useful capability for industry for testing film cooling configurations.

REFERENCES

1. SCHULTZ, D.L.; JONES, T.V.; OLDFIELD, M.L.G.; DANIELS, L.C.: A new transient facility for the measurement of heat transfer rates. AGARD CP 229 "Heat Transfer Problems in Gas Turbine Engines"; Paper 31, 1977.
2. JONES, T.V.; SCHULTZ, D.L.; HENDLEY, A.D.: On the flow in an isentropic free piston tunnel. ARC R&M 3731, January 1973.
3. VILLE, J-P.; CUNAT, D.; RICHARDS, B.E.: The measurement of film cooling effectiveness in short duration wind tunnel. VKI TN 127, December 1978.
4. BACKX, E.: The total temperature in the Longshot wind tunnel, its measurement and evaluation. VKI TN 98, Paril 1974.
5. CONSIGNY, H.; CHAN, C.K.; RICHARDS, B.E.: The effect of pressure gradient and external turbulence on heat transfer to a cold flat plate. VKI TN 128, February 1979.
6. GAUNTNER, D.J. & SUCEC, J.: Method for calculating convective heat transfer coefficients over turbine vane surfaces. NASA TP 1134, January 1978.
7. BRADSHAW, P. & UNSWORTH, K.: An improved Fortran program for the Bradshaw-Ferriss-Atwell method of calculating turbulent shear layers. Imperial Coll. Aero R 74-02, February 1974.
8. PATANKAR, S.V. & SPALDING, D.B.: Heat and mass transfer in boundary layers. Intertext Books, London, 1970.
9. GEORGIOU, D.P.; GODARD, M.; RICHARDS, B.E.: Experimental study of the iso-heat-transfer rates on the end wall of a cascade. ASME P 79 GT 20, March 1979.
10. WITNEY, W.J. et al.: Cold air investigation of a turbine for a high temperature engine application; Part 1. NASA TN D 3751, 1967.

ACKNOWLEDGEMENTS

The development of the tunnel was supported by VKI, encouragement being given by Professors Ginoux, Chauvin and Wendt.
The tunnel would not have developed without the assistance and interest of a number of graduate students (particularly C. Appels, J-P. Ville, and H. Consigny) and Professor C. Sieverding, the VKI design office, the electronics department, the workshops and F. Vandenbroeck, mechanic under the guidance of R. Conniasselle, technical engineer. Useful discussions were held with the Oxford University group under Dr D. Schultz.

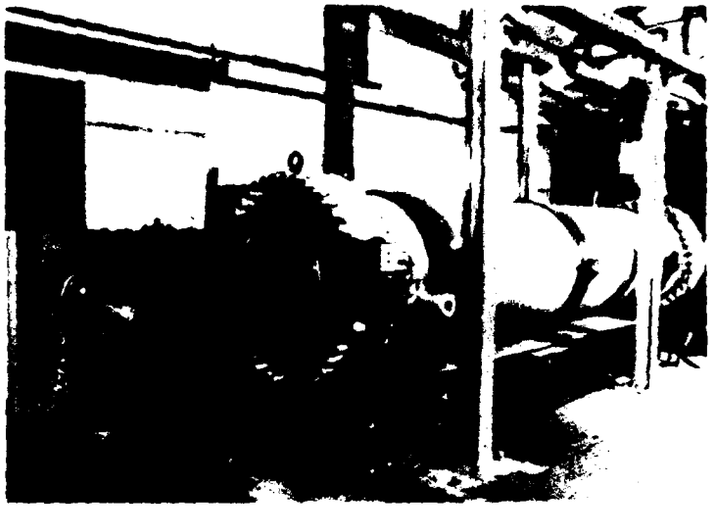

FIG. 1 - PHOTOGRAPH OF TUNNEL CT2

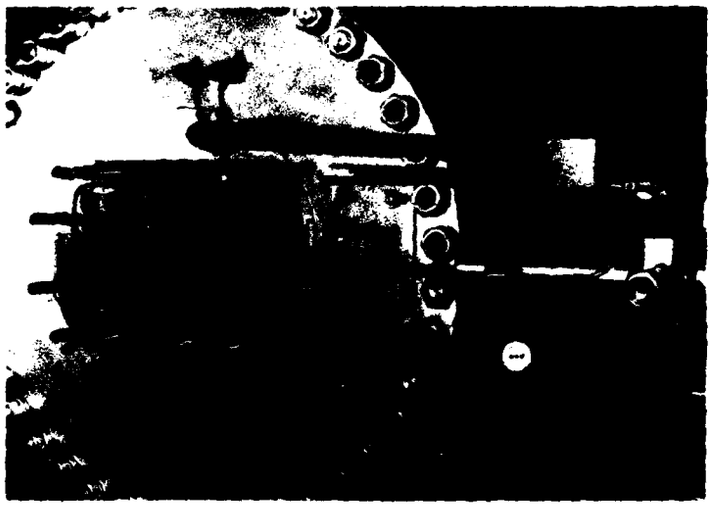

FIG. 2 - PHOTOGRAPH OF GATE VALVE

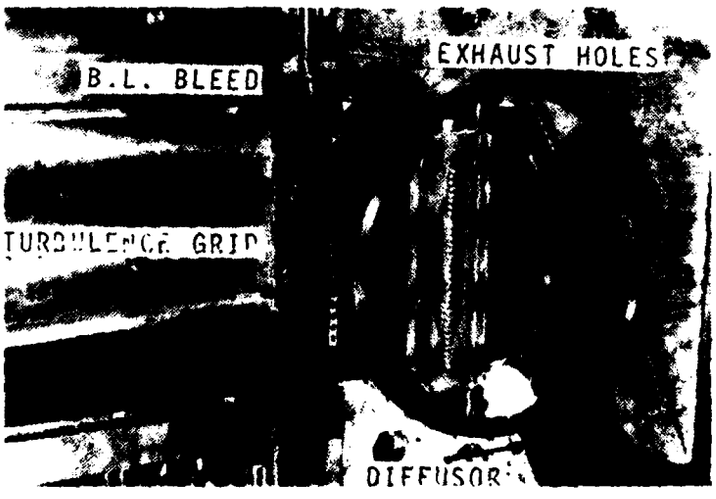

FIG. 3 - PHOTOGRAPH OF CASCADE OF BLADES

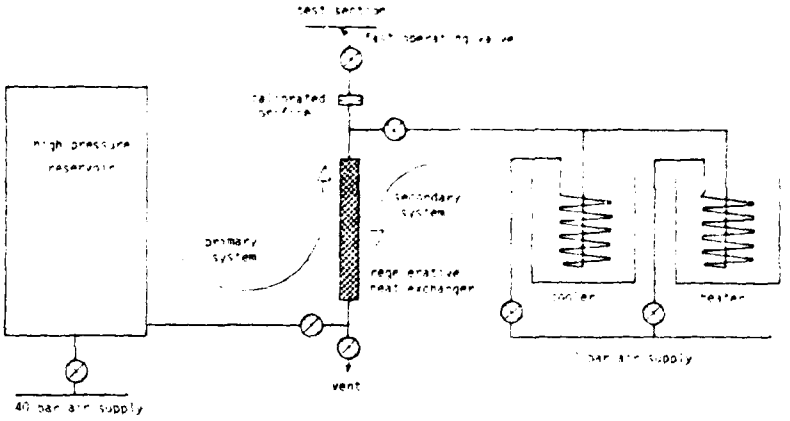

FIG. 4 - SCHEMATIC OF SECONDARY GAS AIR SUPPLY

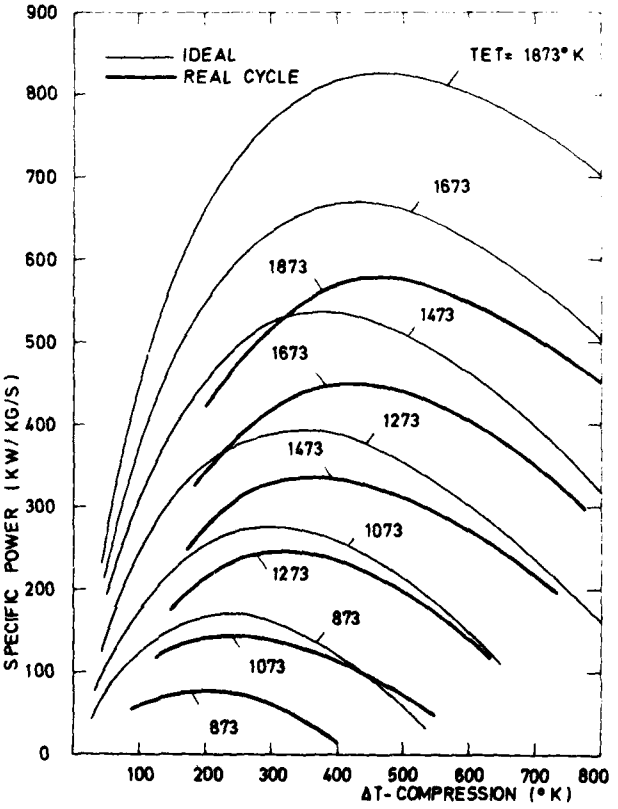

FIG. 5 - CHANNEL FLOW MODEL

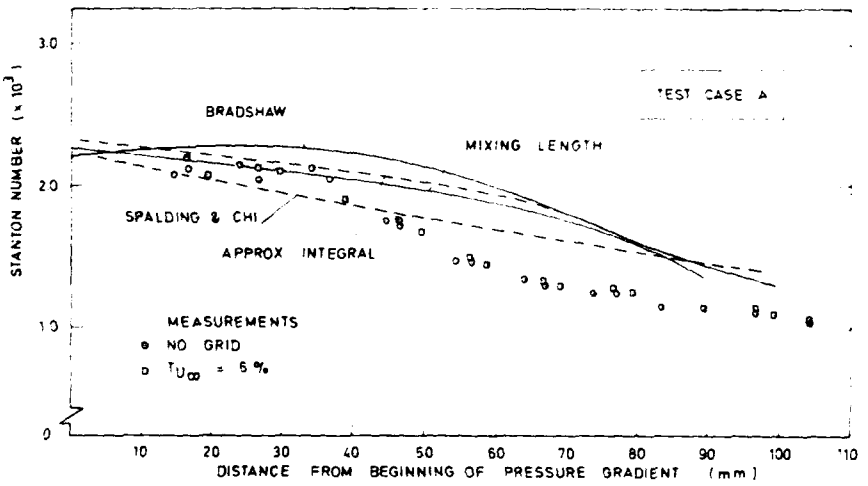

FIG 7 - INFLUENCE OF TURBULENCE AND PRESSURE GRADIENT ON HEAT TRANSFER IN A TURBULENT BOUNDARY LAYER

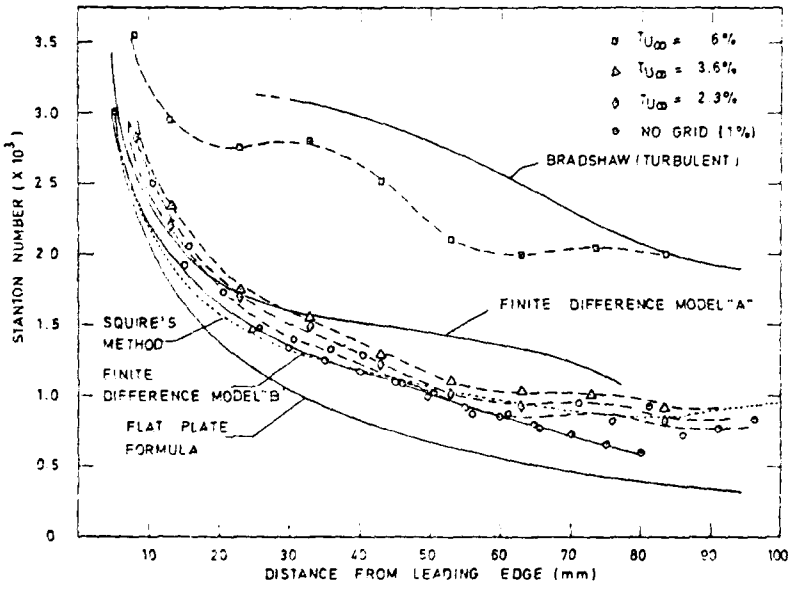

FIG 6 - INFLUENCE OF TURBULENCE AND PRESSURE GRADIENT ON HEAT TRANSFER IN A LAMINAR BOUNDARY LAYER.

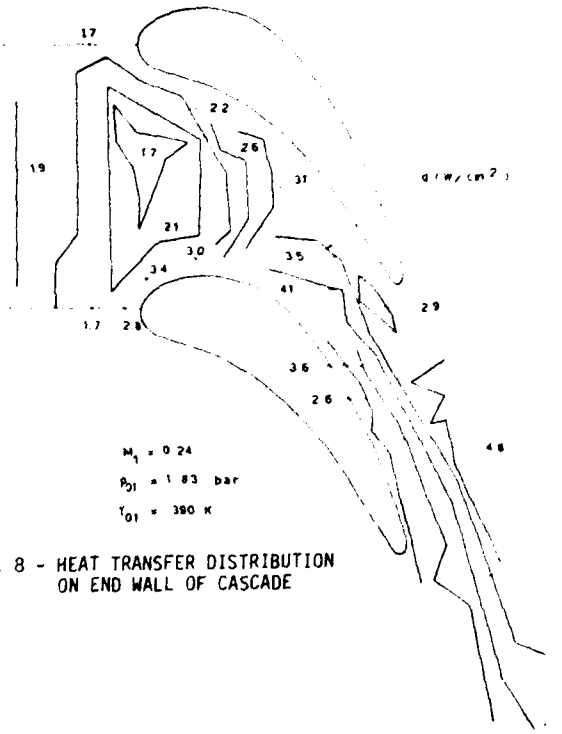

FIG. 8 - HEAT TRANSFER DISTRIBUTION ON END WALL OF CASCADE

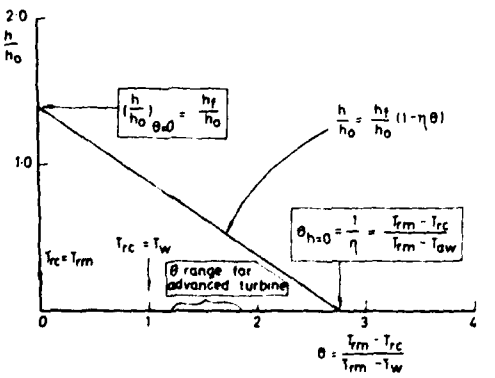

FIG. 9 VARIATION OF HEAT TRANSFER COEFFICIENT, h WITH THE COOLANT TEMPERATURE PARAMETER, θ FOR GIVEN EXTERNAL FLOW CONDITION, x, m AND HOLE GEOMETRY

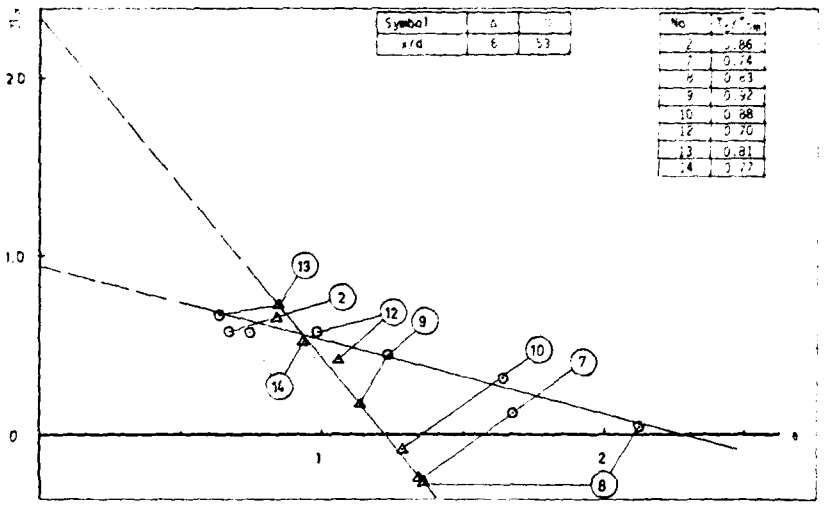

FIG. 10 - REDUCED HEAT TRANSFER COEFFICIENT VS TEMPERATURE PARAMETER θ_1, m = 1.4

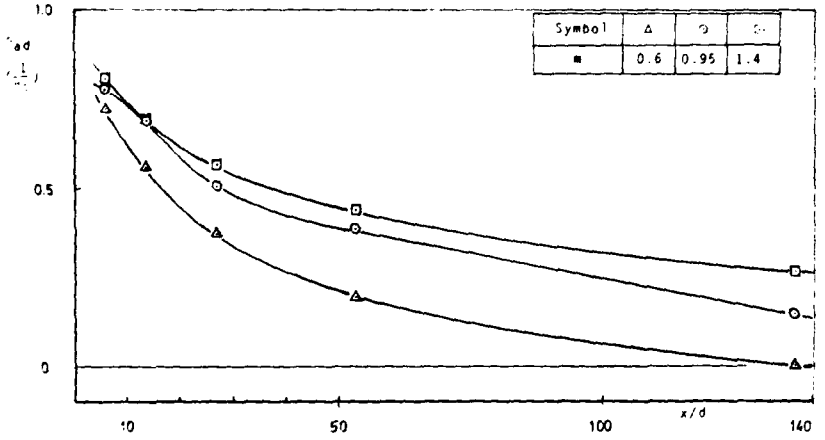

FIG. 11 - ADIABATIC WALL EFFECTIVENESS ON A FILM COOLED FLAT PLATE

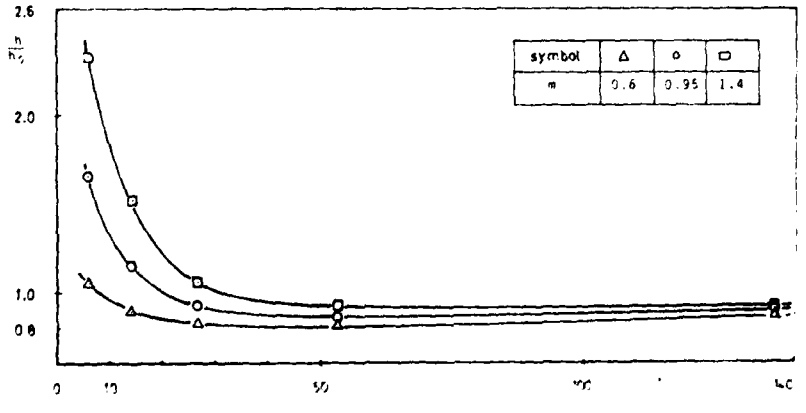

DISCUSSION

G.Winterfeld, Ge

One of the problems with measurements in cascades with a finite number of blades is to achieve a periodic flow Could you, please, comment on how to verify this condition in a short-duration blow-down facility?

Author's Reply

Periodicity was verified in a number of ways. Pressure distributions on the end walls downstream of the blade rows were measured over the central three passages. Oil visualisation and Schlieren observation of the same regions were also used to this end. From six to eight blades, giving five to seven passages, have been used to achieve as closely as possible flow periodicity. To justify the use of transient facilities for cascade testing, the same model has been tested in both a blow-down ambient temperature cascade (VKI tunnel C3) and the transient tunnel. Identical results in side wall pressures downstream of the blade row were obtained, in both cases demonstrating flow periodicity.

D.K.Hennecke, Ge

I feel somewhat uneasy about simulating high levels of free stream turbulence intensity and structure in a short duration test facility. How have you convinced yourself that your tests are representative?

Author's Reply

These are short duration measurements but nevertheless they are measurements taken in times of the order of one tenth to one half a second, when generally we feel that the flow fields that are set up can be considered to be virtually quasi-steady. I think that's as far as we have gone as regards the thinking on the effects of turbulence.

HEAT TRANSFER RATE AND FILM COOLING EFFECTIVENESS MEASUREMENTS IN A TRANSIENT CASCADE.

D. L. Schultz, M. L. G. Oldfield and T. V. Jones
Department of Engineering Science,
University of Oxford, Parks Road,
Oxford, OX1 3PJ.

Summary: A transient cascade especially useful for heat transfer rate measurements is briefly described. The facility employs a free piston which compresses the test gas to temperatures around 450 K and pressures of about 3.5 - 7.5 Atm. The model is initially at room temperature and it is necessary to attain the correct gas-to-wall temperature ratio. The exit Mach number is set by the inlet total pressure and the pressure in the exit dump tank. Thin film heat transfer gauges are used for the measurement of heat transfer rate, deposited on machineable glass ceramic blades. The inherently fast response of these transducers makes them useful for the investigation of boundary layer transition on blade surfaces and some typical results are included.

Introduction: A new type of transient cascade has been developed at Oxford which has substantially improved knowledge of the distribution of heat transfer rates over turbine blading. The cascade has been described in detail at a previous AGARD conference (1) but a very brief review of the principles is included here for completeness. The main features are illustrated in Fig. 1 where it will be seen that it comprises a pump tube in which a free piston is driven by a bank of high pressure cylinders normally at 130 Atm. The test gas ahead of the piston is compressed in about 0.75 seconds, depending on operating conditions, until the desired total pressure and hence temperature are attained. The total pressure is measured by a fast response pressure transducer whose output triggers the gate valve, Fig. 2. This valve opens in approximately 0.03 secs. and the compressed and heated test gas passes over the cascade into the dump tank. If the volumetric flow rate at throat conditions $(\rho^*a^*A^*)_b$ is made equal to that from the high pressure reservoir through a throat located between the reservoir and pump tube $(\rho^*a^*A^*)_r$ then the total pressure ahead of the piston will be maintained constant until the piston reaches the end of the pump tube. The flow duration thus depends on the blade throat area and total pressure (hence total temperature) for a given pump tube volume. For typical cascade throat areas the flow duration in the OUEL cascade varies between 0.3 and 0.5 secs. at total temperatures around 450 K. A more detailed analysis of the performance of this type of cascade is given in Ref. (2). The finite piston mass, 17 kg in the present cascade, would result in oscillations in total pressure when the gate valve opens but a method of compensating for these by altering the volumetric flow rate has been developed and described in Ref. (1). With 'compensation' in use the total pressure may be maintained constant to within about ± 1% provided the blade throat area, and hence the mass flow rate demanded from the driver cylinders is not too great.

Simulation: It is of course essential to achieve the correct Reynolds and Mach numbers for heat transfer and aerodynamic measurements. In addition it can be shown, Ref. (3), that temperature scaling requires the gas/metal (Tg/Tw) for uncooled and gas/metal/coolant (Tg/Tm/Tc) for cooled blades to be correct. Operation at the correct gas/metal temperature ratio of say 1.5/1 requires a test gas temperature of 430 K if the model is initially at room temperature, 288 K. This low temperature also makes full scale Reynolds number simulation more straightforward because of the rapid change in viscosity with temperature. For example the unit Reynolds number Re/mPa at 1500 K is 22.22 at M = 1.10 and 93.63 at 430 K so that engine operating Reynolds numbers may be correctly simulated by pressures which are only 0.25 of engine full scale. Since in general the geometric scale is also increased in cascade testing by factors around 1.5 to 2.0 for ease of instrumentation it can be seen that the total pressure is reduced to between 0.17 and 0.25 of engine full scale for full scale Reynolds number and temperature ratio simulation. The transient cascade at OUEL is normally operated at total pressures between 3.5 and 7.5 Atm. for full scale Reynolds numbers up to 1.7×10^6 based on true chord and exit Mach number. Changes of exit Mach number are achieved by adjusting the exit pressure set by the dump tank, Fig. 1, although it is necessary to measure the cascade exit pressure at some predetermined location closer to the blades because there are inevitably pressure gradients in the exit duct.

Of the engine conditions which should be simulated the inlet turbulence level and its scale are the most difficult. Detailed knowledge of the characteristics of turbulence at inlet to even first stage guide vanes is very limited and what does exist indicates, Ref. (4), that the turbulence is extremely inhomogeneous with levels varying from 12 to 14 u'/U, with levels up to 18% at blade root and tip caused by the secondary flow. The simulation of such spatial non-uniformities is clearly unprofitable in stationary cascade studies but even the attainment of an homogeneous level approaching 10% has not so far been possible. In the OUEL cascade turbulence levels of approximately 4% can be achieved using conventional upstream bar grids. This has been effective in promoting transition early on the suction surfaces of blades and N.G.V.'s and is acceptable although by no means as high as would be desired. Turbulence levels in the OUEL cascade are measured with a conventional constant temperature hot-wire anemometer operation of the wire

through a range of overheats enables both Re' $\overline{Re}$ and To' $\overline{To}$ to be determined, Ref. (6). The hot wire is of course sensitive to fluctuations in total temperature and in the cascade these have been found to be 0.2% under conditions in which the $\sqrt{(Re')^2}/\overline{Re}$ = u'/U fluctuations were 4.2%. The value of u'/U found from hot wire measurements agreed well with that deduced from the stagnation line heat transfer rate on a circular cylinder in cross flow. The enhancement of heat transfer rate due to free stream turbulence is well documented over a wide range of conditions and serves as a useful check on the hot wire measurements. A second feature of the flow in an engine whose effect should be understood is wake interaction with the passage flow and blade boundary layers. Much more work remains to be done before the effects of this phenomena on boundary layer transition and heat transfer rates is understood. Evans at Cambridge has made a detailed study of wake/boundary layer interaction effects on compressor blading but to date there are no similar results available for turbine blade profiles. A study of this phenomena is now in progress at OUEL.

Instrumentation: The short flow duration of the free piston compressor requires high frequency pressure instrumentation but conventional semiconductor transducers connected to 100 - 150 mm lengths of 1.5 mm bore tubing have proved satisfactory, having time constants less than 0.010 secs. Differential transducers (National Semiconductor LX 1620 D) are generally used with the reference total pressure taken from a larger bore tube on one of the lower blades in the cascade so that differential feed to 10 or more transducers can be made without undue degradation of the frequency response.

One of the most useful features of transient testing is the ease with which heat transfer measurements may be made. The method utilises the measurement of the time dependent variation of surface temperature, which has been fully described in AGARD AG - 165, Ref. (5). Machineable glass ceramic blades (Corning 'MACOR') are machined on a numerically controlled mill, the surface is polished and the thin film sensors, an alloy of platinum and silver, deposited by hand painting 'Hanovia Liquid Bright Platinum 05-X' and firing at 650 C. Several coats are applied to achieve a suitably robust film of low resistance and tab leads of gold to reduce the lead resistance, Fig. 3. The temperature coefficient of resistance must be known and is found by heating the entire blade in a temperature controlled bath.

The linear heat conduction equation

$$\frac{\partial^2 T}{\partial x^2} = \frac{1}{\alpha}\frac{\partial T}{\partial t} \tag{1}$$

may be solved for the heat transfer rate at the surface $\dot{q}_{x=0} = -(k\frac{\partial T}{\partial x})_{x=0}$ giving

$$\dot{q}(s) = \sqrt{\rho c k}\ \sqrt{s}\ T(s) \tag{2}$$

s being the Laplace variable.

In the simplest case of $\dot{q}_{x=0}$ constant the surface temperature becomes

$$T = \frac{2\dot{q}\sqrt{t}}{\sqrt{\pi \rho c k}} \tag{3}$$

If the heat transfer rate is not constant it may be obtained from Eqn. (2) above as shown in Ref. (5),

$$\dot{q}(t) = \sqrt{\frac{\rho c k}{\pi}}\left[\frac{T(t)}{\sqrt{t}} + \frac{1}{2}\int_0^t \frac{T(t) - T(\tau)}{(t-\tau)^{3/2}} d\tau\right] \tag{4}$$

More readily an electrical analogue may be used to convert directly from surface temperature to heat transfer rate. The one-dimensional heat conduction process is directly analogous to the conduction of electric waves in a simple R-C transmission line. The equation for line voltage V in terms of t and RC is

$$\frac{\partial^2 V}{\partial x^2} = RC\frac{\partial V}{\partial t} \tag{5}$$

So that the resistive element R is the analogue of the thermal conductance $1/k$ and the capacitance C the analogue of the heat capacity ρC in the solid. The current into the analogue circuit which corresponds to the heat transfer rate is measured, usually by means of a current-to-voltage converter, Ref. (6), Fig. 4. The increase in blade temperature during the test can reach 50 - 75 C and in order to determine the isothermal heat transfer rate the heat transfer rate and surface temperature are cross plotted as in Fig. 5(b) and extrapolation to $\Delta T_s = 0$ performed by the same computer which acquires and processes other data. The computer installation at OUEL comprises a PDP 11/34 with 32 input channels from blade transducers, either pressure transducers or heat transfer gauges, and cascade transducers monitoring inlet total and exit static pressures. The computer is used to calibrate the pressure transducers on-line by pressurising the entire working section. The calibration data is stored on disc, incorporated in a cascade run-control programme and automatically used to analyse the test data. The test data is then printed out in 2 mins. after the completion of the run and gives the blade pressure or

heat transfer rate distribution or loss coefficient measurement together with all the necessary experimental values of cascade operating conditions. Inlet total temperature is normally calculated from the isentropic compression ratio but this parameter has been measured using a thermocouple and found to agree to within 1% of the predicted value at temperatures up to 450 K.

A further valuable feature of fast response heat transfer gauges is the ability it gives to differentiate between laminar, transitional and turbulent boundary layers. Referring to Fig. 6 a typical laminar heat transfer rate record from a thin film gauge would be the smooth trace in (a). Turbulent spots passing over the gauge cause upward spikes from increased heat transfer rate, (b). In the centre of a transition zone the signals are completely random (c), and in a fully developed turbulent boundary layer the trace shows high frequency fluctuations of an approximately constant magnitude (e). Before the boundary layer is fully turbulent downward spikes towards the laminar transitional regime can be observed (d). This phenomena, used by Schubauer and Klebanoff, Ref. (7), with hot wire anemometers, has been observed on the suction surface of a number of guide vane and rotor profiles and has greatly assisted the identification of boundary layer transition. Similar thin film heat transfer gauges have been used by Oldfield et al., Refs. (8) and (9), to determine the location and extent of transitional flow on a blade in the large continuous flow cascade at DFVLR, Braunschweig. In this case the thin film is maintained at a constant overheat temperature by means of a conventional hot-wire anemometer feedback bridge (DISA). Early work on this thin film technique was done by Bellhouse and Schultz, Ref. (10), and Owen, Ref. (11), using thin film gauges in sub- and supersonic tunnels.

Results: The most useful data from the isentropic free piston compressor is perhaps the heat transfer rate distribution. Such a distribution on a rotor blade is illustrated in Fig. 7(a) and compared there with current predictions. The form and level of the heat transfer rate on the pressure surface is seen to be quite well predicted. On the suction surface all current theoretical methods are less reliable in the transition zone. It can be seen from Fig. 7(a) that the final turbulent heat transfer level on the suction surface is in close agreement with the theoretical value although neither is entirely satisfactory during transition. In these circumstances measurements of high frequency fluctuations in heat transfer rate are helpful in identifying the extent of transition. In this case the ratio of peak-to-peak heat transfer rate to mean is shown in Fig. 7(b) in relation to the mean levels. The bandwidth of the measuring system was limited to about 3 kHz and is therefore much less than optimum but the results reveal the usefulness of the method which has been successfully applied to the identification of transition zones on several blade profiles. A 100 kHz bandwidth analogue system has been developed for further studies using this technique.

A complete heat transfer rate survey on a nozzle guide vane is shown in Fig. 8. The variation in Reynolds number from 0.4 to 0.8 x 10^6/m is sufficient to cause transition on the suction and pressure surface. On the pressure surface an increase in free stream turbulence level from below 1% without an upstream grid to 4% at Re = 0.8 x 10^6/m is sufficient to cause immediate transition again on the pressure surface and does not alter the levels on the suction surface. This evidence suggests that although the 4% u'/U turbulence level which can be achieved is much lower than in the engine environment it is sufficiently high to cause natural transition on blade surfaces. Increase in Reynolds number to 1.2 x 10^6/m affects the overall level of heat transfer rate as would be expected and results in no further alteration in the state of the boundary layer on either pressure or suction surface.

Film cooling studies on the pressure surface of the same profile have been made over a range of coolant flows $\rho_c u_c/\rho_\infty u_\infty$ from 0.5 to 4.0. Typical results shown in Fig. 9 show the effect of low, 0.75, and high, 2.00, coolant flow rates. These results are consistent with those obtained on a flat plate by Smith et al., Ref. (12), who showed that high coolant flow rates can increase the heat transfer rate just downstream of the injection holes. Nevertheless, there is a marked reduction in heat transfer rate far downstream at the higher coolant flow rate. In this experiment the coolant temperature was the same as the blade.

Conclusion: The transient cascade has been shown to be a useful facility for a range of measurements on turbine blading under full scale engine Reynolds, Mach numbers and temperature ratios. Although the free stream turbulence level is limited to about 4% in the OUEL cascade present evidence suggests that it is sufficiently high to cause natural transition near the leading edges of both rotor blades and vanes. The measurement of the fluctuations in heat transfer rate have proved useful in identifying the transition region on the blade surface.

While such short duration techniques cannot replace full scale tests the detail which is obtainable, particularly in heat transfer rate measurements provides a relatively inexpensive check on design methods .

Acknowledgements: The free piston cascade was developed with support from the Science Research Council, Rolls-Royce Aero Division and the Ministry of Defence (Procurement Executive). The authors acknowledge the assistance of the staff of Rolls-Royce Aero Division in the current research programme and express their thanks for permission to publish some of the data presented in this paper.

References:

1. D. L. Schultz, T. V. Jones, M. L. G. Oldfield and L. C. Daniels. A new transient cascade facility for the measurement of heat transfer rates. 1977. AGARD - CP 229.

2. T. V. Jones, D. L. Schultz and A. D. Hendley. On the flow in an isentropic light piston tunnel. 1973. Aero. Res. Council R. and M. No. 3731.

3. R. S. Colladay and P. S. Stepka. Similarity Constraints in Testing of Cooled Engine Parts. NASA TN D-7707.

4. H. J. Schafer, B. Koch and H. J. Pfeifer. Application of LDV Techniques to High Speed Combustion Flows. September 1977. International Congress on Instrumentation in Aerospace Simulation Facilities. Royal Military College of Science, Shrivenham. IEEE 77 CH 1251-8 AES.

5. D. L. Schultz and T. V. Jones. Heat transfer research in short duration hypersonic facilities. 1973. AGARD AG - 165.

6. M. L. G. Oldfield, T. V. Jones and D. L. Schultz. An on-line interactive mini-computer system for heat transfer measurements in a transient turbine cascade. 1978. IEEE Trans. AES - 14. pp. 738 - 749.

7. G. B. Schubauer and P. S. Klebanoff. Contributions on the mechanics of boundary layer transition. 1955. NACA TN 3489.

8. M. L. G. Oldfield, R. Kiock, A. T. Holmes, C. G. Graham. Boundary layer studies on highly loaded cascades using heated thin films and a traversing probe. March 9 - 13. 1980. 25th Annual International Gas Turbine Conference. ASME. New Orleans.

9. M. L. G. Oldfield and R. Kiock. The detection of boundary layer transition on a gas turbine blade by means of a pitot probe and thin film technique. March 22 - 23. 1979. Symposium on Measurements in Transonic and Supersonic Cascade Flow. C.E.G.B. Leatherhead. U.K.

10. B. J. Bellhouse and D. L. Schultz. Determination of mean and dynamic friction, separation and transition in a low speed flow with a thin film heated element. 1966. Journal of Fluid Mechanics. 24. pp. 379 - 400.

11. F. K. Owen. Transition experiments on a flat plate at subsonic and supersonic speeds. 1970. AIAA J. 8. No. 3. pp. 518 - 523.

12. M. R. Smith, T. V. Jones and D. L. Schultz. Film cooling effectiveness from rows of holes under simulated gas turbine conditions. 1973. Aero. Res. Council C.P. No. 1303.

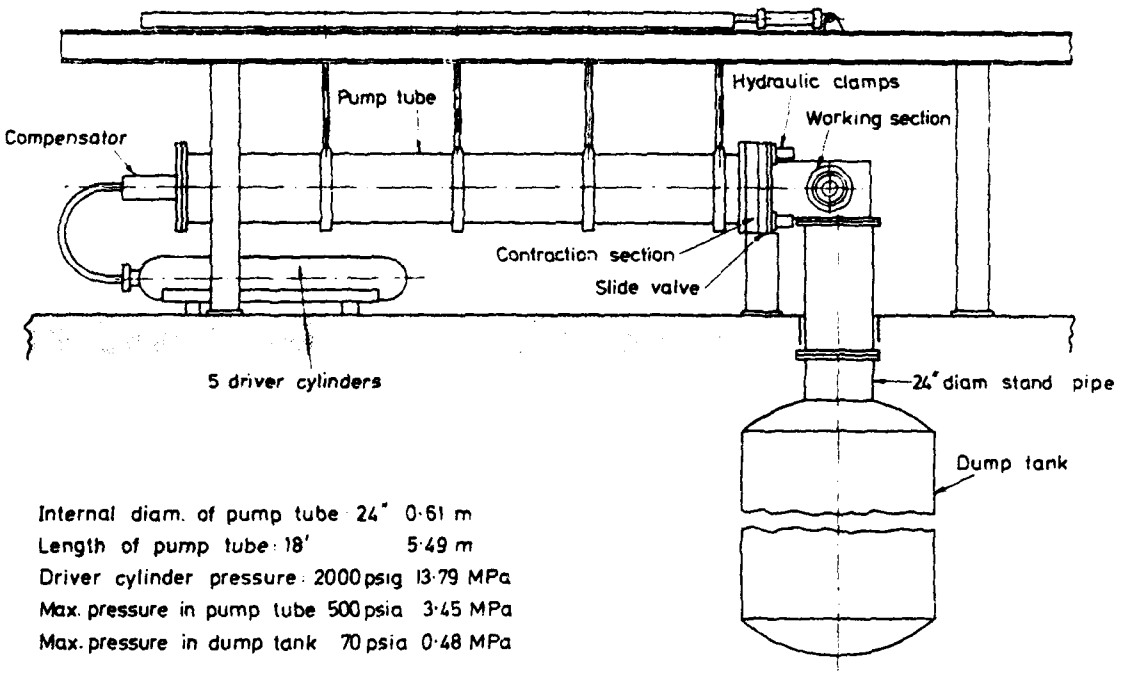

Fig. 1
General arrangement of OUEL transient cascade facility.

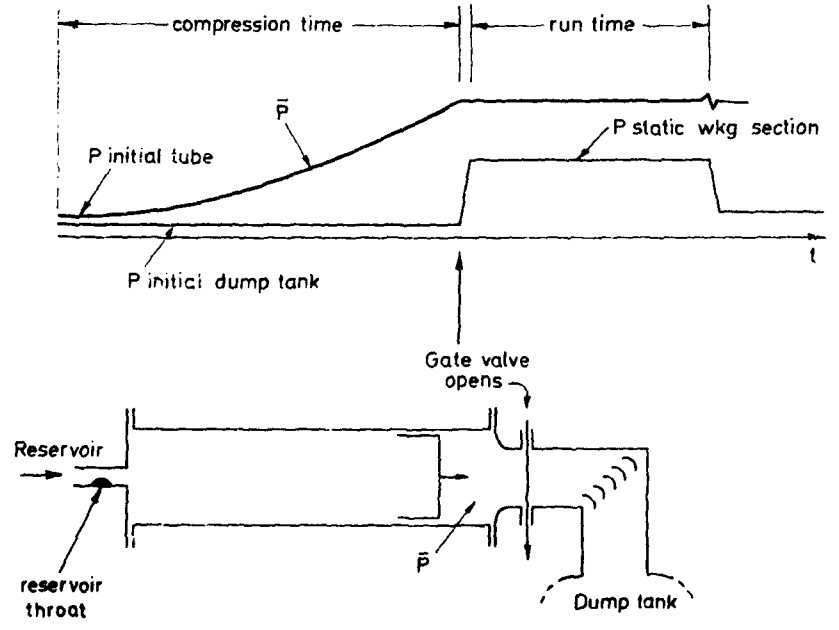

Fig. 2.

Idealised pressure-time history during compression. Gate valve is opened when pressure in pump tube $\bar{P}$ reaches predetermined value

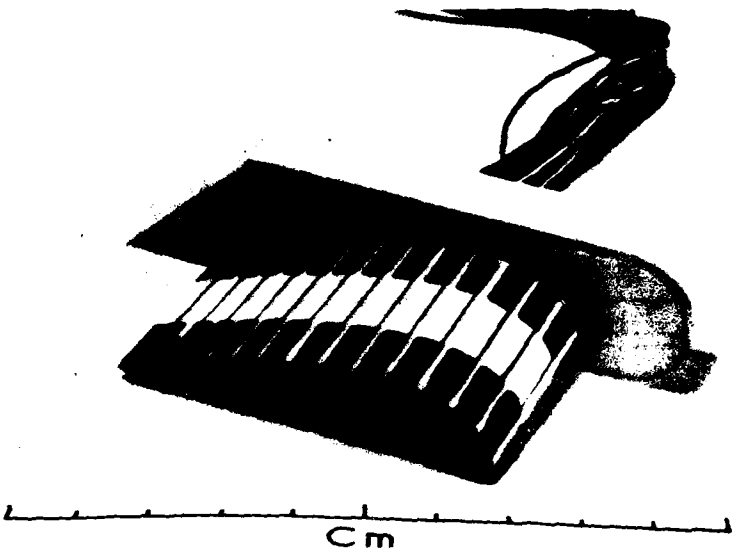

Fig.3.
NGV in machineable glass ceramic.

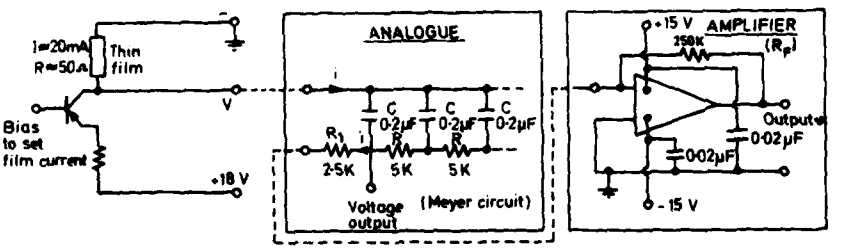

Fig. 4.

Transistor constant current supply for thin film resistance thermometers, analogue circuit and current-to-voltage converter.

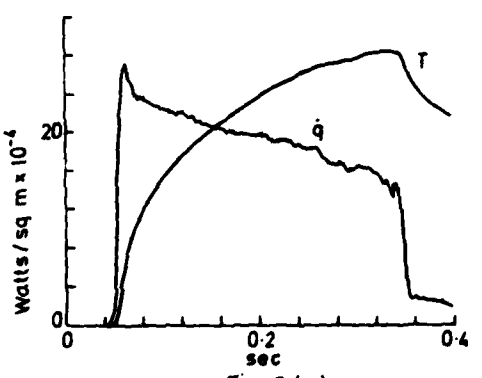

Fig. 5.(a)

Variation of surface temperature T and heat transfer rate $\dot{q}$ during run.

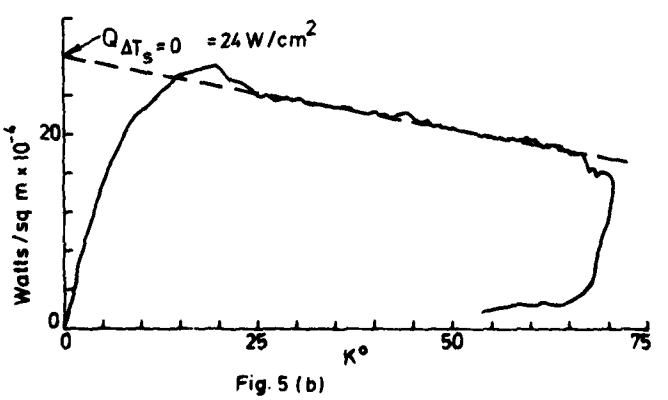

Fig. 5 (b)

Heat transfer rate versus surface temperature Data from 5(a) Run 734

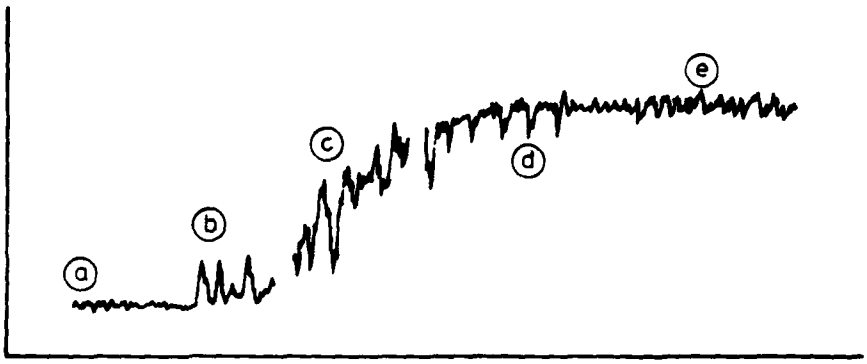

Fig. 6.

Thin film heat transfer gauges signals in laminar transitional and turbulent flow.

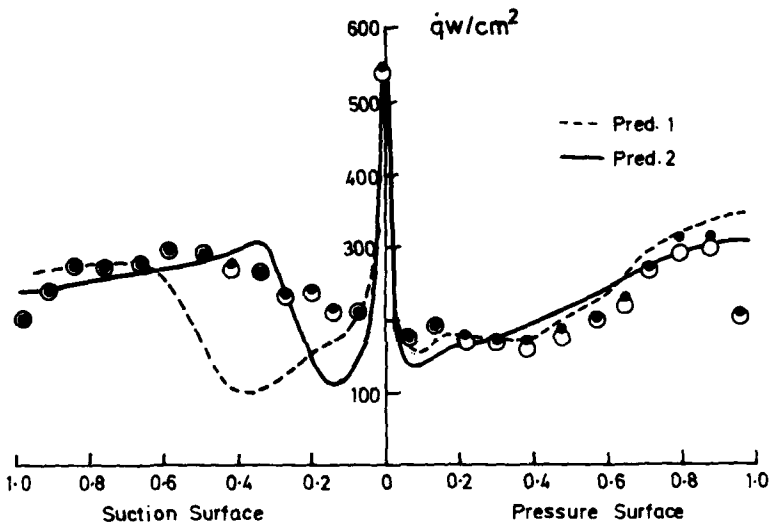

Fig 7 (a)

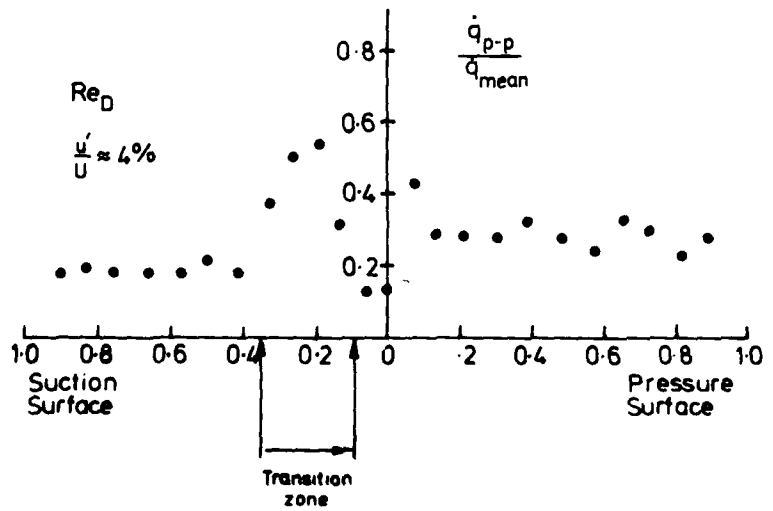

Fig 7 (b)

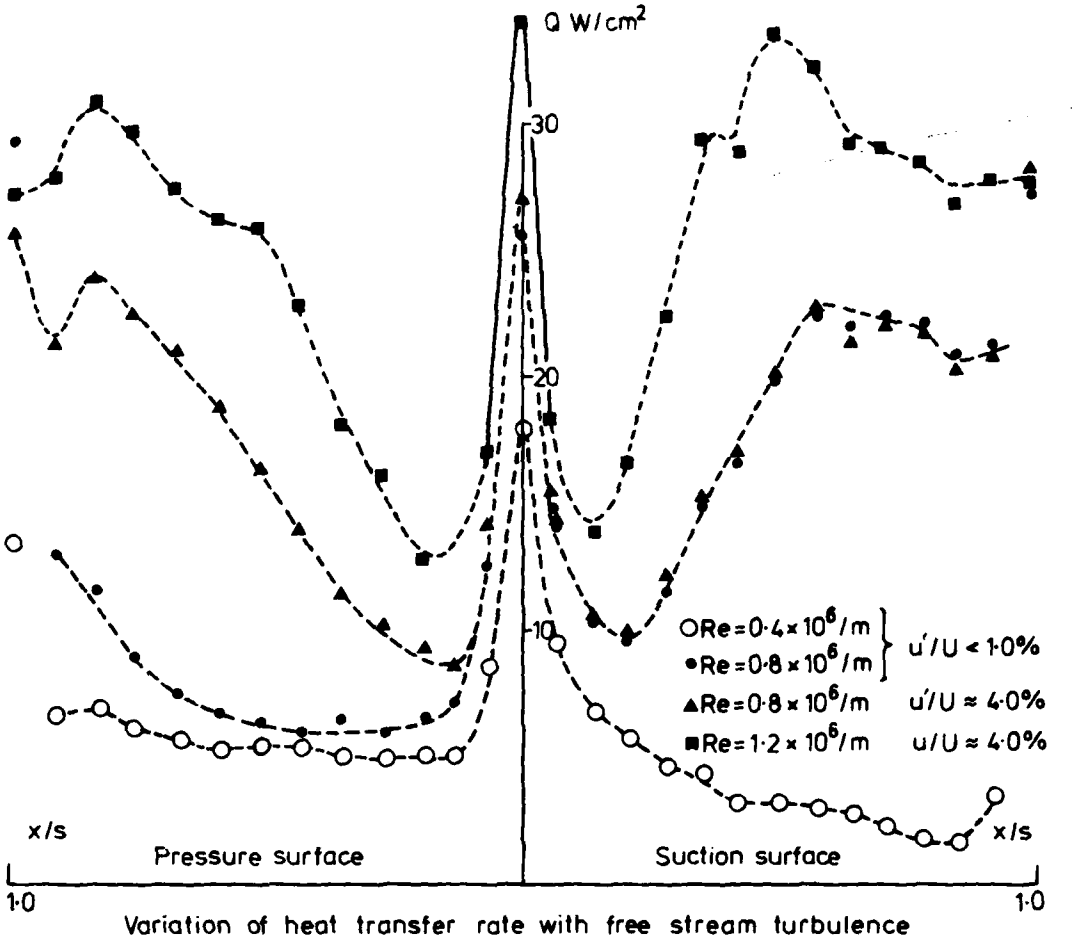

Variation of heat transfer rate with free stream turbulence and unit Reynolds number on N.G.V.

Fig. 8.

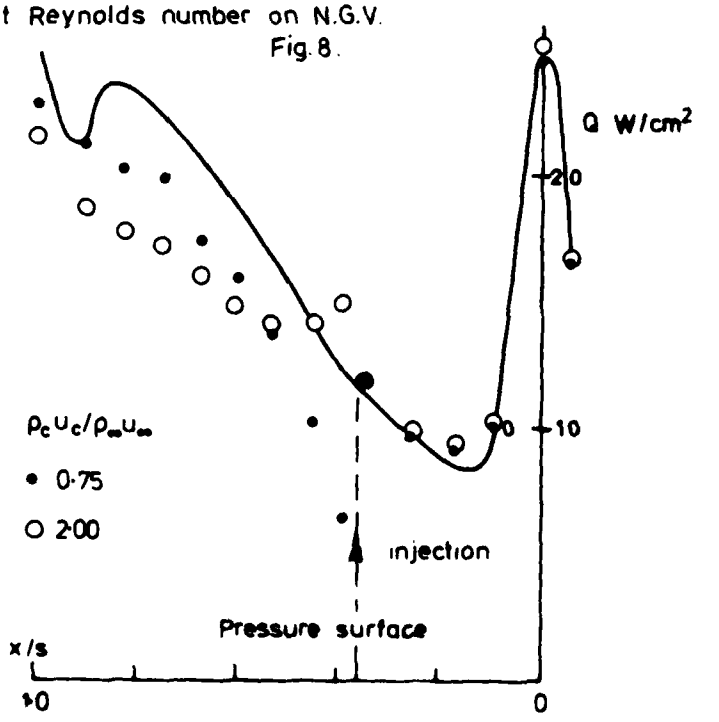

Fig.9

Variation of heat transfer rate on NGV pressure surface with coolant injection

DISCUSSION

W.J.Priddy, UK

Dr Schultz, you state that a fraction of a second is adequate time to allow for the turbulence to settle in your transient facility. There is a range of frequencies present in turbulence including very large scales associated with low frequency. The different frequencies interact through a cascade of energy transfer between the eddies, where the development of the 'high frequency' eddies is dependent on the 'low frequency' scales. Therefore, the time scale for the turbulence to fully develop is dependent on the largest and 'slowest' scales. In view of this, how can you be certain that the turbulence has fully developed?

Author's Reply

If we assume, for example, that the mean blade Mach number is 0.5 and the true chord is 0.05 m then the average transit time through the passage would be of the order of 0.3 milliseconds, representing a frequency of about 1700 Hz. Any frequency below this relates to changes in the mean cascade velocity and their scale has little or no effect on transition processes.

The turbulence structure behind the grids we use is established in the time scale of the experiments. It only takes five milliseconds for the wakes behind the turbulence grid bars to extend to 100 bar diameters when the inlet Mach number is around 0.3, typical of our cascade.

STUDIES OF TURBULENCE CHARACTERISTICS AND THEIR EFFECTS UPON THE DISTRIBUTION OF HEAT TRANSFER TO TURBINE BLADING

by

F.J. BAYLEY, Professor of Mechanical Engineering and
Pro-Vice-Chancellor(Science),
University of Sussex, BRIGHTON BN1 9QT, U.K.

W.J. PRIDDY, Research Fellow in Mechanical Engineering,
University of Sussex, BRIGHTON BN1 9QT, U.K.

In this paper two techniques are used to determine the distribution of heat transfer coefficient around turbine blade sections. Data are reported from cascade tests with a steady mainstream and then from tests in which the turbulence intensity and frequency were systematically varied. A provisional correlation of the data is described.

Nomenclature

b.p.f.	Blade passing frequency, Hz.	Nu_o	Nusselt number in steady flow
c	Blade chord, m.	u_∞	Mainstream velocity, m/s
f_b	Bar passing frequency, Hz.	u'	Root mean square velocity
$\dot{m}$	Mainstream rate of flow, kg/s.		fluctuation, m/s.
M_2	Exit Mach number.	Re	Reynolds number.
N	Rotational speed of cage,	x	Distance around blade surface, m.
	rev/min.	X	Distance of blade cascade from
Nu	Nusselt number		cage, mm.
ν	Kinematic Viscosity, m^2/s.		

Introduction

It is now generally accepted that significant differences are found between measurements of convective heat transfer to turbine blading in laboratory cascades and deductions from engine data. Qualitatively these differences are explicable through the different turbulence characteristics of the flows in cascades and those in the demanding environment of an engine, and certainly many workers have demonstrated experimentally and theoretically that different turbulence parameters have varying and usually significant effects upon local convective heat transfer rates. Quantitatively, however, the situation is less satisfactory, certainly from the designer's point of view, dictated by his requirement to make reliable predictions of blade life and thus of local temperatures around a blade surface. Not least the quantitative difficulties arise from the problems of measuring flows within an engine, but even if these were overcome uncertainties would remain as to the properties of real flows which characterise the turbulence and its effect upon local heat transfer. Turbulence intensity has traditionally been regarded as the principal turbulence parameter, but many workers have demonstrated that other factors are important and Dyban and Epik (1), for example, suggest that each of the three components of velocity fluctuation, the energy spectrum, the correlation coefficient and the so called intermittency factor need to be known to define precisely a turbulent flow. Many modern turbine blade sections, even at the high Reynolds numbers at which they operate manifest considerable areas over which the boundary layer remains laminar in a steady, low turbulence stream. The superimposition of main stream velocity fluctuations associated with artificially induced mainstream turbulence is well known to affect dramatically heat transfer rates under such conditions, and Ishigaki (2) has shown theoretically that under such conditions the frequency of the perturbations, as well as their intensity, or amplitude, is important in determining the enhancement of the convection process. Clearly such effects can be important in turbine blade design for as rotor speed changes so will the frequency of the perturbations in flow velocity which the blades experience.

This paper describes a continuing programme of research in the Thermofluid Mechanics Research Centre of the University of Sussex which is attempting to separate the effects of some of the different turbulence parameters. A previous paper describing this work (3) showed how in experiments upon a modern rotor blade section there appeared to be a clear and separable effect of frequency, over parts of the blade section at least. This early work however involved intensities of turbulence generally higher than might be reasonably expected in an engine, and frequencies lower than would be typical of those experienced by rotor blades, for example, passing through the wakes of stator blades.

AD-A092 953 ADVISORY GROUP FOR AEROSPACE RESEARCH AND DEVELOPMENT--ETC F/G 21/2
TESTING AND MEASUREMENT TECHNIQUES IN HEAT TRANSFER AND COMBUST--ETC(U)
SEP 80
UNCLASSIFIED AGARD-CP-281

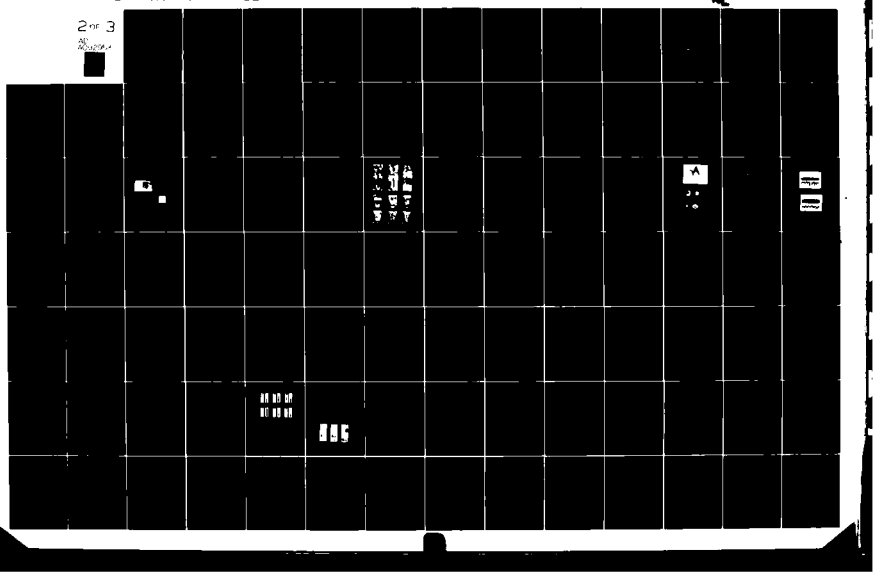

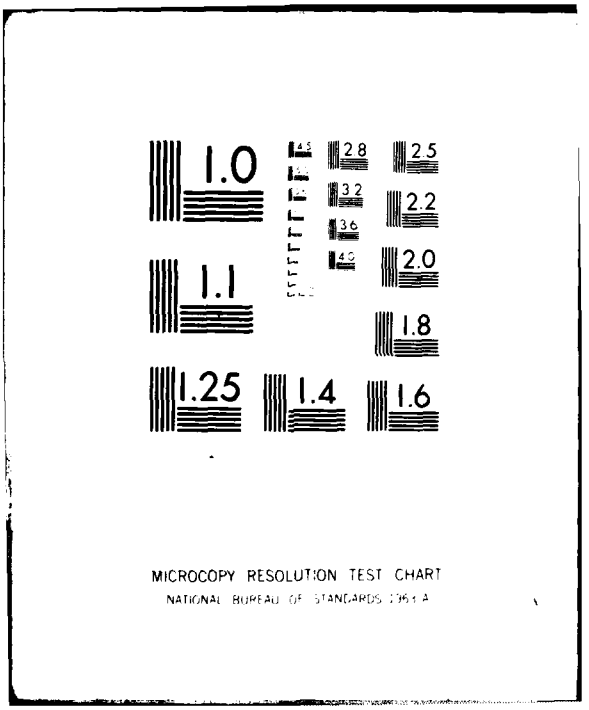
1.0
1.1
1.25
1.4
1.6
1.8
2.0
2.2
2.5
2.8
3.2
3.6
4.0
MICROCOPY RESOLUTION TEST CHART
NATIONAL BUREAU OF STANDARDS 1963 A

present paper some of the deficiencies of the earlier work have been made good and some preliminary attempts are reported at correlating the magnitude of the observed effects following the predictions of the theoretical work of reference (2).

The Turbulence Generator

The cascade tunnel used for the present work typically yielded a turbulence intensity of less than one percent at the blade leading edges. This level of turbulence was enhanced for part of the test programme by a generator of the general form described in reference (3). This comprises a squirrel cage which can be rotated at varying speeds, thus producing a perturbation frequency determined by this speed and the number of bars in the cage, which for the current part of the programme has been kept at thirty. The intensity of the turbulence is determined largely, again as described in detail in (3), by the diameter of the bars, but also by the distance downstream from the cage. Compared with the earlier apparatus of (3) the current design enables the distance between the cage and the leading edges of the blades in the cascade to be varied between 6.4 mm and 38 mm giving an additional control of the turbulence characteristics. Even more important, the facility to operate close to the cage has enabled the effects of the peak frequencies upon the heat transfer to be observed. Thus the current cage design, shown in the drawing of the apparatus, Fig. 1, which incorporates carbon fibre bars 2.4 mm in diameter, can be rotated at up to 20,000 rev/min, giving a bar passing frequency, with 30 bars, of 10 kHz. In the earlier apparatus, with a fixed distance of 46 mm between cage and blades, the high frequency perturbations were found not to persist in the flow over this distance, which was not, of course, typical of blade inter-row spacing in modern engine design.

The turbulence characteristics of the flows behind the cage have been determined by a hot wire anemometer using a single filament set normal to the mainstream flow direction and traversed over the cascade entrance plane. The signals were analysed by standard Disa anemometer circuitry to yield the usual turbulence intensity, defined as the rms streamwise velocity fluctuation expressed as a percentage of the average mainstream absolute velocity. In this phase of the work no attempt has been made to distinguish component fluctuations nor to attempt spatial correlation of the perturbations. The work has concentrated on the gross characteristics of the flow, and in particular its frequency characteristics. Determination of these has been facilitated in the current programme of work, compared with the earlier, by the use of a Solartron 1510 spectrum analyser. This instrument analysed the signals from the anemometer online to yield directly the power spectra of the fluctuating flow. Some typical examples of these are reproduced as Fig. 2. and in all cases the distinct 'spike' at the bar passing frequency is noteworthy, and is now found to be distinguishable further downstream at the higher frequencies than was the case in the earlier programme of work.

Figures 3a and 3b show how independent was the turbulence intensity of frequency and rate of mainstream flow, as also was found in our earlier work (3). The effect upon this parameter of distance from the cage is shown by Fig. 3c and the observations follow generally accepted trends.

For the whole programme of work reported here measurements were made of turbulence characteristics only at the blade leading edges, for current instrumentation does not allow measurements through the blade passages.

Measurements of Heat Transfer

The present programme of work has given the opportunity of comparing two different procedures for determining the distribution of convective heat transfer rate around a turbine blade section. In the past and for some of the present work use has been made of the method developed by our former colleague Dr. A.B. Turner (4). In this, the two-dimensional Laplacian conduction equations are solved by a finite element method on a digital computer using boundary conditions of measured temperature distribution around the blade outer surface and heat transfer rates at the surfaces of internal passages conveying cooling air. The procedure yields the normal temperature gradient and hence the heat transfer rate at the outer surface. This has proved to be a powerful technique and is sensitive enough to show clearly sharp changes of heat transfer rate, as at the laminar-turbulent transition. It is however expensive of computer and user time and especially is this the case when blade sections with long thin trailing edges are examined, for even with the largest computer at our disposal it is difficult to arrange for sufficient elements for an accurate solution to be contained within these regions.

The alternative procedure which has been adopted for most of the current programme is to model the blade section as a hollow shell, about 1mm thick, in a metal plastic composite material. This has a thermal conductivity of about 1 W/mK, so that the typical heat fluxes under the test conditions, in which the mainstream total temperature is about 100°C and the cooling air temperature inside the shell about 20°C, produce temperature drops through the wall of the order 10°C. These can be accurately measured by thermocouples formed from fine (0.2 mm diameter) wires buried in the inner and outer surfaces. The differences between inner and outer temperatures are readily converted on-line to heat transfer coefficients by a simple data reduction programme, and outputs like those of Figures 4, 5 and 6 can be obtained as the rig is running.

Observations in the Unperturbed Flow

Figure 4 compares the distributions of heat transfer coefficient observed in comparable tests on a rotor blade section using the two techniques of measurement. The abscissa of this figure and throughout is defined as the distance measured around the surface from the leading edge stagnation point divided by the plan or true chord and expressed as a percentage. Data beyond the 80 per cent point on the pressure (or concave) surface and 120 per cent on the suction (or convex) surface are of no significance since in these trailing edge regions the physical scale of the blade made impossible accurate modelling by either analytical technique.

Beyond the clearly defined laminar turbulent transition region on the suction surface the agreement between the two methods of determining the heat transfer coefficients is not satisfactory, and this was consistently the case through the whole range of conditions covered in this total programme. The heat fluxes to the thin-shell blade were usually about one-half those on the steel blade used for the Laplacian analysis, and there is some possibility that the boundary layer was more stable with thus a tendency to lower coefficients in the former case. It is more likely, however, that the ill-conditioned nature of the numerical representation of the conduction equations in this region made for errors in the steel blade analysis, and the thin-shell data is thought to be the more reliable. This ill-conditioning is also the cause of the oscillations in heat transfer coefficient observed elsewhere on the steel blade, although in these other regions the mean values are in good agreement with the observations from the thin-shell blade. An error simulation study of the Laplacian results showed them to be sensitive to quite small perturbations; for example, a perturbation of as little as $0.5^{\circ}C$ in surface temperature could under certain conditions lead to variations of ± 15 per cent in computed, surface-average heat transfer coefficients. A full study of the factors affecting numerical solutions of the conduction equations has recently been published by our colleague, Dr. J.M. Owen (5). Thus although the finite element solution has proved a useful and powerful technique of heat transfer analysis, we have for the remainder of the programme concentrated upon the more convenient thin-shell method of testing.

Fig. 5 shows how the distribution of heat transfer coefficient around this same rotor blade section changed as the exit velocity from the cascade, and hence Reynolds number and Mach number, was varied. In this method of representing a range of results the exit Reynolds number is shown in the left-hand abscissa, and its value for a particular curve indicated by the short horizontal line. This also shows the zero point for the heat transfer coefficient for each curve, and the absolute value of this coefficient may be obtained as the height above the corresponding zero line for each distribution curve using the scale at the right-hand coordinate. The simplicity of the thin-shell analytical technique allows these contours of heat transfer coefficient to be drawn by the on-line computer as the test rig is running, and a similar plot is shown as Fig. 6 for a typical nozzle guide vane of low turning angle.

These heat transfer data from the thin-shell blade sections allow comparison with existing prediction techniques for the relevant flow conditions. In Figures 7a and 7b, the distribution of heat transfer around the two blade sections tested are compared with simple flat plate predictions for the highest exit Reynolds numbers in each case. Local Reynolds numbers were computed from measured pressure distributions around each section, and we immediately observe that the turbulent boundary layer predictions are quite inappropriate. The leading edge data are slightly overestimated for the conditions shown using the form proposed in (6), and all our observation show that consistently the rotor blade has behaved more predictably in this region. The predictions from laminar flat plate theory (for example, from ref. 7) are in good agreement with our measurements over substantial parts of both blade sections and for most of the tested range of flow conditions. Indeed, the only exception to this observation is that shown for the pressure surface of the rotor blade in Fig. 7a. The heat transfer coefficient just downstream of the leading edge is in good agreement with theoretical prediction, and at lower exit Reynold numbers this agreement persists downstream, as on the nozzle blade, Fig. 7b. At this high flow on the rotor blade, however, it is observed that the heat transfer coefficient on the pressure surface rises towards the trailing edge and this could be attributed to the development of Taylor-Goertler vertices. The procedure of Smith (8), for example, predicts their onset over most of the pressure surface of this blade at this flow condition; unfortunately a similar prediction is made for the nozzle blade where almost no increase in heat transfer is observed. The slight oscillation in coefficient along the surface of both blades gives some credence to such a hypothesis, however, although it is clear that there is much uncertainty about the quantitative effects of such phenomena. A possible resolution of the discrepancy may be in the value of the acceleration parameter $\nu/u_{\infty}^2 . \frac{du_{\infty}}{dx}$. This only falls below the critical value of $2.6\ 10^{-6}$ associated with relaminarisation of turbulent boundary layers, at the highest flow rate on the rotor blade, and towards the rear of the nozzle blade, where there appears a slight rise in heat transfer. Further study of these phenomena are clearly called for.

It is particularly obvious from these results, as indeed is well known, that the prediction of the laminar-turbulent transition region, both in placing and extent, is of crucial importance if turbine blade designers are to make an accurate estimate of the distribution of heat transfer rates in steady flows at least. None of the many available procedures, empirical or otherwise, predicts the clearly observed transitions in the present programme. There is some evidence that separation is the triggering mechanism on the suction surface of the rotor blade, a point of view based on approximate estimates of the development of the momentum boundary layer thickness, and reinforced by the observed reduction in heat transfer just upstream of the transition on this blade. Similar trends in the heat transfer data for the nozzle blade point the same way but this transition mechanism is not, however, confirmed by the boundary layer analysis.

Effect of the Flow Perturbations

A set of tests was conducted on the rotor blade with the turbulence generator rotated upstream of the cascade at speeds ranging in 1000 rev/min steps up to the maximum of 20,000, and at distances from the leading edge of the instrumental blade varied over the available range. The turbulence conditions covered thus ranged between 15 and 32 per cent intensity and bar passing frequencies between 4 and 10 kHz.

The effects of turbulence intensities which might not unreasonably be expected in an engine are shown as Fig. 8. for the rotor blade. The striking effect of the perturbations upon the heat transfer to the pressure surface in particular is noteworthy, and even the intermediate turbulence intensity more than trebles the convective coefficients on this surface. Effects are less on the suction surface and indeed downstream of the previously observed transition region, which is now almost wholly suppressed, there is little enhancement, as many other investigators have found (9). Further upstream there is some increase in heat transfer, surprisingly rather more evident with the lower intensity represented in this figure, although here the separation referred to in the steady flow work may be complicating the picture.

The effect of frequency upon the distribution of heat transfer as the intensity of the perturbation and the mainstream Reynolds number are held constant, is shown in Fig. 9. Although the effects are less dramatic than those resulting from the change from a steady to an unsteady flow, there is nevertheless an increase in the rate of heat transfer to most of the blade surface as the characteristic fundamental frequency of the perturbations is raised.

Such an effect was predicted by Ishegaki (2), who derived from his theoretical analysis the parameter

$$\left(\frac{u'}{u_\infty}\right)^2 \left(\frac{f_b c}{u_\infty}\right)^{\frac{1}{2}}$$

in which u' is the r.m.s. velocity fluctuation superimposed on the mainstream velocity, u_∞, so that (u'/u_∞) is the usual turbulence intensity. The second group is the so-called Strouhal number in which f_b is the frequency of disturbance, in this case the blade passing frequency, and c a characteristic length, in this case the chord, or the appropriate fraction, of the blade.

Fig. 10 shows all the data from the present rotor blade test programme represented in terms of a modified version of this parameter. Following the practice adopted in our earlier work (3), for convenience the blade has been divided into four principal regions, the leading edge, the pressure surface, and the upstream and downstream halves of the suction surface. As has already been seen there is a negligible effect of the perturbations on the latter region, so that this figure shows the results only for the remaining three regions of the blade surface, as indicated.

The abscissa is the Ishigaki parameter modified by multiplication by the mainstream Reynolds number appropriate to each of the blade regions represented. The exit values are used for the pressure surface, the midsurface distance and exit velocity for the upstream suction surface, and the cascade inlet velocity and radius of curvature for the leading edge. Because of the scales adopted all the data for the latter region is compressed together near the origin, and is therefore shown only as average values for the two different intensities systematically studied.

The heat transfer rate in the ordinate of Fig. 10. is represented in the normalised form as the ratio of the surface-average coefficient measured in the unsteady flow to that at the corresponding conditions in the unperturbed flow. The resulting correlation is not complete and differences in the effects of the perturbations are apparent upon the three blade regions distinguished. It is not possible yet to determine whether this is due to variations in local turbulence conditions around the blade, which cannot be measured in the current phase of the work, or to more fundamental variations in local flow stability, for example. Nevertheless the correlation of Fig. 10 is not discouraging but further work is required to resolve the uncertainties which remain.

Conclusion

The thin-shell technique for measurement of blade heat transfer coefficients is shown to be a reliable and convenient method to apply. With it, some understanding of boundary layer behaviour in both a steady and turbulent mainstream has already been gained. When the requirement is to test at elevated gas temperature, for example downstream of a combustion chamber, the so-called Laplace method for a high temperature metal blade is a powerful alternative. This solution, however, demands a precise knowledge of the boundary conditions.

An encouraging correlation for the blade heat transfer in turbulent conditions has been made but points to the need for further research. The turbulence frequency and intensity parameters appear both to be significant.

References

1. Dyban, I. and Epik, H. — 'Calculation of convective heat transfer from statistical characteristics of turbulence', Heat Transfer Soviet Research Vol. 9, No. 4, 1977.

2. Ishigaki, H. — 'The effect of oscillation on flat plate heat transfer' J. Fluid Mech., P.437, Vol. 47, 1971.

3. Bayley, F.J. and Milligan, R.W. — 'The effect of free stream turbulence upon heat transfer to turbine blading', AGARD PEP conference on High Temperature Problems in Gas Turbine Engines, paper No. 37, 1977.

4. Turner, A.B. — 'Local heat transfer measurements on a gas turbine blade', I.Mech.E. Jnl. of Mech.Eng.Sci., Vol. 13, No. 1, 1971.

5. Owen J.M. — 'On the computation of heat transfer coefficients from imperfect temperature measurements'. I.Mech.E. Jnl. of Mech.Eng.Sci., 21(5), Oct. 1979.

6. Goldstein, S. (ed) — 'Modern developments in fluid dynamics', Clarendon Press, Oxford, 1972.

7. Bayley, F.J., Owen, J.M. and Turner, A.B. — 'Heat Transfer, Nelson, 1972.

8. Smith, A.M. — 'On the growth of Taylor-Goertler vortices along highly concave walls', Quart.App.Maths, 1955, 8(3), pp. 233-262.

9. Brown, A. and Martin, B.W. — 'Heat transfer to turbine blades with special reference to the effects of mainstream turbulence', ASME Gas Turbine Conference, paper No. 79-GT-26, 1979.

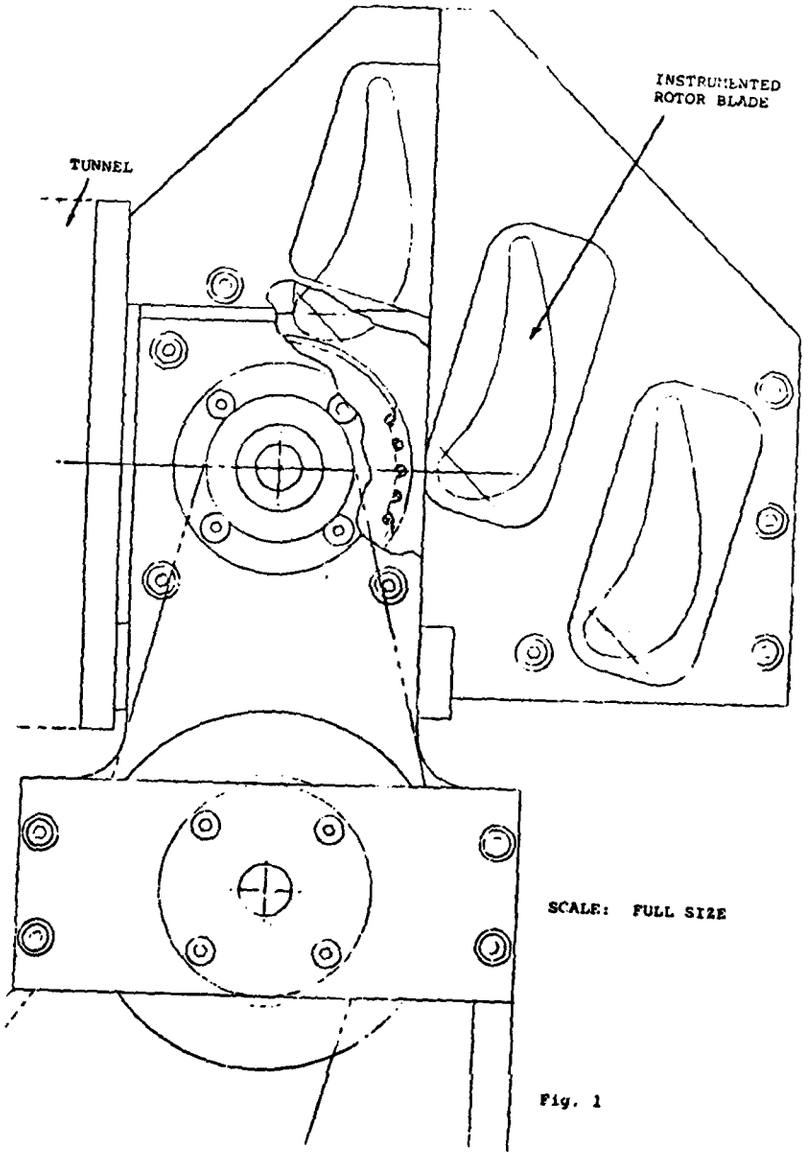

SCALE: FULL SIZE

Fig. 1

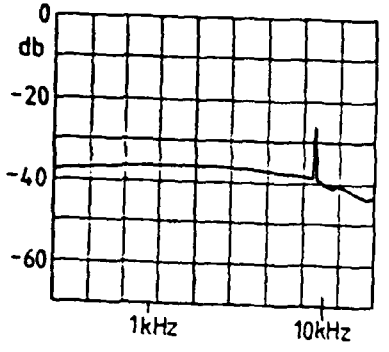

X = 12mm N = 20,000 rev/min

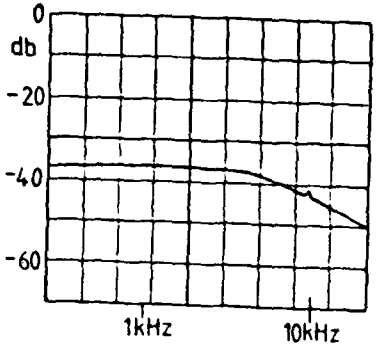

X = 50mm N = 20,000 rev/min

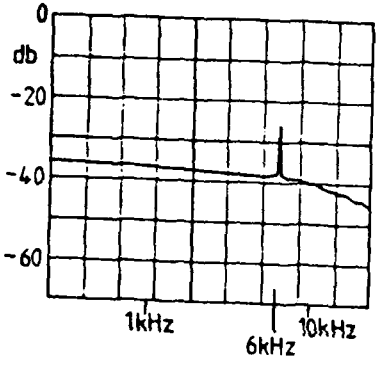

Fig 2 Power spectra (dB : log f)
Effect of speed and distance of cage

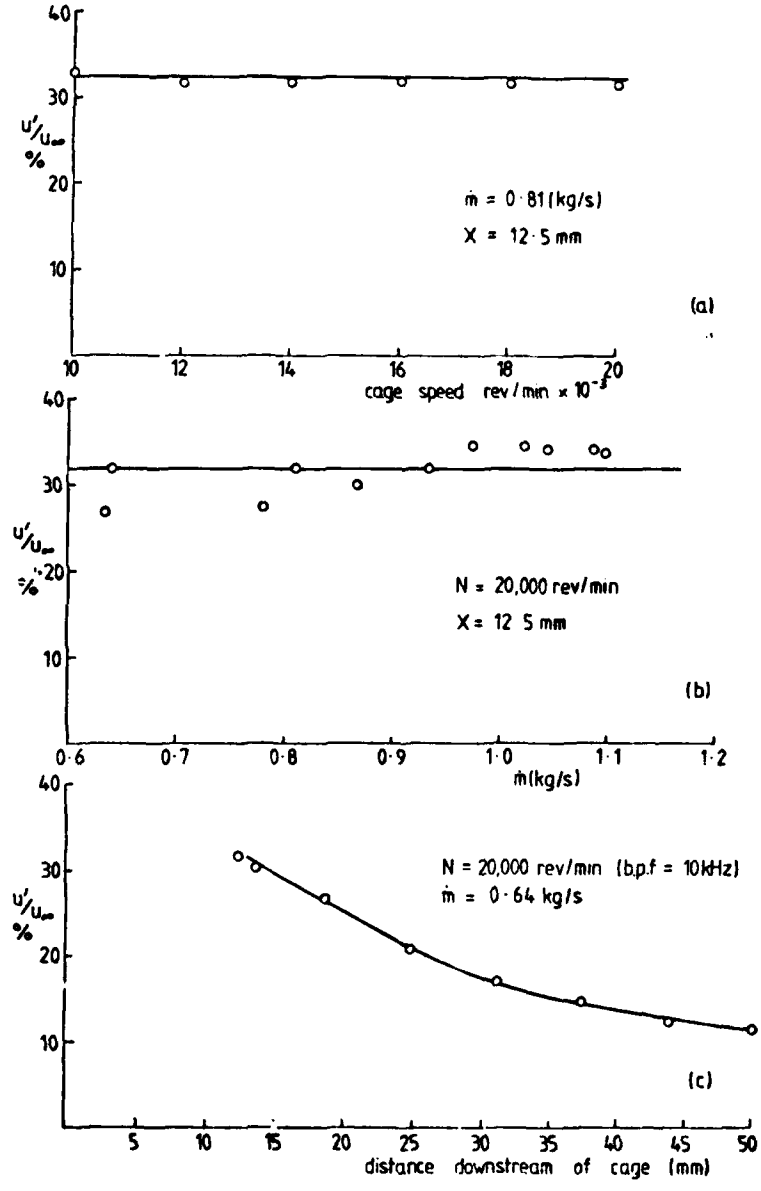

Fig. 3 Turbulence intensity

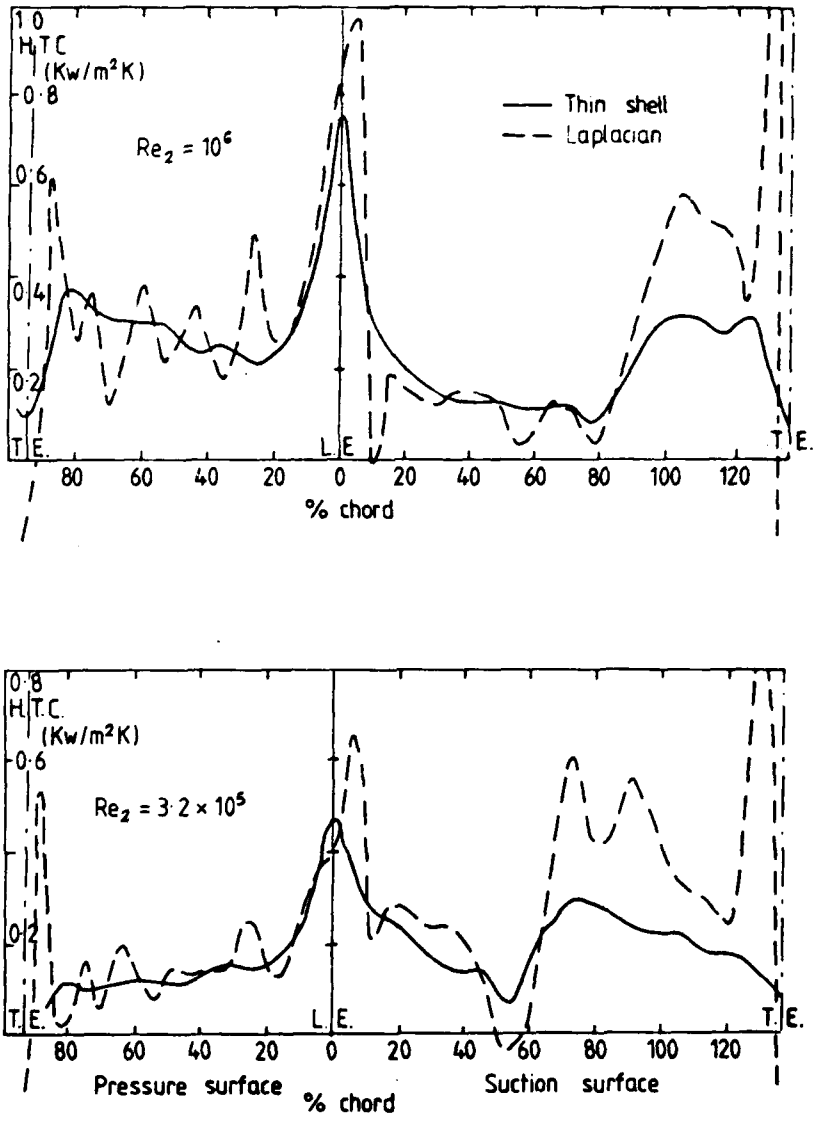

Fig. 4 Local heat transfer coefficient : comparison between Laplacian and thin - shell results

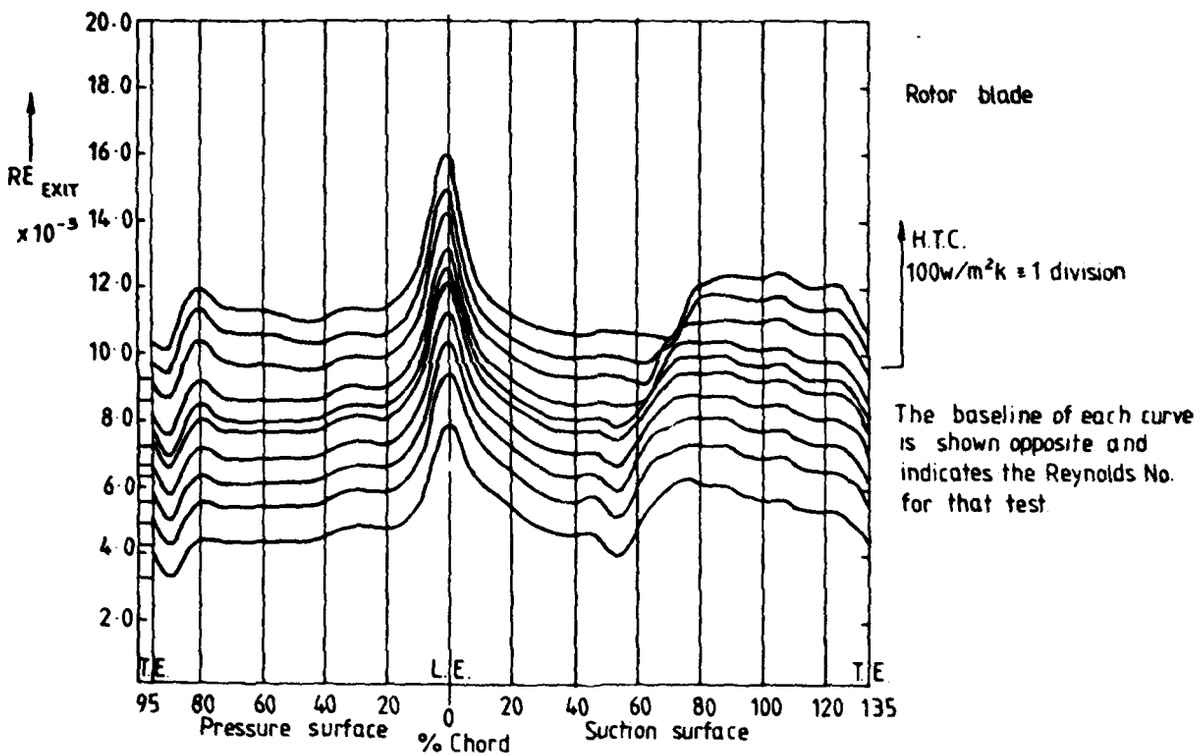

Fig. 5 Distribution of Heat Transfer in Steady Flow

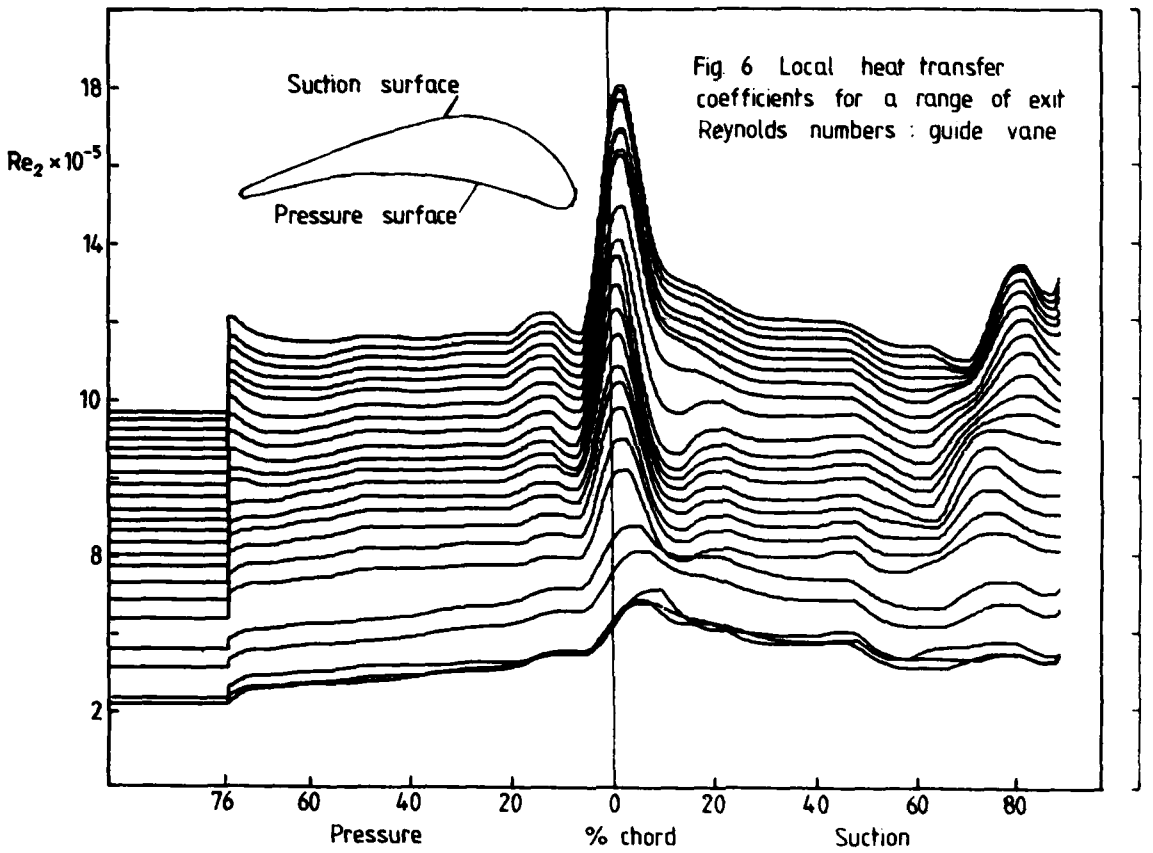

Fig. 6 Local heat transfer coefficients for a range of exit Reynolds numbers : guide vane

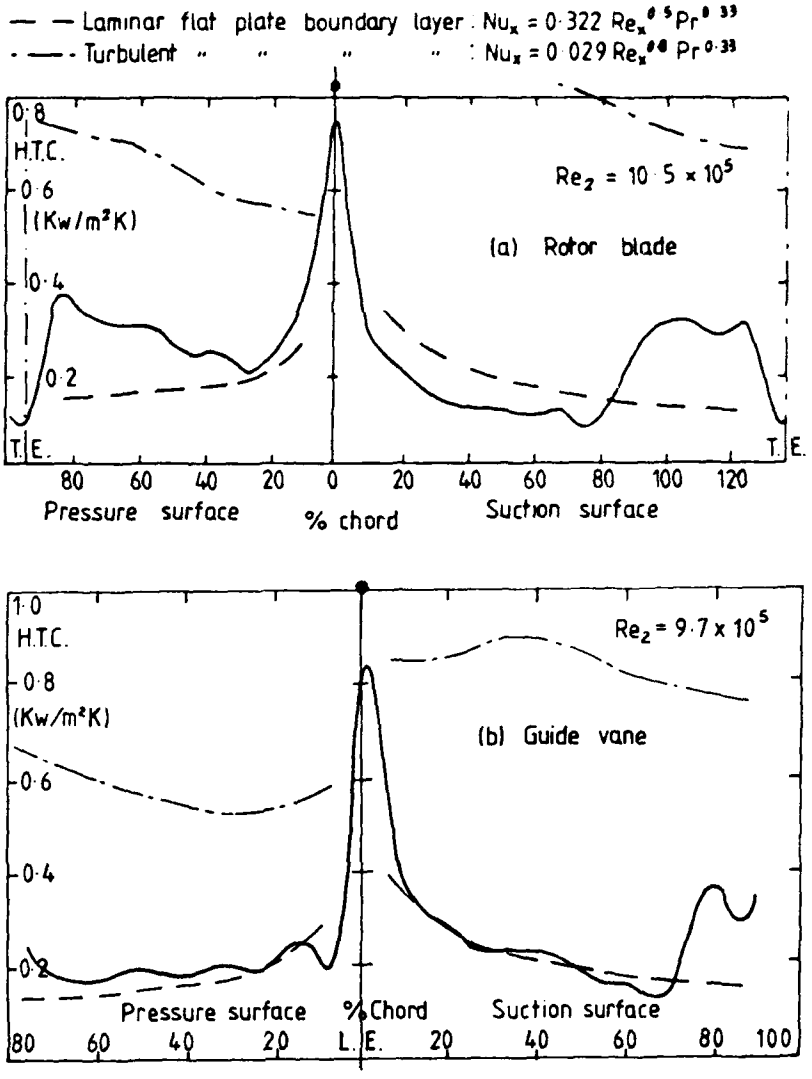

Fig. 7 Experimental and predicted heat transfer coefficients

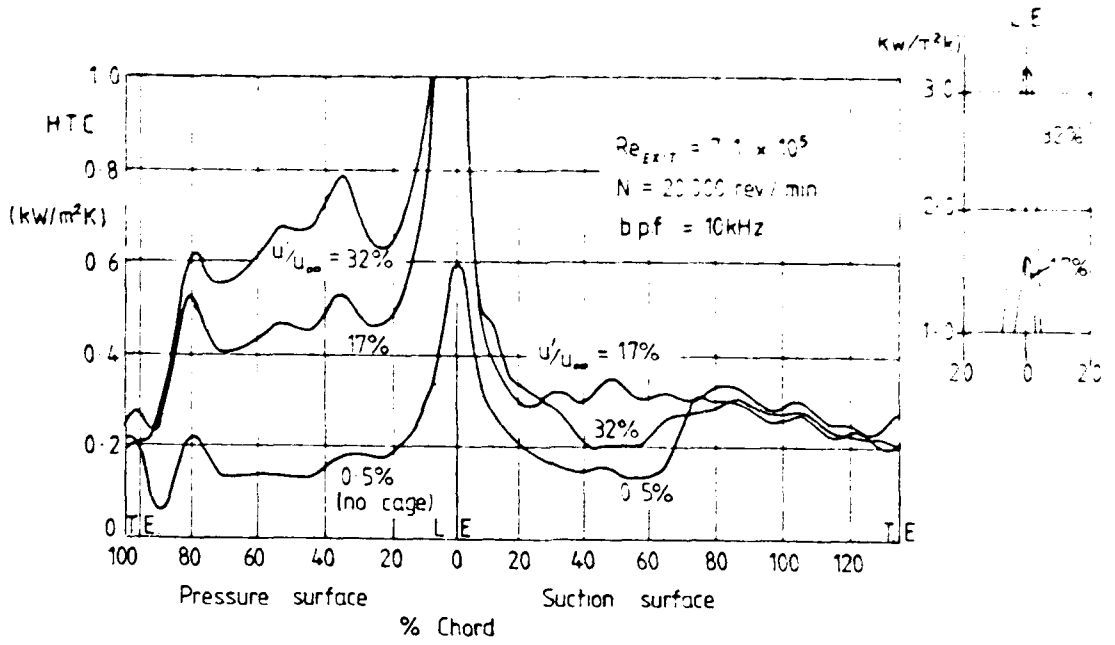

Fig 8 Variation of heat transfer coefficient distribution with turbulence intensity

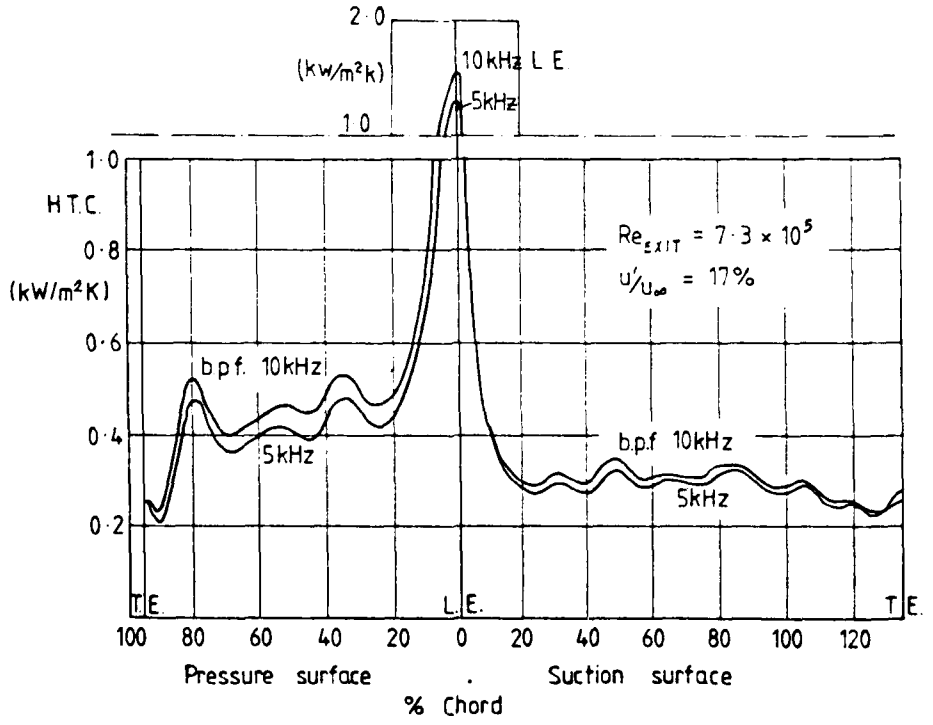

Fig. 9 Variation of heat transfer coefficient distribution with blade passing frequency

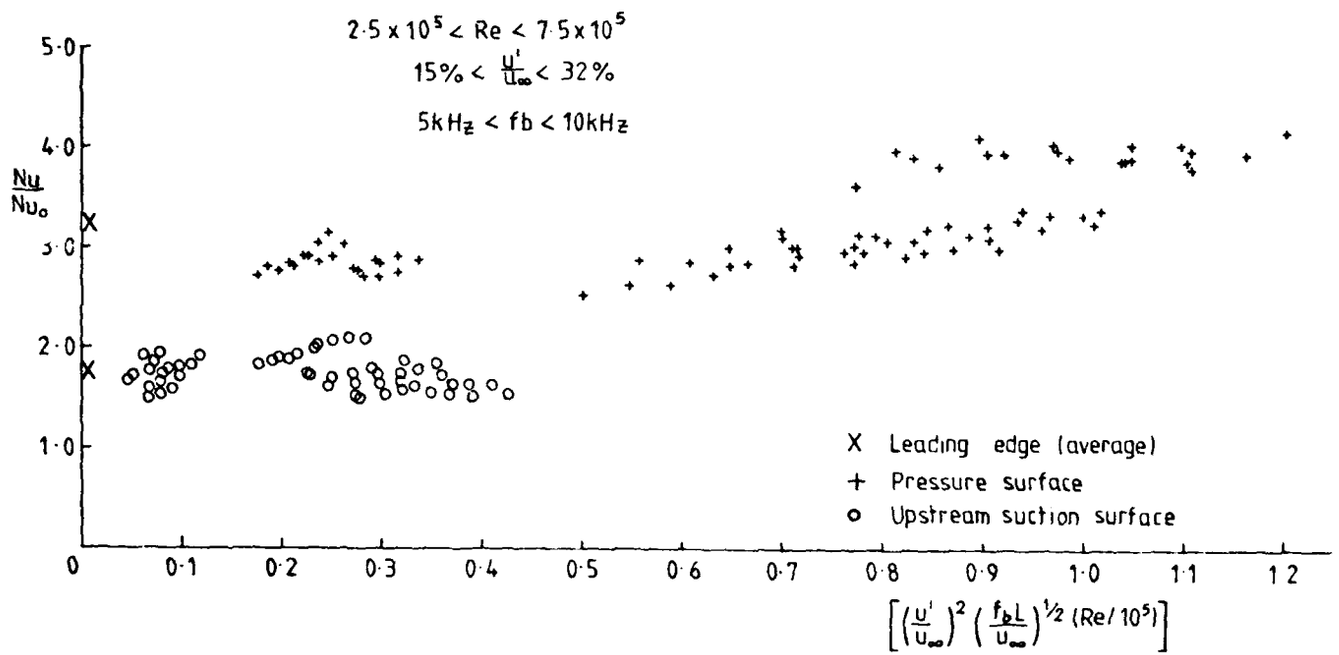

Fig 10 Variation in heat transfer with turbulence over three blade regions

DISCUSSION

M.L.G.Oldfield, UK

You have simulated characteristic blade passing frequencies with the squirrel cage, but the bars are closer together than an upstream nozzle guide vane row of blades would be. Have you considered using fewer bars rotating at a higher velocity, so that the nozzle guide vane wake passing velocity and wake spacing can also be simulated?

Author's Reply

In effect we have attempted to walk before we run and concentrated on the turbulence frequency as an individual parameter as well as the turbulence intensity. Presumably a phase lock averaging technique could be applied to study the velocity defect of the wakes simulated upstream of the cascade blades. The spacing of the passing bars and their speed might then be adjusted to simulate correctly the relative wake velocity and spacing produced in a turbine by the upstream blade row. However, the configuration will depend on the particular engine and stage under consideration, whereas ours is a general study of the blade passing effect. It might also prove not possible to control all three parameters, namely frequency, wake spacing and velocity defect, independntly of each other in a model rig.

CORRELATION MEASUREMENT OF VELOCITY AND TEMPERATURE FLUCTUATIONS IN A FREE JET DIFFUSION FLAME

by

V. Wittmer and R. Günther
Universität Karlsruhe (TH)
Engler-Bunte-Institut
Lehrstuhl und Bereich Feuerungstechnik
Richard-Willstätter-Allee 5
7500 Karlsruhe 1
Germany

SUMMARY

In the present paper a free jet diffusion flame was studied. The measurement techniques used were the laser-Doppler-anemometry (LDA) and a compensated thermocouple. With LDA the fields of both the mean axial and radial velocities and their fluctuations were measured. The local mean and fluctuating temperature were measured after determining the frequency response. The time constant was measured assuming the transfer function of the thermocouple to be a first order lag. The results of the temperature measurement show, that the maximum of the temperature fluctuations is outside of the reaction zone. In a traverse plane the correlation of the fluctuating axial and radial velocities has the maximum at the location of the highest gradient of the axial velocity. The correlation of fluctuating velocity and temperature becomes zero in the reaction zone.

NOMENCLATURE

d		nozzle diameter
k		constant
P		probability density function
R		correlation coefficient
t		time
T		temperature
$\dot{T}$		derivative of temperature with respect to time
$\overline{T}$,	$\sqrt{\overline{T'^2}}$	mean and fluctuating temperature
u		velocity
$\overline{u}$,	$\sqrt{\overline{u'^2}}$	mean and fluctuating velocity (axial)
$\overline{v}$,	$\sqrt{\overline{v'^2}}$	mean and fluctuating velocity (radial)
x		(axial) coordinate
y		(radial) coordinate
τ		time constant

Subscripts

c	corrected
g	gas
i	index
m	axial quantity
s	thermocouple

1. INTRODUCTION

A common flame in industrial practice is the turbulent diffusion flame. This flame burns in a shear layer that is turbulent. In contrast to premixed flames the diffusion flame entrains its combustion air from its surrounding. Turbulent mixing of fuel and air controls the combustion process.

In order to study the behaviour of a turbulent flame both mean and fluctuating values of velocity, temperature and concentration must be studied. At the present time it is not possible to calculate those quantities from theory alone. Experimental values are needed as a basis and point of comparison of mathematical models. In particular, the measurement of the correlation of physical quantities is necessary to interpret the processes in a turbulent flame.

In the present paper the turbulent velocity and temperature fields and the correla-

tion of velocity and temperature fluctuations were measured.

2. FLAME AND BURNER SYSTEM

The gas leaves a conical nozzle with a diameter of 8 mm with an exit velocity of 71 m/s (Re = $3.7 \cdot 10^4$). This type of nozzle was chosen to avoid agglomeration of particle in the nozzle. The particles were necessary for seeding the gas for laser-Doppler-anemometry. Because of the high exit velocity the flame has to be stabilized, for which a ring-shaped jet of oxygen (450 l/h) was used.

The whole burner system could be traversed in the horizontal direction.

3. VELOCITY MEASUREMENT

The laser-Doppler-anemometry (LDA) was used for the measurement of the following velocity components:

$\bar{u}$, $\sqrt{\overline{u'^2}}$, $\bar{v}$, $\sqrt{\overline{v'^2}}$, $\overline{u'v'}$.

The optical arrangement (Fig. 1) consisted of an Argon Ion laser, beam splitter, two Bragg cells and the focussing lens. Beam splitter and Bragg cells formed a rotatable unit. The laser was operated in the green line with a power of about 0.5 Watt. The frequency shifting by Bragg cells is necessary for high turbulence measurements. The fringe distance in the measurement volume of the LDA system was 4 µm. The forward scattered light passed an optical system consisting of two lenses which enlarged the measurement volume by a factor of 1.5 . The LDA signal collected by a photomultiplier was analyzed in a TSI tracker. Its voltage output and trigger output (to avoid measurements during dropout time) were connected with a signal analysis computer (Deutsche Intertechnique, PS 400) which sampled the signal and calculated the velocity. Since an LDA system gives a higher weighting to higher velocities, a correction as suggested by Durst was used, Eq.(1).

$$P_c(u_i) = P(u_i)/u_i \qquad (1)$$

The meaning of this equation is, that the probability of a given velocity is divided by that velocity.

The radial components of the velocity and $\overline{u'v'}$ term were measured by rotating the optical system. By measuring in three directions (30^o, 0^o, -30^o) it is possible with the geometrical relationship to calculate these quantities [2] :

3.1 Seeding System

For seeding MgO particles were used. The gas was seeded as well as the air stream. This stream was introduced by a cylinder with a diameter of 0.6 m surrounding the gas nozzle. The cylinder is covered by a perforated plate and contained sieves for a uniform velocity distribution (Fig. 1). The exit velocity of the air stream is only 0.4 m/s, so that the flame burned as a free jet.

4. TEMPERATURE MEASUREMENT

In a turbulent flame the temperature of the fluid can change very quickly. The fluctuations can range up to 10 kHz. An uncompensated thermocouple responds too slowly to reproduce all fluctuations with the same accuracy. The principle of the compensated measuring technique, which was first proposed by Kunugi [3] , is to match the frequency response of the thermocouple.

The frequency response of a thermocouple can be described by a simple heat transfer equation, Eq.(2)

$$\tau \cdot \dot{T}_s + T_s - T_g = 0 \qquad (2)$$

It can be seen that equation 2 represents a first order lag. Knowing the geometry and the physical properties of the thermocouple it is possible to find the time constant τ [4, 5] . In the present paper the behaviour of the thermocouple is modelled as a first order lag to determine the time constant. In general

$$\tau\dot{y}(t) + y(t) = k\, x\,(t) \qquad (3)$$

from which the response to a step function is

$$y(t) = k \cdot e^{-t/\tau} \qquad (4)$$

Thus

$$y(\tau) = 0.368\; y\;(t = 0) \qquad (5)$$

or in general, if the value for t = 0 is not used

$$y(t + \tau)/y(t) = 0.368 \qquad (6)$$

Eq.(5), (6) are equivalent to determining τ by finding the intercept of the tangent to the curve with the time axis (Fig. 2).

4.1 Experimental Apparatus

To find the time constant the thermocouple was heated by a pulsed electrical current (Fig. 3). The response curve was sampled by a signal-analysis-computer and τ was calculated with the help of Eq.(5). The resulting compensated signal was filtered by low pass filters. The filter cut off frequency was determined by a frequency analysis. During the analysis the frequency was found after which the electronical noise became greater than the signal. Since the compensating network amplified noise and signal in the same way up to this cut off frequency, the noise was subtracted by an energy balance. By Eq.(7) the true RMS-value of the temperature was determined

$$RMS^2_{true} = RMS^2_{measured} - RMS^2_{noise} \qquad (7)$$

The RMS_{noise} quantity is dependent on low pass filter and time constant and was calibrated before measurement.

For the measurements a butt welded Pt-PtRh (10%) thermocouple with a diameter of 0.05 mm was used.

5. CORRELATION MEASUREMENT

A combination of the measurement techniques LDA and compensated thermocouple allowed the determination of the correlation of temperature and velocity fluctuations. The relationship of these two quantities is given by Eq.(8):

$$R = \overline{u'T'} / \sqrt{\overline{u'^2}} \cdot \sqrt{\overline{T'^2}} \; ; \quad -1 \leq R \leq +1 \qquad (8)$$

The physical significance of a negative R is that a high temperature occurs with a low velocity and vice versa. If R = 0 there is no dependence of the two fluctuating quantities. If R is positive, then a high (low) temperature coincides with a high (low) velocity.

5.1 Experimental Apparatus

For the correlation measurement the signals of velocity and temperature are to be measured simultaneously (Fig. 1). The trigger signal of the tracker was used to synchronize the simultaneous measurement. The correlation was calculated by the signal-analysis-computer in the following way. The correlation may be expressed in terms of the time averaged velocity-temperature uT and the product of the mean velocity and mean temperature as

$$\overline{u'T'} = \overline{uT} - \bar{u}\bar{T} \qquad (9)$$

For the measurement the thermocouple was located directly above the LDA measurement volume.

6. RESULTS

The results of axial (Fig. 4) and radial (Fig. 5) distribution of the measured quantities are plotted with the same abscissa scale, so the various physical values may be compared.

Fig. 4 shows the distribution along the flame axis in dimensionless distance x/d of the axial mean velocity $\bar{u}$, the fluctuating velocity $\sqrt{\overline{u'^2}}$, the turbulence intensity Tu calculated from these both and the radial fluctuating velocity $\sqrt{\overline{v'^2}}$. Furthermore, the mean temperature $\bar{T}$, the fluctuating quantity $\sqrt{\overline{T'^2}}$ and the correlation coefficient are plotted.

The decay of the mean velocity along the axis is typical for a jet. Not typical, however, is the appearance of an acceleration right after the nozzle. This increase of the velocity at x/d = 10 with the value of the exit velocity must be a result of an explosive expansion of the jet on ignition and the restricting influence of the oxygen stabilization on the jet. The effect is not a fault of the measurement technique (LDA) since it was also observed in probe measurements. This initial acceleration was also found in measurements of a concentric diffusion flame [6]. The axial fluctuating velocity $\sqrt{\overline{u'^2}}$ shows a distribution similar to that of the mean velocity. Large values occur at x/d = 10. Further from the nozzle the fluctuating velocity decreases. The turbulence intensity increases with the nozzle distance and remains constant 20% past x/d = 100. The radial velocity fluctuations $\sqrt{\overline{v'^2}}$ do not behave isotropically with respect to $\sqrt{\overline{u'^2}}$. Some isotropy is to be seen near the nozzle exit, but further downstream the ratio of $\sqrt{\overline{v'^2}} / \sqrt{\overline{u'^2}}$ becomes nearly 0.5 .

The distribution of the mean temperature in °C along the flame axis shows, that the temperature maximum lies between x/d = 110 and x/d = 120. At these points the reaction zone reaches the axis. The temperature fluctuations have a constant value up to x/d = 60 and then they increase sharply. They reach the maximum at a location where the mean temperature is already decreasing. The occurence of the maximum fluctuation outside the reaction zone is also observed in radial profiles. This results from the fact that the combustion air reacts very quickly with the gas in the reaction zone. Outside this zone eddies of cold air and hot gas can exist side by side so that high fluctuations of temperature are found. The increasing fluctuations and the higher mean temperatures in the range from x/d = 80 to x/d = 110 indicate that the reaction takes place intermittently

on the axis.

The correlation coefficient R of fluctuating temperature and velocity is nearly constant and positive up to the reaction zone. The value of R passes through zero inside the main reaction zone and becomes negative further downstream. This behaviour is also observed in the radial profiles.

Fig. 5 shows the radial profiles of the various measured values at x/d = 60 in the dimensionless scale y/d. In addition to the quantities on the axis the mean radial velocity $\bar{v}$ and the shear stress term $\overline{u'v'}$ are represented. The quantities of velocity are normalized with the mean velocity on the axis with the exception of the fluctuating values.

The shear stress term $\overline{u'v'}$ has its maximum at the point of the steepest gradient of the mean velocity $\bar{u}$, where the fluctuating velocities in axial and radial direction are also largest. The profile of the mean temperature $\bar{T}$ ranges from 1050°C on the axis to 1400°C in the reaction zone. The temperature fluctuations increase up to a point sharply after the reaction zone.

The correlation R of fluctuating velocity and temperature is similar to that on the axis. From the middle of the flame outwards the coefficients are positive, pass zero in the reaction zone and then become negative. A check was made as to whether this change of sign was influenced by the seeding system of the LDA. The particles supplied to the jet represent gas and those for the combustion air represent air. Different methods of seeding (particles only in the gas stream or only in the combustion air), however, did not change the behaviour of the coefficients. The negative coefficient indicates that quickly moving eddies occur with low temperature and slow eddies with high temperature. Between the middle of the flame and the reaction zone temperature and velocity fluctuations are in phase.

The measurement of $\overline{u'T'}$ indicates that the $\overline{u'\rho'}$ correlation (velocity-density fluctuation) must have the same behaviour with reversed tendency in the sign, because temperature and density are inversely proportional. Measurements of the velocity and concentration correlation ($\overline{u'c'}$) should give the reversed tendency.

7. CONCLUSION

The application of LDA and compensated thermocouple in flames allow local turbulent properties of the reacting flow to be studied. In particular, the temperature measurement and the correlation velocity-temperature fluctuation give information about the density. The results of the measurements of the flow and temperature field give insight into the relationship of reaction and fluid mechanics.

8. REFERENCES

[1] Durst, F., Whitelaw, J.H.: Theoretical considerations of significance to the design of optical anemometers. Imp. Coll., Mech. Eng. Dept., Report ET/TN/A 15 (1972).

[2] Kleine, R.: Anwendung der Laser-Doppler-Anemometrie zur Bestimmung der turbulenten Flammengeschwindigkeit, Thesis, Universität Karlsruhe (T.H.) (1974).

[3] Kunugi, M., Jinno, H.: 7th Symposium (Intern.) on Comb. 1959, p. 942.

[4] Lenz, W., Günther, R., Hellat, J.: Measurements of fluctuating temperature in enclosed swirling flames, Meeting "Fluid Mechanics of Combustion Processes" 1977, Cleveland, USA.

[5] Lenz, W., Günther, R.: Measurement of fluctuating temperatures in a free jet diffusion flame, Comb. and Flame 37 (1980), p. 63-70.

[6] Günther, R., Wittmer, V.: The turbulent reaction field in a concentric diffusion flame, (to be published).

9. CAPTIONS

Fig. 1: Experimental apparatus

Fig. 2: Step function of a 1st order lag.

Fig. 3: Pulsed heated thermocouple.

Fig. 4: Axial distribution of velocity, temperature and correlation coefficient R.

Fig. 5: Radial distribution of velocity temperature and correlation coefficient R at x/d = 60.

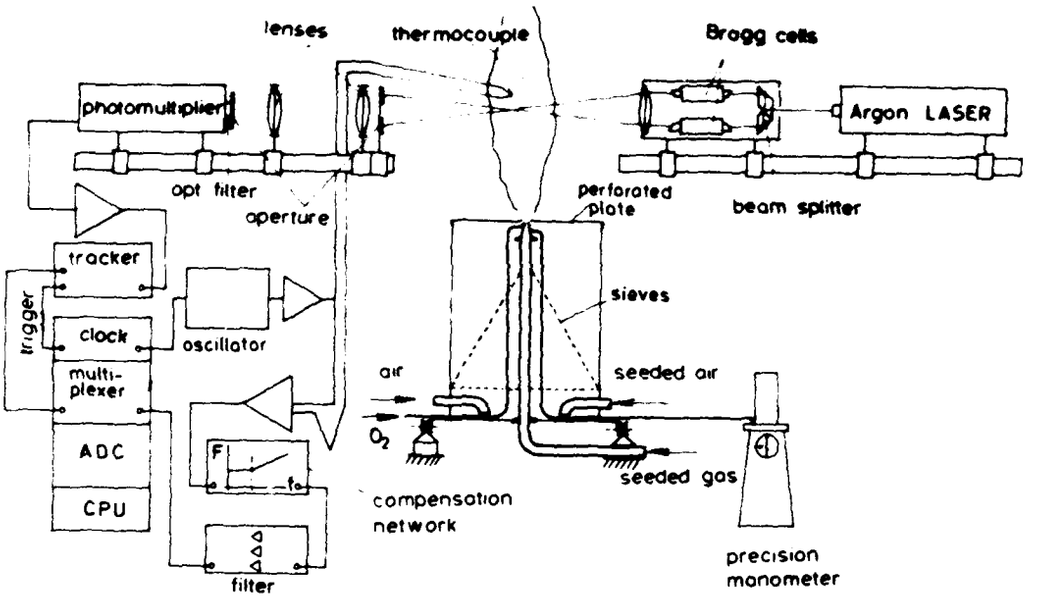

Fig.1

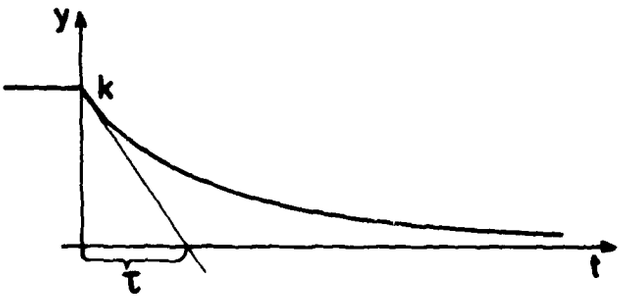

Fig. 2

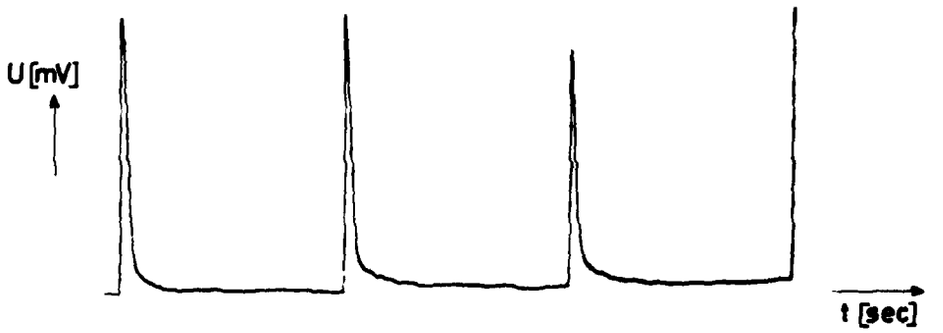

Fig.3

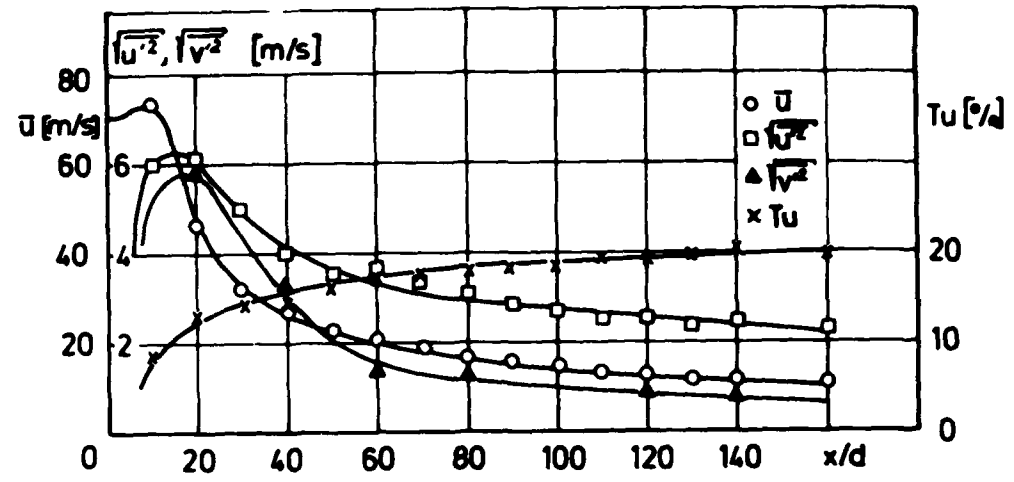

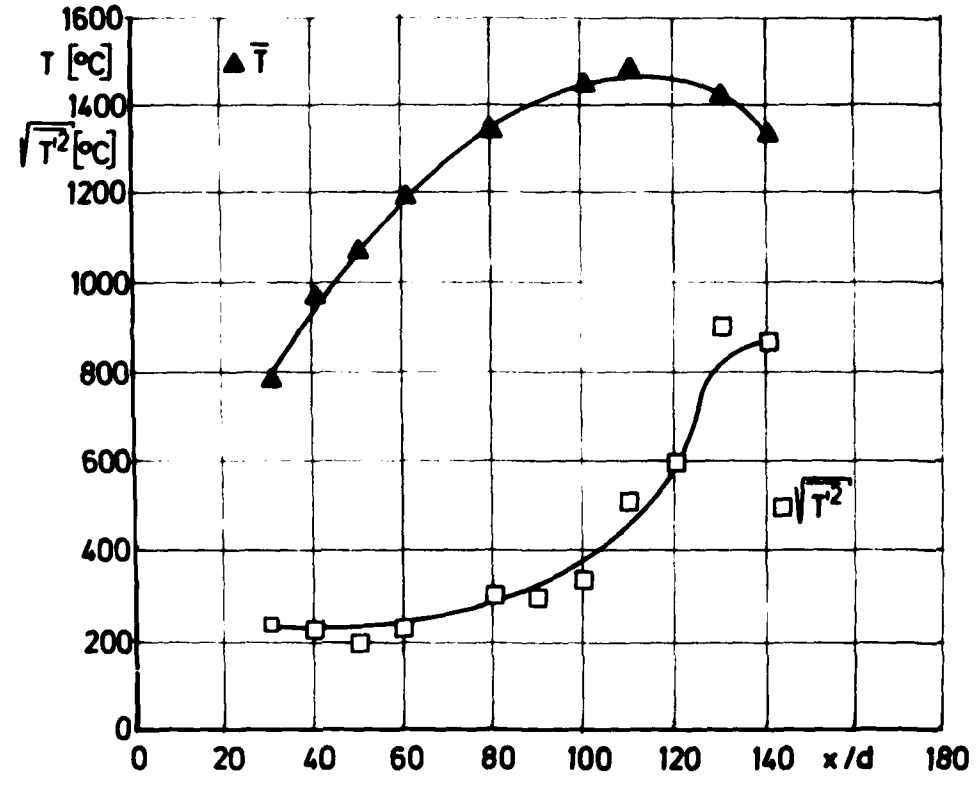

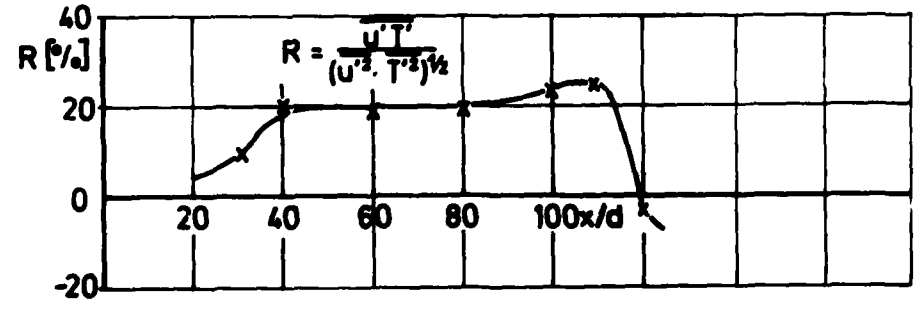

Fig.4

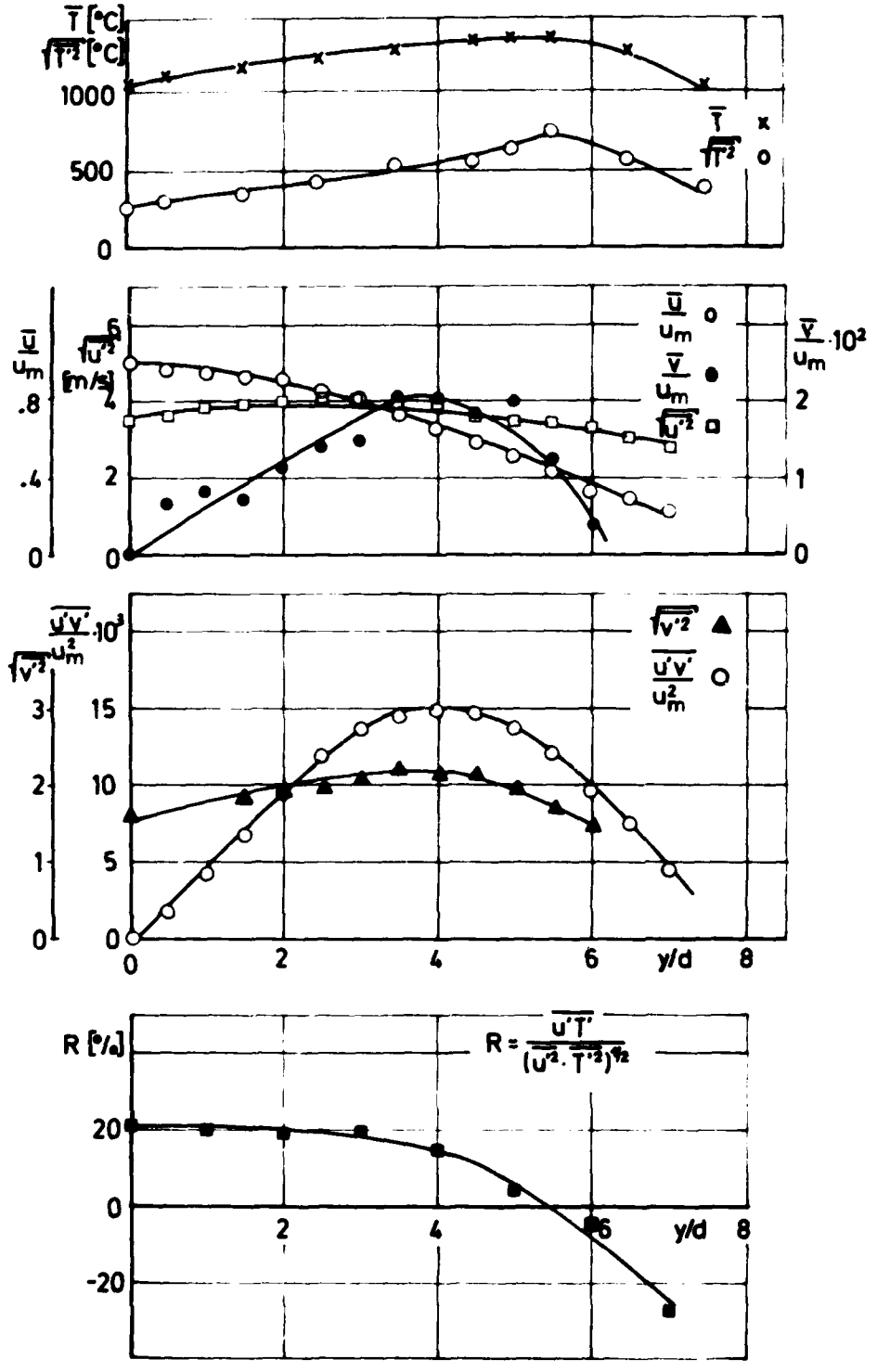
$\overline{T}$ [°C]
$\sqrt{T'^2}$ [°C]
1000
500
0
$\frac{\overline{T}}{\sqrt{T'^2}}$ x o
$\frac{\overline{u}}{u_m}$ o
$\frac{\overline{v}}{u_m}$ ●
$\frac{\sqrt{u'^2}}{u_m}$ □
$\frac{\overline{v}}{u_m} \cdot 10^2$
$\sqrt{u'^2}$ [m/s]
.8
.4
0
6
4
2
2
1
0
$\frac{\overline{u'v'}}{u_m^2} \cdot 10^3$
$\sqrt{v'^2}$
$\sqrt{v'^2}$ ▲
$\frac{\overline{u'v'}}{u_m^2}$ O
3
2
1
0
15
10
5
0
0
2
4
6
y/d
8
R [%]
$R = \frac{\overline{u'T'}}{(\overline{u'^2} \cdot \overline{T'^2})^{1/2}}$
20
0
-20
2
4
6
y/d
8

Fig. 5

DISCUSSION

J.H.Whitelaw, UK

(1) The correlation of discontinuous and continuous signals, each with significant uncertainties, may result in errors. Would you please give an estimate of the error bounds associated with your correlation measurements?

(2) Did you try to measure $v'\overline{T'}$?

Author's Reply

(1) Comparing the data measured at the same point in the flow, we estimate the error of the correlation coefficient to be within 10% of the measured value.

(2) At the moment we are not able to measure $\overline{v'}\,\overline{T'}$ with our experimental equipment.

F.C.Gouldin, US

My questions concern the correction of laser velocimetry data for seeding and velocity bias. First, I notice from your paper that at least the axial velocity data are corrected for velocity bias by weighting the velocity with the reciprocal of the velocity magnitude. Were radial velocity data corrected in a similar manner and, if so, was the reciprocal of the radial velocity magnitude used as the weighting factor?

Secondly, have you considered the influence of seeding particle density bias on your results? In particular I am concerned that your velocity data, corrected for velocity bias, are in fact density weighted due to seeding bias.

Author's Reply

(1) For the radial components we measured the PDF's in three directions (described in the paper). Each PDF was weighted; so the radial velocity is weighted too.

(2) I did not consider the seeding bias errors, but the velocity bias error. I think we do not need to correct for the seed density, because for our measurement a continuous (time resolved) signal was not necessary.

VELOCITY AND TURBULENCE MEASUREMENTS IN TURBULENT FLAMES USING THE L2F TECHNIQUE

by

H. Eickhoff and R. Schodl
DFVLR-Institut für Antriebstechnik
Linder Höhe, 5 Köln 90, W. Germany

SUMMARY

For measuring the flow properties within turbulent diffusion flames a L2F-velocimeter was applied.

Considering the problem of seeding, some basic investigations were carried out within a round free jet. The optically measured mean velocity and turbulence intensities were compared with pitot-tube and hot wire data respectively. The results which are presented and discussed indicate the capability of the L2F velocimeter when it is applied to highly turbulent flows. Mean velocity and turbulence have been measured in hydrogen-air and propane-air diffusion flames under different initial conditions. The results are discussed with regard to the influence of combustion on the turbulent flow field.

1. INTRODUCTION

Combustion influences the turbulent flow field and the interaction between chemical reactions and fluid mechanics is quite complex. There has been made much progress in the development of turbulence models to predict non reacting turbulent flows which now are applied to flows with combustion also. These models containing more or less empirical input need further experimental verification and control, respectively. By the laser technique velocity and turbulence measurements became possible without disturbing the flame and the laser-Doppler-technique has been applied to some diffusion flames.
For the present investigation a different technique, the Laser-Two-Focus (L2F)-method in a comparative study of a series of propane- and hydrogen-flames was applied to investigate the influence of combustion on the turbulent flow field under a variety of different conditions.

2. MEASURING METHOD

The experimental flow studies within turbulent diffusion flames were carried out by using a Laser-Two-Focus velocimeter that is available in the institute. Although this technique has been originally developed for flow investigations within high speed turbomachine rotors it also operates very satisfactorily in turbulent flames.

2.1 Description of the L2F-technique

The worse test conditions in turbomachines (backscatter mode, high flow velocities, flow unsteadyness, narrow blade channels associated with strong background radiation etc.) initiated in 1972 the development of the Laser-Two-Focus-velocimeter (L2F).
This method - the basic idea was originally proposed by Tanner [1] for the application in low turbulent flows - is quite different from the well-known Doppler velocimeter insofar that the fringe pattern within the probe volume is substituted by two discrete parallel light beams forming a light gate and allowing to concentrate the available laser light to very high intensity in the probe volume which leads to favourable signal-to-noise ratios even in worse background radiation situations as in turbomachines.

In order to enable velocity measurements also in highly turbulent flows new optics and a new data processing system have been developed. As a result a very compact apparatus (Fig.1) is now available which is easy to handle and which allows to change the measuring point without any readjustment of the optical parts.

The details within the L2F-probe volume are shown in Fig.2. Due to focusing both

beams have a converging-diverging cross-section with a minimum beam diameter of 10 to 15 µm. The distance between the beams is fixed to about 0.4 mm, whereas the length of the probe volume along the optical axis is limited to ± 0.5 mm from the focal plane. A particle passing through both the light beams emits two successive scattered light pulses, the time interval of which corresponds to the flow velocity perpendicular to the optical axis. The occurrence of those "relevant" double pulses requires however that the plane of the laser beams is parallel to the flow direction which consequently can be determined by turning the plane.

The details of the L2F concept are illustrated in Fig.3. The center of a polarization (Rochon) prism used to split the initial laser beam is located at the focal point of the following lens L_1. Thus, the beam axes leave the lens parallel to each other while the beams themselves are highly focused at the second focal plane of L_1 as shown in detail "A". With the help of lens system L_2 the "light-gate" is forwarded to the probe volume; its distance to the optical device can be adjusted to the actual test environment by applying lens systems L_2 of various focal length. The useful back-scattered light emitted by particles passing through the probe volume is gathered also by lens system L_2 in a confocal way and deflected at the perforated mirror to the microscope optics, which - together with the succeeding dual hole aperture - allows each photomultiplier to be adjusted to one laser beam in the probe volume. Furthermore microscope and aperture minimize the background radiation such that measurements close to walls (≥ 0.5 mm) become possible. The setting angle α (Fig.2) of the laser beams' plane is varied by rotating the beam splitter (Rochon prism). Flight-time measurement and signal processing are performed with modern electronics of high time-response, operating in a start/stop mode.

In laminar flows only a few measurements are needed to evaluate the velocity vector. Turbulent flows, however, require a considerably larger number of individual measurements. In order to analyse turbulent flows adequately, it is expedient to adjust the setting angle α in 8 - 10 steps around the mean flow direction and to take up to 1 000 measurements at each angle step. The collected data are stored and classified along the time axis by means of a multichannel-analyzer (probability density distributions).

Fig.4 shows an oscillogram containing various probability density distributions corresponding to different angles α with respect to the mean flow direction. The x-axis represents the transit time of the particles between the two beams. The quantity of each time-measurement is arranged along the ordinate. Each distribution represents the same number of measuring events. The probability that a particle travelling along with the flow will be irradiated by both laser beams is maximum at the angle position $\alpha = 0^{\circ}$ corresponding to the mean flow direction. The peak of the distribution curve determines the mean velocity, whereas the width of the curve near the baseline indicates the maximum velocity fluctuations. As α increases the probability of particle irradiation by both laser beams decreases rapidly and is - in this case - at $\alpha = 1.5^{\circ}$ practically nonexistent. Negative values of α yield the same results. A combination of all data leads to a two dimensional probability density distribution depending on time difference (velocity $^{-1}$) and angle (setting angle α, see Fig.5) which allow to calculate the mean flow vector (direction and magnitude), the turbulence intensities (in different directions), the Reynold's shear stresses, the skewness-factors, etc. More details on the technique are given in ref.[2] and [3].

2.2 Measurements within a round free jet

To ensure the applicability of the L2F velocimeter to highly turbulent flows some basic investigations were carried out within a round turbulent free jet.

The nozzle had a diameter of 10 mm and was the same as it was employed to the diffusion flames. The test flow was generated by a small centrifugal compressor that sucked the air from the environmental laboratory. By this way the free jet air as well as the

surrounding air were equally seeded by natural dust particles such that no biasing error due to different seeding rates had to be considered.

In order to avoid the particle biasing error, the measured probability distributions were corrected by dividing each value of the histogram by the corresponding velocity $\bar{u}$. This correction as well as the calculation of the axial mean velocity $\bar{u}$, the mean flow angle $\bar{\gamma}$ and the axial turbulence intensity u'^2/u as well as the radial turbulence intensity v'^2/u were performed by a computer that worked on-line to the L2F-electronics.

To verify the optically measured data pitot probe and hot wire measurements were carried out within the same free jet. The pitot probe which was insensitive against flow angle variations was used to measure the mean velocity. The data were corrected by the Goldstein formula considering the local turbulence intensities. The axial turbulence intensities were measured by a hot wire. This measurements were supported by the DFVLR-Abteilung für Turbulenzforschung, Berlin.

In Fig.6 the mean velocity profile measured on the axis of the free jet and the radial turbulence intensities are plotted against x/d (x represents the distance of the measuring point from the nozzle outlet, d the diameter of the nozzle). - The optically measured axial mean velocities $\bar{u}$ which are referred to the mean velocity $\bar{u}_o$ at nozzle exit (open circle symbols) agree within an error smaller than 1 % with the corrected pitot probe data (solid line). The reproductivity of both data was within the same range ($\bar{u}_o$ = 90 m/s, Re = $6 \cdot 10^4$).

The radial turbulence intensities were only optically measured (triangles in Fig.6). The range of uncertainty which increases with flow turbulence is indicated in the diagram. When comparing these data with the axial turbulence intensities (see Fig.7) the flow turbulence is found to be rather isotropic up to x/d = 10. At higher values of x/d the radial turbulence intensity is always lower than the axial one as it is well known from other free jet measurements. The agreement of the optically measured turbulence intensities with the hot wire data (see Fig.7) is also very good except the deviations at higher turbulence intensities.

As it is shown by these results the L2F velocimeter is an instrument appropriate for performing measurements within turbulent flows. This, however, in true as far as the turbulence intensity does not exceed 35 %. Beyond that limit a considerable portion of the statistically fluctuating velocities approach sero which can not be measured by the L2F-technique. In this case a Laser Doppler velocimeter with frequency shifting is recommandable.

3. FLAME MEASUREMENTS

3.1 Experimental Arrangement and Conditions

The measurements were performed with an argon ion laser at 100 mW power and 5145 Å wave length. The experimental test rig is shown in Fig.9. The L2F-system was fixed and the axial position of the measuring point was varied by moving the burner along the axis of the working section.

Measurements have been performed with propane and hydrogen as the fuel, respectively. The central fuel jet issuing from a contured nozzle was seeded with SiO_2-particles. Initial conditions of the different flames investigated are listed in table 1. The maximum external air velocity was 1 m/s.

TABLE 1:

Flame No.	$u_o [\frac{m}{s}]$	O_2	Flame No.	$u_o [\frac{m}{s}]$
1	54	$+O_2$	5	115
2	54	-	6	195
3	40	$+O_2$	H_2 - jet	195
4	40	-		

a) propane, d = 10 mm b) hydrogen, d = 5 mm

In order to get propane-flames burning stable at the nozzle exit a small amount of oxygen was added through a concentric nozzle as shown in Fig.9A. Flames No.2 and 4, Table 1a, without oxygen addition are lifted with ignition taking place at about x/d = 20. Furthermore hydrogen-flames at two different nozzle - exit velocities u_o = 115 and 195 m/sec burning stable at x/d = 0 were investigated together with a non burning hydrogen jet, Table 1b.

When optical velocimeters are applied to diffusion flames the problem of seeding must be considered because artificial seeding is required which must be resistant to the high temperatures. It is difficult to ensure an equal seeding rate of the internal nozzle flow and of the surrounding air; it is much easier to seed only the internal flow, that, however, will probably lead to biased measurements.

In order to estimate experimentally these errors which have been discussed by Glass and Bilger [5] free jet tests were performed with an alternate seeding of the internal nozzle flow and of the environmental air. The various results of these measurements are shown in Fig.8. In comparison to the pitot probe data the optically measured velocities turn out to be somewhat higher in the case of internal nozzle flow seeding and lower in the case of only seeding the environmental air. The influence of the different seeding on the turbulence intensities is opposite compared to the hot wire data.
As the experimental arrangement for the flame measurements did not allow uniform seeding, the cold flow investigations of the seeding bias effect may be taken as an indication of the possible error of a few percents with central seeding only.

3.2 Results and Discussion of Turbulence Measurements

In Fig.10 the centreline axial turbulence intensity and velocity for two propane flames (No. 1 and No.2) with the same nozzle exit velocity of u_o = 54 m/sec are shown. Flame No.1, burning at x/d = 0 by oxygen stabilization has a lower turbulence intensity up to x/d = 40 compared to flame No.2 which is lifted up to about x/d = 20. With the onset of combustion in flame No.2 the turbulence intensity decreases and downstream is even lower than in flame No.2. This is due to different reasons among which the buoyancy is an important one; the influence of buoyancy on the propane flames can also be seen from Fig.13 where the axial velocities on the centreline are shown.

Although the turbulence intensities in the two flames are very different, the dashed lines in Fig.10 indicate nearly the same maximum turbulence velocities of about 5 m/sec. In the next Fig.11 centreline axial turbulence intensities of all four propane flames are compared to the turbulence intensity in an air jet.

Radial profiles at x/d = 15 of the local axial turbulence intensity and velocity of flame No.1 and flame No.2 which at this axial position is a non burning propane jet are compared in Fig.12. Due to the smaller width of the flame (No.1), the turbulence intensity increases more rapidly in radial direction. In contrast to the behaviour of non

reacting turbulent jets the fluctuating velocity $(\overline{u'^2})^{1/2}$ strongly increases in radial direction and has a maximum value of about twice that on the centreline.

Mean axial velocities on the centreline of a H_2-jet and of a H_2-flame, No.6, are compared to those of propane flames No.1 - 4 in Fig.13. The more rapid spreading of the H_2-jet and H_2-flame becomes obvious. There is nearly no decrease of axial velocity in the propane flames up to x/d = 15.

In the next Fig.14 the centreline axial turbulence intensities in the two H_2-flames No. 5 and 6 being not very different from each other are compared to the turbulence intensities in the two propane flames No.1 and 3, which are not lifted.
The turbulence intensities in the hydrogen flames being much larger over the whole x/d-range than in the propane flames are at the first ten nozzle diameters even larger than in the air jet, Fig.15. But if comparing these results, the Reynolds-number dependence of $(\overline{u'^2})^{1/2}/u$ in turbulent jets has to be considered also. The upper curve representing the non burning H_2-jet indicates only a slightly higher turbulence intensity compared to the H_2-flame.

3.3 Flow Vizualisation

Comparing the results of the measurements in the propane- and hydrogen-flames the largest differences are observed within the region of developing turbulence.
Although no quantitative results could be expected a series of Schlieren pictures had been made in order to study the structure of the flow in the initial regions of the flames.

Figures 16, a - c show pictures of propane diffusion flames at different nozzle exit velocities, the nozzle diameter being 5 mm. Flames a and b, Fig.16, are burning stable at the nozzle exit without O_2-addition, flame c is stabilized by oxygen. The light part of nearly cylindrical shape inside indicates the reacting interface and the onset of inner instability of the laminar shear layer can be observed at about x/d = 2-3. Detailed investigations of the stability of the laminar shear layer in some turbulent diffusion flames have been performed by Recknagel [6]. Michalke [7] has studied theoretically the influence of variable density on the stability of a laminar shear layer.

The outer dark region indicates the preheat zone and it seems that there is no strong interaction between this flow regime and the inner jet, the non reacting interface of low density separating both regions. This becomes obvious also from the onset of ring vortices in the preheat zone far downstream.
Fig.16.b shows a similar situation with the onset of inner instability nearer to the nozzle and a less orderly structure of the flow. Extensive measurements in the initial region of propane diffusion flames at low velocities have been performed by Yule and Chigier [8] and the coherent structure of the flow field has been discussed in detail. From Fig.16.c the onset of fully turbulent flow downstream at x/d = 15 - 20 can be seen, the vortical structure near the nozzle being caused by the oxygen flow.

Figures 17.d - i indicate the different behaviour of hydrogen flames. Beginning with an orderly structure of ring vortices in the preheat zone the flow becomes fully turbulent near the nozzle. Up to the onset of turbulent flow the reacting interface of nearly cylindrical shape can be identified inside the preheat zone. A similar structure as in non reacting plane shear flows [9] with regard to longitudinal streaks (Fig.17, g and h) can be observed. From the Schlieren pictures it becomes obvious also that the hydrogen diffusion flames which have been investigated by the L2F method are fully turbulent immediately behind the nozzle. Detailed measurements in a hydrogen-diffusion-flame which had a regular structure of ring vortices up to x/d = 20 have been made by Altgeld [10].

4. CONCLUSIONS

As it was proved by free jet tests the L2F-velocimeter operates very satisfactorily and no additional problems arised when it was applied to turbulent diffusion flames. Although only the internal nozzle flow was seeded the resultant measuring errors were found to be rather small.

Concerning the turbulence in diffusion flames several influences of combustion can be identified. The region of developing turbulence is strongly influenced if the density in the initial region is remarkably changed by combustion. Variable density influences the stability of a free shear layer [6, 7] and similarly it acts on the development of turbulence.
Heat release by combustion may have a damping effect on the turbulence as can be concluded from the measurements in those propane flames with ignition taking place downstream at about x/d = 20. This was pointed out also by Bray [11], who discussed the turbulence energy equation for variable density flows. Furthermore buoyancy has an damping influence on the turbulence intensity.

Concerning the capability of turbulence models to predict diffusion flames the present experimental results explain the fact that turbulent hydrogen diffusion flames reasonably well can be predicted by the k-ε-model [12], which has been extensively tested for constant density flows. With regard to hydrocarbon flames the flow field is strongly influenced by the region of developing turbulence and this is out of the scope of the k-ε-model. However, the influence of variable density on the turbulent mixing process partially can be accounted for by a density dependent term in the shear stress expression [13].

REFERENCES

[1] Tanner, L.H.: "A Particle Timing Laser Velocity Meter". Optics and Laser Technology, pp.108-110, June 1973.

[2] Schodl, R.: "Laser-Two-Focus-Velocimetry (L2F) for Use in Aero-Engines". AGARD-LS-90 (1977).

[3] Schodl, R.: "Development of the Laser-Two-Focus Method for Non-Intrusive Measurement of Flow Vectors, particularly in Turbomachines". ESA-TT-528. (1979).

[4] McLaughlin, D.C., and Tiederman, W.G.: "Biasing Correction for Individual Realization of Laser Anemometer Measurements in Turbulent Flows". The Physics of Fluids, Vol.16, No.12 (1973).

[5] Glass, M., and Bilger, R.W.: "The Turbulent Jet Diffusion Flame in a Co-Flowing-Stream - Some Velocity Measurements". Combustion Science and Technology (1978), Vol.18, pp.165-177.

[6] Recknagel, J.: "Untersuchungen zur Stabilität der Trennungsschicht bei Freistrahlflammen". Diss.Univ.Karlsruhe (1969).

[7] Michalke, A.: "Der Einfluß variabler Dichte auf die Instabilität einer freien Scherschicht". Ing.-Archiv 40 (1971), pp.29-39, Springer-Verlag.

[8] Yule, A.J., and Chigier, N.A.: "Coherent Structures in Turbulent Flames". AFOSR-77-3414, Univ.of Sheffield (1979).

[9] Bernal, L.P., et al: "On the Development of Three Dimensional Small Scales in Turbulent Mixing Layers". 2nd Symp.on Turbulent Shear Flows, London (1979), 8.1.-8.6.

[10] Altgeld, J.H.: "Laser-Doppler-Messungen in einer turbulenten Wasserstoff-Luft-Diffusionsflamme". Diss.TH Aachen (1979).

[11] Bray, K.N.C.: "Kinetic Energy of Turbulence in Flames". AASU Rep. No.332 (1974), Univ. of Southampton.

[12] Bilger, R.W.: "Turbulent Jet Diffusion Flames Prog. Energy". Combust.Sci.(1976), Vol.1, pp.87-109.

[13] Eickhoff, H., Grethe, K., and F. Thiele: "Turbulent Reaction and Transport Phenomena in Jet Flames". AGARD-CPP-275 (1979).

FIGURES

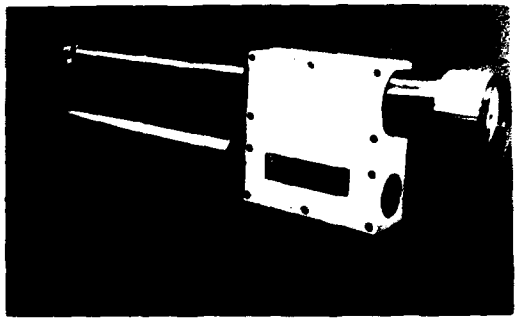

Fig.1 Photograph of the Laser-Two-Focus Velocimeter

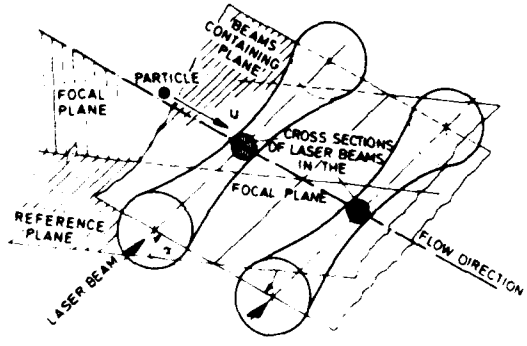

Fig.2 Laser-Two-Focus probe volume (principle sketch)

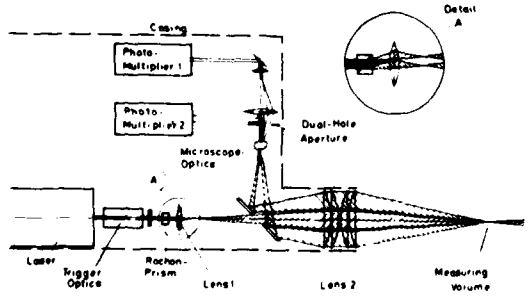

Fig.3 Optical set-up of Laser-Two-Focus velocimeter

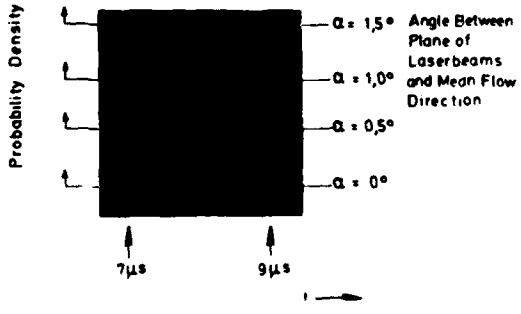

Fig.4 Output-signal of the electronic data processing system

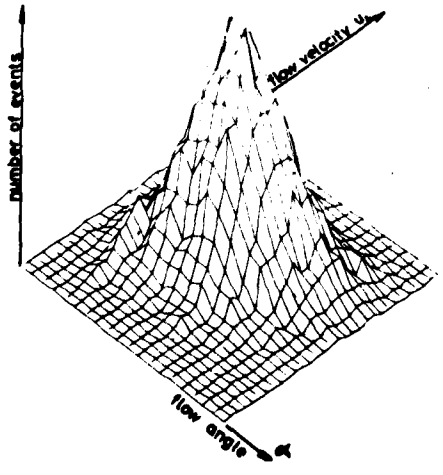

Fig.5 Measured two-dimensional probability distribution

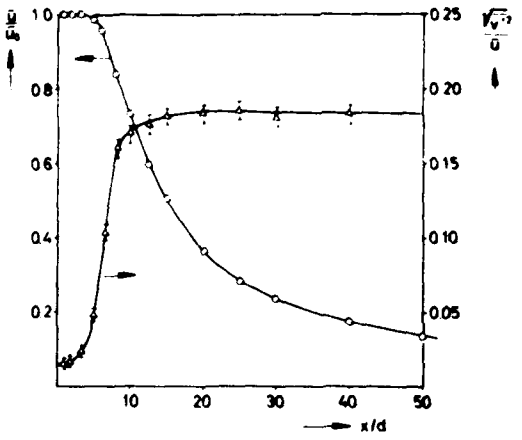

Fig.6 Results of different measurements on the axis of a turbulent free jet

— axial mean velocity measured by a corrected pitot probe

o axial mean velocity measured by the L2F velocimeter

Δ radial turbulence intensity measured by the L2F velocimeter

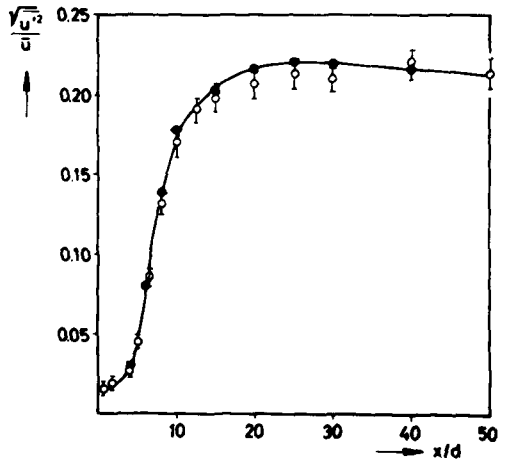

Fig.7 Axial turbulence intensity within a turbulent free jet

results of different measurements

● Hotwire-measurements

o L2F-measurements

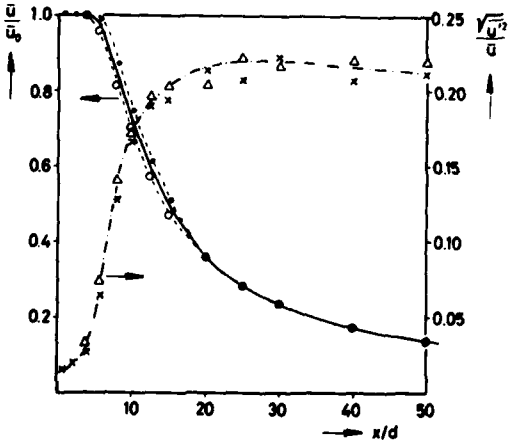

Fig.8 Results of L2F-measurements within a turbulent free jet
- the seeding was varied.

● axial mean velocity
- seeding the internal nozzle flow

o axial mean velocity
- seeding only the environmental air

x axial turbulence intensity
- seeding the internal nozzle flow

Δ axial turbulence intensity
- seeding only the environmental air

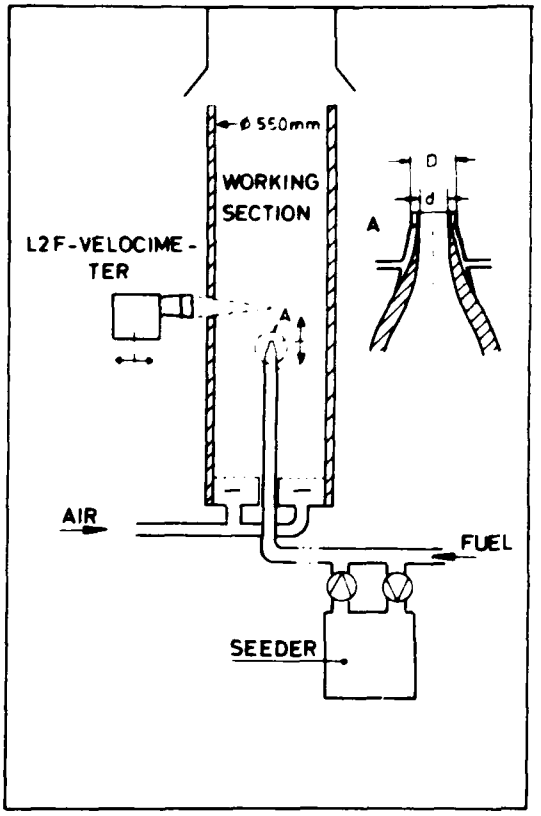

Fig.9 Experimental test rig

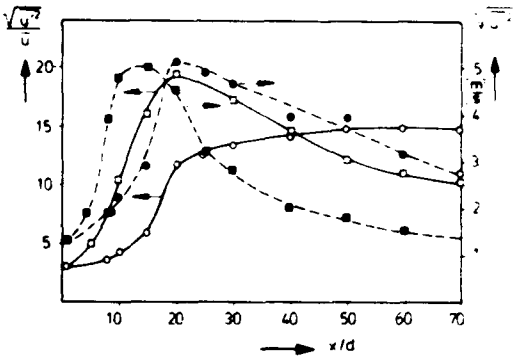

Fig.10 Centreline axial turbulence intensity and velocity

—o— —●— flame 1; propane
—□— —■— flame 2

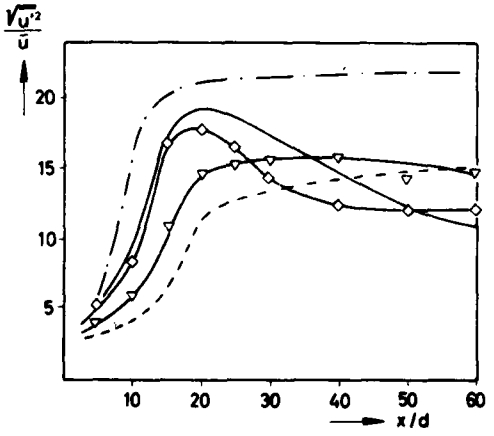

Fig.11 Centreline axial turbulence intensities in propane flames

—▽— flame 3; —◇— flame 4,
--- flame 1; —— flame 2;
—·— air jet

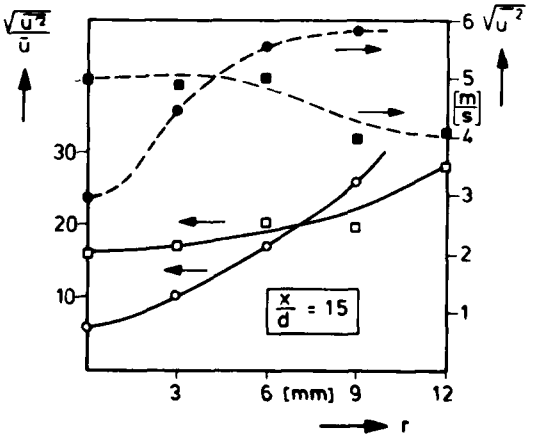

Fig.12 Radial profile of axial turbulence intensity and velocity

—o— —●—propane flame 1
—□— —■—propane jet (flame 2)

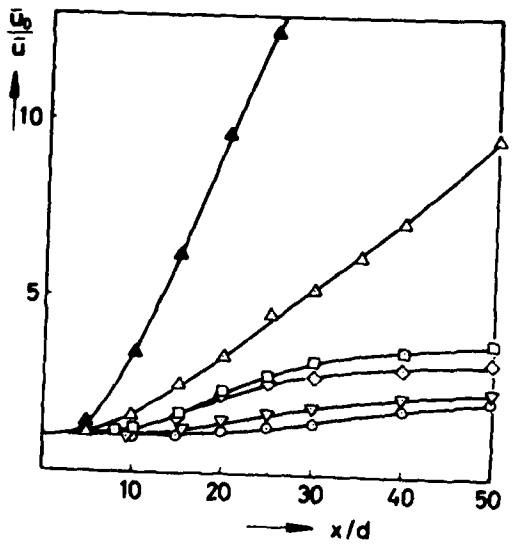

Fig.13 Velocity-ratios $\tilde{u}_o/\bar{u}$ on centreline

—▲— H_2-jet; —△— H_2-flame 6;
-o-□▽◇ propane flames 1,2,3,4

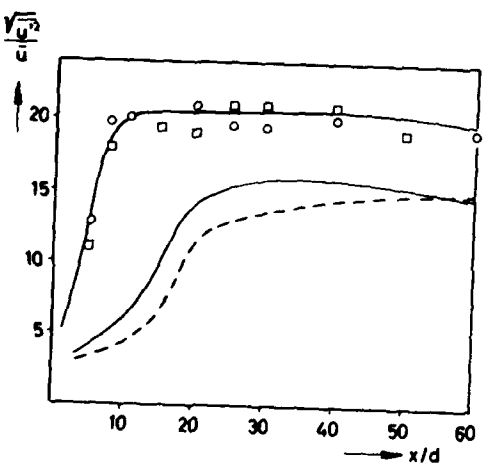

Fig.14 Centreline axial turbulence intensities

—o—flame 5 } H_2
—□—flame 6 }

——flame 3 } propane
----flame 1 }

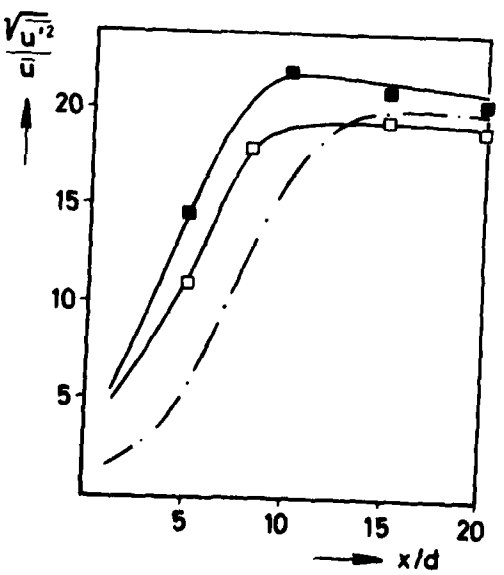

Fig.15 Centreline axial turbulence intensities

—●— H_2-jet; -o- H_2-flame 6;
-·- air jet

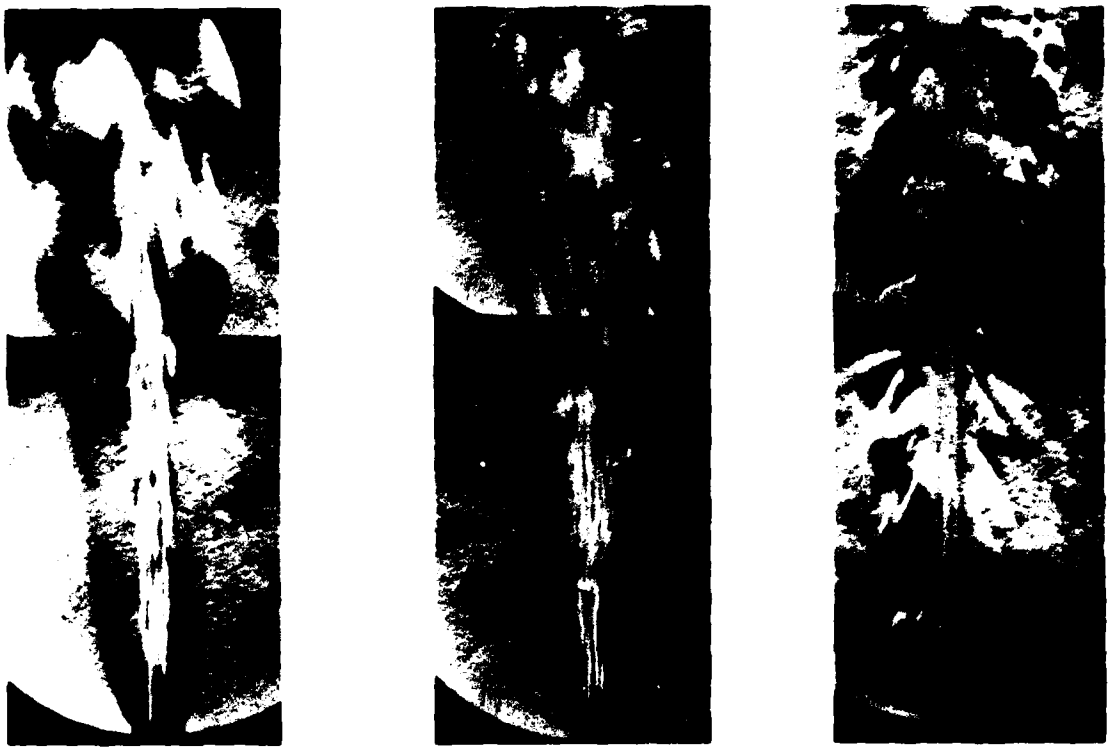

a) u_o = 6,5 m/s b) u_o = 15 m/s; c) u_o = 56 m/s

Fig.16 Schlieren pictures of propane flames; (d = 5 cm); exposure time 1/1000 s.

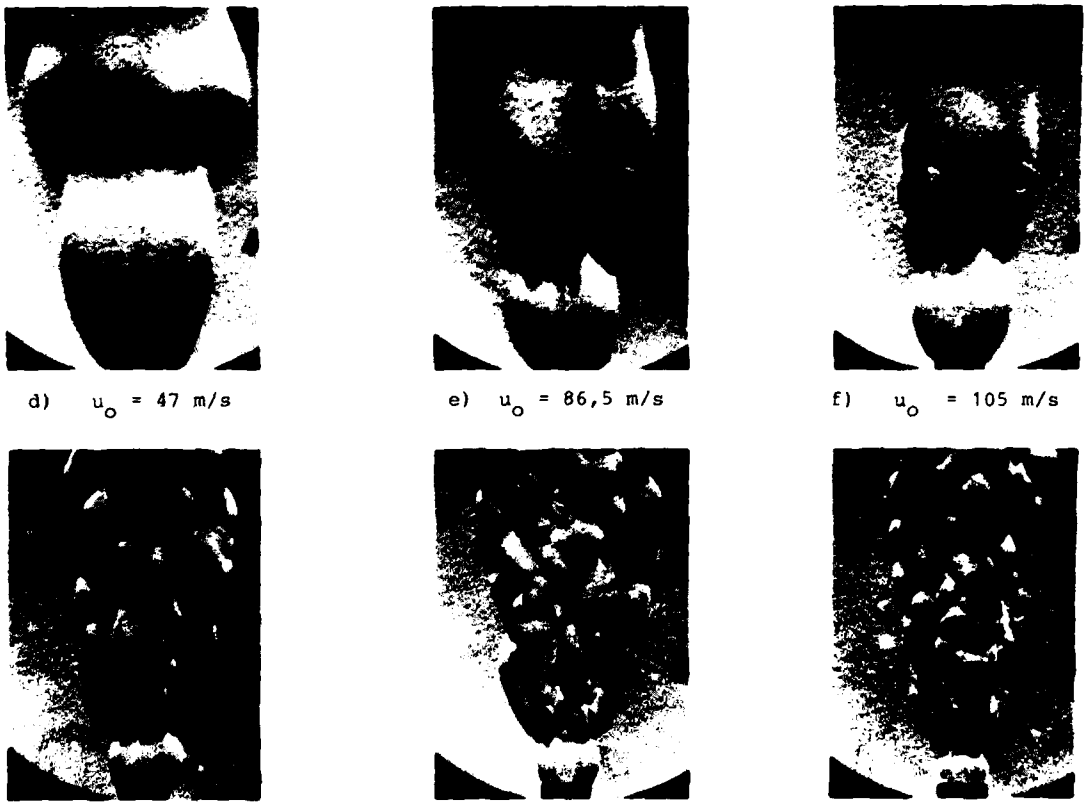

d) u_o = 47 m/s e) u_o = 86,5 m/s f) u_o = 105 m/s

g) u_o = 136 m/s h) u_o = 195 m/s i) 315 m/s

Fig.17 Schlieren picture of hydrogen flames; (d = 5 cm); exposure time 1/1000 s.

DISCUSSION

G.Kappler, Ge

(1) Did you have to seed your flame or was seeding only necessary in order to reduce measuring time?

(2) Could you comment on the application of the L2F method for measurements in a real combustor primary zone? Will the seeds really follow the highly turbulent flow with sharp and sudden changes of flow direction?

Author's Reply

(1) In flames seeding is absolutely necessary.

(2) The L2F technique can be applied to every turbulent flow if the level of turbulence does not exceed a value of about 35%.

It is a basic problem how far particles exactly follow a highly turbulent flow. Shock-experiments have been performed indicating that small particles follow rapid changes.

J.H.Whitelaw, UK

(1) Over a number of years, the turbulence intensity in a fully developed jet seems to have decreased to an accepted level of around 25%. Your results show 22.5%. Can you explain this further reduction?

(2) The influence of seeding is known to be negligible on the centre line but significant at large radii.

(3) A comparison between a mixing layer, such as that of Brown and Roshko, and a jet should be undertaken with great care. In the two dimensional mixing layer, the structure is also two dimensional and is destroyed by small amounts of turbulence in either of the free stream flows.

Author's Reply

(1) Obviously the level of turbulence depends on the measuring technique. It is difficult to give a conclusive answer.

(2) Our comparison shows quantitative data concerning the influence of seeding on the axis. It is true that with increasing radii the outer flow must be seeded also.

(3) The comparison was made based on short-time Schlieren pictures not shown in the written report. Of course such a comparison must be made carefully. The main difference seems to be not the fact that we have a flow of rotational symmetry, but that there is a flame which has a decoupling effect, separating an inner flow with high frequency vortices and an outer flow of low frequency vortices. The different stages of developing turbulence, including orderly structures, are very similar to those in a plane shear layer.

M.Ballarin, Fr

Can you compare approximately the time necessary to do measurements in flows where the levels of turbulence are respectively 10% and 30%?

Author's Reply

I cannot give exact values, but with higher levels of turbulence the measuring time increases rapidly.

W.G.Alwang, US

Is it possible with the L2F to measure velocity cross correlations and velocity-temperature cross correlations?

Author's Reply

I don't know whether it is possible to measure velocity-temperature cross correlations, I did not consider this point. I don't see that it could be possible; but it is possible of course to measure velocity cross correlations.

VELOCITY MEASUREMENT TECHNIQUES IN LIQUID SPRAYS USING LASER DOPPLER VELOCIMETRY

M.L. RIETHMULLER
Associate Professor

J-M. BUCHLIN
Assistant Professor

von Karman Institute for Fluid Dynamics
Chaussée de Waterloo, 72
B-1640 Rhode Saint Genèse, Belgium

SUMMARY

In many applications there exists a velocity lag between droplets and a surrounding gas. The measurement of gas velocity must therefore be performed separately from the measurement of droplet velocity. This is the objective of a technique implemented in order to measure gas velocity in the presence of droplets. A laser velocimeter adjusted for reference beam mode has been used in a water spray. Satisfactory results are obtained and it is shown that, providing the gas flow is correctly seeded with small particles a velocity measurement of gas velocity is yielded even with a large number of droplets.

1. INTRODUCTION

Spraying of liquids is encountered in a wide range of applications such as cyclone separators, dryers, humidification towers, combustors. In most cases the spraying mechanism involves a mixing and entrainment of gas. Numerical models of this process have been developed and there is a need for experimental validation in order to qualify these models. For more than eight years it has been possible to measure the velocity of droplets using a laser doppler velocimeter. Other means have been used in the past all based on photographic techniques. These techniques involved tedius data reductions and the laser doppler velocimeter appeared as an important improvement. The investigations in spraying processes have now advanced such that the measurement of the velocity of droplets is no more sufficient. Since a considerable velocity lag exists between droplets and gas entrained, it is necessary to make available an instrument that measures the gas velocity in the presence of droplets. Since optical techniques appear to be the most convenient ones, it was a logical step to adapt the laser doppler velocimeter to gas velocity in the presence of droplets.

2. STATEMENT OF THE PROBLEM

The problem of measurement of gas entrainment is best illustrated by the laser photograph of figure 1. Smoke is visualizing the gas streamlines while the droplets are clearly visible. Gas is entrained perpendicular to the edge of the spray and is then directly turned downward. However, the gas does not follow the droplet trajectories. In this picture, droplets are made fluorescent with a suitable dye. Oil smoke is the tracer for the gas. If a standard laser velocimeter, adjusted for gas measurement is used, signals are yielded by the scattering of light by oil smoke particles but also by laser droplets. It is therefore very difficult to discriminate between smoke and droplets.

Because of the framework in which the present investigation has been performed, industrial water spray nozzles such as the one shown on figure 2 have been used. The nozzle shown produces a full cone spray of coarse droplets : mean drop diameter is ranging from 0.1 mm to 1 mm. Since particles suitable for seeding are in the range of .1 to 1 x 10^{-3} mm we have to solve a problem of measurement of the velocity of two very different particle sizes and thus of two very different ranges of scattering levels.

3. MEASUREMENT TECHNIQUE

3.1 Principles

Laser doppler velocimetry has now become a well known technique and is widely used. Most applications are based on the use of the crossed beam mode in which the measurement volume is obtained by the intersection of two laser beams of equal intensity. This mode is also sometimes called fringe mode (Ref. 1). In this configuration, receiving optic unit may be placed anywhere in space.

Another technique used more often in water flows (Ref. 2) is the reference beam mode. Figure 3 illustrates the basic principle of this mode. In this configuration, the photodetector is aligned with one of the two beams which is of much lower intensity than the other one.

If a very small particle crosses the crossover region of the two beams, it scatters light from the intense beam 2 in all directions and in particular to the photodetector. The latter is also aligned with the reference beam and an heterodyning process occurs between scattered radiation and reference beam thus providing doppler difference. The performance of such a system can only be retained if the following conditions are fulfilled:

- proper matching between reference beam and scattering light level;
- alignement of photodetector with respect to the reference beam;
- reference beam must not be obstructed by scattering particles.

The last requirement implies that doppler signals of significant quality are only obtained with small particles.

It has already been shown that the crossed beam mode is perfectly suited to the measurement of the velocity of large particles. The suitable optical arrangements are described in references 3 and 4.

Because of the last requirement for good performances of reference beam mode, this arrangement appears to be very poorly adapted to large particle measurement. This disadvantage might be taken to the advantage of the measurement of small particles since it will only respond to the small tracers entrained by the gas. Although a large amount of light might reach the photodetector when a large particle crosses the probe volume, the doppler component of the signal will only be very weak if existent.

We can therefore adapt a laser doppler velocimeter to the task of measuring either droplet velocity (crossed beam) or gas velocity (reference beam). Such a method has already been used in two phase gas/liquid flows where both liquid and bubble velocity had to be measured. An example of such development is shown in reference 5.

3.2 Practical arrangement

The practical arrangement used for the implementation of the present reference beam technique is shown at figure 4. The laser is a HeNe of 15 mW, the illuminating optic unit is detailed on figure 5. Neutral density filters are used in order to adjust the intensity level of the reference beam. In the present case, the diameter of the probe volume is of the order of 0.15 mm.

Behind the photomultiplier, the electronic chain is essentially made out of a period counter (VKI DO 78-3A). An oscilloscope is used to monitor the signal yielded by the photomultiplier. The ratio between the intensity of the reference beam and the main one is of the order of 1 to 1000. This ratio is to be carefully adjusted for optimum signal to noise ratio.

An oil smoke generator is used in order to provide scattering tracers. The smoke is injected in a chamber installed above the spray nozzle with an outlet surrounding it. This ensures that a proper seeding is obtained.

The nozzle is installed in a special facility provided with pumps, metering units and water collector. Illuminating and receiving optic units are installed at about 1.5 meter apart and each of them is protected against water droplets.

3.3 Application of the measurement technique

The working principle of the measurement technique is best illustrated by the oscilloscope traces shown on figure 6. The bottom trace is the signal yielded by the photodetector. Each negative peak corresponds to the passage of a large drop in the reference beam. The upper trace is the corresponding filtered signal as shown after amplification. This is the doppler component of the bottom signal. The comparison between upper and lower traces clearly shows that to each passage of a drop corresponds an absence of doppler component. This figure demonstrates that the system actually works correctly : large drops do obstruct reference beam and therefore cancel out doppler signals. It can therefo e be concluded that the velocity measured will be that of gas tracers and not that of the large drops.

A verification of the correct behaviour of the system is made by comparing the number of signals yielded by the doppler processor with and without smoke. With a proper trigger level adjustment, the ratio between these numbers is larger than 50. Even when the measurements are performed without external seeding a certain number of signals are still processed. They correspond to smaller droplets, always present in a spray and to very few drops which cross the probe volume at its outside boundary. In actual measurement these spurious measurements only account for less than 1% error.

3.4 Limitations of the technique

Although, the use of reference beam mode allows a proper measurement of gas velocity in the presence of droplets, this technique has its limitations. The reference beam is obstructed by all drops which are crossing it and which are of sufficiently large diameter. This means that not only those droplets crossing the probe volume will cause a drop in the signal, but also those which are crossing it along the whole length. Fortunately, the reference beam has its minimum diameter at the probe volume and rapidly diverges. This limits the length over which the droplets are completely obstructing the beam. However, when the concentration of droplets increases, there is always more than one droplet at a time crossing the reference beam. This causes the system to be saturated, no proper measurement can be taken anymore. This type of limitation is illustrated at figure 7. The bottom trace shows the signal yielded by the photomultipliers : individual passage of droplets can hardly be detected. With a higher concentration, the signal becomes essentially made out of noise.

Another limitation of the method lies in the relative size of probe volume compared to droplet diameter. For the technique to work at its optimum, droplets should be much larger than probe volume.

These two limitations could be overcome by using a beam expander between the laser and the illuminating optic unit : this would result in a reference beam of larger diameter almost everywhere but the probe volume which would be considerably reduced in size. Such an improvement has still to be tested.

4. EXAMPLES OF MEASUREMENT

Measurements of both droplet and gas velocities have been performed in an industrial water spray. Droplet velocity measurement is usually made with a crossed beam arrangement whereas reference beam mode is used for gas velocity (smoke tracers). Velocities measured in a spray at a distance of 500 mm from the nozzle orifice and 100 mm from the centerline is presented at figure 8 for different water flow rates. As expected, entrained gas velocity is always lower than droplet one. Both velocities increase with water flow rate.

Further measurements are presented in figure 9. The upper graph represents the velocity of droplets. Velocity of gas is shown on the lower one. The measurements have been made at three different locations. The results obtained are in good agreement with expected trends: gas and droplet velocities are decreasing with increasing distance from nozzle. Centerline velocities are also higher than velocities measured along the transversal direction.

During these qualification measurements, it was found that a reliable result could only be obtained after careful adjustment of the optical set-up and proper tuning of the doppler processor. Most sensitive parameters are the ratio of light intensity between reference beam and main one and trigger level adjustment on the processor. This system allows a discrimination between noise and signal which is critical at high flow rates. Finally, seeding level of the gas must be constant and a rather high concentration of tracers is required.

5. FURTHER DEVELOPMENTS AND RECOMMENDATIONS

The present measurement technique has been implemented using already existing equipment. Considerable improvements in the range of operation and convenience of use would be obtained if a specialized optical arrangement is developed for this particular technique. Both illuminating and receiving units could be optimized : illuminating ones should include a beam expander and variable beam splitting ratio. Receiving one could be optimized with other kinds of photodetectors.

In the processing chain, some tests have been made with a large particle detector controlling an inhibition of the processing. This device proved to improve the discrimination between tracers and larger droplets. Although this was not needed in the present application, it could allow an extension of the range of operation for smaller droplets.

6. CONCLUSION

A laser velocimeter of reference beam type has been used to measure gas velocity in a water spray. Although the adjustment of the optical system is somewhat delicate, good results have been obtained. Examples of measurement are shown and demonstrate the usefulness of such a technique. Limitations in the range of operation have been found but modifications that would improve this range are suggested. The overall results obtained here represented a strong encouragement to further develop the application of reference beam modes in two phase flows.

REFERENCES

1. DURST, F.; MELLING, A. & WHITELAW, J.W.: Principles and practice of laser doppler anemometry. Academic Press, 1976.
2. OLDENGARM, J.; VAN KRIEKEN, A.H.; & RATERINK, H.: Laser doppler velocimeter with optical frequency shifting. Optics and Laser Technology 5, 1973, pp 249.
3. RIETHMULLER, M.L.: Optical measurement of velocity in particulate flows. VKI LS 54, 1973, "Measurements of velocities in single and two-phase flows".
4. RIETHMULLER, M.L. & GINOUX, J.J.: The application of a laser doppler velocimeter to the velocity measurement of solid particles pneumatically transported. Proc. Pneumotransport 2, Paper D 3, BHRA Fluid Eng., 1973.
5. DAVIES, W.E.R.: Velocity measurements in bubbly two-phase flows using laser doppler anemometry. UTIAS TN 184, 1973.

Fig.1 Visualization of the entrainment

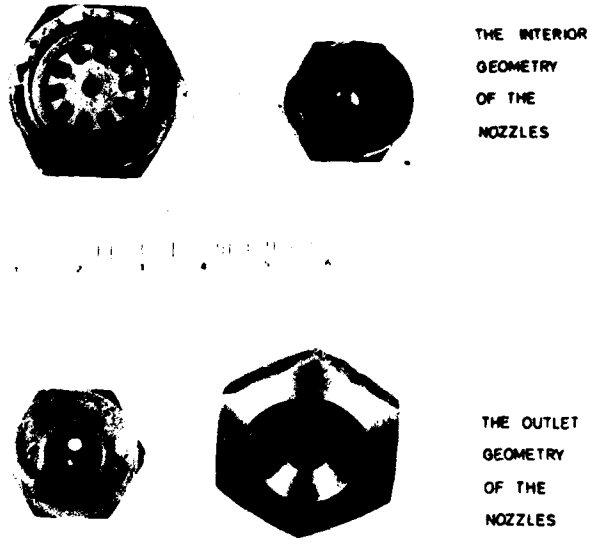

LEFT NOZZLE	: TYP SZ 2	RIGHT NOZZLE	: TYP SZ 1
NOZZLE No	402924	NOZZLE No	402 843
ANGLE	: 60° ∢	ANGLE	45° ∢
DIAMETER	5,8 mm ϕ	DIAMETER	4,4 mm ϕ
MATERIAL	. BRASS	MATERIAL	: BRASS

Fig.2 Industrial nozzles

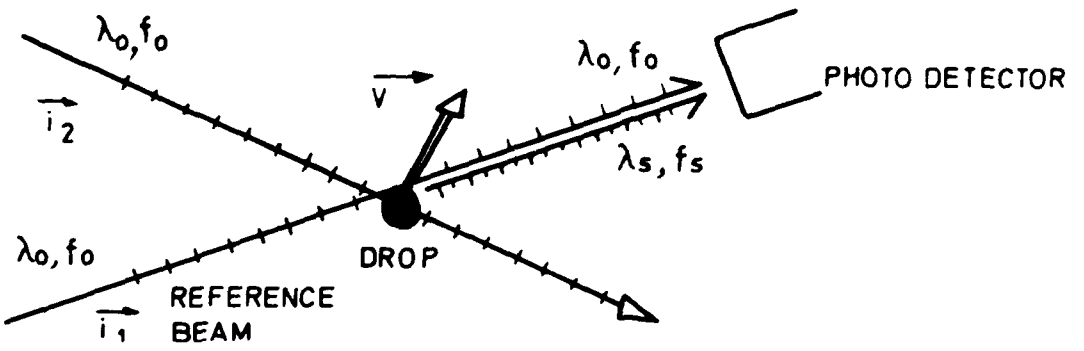

Fig.3 Reference beam mode – principles

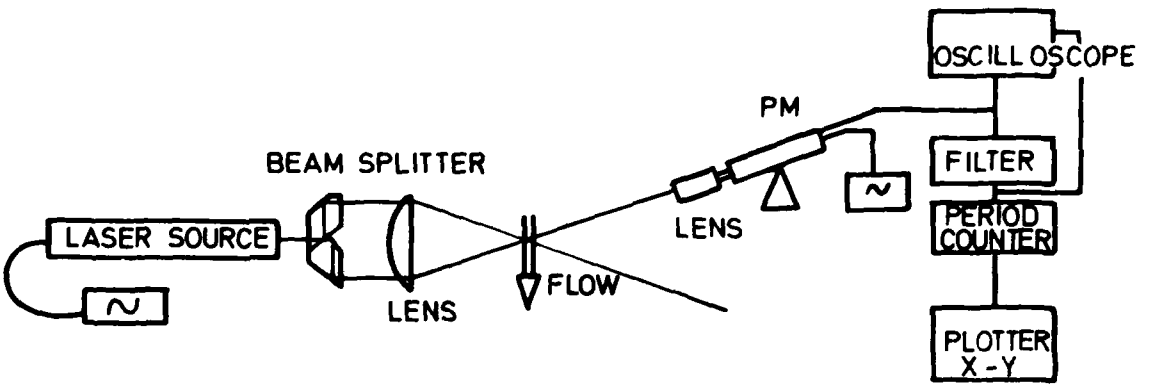

Fig.4 Reference beam mode – practical arrangement

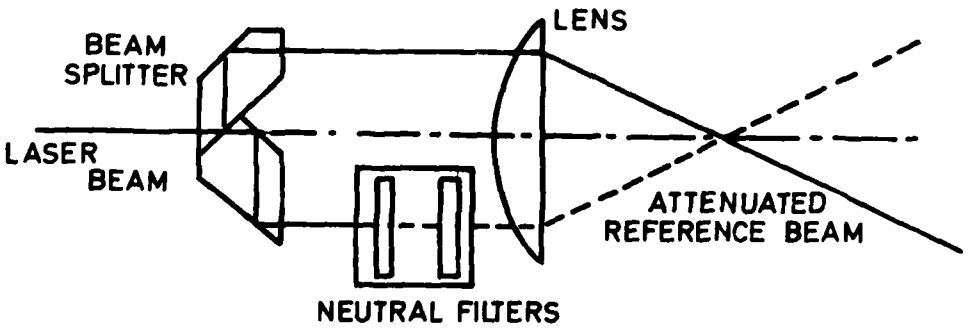

Fig.5 Detail of illuminating optic unit

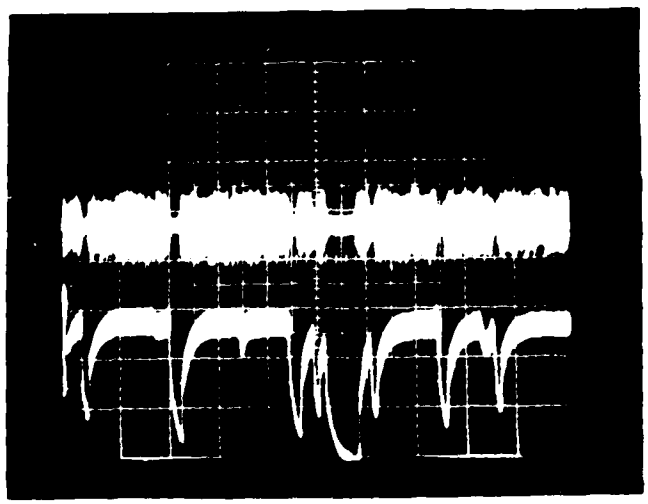

Fig.6 Signals yielded by the photodetector

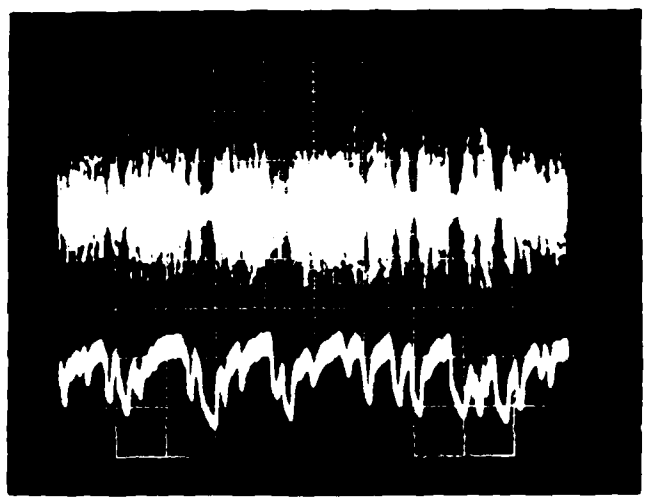

Fig.7 Signals yielded by the photodetectors. Saturation

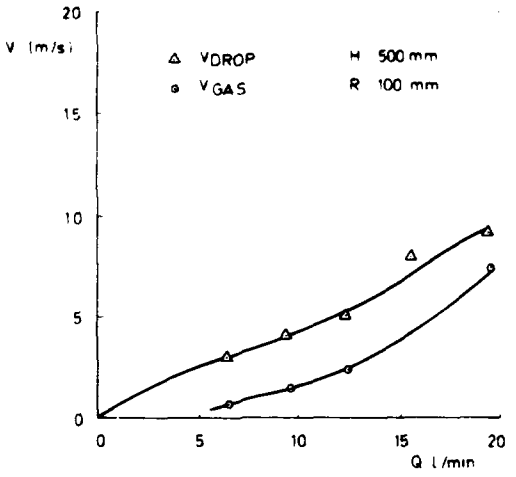

Fig.8 Velocity versus water rate

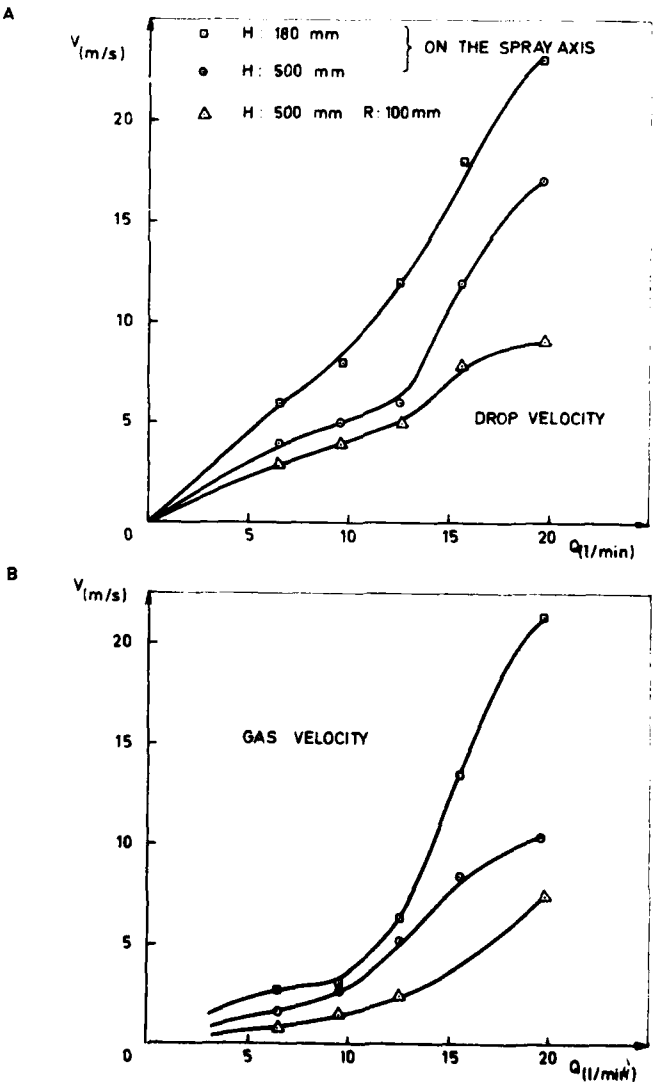

Fig.9 Axial velocity change versus water rate

MÉTHODES DE MESURE A COURT TEMPS DE RÉPONSE POUR LA DÉTERMINATION DES FLUCTUATIONS DE VITESSE ET TEMPÉRATURE DANS LES ÉCOULEMENTS A TEMPÉRATURE ÉLEVÉE

par Marc CHARPENEL, Yves LE BOT, Philippe MAGRE, Jean LABBÉ et Pierre MOREAU

Office National d'Etudes et de Recherches Aérospatiales (ONERA)
92320 Châtillon, France

SOMMAIRE

Un appareil optique utilisant une méthode d'émission et absorption simultanées en infrarouge pour la mesure des températures instantanées de gaz et des sondes de pression d'arrêt à court temps de réponse pour mesurer le taux de turbulence ont été développés pour caractériser l'aspect instationnaire des écoulements à température élevée.

Ces deux techniques expérimentales sont présentées et les résultats obtenus sur des écoulements turbulents chauds sont analysés et comparés avec les indications plus classiques de la vélocimétrie laser. L'extension de ces techniques de mesure à l'obtention de spectres de turbulence et à la détermination de l'échelle intégrale par la méthode optique des faisceaux croisés est également examinée.

SUMMARY

An optical device using an infrared simultaneous emission and absorption method for measurements of instantaneous gas temperatures, and total pressure probes with a short response time in order to measure the turbulence level have been developed to characterize the unsteadiness of high temperature flows.

These two experimental techniques are described and the results obtained on hot turbulent flows are analyzed and compared with more classical indications given by laser velocimetry. The further application of these techniques to obtain the turbulence spectra and to determine the integral scale by the optical method of crossed beams is also examined.

1 - INTRODUCTION

Dans les foyers de turbomachines la combustion s'accompagne de fluctuations des concentrations, de la température et de la vitesse d'éjection des gaz. Ces fluctuations ont une influence sur le rendement et sur les productions de polluants dans la chambre de combustion, mais aussi sur les conditions de transfert thermique au niveau de la turbine. Cela a conduit à rechercher des méthodes appropriées de qualification de l'aspect instationnaire des écoulements chauds et notamment de la température et de la vitesse.

Les méthodes classiques de détermination de la turbulence au moyen d'anémomètres ou de thermomètres à fil ou à film chaud ne peuvent plus être utilisées aux niveaux de température régnant à la sortie de la chambre de combustion ou à l'entrée de la turbine. Les techniques d'avenir telles que l'anémométrie laser pour la mesure de vitesses ou la diffusion Raman anti-stoke cohérente pour la mesure des concentrations et de la température sont de mise en oeuvre difficile et les conditions de leur utilisation ne sont pas toujours réunies. Aussi toute méthode, même moins performante, mais susceptible de fournir des indications sur le caractère instationnaire de l'écoulement est à retenir. C'est pourquoi l'ONERA a développé des sondes de pression d'arrêt à court temps de réponse pour caractériser de manière indirecte les fluctuations de vitesse et un appareil optique de mesure de la température des gaz utilisant une méthode d'émission et absorption simultanée en infrarouge. Ces méthodes de mesure ne sont pas sans défaut : La pyrométrie infrarouge intègre les fluctuations de température le long du faisceau optique et la mesure de pression d'arrêt est une méthode perturbatrice de l'écoulement qui nécessite en outre la recherche d'une relation de correspondance pouvant exister entre fluctuations de pression et fluctuations de vitesse.

La description de ces deux techniques expérimentales est présentée et les résultats obtenus sur des écoulements turbulents chauds analysés. En outre l'utilisation sur ces mêmes écoulements de la vélocimétrie laser pour la mesure locale et instantanée de la vitesse permet de valider, à haute température, la relation entre fluctuations de vitesse et de pression trouvée à température modérée par comparaison avec les mesures effectuées au moyen de sondes à film chaud. L'extension de ces techniques de mesure à l'obtention de spectres de turbulence et à la détermination de l'échelle intégrale par la méthode des faisceaux croisés est également examinée.

2 - PRINCIPE DES DIFFERENTES METHODES DE MESURE DEVELOPPEES

2.1 - Mesures de pression instationnaire

Les mesures de pression nécessitent la mise en oeuvre de sondes refroidies comportant un élément sensible dont la protection contre l'environnement à haute température dans des gaz souvent réactifs doit être assurée. L'élément sensible est un capteur piezoélectrique ONERA, 20H47 ou 20H48, plus ou moins protégé suivant la durée de vie prévue pour la sonde et la bande passante souhaitée.

Travail effectué sous contrats de la DRET (Direction des Recherches, Etudes et Techniques)
de la SNECMA (Sté Nationale d'Etudes et de Construction de Moteurs d'Aviation)

La figure 1a montre le schéma d'une sonde d'arrêt de forme classique comportant un capteur affleurant. Une circulation d'eau maintient la structure de la sonde à une température convenable et une protection de la surface sensible est assurée au moyen d'un élastomère qui se carbonise progressivement. La durée de vie du capteur, variable avec les conditions d'essais, est de l'ordre de 30 minutes à 1300 K sous 1 bar. La bande passante est très élevée (300 kHz environ).

Dans le montage de la figure 1b le corps de la sonde est cylindrique et le capteur, toujours protégé par un élastomère, est placé au fond d'une cavité face à l'écoulement et ses performances sont semblables à celles de la précédente. Par contre dans la sonde cylindrique de la figure 1c l'élément sensible est placé latéralement dans une cavité refroidie. Sa bande passante n'est plus que de 10 kHz environ mais la durée de vie semble très grande pour une température ne dépassant pas 1800 K.

Des études effectuées à température modérée ont montré que les fluctuations de pression d'arrêt, $\tilde{P}_{rms}$, et les fluctuations de vitesse, $\tilde{V}_{rms}$, mesurées au moyen d'une sonde à film chaud, sont reliées par la relation :

$$\frac{\tilde{P}_{rms}}{\rho V^2} = K \frac{\tilde{V}_{rms}}{V} \qquad (1)$$

où l'on peut prendre pour ρ et V les valeurs moyennes de la masse volumique et de la vitesse.

L'analyse de ces mesures effectuées dans des conditions d'essais variées au moyen de divers types de sondes montre que le coefficient K est de l'ordre de 2. Une conclusion analogue est également proposée dans [1]. Un bon recoupement entre les densités spectrales énergétiques des deux types de mesure est également observé (figure 2).

La relation de proportionnalité entre les fluctuations de pression d'arrêt et les fluctuations de vitesse s'explique s'il est possible de négliger les fluctuations de pression statique. Effectivement les études de Batchelor [2] conduisent, dans le cas de la turbulence homogène, à relier fluctuations de pression statique et fluctuations de vitesse sous la forme :

$$\tilde{p}_{rms} = 0{,}58\, \rho\, \tilde{V}^2_{rms}$$

Ce terme est évidemment généralement très faible devant la fluctuation de pression d'arrêt $\tilde{P}_{rms}$.

Ces conclusions laissent supposer que l'effet d'intégration de la mesure par sonde est négligeable. Ce résultat demande toutefois à être confirmé par des essais effectués dans des écoulements variés afin de préciser notamment l'influence de l'échelle de la turbulence.

2.2 - Mesures des températures de gaz instantanées

La méthode optique de mesure de température des gaz mise au point à l'ONERA pour les gaz à hautes températures issus des moteurs fusée [3], et fonctionnant dans le visible, a été adaptée, par transposition dans l'infrarouge, aux écoulements gazeux des bancs thermiques dont la température est beaucoup plus basse [4].

La méthode consiste à enregistrer simultanément, grâce à deux détecteurs, les signaux monochromatiques provenant d'une part, d'une source de référence après traversée de la flamme et d'autre part, de la flamme seule. La connaissance de la température de luminance monochromatique de la source permet alors de calculer à chaque instant la température moyenne de la flamme ainsi que son facteur d'émission. Le temps de réponse n'est limité que par la constante de temps des récepteurs et celle de l'enregistrement des signaux.

L'application de cette méthode dans le visible, sur des flammes généralement transparentes dans ce domaine spectral, nécessite l'addition d'un sel de sodium qui augmente l'émissivité de la flamme sur les raies de résonance du sodium. L'intervalle spectral est alors imposé par un monochromateur et on utilise des photomultiplicateurs dont le temps de réponse est de l'ordre de la microseconde. Les appareils ainsi équipés, et maintenant commercialisés sous le nom de MT4, ont été utilisés dans de nombreuses applications sur des flammes dont la température était comprise entre 1 400 K et 5 000 K.

La transposition dans l'infrarouge permet, en utilisant l'émission propre des gaz due soit à la vapeur d'eau soit au gaz carbonique, de s'affranchir de tout ensemencement. Les raies émises sont alors suffisamment serrées pour admettre une faible résolution spectrale qui, jointe à l'utilisation de détecteurs à l'antimoniure d'indium refroidis à l'azote liquide, permet la mesure de températures aussi basses que 600 K. L'intervalle spectral est imposé par un simple filtre interférentiel de largeur relative 4 %, ce qui simplifie considérablement l'appareil.

Le schéma optique du dispositif qui permet de discriminer les signaux provenant de la source et de la flamme est présenté figure 3. L'image de la source S est formée dans le plan C par la lentille L4. La lentille L2 en reforme une image dans le plan de la flamme. L'optique L3, qui supporte le diaphragme d'ouverture, conjugue les plans images précédents sur le diaphragme de champ D. La lentille L4 permet le transport de l'image monochromatique, isolée par le monochromateur M, sur le miroir prismatique P qui la divise en deux parties sensiblement égales. Grâce aux lentilles L5 une moitié de l'énergie arrive sur un récepteur R1, l'autre moitié sur un récepteur R2. Un couteau placé dans le plan C peut être déplacé de façon à diviser l'image exactement comme le miroir prismatique. L'un des récepteurs, par exemple R2, ne reçoit alors plus aucune énergie provenant de la source, alors que le signal délivré par R1 n'a pas changé.

Si la flamme est homogène en température les signaux Y1 et Y2 délivrés par R1 et R2 sont donnés par les relations suivantes [3] :

$$Y_1 = K_1 L(\lambda, T_{LS}).(1-\varepsilon) + K_2 L(\lambda, T_F).\varepsilon$$

$$Y_2 = K_2 L(\lambda, T_F).\varepsilon$$

Compte tenu des différences de sensibilité des détecteurs et des étendues géométriques des faisceaux incidents, les coefficients de proportionnalité K_1 et K_2 ne sont pas identiques mais il est toujours possible de les égaler en jouant sur les étages d'amplification.

$\mathcal{E}$ est le facteur d'émission défini par :

$$\mathcal{E}(\lambda) = 1 - \exp\left[- \int_0^{\ell} \alpha(\lambda, x)\, dx \right]$$

où $\alpha(\lambda, x)$ est le coefficient d'émission monochromatique local égal au coefficient d'absorption d'après la loi de Kirchoff.

On remarquera que $\mathcal{E}$ dépend de l'épaisseur de la flamme ℓ. La connaissance de la luminance monochromatique de la source $L(\lambda, T_{LS})$ permet alors de calculer à chaque instant, par la résolution de ce système de deux équations, les inconnues $L(\lambda, T_F)$ et $\mathcal{E}(\lambda)$ où $L(\lambda, T_F)$ est la luminance monochromatique du corps noir à la température de la flamme T_F. Un calculateur analogique permet d'effectuer ce calcul en temps réel. La loi de Planck pour la longueur d'onde λ permet ensuite de remonter à la température de la flamme.

Le calcul d'erreur montre que la précision de la mesure est d'autant plus grande :

- que l'on travaille au plus près du point de renversement défini par l'égalité des températures de la flamme et de la source,
- et que le facteur d'émission de la flamme $\mathcal{E}$ est proche de l'unité.

Cette précision peut être de l'ordre du pourcent.

L'étude détaillée [4] du principe de mesure nous a permis de souligner que la température mesurée n'a de signification claire que si la température de la flamme est uniforme sur tout le volume gazeux traversé par les faisceaux optiques et que la mesure intéresse tout ce volume. Malgré cela, lorsque toutes les caractéristiques du milieu (concentrations, température) varient en tout point et à tout instant de façon aléatoire, on montre qu'il est possible de découpler les fluctuations de température et d'émissivité à condition que la turbulence soit statistiquement homogène et que les fluctuations d'émissivité soient de faible amplitude vis-à-vis de la valeur moyenne. Pour cela on se place sur une bande d'émission pour laquelle le facteur d'émission est très faible et on travaille au point de renversement défini par l'égalité de la température de la source et de la température moyenne de la flamme.

Dans ces conditions, et pour un faisceau optique très étroit en comparaison de l'échelle intégrale de la turbulence, on montre que les fluctuations du signal Y_1, notées $\tilde{Y}_1(t)$, sont données par l'intégrale sur le trajet optique des fluctuations de la luminance du corps noir $\tilde{L}_F(T_F(x,t))$ à la température locale de la flamme $T_F(x,t)$

$$\tilde{Y}_1(t) = K_1 . \bar{\alpha} . \int_0^{\ell} \tilde{L}_F(T_F(x,t))\, dx$$

$\bar{\alpha}$ est la valeur moyenne du coefficient d'émission, indépendant de x et de t puisque le milieu est supposé statistiquement homogène.

Si les fluctuations de température sont de suffisamment faible amplitude il est possible de linéariser la loi de luminance $L(T)$ au voisinage de la température moyenne $\bar{T}_F$ et obtenir ainsi l'intégrale des fluctuations de température sur le trajet optique :

$$\tilde{Y}_1(t) \simeq K_1 . \bar{\alpha}\, \ell . \frac{\partial L}{\partial T}(\bar{T}_F) . \frac{1}{\ell} \int_0^{\ell} \tilde{T}_F(x,t)\, dx$$

avec $\ell\bar{\alpha} = \bar{\mathcal{E}}$ le facteur d'émission moyen.

Cette relation peut encore s'écrire, en faisant apparaître une température moyenne instantanée équivalente $\Omega(t)$, de fluctuation $\tilde{\Omega}(t)$, :

$$\tilde{Y}_1(t) \simeq K_1 . \bar{\alpha}\, \ell . \frac{\partial L}{\partial T}(\bar{T}_F) . \tilde{\Omega}(t)$$

avec,

$$\tilde{\Omega}(t) = \frac{1}{\ell} \int_0^{\ell} \tilde{T}_F(x,t)\, dx$$

Evidemment la mesure des fluctuations de température est affectée par l'intégration sur le trajet optique. On montre [4] que, lorsque la longueur d'intégration ℓ est grande devant l'échelle intégrale de la turbulence Λ, variance mesurée $\overline{\tilde{\Omega}^2}$ et variance locale $\overline{\tilde{T}^2}$ sont proportionnelles. Le rapport de proportionnalité est trouvé égal au rapport du double de l'échelle intégrale à la longueur d'intégration :

$$\overline{\tilde{\Omega}^2} = 2 . \frac{\Lambda}{\ell} . \overline{\tilde{T}^2}$$

L'effet d'intégration peut donc être très important et il est nécessaire, pour remonter à la variance locale, de déterminer l'échelle intégrale.

2.3 - Mesure de l'échelle intégrale

a) Faisceaux orthogonaux

Cette technique consiste à mesurer le niveau de corrélation entre deux mesures optiques sur deux trajets orthogonaux et progressivement éloignés l'un de l'autre comme le montre la figure 4. Les points A et B délimitent la plus courte distance d des deux droites. Si l'on découpe les deux trajets optiques en intervalles de longueur 2Λ (en prenant A et B comme point milieu de l'un des intervalles), chacune des mesures $\tilde{\Omega}_1$ et $\tilde{\Omega}_2$ est la moyenne des grandeurs indépendantes attachées à chacun des éléments constituant l'un des trajets optiques. On conçoit que seuls les deux intervalles incluant le point A ou B donneront une contribution notable à la corrélation entre $\tilde{\Omega}_1$ et $\tilde{\Omega}_2$ puisque la distance entre tous les points des autres intervalles sera supérieure à l'échelle intégrale Λ.

Si on appelle $\beta(d)$ la fonction de corrélation ainsi obtenue, on montre [4] qu'elle est reliée à la fonction de corrélation à 2 points dans le milieu $R(\delta)$ par :

$$\beta(d) = \frac{2\pi}{l_1 l_2} \int_d^\infty R(\xi)\, \xi\, d\xi$$

En particulier la corrélation en faisceaux croisés, pour d = 0, est donnée par :

$$\beta(0) = \frac{2\pi}{l_1 l_2}\, \overline{\tilde{T}}^2\, \Lambda'^2$$

où Λ' est une échelle intégrale différente de celle utilisée jusqu'ici et définie par :

$$\Lambda'^2 = \frac{1}{\overline{\tilde{T}}^2} \int_0^\infty R(\xi)\, \xi\, d\xi$$

La normalisation de $\beta(d)$ par $\beta(0)$ permet de définir la fonction sans dimension $\eta(d)$

$$\eta(d) = \frac{\beta(d)}{\beta(0)} = \frac{1}{\overline{\tilde{T}}^2\, \Lambda'^2} \int_d^\infty R(\xi)\, \xi\, d\xi$$

dont l'inversion donne :

$$R(\xi) = -2.\, \overline{\tilde{T}}^2.\, \Lambda'^2 \left[\frac{\partial \eta(d^2)}{\partial (d^2)}\right]_{d=\xi}$$

On voit qu'il est nécessaire pour obtenir R de tracer η en fonction du paramètre d^2 et d'en prendre la dérivée. La valeur de cette dérivée à l'origine permet de calculer Λ' :

$$\left[\frac{\partial \eta(d^2)}{\partial (d^2)}\right]_{d=0} = -\frac{1}{2\,\Lambda'^2}$$

Enfin l'intégration de cette fonction dérivée sur d permet d'obtenir une relation entre Λ et Λ' et donc de calculer Λ :

$$\Lambda = \frac{1}{\overline{\tilde{T}}^2} \int_0^\infty R(\xi)\, d\xi = -2\,\Lambda'^2 \int_0^\infty \frac{\partial \eta(d^2)}{\partial (d^2)}\, dt$$

La méthode des faisceaux orthogonaux permet donc bien de déterminer l'échelle intégrale ; elle permet, mieux encore, d'obtenir la fonction de corrélation à deux points, mais a pour inconvénient d'être longue (il faut effectuer des mesures point par point) et assez peu précise (la fonction R s'obtient par dérivation de la fonction η). Aussi on a recherché et on propose une mesure plus simple dérivée de celle-ci. Elle consiste à mesurer la corrélation normalisée en faisceaux croisés.

b) Corrélation normalisée en faisceaux croisés

Il est toujours difficile d'effectuer des mesures absolues et ceci est également vrai pour les corrélations. Ce que donne le traitement numérique c'est la corrélation normalisée par les valeurs quadratiques moyennes des mesures $\tilde{\Omega}_1$ et $\tilde{\Omega}_2$. Or nous avons donné une expression de ces valeurs quadratiques moyennes :

$$\left(\overline{\tilde{\Omega}_1^2}\right)^{1/2} = \left(\overline{\tilde{T}}^2\, \frac{2\Lambda}{l_1}\right)^{1/2} \quad \text{et} \quad \left(\overline{\tilde{\Omega}_2^2}\right)^{1/2} = \left(\overline{\tilde{T}}^2\, \frac{2\Lambda}{l_2}\right)^{1/2}$$

La corrélation en faisceaux croisés donnée par

$$\beta(0) = \frac{2\pi}{l_1 l_2}\, \overline{\tilde{T}}^2\, \Lambda'^2$$

devient après normalisation

$$\rho(0) = \frac{\beta(0)}{\left(\overline{\tilde{\Omega}_1^2}.\, \overline{\tilde{\Omega}_2^2}\right)^{1/2}} = \frac{\pi}{\sqrt{l_1 l_2}} \cdot \frac{\Lambda'^2}{\Lambda}$$

Pour aller plus loin on admet que les deux échelles intégrales Λ et Λ' sont voisines. C'est le cas lorsque l'on admet pour la fonction de corrélation R une loi exponentielle ; on a alors rigoureusement $\Lambda' = \Lambda$. Pour une gaussienne on trouve :

$$\Lambda' = \sqrt{\frac{4}{2\pi}}\,\Lambda \simeq 0{,}8\,\Lambda$$

Or ce sont deux cas extrêmes correspondant à un nombre de Reynolds de turbulence soit très grand (cas de l'exponentielle) soit très faible (cas de la gaussienne) [5]. On admettra que pour les Reynolds intermédiaires cette quasi-égalité tient encore. Dans ces conditions la corrélation normalisée en faisceaux croisés, jointe à la connaissance des longueurs d'intégration l_1 et l_2, permet de calculer l'échelle intégrale :

$$\Lambda = \frac{\rho(0)}{\pi} \sqrt{l_1 l_2}$$

Il est à remarquer que la méthode des faisceaux orthogonaux ne faisait pas intervenir les longueurs d'intégration. Les deux méthodes sont donc indépendantes. Dans les deux cas, les corrélations sont d'autant plus faibles, donc difficiles à mesurer, que ces longueurs sont grandes devant l'échelle intégrale.

c) Influence de l'épaisseur des faisceaux

Tous ces résultats supposent les faisceaux optiques infiniment étroits, ce qui n'est pas physiquement réalisable. On montre [ ] que l'intégration supplémentaire sur les dimensions transversales des faisceaux apporte une contribution négligeable si l'épaisseur des faisceaux, e, est petite devant l'échelle intégrale Λ. Les termes correctifs sont en effet d'ordre $(e/2\Lambda)^2$ et pour des faisceaux larges de 2 mm et une échelle intégrale d'environ 1 cm la précision des mesures est encore de 1 pour cent.

2.4 - Vélocimétrie laser

Le principe de cet appareil consiste à créer dans la zone d'intersection de deux faisceaux laser de même longueur d'onde (514,5 nm), un réseau de franges d'interférences optiques régulièrement espacées. Le passage à travers celles-ci de particules diffusantes entraînées par le fluide donne naissance à une succession d'émissions lumineuses dont la fréquence est proportionnelle à la vitesse des particules dans la direction perpendiculaire aux franges. Si ces particules sont suffisamment petites, leur propre vitesse instantanée est très sensiblement celle du fluide porteur. Pour des raisons de compatibilité avec la température du fluide, le matériau retenu est une poudre ultra-fine de dioxyde de zirconium dont le diamètre caractéristique est de l'ordre du micron. Mises en suspension dans un jet d'air par un dispositif à double flux tourbillonnaire, elles sont injectées dans la soufflerie, en amont du foyer. L'interfrange est de 17,4 m et le diamètre du volume de mesure d'environ 120 μm.

Les signaux lumineux captés par un télescope type Cassegrain sont successivement validés (pour séparer grosses et petites particules) puis filtrés et mis en forme par un compteur-fréquencemètre. La cadence d'acquisition de ce compteur est faible, inférieure à 300 par seconde. Ce compteur est relié à un ordinateur gérant l'acquisition des données de la soufflerie. Lorsque le nombre de particules validées est suffisant (1 000 particules au minimum) l'ordinateur calcule la vitesse moyenne et son écart type en supposant la distribution gaussienne.

Les signaux captés et mis en mémoire dans l'ordinateur sont ensuite transférés sur une bande magnétique et mis en réserve pour un traitement ultérieur comme par exemple le calcul de la distribution des vitesses (histogrammes).

Lorsqu'il s'agit d'obtenir des spectres de turbulence de vitesse d'écoulement un compteur rapide du type DISA, permettant l'acquisition d'une mesure toutes les 10 microsecondes, est utilisé. Dans ces conditions la limitation de la bande passante n'est plus due au compteur mais à l'insuffisance du flux en particules (plusieurs milliers de particules sont nécessaires par seconde). Bien entendu, la discrétisation du signal pose un problème de traitement. On le résoud facilement grâce à l'utilisation de la tension analogique proportionnelle à la fréquence instantanée mesurée que délivre l'appareil. Cette tension analogique subsiste entre deux mesures successives si bien que le signal présente l'allure de marches d'escalier qui se rapprochent d'autant plus du signal réel que les mesures sont plus serrées. Ce signal est traité comme un signal continu.

3 - EXEMPLES D'APPLICATIONS

3.1 - Mesure du taux de turbulence aérodynamique au moyen de sondes de pression d'arrêt

Les taux de turbulence mesurés, d'une part au moyen d'une sonde de pression d'arrêt à court temps de réponse et d'autre part par vélocimétrie laser, ont été comparés lors de la caractérisation de l'écoulement issu d'une chambre de combustion industrielle. Les mesures ont été effectuées à mi-hauteur de veine sur un secteur angulaire de l'ordre de 90°. La figure 5 résume les résultats obtenus. Un bon accord apparaît entre les indications des deux techniques de mesures utilisées, confirmant ainsi à haute température la relation de correspondance entre fluctuations de pression d'arrêt et de vitesse d'écoulement établie à partir d'études sur des écoulements à température modérée.

Les variations azimutales du taux de turbulence observées sur la figure 5 sont liées à la géométrie particulière de la chambre de combustion expérimentée (présence des cannes de prévaporisation et des orifices de dilution).

3.2 - Caractérisation des fluctuations de température et de vitesse d'écoulement dans un montage d'étude de la combustion turbulente

La méthode optique de mesure des fluctuations de température et la vélocimétrie laser ont été appliquées à l'analyse de l'écoulement dans un montage d'étude de la combustion turbulente.

Dans ce dispositif expérimental un écoulement prémélangé air-méthane est enflammé et la combustion stabilisée par un écoulement parallèle de gaz à haute température issus d'un foyer auxiliaire (figure 6). La veine est bidimensionnelle, de section 100 x 100 mm, et la conduite d'arrivée des gaz de stabilisation a pour hauteur 19 mm. La vitesse initiale moyenne de l'écoulement frais est de l'ordre de 55 m/s, la richesse 0,8, et la température 600 K. La vitesse moyenne des gaz chauds est d'environ 110 m/s et leur température 2 000 K.

L'installation d'essais n'étant pas refroidie, seuls sont possibles des essais de courte durée (environ 30 s).

3.2.1 - Analyse de la turbulence thermique

Les mesures de fluctuations de température par pyrométrie optique ont été limitées à l'exploration d'un plan situé à 42 mm du point de confluence des deux écoulements pour différentes distances à la paroi inférieure : 10, 15, 20, 25, 30 et 45 mm. Ces points de mesure sont indiqués sur le schéma de la figure 6.

Au contraire des gaz chauds issus d'une combustion, les gaz frais contiennent très peu de gaz carbonique et de vapeur d'eau et les émissivités des uns et des autres sont très différentes. Pour les rapprocher il a été nécessaire d'introduire dans les gaz frais une faible proportion de gaz carbonique et d'utiliser la longueur d'onde 4,25 μm pour laquelle ce gaz présente un maximum d'émission. A cette longueur d'onde le hublot de silice est opaque et le passage du faisceau infrarouge a été assuré grâce à deux orifices de 8 mm de diamètre percés face à face dans les éléments mobiles des parois latérales. La translation de ces parois permet le déplacement du point de mesure. Les essais ont été effectués à richesse égale à 0,8 mais aussi à richesse nulle, donc sans inflammation : on a alors simplement un mélange des deux écoulements de températures différentes.

Les mesures instantanées sont enregistrées sur bande magnétique analogique, en vue de leur traitement en temps différé. La numérisation d'un essai de 30 secondes fournit ainsi 625 000 points de mesure, soit un point toutes les 25 μs. Ces 625 000 points de mesure permettent de tracer avec précision les histogrammes relatifs à la température. Ce calcul s'effectue par valeurs discrètes de pas 10 K.

Les figures 7 et 8 présentent les histogrammes obtenus pour la richesse 0,8 et la richesse nulle pour une exploration verticale. Les fluctuations sont importantes et fortement non gaussiennes, le pic de gaz chauds s'estompant progressivement pour laisser place à un pic de plus en plus étroit vers les basses températures. On en déduit les profils de température moyenne et les écarts types correspondants (figure 9). La différence est peu sensible entre les deux conditions d'essais ; cela tient sans doute au choix de la section de mesure, encore très proche du point de confluence des deux écoulements.

3.2.2 - Analyse des fluctuations de vitesse d'écoulement

Pendant les essais les mesures de vitesse instantanée effectuées par vélocimétrie laser sont enregistrées sur bande magnétique numérique en vue de leur analyse en temps différé.

Un programme de traitement permet de tracer les histogrammes dont un exemple est donné figure 10. Il correspond à la première section de mesure située à 42 mm en aval de la confluence des deux écoulements. On peut distinguer plusieurs formes d'histogrammes correspondant à diverses zones successives dans le foyer :

- Dans les gaz frais près de la paroi supérieure du foyer, (γ = 90 mm), l'histogramme présente un seul pic centré à 65 m/s et correspondant à l'écoulement initial à 55 m/s. La différence des vitesses s'explique d'une part par une légère accélération de l'écoulement et d'autre part par le fait que les vitesses initiales sont calculées sans tenir compte des couches limites. On note également sur cet histogramme un petit pic, centré à 35 m/s, correspondant à des signaux imparfaitement éliminés par le système de validation ; ces valeurs erronées ont une très grande importance sur le résultat du calcul de la turbulence : elles doivent être écartées avant d'effectuer ce calcul.

- Toujours dans les gaz frais, mais plus près de la zone de combustion (γ = 30 mm), l'histogramme devient plus large, ce qui correspond à une augmentation de la turbulence.

- Au début de la zone de mélange et combustion (γ = 20 mm) l'histogramme se déforme et présente alors un sillage important vers les fortes vitesses.

- Au centre de cette zone de mélange (γ = 15 mm) on obtient un histogramme à deux pics, de hauteurs sensiblement égales, correspondant aux deux écoulements.

- Enfin, dans le sillage des gaz de stabilisation (γ = 10 mm) on retrouve un histogramme à un seul pic provenant de l'écoulement chaud.

La connaissance des histogrammes est nécessaire avant le calcul des vitesses moyennes et des écarts-types car elle permet d'éliminer les valeurs provenant d'une validation injustifiée et qui peuvent induire des erreurs importantes, notamment sur la turbulence. Les profils transversaux de vitesse moyenne et de fluctuation de vitesse sont donnés sur la figure 11. Le taux de turbulence maximum dans la zone de mélange et combustion atteint près de 25 %.

La comparaison des fluctuations de vitesse ainsi déterminées avec celles déduites des mesures de fluctuations de pression d'arrêt de l'écoulement est en cours.

3.3 - Utilisation de ces méthodes de mesure pour l'obtention de spectres et échelles de turbulence

Les différentes techniques de mesure présentées peuvent permettre une caractérisation plus complète de la turbulence, par exemple l'obtention de spectres ou la détermination de l'échelle intégrale. Ces possibilités ont tout d'abord été exploitées sur un montage expérimental fonctionnant à température modérée.

Ce montage représente un secteur de la zone de dilution d'un foyer annulaire (figure 12). Il comporte essentiellement un canal démontable de section rectangulaire (300 x 100 mm) monté à la suite d'un foyer générateur de gaz chauds. La disposition interne comporte :

- une veine centrale recevant directement les gaz issus du foyer ;
- deux veines situées de part et d'autre de la première, au-dessus et au-dessous, alimentées en air frais par deux conduites indépendantes ;
- les parois constituées de plusieurs éléments en tôle séparant les veines latérales de la veine centrale. Ces parois permettent d'une part le passage de l'air de dilution au moyen d'une série d'orifices circulaires, d'autre part leur propre refroidissement grâce à la création de films fluides localisés aux raccordements de deux tôles successives.

Les trois veines, distinctes à l'entrée, n'en constituent plus qu'une seule à la sortie, les écoulements latéraux étant astreints, par ce dispositif, à se mélanger à l'écoulement central. Enfin, le rétrécissement terminal, provoquant une accélération de l'écoulement, permet d'atteindre un nombre de Mach du même

ordre que celui observé dans la réalité à l'entrée du distributeur de la turbine ($M \simeq 0,2$). La température est environ 600 à 650 K.

3.3.1 - Mesure de l'échelle intégrale

a) Technique des faisceaux orthogonaux

La mesure de l'échelle intégrale de la turbulence s'effectue en utilisant deux pyromètres qui intègrent l'émission infrarouge du jet sur deux trajets orthogonaux. L'un d'eux, maintenu fixe, est placé verticalement au-dessus de la veine, à environ 70 mm du plan de sortie ; l'autre est horizontal et peut être translaté axialement.

La figure 13 présente les courbes de corrélation spatio-temporelles obtenues à partir des deux mesures. Chaque courbe correspond à une position relative des deux faisceaux, t étant le paramètre de corrélation temporelle et d la plus courte distance entre les deux faisceaux. d est modifié par pas de 10 mm sauf à l'approche de l'intersection où le pas est resserré à 2 mm. Pour ne pas surcharger la figure les courbes correspondantes n'y figurent pas. A une légère atténuation près les courbes se déduisent les unes des autres par une translation. Ceci s'explique si l'on admet l'hypothèse de Taylor de turbulence gelée ; effectivement, si on porte sur un diagramme l'abscisse t_{max} relative au maximum des courbes de corrélation, en fonction de la distance d, on obtient une droite (figure 14), et la vitesse définie par la pente de cette droite (84 m/s) est proche de la vitesse attendue pour le jet.

Les points à déphasage nul ($t = 0$) permettent de tracer la courbe de corrélation $\rho(d)$ qui présente un maximum pour $d = 0$ (figure 15). On a vu qu'il est nécessaire, pour obtenir la fonction de corrélation à 2 points, de tracer $\rho(d)$ en fonction du paramètre d^2 au lieu de d et d'en prendre la dérivée. On obtient ainsi une courbe beaucoup plus étroite qui représente, à un coefficient près, la fonction de corrélation cherchée. (figure 15)

La valeur à l'origine permet de calculer l'échelle intégrale Λ' et l'intégration sur d permet de calculer l'échelle intégrale Λ. On les trouve très proche l'une de l'autre :

$$\Lambda' = 0,74 \text{ cm} \quad \text{et} \quad \Lambda = 0,72 \text{ cm}$$

ce qui est une justification supplémentaire de l'approximation qui consiste à les supposer égales. Il faut cependant noter que ces mesures ne sont qu'approximatives. En particulier le calcul par intégration est arrêté arbitrairement au premier zéro de la courbe de corrélation. On suppose que la contribution du reste de la courbe, alternativement positive et négative, est négligeable.

b) Corrélation en faisceaux croisés

Une autre méthode pour atteindre Λ est d'utiliser la corrélation normalisée en faisceaux croisés donnée par :

$$\rho(o) = \frac{\pi \Lambda}{\sqrt{l_1 l_2}} = 0,24.$$

Cette détermination fait intervenir les longueurs d'intégration l_1 et l_2. Dans le cas présent :

$$l_1 \simeq 5 \text{ cm} \quad \text{et} \quad l_2 \simeq 30 \text{ cm}$$

On en déduit une échelle intégrale $\Lambda = 0,94$ cm qui est du même ordre de grandeur que celle déterminée par la méthode des faisceaux orthogonaux ($\Lambda = 0,72$ cm).

3.3.2 - Spectres de turbulence

A titre de comparaison il a été porté sur une même figure (16) les densités spectrales énergétiques dérivées de l'analyse des signaux obtenus par les trois techniques de mesure : la sonde de pression d'arrêt, le pyromètre optique et la vélocimétrie laser. Les trois spectres sont très semblables et on ne remarque pas de rupture de pente sur le spectre de vitesse, ce qui laisse penser que le flux en particules était suffisant pour que le spectre soit réaliste au-dessus de 10 kHz. Les pics de densité spectrale de faible énergie observés aux basses fréquences doivent être attribués à des instabilités du foyer amont. La concordance entre ces trois spectres peut surprendre puisque l'un au moins d'entre eux (le spectre de température) est modifié par l'effet d'intégration. Cependant la représentation utilisant une échelle logarithmique peut être trompeuse. On peut en effet montrer [4] que l'effet d'intégration se fait sentir dans tout le spectre de telle sorte que l'intégration de celui-ci conduise à une variance atténuée dans le rapport $l/2\Lambda$. Ce rapport est ici assez faible, égal à 1,44.

Sur le montage d'étude de la combustion turbulente, seuls les spectres résultant des mesures de température ont été jusqu'ici obtenus (figure 17). Ces spectres correspondent aux points Y = 20 et Y = 25 mm, avec et sans inflammation des gaz frais. On note dans tous les cas la présence d'un pic très important à la fréquence de 800 Hz qui peut s'expliquer par un battement de la flamme entrainant ainsi le fort étalement des histogrammes. Un autre pic à la fréquence de 1 300 Hz apparaît seulement en absence d'inflammation. Il n'est évidemment pas question dans ces conditions "instationnaires" d'appliquer aux fluctuations de température la correction d'effet d'intégration due à la turbulence à petite échelle. Celle-ci ne peut être envisagée qu'après séparation des fluctuations dues au mouvement d'ensemble et de celles dues à la turbulence et par la mise en oeuvre d'une méthode d'analyse conditionnelle.

4 - CONCLUSION

La caractérisation de l'aspect instationnaire des écoulements à température élevée, notamment dans les foyers et les turbines où la technique classique de l'anémométrie à fil chaud ne peut plus être employée, a conduit l'ONERA à étudier des méthodes nouvelles de mesure des fluctuations de vitesse et de température. C'est ainsi que des sondes de pression d'arrêt à court temps de réponse pour la mesure des fluctuations de vitesse et un appareil optique utilisant une méthode d'émission et absorption simultanées en infrarouge pour la mesure des températures de gaz ont été développées. Ces techniques de mesure ne donnent pas au contraire de techniques d'avenir telles que l'anémométrie laser pour la mesure de vitesse ou la diffusion Raman anti-stoke cohérente pour la mesure des concentrations et de la température, la structure fine de l'écoulement mais elles sont plus faciles à utiliser sur des bancs d'essais industriels.

L'analyse des mesures effectuées à température modérée à l'aide de sondes de pression et de films chauds montre qu'il existe une relation de proportionnalité entre les fluctuations de pression d'arrêt et les fluctuations de vitesse. L'utilisation de cette relation permet donc la mesure de la turbulence de vitesse par l'intermédiaire des mesures de pression d'arrêt. Ce résultat demandait toutefois à être confirmé par des mesures dans des écoulements à plus haute température en les comparant à des mesures par vélocimétrie laser. Cette comparaison a été effectuée pour la première fois à la sortie d'une chambre de combustion à la température moyenne de 1 330 K. La bon accord observé justifie l'utilisation des sondes de pression d'arrêt pour qualifier la turbulence des écoulements chauds.

La technique de mesure des températures par pyrométrie infrarouge a été expérimentée dans un montage d'étude de la combustion turbulente où la température des gaz est comprise entre 600 et 2 000 K. La comparaison des histogrammes de température obtenus par la pyrométrie aux histogrammes de vitesse déterminés par anémométrie laser montre l'intérêt de cette technique malgré l'inconvénient de l'intégration des températures le long du faisceau optique. Sur ce montage, l'analyse spectrale du signal de mesure pyrométrique montre que la flamme n'est pas stationnaire, et il n'est pas possible, dans ces conditions, d'appliquer la correction d'effet d'intégration due à la turbulence à petite échelle.

Au contraire, dans le cas où le milieu est statistiquement homogène, on montre qu'il est possible de remonter à la variance locale de la température si l'on connait l'échelle intégrale de la turbulence. Celle-ci peut être obtenue par des corrélations entre deux mesures optiques croisées. Un exemple d'utilisation de cette technique, sur un montage d'étude de la dilution, est présenté. Sur ce même montage on a également comparé les spectres obtenus par les trois techniques de mesure : la sonde de pression d'arrêt, le pyromètre optique et la vélocimétrie laser. Ils sont très comparables.

BIBLIOGRAPHIE

1 - C. FREEMAN
The relationship between steady and unsteady spatial distorsion. Dans "Unsteady phenomena in turbomachinery" - AGARD-CP n° 177, 1975.

2 - J.O. HINZE
"Turbulence" - Mac Graw Hill, 1959, p.

3 - A. MOUTET, C. VERET, L. NADAUD
Méthodes optiques de mesure instantanée de la température des flammes - Recherche Aérospatiale 68 - Janv.-Fév. 1959.

4 - M. CHARPENEL
Mesures instantanées par pyrométrie infrarouge de températures de gaz de combustion - Application à la turbulence thermique - Revue de Physique Appliquée - Tome 14, mars 1979, p. 491.

5 - A. FAVRE, L.S.G. KOVASZNAY, R. DUMAS, J. GAVIGLIO et M. COANTIC
La turbulence en mécanique des fluides - (Gauthiers-Villars) 1976, p. 94 et p. 101.

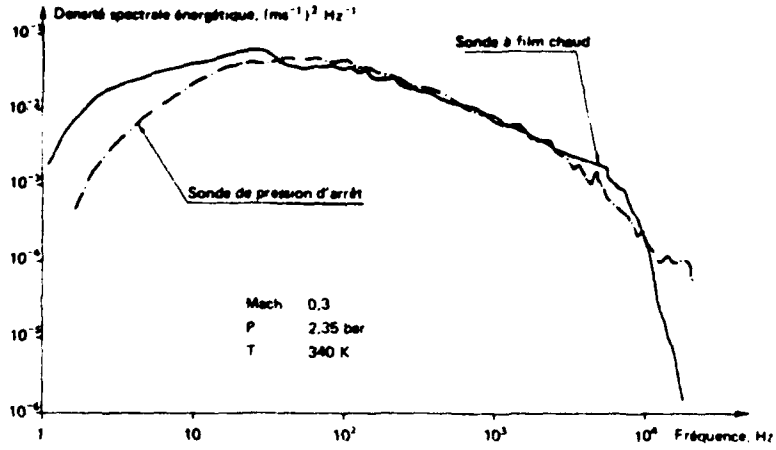

Fig. 1 – Comparaison des densités spectrales de fluctuations de vitesse d'écoulement obtenues à partir de la réponse d'une sonde à film chaud et de celles déduites des fluctuations de pression d'arrêt.

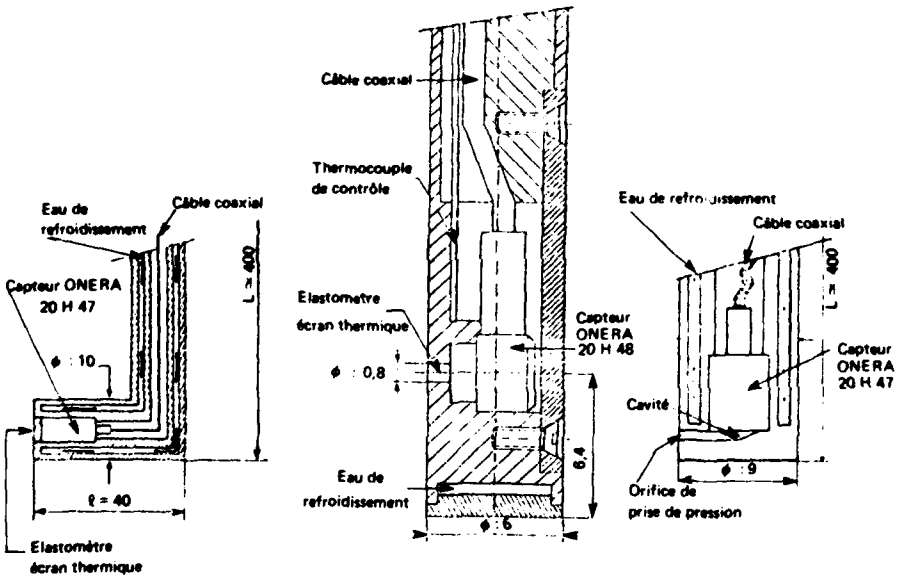

a. Sonde du type Pitot. *b. Sonde cylindrique à large bande passante.* *c. Sonde cylindrique à cavité.*

Fig. 2 – Représentation de trois types de sondes de pression d'arrêt à court temps de réponse utilisées pour la caractérisation de la turbulence des écoulements à température élevée. (cotes en mm).

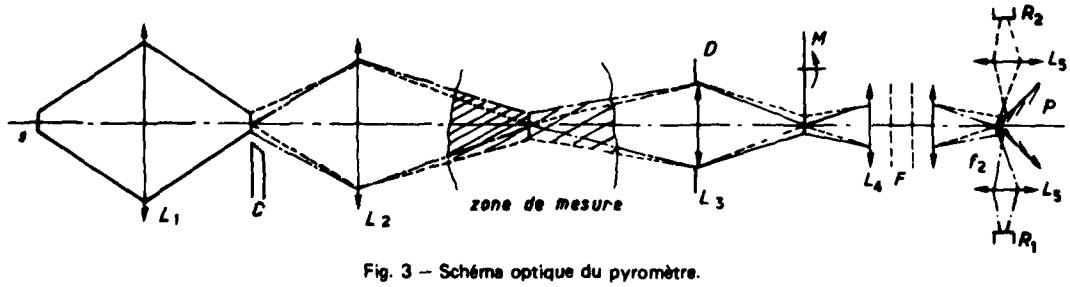

Fig. 3 – Schéma optique du pyromètre.

S : Source C : Couteau D : Diaphragme d'ouverture
F : Filtre interférentiel M : Modulateur P : Prisme séparateur
R_1 , R_2 : Récepteurs.

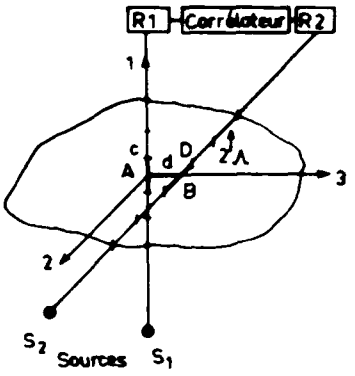

Fig. 4 – Technique des faisceaux orthogonaux

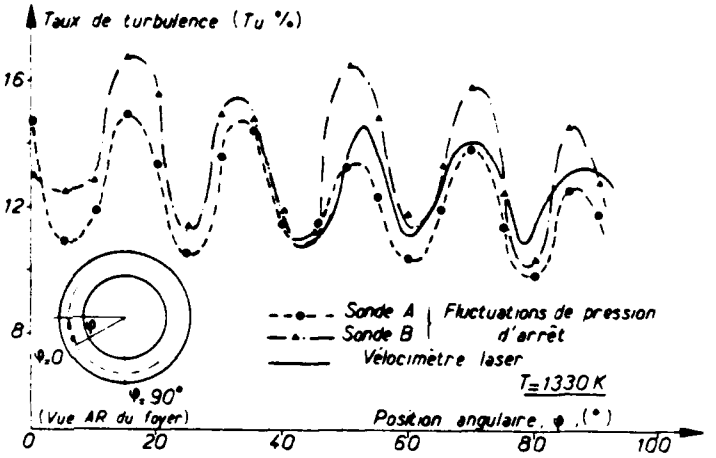

Fig. 5 – Profil angulaire du taux de turbulence de l'écoulement à mi-hauteur de veine à la sortie de la chambre de combustion.
Comparaison des mesures par vélocimétrie laser et par sonde de pression à court temps de réponse.

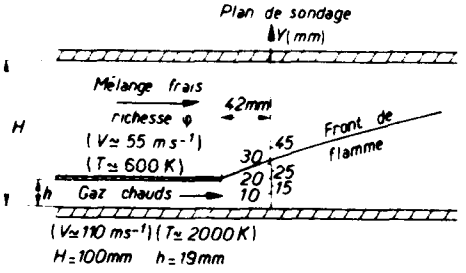

Fig. 6 – Schéma du foyer d'étude de la combustion turbulente. Localisation des points de mesure.

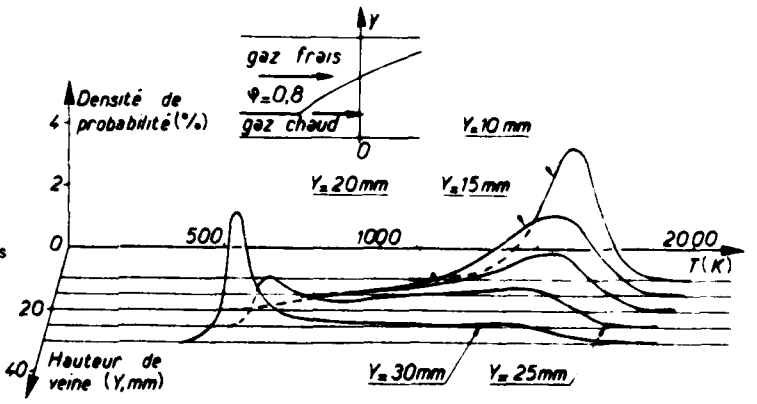

Fig. 7 – Foyer d'étude de la combustion turbulente. Cas d'une richesse $\varphi = 0,8$. Histogrammes de températures instantanées mesurées par pyrométrie optique.

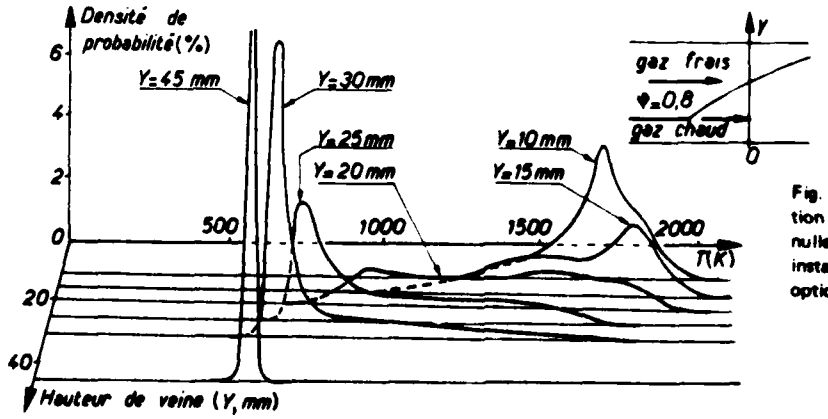

Fig. 8 – Foyer d'étude de la combustion turbulente. Cas d'une richesse nulle. Histogrammes de températures instantanées mesurées par pyrométrie optique.

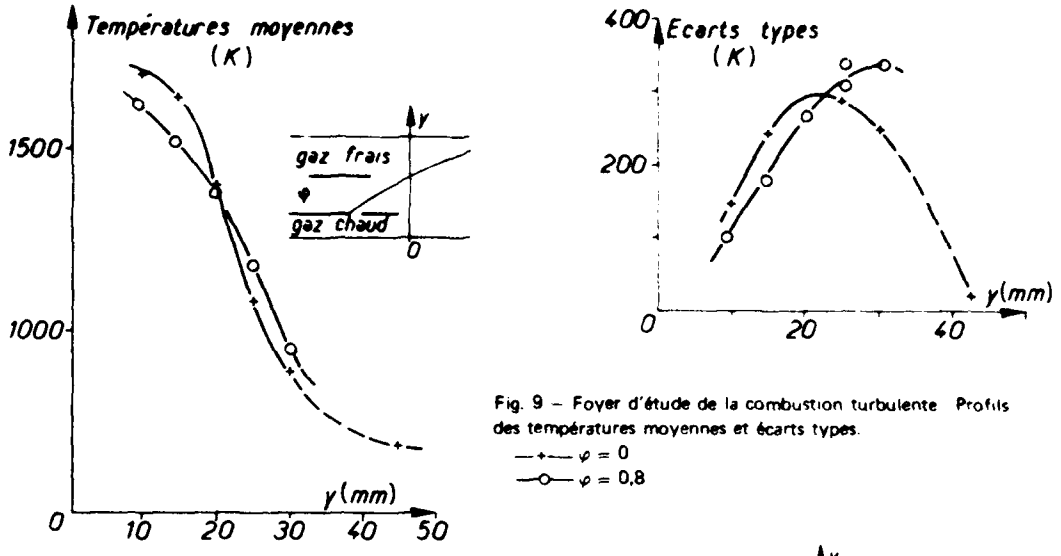

Fig. 9 – Foyer d'étude de la combustion turbulente Profils des températures moyennes et écarts types.
—+— $\varphi = 0$
—○— $\varphi = 0,8$

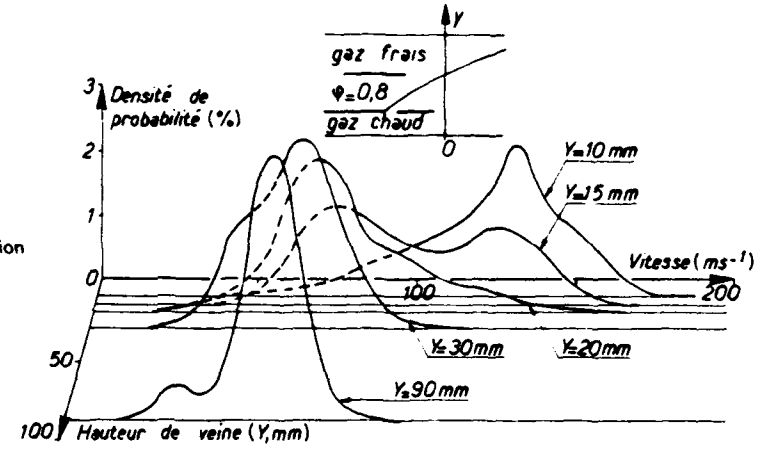

Fig. 10 – Foyer d'étude de la combustion turbulente. Cas d'une richesse $\varphi = 0,8$. Histogrammes de vitesses instantanées mesurées par vélocimétrie laser.

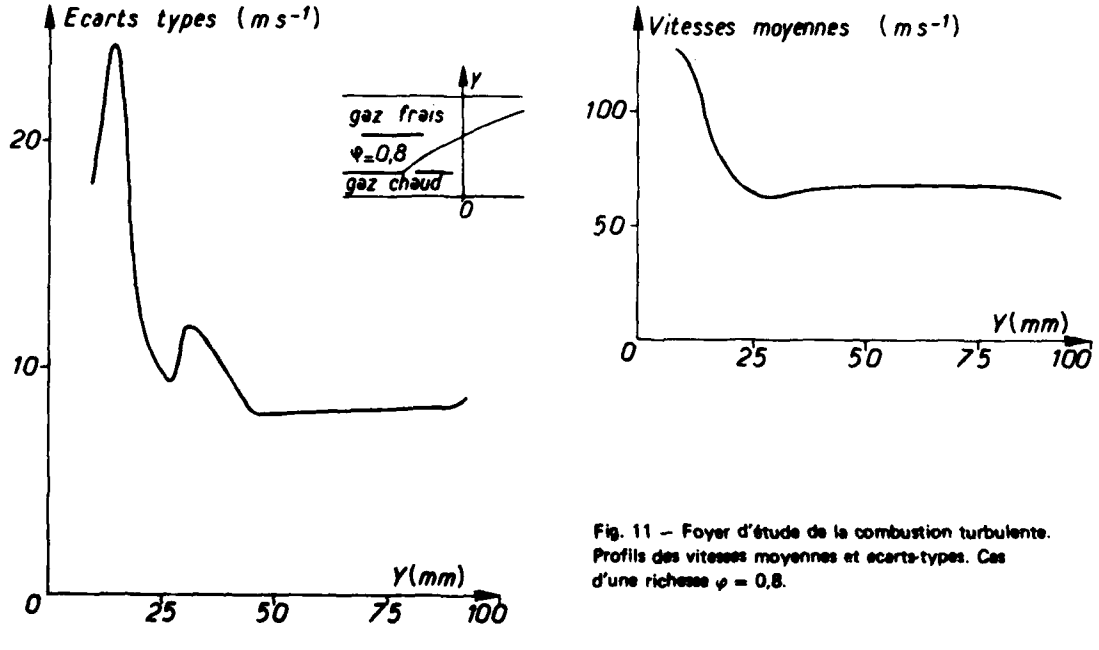

Fig. 11 – Foyer d'étude de la combustion turbulente. Profils des vitesses moyennes et écarts-types. Cas d'une richesse $\varphi = 0,8$.

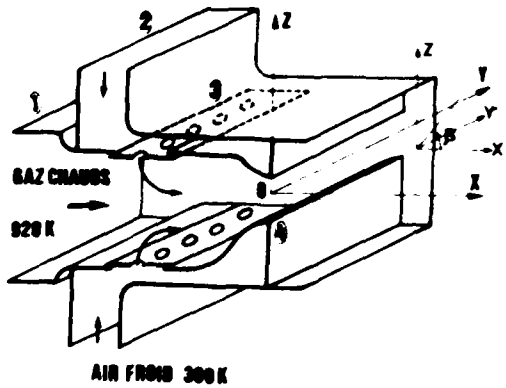

Fig. 12 – Coupe schématique du dispositif d'étude de la dilution.
1 – Canal d'injection principale
2 – Canal d'injection secondaire
3 – Injecteurs amovibles
4 – Convergent de sortie.

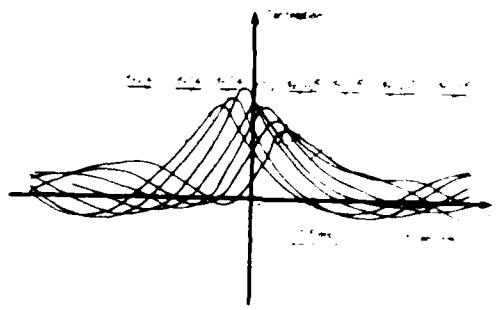

Fig. 13 – Foyer de dilution corrélations spatio temporelles

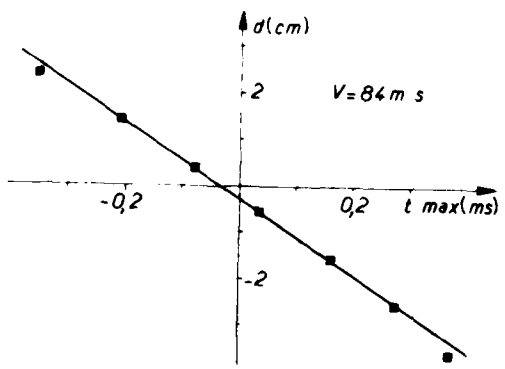

Fig. 14 – Foyer de dilution : déplacement des maximums de corrélation.

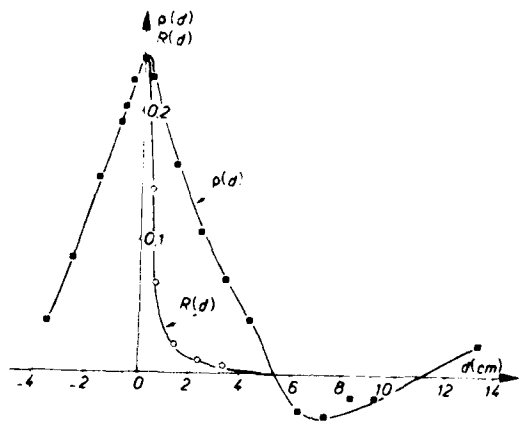

Fig. 15 – Foyer de dilution : corrélations ρ(d) et R(d).

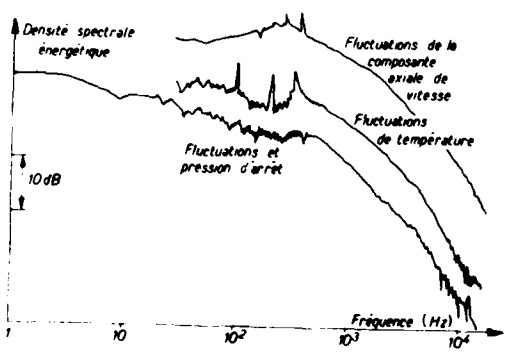

Fig. 16 – Comparaison des spectres de température, de pression et de vitesse d'écoulement en un même point à la sortie du foyer de dilution.

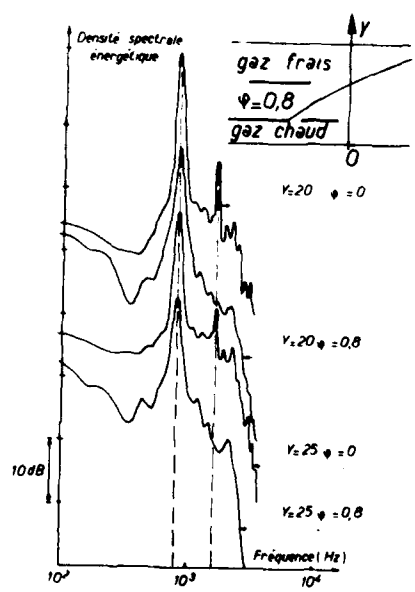

Fig. 17 – Foyer d'étude de la combustion turbulente. Spectres d'émission de la flamme.

DISCUSSION

D.L.Schultz, UK

Is the constant k = 2 based on theoretical or experimental results? You say in your paper that k is of "order" 2 and I would like to know what the range of k might be.

Réponse d'auteur

Ce résultat est essentiellement expérimental, obtenu sur diverses expériences à températures variées. Ce résultat est à environ 10% près c'est à dire que l'on peut obtenir aussi bien un coefficient de 1.8 au 2.2. Une justification théorique a été présentée en référence (1) dans le papier écrit.

M.Mouranche, Fr

L'utilisation de la pyrométrie optique que vous avez décrite pour la mesure des températures de gaz est très séduisant. Quelles sont ses limitations d'emploi sur les montages d'essai de combustion?

Réponse d'auteur

La seule condition d'utilisation comme pour beaucoup de méthodes optiques est de disposer de deux orifices pour faire traverser le faisceau optique. Il est également nécessaire qu'il n'y ait pus de particules solides de trop grande dimension dans le gaz; mais la principale limitation de la méthode résulte de l'integration des températures sur le chemin optique.

VELOCITY AND TEMPERATURE MEASUREMENTS IN A PREMIXED FLAME WITHIN AN AXISYMMETRIC COMBUSTOR

by

A.M.K.P. Taylor and J.H. Whitelaw
Imperial College of Science and Technology
London SW7 2BX, England.

SUMMARY

Measurements of velocity, temperature and noise characteristics are reported for a premixed natural-gas, air flame stabilised on a disc baffle located on the axis of a round pipe and for a corresponding isothermal flow. The stability limits of the flame are identified and measurements of mean axial velocity, the variance of the corresponding fluctuations and noise intensity provided for equivalence ratios in the range 0.7 to 1.6. Centre-line distributions of mean axial velocity, the variance of the corresponding fluctuations and mean temperature are reported and an analysis presented of the uncertainties of the laser-anemometer instrumentation and bare-wire thermocouple measurements. It is shown that the range of equivalence ratios which allow stable combustion is comparatively small; that the maximum and minimum mean velocities and the length of the recirculation region are increased by combustion; and that the centre-line distribution of mean temperature is comparatively uniform for more than 3 baffle diameters downstream.

LIST OF SYMBOLS

$\overline{h}$	Mean surface heat transfer coefficient	
$\overline{h'T'_g}$, $\overline{h'T'_w}$	Correlation between fluctuating surface heat transfer coefficient and fluctuating gas/wire temperature	Eq. 2
N	Population size; Eq. 1	
$\overline{p}$, p'	Mean, fluctuating pressure	
r	Radial distance	
R	Radius of combustor	
$\overline{T}$, T'	Mean, fluctuating temperature	
$\overline{T}_g$, $\overline{T}_w$	Mean temperature of gas and wire; Eq. 2	
U	Mean axial velocity	
U_o	Annular bulk velocity	
$[U_n]$	n^{th} sample of axial velocity; Eq. 1	
$\overline{u^2}$, $\overline{v^2}$	Variance of axial, radial velocity fluctuations	
$\overline{uv}$	One-point correlation	
ϕ	$\frac{\text{(volumetric) fuel/air ratio}}{\text{stoichiometric (volumetric) fuel/air ratio}}$	

1. INTRODUCTION

The two main purposes of this paper are to present measurements of the velocity and temperature characteristics of bluff-body stabilised, premixed methane-air flames and to assess the precision of the results. Laser-Doppler anemometry was used for measurements of mean velocity and related one point correlations, and bare-wire thermocouples gave values of mean temperature. The flow arrangement comprised a 80mm diameter pipe with a 39.8mm diameter stabiliser disc and measurements were obtained at (volumetric) equivalence ratios of between 0.70 and 1.6 and upstream cold-flow pipe Reynolds numbers of approximately 33,000.

The flow configuration is relevant to the afterburners of gas-turbine combustors and the assessment of the precision is relevant to velocity and temperature measurements in a wide range of combusting flows. Stabilised, premixed flames have previously been investigated in, for example, references 1 to 6. Assessments of the precision of velocity measurements in combusting flows have been reported for example, in references 7 and 8 and that of temperature measurements in references 9 to 11.

In the present paper the velocity, temperature and sound-intensity results are presented in section 3, which is preceeded by a description of the geometry and instrumentation in Section 2. Section 4 provides careful consideration of error sources and the paper ends with summary conclusions.

2. FLOW AND INSTRUMENTATION ARRANGEMENTS

Figure 1 presents a line diagram of the flow configuration and shows the mild-steel pipe of 1.83m length coupled to a supply system for air and town gas (94% CH_4). Measurements have been obtained with the baffle located 0.8m from the open end of the

pipe. As shown, vitreous silica plate windows were set into the combustor wall and allowed optical access for the laser-Doppler anemometer. The inside diameter of the pipe was circular to within 1mm except near the windows where this figure decreased to around 3mm. The flow rates of town gas and air were measured with orifice plates and manometers: the accuracy of the measurements was of the order of 3% with a reproducibility of 0.5%.

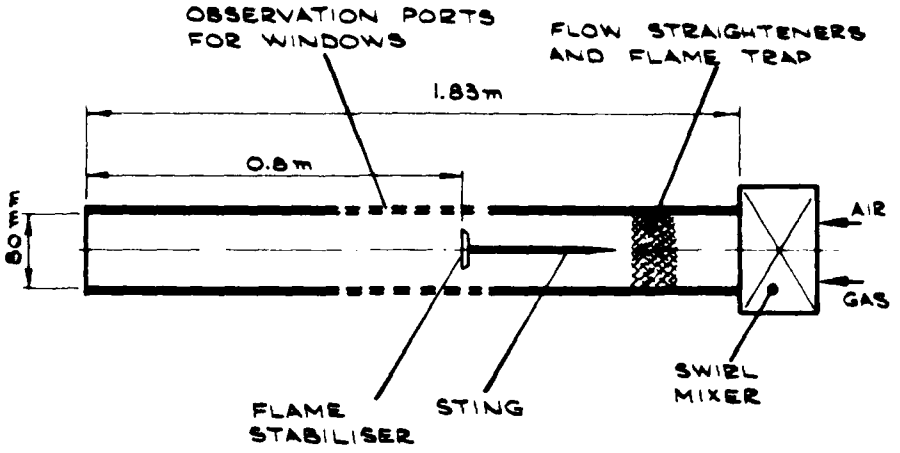

FIG.1. LINE DIAGRAM OF FLOW CONFIGURATION.

Velocity characteristics were obtained with the laser-Doppler anemometer operating in a forward-scatter, fringe mode with the optical characteristics of table 1. The Doppler signals were detected by a photomultiplier (RCA Model 4836) and processed by a spectrum analyser (Hewlett-Packard model 141T/8552A/8553B) interfaced to a microprocessor (Intersil Model IM6101), as described in reference 12. The probability density function of velocity was obtained by counting the occurrence of doppler signals in the frequency spectrum. Signals were distinguished from noise by setting a threshold level of occurrence in the frequency spectrum. The flow was seeded with titanium dioxide particles which, before their introduction, had a nominal diameter of 0.45μm. The maximum data rate observed at the photomultiplier output was of the order of 5000 signals/s; approximately 10 minutes were required to form the mean and variance from 10,000 (or more) signals.

TABLE 1	Optical characteristics
Laser power	600 mW
Laser wavelength	514.5 nm
Fringe spacing	2.23 μm
Length of measuring volume at $1/e^2$ intensity	2 mm
Diameter of measuring volume at $1/e^2$ intensity	200 μm
Frequency shift	21 MHz

The optical components of the anemometer were assembled on a bench and translated in two orthogonal planes by a milling-table arrangement which allowed location to better than 0.1mm.

Temperatures were measured with a bare-wire thermocouple (platinum: 13% rhodium-platinum) constructed from 80μm diameter wire. The hot junction was formed at the centre of a 10mm length of wire and had a diameter of approximately 90μm. The thermocouple was calibrated for radiation effects in the manner described in reference 11 and was inserted into the flow, through plugs located in the combustor wall, and traversed with the milling-table.

Sound intensity levels were measured with a microphone (General Radio Model 1560-P4) which was located approximately 2m from the combustor. The signal from the microphone was analysed with a spectrum analyser (General Radio Model 1564-A).

3. RESULTS

Confined, bluff-body stabilised flames are known to have limited ranges of stable combustion and can also have fluctuation energy concentrated at discrete frequencies As a consequence, the stability characteristics of the combusting flow was investigated over a range of equivalence ratio, ϕ, and are described in the following subsection. This is followed by two subsections describing the detailed velocity and temperature results, respectively, at ϕ = 0.70.

3.1 Influence of equivalence ratio

The stability characteristics of the flames were examined in the range of equivalence ratio from around 0.5 to 1.6 by visual observation and by the measurement of sound intensity and velocity characteristics.

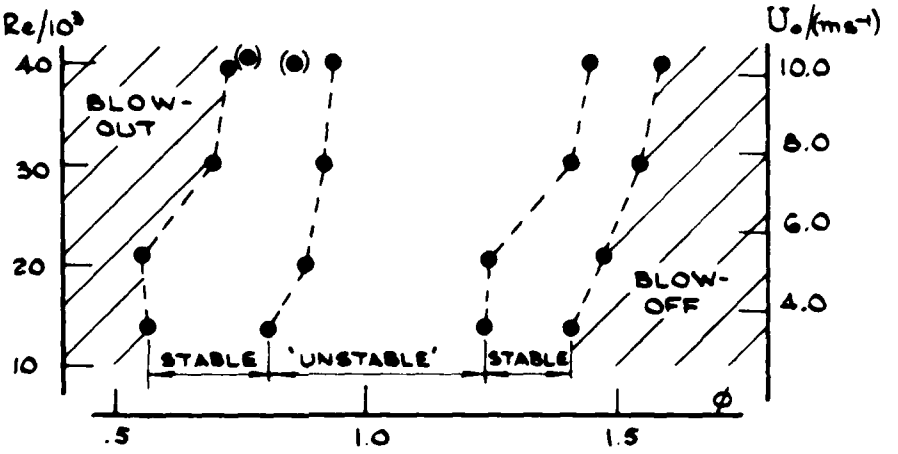

FIG.2. FLAME EXTINCTION DATA WITH U_o AS PARAMETER.

Figure 2 shows the stability limits of the flame as a function of (annular) bulk air velocity, U_o and equivalence ratio. The shaded areas define the familiar fuel-rich and -lean extinction limits. Adjacent to these limits are regions, designated as 'stable', which refer to the presence of the flame only downstream of the bluff-body. Between these regions is a range marked 'unstable' which corresponds to operation with a flame visible upstream of the baffle. At small values of U_o ($\lesssim$6ms^{-1}) flashback occurred, with the flame attaching to the boundary layer of the sting upstream of the baffle. At values of U_o appropriate to the data presented here (U_o = 8.3 ms^{-1}), the flame was unattached to the sting. The boundary between each flow regime is subject to an uncertainty of $\pm 0.03\phi$.

Figure 3 shows the related sound output from the combustor. The sound level within the 'stable' regions was relatively low, being less than 10dB above the equivalent (inert) air flow. As the 'unstable' range was approached the sound level increased markedly (15dB), together with the variance of velocity which is shown in figure 4.

The flow pulsations were so violent that damage occurred to the glass observation windows, thereby limiting the extent of measurement in the 'unstable' region. The appearance of the probability density function of axial velocity in this region was either heavily skewed or bimodal, the latter suggesting a harmonic oscillation of velocity. Frequency analysis of the sound level confirmed the presence of a preferred frequency of about 80Hz which corresponded to an acoustic quarter-wave arrangement.

Figure 5 indicates a large variation of mean velocity, at x/R=1.63 and r/R=0, as the equivalence ratio is altered. This is due to a related change in the length of the recirculation region since, as figure 6a confirms, a small change in this length can result in a large change in velocity. In addition, however, equivalence ratios of the order of unity undoubtedly cause much higher centre-line velocities since the maximum value of U/U_o of figure 6a is around 1.5 and that of figure 4 is around 3.0.

3.2 Velocity characteristics

Figs. 6a and b present the centreline values of the mean and variance of axial velocity in reacting and non-reacting flow. The length of the recirculation zone is about 40% greater in combustion as compared with the isothermal flow. Similarly large increases have been reported by Winterfeld, reference 5, for confined flows; in contrast, Durao and Whitelaw, reference 13, measured a smaller ($\lesssim$5%) increase for unconfined

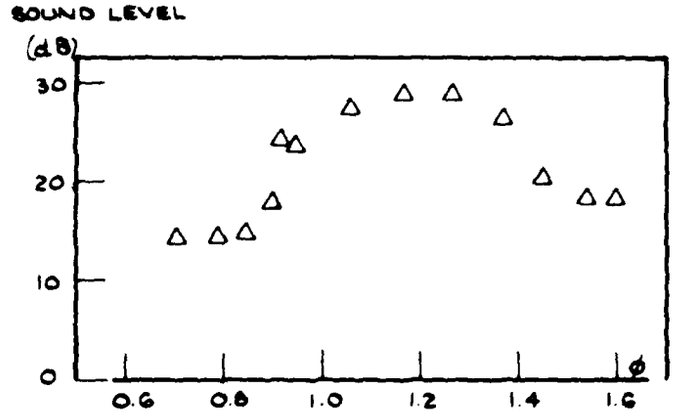

FIG.3. SOUND LEVEL AS A FUNCTION OF EQUIVALENCE RATIO.

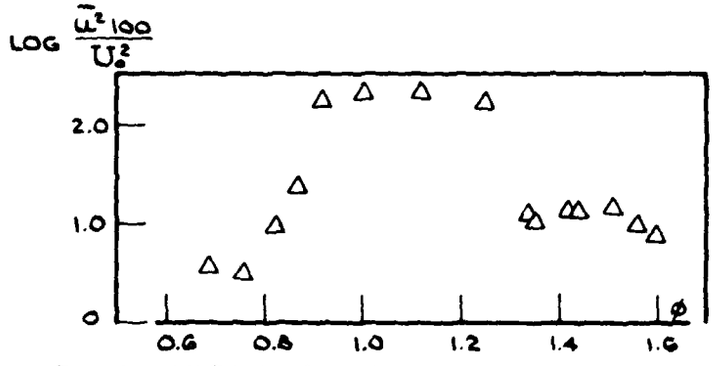

FIG.4. VARIANCE OF VELOCITY AS A FUNCTION OF EQUIVALENCE RATIO. $\left(\frac{r}{R}=0,\ \frac{x}{R}=1.63\right)$

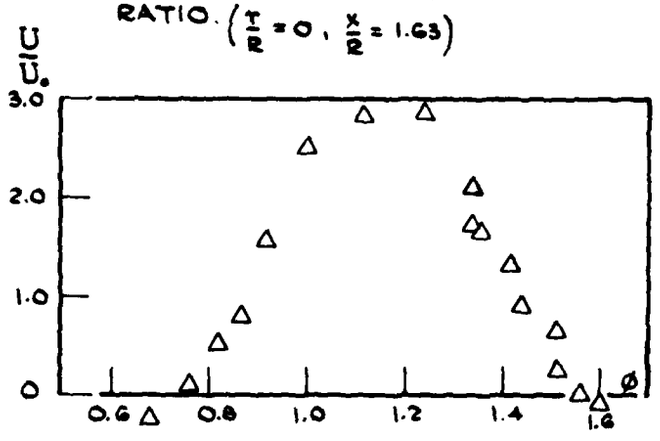

FIG.5. MEAN VELOCITY AS A FUNCTION OF EQUIVALENCE RATIO $\left(\frac{r}{R}=0,\ \frac{x}{R}=1.63\right)$

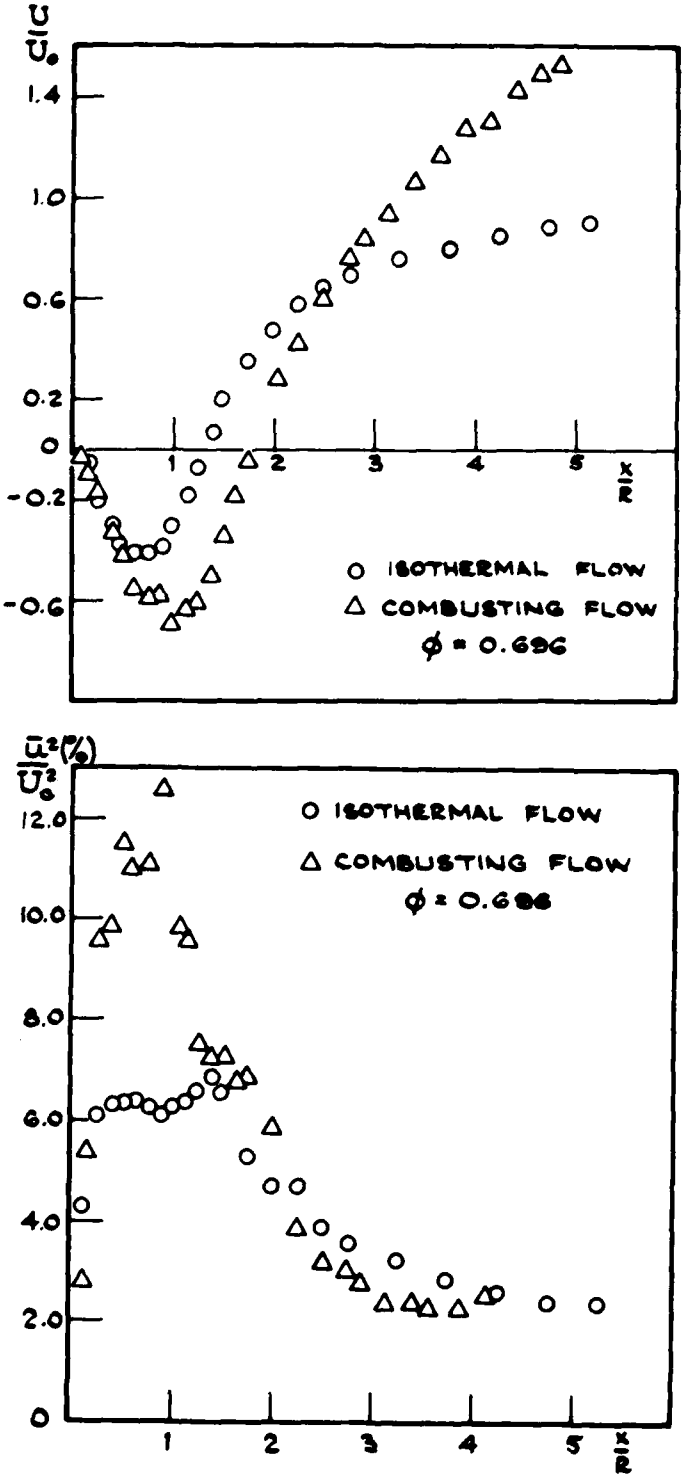

FIG. 6. CENTRELINE PROFILES OF THE MEAN (a) AND VARIANCE (b) OF AXIAL VELOCITY.

flows. Downstream of the recirculation zone, the axial velocity continues to accelerate faster than in isothermal flow. This is a result of the greater velocities away from the axis which come about through the increased volume of the gases.

The large values of $\overline{u^2}$ within the recirculation zone imply that the flow is indeed fully turbulent, and that no laminarisation has occurred. The magnitudes in the reacting flow are, at most, double those in the equivalent isothermal flow. By implication, turbulence levels throughout the recirculation zone will have increased, although momentum transfer will be nett reduced (compared to isothermal flow) because of the fall in density. By analogy, mass transfer, which is crucial to the mechanism of flame stabilisation, will also have been reduced. This expectation is confirmed by the residence time measurement of reference 5.

As the equivalence ratio tends to stoichiometric, figures 3 and 4, the length of the recirculation zone becomes smaller while the levels of $\overline{u^2}$ greatly increase. The decrease in the recirculation zone length (a trend that has also been reported by reference 5)which would tend to reduce the flame holding ability of the bluff-body, is more than compensated for by the increase in the level of $\overline{u^2}$. However, the evidence of spectral analysis of the sound level suggests that combustion-induced acoustic oscillations play an ever larger role, and the variation of $\overline{u^2}$ and the appearance of bimodal probability density functions of U are further confirmation of this. The presence of the flame upstream of the baffle is thus probably a result of both bulk transport of reacting gas by the oscillations, together with the instantaneous velocity falling below the flame speed. The violence of the fluctuations, together with a flame front which no longer develops from the bluff-body tip, make it uncertain to what extent simple models of bluff-body physics (based on a well-stirred reactor) still apply.

3.3 Temperature distribution

The mean temperature profile on the centreline, figure 7, is quite uniform, except for the area immediately adjacent to the bluff-body. It suggests rapid mixing and that the 'well-stirred reactor' model of the recirculation zone is qualitatively correct, although it is certain that radial profiles of temperature would show greater variations. The velocity fluctuations on the centre line correspond to intensities of greater than 15% even at x/R of 5 and to much larger values for x/R < 5; they suggest large temperature fluctuations and that the adiabatic flame temperature will be approached, on the centre line and over much of the range of figure 6, for a significant period of time.

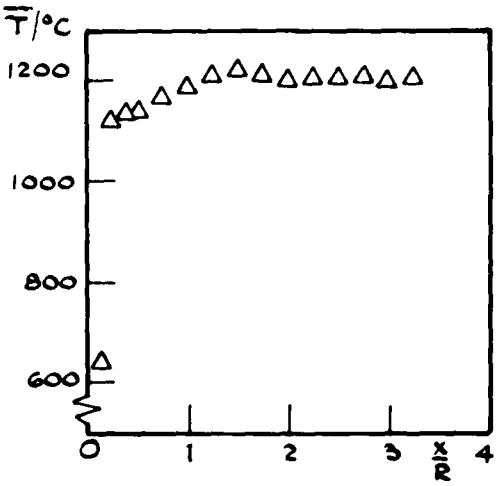

FIG.7. CENTRE-LINE PROFILES OF MEAN TEMPERATURE.

4. Discussion of measurement accuracy

The purpose of this section is to appraise the accuracy of the measurements of the previous section and to comment on the accuracy of the measurement of velocity and temperature of combusting flows in general. The discussion is again presented in three parts which correspond closely to those of the previous section.

4.1 Equivalence ratio and flow symmetry

The results of figures 2 to 5 imply that the equivalence ratio should be maintained constant, at a known value, within limits which depend upon the value of ϕ and the required constancy of the combusting flow. A variation in ϕ from 0.80 to 0.81, for example, can result in a 10% change in the mean velocity on the centre line. In the present case, the equivalence ratio was determined by measuring the volume flows of gas with orifice meters and the expected accuracy of the resulting value was of order 3% with a constancy of around 1%.

The flow symmetry was tested, in detail, with non-combusting flow and showed asymmetries of less than 5% of the bulk velocity. These were caused, at least in part, by the departures from circularity of the combustor pipe previously referred to in Section 2.

4.2 Velocity characteristics

Table II identifies sources of possible error appropriate to the present laser-Doppler anemometer: the influences of refraction index gradients on signal quality and of the TiO_2 particle on the combustion process are not considered since, according to reference 14, they are expected to be negligible.

TABLE II: Possible sources of error in velocity measurements

ERROR SOURCE
Finite Transit time broadening
Mean Velocity gradient broadening
Particle concentration broadening
Instrument noise
Size of population used for evaluation of mean and variance
Velocity weighting of particle statistics
Density weighting of particle statistics

The magnitude of the first four effects can be determined from a knowledge of the flow and of the standard formulae given, for example, in reference 14. Taken together, they imply an uncertainty in mean velocity which is less than 0.5% of the maximum velocity and an uncertainty in the variance of velocity fluctuations corresponding to an overestimation of up to around 1%. It should be noted that steeper gradients than those encountered here can occur when radial profiles are measured and usually result in larger uncertainties.

The number of velocity values used to form the mean and variance was at least 10,000 and, according to the analysis of reference 15, implies uncertainties (which depend on the standard deviation for mean velocity alone) of $\pm$1% and $\pm$3% in the mean and variance of velocity respectively, at 95% confidence limits.

The uncertainties associated with the last two items of Table II are more difficult to quantify and, as will be indicated, are potentially longer than those discussed in the previous two paragraphs. The importance of the averaging procedure (convection weighting) has been assessed in a number of papers, for example references 16 to 21, and depends on the relative time scale of particle arrival, the sampling rate of the instrumentation and the frequency of the energy containing turbulence. In the present flow, the time scale of particle arrival is greater than that of the sampling, which is limited to a minimum of 42μs between successive measurement. The measurements are therefore controlled by the particle arrival rate, not by the sampling technique, and an error will result with averages formed from the expression

$$\bar{U} = \frac{1}{N} \sum_{n=1}^{N} [U_n] \qquad (1)$$

as they were in this paper.

Averaging algorithms which properly account for "velocity weighting" require knowledge of the joint velocity probability density distribution for three components of velocity (refs. 16 & 19). A "one-dimensional" correction can be applied to the data and its validity is restricted (refs. 16 & 18) to flows in which the velocity components, normal to the velocity component measured, are small. Measurements on the centreline of the transverse fluctuating component of velocity in isothermal flow (reference 22) show that ($\overline{v^2}/\overline{u^2} \gtrsim 1$), so that application of the "one-dimensional" correction is not justified.

An exact value cannot therefore not be obtained without three-dimensional measurements and, even then, may be complicated by the existence of signal amplitude bias as discussed in references 21 and 23. An estimate of velocity weighting for this flow can be obtained by using the (calculated) corrections for $\overline{v^2}/\overline{u^2} = 1$ and $\overline{uv} = 0$ given in reference 17. This analysis suggests that the magnitude of U/U_o is too large by about 0.08 U/U_o, and $\overline{u^2}/U_o^2$ too small by about 0.024 $\overline{u^2}/U_o^2$, at $x/R = 0.75$. These values are expected to be the largest that will apply within the recirculation zone: downstream (at, say, $x/R = 4.50$) the errors will be +1% and -2% of the local value of mean and variance.

The error arising from local fluctuations in the volumetric seeding concentration requires measurements, or assumptions, concerning the magnitudes of the fluctuations of temperature and pressure, so as to make use of the estimates provided by reference 24. In this case, $\sqrt{\overline{T'^2}}/\overline{T}$ and $\sqrt{\overline{p'^2}}/\overline{p}$ have been taken as 0.20 and 0.03 respectively. The latter value is the maximum expected, and will occur in the presence of violent combustion-induced oscillations (25). The only important error is that caused by the temperature fluctuations in the value of mean velocity, amounting to a possible 5% underestimation of

the local value.

The above arguments suggest that the errors depend on the turbulence intensity, and that they can only be estimated. The probable uncertainty in the mean and variance measurements are of the order ±2% in both mean and variance downstream of the recirculation zone but may be up to ±5% and an underestimation of about 25% in the local values of mean and variance respectively within the recirculation zone.

4.3 Temperature characteristics

Bare-wire thermocouples were preferred to a suction pyrometer partly on grounds of size but also because of the dependence of pyrometer measurements on suction velocity as shown, for example, in reference 11. They have, however, the disadvantage of greater fragility, particularly with the 80μm diameter wire used. Indeed, measurements with equivalence ratios around unity proved to be very difficult due to frequent breakage in the corresponding pulsating flow.

The thermocouples were arranged, as described in section 2, and had a probable conduction error of less than 0.1%. The magnitude of the radiation correction has been shown to be of order 80°C at 1400°C in a free flame and, with the lower temperatures and confined nature of the present arrangement was certainly less than 40°C and probably much less.

In addition to radiation and conduction effects, the relationship between the wire and gas temperature involves the correlations between an 'overall' heat-transfer coefficient and the gas and wire temperatures,

$$\text{i.e. } \bar{T}_w = \bar{T}_g + \overline{h'T_g'}/\bar{h} - \overline{h'Tw'}/\bar{h} \quad - \text{radiation-conduction.} \qquad (2)$$

For an infinitely small thermocouple junction, Tg' and Tw' are identical and the influence of the correlations is zero. The results of reference 11 show that the influence of the correlations is also zero for a 40μm thermocouple. A reasonable assessment of the accuracy of the present measurements is, therefore -50°C, + 20°C.

5. SUMMARY CONCLUSIONS

The following main conclusions may be extracted from the preceeding text:

1. Combustion-induced oscillations become increasingly important as the equivalence ratio approaches unity, where the flow is dominated by an acoustic oscillation associated with greatly increased sound intensities and velocity variance. The range of equivalence ratios for which stable combustion can be achieved is quantitied and shown to be small.

2. Centre-line distributions of mean axial velocity and the variance of the corresponding fluctuations have been obtained at a volumetric equivalence ratio of 0.7 and in isothermal air flow and have the same general shape. The maximum negative and positive velocities are larger for the combusting flow and the recirculation length is larger by around 40%. The velocity variance is generally larger for the combusting flow and much larger (x2) in the recirculation region. The mean temperature distribution is comparatively uniform, consistent with a well-stirred reactor assumption.

3. The uncertainties in the measurements are considered and shown to be significant. Small changes in equivalence ratio give rise to significant changes in the length of the recirculation region and to local flow properties. The velocity measurements, in regions of high values of velocity variance, are subject to uncertainties which cannot be quantified exactly; the mean and variance of velocity can be subject to errors of up to ±5% and -25% respectively although the corresponding figures away from the recirculation region are of the order of 2% in each quantity. The mean-temperature values are subject to uncertainties of around +20°C, -50°C.

1. Longwell, J.P., Chenevey, J.E., Clark, W.W., Frost, E.E. "Flame Stabilisation by baffles in a high velocity gas stream". Third Symposium on Combustion and Flame and Explosion Phenomena, Baltimore, Maryland. Williams & Wilkins Company, 1949, pp.40-44.

2. Barrère, M. and Mestre, A. "Stabilisation des flammes par des obstacles". Selected Combustion Problems, London. Butterworths Scientific Publications, 1954, pp.426-446.

3. DeZubay, E.A. "Characteristics of disk-controlled flame". Aero Digest, July 1950.

4. Clare, H., Durão, D.F.G., Melling, A., Whitelaw, J.H. "Flame Stabilisation of a V-gutter stabilized flame by Laser Anemometry and Schlieren photography". Applications of Non-Intrusive Instrumentation in Fluid Flow Research, AGARD-CP-193, 1976, Paper no. 26.

5. Winterfeld, G. "On processes of turbulent exchange behind flame holders". Tenth Symposium (International) on Combustion, The Combustion Institute, 1965, pp.1265-1275.

6. El-Banhawy, Y., Melling, A., Whitelaw, J.H. "Combustion-Driven Oscillations in a small Tube" Combustion and Flame, Vol.33, 1978, pp.281-290.

7. Self, S. and Whitelaw, J.H. "Laser Anemometry for Combustion Research". Combustion Science and Technology, Vol.13, 1976, pp.171-197.

8. Durão, D.F.G. and Whitelaw, J.H. "Critical Review of Laser Anemometry Measurements in Combusting Flows", in Progress in Aeronautics and Astronautics, Volume 53 Experimental Diagnostics in Gas Phase Combustion Systems, 1977, pp.357-372.

9. Bilger, R.W. "Probe measurements in turbulent combustion." ibid., pp.49-69.

10. Moneib, H. "Experimental study of the fluctuating temperature in inert and reacting turbulent jets". Ph.D. Thesis, University of London, 1980.

11. Attya, A.M. "Temperature and species concentration measurements in unconfined kerosene spray flames", 1980. Fluids Section, Mechanical Engineering Dept., Imperial College. Report FS/80/15.

12. Durão, D.F.G., Laker, J., Whitelaw, J.H. "A micro-processor controlled frequency analyser for laser-Doppler anemometry", 1978. Fluids Section, Mechanical Engineering Dept., Imperial College. Report FS/78/21.

13. Durão, D.F.G. and Whitelaw, J.H. "Velocity characteristics of disk-stabilised diffusion and premixed flames", in Progress in Aeronautics and Astronautics, Volume 53: Experimental Diagnostics in Gas Phase combustion systems, 1977, pp.395-409.

14. Durst, F., Melling, A., Whitelaw, J.H. "Principles and practice of laser-Doppler anemometry". London, Academic Press, 1976.

15. Yanta, W.J. "Turbulence measurements with a laser-Doppler velocimeter". 1973 Naval Ordnance Laboratory NOLTR 73-94, pp.11-13.

16. Dimotakis, P.E. "Single scattering particle laser-Doppler measurements of turbulence". Application of non-intrusive instrumentation in fluid flow research, AGARD-CP-193, 1976. Paper no.10.

17. McLaughlin, D.K. and Tiederman, W.G. "Biasing correction for individual realization of laser anemometer measurements in turbulent flows". The Physics of Fluids, Vol.16, no.12, December 1973.

18. Barnett, D.O. and Bentley, H.T. (1974). "Statistical bias of individual realization laser anemometers". Proceedings of the second international workshop on laser velocimetry. Vol.I, pp.428-444.

19. Buchhave, P. "Biasing Errors in individual particle measurements with the LDA-Counter signal processor". Proceedings of the LDA-Symposium, Copenhagen 1975, pp.258-278.

20. Durão, D.F.G. and Whitelaw, J.H. "The influence of sampling procedures on velocity bias in turbulent flows". ibid., pp.138-149.

21. Durão, D.F.G. and Whitelaw, J.H. "Bias effects in laser-Doppler anemometry". J. Phys. E: Sci. Instrum., Vol.13, 1980, pp.442-445.

22. Taylor, A.M.K.P. Ph.D. Thesis, University of London. In preparation.

23. Durão, D.F.G. and Whitelaw, J.H. "Relationship between velocity and signal quality in laser-Doppler anemometry". J.Phys.E: Sci. Instrum., Vol.12, 1979, pp.47-50.

24. Asalor, J.O. and Whitelaw, J.H. "The influence of combustion-induced particle concentration variations in laser-Doppler anemometry". Proceedings of the LDA Symposium, Copenhagen, 1975, pp.115-137.

25. Sherwood, M. Private Communication.

ACKNOWLEDGEMENT

Financial support from the Science Research Council is gratefully acknowledged.

DISCUSSION

F.C.Gouldin, US

In your presentation you noted the presence in the combustor of a flame sheet which begins at or near the edge of the flame stabiliser and extends downstream, and you referred to the recirculation zone behind the stabiliser as a stirred reactor. By flame sheet I assume you mean a thin reaction zone in which fuel and air react to form products. If this interpretation is true, what are the significant reactions occurring in the stirred reactor region of the stabiliser wake?

Author's Reply

The phrase "well stirred reactor" refers to a (mathematical) model sometimes used to describe the mechanism of stabilisation behind a bluff body. Its usefulness lies in being able to assign one representative value of any quantity to the reacted and unreacted gases. The "reactor" extends into both reacted and unreacted gases. Whilst there are no reactions taking place within the recirculation zone, the products (and temperature) are uniformly distributed in space (well-stirred). In the present case, for example, 1200°C would be a good estimate of the temperature of burnt gases within the recirculation zone.

A.M.Mellor, US

Did you observe the flashback phenomenon if the pipe was terminated in the plane of the disc?

Author's Reply

I do not recollect having observed flashback for the (few) experiments conducted under conditions when the pipe was terminated in the plane of the disc.

M.Nina, Po

(1) The size of the recirculation zone depends on the value of ϕ: in your Figure 6 you compare centre-line velocity profiles, isothermal and $\phi = 0.696$. Is there a reason for choosing this value?

(2) Could you tell us more about your fine-wire thermocouple problems, such as life time and reasons and locations of breakages?

Author's Reply

(1) The only significance of $\phi = 0.696$ ($\phi = 0.70$ to within the limits of reproducibility) was that it was an operating point which lay far from the 'unstable' range of operation.

(2) The lifetime of the thermocouple was principally determined by the equivalence ratio. Breakage would occur close to the thermocouple bead. Values of equivalence ratio much greater than about 0.7–0.8 resulted in almost immediate breakage. We interpret this as a result of instantaneous values of temperature being much higher than the mean, thus approaching the fusion temperature of the metals.

N.I.Hay, UK

I would like to ask two questions: the first, under unstable conditions what was the pressure ratio across the flow straightener and did any swirl survive downstream of it? The second question, did the flame stabilise on the flame trap upstream of the baffle?

Author's Reply

(1a) We have no information on the pressure drop across the flow straightener.

(1b) We observed no swirl downstream of the straightener.

(2) The flame would not normally stabilise on the trap upstream of the baffle. The exception to this behaviour arose if, after prolonged operation in the 'unstable' mode, the flame trap (a wire mesh screen) was shaken out of its position.

J.S.Lewis, UK

Will you attempt to include the unstable mode of operation in your theoretical model of this test rig? If so, will you require measurements to be made during unstable operation?

Author's Reply

Some of the measurements represented in the first three graphs were for unstable combustion and they gave the impression from the probability density, which was bimodal, that perhaps the vibrations may have been sinusoidal. The output of the thermocouple, all of the five seconds that it lasted, seemed to indicate that we had a periodic fluctuation but we certainly wouldn't attempt to model that kind of flow. However, I believe that you have done some work using a program on combustion induced oscillations.

C.Winterfeld, Ge

The correlation of the results has been done in a way which is different from that normally used in the literature. Could the authors please comment, on how their results compare with former works reported in the literature?

Author's Reply

That's true, yes. I believe that your own paper presented at the Combustion Symposium indicated that as one increases the equivalence ratio the recirculation length becomes shorter. We did not make detailed enough measurements, because as I pointed out the thing kept coming to bits, of how much shorter the recirculation length became. All we know is that it did become shorter because we measured it at a point which was negative when we started off, it then became positive velocity, and then finally ended up at the rich extinction limit as a negative velocity again, but we had no idea of just how the recirculation length itself varied. As to your point on the way we present the data, I agree that all papers represent it as on the diameter of the baffle. The reason I present it as a function of the radius of the containing pipe is historical and hangs over from my isothermal work. Also, it was convenient to normalise it in that fashion.

THE USE OF OPTICAL TECHNIQUES IN THE INTERPRETATION OF HEAT TRANSFER MEASUREMENTS

J.M. Owen and J.R. Pincombe
School of Engineering and Applied Sciences
University of Sussex
Falmer, Brighton, BN1 9QT, U.K.

SUMMARY

Optical techniques have been used to study the flow structure, and to gain a better understanding, of the convective heat transfer inside rotating cavities. Flow visualization has been used to determine the amount of coolant necessary to seal an air-cooled rotor-stator system, to delineate regimes of vortex breakdown in rotating cavities with axial throughflow, and to identify the flow regimes in a rotating cavity with a radial outflow of coolant. LDA measurements of the radial and tangential components of velocity inside the rotating cavity have been used to correlate the flow visualization results. For the radial outflow case, these velocity measurements are in good agreement with theoretical predictions. Measured Nusselt numbers reveal the presence of heat transfer regimes corresponding to those identified by the optical techniques.

LIST OF SYMBOLS

a	inlet radius
b	outer radius
$C_w \equiv Q/\nu b$	dimensionless flow rate
$D \equiv (\nu/\Omega)^{\frac{1}{2}}$	Ekman layer thickness parameter
$G \equiv s/b$	gap ratio
$G_c \equiv s_c/b$	shroud clearance ratio
$\overline{Nu}$	mean Nusselt number
Q	coolant volumetric flow rate
r	radial coordinate
$Re_r \equiv C_w b/2\pi r$	radial Reynolds number
$Re_z \equiv 2\bar{W}a/\nu$	axial Reynolds number
$Re_\theta \equiv \Omega b^2/\nu$	rotational Reynolds number
s, s_c	axial gap between the rotor and stator or rotor and shroud, respectively
u, v	radial, tangential components of velocity in a rotating frame
$\bar{v}, \bar{v}_o$	tangential component of the potential core in a rotating and stationary frame respectively
V_r, V_θ	radial, tangential components of velocity in a stationary frame
$\bar{W}$	bulk-average axial velocity in inlet pipe
z	axial coordinate measured from rotor
β	volume expansion coefficient
ΔT	temperature difference between the disc tip and the coolant
Δ_E, Δ_K	thickness of the inner and outer layers respectively
$\epsilon \equiv \bar{W}/\Omega a$	axial Rossby number
$\epsilon_r \equiv Q/4\pi r\Omega D$	radial Rossby number
$\lambda_{\theta o} \equiv \frac{1}{2}\beta\Delta T\Omega r/\bar{v}_o$	buoyancy parameter
ν	kinematic viscosity
ρ	density
Ω	rotational speed

Subscripts

o	$\Delta T = 0$

1 INTRODUCTION

In this paper, it is shown how the techniques of flow visualization and laser doppler anemometry (LDA) can be used to complement each other and to add to a better understanding of flow structure and convective heat transfer. In order to gain insight into the flow around turbine and compressor discs in gas turbine engines, the techniques have been applied to the study of flow inside the cavity between a rotating and a stationary disc and in the cavity between two corotating discs. Although the application is specialized, the techniques should be applicable to many other flow systems.

Fig. 1a shows a simplified model of an air-cooled turbine disc rotating close to a stator, and flow visualization has been used to examine the flow structure and to quantify the amount of coolant necessary to 'seal' the cavity (that is, to prevent the ingress of hot gas into the cavity). Fig. 1b shows a model of corotating compressor discs through the centre of which is an axial flow of air (simulating cooling air on its way to the turbine blades). The flow in this configuration is extremely complex, and the occurrence of vortex breakdown (1) can dramatically alter the flow structure and heat transfer inside the cavity. Fig. 1c shows a simplified model of air-cooled corotating turbine discs, and a number of regimes of heat transfer have been identified by Owen and Bilimoria (2). In the latter case, flow visualization and LDA measurements have provided an understanding of the flow structure and have enabled a simple theoretical model to be developed and tested(3).

A brief description of the experimental rigs and the optical instrumentation is presented in Section 2. Sections 3 and 4 describe the application of flow visualization and LDA, respectively, to the three rotating cavities described above.

2. EXPERIMENTAL APPARATUS

2.1 The rotating cavities

For the rotor-stator cavity shown in Fig. 1a, the rotor was a plane aluminium disc of radius b = 190 mm, and the stator and shroud were made from perspex. The gap, s, between the rotor and stator was 19 mm ($G = 0.1$, $G = s/b$) and the shroud clearance, s_c, was varied from 0.48 to 7.6 mm ($0.0025 < G_c < 0.04$, $G_c = s_c/b$). The rotor was driven up to 4000 rev/min ($Re_\theta = 10^6$, $Re_\theta = \Omega b^2/\nu$) by means of a variable-speed electric motor, and the coolant flow rate was supplied through the inlet pipe (a = 19 mm) at rates up to 0.06 m^3/s ($C_w = 2 \times 10^4$, $C_w = Q/\nu b$).

For the rotating cavity with axial throughflow shown in Fig. 1b, two different rigs were used. The isothermal rig comprised two perspex discs, of radius b = 190 mm, and a perspex shroud. The radius of the rotating inlet and outlet pipes was a = 19 mm, and the spacing between the discs was varied from $G = 0.133$ to 0.53. The cavity was rotated up to $Re_\theta = 4 \times 10^5$, and axial Reynolds numbers of $Re_z = 10^5$ ($Re_z = 2\bar{W}a/\nu$, $\bar{W}$ being the bulk-average velocity in the inlet pipe) were produced. The heat transfer rig was twice the size of the isothermal rig, and the discs were made from stainless steel and instrumented with thermocouples. The maximum axial and rotational Reynolds numbers on the heat transfer rig were 6×10^5 and 2.5×10^6, respectively.

The rotating cavity with radial outflow shown in Fig. 1c was based on the isothermal and heat transfer rigs described above. The only difference was that the perspex shroud contained thirty holes equi-spaced on the mid-axial plane. In the isothermal rig, the holes were 12.7 mm diameter; in the heat transfer rig, the holes were 25.4 mm diameter.

2.2 Flow visualization apparatus

Illumination of the cavity was achieved using either a ½ mW He Ne laser or, for photographic purposes, a 2 W argon-ion laser. As shown in Fig. 2, the illuminating laser was used in conjunction with a cylindrical and a collimating lens to produce 'slit illumination' in a plane through the axis of rotation (hereafter referred to as 'the r-z plane'). The focal lengths of the lenses were chosen to produce a beam that, viewed normal to the r-z plane, was slightly wider than the cavity width, s; viewed normal to the r-θ plane, the beam was brought to a focus at the axis of rotation of the cavity. The resulting 'sheet' of light was, depending on the laser and lenses used, approximately 1 mm thickness.

For photography, an Olympus OM2 camera (operating in the 'aperture preferred' mode) was arranged with the axis of its lens normal to the illuminated plane. With an f 1.8 lens and ASA 1600 film, a minimum exposure time of 1/60 s was required for the air flows, seeded with oil particles, as described below. For video recordings, a Sony video camera and monitor were used in conjunction with a Sony video tape-recorder which facilitated play-back in slow motion.

For flow visualization, the coolant air was 'seeded' by means of a Concept smoke generator. This vapourized Shell Ondina oil, and the resulting 'smoke' was driven-off with carbon dioxide. The size of the oil particles was approximately 0.8 μm diameter. For laser doppler anemometry, the air was seeded by means of a Norgren 'micro-fog lubricator' which generated particles of approximately 2 μm diameter.

2.3 The laser doppler anemometer

For measurements in the isothermal rotating cavity rig shown in Figs. 1b and 1c, the LDA optics were arranged in a forward-scatter real-fringe mode. This is illustrated in Fig.2 where the incident beams are arranged to detect the radial component of velocity.

For forward-scatter, the transmitting optics comprised a 5 mW He Ne laser (wavelength 632.8 nm), a rotating diffraction grating, steering prisms and transmitting lens. The receiving optics comprised an f 1.8 50 mm lens, 50 μm adjustable pinhole and an EMI 9558 B photomultiplier tube, all of which were contained in a single housing.

The diffraction grating was a bleached radial grating with 21,600 lines on an effective diameter of 133 mm. Approximately 50 per cent of the incident light was transmitted in the first-order beams, and a rotational speed of 2570 rev/min produced a frequency shift of 1.85 MHz. The grating could be yawed about its optical axis, allowing measurements to be made in either of two orthogonal directions. The emergent first-order beams were reflected by steering prisms to create two parallel beams, with a separation distance of 50 mm, which were focussed at the optical probe volume by the transmitting lens. For forward scatter, with a transmitting lens of 200 mm focal length, the probe volume was approximately 0.25 mm diameter and 2 mm long, and the fringe spacing was approximately 2.5 μm.

For the heat transfer rig, where the only optical access was through the perspex shroud, the LDA optics were arranged in back-scatter. Under these conditions, the 2 W argon-ion laser (wavelength, 514 nm) was used in conjunction with a conventional beam splitting cube. A beam separation of 30 mm and a transmitting lens of focal length 300 mm was used. As velocity measurements in back-scatter were limited to the tangential component of velocity in the fluid core, well away from the disc surfaces, no frequency shifting was necessary.

The doppler signal from the photomultiplier was processed by a Cambridge Consultants tracking filter, which had an upper frequency limit of 15 MHz. The tracker output voltage, which was proportional to the magnitude of the velocity component being measured, was passed into either a Solartron Time-Domain Analyzer

or a Solartron Digital Spectrum Analyzer. The former provided true time-average and r.m.s. values; the latter provided the power spectrum of the measured component of velocity.

3 FLOW VISUALIZATION

3.1 Sealing an air-cooled turbine disc

Fig. 1a shows the geometry examined in this investigation. Previous tests on a similar geometry (4) showed that the minimum dimensionless flow rate, $C_{w,min}$ necessary to prevent ingress of external fluid into the cavity between the rotor and stator could be estimated from

$$C_{w,min} = 0.61\, G_c\, Re_\theta \qquad (1)$$

The above relationship was based on pressure measurements obtained on the stator and shroud for clearance ratios of $G_c = 0.0033$ and 0.0067.

Using the rig described in Section 2.1, flow visualization was used to supplement the pressure measurements for values of G_c from 0.0025 to 0.04. Using the argon-ion laser and the optics described in Section 2.2, slit illumination in the r-z plane enabled the flow structure to be studied. The injection of smoke into the main 'coolant' air supply entering at the centre of stator ('central seeding') revealed the basic flow patterns; injection of smoke at the outside of the cavity ('peripheral seeding') revealed the point at which ingress first occurred and the extent of subsequent penetration of external flow into the cavity.

Photographs obtained using both central and peripheral seeding at $Re_\theta = 5 \times 10^4$, $G_c = 0.01$ and 0.02, and $C_w = 280$, 395 and 485 are shown in Fig. 3. It should be pointed out that, for each flow condition, a sequence of photographs was taken from the time that smoke entered the cavity to the time when no further changes in smoke patterns were discernible. The particular photographs that appear in Fig. 3 were chosen to provide the maximum information on the flow structure. It should also be noted that the lower half of the cavity is shown (that is, the 'coolant' flow enters near the top left-hand side and leaves near the bottom right-hand side of the photograph) and reflections cause mirror images (particularly on the stator side).

Referring to Fig. 3 for $G_c = 0.01$ and $C_w = 280$, the flow in the cavity is mainly laminar although, using central seeding, large instabilities in the reverse flow near the stator are clearly visible for $r/b \geq 0.6$: using peripheral seeding, smaller instabilities of the main flow near the rotor can be seen at $r/b \geq 0.4$. Similar effects are visible for $G_c = 0.02$, $C_w = 280$. For this flow rate, the secondary flow in the cavity creates one large recirculation zone centred at $r/b \simeq 0.6$, $z/s \simeq 0.7$.

For $G_c = 0.01$, $C_w = 395$, central seeding shows that the stator instabilities have spread towards the centre of the cavity and that rotor instabilities have increased in size. The nature of the rotor instabilities are clearly visible with central seeding at $G_c = 0.02$, and two large vortices can be seen near $r/b \simeq 0.5$. For $G_c = 0.01$, $C_w = 485$, central seeding reveals that the rotor vortices have grown in size, and in number, and have interacted with the stator vortices to effectively divide the cavity into inner and outer recirulation zones. This effect can also be seen for $G_c = 0.02$, $C_w = 485$, and peripheral seeding reveals the presence of an inner zone for $r/b \leq 0.4$ and an outer zone for $r/b \geq 0.6$. Further increase in flow rate causes an increase in turbulence in the cavity, but the overall flow structure is not materially altered. Increasing the rotational speed does not significantly affect the sequence of events described above. However, at high rotational speeds, clear flow visualization is more difficult to achieve.

In order to determine incipient ingress, the rotational speed was kept constant and the flow rate was slowly increased until smoke, injected at the periphery, failed to enter the cavity. The values of $C_{w,min}$ obtained in this way were consistently greater than those deduced from pressure measurements suggesting that flow visualization provided a more sensitive test for ingress. For the range of clearance ratios tested, the results were correlated (See (5)) by

$$C_{w,min} = 0.14\, G_c^{0.66} Re_\theta \qquad (2)$$

3.2 The rotating cavity with axial throughflow

Fig. 1b shows the geometry that was studied by Owen and Bilimoria (2) who observed that relatively small changes in rotational speed or axial flow rate could, under certain conditions, cause dramatic increases in heat transfer rates. With the isothermal rig described in Section 2, Owen and Pincombe (1) used flow visualization to show that vortex breakdown could occur; this phenomenon could dramatically alter the flow structure (and hence alter the heat transfer) inside the cavity.

Using the ½ mW He Ne laser to illuminate the r-z plane, it was possible to visualize the flow structure and to identify the onset of vortex breakdown. Typical flow patterns for $G = 0.53$ and $Re_z = 5000$ (turbulent flow) are shown in Fig. 4 where the shading is used to represent regions where the smoke penetrated quickly by convection and dashed lines are used to imply intermittency or uncertainty.

A powerful axisymmetric toroidal vortex centred at $r/b \simeq 0.8$, $z/s \simeq 0.5$ caused smoke to fill the entire cavity, as shown in Fig. 4a. No obvious effect of rotational speed was seen until the Rossby number, ϵ (where $\epsilon \equiv W/\Omega s = 50\, Re_z / Re_\theta$), was reduced from ∞ (the stationary value) to $\epsilon \simeq 100$, where an occasional precession of the main axial jet about the central axis could be seen. As the Rossby number was further reduced, the jet precession occurred more regularly and eventually became continuous, as illustrated in Fig.4b. This form a spiral vortex breakdown was termed 'mode Ia' breakdown, ('mode I' is used for all spiral vortex breakdowns; 'mode II' is used for all axisymmetric vortex breakdowns), and it reached its

maximum intensity at $\epsilon \simeq 21$, whereafter, at higher rotational speeds, the jet suddenly stopped precessing. If for $\epsilon < 21$, when the jet had resumed its central position, the Rossby number was increased (by speed reduction or by flow increase), the jet did not resume its precession until $\epsilon > 23$.

For $\epsilon < 21$, the jet appeared to be axisymmetric with occasional oscillations of the jet boundaries, and this was termed mode IIa. Occasional excursions of the jet into the cavity were observed; and for $\epsilon \leq 10$, an inner core of smoke with imprecise boundaries was formed as shown in Fig. 4c. As ϵ was further reduced, the core shrank in size and the occurrence of the excursion of the jet into the cavity increased.

At $\epsilon \simeq 2.6$, the jet took on the appearance of a flickering flame, as shown in Fig. 4d, and this was termed mode Ib. No further change in behaviour occurred until $\epsilon \simeq 1.5$ when signs of intermittent reverse flow were observed at the downstream end of the jet. A further increase in speed caused the smoke core to expand in size to reach a maximum value at $\epsilon \simeq 1$. This form of breakdown, termed IIb, is shown in Fig.4e.

The boundaries of these four modes of vortex breakdown were delineated for a range of flow rates, and the results are shown in Fig. 5.

3.3 The rotating cavity with radial outflow

Referring to the geometry shown in Fig. 1c, Hide (6) analysed the case of a rotating cavity with a laminar source-sink flow by considering the flow structure to comprise four regions:

(i) an inner layer of thickness Δ_E;

(ii) separate Ekman layers with a thickness of 3D ($D \equiv (\nu/\Omega)^{\frac{1}{2}}$) on each disc;

(iii) an outer layer of thickness Δ_K;

(iv) a potential core in which the axial and radial components of velocity are zero.

Flow visualization was used by Owen and Pincombe (7) to study the flow structure for the case of a uniform source where the flow enters radially (Hide's case) and the case where the flow enters axially (the gas turbine case). The isothermal cavity rig described in Section 2 was used where, for the radial inlet case, a rotating tubular gauge located at $r = a$ was used to create a uniform source flow. The r-z plane was illuminated by the argon-ion laser, and by pulsing the smoke generator it was possible to observe the flow structure. Photographs were taken in side scatter, and typical examples of the flow structure for the radial and axial inlet cases can be seen in Fig.6.

It should be noted that smoke is injected into the air flow on the left-hand-side of the cavity, and the mirror images on the disc surfaces at $z = 0$, s should be ignored. Figs. 6a and b, show the inner and outer layers, Ekman layers and potential core (which stands out as a black region into which the white smoke has not penetrated) for the radial and axial inlet cases, respectively, at $C_w = 79$ and $Re_\theta = 2.5 \times 10^4$. For the axial inlet case, the asymmetry of the central axial jet is attributed to vortex breakdown. Also, although the flow is predominantly laminar, cellular disturbances can be seen on the Ekman layers for both inlet cases. These disturbances increase with increasing values of $Re_r (Re_r \equiv C_w b/2\pi r)$, and for $Re_r \geq 140$ 'finger-like' disturbances were clearly visible; it was believed that these finger-like disturbances signalled the onset of turbulence.

Fig. 6c shows the axial inlet case at a higher flow rate, $C_w = 314$, $Re_\theta = 2.5 \times 10^4$. Unlike the previous case, the axial jet impinges axisymmetrically on the downstream disc to form a radial wall jet. At $r/b \simeq 0.5$, this jet separates from the downstream disc, effectively dividing the cavity into two distinct flow systems: the inner system (formerly considered to be the inner 'layer'), is bounded by the central axial jet, boundary layers in each disc, and the 'separation layer' for $0.5 \leq r/b \leq 0.75$; the outer system is bounded by the separation layer, Ekman layers on each disc, and the outer layer at $r/b \simeq 1$. A distinction is made in the terms 'Ekman layers', where convective acceleration is weak and the flow rate up each disc is equal to half the total flow rate, and 'boundary layers', where convective acceleration is strong and the flows in the two boundary layers are unequal.

Flow visualization has also been used to study radial outflow on the heat transfer rig described in Section 2. Under heated conditions four regimes of flow have been identified:

(a) the inner and outer layers fill the entire cavity;
(b) Ekman layers exist;
(c) the inner layer oscillates;
(d) the flow becomes chaotic.

For a given flow rate and with the downstream disc heated, the flow moves from regime (a) to (b) to (c) to (d) as the rotational speed is increased. The first three regimes correspond to the heat transfer regimes identified by Owen and Bilimoria (2), and regime (d) is believed to signal the onset of free convection inside the cavity.

Further details of the flow visualization can be found in (2) and (7). The use of laser doppler anemometry to quantify the flow in these rotating cavities is discussed in Section 4.

4 MEASUREMENTS BY LASER DOPPLER ANEMOMETRY

4.1 The rotating cavity with axial throughflow

For the isothermal rotating cavity rig described in Section 2, measurements of the radial and tangential components of velocity were made by 'looking through' the perspex discs, and measurements of the axial and tangential components were made 'looking through' the shroud. In both cases, forward scatter was employed using the 5 mW He Ne laser.

It was found that, near the centre of the cavity, (r/b = 0.133) the axial throughflow could cause the tangential velocity to exceed the local disc speed by a factor of twenty or more, as can be seen from Fig. 7. As the rotational speed is increased (ε^{-1} is increased) $V_\theta/\Omega r$ tends to unity; that is, at small values of ε, the fluid in the cavity tends to rotate as a solid body. The discontinuity at $\varepsilon^{-1} \simeq 0.045$ ($\varepsilon \simeq 22$) is caused by the change from mode Ia to IIa, as described in Section 3.2.

The various modes of vortex breakdown could also be identified by examination of the power spectrum of the tangential component of velocity. During vortex breakdown there was a good correlation between the visual observation of jet oscillations and the appearance of 'peaks' in the power spectrum. When it was possible to time the visually observed precession of the jet, close agreement was found between the timed results and the frequency of the dominant spectral peak. Examples of the spectra for laminar and turbulent flow are shown in Fig.8. The dominant spike of Figs. 8a, c, e are associated with mode I (spiral) breakdown; the peak plus higher harmonics of Figs.8b, d, f are associated with mode II (axisymmetric) breakdown. The spectral 'signatures' of the vortex breakdowns were used to delineate the boundaries between modes, and the results obtained were consistent with those obtained by flow visualization.

4.2 The rotating cavity with radial outflow

For laminar source-sink flow, Hide (6) has shown that the radial and tangential components of velocity referred to a rotating coordinate system, u and v, respectively, are given by

$$u = -\bar{v}e^{-z/D}\sin(z/D) \tag{3}$$

and

$$v - \bar{v} = -\bar{v}e^{-z/D}\cos(z/D) \tag{4}$$

where

$$\bar{v} = -Q/2\pi rD \tag{5}$$

Q being the volumetric rate. The above equations apply between the inner and outer layers, and are only valid for small values of the radial Rossby number, ε_r ($\varepsilon_r \equiv Q/4\pi r\Omega D$). Faller (8) has obtained an improved estimate for $\bar{v}$, the tangential velocity of the potential core, where

$$\bar{v} = -\frac{Q}{2\pi rD}(1 + 0.3\varepsilon_r + 0.388\varepsilon_r^2 + \ldots) \tag{6}$$

Owen, Pincombe and Onur (3) obtained solutions for the turbulent integral equations using $1/7^{th}$ power law profiles. For isothermal flow,

$$\frac{\bar{v}_o}{\Omega r} = -\frac{2.220\, C_w^{5/8}}{(r/b)^{13/8}Re_\theta^{\frac{1}{4}}} \tag{7}$$

and for non-isothermal flow

$$\bar{v}/\bar{v}_o \simeq 1 - 0.106\lambda_{\theta o} \tag{8}$$

where

$$\lambda_{\theta o} \equiv \tfrac{1}{4}\beta\Delta T\Omega r/\bar{v}_o \tag{9}$$

ΔT being the temperature difference between the heated disc and the cooling air, and the subscript 'o' referring to the isothermal case.

The isothermal rotating cavity rig described in Section 2 was used for the laminar experiments, and measurements were made with the LDA in forward scatter using the 5 mW He Ne laser. Fig. 9 shows a typical comparison between the measured velocity components ($\bar{V}_\theta = \bar{v} + \Omega r$) and those predicted from eqns.(3) and (4) (using eqn. (6) for $\bar{v}$). Measurements were obtained for the radial inlet case of Hide and the axial inlet case applicable to a gas turbine. It can be seen that the inlet conditons have only a weak effect on the flow in the Ekman layers, and agreement between the measured and theoretical values is good.

The heat transfer rig was used to achieve turbulent flow and to produce non-isothermal conditions. The only optical access was through the perspex shroud with the LDA optics arranged radially in the back-scatter mode. The optical quality of the shroud, which contained thirty holes and tended to fog-up with oil particles, made measurement extremely difficult. Measurements were, therefore, limited to the tangential component of velocity in the mid-axial plane (z/s = 0.5).

The effect of flow rate on the transition from laminar to turbulent flow can be clearly seen in Fig.10. The measurements were made in isothermal flow at a gap ratio of G = 0.133 and a radius ratio of r/b = 0.767. For all three values of Re_θ, transition occurs at $C_w \simeq 860$ ($Re_r \simeq 180$), which is the intercept of eqns.(5) and (7). For small radii ($Re_r > 180$), the flow in the Ekman layers is turbulent; for large radii ($Re_r < 180$) the flow is laminar.

In Fig. 11, the radial distribution of the turbulent tangential velocity is shown at G = 0.133 for Re_θ = 0.4, 0.6 and 1.0 x 10^6. For $\beta\Delta T \simeq 0.27$ these three values of Re_θ cause the steady, oscillating and chaotic flow described in Section 3.3. The small reduction in $\bar{V}_\theta$ caused by heating at the two lower values of Re_θ is consistent with that given by eqn.(8). At $Re_\theta = 10^6$, the drop in the isothermal data below the theoretical curve for r/b > 0.9 is attributed to ingress of external fluid into the cavity via the holes in the shroud. At the highest value of Re_θ, heating ($\beta\Delta T \simeq 0.27$) causes chaotic flow which tends to create a forced vortex where $\bar{V}_\theta/\Omega r \simeq 0.6$.

Further details of the velocity measurements, and power spectra obtained from them, are given in (3). The effect of these flows on the heat transfer in a rotating cavity is discussed in Section 5.

5 HEAT TRANSFER IN ROTATING CAVITIES

Using the heat transfer rig described in Section 2.1, Owen and Bilimoria (2) obtained heat transfer rates for the case of the rotating cavity with axial throughflow. It was only by the use of the flow visualization techniques described in Section 3.2, that the dramatic changes of heat transfer that they measured were linked to the occurrence of vortex breakdown.

For the case of the rotating cavity with radial outflow, Owen and Bilimoria identified three regimes of heat transfer. At low rotational speeds, in regime (i), the mean Nusselt numbers(on the heated downstream disc) was independent of Re_θ ; at intermediate speeds, in regime (ii), $\overline{Nu} \propto Re_\theta^{\frac{1}{2}}$; at high speeds,in regime (iii), $\overline{Nu}$ was only weakly dependent on Re_θ. These three regimes were attributed to the cases where (i) the inner and outer layers fill the entire cavity, (ii) Ekman layers begin to develop, (iii) the Ekman layers are fully developed.

Mean Nusselt numbers in the above regimes can be correlated by

regime (i): $$\overline{Nu} = 1.94\, G^{1/6}\, C_w^{2/3} \tag{10}$$

regime (ii): $$\overline{Nu} = 0.0688\, C_w^{1/3}\, Re_\theta^{1/2} \tag{11}$$

regime (iii): $$\overline{Nu} = 4.39 G^{1/9}\, C_w^{1/2}\, Re_\theta^{1/9} \tag{12}$$

The boundary between regimes (i) and (ii) are correlated by

$$G^{-1/6} C_w^{-1/3} Re_\theta^{1/2} = 28 \tag{13}$$

and the boundary between (ii) and (iii) by

$$G^{-1/6} C_w^{-1/4} Re_\theta^{7/12} = 510 \tag{14}$$

In a more recent study (3), the flow visualization described in Section 3.3 revealed that regime (iii) only occurred during heating ($\beta\Delta T \approx 0.27$) and was associated with buoyancy-induced oscillations. It was believed to be the first step towards free convection inside the cavity.

From the solution of the turbulent integral Ekman layer equations, Owen, Pincombe and Onur (3) showed that,

$$\overline{Nu} = c\, C_w^{3/8}\, Re_\theta^{1/2} (1 + 0.0532\lambda_{\theta o}) \tag{15}$$

where, for a Prandtl number of unity and a quadratic temperature rise over the rotating disc, $C = 0.0791$. The experiemntal data were obtained for air ($Pr = 0.71$), and as no allowance was made in the theoretical model for the presence of inner and outer layers, it is not surprising that the agreement between eqn.(11) (for the Ekman layer regime) and eqn.(15) is not perfect.

Using eqn.(15), a regression fit was made on the regime (ii) data, and the 'best' value of c was found to be 0.0453. For 62 data points for $G = 0.133$, 0.267 and 0.4, $900 < C_w < 8.4 \times 10^4$, $10^5 < Re_\theta < 2 \times 10^6$, the correlation coefficient was 0.994. Fig.12 shows the comparison between eqn.(15) with $c = 0.0453$, and the measured mean Nusselt numbers. Apart from the overestimate at small values of C_w, the fit in regime (ii) is good; the fit is obviously not effective in regime (i), (where $\overline{Nu}$ is virtually independent of Re_θ), or in regime (iii) (where buoyancy causes oscillating, and eventually chaotic, flow).

6 CONCLUSIONS

Flow visualization and laser doppler anemometry have been used to provide a better understanding of flow structure and convective heat transfer inside rotating cavities. Three different gas turbine configurations have been studied.

In the first, a model of an air-cooled gas turbine disc rotating close to a stator has been used to study the ingress of hot gas into the system. Flow visualization has been used to examine the flow structure and to identify the point at which ingress first appears.

In the second, a model of corotating compressor discs with an axial throughflow of coolant has been studied. Using flow visualization and LDA, vortex breakdown has been identified and formerly inexplicable heat transfer behaviour has been explained.

In the third, a model of corotating turbine discs with a radial outflow of coolant has been examined. Flow visualization has been used to determine the flow structure and to identify the different flow regimes. LDA has been used to measure the velocity distribution between the rotating discs, and the results have been compared with theoretical models. The different heat transfer regimes, delineated from correlations of the mean Nusselt numbers, correspond to the regimes identified by the flow visualization and LDA measurements.

REFERENCES

1. Owen, J.M. and Pincombe,J.R. 'Vortex breakdown in a rotating cylindrical cavity'. J.Fluid Mech. 90, 1979, p.109.

2. Owen, J.M. and Bilimoria, E.D. 'Heat transfer in rotating cylindrical cavities', J.Mech.Engng.Sci. 19, 1977, p.175.

3. Owen, J.M., Pincombe,J.R. and Onur,H. 'Velocity measurements in a heated rotating cavity with a radial outflow of coolant', 1979. Mech.Engng.Rep. No. TPMRC/4, School of Engng and Appl.Sciences, University of Sussex, Brighton, U.K.

4. Bayley, F.J. and Owen, J.M. 'The fluid dynamics of a shrouded disk system'. J.Engng Power, Trans. ASME, Series A, 92, 197 , .333.

5. Owen, J.M. and Phadke,U.P. 'An investigation of ingress for a simple shrouded rotating disk system with a radial outflow of coolant'. ASME Paper No. 80-GT-49, 25th Annual Gas Turbine Conference, New Orleans, 1980.

6. Hide, R. 'On source-sink flows in a rotating fluid'. J.Fluid Mech. 32, 1968, p.737.

7. Owen, J.M. and Pincombe, J.R. 'Velocity measurements inside a rotating cylindrical cavity with a radial outflow of fluid'. J.Fluid Mech. To be published.

8. Faller, A.J. 'An experimental study of the instability of the laminar Ekman boundary layer'. J. Fluid Mech. 15, 1963, p.560.

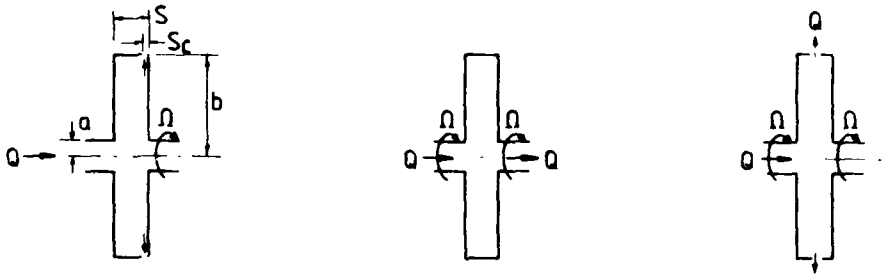

(a) Rotor-stator system

(b) Rotating cavity with axial through-flow

(c) Rotating cavity with radial outflow

Fig. 1 Schematic diagram of rotating disc systems.

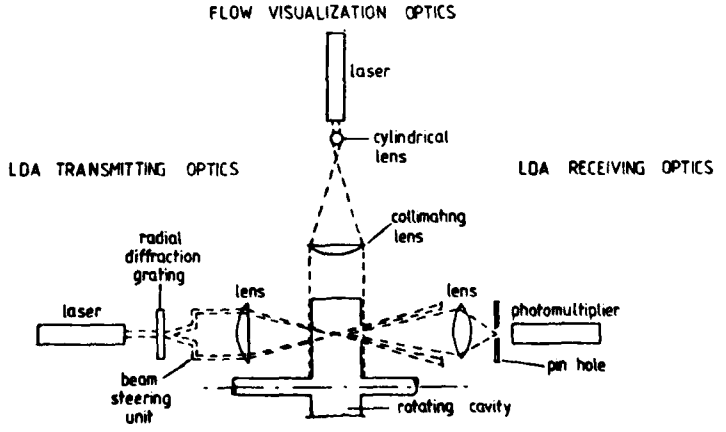

Fig. 2 Schematic diagram of flow visualization and LDA optics

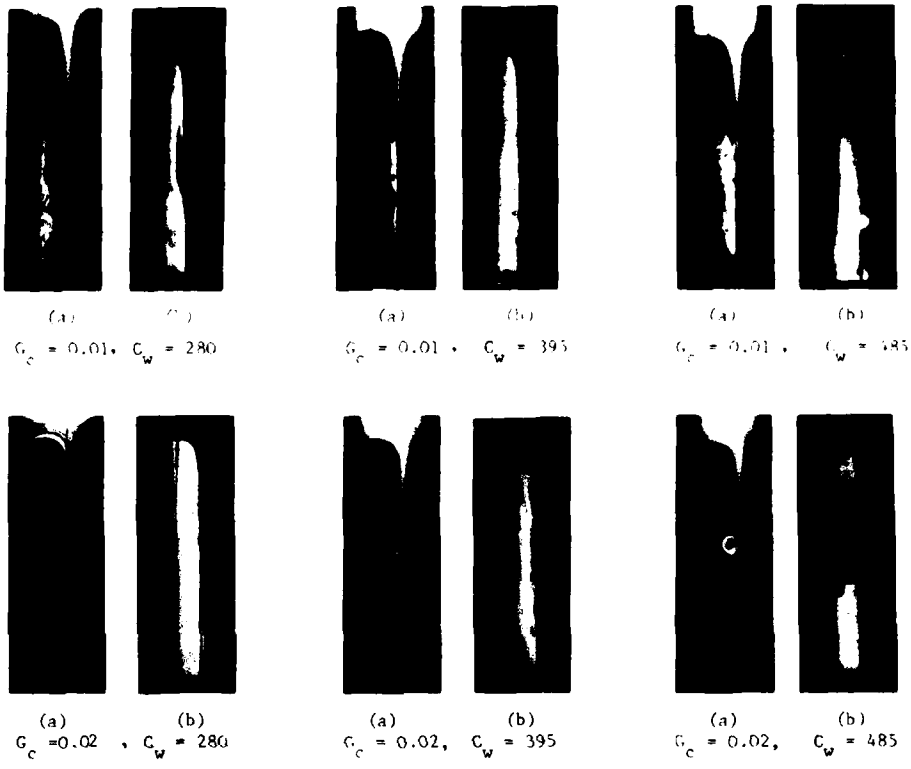

Fig. 3 The flow structure between a rotor and stator for G = 0.1, $Re_\theta = 5 \times 10^4$.

(a) central seeding; (b) peripheral seeding.

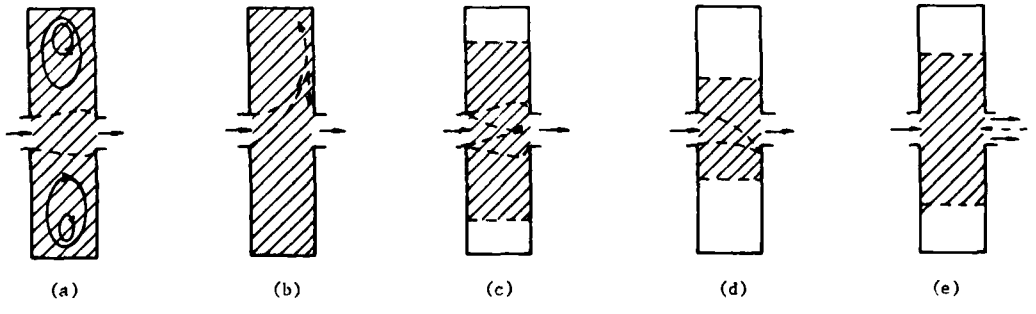

Fig. 4 Visual impressions of flow inside a rotating cavity with turbulent axial throughflow for G = 0.53, Re_z = 5000.

	(a)	(b)	(c)	(d)	(e)
Rossby number, ε	∞	25	4	2	1

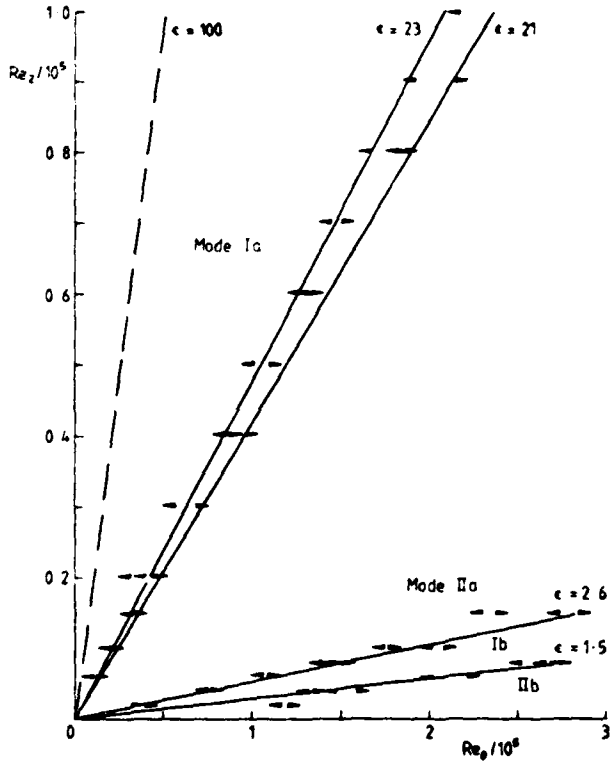

Fig. 5 Regimesof vortex breakdown in a rotating cavity with turbulent axial throughflow for G = 0.53.
— Re_θ increasing; — Re_θ decreasing.

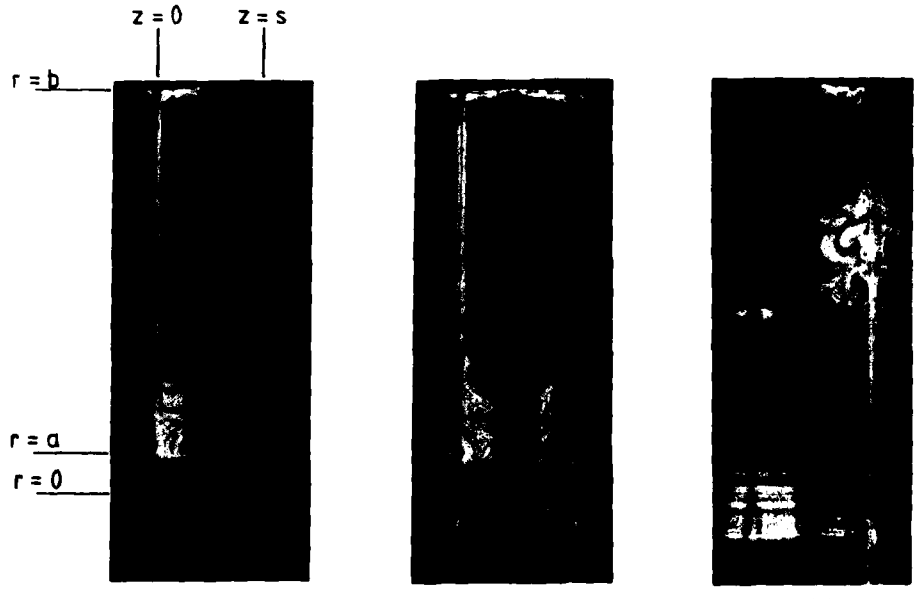

(a) radial inlet, C_w=79 (b) axial inlet, C_w=79 (c) axial inlet, C_w= 314

Fig.6 Flow visualization inside a rotating cavity with a radial outflow for G = 0.267, $Re_\theta = 2.5 \times 10^4$

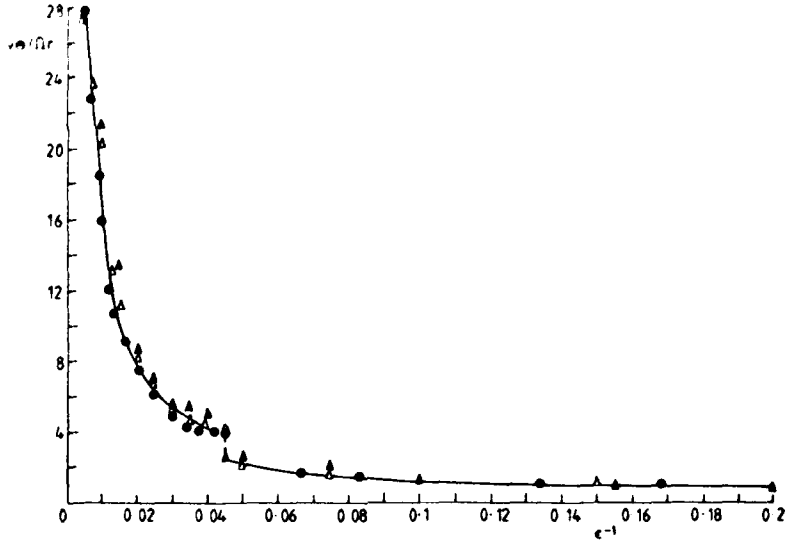

Fig.7. Tangential velocity variation for the rotating cavity with turbulent axial throughflow for G = 0.53, r/b = 0.133, z/s = 0.189.
▲, $Re_z = 10^4$; △, $Re_z = 2 \times 10^4$; ●, $Re_z = 3 \times 10^4$

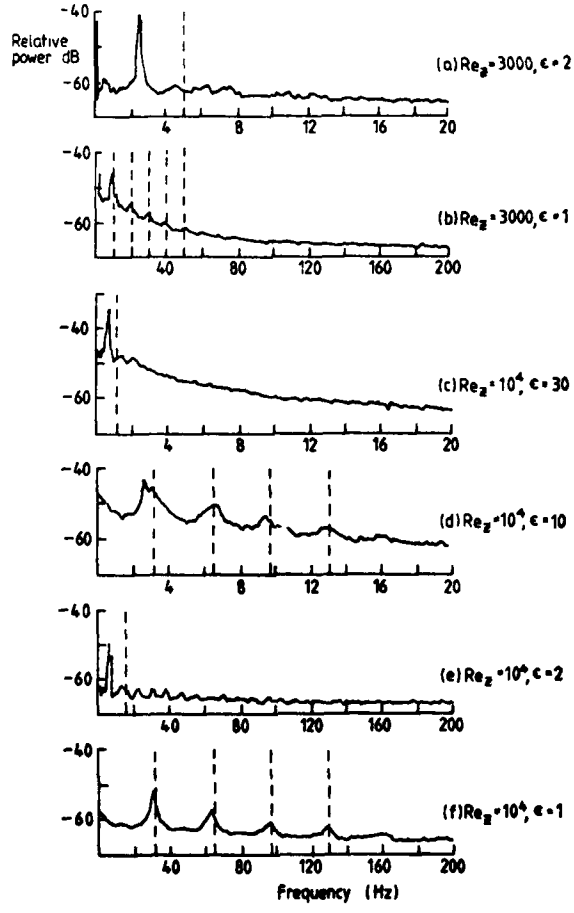

Fig.8. Power spectrum of the tangential component of velocity for the rotating cavity with axial throughflow for G = 0.53, r/b = 0.53, z/s = 0.5.

------ cavity rotational frequency and harmonics.

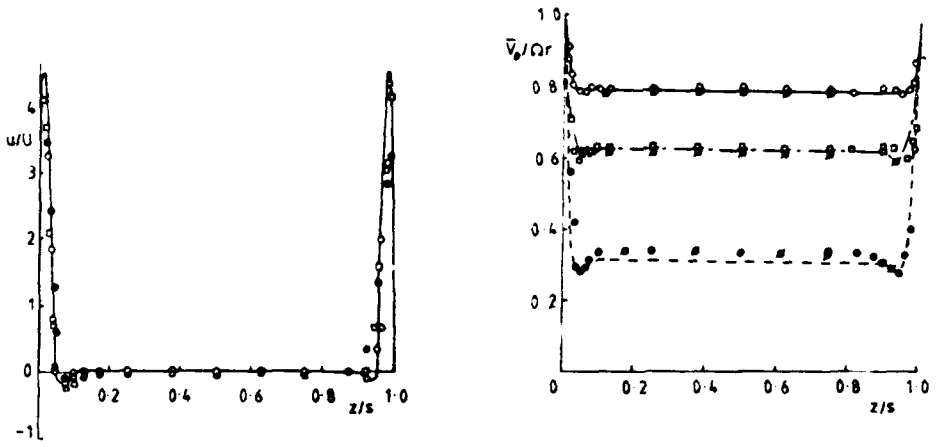

Fig. 9 The axial distribution of radial and tangential components of velocity in a rotating cavity with a radial outflow for G = 0.267, $Re_\theta = 5 \times 10^4$, r/b = 0.833.

ε_r	0.098	0.170	0.310	
Eqns.(3) and(4)	———	— - —	-----	
axial inlet	o	□	●	measured values
radial inlet	ϕ	⊠	♦	measured values

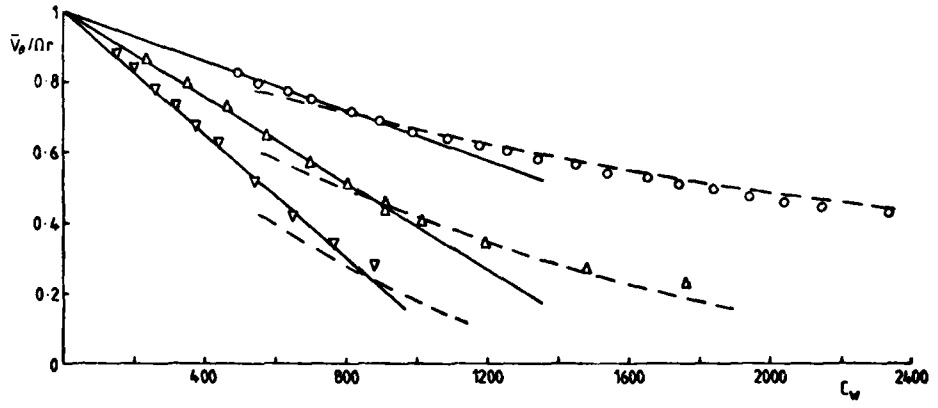

Fig. 10. The effect of flow rate on the tangential velocity in a rotating cavity with radial outflow for G = 0.133, r/b = 0.767, z/s = 0.5.
∇, $Re_\theta = 10^5$; Δ, $Re_\theta = 2 \times 10^5$; o, $Re_\theta = 6 \times 10^5$; ——— eqn(5); ------ eqn.(7).

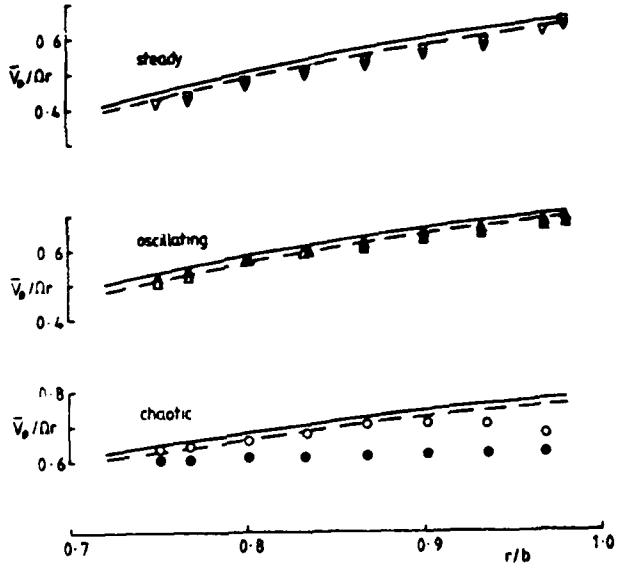

Fig. 11 The effect of heating on the tangential velocity in a rotating cavity with radial outflow for G = 0.133, z/s = 0.5.

	▽	▼	△	▲	○	●
C_w	1540	1540	1600	1600	1790	1790
$Re_\theta/10^6$	0.4	0.4	0.6	0.6	1.0	1.0
$\beta\Delta T$	0	0.27	0	0.27	0	0.27

—— eqn.(7); - - - eqn.(8), $\beta\Delta T$ = 0.27

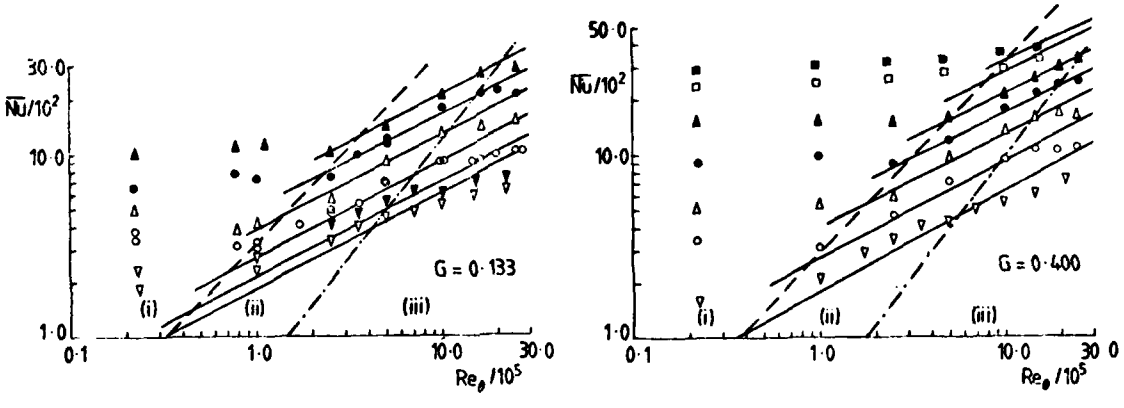

Fig. 12 Mean Nusselt numbers for the heated downstream disc in a rotating cavity with radial outflow for $\beta\Delta T$ = 0.27

Symbol	▽	▼	0	△	●	▲	□	■
$C_w/10^4$	0.09	0.14	0.28	0.71	1.42	2.83	5.70	8.40

- - - eqn(13); —— - —— eqn (14); ——— (eqn(15)(c = 0.0453)

APPLICATION DE LA SPECTROSCOPIE U.V. AU DOSAGE DE L'OXYDE NITRIQUE

J.Ph. DURAND[x] et J.C. BELLET

Laboratoire d'Energétique et de Détonique
E.N.S.M.A. - Université de Poitiers
86034 POITIERS - FRANCE

RESUME -

L'objectif des travaux présentés ici était de confronter, dans des conditions expérimentales très différentes, des mesures de concentration de l'oxyde nitrique NO dans des produits de combustion, effectuées simultanément par spectrométrie d'absorption U.V. et par prélèvement et dosage à l'aide d'un analyseur à chimiluminescence. Les travaux ont montré qu'il faut tenir compte des absorptions parasites de l'oxygène et de l'anhydride carbonique dès que les températures dépassent environ 700 K pour la bande γ(1,0) et 900 K pour la bande γ(0,0). De plus des mesures effectuées dans le jet d'un turboréacteur au banc d'essai à la SNECMA ont montré que d'autres espèces parasites non encore identifiées (probablement des imbrûlés) interféraient avec la mesure.

1 - INTRODUCTION -

La validation expérimentale des modèles de formation des oxydes d'azote dans les foyers de turbomachine, comme l'application de normes concernant les quantités d'oxyde nitrique émises par les moteurs, implique que l'on puisse faire confiance aux méthodes de mesure de concentration utilisées. La méthode la plus couramment employée est le prélèvement par sonde et le dosage à l'aide d'un analyseur à chimiluminescence. Or les sondes peuvent être le siège de réactions de réduction ou d'oxydation de NO /cf. par exemple : réf. 1/, entraînant une sous-estimation de la concentration réelle au point de mesure. C'est ainsi que la concentration en NO_2 indiquée par l'analyseur peut être interprétée soit comme étant celle réellement présente dans la flamme, soit comme résultant d'une oxydation de NO ayant lieu au cours du prélèvement /2,3,4/.

Par ailleurs les conclusions des confrontations entre mesures par prélèvement et mesures par absorption U.V. ne concordent pas : les résultats traduisent soit un bon accord entre les deux types de mesure /5,6/, soit un désaccord important, la mesure par absorption U.V. indiquant alors une concentration de NO supérieure à celle donnée par les prélèvements et analyses /7,8/.

Ces différences d'interprétation pouvant résulter de conditions expérimentales ou de modes opératoires différents, il nous a paru utile de reprendre la confrontation entre mesures par prélèvement et analyse, en appliquant les mêmes techniques dans trois sortes d'écoulement différents : gaz brûlés produits par un brûleur type MEKER, foyer tubulaire et jet d'un turboréacteur.

2 - METHODE DE MESURE PAR ABSORPTION U.V. -

2.1 - Expression du taux de transmission -

Les bases de la méthode de mesure de la concentration de NO par mesure d'absorption dans l'ultra-violet peuvent être trouvées dans les ouvrages de HERZBERG /9/ et de PENNER /10/, ainsi que dans les travaux de DAVIS et al. /11/ et de MUELLER /5/. Nous avons toutefois déterminé, à l'aide de notre propre montage expérimental et de mélanges étalons $NO-N_2$, les valeurs des paramètres d'élargissement de raie pour les deux bandes γ(1,0) et γ(0,0), qui sont les plus intenses, et trouvé respectivement 1810 K/bar et 1860 K/bar.

En raison de la structure très fine du spectre de rotation de la molécule de NO, il serait nécessaire d'utiliser un spectrographe à très haute résolution pour en séparer les raies. C'est pourquoi on effectue la mesure pour un intervalle de fréquence Δν correspondant à une résolution moyenne, en tenant compte, dans le calcul, de l'absorption résultant de l'ensemble des raies correspondantes.

Pour un milieu absorbant homogène d'épaisseur b, le taux de transmission de la lumière issue d'une source lumineuse, peut s'écrire sous la forme :

$$\tau_{\Delta\nu} = \int_{\Delta\nu} \frac{e_{s_\nu}}{\int_{\Delta\nu} e_{s_\nu}\, d\nu} e^{-bk_\nu}\, d\nu \qquad (2\text{-}1)$$

où e_{s_ν} est le coefficient spectral d'émission de la source, et k_ν le coefficient spectral d'absorption du milieu.

Pour un milieu optiquement mince où $b\, k_\nu \ll 1$, on peut écrire :

$$\tau_{\Delta\nu} = 1 - \int_{\Delta\nu} \frac{e_{s_\nu}}{\int_{\Delta\nu} e_{s_\nu}\, d\nu} b\, k_\nu\, d\nu \qquad (2\text{-}2)$$

Or pour un milieu absorbant à la pression p où la fraction molaire de NO est X_{NO}, k_ν est de la forme :

$$k_\nu = X_{NO}\, p\, B_\nu\, (T)$$

---

x - Affiliation présente : SNIAS, Service pyrotechnique, B.P. 96 - 78130 LES MUREAUX.

où $B_\nu(T)$ est une fonction de la température.
Si l'on pose :

$$S_\nu = \frac{e_{s_\nu}}{\int_{\Delta\nu} e_{s_\nu}\, d\nu}$$

on obtient une relation linéaire :

$$\tau_{\Delta\nu} = 1 - bp\, X_{NO} \int_{\Delta\nu} S_\nu\, B_\nu(T)\, d\nu \qquad (2-3)$$

Si le milieu n'est pas optiquement mince, il faut tenir compte des autres termes du développement de e^{-bk_ν}. On peut montrer /12/ que, pour des taux d'absorption de 15% au maximum, et pour $\Delta\nu = 1{,}5$ Å on commet une erreur inférieure à 1% en écrivant :

$$\tau_{\Delta\nu} = \exp\left(- bp\, X_{NO} \int_{\Delta\nu} S_\nu\, B_\nu(T)\, d\nu\right) \qquad (2-4)$$

Ce qui signifie que le milieu suit une loi de LAMBERT.
Si l'on note :

$$f_\nu(T) = \int_{\Delta\nu} S_\nu\, B_\nu(T)\, d\nu$$

on peut écrire :

$$\tau_{\Delta\nu} = \exp\left(- bp\, X_{NO}\, f_\nu(T)\right) \qquad (2-5)$$

ou :
$$X_{NO} = - \frac{\operatorname{Ln} \tau_{\Delta\nu}}{b\, p\, f_\nu(T)}$$

Dans le cas d'un milieu non homogène, on peut écrire :

$$\tau_{\Delta\nu} = \exp\left(- p \int_0^b X_{NO}\, f_\nu(T)\, dx\right) \qquad (2-6)$$

Si le milieu comporte des espèces absorbantes autres que NO, de fractions molaires X_i, dont l'absorption suit également une loi de LAMBERT avec une fonction $g_{i\nu}(T)$ connue, équivalente de la fonction $f_\nu(T)$ pour NO, le taux de transmission devient alors :

$$\tau_{\Delta\nu} = \exp\left(- p \int_0^b X_{NO}\, f_\nu(T)\, dx\right) \exp\left(- p \sum_i \int_0^b X_i\, g_{i_\nu}(T)\, dx\right) \qquad (2-7)$$

d'où l'on peut déduire le taux d'absorption qui correspondrait à l'absorption par NO seul.

Les données de la littérature, en particulier les formules empiriques proposées par WHITING /13/, permettent de calculer pour un intervalle $\Delta\nu$ donné la fonction $f_\nu(T)$ pour les bandes $\gamma(1,0)$ et $\gamma(0,0)$. La figure 1 représente les variations de $f_\nu(T)$ pour $\Delta\nu = 1{,}37$ Å, valeur correspondant à nos conditions de mesure. Afin de faciliter les calculs nous avons déterminé, par des régressions logarithmiques, des expressions analytiques approchées qui sont résumées dans le tableau 1 pour X_{NO} en ppm.

bande $\gamma(1,0)$	294 K < T < 800 K	$f(T) = 1{,}242.10^{-1} T^{-1{,}167} + 6{,}774.10^{-5} \exp(-2{,}312.10^{-3} T)$
	800 K < T < 1600 K	$f(T) = 1{,}638\ T^{-1{,}623} + 8{,}831.10^{-5} \exp(-1{,}379.10^{-3} T)$
bande $\gamma(0,0)$	294 K < T < 800 K	$f(T) = 8{,}857.10^{-2}\ T^{-1{,}205}$
	800 K < T < 1600 K	$f(T) = 9{,}063.10^{-7} \exp(1{,}676.10^{3}/T) + 6{,}197.10^{-5} \exp(-1{,}397.10^{-3} T)$

TABLEAU 1 - Formes analytiques approchées de la fonction $f_\nu(T)$ pour X_{NO} en ppm.

2.2 - Dispositif de mesure et sensibilité -

Deux sources de lumière ont été utilisées :
- une lampe au deuterium (type BOWE de JOBIN-YVON),
- une lampe à cathode creuse réalisée au laboratoire d'après un schéma proposé par MUELLER /5/.

L'analyseur de spectre utilise était un monochromateur JOBIN-YVON type HRS 1 équipé d'un photomultiplicateur EMI type 9558 QB. Dans les conditions de nos mesures, sa résolution était de 1,37 Å.

Le seuil de sensibilité de la mesure à une température T a été défini par le produit X_{NO} b p correspondant à un taux d'absorption de 5%, soit une erreur relative de 10%. Le tableau 2 résume les valeurs de ce seuil pour les deux sources utilisées et pour les deux bandes $\gamma(1,0)$ et $\gamma(0,0)$, dans l'intervalle de température 294 K < T < 2000 K.

		T °K				
Bande	Lampe à décharge	K_{ν} ff (pression atm)				
	Lampe au deutérium					
Bande	Lampe à décharge					
	Lampe au deutérium					

TABLEAU 2 - Seuils de sensibilité de la méthode de mesure suivant la température.

3 - METHODE DE MESURE PAR PRELEVEMENT -

Pour le prélèvement d'échantillons gazeux dans l'écoulement, trois types de sondes en acier inoxydable refroidi ont été utilisés, afin de comparer les résultats auxquels elles conduisaient.

Deux des sondes avaient un tube de prélèvement de diamètre intérieur constant de 1 mm, et ne différaient que par leurs géométries, l'une ayant l'orifice de prélèvement à l'extrémité d'une pointe effilée orientée dans le sens de l'écoulement (fig. 6a), et l'autre ayant cet orifice sur le côté de la hampe (fig. 6b). Le débit dans ces deux sondes était réglé de façon que la vitesse d'aspiration à l'entrée soit égale à celle de l'écoulement. La troisième sonde avait une forme identique à la première, mais le tube de prélèvement était rétreint à son extrémité de façon que l'orifice constitue un col sonique de diamètre 0,5 mm.

Les lignes de liaisons entre les sondes et l'analyseur étaient aussi en acier inoxydable et avaient un diamètre intérieur de 3 mm. Elles comportaient une partie plongée dans la glace fondante afin de condenser le plus possible la vapeur d'eau dont la présence peut modifier la réponse de l'analyseur à chimiluminescence.

Ce dernier était un THERMOELECTRON modèle 10 A. Suivant les recommandations faites par divers auteurs /3,14/ nous en avons réglé la température du convertisseur entre 350 et 400°C. Afin de tenir compte de la présence de CO_2 dans les échantillons analysés, nous avons effectué un étalonnage de l'analyseur à l'aide de mélanges étalons NO - N_2 - CO_2, et avons constaté que la présence de CO_2 entraîne une surestimation de la concentration réelle en NO, qui ne dépasse pas toutefois 5% pour une fraction molaire de CO_2 de 20% (fig. 3).

Par ailleurs les autres espèces stables présentes dans les gaz étaient dosées par analyse chromatographique, la fraction molaire de vapeur d'eau étant déduite d'un bilan atomique à partir de la composition des gaz frais.

4 - MONTAGES EXPERIMENTAUX -

Trois montages expérimentaux, réalisés au Laboratoire, ont été utilisés pour la comparaison entre mesure par absorption U.V. et mesure par prélèvement : un petit brûleur à flamme stabilisée sur une grille type MEKER, un foyer tubulaire à combustion stabilisée par mélange turbulent de gaz brûlés avec les gaz frais, et un four aménagé pour y faire des mesures d'absorption dans des mélanges étalons. Le combustible utilisé était du propane.

4.1 - Le brûleur type MEKER -

Ce brûleur (fig. 4) vertical de section constante 86 mm x 104 mm, comporte à sa base une grille en laiton analogue à celle d'un brûleur MEKER, avec une maille carrée de 2 mm de côté. Au-dessus de cette grille sont superposés dans l'ordre :

- un tronçon de 5 cm de haut, revêtu intérieurement de matériau réfractaire,
- deux grilles croisées refroidies par eau permettant de refroidir les gaz à une même température pour plusieurs valeurs de la richesse (en adaptant le débit du mélange frais),
- un tronçon de mesure de 13 cm de haut, muni de vitres en quartz transparent au rayonnement U.V. et de passages pour sonde à thermocouple ou sonde de prélèvement.

Ce brûleur permettait d'effectuer des mesures dans des produits de combustion à des températures comprises entre 950 K et 1250 K, et pour des richesses de mélange frais variant de 0,5 à 1,5.

4.2 - Le foyer tubulaire -

Le foyer tubulaire a été réalisé pour permettre l'étude de la variation des vitesses de réactions au cours de la combustion turbulente d'un mélange hydrocarbure-air stabilisée par mélange de gaz brûlés avec les gaz frais /15/ (fig. 5). Les gaz brûlés, produits par une chambre de combustion spéciale, sont mélangés rapidement avec les gaz frais à l'aide d'un "mélangeur" comportant 100 conduits de passage des gaz brûlés et 81 injecteurs de gaz frais disposés sur sa face aval à l'entrée de la veine d'expérimentation de section constante 10 cm x 10 cm, pourvue de parois réfractaires.

On peut donc, dans cette veine, stabiliser une zone de combustion distribuée en réglant le rapport des deux débits de gaz brûlés et de gaz frais de telle sorte que la température du mélange formé provoque son inflammation spontanée à une distance voulue en aval des injecteurs. La longueur de cette zone de combustion était d'environ 70 cm.

4.3 - Le four à gaz étalons -

Afin de pouvoir étudier la variation en fonction de la température de l'absorption due à certains gaz, nous avons aménagé un four électrique pour pouvoir y introduire des mélanges de composition connue et en mesurer le taux d'absorption pour les longueurs d'ondes étudiées. Pour cela nous avons disposé à l'intérieur de ce four un tube en silice, de longueur 44 cm et de diamètre intérieur 4 cm, comportant à chaque extrémité un bouchon en matériau réfractaire muni d'un hublot en quartz transparent dans l'U.V. et un tube de raccordement pour le

passage des gaz introduits.

5 - RESULTATS ET INTERPRETATION -

5.1 - Expériences sur le brûleur type MEKER -

Nous avons mesuré simultanément, par prélèvement et analyse et par absorption U.V., la concentration de NO dans l'écoulement de gaz brûlés du brûleur type MEKER pour trois valeurs de la richesse (0,63 ; 0,71 et 1,13), en réglant chaque fois le débit de manière que la température mesurée par thermocouple sur l'axe dans le plan de mesure soit de 1100 ± 5 K. La source utilisée était la lampe à décharge. De plus, pour faire varier la concentration de NO sans modifier la température, nous avons aussi effectué des mesures en injectant dans les gaz frais de l'ammoniac, qui se transforme en NO en proportion plus ou moins importante selon la richesse.

Les résultats des mesures par prélèvement ont montré que les rapports des fractions molaires X_{NO_2}/X_{NO_x} étaient toujours faibles, compris entre 0,04 et 0,12 (quelque soit le type de sonde utilisé).

Pour confronter les deux types de mesures, nous avons représenté sur la figure 4 les variations de - Log τ pour la bande γ(1,0) en fonction des valeurs de X_{NO} mesurées par prélèvement sur l'axe du brûleur (cf. relation 2-5). Ces résultats mettent en évidence par extrapolation un taux de transmission inférieur à 1 pour $X_{NO} = 0$. On sait [14,17] que l'oxygène moléculaire absorbe à haute température au niveau des bandes γ(1,0) et γ(0,0).

Mais comme le taux d'absorption parasite mis en évidence dépend très peu de la richesse, il apparaît qu'au moins une autre des espèces présentes dans les gaz brûlés doit interférer avec la mesure. C'est pourquoi nous avons entrepris des mesures d'absorption concernant ces espèces à l'aide du four décrit au § 4.3.

5.2 - Détermination des absorptions parasites -

5.2.1 - Nous avons mesuré, pour les deux bandes γ(1,0) et γ(0,0) en utilisant la lampe à décharge, la variation en fonction de la température (jusqu'à 1270 K) de l'absorption de divers mélanges constitués par chacun des gaz étudiés dilué dans de l'argon. Nous avons constaté que l'absorption de CO_2 ne peut être négligé dès 700 K pour la bande γ(1,0) et dès 900 K pour la bande γ(0,0), et celle de O_2 dès 800 K pour γ(1,0) et dès 1000 K pour γ(0,0).(fig. 7 et 8)

Nous avons aussi cherché à donner pour les taux d'absorptions correspondants des expressions approchées. Comme le milieu absorbant n'est optiquement mince que pour les faibles taux d'absorption, nous avons supposé que la variation en fonction de l'épaisseur optique du milieu suit une loi de LAMBERT, ce qui peut se justifier par le fait que les absorptions de O_2 et de CO_2 s'étendent continûment sur l'ensemble des bandes γ de NO et peuvent donc être considérées comme constantes sur chacune des bandes de largeur Δν. Nous avons donc considéré que le taux de transmission τ de la lumière à travers le mélange dans le four pouvait être écrit sous la forme :

$$\tau = \exp\left(- p\, X_i\, l_e\, g_{i\nu}(T)\right) \qquad (5\text{-}1)$$

où X_i est la fraction molaire de l'espèce considérée, l_e la longueur effective du chemin optique dans le four et $g_{i\nu}(T)$ la loi d'absorption en fonction de la température. En supposant cette dernière de la forme :

$$g_{i\nu}(T) = a \exp(b\,T)$$

ou $$g_{i\nu}(T) = a \exp(- b/T)$$

nous avons obtenu les expressions résumées dans le tableau 3 (pour X_i sans dimension) et

espèce	Longueur d'onde (Å)	g(T) = a exp(bT) ou a exp(-b/T) avec a ($cm^{-1}atm^{-1}$) et b(K ou K^{-1})
CO_2	2147.1	$4{,}52.10^{-5}\ \exp(5{,}76.10^{-3}T)$
O_2	2147.1	$4{,}14\ \exp(-\ 6{,}87.10^{3}/T)$
CO_2	2261.0	$1{,}81.10^{-6}\ \exp(7{,}35.10^{-3}/T)$
O_2	2261.0	$2{,}02.10^{-6}\ \exp(6{,}25.10^{-3}T)$

TABLEAU 3

porté les variations correspondantes de α = 1 - τ sur les figures 7 et 8.

5.2.2 - Nous avons utilisé ces lois pour calculer le taux d'absorption parasite dans les gaz brûlés du brûleur type MEKER. Pour cela nous avons intégré les lois d'absorption de O_2 et CO_2 le long du trajet optique en prenant la température mesurée le long de ce trajet. Nous avons ainsi obtenu un taux d'absorption parasite de 2,0 ± 0,2%, quelle que soit la richesse, alors que les valeurs extrapolées à partir des résultats expérimentaux (cf. fig.6) donne un taux d'absorption parasite compris entre 2 et 2,5% avec une précision de 0,5%. A la précision des mesures, il apparaît donc que l'on peut admettre que l'absorption parasite mise en évidence était bien due à l'oxygène et à l'anhydride carbonique.

5.3 - Interprétation des expériences sur le brûleur MEKER -

Pour confronter les résultats des deux méthodes de mesures, nous avons dû tenir compte de la présence de couches limites thermiques dans lesquelles la concentration de NO est encore importante et l'absorption correspondante d'autant moins négligeable que l'absorption de NO augmente quand la température diminue. En utilisant les profils de concentration de NO et de température mesurés par prélèvement et par thermocouple le long du chemin optique, et en procédant par des régressions logarithmiques à partir des valeurs sur l'axe, nous avons déterminé une "longueur d'absorption équivalente" qui est celle du chemin optique qui donnerait le même taux d'absorption pour des températures et concentrations uniformes et égales aux valeurs mesurées sur l'axe. Nous avons vérifié que cette "longueur d'absorption équivalente" était constante à ± 5% pour l'ensemble des conditions de mesure, et égale à 10,9 cm en moyenne au lieu de 11 cm.

Nous avons ainsi représenté sur la figure 9 :

- d'une part les fractions molaires de NO et NO_x mesurées par prélèvement sur l'axe pour la richesse $\phi = 0,7$, en fonction de la valeur mesurée de τ_{λ},
- d'autre part la droite représentant l'équation 2-5 pour la même température et pour la "longueur équivalente d'absorption" déterminée précédemment, compte tenu de l'absorption parasite de O_2 et CO_2.

On constate que les valeurs de X_{NO} déduites des mesures optiques sont légèrement supérieures aux fractions molaires déterminées par prélèvement et analyses, de 17% en moyenne pour NO_x et de 23% en moyenne pour NO, la précision des mesures étant d'environ 11% pour les deux méthodes. Ces résultats sembleraient donc indiquer que, dans ces conditions expérimentales, le NO_2 dosé proviendrait d'une oxydation de NO lors du prélèvement, et que de plus il y aurait une légère réduction de NO au cours de ce prélèvement (à moins qu'il y ait une absorption parasite supplémentaire due à une espèce en très faible concentration...

5.4 - Expériences sur le foyer tubulaire -

Deux séries d'expériences ont été effectuées avec le foyer tubulaire :

- les unes sans combustion dans la veine d'expérience (richesse $\phi_2 = 0$), c'est-à-dire en écoulement de gaz brûlés dilués par l'air injecté,
- les autres avec une zone de combustion stabilisée par auto-inflammation du mélange formé à environ 20 cm en aval du mélangeur et pour une richesse $\phi_2 = 0,45$.

Dans les deux cas le débit total était de 300 g/s et la température de mélange immédiatement en aval du mélangeur de 1150 K.

Les mesures ont été effectuées à 25 cm en aval du mélangeur, c'est-à-dire au début de la zone de combustion lorsque $\phi_2 = 0,45$. Les résultats obtenus par prélèvement avec la sonde type b (fig. 2b) sont résumés sur la figure 10. Avec la sonde type a les résultats obtenus étaient presque identiques. Par contre avec la sonde à col sonique la fraction molaire de NO_2 obtenue était, pour $\phi_2 = 0$ et pour $\phi_2 = 0,45$, environ la moitié de celle obtenue avec les sondes sans col sonique. Ce dernier résultat tend à prouver que le NO_2 détecté par prélèvement et analyse provient d'une oxydation de NO en proportion variable suivant le type de sonde utilisé. De plus il apparaît que cette transformation de NO en NO_2 est beaucoup plus importante en présence de combustion ($\phi_2 = 0,45$).

Les mesures d'absorption effectuées dans la même section de la veine ont été interprétées :

- en calculant les absorptions parasites dues à O_2 et CO_2, à partir des profils des concentrations et de la température le long du chemin optique,
- en estimant, à partir du profil de la température et de celui de la concentration de NO obtenu par prélèvement et analyse, une "longueur équivalente d'absorption" pour NO (cf. § 5.3) qui a été trouvée égale à 12,1 cm au lieu de 10 cm.

En absence de combustion ($\phi_2 = 0$) on a obtenu ainsi une valeur de X_{NO} supérieure de 25% à celle de X_{NO_x} mesurée sur l'axe par prélèvement. Ce résultat conduit aux mêmes conclusions que les expériences effectuées avec le brûleur type MEKER, c'est-à-dire que, non seulement le NO_2 dosé proviendrait d'une oxydation de NO lors du prélèvement, mais qu'il y aurait de plus soit réduction de NO, soit absorption parasite supplémentaire due à une autre espèce que O_2 et CO_2.

En présence de combustion ($\phi_2 = 0,45$) nous avons constaté une augmentation très importante du taux d'absorption, qui était environ le double de celui mesuré sans combustion ($\phi_2 = 0$). Cette augmentation ne correspond probablement pas à une augmentation correspondante de X_{NO}, (puisque les mesures par prélèvement et analyse n'indiquent pas d'augmentation de X_{NO_x}), mais plus vraisemblablement à une absorption par certains hydrocarbures résultant de la fragmentation du propane et présents en concentrations relativement importante au début de la zone de combustion /15/.

6 - MESURES DANS LE JET D'UN TURBOREACTEUR -

Des confrontations ont également été effectuées à la SNECMA dans le jet d'un turboréacteur "LARZAC" au banc d'essai. Les mesures ont été effectuées à 3 cm en aval de la section de sortie de la tuyère. Elles ont montré que, lorsque l'on faisait varier le régime du moteur depuis le maximum jusqu'au ralenti :

- les mesures par prélèvement et analyses indiquaient une fraction molaire de NO décroissant rapidement de 77 ppm à 4 ppm,
- le taux d'absorption mesuré pour la bande $\gamma(0,0)$ décroissait d'abord de 8,7% à 5,3% pour ensuite augmenter régulièrement jusqu'à 38%.

L'absorption parasite due à O_2 et à CO_2 restant inférieure à 1%, et le taux d'absorption mesuré pour le régime maximal correspondant à environ 140 ppm, les résultats mettent clairement en évidence la présence d'une absorption parasite supplémentaire augmentant quand le régime du moteur décroît, c'est-à-dire en fait quand les concentrations des imbrûlés croissent (celles de CO et de CH_x atteignent entre 2000 et 3000 ppm au ralenti).

[illegible] -

Nos travaux ont contribué à rendre plus aisée l'application de la spectroscopie U.V. à la mesure de concentration de l'oxyde nitrique :

- en proposant des expressions analytiques approchées simples reliant la fraction molaire de NO et le taux de transmission mesuré pour les bandes γ 1,0 et γ 0,0,
- en mettant en évidence les absorptions parasites de l'oxygène et du gaz carbonique, qui ne peuvent être négligées dès 700 K pour γ 1,0 et dès 900 K pour γ 0,0, et en proposant également des expressions analytiques approchées des taux d'absorption correspondants.

Toutefois il est apparu que des espèces autres que l'oxygène et l'anhydride carbonique, vraisemblablement des imbrûlés, interfèrent avec les mesures de concentration de l'oxyde nitrique par absorption U.V. et sont, au moins pour une part, responsables des écarts constatés avec les mesures par prélèvement et analyse. Il est donc nécessaire de les identifier et de les mesurer avant de pouvoir interpréter correctement la confrontation entre les deux méthodes de mesure.

REMERCIEMENTS -

Ces travaux ont été effectués dans le cadre du contrat n° 145.243 YY conclu avec la SNECMA, que les auteurs tiennent à remercier. Ils remercient également M. Daniel PALAISE pour l'efficacité et le soin qu'il a apportés dans sa contribution à la conduite des expériences.

REFERENCES -

/1/ - DE SOETE G., "Mécanismes physico-chimiques de formation et de réduction de NO_x dans les flammes d'hydrocarbures", Rapport I.F.P. n° 25862, 1978.

/2/ - CERNANSKY N.P., "Sampling and measuring for NO and NO_2 in Combustion systems", Experimental diagnostics in gas phase combustion systems, Ed. B.T. ZINN, Progress in Astronautics and Aeronautics, volume 53, AIAA, New York, 1977, p. 33.

/3/ - DE SOETE G., "Formation d'oxydes d'azote dans les flammes : le mécanisme de formation du prompt NO", Rapport I.F.P. n° 21832, 1973.

/4/ - MERRYMAN E.L. and LEVY A., "Nitrogen oxide formation in flames : the role of NO_2 and fuel nitrogen", XVth Symposium (International) on Combustion, the Combustion Institute, p. 1039, 1975.

/5/ - MUELLER F.J., "Direkte spektroskopische Bestimmung der lokalen NO Koncentration in einer laminaren Methan-Flamme", Dissertation, T.H. Aachen, 1975.

/6/ - MEINEL H. and JUST T., "Measurement of NO_x exhaust emissions by a new NDUV analyzer ", Experimental diagnostics in gas phase combustion systems, Ed. B.T. ZINN, Progress in Astronautics and Aeronautics, vol. 53, AIAA, New York 1977, p. 177.

/7/ - PEW J.D., McGREGOR W.K. and GLASSMAN H.N., "Resonance absorption measurements of NO concentration in combustor exhaust", Experimental diagnostics in gas phase combustion systems, Ed. B.T. ZINN, Progress in Astronautics and Aeronautics, vol. 53, AIAA, New York, 1977, p. 187.

/8/ - PEW J.D., BRYSON R.J. and LOWRY H.S., "Optical in situ versus probe measurements of nitric oxide concentration as a function of axial position in a combustor exhaust", AEDC-TR-78-32, 1978.

/9/ - HERZBERG G., "Molecular spectra and molecular structure, I. Spectra of diatomic molecules", D. van Nostrand Company Inc., New York, 1950.

/10/ - PENNER S.S., "Quantitative molecular spectroscopy and gas emissivities", Addison-Wesley Publishing Company Inc., Pergamon Press, 1959.

/11/ - DAVIS M., McGREGOR W.K., PEW J.D. and GLASSMAN H.N., "Transmission of Doppler broadened resonance radiation through absorbing media with combined Doppler and pressure broadening (Nitric Oxide gamma bands as an example)", AEDC-TR-76-12, 1976.

/12/ - DURAND J.Ph., "Application de la spectroscopie U.V. à la mesure de la concentration de l'oxyde nitrique dans des produits de combustion", Thèse de Docteur-Ingénieur, Poitiers, 1980.

/13/ - WHITING E., "An empirical approximation to the VOIGT Profile", J. Quant. Spectr. Radiat. Transf., vol. 8, 1968, p. 1379.

/14/ - DUTERQUE J., "Conditions d'emploi des appareils de chimiluminescence dans l'analyse des oxydes d'azote", Rapport technique n° 1311849 EH, 1978.

/15/ - BELLET J.C., MERLIN J., BAUER P. et KAGEYAMA T., "Expériences sur la combustion turbulente du propane en foyer tubulaire", communication présentée au VIth International Colloquium on Gasdynamics of Explosions and Reactive Systems, Stockholm, 1977.

/16/ - GAYDON A.G., "The Spectroscopy of Flames", Chapman and Hall, London, 1974.

/17/ - BOWMAN C.T., "Investigation of nitric oxide formation kinetics in combustion processes : the hydrocarbon-oxygen-nitrogen reaction", Comb. Sci. Techn., vol. 3, 1971, p. 37.

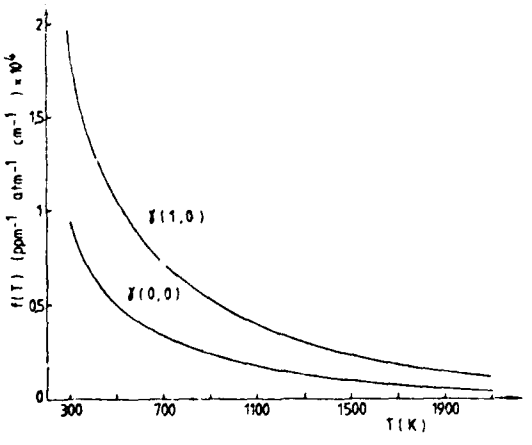

Fig. 1 - Variation de $f_\nu(T)$ en fonction de la température pour $\gamma(1,0)$ et $\gamma(0,0)$.

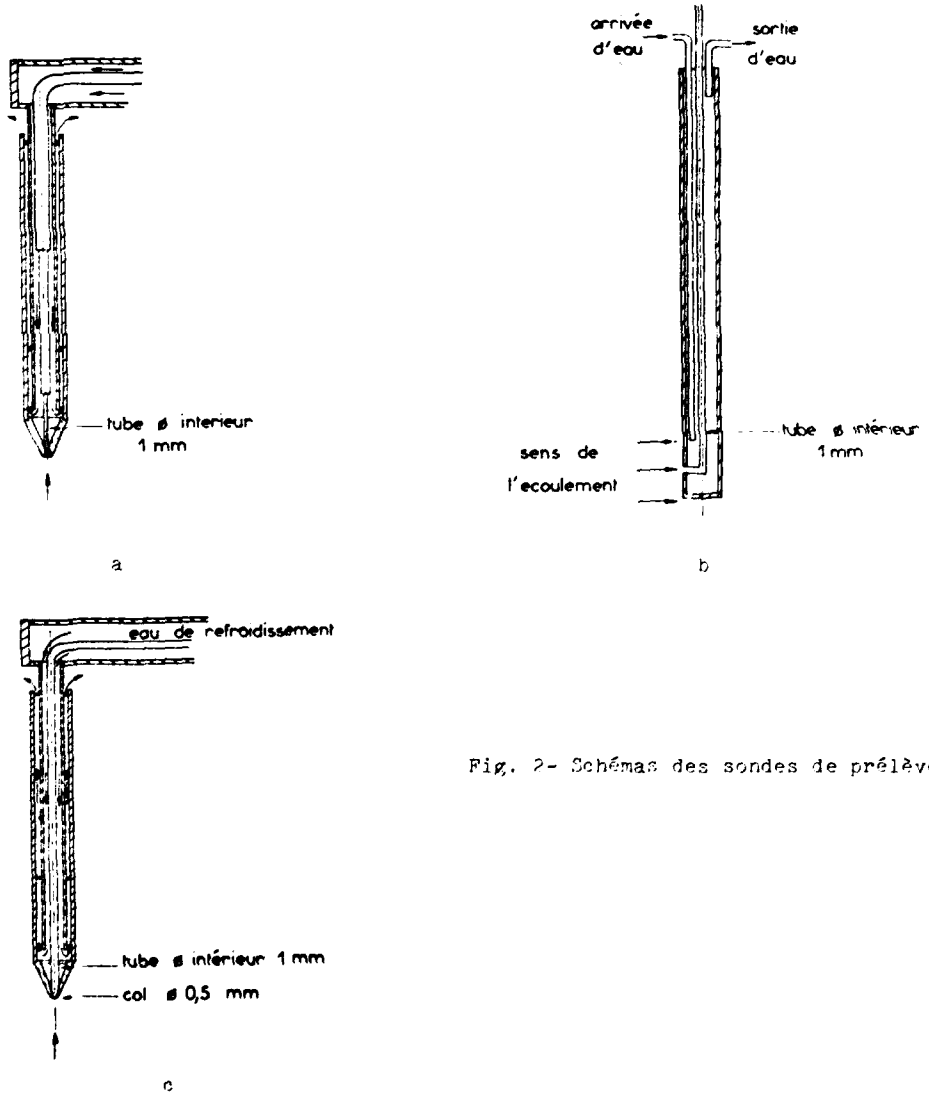

Fig. 2- Schémas des sondes de prélèvement.

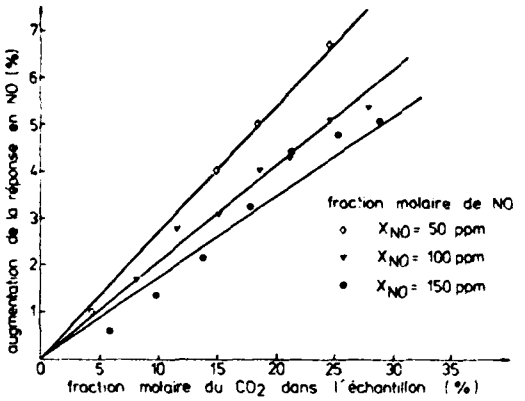

Fig. 3 - Influence de la fraction molaire de CO_2 sur la réponse en NO de l'analyseur Thermo-électron 10 A.

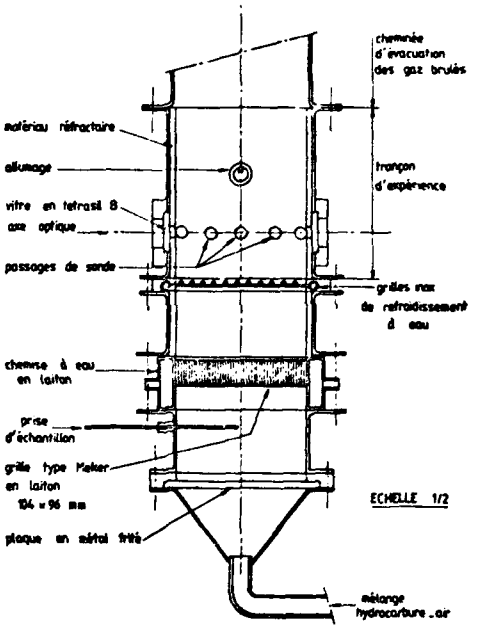

Fig. 4 - Schéma du brûleur type MEKER.

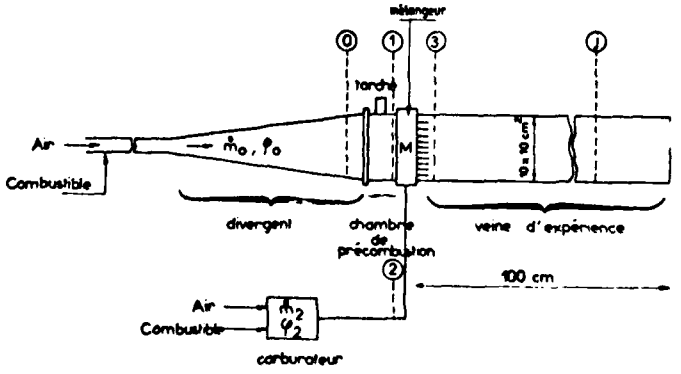

Fig. 5 - Schéma du foyer tubulaire.

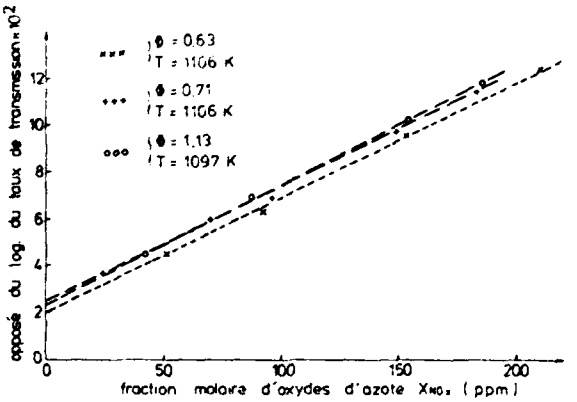

Fig. 6 - Variation de - Ln $\tau_{\Delta\nu}$ en fonction de la fraction molaire de NO_x mesurée par prélèvement.

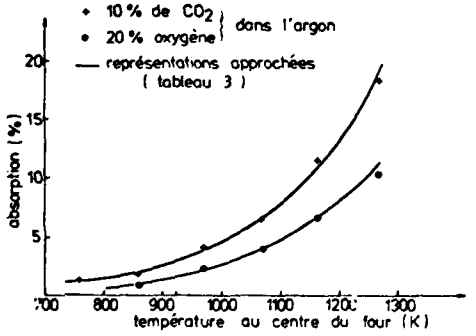

Fig. 7 - Variation de l'absorption par O_2 et CO_2 en fonction de la température pour $\gamma(1,0)$.

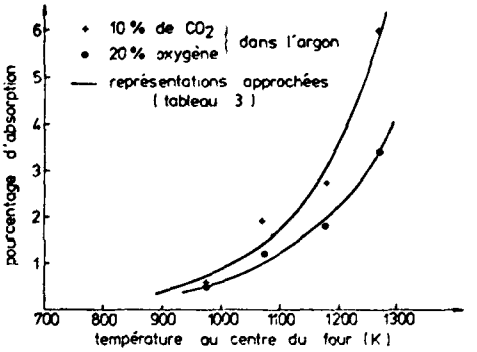

Fig. 8 - Variation de l'absorption par O_2 et CO_2 en fonction de la température pour $\gamma(0,0)$.

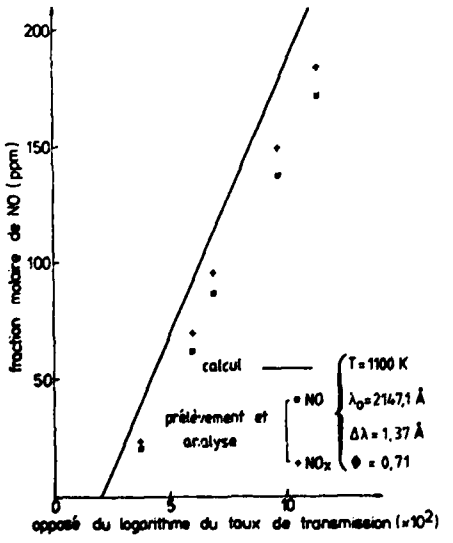

Fig. 9 - Confrontation entre les fractions molaires calculées à partir des mesures d'absorption et mesurées par prélèvement et analyse.

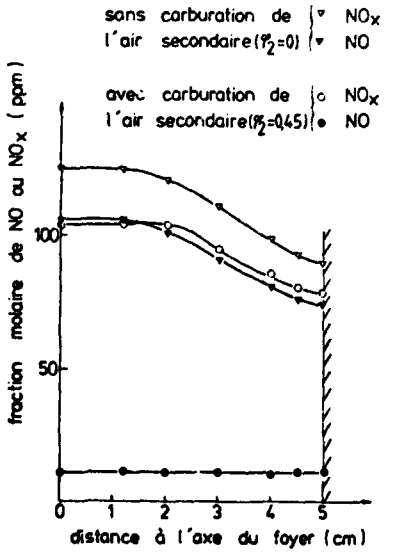

Fig.10 - Fractions molaires de NO et NO_x mesurées par prélèvement dans le foyer tubulaire à 25 cm en aval du mélangeur.

DISCUSSION

A.M.Mellor, US

Why does CO_2 give a positive interference in your chemiluminescence analyser? It usually gives a negative interference due to quenching of NO_2.

Réponse d'auteur

Nous avons en effet constate que, avec l'analyseur "Thermoélectron" model 10A, dont nous disposions, la réponse obtenue avec un mélange NO N_2-CO_2 etait supérieure a celle correspondant a l'etalormage, effectue avec un mélange NO-N_2 contenant la même fraction molaire de NO. Nous avons que des auteurs, ayant utilise un modèle 12A, indiquent un effect de sens oppose. Cette différence dans l'efficacité relative des "figeages" par N_2 et par CO_2 est peut-être due a des différences dans les conditions de functionnement des analyseurs (dilution de l'échantillon analyse, pression dans la chambre de réaction, . . .).

A.Eckbreth, US

I would like to make a comment I believe relevant. The FAA-DOT (Federal Aviation Administration Department of Transportation) in the United States have of course been concerned about the discrepancy between probe and optical measurements of NO. In a three year study conducted at the United Technologies Research Centre under their sponsorship, Zabielski, Saery and Colket have investigated this problem in some detail. The study roughly parallels the investigation described, that is, measurements in a flat flame burner, practical devices, a swirl burner and the exhaust of a JT-12 can. The NO absorption measurements were made using an NO resonance lamp. Over a wide range of stoichiometries, optical and probe measurements were found to agree always within 25%. Details of this work will soon be available in an FAA-DOT approved final report and, I believe, a paper at the XVIIIth Combustion Symposium.

Réponse d'auteur

Il est probable que les ecants de 25% entre les deux méthodes de mesure, que vous mentionnez, sont dus aussi à des absorptions parasites. Je peux vous préciser qu'a des température de quelques certaines de degrés C, les absorptions par C_2H_2, C_3H_6, C_3H_8, C_4H_{10} (et dans une moindre mesure, C_2H_4 et C_2H_6) sont très sensibles pour des concentrations de l'ordre de 1000 p.p.m. Par contre nous n'avons constate aucune interférence avec CO ou CH_4.

DIAGNOSTICS DES COMBUSTIONS PAR D.R.A.S.C.

par B. Attal, M. Péalat et J.P. Taran

Office National d'Etudes et de Recherches Aérospatiales
92320 Châtillon - FRANCE

RESUME

Les spectromètres DRASC mis au point à l'ONERA sont présentés dans cet exposé.

L'instrument de DRASC non résonnante permet la mise en oeuvre de la technique BOXCARS et l'élimination du fond non résonnant. Sa résolution spectrale est de 0,7 cm^{-1} ; elle peut être réduite à 0,07 cm^{-1} par simple mise en place d'un élément optique sans réalignement du montage. Un mode de fonctionnement en bande large est aussi prévu pour la spectroscopie multiplex.

Des résultats caractéristiques obtenus dans un foyer de simulation de turbomachine sont présentés. La détectivité est comprise généralement entre 100 et 1000 ppm.

La DRASC résonnante permettra des gains en détectivité compris entre 100 et 1000 comme le laissent espérer les résultats récemment obtenus sur I_2.

1 - INTRODUCTION

La Diffusion Raman Anti-Stokes Cohérente (DRASC) est une des meilleures techniques, sinon la meilleure, pour les diagnostics ponctuels et non intrusifs dans les combustions. Il y a plusieurs années que la faisabilité des mesures de concentration /1/ et de température /2/ a été démontrée à l'ONERA.

Depuis, des progrès considérables ont été réalisés dans la mise en oeuvre de cette technique /3-6/, aussi ses performances ont été fortement améliorées : amélioration de la détectivité /9-13/ et de la résolution spatiale /8/, augmentation de la vitesse d'acquisition des spectres /7/. Récemment plusieurs tentatives pour étudier des brûleurs d'intérêt pratique ont été couronnées de succès et ont fait l'objet de publications /14-16/.

Dans ce contexte, le but de la présente communication est de donner un compte-rendu des progrès réalisés à l'ONERA sur les techniques de DRASC. Le travail a été poursuivi dans plusieurs directions :

1 - amélioration de l'équipement existant afin d'accroître la fiabilité, la résolution spatiale et la détectivité des spectromètres DRASC ;

2 - mise au point de méthodes de calcul pour améliorer la réduction des données et pour tenir compte de certains effets (tels que variation de la largeur des raies en fonction de la température et des nombres quantiques de vibration et de rotation) ;

3 - étude théorique de la DRASC résonnante afin d'en évaluer les possibilités d'application à la détection de gaz à l'état de trace ;

4 - mesures de température et de concentrations dans des brûleurs et des écoulements d'intérêt pratique.

2 - DEVELOPPEMENT DU SPECTROMETRE DRASC

Le principal intérêt de la DRASC réside dans la puissance considérable du signal diffusé. Avec les lasers à rubis ou à Yag disponibles sur le marché, les émissions anti-Stokes cohérente de N_2 et de O_2 de l'air sont facilement visibles sur un écran. La démonstration du processus de diffusion est donc simple et claire. Le lecteur est cependant mis en garde : en effet, il est très délicat d'effectuer des mesures précises et reproductibles de température et de concentrations. A dire vrai, la DRASC avec des sources laser pulsées souffre d'un manque de reproductibilité du signal . Ceci résulte des instabilités en puissance et en fréquence des lasers et de leur instabilité de direction. Si l'on ne prend pas de précautions, les fluctuations de puissance du signal sont de ± 30 % ; avec un bloc source très bien construit et avec une voie de référence, on peut espérer une précision relative sur la mesure de susceptibilité de ± 5 %.

La présence dans le spectre d'un fond continu dû à un terme de susceptibilité non résonnante est la deuxième difficulté majeure rencontrée en DRASC. Les raies Raman les plus faibles sortent peu de ce fond continu et il est impossible de mesurer les concentrations des espèces à l'état de trace.

Avec une précision des mesures de ± 5 %, la détectivité est de l'ordre de 0,1 % à 1 % dans les flammes en utilisant une seule impulsion laser par position spectrale. Deux techniques peuvent être utilisées pour réduire le fond non résonnant et pour améliorer la détectivité:(i) élimination du fond par un choix judicieux des polarisations des lasers /9 - 13/, (ii) augmentation par résonance électronique de la réponse de la molécule étudiée /6, 18, 19/.

DRASC NON RESONNANTE

Pendant plusieurs années, l'ONERA a expérimenté sur des flammes un spectromètre DRASC construit autour d'un laser à rubis et dont la description se trouve en référence 6. Récemment, l'Office s'est pourvu d'un système à YAG doublé, choisi en raison de sa puissance crête et de son taux de répétition plus élevé. Ce spectromètre a été mis au point conjointement par l'ONERA et QUANTEL à partir de l'expérience acquise sur le spectromètre DRASC à rubis.

BLOC SOURCE

Les composants optiques des sources laser et les optiques permettant d'en combiner les faisceaux sont fixés directement sur une table en fonte d'aluminium de 50 cm par 150 cm (figure 1). L'oscillateur à Yag est déclenché passivement. Equipé du système Polarex et d'un amplificateur, le système délivre plus de 120 mJ à 5320 Å à la sortie du doubleur de fréquence pour une durée d'impulsion de 10 ns et une cadence de répétition de 1 à 10 Hz (faisceau à ω_1). Le faisceau est monomode longitudinal sur 95 % des tirs et la stabilité en fréquence est alors meilleure que $\pm 0{,}01$ cm^{-1}. Ces caractéristiques sont obtenues grâce à l'utilisation d'une cavité stable pour l'oscillateur Yag. Un deuxième doubleur est utilisé pour convertir le résidu d'infrarouge sortant du premier doubleur. Ainsi, 40 mJ supplémentaires à 5320 Å sont récupérés pour pomper la chaine composée d'un laser à colorant et d'un étage amplificateur. Elle produit le faisceau "Stokes" à ω_2. Le laser à colorant est accordé sur toute sa plage grâce au système composé d'un réseau fixe utilisé en incidence élevée et d'un miroir orientable devant le réseau. Cette configuration développée par QUANTEL pour ses lasers à colorant a, par ailleurs, été proposée par Shashan et al. et par Littman et al /20/. La largeur de raie est de 0,7 cm^{-1} ; elle peut être réduite à 0,07 cm^{-1} après insertion d'un expanseur de faisceau à prismes. Cette opération maintient l'alignement de la cavité d'une manière très précise. Elle provoque toutefois un léger déplacement du centre de la raie.

Avec 40 mJ d'énergie de pompage, la chaîne à colorant délivre de 1 à 3 mJ dans la bande utile en DRASC, c'est-à-dire 560 nm-700 nm. Cette énergie est d'autre part pratiquement indépendante de la largeur de raie choisie.

Le mécanisme d'accord du laser à colorant est commandé par un moteur pas à pas. Celui-ci peut être embrayé sur un mouvement grossier qui permet le balayage de toute la plage de 560 nm à 700 nm ou sur un mouvement fin qui permet alors l'exploration de 6 nm autour d'une position quelconque avec une finesse d'analyse de 0,007 cm^{-1}. Un mode de fonctionnement en large bande est aussi prévu pour le laser à colorant, donnant une largeur de raie de l'ordre de 100 cm^{-1} . L'accord est alors réalisé à l'aide d'un filtre interférentiel ; ce mode de fonctionnement est utilisé pour les expériences DRASC multiplex /7/ avec un spectrographe et un analyseur optique OMA.

EQUIPEMENTS ANNEXES ET MONTAGE DE DETECTION

Un espace de 60 cm x 30 cm est prévu sur la table pour le montage des optiques d'adaptation et de superposition des faisceaux laser ainsi que pour les optiques nécessaires à l'élimination du fond non résonnant /9 - 13/ et à la technique des faisceaux croisés (Boxcars) /8/. Ainsi nous utilisons :

- des télescopes pour adapter les divergences des faisceaux ;
- des lames à faces parallèles pour les translater ainsi que pour les dédoubler dans le cas du montage BOXCARS ;
- un miroir dichroïque pour l'alignement et la superposition des deux faisceaux laser ;
- des lames $\lambda/2$ et $\lambda/4$ et des polariseurs pour l'élimination du fond non résonnant.

Le miroir dichroïque est monté sur une platine de rotation très robuste ayant une sensibilité d'alignement meilleure que 10 µrad. Une petite fraction (≃ 5 %) des faisceaux laser est par la suite prélevée pour la voie de référence.Nous examinerons maintenant le système de détection et le problème d'élimination du fond non résonnant.

Le montage de détection, y compris le bras de référence, est installé sur une autre table de 50 cm x 150 cm (figure 2). Toutes les lentilles de focalisation sont des achromats non collés traités A.R. entre 400 nm et 700 nm.

Les signaux anti-Stokes sont filtrés grâce à des doubles monochromateurs de dispersion totale nulle précédés de filtres dichroïques. Ces derniers bloquent l'essentiel du rayonnement des lasers de façon à éviter les problèmes de claquage sur les diaphragmes des

monochromateurs. La détection est faite à l'aide de photomultiplicateurs intégrés dans les monochromateurs.

Le niveau du signal anti-Stokes dans les voies signal et référence est ajusté entre 10^3 et 10^4 photoélectrons par coup, ce qui correspond à une incertitude de Poisson de l'ordre de quelques pour cents. Des signaux plus intenses peuvent provoquer une saturation des photomultiplicateurs tandis que des signaux plus faibles donnent des niveaux d'incertitude inacceptables.

Les voies signal et référence ont, dans la mesure du possible, une géométrie identique, surtout lorsque la configuration BOXCARS est utilisée. La cuve de référence contient 50 bars d'argon ; au delà de cette pression des problèmes de claquage et de phase matching viennent perturber le fonctionnement de la voie de référence. Le signal de référence est habituellement plus fort que nécessaire et doit être atténué ; ainsi il reste suffisant même lorsque la configuration BOXCARS et l'élimination du fond non résonnant sont utilisées simultanément. (voir plus loin).

Dans les deux voies, le niveau du signal est maintenu au niveau prévu de 10^4 photoélectrons en ajustant la puissance des faisceaux laser à l'aide d'atténuateurs ce qui évite la saturation Raman au centre de la raie. Les impulsions délivrées par les photomultiplicateurs sont traitées par une électronique munie de portes rapides (durée d'ouverture : 50 ns). Elle calcule leurs rapports, la racine carrée de ceux-ci, puis leur moyenne pour un nombre fixé n d'impulsions laser (n = 1 à 10 en pratique). Cette électronique élimine aussi toute mesure pour laquelle le signal ou la référence s'écarte de ± 35 % de leur valeur moyenne respective.

Cette électronique commande aussi l'avance du laser à colorant lorsque les n coups ont été obtenus et trace le spectre en temps réel.

Pour la DRASC multiplex , nous utilisons un spectrographe et un analyseur optique multicanal (OMA_2 de PAR - EGG). L'élément dispersif dans le spectrographe est un réseau holographique concave de 2100 traits au mm, corrigé des aberrations et de 750 mm de rayon de courbure. La résolution spectrale de l'ensemble spectrographe-détecteur est de 1 cm^{-1} . Les spectres de signal et de référence sont enregistrés simultanément sur le vidicon. Leur rapport est calculé canal par canal donnant ainsi naissance à un nouveau spectre dont la racine carrée et, si nécessaire, une moyenne sont calculées par la suite. L'enregistrement du spectre de référence est d'une nécessité vitale car le spectre du laser à colorant n'est pas reproductible et montre d'appréciables modulations.

La technique d'élimination du fond non résonnant par l'utilisation des propriétés du tenseur de susceptibilité non linéaire du 3ème ordre a été discutée en détail pour les faisceaux colinéaires, et plusieurs configurations de polarisation ont été proposées /9 - 13/. La configuration BOXCARS offre plus de souplesse car les deux faisceaux "laser" à ω_1 sont maintenant séparés et peuvent donc avoir différentespolarisations $\hat{e}_1$ et $\hat{e}_1'$. Dans la zone de recouvrement de ces deux faisceaux et du faisceau Stokes, nous pouvons supposer, pour simplifier, que tous les vecteurs k sont alignés et que les polarisations des champs électriques sont dans un plan perpendiculaire aux vecteurs k, suivant l'alignement de la figure 3. Nous supposons le vecteur polarisation du champ Stokes $\hat{e}_2$ aligné suivant l'axe X.Si nous supposons aussi que le tenseur de susceptibilité non résonnante possède la symétrie de Kleinman, nous pouvons écrire le vecteur de polarisation anti-Stokes de la manière suivante :

$$\underline{P} = \underline{P}_{nr} + \underline{P}_r$$

avec $$\underline{P}_{nr} \alpha \begin{vmatrix} \cos(\theta + \psi) + 2\cos(\theta - \psi) \\ \sin(\theta + \psi) \end{vmatrix} , \quad \underline{P}_r \alpha \begin{vmatrix} 4(a+b)\cos\theta\cos\psi + 2b\sin\theta\sin\psi \\ (2a+b)\sin(\theta+\psi) \end{vmatrix}$$

en utilisant les notations de Rahn et coll. /12/. Pour obtenir une réjection totale de la contribution non résonnante, nous interposons un analyseur orthogonal à $\underline{P}_{nr}$, recueillant ainsi de la lumière polarisée suivant $\hat{e}_a$ et d'amplitude $\hat{e}_a \cdot \underline{P}_r$. Lorsque $b = 0$, nous avons :

$$(1) \qquad \hat{e}_a \cdot \underline{P}_r = \frac{\sin 2\theta + \sin 2\psi}{\left[3 + 2(\cos 2(\theta - \psi) + \cos 2\theta + \cos 2\psi)\right]^{1/2}}$$

qui conserve la symétrie en θ et ψ .

Cette expression est représentée figure 4 ; elle présente un maximum étendu qui comprend la solution de Rahn et coll. /12/ ($\theta = \psi = 60°$) ainsi que celle proposée par Levenson et al /9/ ($\theta = 45°$, $\psi = 90°$). Nous remarquons que toute solution en θ et ψ telle que

$$(2) \qquad (90° - \psi)^2 + (90° + \theta)^2 = 1800$$

expression trouvée d'une façon empirique et qui correspond au cercle de rayon 42,4°centré à $\theta = 90°$, $\psi = 90°$, donne un résultat supérieur à 0,98 et est donc acceptable (mis à part les singularités en $\psi = -\theta = 60°$ et $\psi = -\theta = 120°$). Ceci donne une souplesse instrumentale considérable. La solution la plus élégante est probablement obtenue avec $\theta = \pm 45°$, $\psi = 90°$ puisque dans ce cas $\underline{P}_{nr}$ est aligné avec $\hat{e}_1$ (figure 5). On peut ainsi choisir les polarisations $\hat{e}_2$ et $\hat{e}_1$ pour les faisceaux laser et Stokes superposés et $\hat{e}_1$

pour l'autre faisceau. Le faisceau anti-Stokes utile est émis le long de ce dernier : puisque l'analyseur doit être orienté d'une façon précise à angle droit de $\hat{e}_1$, le faisceau ω_1 est éliminé complètement . Bien que cette solution paraisse séduisante, nous avons préféré celle où $\theta = \psi = 60°$ qui permet un alignement plus facile. La figure 6 donne le schéma de cet arrangement montrant la lentille de focalisation (à gauche) et celle de recollimation (à droite), les zones illuminées par les faisceaux laser sur ces lentilles et les polarisations des faisceaux laser.

Le faisceau à ω_2 est polarisé horizontalement tandis que les deux faisceaux parallèles ayant la fréquence ω_1 sont polarisés linéairement à 60° du vecteur de polarisation de ω_2. Cet angle est obtenu grâce à une lame demi-onde (figure 1). Un faible degré d'ellipticité est également obtenu grâce à une lame quart d'onde afin de compenser les biréfringences des divers composants optiques situés entre la lame demi-onde et le volume de mesure (notamment le séparateur de faisceau (BS), les fenêtres et les lentilles). Le faisceau anti-Stokes, émis à $\omega_3 = 2\omega_1 - \omega_2$ dans la direction où aucun faisceau ω_2 n'est présent, est filtré grâce à un polariseur de Glan. Ainsi qu'il en est question en /12/, il est parfois nécessaire de modifier légèrement les angles de 60° afin de réduire le fond non résonnant résiduel, cette correction étant fonction de la composition du milieu étudié. Bien entendu, pour des raisons évidentes, on ne dispose pas de filtre polarisant sur le faisceau anti-Stokes de la voie référence.

CARACTERISTIQUES DU SPECTROMETRE DRASC

Les performances d'un spectromètre DRASC sont caractérisées par la résolution spatiale, la stabilité, l'élimination du fond non résonnant et la résolution spectrale.

- La résolution spatiale et l'efficacité de la création du signal anti-Stokes sont optimales quand les faisceaux sont limités par la diffraction, que leurs diamètres sont égaux et que leurs directions sont soigneusement alignées.

Pour des faisceaux limités par la diffraction, l'alignement est alors délicat et difficile à maintenir. La figure 7 donne la puissance anti-Stokes du signal de référence de notre montage en fonction de l'angle entre les faisceaux laser à ω_1 et ω_2 dans l'arrangement colinéaire (une courbe similaire est obtenue en utilisant la voie signal). Les faisceaux sont focalisés au moyen d'un achromat de 20 cm de focale. La courbe, très pointue, montre que l'alignement est extrêmement critique si on utilise des faisceaux limités par la diffraction.

Cet alignement peut être maintenu sur notre montage pendant plusieurs mois sans réajustement. Quant au laser à colorant, sa direction change de moins de 10 µrd entre 560 nm et 700 nm ; aucune correction n'est donc nécessaire car cette valeur est très inférieure à l'angle de diffraction des deux faisceaux laser (150 µrd environ). En outre le rapport des signaux de mesure et de référence reste constant à ± 5 % pour un défaut d'alignement inférieur à 100 µrd, ce qui garantit la reproductibilité des mesures. Une évaluation de la résolution spatiale longitudinale peut être obtenue en translatant une lame couvre-objet de microscope le long de la région focale, et en enregistrant la racine carrée du signal non résonnant produit dans le verre en fonction de la position de la lame. Les résultats sont semblables à ceux présentés dans la figure 14 de la référence 6. Pour un achromat convergent de 40 cm de focale, la résolution spatiale transversale est de 60 µm ; avec la configuration en faisceaux croisés dite BOXCARS, nous obtenons une résolution longitudinale inférieure à 3 mm pour une distance de 8 mm entre les faisceaux parallèles, leurs diamètres étant de 6 mm. Cette résolution varie comme f^{-2} en fonction de la distance focale f de la lentille.

- Un excellent test des performances d'un spectromètre DRASC est son aptitude à détecter le CO_2 atmosphérique. La figure 8 présente ces spectres enregistrés avec une résolution spectrale de 0,7 cm^{-1} avec (a) et sans (b) suppression du fond non résonnant, la technique BOXCARS donnant une résolution spatiale de 1 mm dans les voies signal et référence. L'écart type des fluctuations est de ± 2 % pour une moyenne calculée sur 10 tirs laser par position spectrale ; aussi nous pouvons détecter 15 ppm de CO_2 dans l'air pour un rapport S/B unité. Lorsque les polarisations des faisceaux ω_1 et ω_2 sont parallèles, la faible pente négative du fond non résonnant est due à la présence de l'aile de la branche Q de O_2 située à 1556 cm^{-1}.

Lorsque nous orientons les polarisations des faisceaux à 60° l'une de l'autre suivant le schéma de la figure 6, nous espérons un accroissement considérable de la détectivité due à la disparition du fond non résonnant. Ce fond est abaissé en dessous du niveau de bruit de notre électronique, sa réduction étant supérieure à un facteur 30. Dans le même temps cependant, la raie Raman de CO_2 , qui est fortement polarisée, voit son intensité réduite d'un facteur 4. La détectivité est par conséquent augmentée d'un ordre de grandeur. Deux faibles raies de l'oxygène deviennent également visibles dans le spectre.

Quand nous utilisons la résolution spectrale de 0,07 cm^{-1} , l'intensité de la raie de CO_2 est trois fois plus grande car son contour est alors pratiquement résolu. Ce résultat montre qu'une très bonne résolution spectrale est essentielle à l'obtention d'une bonne détectivité dans les flammes si nous gardons à l'esprit que les largeurs des raies Raman y diminuent approximativement comme $(273/T)^{1/2}$

Le résultat d'une expérience de DRASC multiplex sur cette même raie du CO_2 est présenté sur la figure 9. Une moyenne sur 10 spectres fut effectuée afin de rendre la comparaison avec la figure 8 plus facile. Le rapport signal/bruit et le niveau du fond apparaissent dégradés bien que la technique BOXCARS n'ait pas été utilisée pour ces enregistrements (ce qui aurait conduit à recueillir 30 fois moins de signal anti-Stokes).

Cette dégradation des performances s'explique par la diminution de la densité spectrale de puissance du laser a colorant dans le mode en bande large, par une résolution du système (OMA + spectrographe) moins bonne et par la présence d'un peu de lumière parasite.

DRASC RESONNANTE

L'ONERA étudie activement l'augmentation résonnante de la DRASC : les mécanismes physiques ont été décrits en détail de même que le contenu des spectres et la forme des raies pour les gaz. Ces études ont été partiellement confirmées par des expériences /6 - 18 - 19/ tandis que les problèmes d'élargissement Doppler ont été récemment abordés. Ces premières expériences ont montré que la DRASC résonnante dans les gaz est d'une utilisation pratique difficile. Sa mise en oeuvre demande un soin extrême. En effet, aux difficultés générales rencontrées avec la DRASC hors résonance, s'ajoutent des problèmes presque insolubles de saturation à un photon, d'élargissement Stark, de stabilité spectrale et de mesure précise des longueurs d'onde émises. Ainsi les lasers déclenchés de forte puissance ne présentent pas en général la stabilité spectrale nécessaire et risquent de causer une très forte saturation, tandis que les lasers continus, qui conviennent parfaitement pour la spectroscopie à haute résolution et ne provoquent pas de saturation, risquent de conduire à un échauffement important des échantillons. Nous avons donc choisi d'utiliser des lasers à colorant pompés par flashes, car ils offrent un compromis raisonnable entre ces deux extrêmes.

Les lasers à colorant sont présentés sur la figure 10. Les deux cuves de colorant sont montées dans une seule tête "flash" de façon à ce que les impulsions laser soient synchrones. Quatre flashes à ablation réfroidis par eau sont utilisés pour le pompage avec une énergie de décharge de 300 à 400 J. Les cavités laser sont montées sur un bloc de céramique de 80 cm de long. Deux techniques sont utilisées pour l'accord des lasers. Le "laser" de fréquence ω_1 est accordé au moyen d'un filtre interférentiel et de deux étalons Fabry Pérot en silice de 0,1 et 1 mm d'épaisseur de 83 % de réflexion. Le laser "Stokes" de fréquence ω_2 est accordé grâce à un réseau utilisé dans le deuxième ordre de 1200 traits/mm monté en Littrow avec système expanseur de faisceau à prismes. Les deux oscillateurs délivrent des faisceaux de 2 mm de diamètre avec une divergence inférieure à 1,5 fois la limite de diffraction. La puissance crête est comprise entre 1 et 10 kW entre 500 nm et 650 nm pour une durée d'impulsion d'environ 1 µs. La largeur de raie est typiquement de 0,01 cm^{-1} à ω_1 et 0,07 cm^{-1} à ω_2. Les deux lasers sont polarisés horizontalement.

Les cavités laser sont installées sur une table de fonte d'aluminium de 50 cm x 150 cm. Les faisceaux sont combinés au moyen d'un miroir dichroïque monté dans une mécanique ayant une stabilité d'alignement de l'ordre de 20 µrad. Ils sont ensuite focalisés dans la cuve de référence (50 bars d'argon) puis recollimatés. Le signal anti-Stokes créé dans cette cuve est séparé des faisceaux excitateurs au moyen d'une lame dichroïque puis envoyé vers un monochromateur pour filtrage et détection. Les faisceaux de pompe transmis par la lame dichroïque sont filtrés à l'aide d'un verre Schott OG 570 puis focalisés dans la cuve de mesure (focale = 30 cm). Cette focalisation relativement faible permet de réduire au maximum les problèmes de saturation à un photon ; mais elle impose par contre d'utiliser une cuve de longueur suffisante afin d'éviter la création de signal anti-Stokes dans les fenêtres ; ceci nous contraint à utiliser une pression plus basse dans la cuve de mesure pour réduire les pertes par absorption. Pour les résultats décrits ci-dessous, la longueur de cuve optimale a été de 6 à 8 cm pour une pression de vapeur d'iode de 0,5 à 2 mb. La cuve a été réalisée avec un tube épais en silice de 4 cm de diamètre dont les extrémités sont coupées à l'incidence de Brewster. Nous avons fixé deux fenêtres en CaF_2 sur ces extrémités polies.

Les spectres sont enregistrés en accordant ω_1 à la fréquence désirée puis en balayant les spectres de quelques gaz bien connus tels que CO_2, O_2 et H_2 afin d'étalonner le mécanisme de balayage de ω_2. La cuve est ensuite remplie du gaz à étudier. Le niveau du signal anti-Stokes est maintenu à quelques centaines de photoélectron de façon à prévenir les risques de saturation de l'absorption. A cette fin, des verres neutres parallèles et calibrés sont placés devant la cuve si nécessaire.

Les règles permettant l'interprétation des spectres de DRASC résonnante ont été présentées récemment /6 - 18 - 19/ et nous en résumerons simplement les résultats. Ces règles sont déduites de l'expression de la susceptibilité /6/ :

$$X_r = \frac{N}{\hbar^3} \frac{1}{(\omega_{ba} - \omega_1 + \omega_2 - i\Gamma_{ba})}$$

$$(3) \quad X\Bigg\{\Sigma_{n'} \frac{\mu_{an'}\,\mu_{n'b}}{\omega_{n'a} - \omega_3 - i\Gamma_{n'a}} \Sigma_n \frac{\mu_{bn}\,\mu_{na}}{\omega_{na} - \omega_1 - i\Gamma_{na}} (\rho^{(o)}_{aa} - \rho^{(o)}_{nn}) - \Sigma_{n'} \frac{\mu_{an'}\,\mu_{n'b}}{\omega_{n'a} - \omega_3 - i\Gamma_{n'a}} \Sigma_n \frac{\mu_{bn}\,\mu_{na}}{\omega_{nb} - \omega_2 + i\Gamma_{nb}} (\rho^{(o)}_{bb} - \rho^{(o)}_{nn})\Bigg\}$$

où N est le nombre de molécule par cm^3 de la molécule étudiée. Les fréquences d'absorption des états $|a\rangle$ et $|b\rangle$ vers l'état $|n\rangle$ sont respectivement ω_{na} et ω_{nb} .

Cette expression suppose l'existence d'une seule résonance Raman (c'est-à-dire que nous ignorons la décomposition en sous-niveaux rotationnels) et l'interaction faible réduisant la nécessité des corrections d'ordre plus élevé sur les populations initiales $\rho_{22}^{(0)}$, $\rho_{bb}^{(0)}$, $\rho_{nn}^{(0)}$. La figure 11 montre trois types de résonance associés au niveau fondamental $|a\rangle$. Nous les appelons "Résonances Raman Exaltées par Laser (figure 11a), Résonances Double-Electroniques (figure 11b) et Résonances Raman Exaltées par l'Anti-Stokes (figure 11c).

Les transitions vibrationnelles fondamentales et leurs harmoniques sont possibles. Il existe aussi des jeux de transitions analogues qui sont associées au niveau $|b\rangle$ si ce dernier est suffisamment peuplé. Leurs propriétés spectrales se déduisent aisément des dénominateurs correspondants qui figurent dans l'équation (3).

Une caractéristique remarquable des transitions "double-électroniques" est que leur position dans le spectre dépend de ω_1 puisque $\omega_1 - \omega_2 = \omega_{n'a} - \omega_1$, contrairement aux raies Raman des types 11a et 11c. Cette propriété facilite l'identification des raies et a été utilisée lors de travaux précédents /18 - 19/. Le spectre de la figure 12 illustre ces propriétés ; ce spectre a été enregistré récemment dans I_2 pur pour deux valeurs de ω_1 et dans la même région spectrale, tout comme ceux de /18 - 19/ avec cependant une meilleure résolution spectrale. Les deux spectres ont été enregistrés à 24 heures d'intervalle. Le laser ω_1 a été accordé chaque fois à une fréquence inférieure de 0,4 cm^{-1} à celle de la raie D_1de N_a à 16 956,2 cm^{-1}de façon à être en résonance sur la raie d'absorption R67 (13-1) (figure 13). La coincidence avec la raie de N_a était vérifiée à travers un monochromateur et grâce à des étalons Fabry Pérot de 0,1 , 1, 10 mm, l'incertitude finale étant de ± 0,05 cm^{-1} . L'observation des spectres de la figure 12 appelle plusieurs commentaires :

1 - il n'y a aucune ambiguité sur l'identité des raies Raman Q(62), Q(63) et Q(67) ; toutefois l'échelle horizontale n'est valable qu'à la précision de l'étalonnage (soit ± 0,05 cm^{-1}) sur l'accord du laser de fréquence ω_2 ;
2 - les positions théoriques de ces raies ne sont pas connues avec une précision supérieure à 0,1 cm^{-1} ;
3 - les deux spectres diffèrent par la position des raies "double-électroniques" ce qui indique une diminution de 0,1 cm^{-1} de ω_1 entre les cas (a) et (b) ; ceci reste dans les limites de l'incertitude sur le positionnement de ω_1 . La diminution de l'intensité des deux raies associées au niveau J = 67 est due au fait que ω_1 s'éloigne de la raie d'absorption R67 (13-1).

INSTRUMENTATION PRATIQUE

De nombreuses études de flammes par DRASC ont été faites ces dernières années /3 - 5 - 8 - 17/. Toutefois l'expérimentation sur des brûleurs d'intérêt pratique vient seulement de commencer. Durant novembre et décembre 1978, nous avons effectué les premières mesures sur foyer de simulation de turbomachine. Ces mesures étaient des mesures moyennes de concentration et de température. Le foyer en question qui a été construit pour des recherches de base en combustion /14/, est alimenté en kérosène. Il donne un écoulement rectangulaire de 10 x 50 cm de 600 g/s à une température de 1100 K (figure 14). Le bloc source du spectromètre DRASC était installé près du brûleur tandis que les optiques de réception (miroirs de renvoi, filtres, lentilles et monochromateurs) étaient montés sur une table séparée disposée sous le jet (figure 15). Dans le voisinage du montage, le niveau de bruit était de 110 dB tandis que la température ambiante variait de 5°C à 16°C. Le bloc source était protégé du bruit à l'aide d'un caisson en contre plaqué de 2 cm d'épaisseur et une couverture électrique maintenait la température du montage au dessus de 13°C. Il ne fut pas nécessaire de protéger le reste de l'appareillage. De nombreux spectres furent enregistrés.

Le spectre de N_2 au centre du jet est typique de ces expériences (figure 16) : le traitement numérique des résultats conduit à une concentration de 78 ± 5 % et une température T = 1150 ± 50 K conformément aux mesures par chromatographie et par thermocouple (qui donnent respectivement 78 % et 1050 K). Nous remarquerons que le fond résonnant, qui est un paramètre essentiel pour l'obtention d'un bon accord entre les spectres théoriques et expérimentaux et donc pour l'obtention d'une température exacte, est d'environ 20 % plus grand que la valeur déduite d'une mesure dans l'air ambiant (en utilisant la loi en 273/T pour le nombre de molécules par unité de volume à pression constante). Nous avons également remarqué que les mesures du fond non résonnant fluctuent de ± 10 % lorsqu'elles sont enregistrées au coup par coup : nous pensons que ces fluctuations sont dues principalement à des variations de la susceptibilité (et donc du nombre de molécules par unité de volume), et non pas à celles du rendement de conversion qui résulteraient des distorsions des ondes laser par les gradients d'indice. En outre, ces fluctuations sont comparables à celles qui peuvent être déduites de mesures par anémométrie laser à la même position dans le jet. D'autres gaz furent étudiés : O_2 , CO_2 (figure 17 et CF_4 . Ce dernier est injecté dans le foyer pendant un court instant, puis sa concentration est contrôlée à différents moments de façon à déterminer le temps de séjour. Une concentration de CF_4 de 1 % est détectable sans élimination du fond non résonnant.

Tous ces résultats furent obtenus sans élimination du fond non résonnant et sans la configuration BOXCARS. L'introduction récente de ces techniques a permis une appréciable amélioration de notre montage ; l'instrumentation future sur des foyers expérimentaux apparaît extrêmement prometteuse.

Aucune recherche systématique sur la DRASC résonnante dans les flammes n'a été rapportée à ce jour. Cependant, une ou deux espèces présentant de l'intérêt en combustion

ont déjà fait l'objet d'études fortuites par DRASC résonnante. Il s'agit de C_2 /17 - 27 - 28/ et de NO_2 /29/. Peu de choses peuvent être déduites de ces spectres car :

1 - les spectres d'absorption-émission de ces espèces ne sont pas encore entièrement interprétés ;
2 - les fréquences laser n'étaient pas connues avec suffisamment de précision ;
3 - les transitions pouvaient être fortement saturées (les puissances laser utilisées étant considérables) ce qui peut altérer les intensités relatives des diverses raies.

Un exemple d'interférence entre C_2 et CO_2 est présenté sur la figure 18. Ce spectre multiplex a été enregistré dans une flamme de bougie, à proximité de la mèche, avec élimination du fond non résonnant par la technique des polarisations croisées. La région spectrale présentée s'étend autour de la raie du CO_2 à 1388 cm^{-1} . L'absence de la bande de combinaison du CO_2 à 1409 cm^{-1} permet d'affirmer que la température est inférieure ou égale à 600 K ; d'après l'intensité de la raie à 1388 cm^{-1} , nous estimons la concentration de CO_2 à 1000 ppm environ. La détectivité n'est pas aussi bonne que celle déduite du spectre de la figure 8a : elle se situe maintenant à 200 ppm environ, à cause de l'interférence d'une série de raies dues à C_2 . Finalement, la présence de C_2 et CO_2 dans une zone où l'on s'attend à trouver seulement du carburant en phase vapeur indique que ces espèces diffusent depuis la zone de réaction vers la mèche ; C_2 devrait donc y être plus proche de l'équilibre de Boltzman que dans les autres régions de la flamme. Les diverses raies de C_2 qui apparaissent dans le spectre de la figure 18 sont probablement composées chacune d'un ensemble de raies car leur largeur ($\simeq$ 2 cm^{-1})est sensiblement plus large que celle de raies uniques élargies par effet Doppler ou par collisions. Nous étudions actuellement l'interprétation de ce spectre sous la forme de transitions de DRASC résonnante du type de celles de la figure 11. Seules les transitions à un photon de type P peuvent donner une contribution appréciable dans cette partie du spectre. Cette recherche est un peu simplifiée si nous notons que le nombre quantique de spin est conservé dans les processus de DRASC ; 20 contributions majeures proportionnelles à $\rho^{(o)}_{aa}$ et du type Q_Ω (v + 1⟵v), P_Ω (v - 1⟵v), P_Ω (v⟵v) ont déjà été mises en évidences (dans les notations de la référence /18/). Pour toutes ces possibilités, on a $2 < v < 4$, $83 < J < 95$ et Ω = 0, 1, 2 suivant le nombre quantique de spin de la transition en résonance /31/. La liste complète des transitions, y compris celles proportionnelles à $\rho^{(o)}_{bb}$ sera publiée ultérieurement /32/.

Finalement la concentration de C_2 ne peut actuellement être déduite de tels spectres. Afin de mieux comprendre et de réduire les problèmes liés aux interférences dues à C_2 dans les flammes, d'autres recherches devront être faites.

Notons ici que les spectromètres DRASC construits autour d'un laser à rubis présentent l'avantage de fonctionner dans une zone spectrale complètement différente, où l'on s'attend à n'observer qu'une influence réduite du C_2.

3 - CONCLUSION

Un spectromètre DRASC sensible et d'une grande souplesse d'emploi a été construit et essayé. Cet instrument offre plusieurs modes d'opération en ce qui concerne la résolution spatiale, la suppression du fond non résonnant et la spectroscopie multiplex. Il allie détectivité, précision de mesure et simplicité d'opération : la détectivité est 1000 ppm ou mieux si le fond non résonnant est annulé, la résolution spatiale est de l'ordre du mm et les mesures peuvent être acquises en une seule impulsion laser. De plus cet appareil est fiable : le transport en camion vers les cellules d'essais du foyer de simulation de turbomachine et les deux mois de fonctionnement sur l'installation n'ont nécessité que de minimes réajustements du montage. La DRASC est donc devenue la meilleure technique optique d'analyse des flammes. Cependant son utilisation est actuellement limitée aux espèces pour lesquelles les données spectroscopiques et les largeurs de raies sont connues, car il est nécessaire de calculer sur ordinateur des spectres théoriques de bonne qualité pour obtenir des dépouillements précis. On peut espérer que le nombre de données spectroscopiques nécessaires pour les différentes espèces importantes en combustion s'accroîtra rapidement.

La DRASC résonnante nécessitera encore de nombreuses années de développement tant du point de vue théorique qu'expérimental. Elle reste une extension très prometteuse de la technique d'analyse chimique par DRASC conventionnelle. Les résultats obtenus récemment dans I_2 montrent que des gains en détectivité compris entre 100 et 1000 peuvent être espérés.

REFERENCES

/1/ - Régnier P.R. et Taran J.P.E., "On the Possibility of Measuring Gas Concentrations by Stimulated Anti-Stokes Scattering", Applied Physics Letters, Vol. 23, No 5, sept. 1973, pp. 240-242.

/2/ - Moya F., Druet S., et Taran J.P.E.,"Gas Spectroscopy and Temperature Measurement by Coherent Raman Anti-Stokes Scattering", Optics Communications, Vol. 12, No 2, Feb. 1975, pp. 169-174.

/3/ - Moya F.S., Druet S., et Taran J.P.E., "Flame investigation by Coherent Anti-Stokes Raman Scattering" dans Experimental Diagnostics in Gas Phase Combustion Systems, Vol. 53, New York, éditeur Zinn B.T., Progress in Astronautics and Aeronautics, AIAA, 1977, pp. 549-575.
Péalat M., Druet S., Attal B., et Taran J.P.E., "Temperature and Concentration Measurements in Reactive Media by Coherent Anti-Stokes Raman Scattering" présentée à 16th International Symposium on Combustion, Aug. 1977, pp. 789-798.

/4/ - Nibler J.W., Shaub W.M., McDonald J.R., et Harvey A.B., "Coherent Anti-Stokes Raman Spectroscopy", dans "Vibrational Spectra and Structure", Vol. 6, Amsterdam, éditeur Durig J.R., Elsevier, 1977, pp. 173-225.

/5/ - Nibler J.W., et Knighten G.V., "Coherent Anti-Stokes Raman Spectroscopy" dans "Topics in Current Physics", chapitre 7, New York, éditeur Weber A., Springer Verlag, Berlin, 1977.

/6/ - Druet S.A.J., et Taran J.P.E., "Coherent Anti-Stokes Raman Spectroscopy", dans "Chemical and Biochemical Applications of Lasers,éditeur Moore C.B., Academic Press, 1979, pp. 187-252.

/7/ - Roh W.B., Schreiber P.W., et Taran J.P.E., "Single Pulse Coherent Anti-Stokes Raman Scattering", Applied Physics Letters, vol. 29, No 3, Aug. 1976, pp. 174-176.

/8/ - Eckbreth A.C., "BOXCARS, Cross-Beam Phase-Matched CARS Generation in Gases", Applied Physics Letters, Vol. 32, No 7, April 1978, pp. 421-423.

/9/ - Song J.J., Eesley G.L., et Levenson M.D., "Background Suppression in Coherent Raman Spectroscopy", Applied Physics Letters, vol. 29, No 9, Nov. 1976, pp. 567-569.

/10/ - Akhmanov S.A., Bunkin A.F., Ivanov S.G., and Koroteev N.I., "Polarization Active Raman Spectroscopy and Coherent Raman Ellipsometry", Soviet Physics JETP, vol. 47, No 4, April 1978, pp. 667-678.

/11/ - Oudar J.L., Smith R.W., and Shen Y.R., "Polarization-Sensitive Coherent Anti-Stokes Raman Spectroscopy", Applied Physics Letters, Vol. 34, No 11, June 1979, pp. 758-760.

/12/ - Rahn L.A., Zych L.J., and Mattern P.L., "Background-Free CARS Studies of Carbon Monoxide in a Flame", Optics Communications, Vol. 30, No 2, Aug. 1979, pp. 249-252.

/13/ - Koroteev N.I., Endemann M., and Byer R.L., "Resolved Structure within the Broad-Band Vibrational Raman Line of Liquid H_2O from Polarization CARS", Physical Review Letters, Vol. 43, No 5, july 1979, pp. 398-401.

/14/ - Taran J.P.E., "CARS Flame Diagnostics", présentée à "CARS Meeting of the Institute of Physics", AERE Harwell, Mars 1979.

/15/ - Switzer G.L., Roquemore W.M., Bradley R.B., Schreiber P.W., and Roh W.B., "CARS Measurements in a Bluff-Body Stabilized Diffusion Flame", Applied Optics, Vol. 18, No 14, July 1979, pp. 2343-2345.

/16/ - Eckbreth A.C., "CARS Thermometry in Practical Combustors", à paraître.

/17/ - Beattie A.C., Black J.D., Gilson T.R., and Greenhalgh D.A., "Coherent Anti-Stokes Raman Spectroscopy in Sooty Diffusion Flames", SPIE Paper N° 158-09, August 1978.

/18/ - Attal B., Schnepp O., and Taran J.P.E., "Resonant CARS in I_2 vapor", Optics Communications, Vol. 24, No 1, Jan. 1978, pp. 77-82.

/19/ - Druet S.A.J., Attal B., Gustafson T.K.G., and Taran J.P.E., "Electronic Resonance Enhancement of CARS", Physical Review, Vol. A18, No 4, Oct. 1978, pp. 1529-1557.

/20/ - Shoshan I., and Oppenheim U.P., "The Use of a Diffraction Grating as a Beam Expander in a Dye Laser Cavity", Optics Communications, Vol. 25, No 3, June 1978, pp. 375-378.
Littman M.G., and Metcalf M.J., "Spectrally Narrow Pulsed Dye Laser without Beam Expander", Applied Optics, Vol. 17, No 14, July 1978, pp. 2224-2227.

/21/ - Druet S.A.J., Taran J.P.E., and Bordé Ch. J., "Line Shape and Doppler Broadening in Resonant CARS and Related Nonlinear Processes through a Diagrammatic Approach", Journal de Physique, Vol. 40, sept. 1979, pp. 819-840 et additif, Journal de Physique, Fév. 1980 (à paraître).

/22/ - Gerstenkorn S., and Luc P., "Atlas du Spectre d'Absorption de la Molécule d'Iode" Editions du Centre National de la Recherche Scientifique, Paris, 1978.
Luc P., "Molecular Constants and Preliminary Polynomial Expansion Parameters Describing the B-X System of the I_2 Molecules", Journal of Molecular Spectroscopy, (à paraître).

/23/ - Kiefer W. and Bernstein H.J., "Vibrational-Rotational Structure in the Resonance Raman Effect of Iodine Vapor", J. Molec. Spectroscopy, Vol. 43, No 3, March 1972, pp. 366-381.

/24/ - Brewer R.G., "Coherent Transients and Pulse Fourier Transform Spectroscopy", présentée à 4th International Conference on Laser Spectroscopy, Rottach-Egern, FRG, 11-15 juin 1979, in "Laser Spectroscopy 4", New York, édité par Walther H., and Rothe K.W., Springer Verlag, Berlin, Heidelberg, 1979, pp. 220-230.

/25/ - Gilson T.R., "Re-determination of some of the Spectroscopic Constants of the Electronic Ground State of di-Nitrogen $^{14}N_2$, $^{14}N^{15}N$ and $^{15}N_2$ Using CARS", (à paraître).

/26/ - Owyoung A., "High Resolution Coherent Raman Spectroscopy of Gases", présentée à 4th International Conference on Laser Spectroscopy, Rottach-Egern, FRG, 11-15 juin 1979, dans "Laser Spectroscopy 4", New York, édité par Walther H. and Rothe K.W., Springer Verlag, Berlin, Heidelberg, 1979, pp. 175-187.

/27/ - Eckbreth A.C., "CARS Diagnostics Investigation of Flames", présentée à 10th Materials Research Symposium on Characterization of High Temperature Vapors and Gases, NBS, Gaithersburg, Maryland, Sept. 1978.

/28/ - Gross K.P., Guthals D.M., and Nibler J.W., "Electronic Three Wave Mixing Spectra of Transient Species Produced by UV Laser Photolysis of Benzene", J. Chemical Physics, Vol. 70, No 10, May 1979, pp. 4673-4680.

/29/ - Guthals D.M., Gross K.P., and Nibler J.W., "Resonant CARS Spectra of NO_2", J. Chemical Physics, Vol. 70, No 5, March 1979, pp. 2393-2398.

/30/ - Sviridov A.G., Sobolev N.N., Novgorodov M.Z., and Arutianova G.A., Journal Quantitative Spectroscopy and Radiative Transfer, Vol. 6, 1966, pp. 875-892.

/31/ - Herzberg G., Lagerquist A., and Malmberg C., "New Electronic Transitions of the C_2 Molecule in Absorption in the Vacuum Ultraviolet Region", Can. J. of Physics, Vol. 47, No 24, Dec. 1969, pp. 2735-2743.

/32/ - Attal B., Druet S.A.J., Muller-Dethlefs K., Péalat M., et Taran J.P.E., (à paraître).

AD-A092 953 ADVISORY GROUP FOR AEROSPACE RESEARCH AND DEVELOPMENT--ETC F/G 21/2
TESTING AND MEASUREMENT TECHNIQUES IN HEAT TRANSFER AND COMBUST--ETC(U)
SEP 80
UNCLASSIFIED AGARD-CP-281

NL

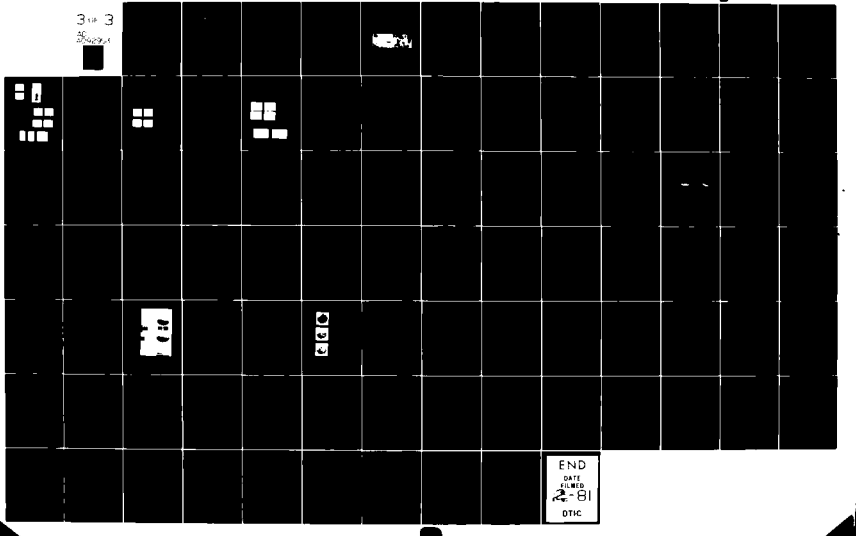

END
DATE FILMED
2-81
DTIC

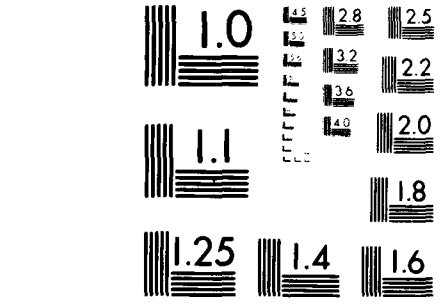

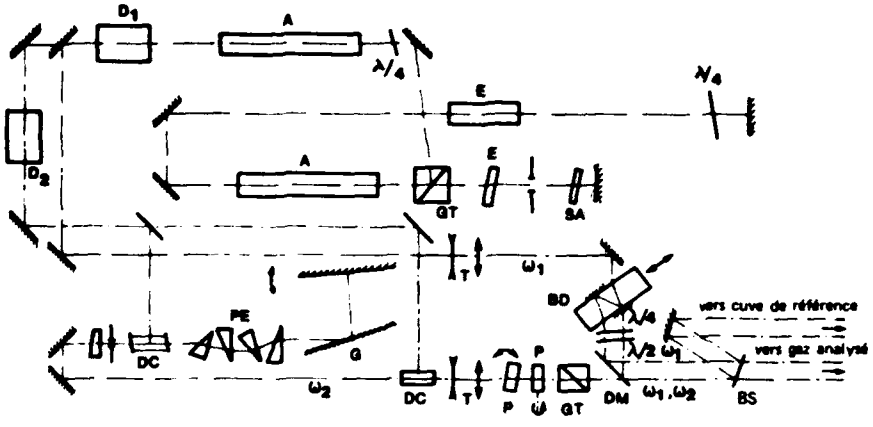

Figure 1 - Bloc source ; A : amplificateur Nd Yag
BD : lame parallèle pour dédoublement en deux faisceaux parallèles pour la technique BOXCARS (la disposition BOXCARS est celle qui est montrée, une translation de la lame permettant de passer à l'arrangement colinéaire sans perte de l'alignement) ;
BS : lame séparatrice pour la voie de référence ;
D_1 et D_2 : doubleurs à KDP ;
DC : cuve de colorant ;
DM : miroir dichroïque ;
E : étalon Fabry Pérot ;
G : réseau ;
GT : prisme de Glan-Tompson ;
P : lame parallèle pour translation des faisceaux ;
PE : expanseur de faisceau à prismes ;
SA : absorbant saturable ;
T : télescope ;
λ/4 et λ/2 : lames quart d'onde et demi-onde, respectivement ;
ω_1 : faisceau "laser" ;
ω_2 : faisceau "Stokes".

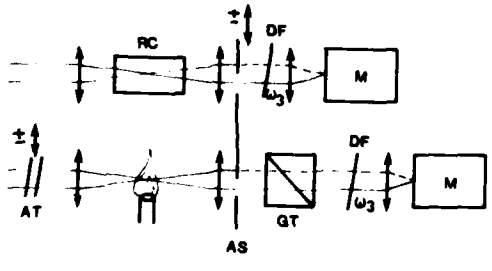

Figure 2 - Schéma des voies signal et référence ;
AS : diaphragme translatable pour le fonctionnement en faisceaux confondus ou BOXCARS (disposition BOXCARS représentée) ;
AT : atténuateurs réglables ;
DF : filtres dichroïques ;
M : monochromateur et détecteur ;
RC : cuve de référence.

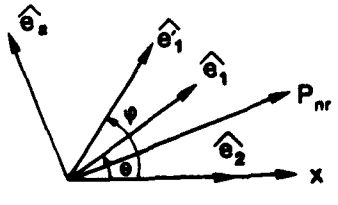

Figure 3 - Vecteurs polarisation des champs électriques dans la zone focale. On suppose une propagation en ondes planes quasi-colinéaires.

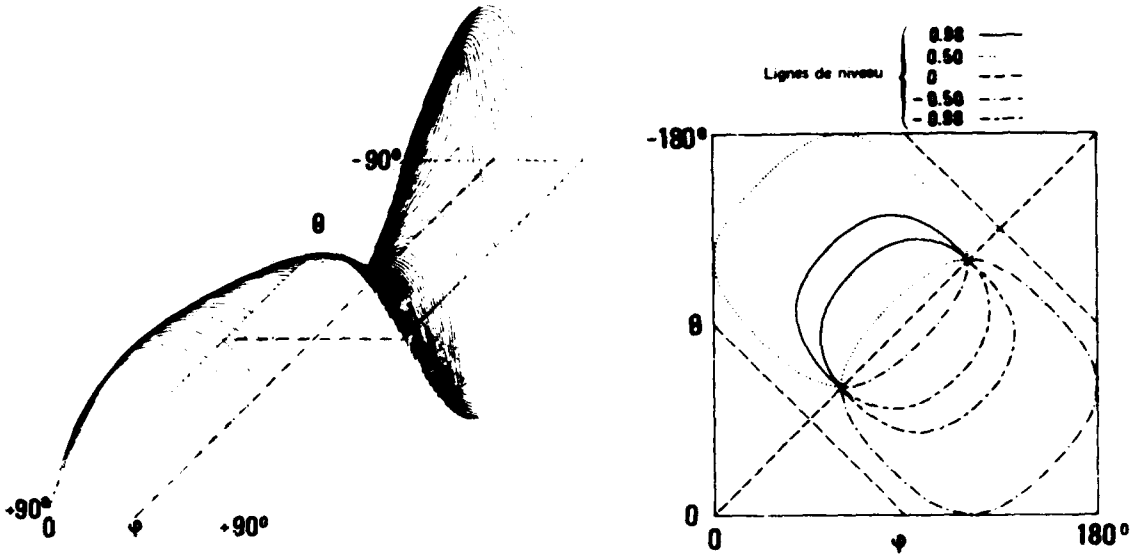

Figure 4 - Perspective et lignes de niveau pour l'amplitude de polarisation anti-Stokes en fonction de θ et ψ . En raison des symétries, nous n'avons figuré la perspective que pour $0 < \psi < \pi/2$ et $-\pi/2 < \theta < \pi/2$ avec des incréments de 2° en θ. Les courbes de niveau sont données pour $-180° < \theta < 0$, $0 < \psi < 180°$. La puissance anti-Stokes est proportionnelle au carré de cette amplitude.

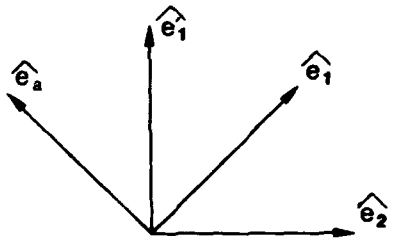

Figure 5 - Une des configurations possibles pour un signal maximum en BOXCARS.

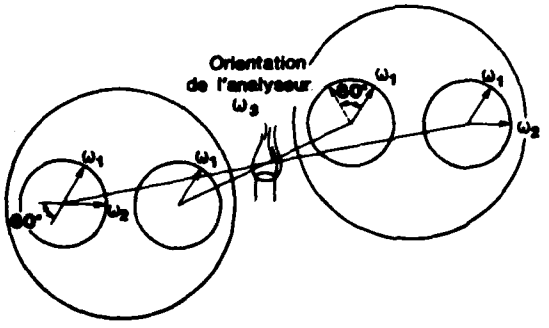

Figure 6 - Arrangement BOXCARS avec élimination du fond non résonnant : on figure les sections droites des faisceaux et leur polarisation dans les plans de la lentille de focalisation (à gauche) et de recollimation (à droite) dans la voie de l'échantillon ; la direction de polarisation du faisceau recueilli à ω_3 est choisie grâce à GT (figure 2). On n'effectue pas de filtrage de polarisation dans le canal de référence.

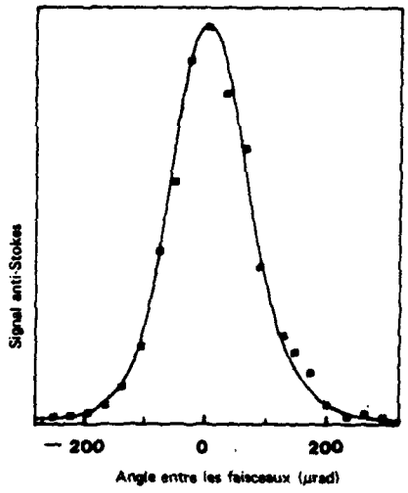

Figure 7 - Signal DRASC obtenu en fonction de l'angle entre les faisceaux laser et Stokes (arrangement colinéaire).

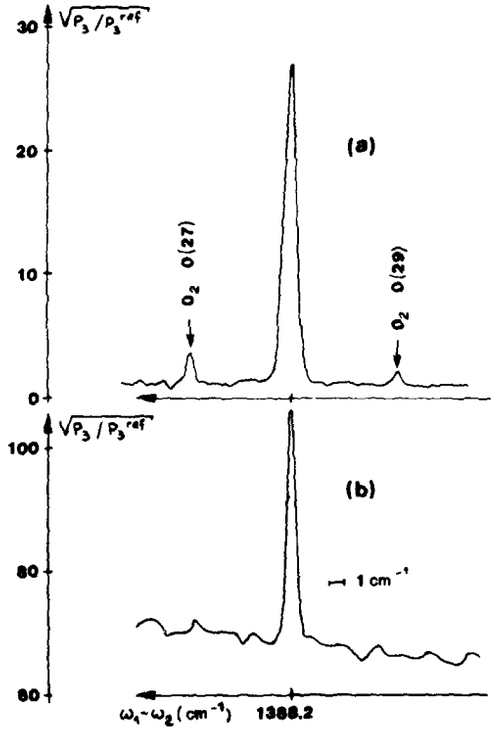

Figure 8 - Spectres du CO_2 de l'air obtenus en faisceaux croisés (BOXCARS) (a) avec élimination du fond non résonnant ; (b) avec polarisation parallèles. P_3 et P_3^{ref} sont les puissances anti-Stokes signal et référence respectivement. Les échelles verticales sont arbitraires.

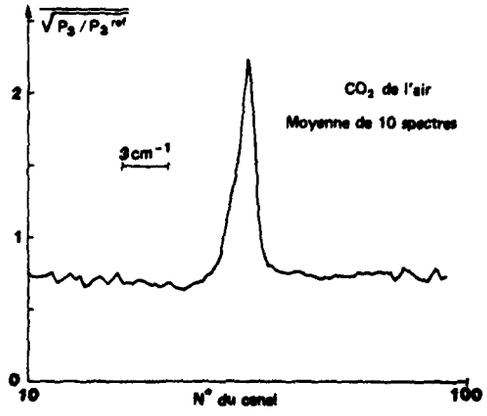

Figure 9 - Spectre pris dans les conditions de la figure 8a avec analyseur optique multicanal et faisceaux colinéaires.

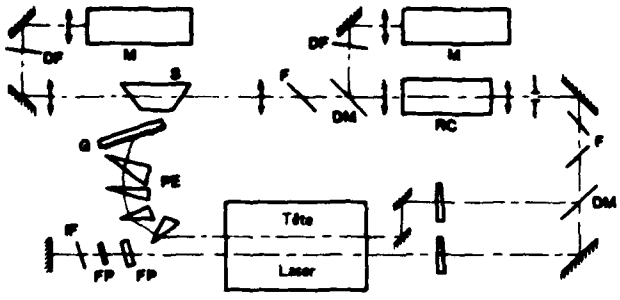

Figure 10 - Schéma du spectromètre DRASC résonnant :

DF : filtre dichroïque ;
DM : miroir dichroïque ;
F : filtre coloré ;
FP : étalon Fabry Pérot ;
IF : filtre interférentiel ;
G : réseau ;
M : monochromateur et détecteur ;
PE : expanseur de faisceau à prismes ;
RC : cuve de référence ;
S : cuve à échantillons.

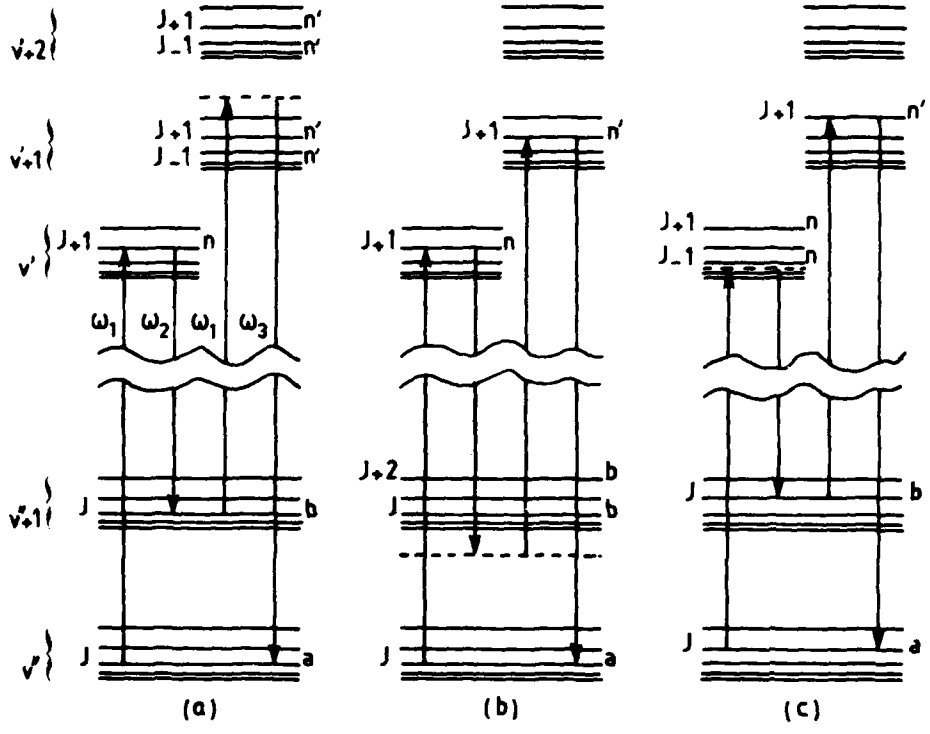

Figure 11 - Diagramme des niveaux d'énergie représentant les états qui contribuent à la DRASC résonnante dans une molécule diatomique : (a) transition vibrationnelle fondamentale ($\Delta v = 1$) exaltée par ω_{na} ; (b) double résonance électronique avec $\omega_1 = \omega_{na}$ et $\omega_3 = \omega_{n'a}$; (c) transition vibrationnelle exaltée par $\omega_{n'a}$: Notons que ces diagrammes ne représentent en aucun cas l'échange d'énergie /6 - 19/, contrairement à une idée largement répandue.

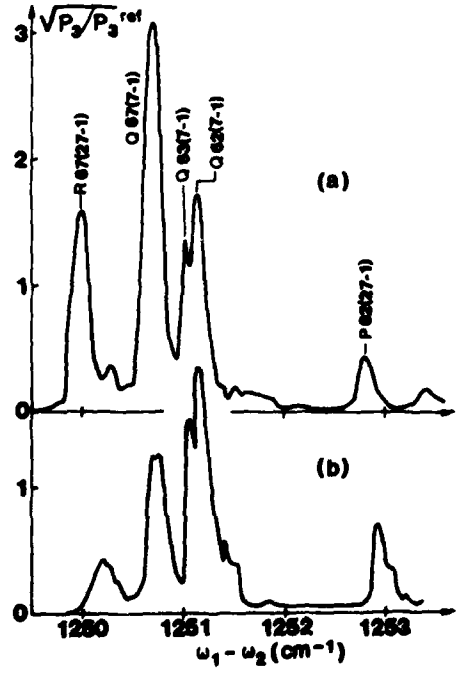

Figure 12 - Spectre du 5ème harmonique de DRASC résonnante dans I_2 pur à 33°C et 0,8 mb. On prend en chaque point la moyenne de trois coups laser successifs.

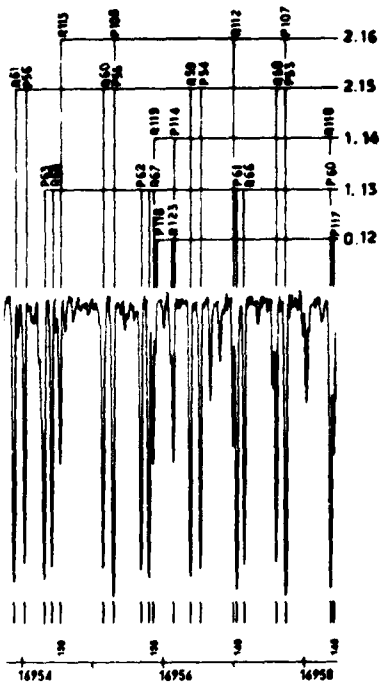

Figure 13 - Spectre d'absorption de I_2 pur à température ambiante et 0,3 mb /22/.

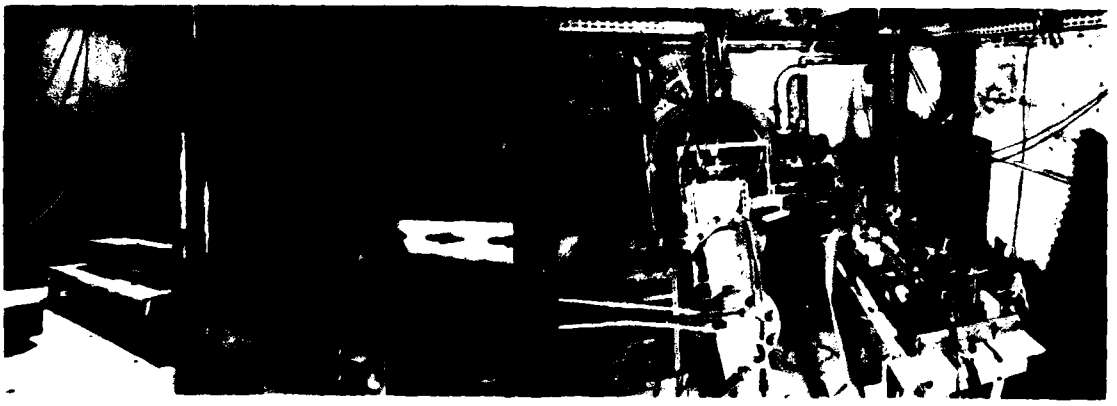

Figure 14 - Vue du foyer allumé. Le spectromètre DRASC est enfermé dans le coffre en contre plaqué (arrière plan); le monochromateur et le détecteur de la voie "échantillon" sont visibles à gauche.

Figure 15 - Vue d'ensemble de l'installation.

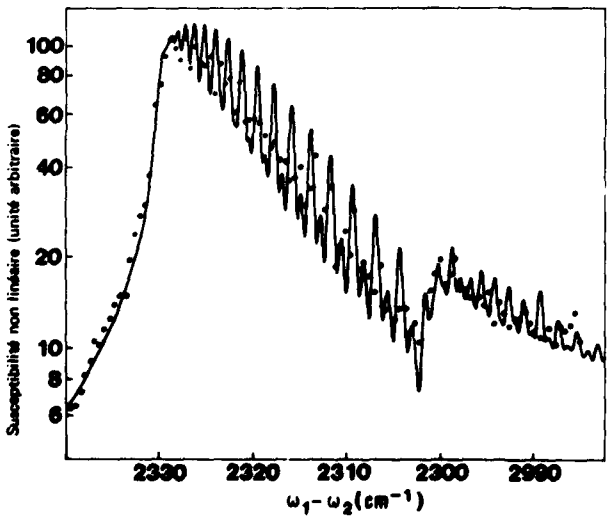

Figure 16 - Spectre moyen de N_2 sur l'axe dans le plan de sortie du foyer; la moyenne de 10 mesures est prise en chaque point. Le traitement des données est effectué avec les constantes spectroscopiques de Gilson /25/ et les valeurs de largeur de raie de Owyoung /26/.

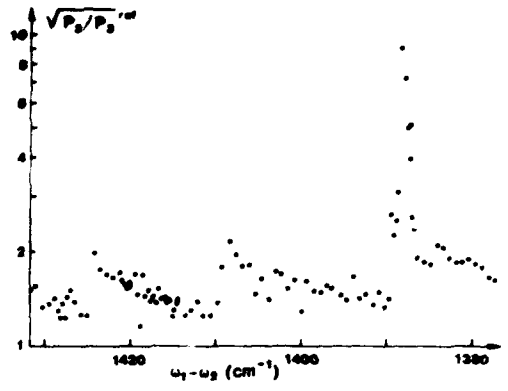

Figure 17 - Spectre moyen de CO_2 relevé au même point que la figure 16 ; la moyenne de 6 mesures est prise en chaque point. Aucun calcul numérique n'a été effectué sur ces spectres de CO_2 ; la concentration de CO_2 mesurée par prélèvement est de 3,36 %. Nous en déduisons que notre sensibilité de détection est de 1000 ppm environ pour ces conditions expérimentales.

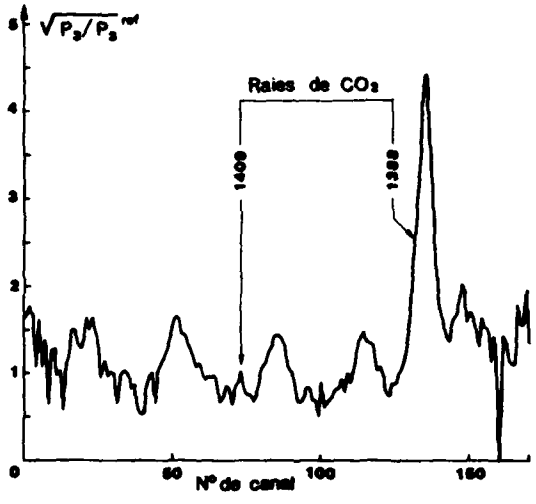

Figure 18 - Spectre multiplex relevé en une seule impulsion dans une flamme de bougie au voisinage de la raie de CO_2 à 1388 cm^{-1}. Les échelles sont les mêmes que pour la figure 9. Le gain de l'étage amplificateur du vidicon est commandé par un générateur d'impulsions pour éliminer le fond lumineux de la flamme.

DISCUSSION

D.A.Greenhalgh, UK

By recording your spectra on a logarithmic scale, do you not cause a bias when fitting due to poor photon statistics in the low signal channels?

Author's Reply

We use a logarithmic scale when we work with a thin dye laser spectrum. In this case, the signal is strong enough to get 10^3 to 10^4 photoelectron counts in each location of the spectrum (by playing with neutral attenuators) so that the accuracy is nearly the same everywhere. Your comment is true for multiplex CARS in which the number of photoelectron counts is limited due to the dynamics of the ISIT detector. In that case we use a linear scale.

A.Eckbreth, US

The change in the nonresonant susceptibility you report for the turbojet combustor is probably due to the change in composition accompanying combustion. In preliminary experiments at our laboratory we have measured the non-resonant susceptibility of water vapour and have found it to be comparable to that of methane, that is, two to three times that of nitrogen. The increase in susceptibility you report is probably due to the water vapour concentration in the exhaust. Would you agree with that?

Author's Reply

Yes, I agree with you.

Investigations of Coherent Anti-Stokes Raman Spectroscopy (CARS) for Practical Combustion Diagnostics

by

Alan C. Eckbreth, Robert J. Hall and John A. Shirley
Senior Research Scientists
United Technologies Research Center
East Hartford, Connecticut 06108, U.S.A.

SUMMARY

Coherent anti-Stokes Raman spectroscopy (CARS) appears very promising for the remote, spatially-and temporally-precise probing of instrumentally hostile combustion environments due to its large signal conversion efficiency and coherent signal nature. CARS is a wave mixing process wherein incident laser beams at frequencies ω_1 and ω_2, with a frequency difference appropriate to the molecular species being probed, interact to generate a coherent signal at frequency $\omega_3 = 2\omega_1 - \omega_2$. By analyzing the spectral distribution of the CARS signal, temperature measurements can be performed. Species concentration measurements derive from the intensity of the CARS radiation or, in certain cases, from its spectral shape. CARS spectra have been recorded in a variety of flames from N_2,O_2,CO, H_2,H_2O, CO_2 and CH_4 and, for the first five generally show very good agreement with computer synthesized spectra. Quite significantly,CARS has been successfully demonstrated with both liquid and gaseous fuels in the primary zone and exhaust of practical combustors. Although thermometry has received the major emphasis, species concentration measurements have been performed for H_2, O_2, and CO.

1. INTRODUCTION

Spatially-precise laser spectroscopy offers the potential for the remote, non-perturbing, in-situ measurement of temperature and species concentrations in combustion processes. Laser techniques are capable of high temporal resolution, although compromises in spatial and/or temporal scale may be necessary in certain measurement applications or parameter ranges. Three approaches, which are inherently spatially and temporally precise, have received much attention in the last several years, namely, spontaneous Raman scattering, coherent anti-Stokes Raman spectroscopy (CARS) and laser-induced fluorescence (Ref.1). For the most part, Raman scattering and CARS are best suited to thermometry and major species concentration measurements, while laser-induced fluorescence is applicable to measurement of flame radicals at trace levels. Raman scattering and laser-induced fluorescence are incoherent scattering processes wherein the generated signal is dispersed into essentially 4π sr. CARS is a coherent wave-mixing process in which the signal emerges as a laser-like beam in a precise direction.

Raman scattering has been widely investigated and is highly developed and understood (Refs.2,3). However, due to its inherent weakness, it is generally limited to application in relatively "clean" flames. With increases in fuel droplet/fragment and soot concentrations, laser-induced interferences, e.g. fluorescences (Ref.4), incandescences (Ref.5), can exceed and mask detection of the Raman signals, often by orders of magnitude. With greater emphasis being directed toward less clean, alternate fuels, stronger diagnostic techniques are required which can operate over a broad range of fuel specifications, stoichiometries and combustion approaches. Both CARS and laser-induced fluorescence appear to possess this capability (Ref. 1), but only CARS has been demonstrated to date in practical combustion environments (Refs.6-9). The two techniques are complementary in regard to their capabilities and have been under development in our (Ref.10) and other laboratories for several years. In this paper, the focus will be restricted to CARS due to space limitations and its potential for near-term practical utilization. The next section of the paper summarizes the theory and application of CARS for combustion diagnostics. Succeeding sections survey the use of CARS for temperature and species concentration measurements in a variety of flame and combustion systems.

2. COHERENT ANTI-STOKES RAMAN SPECTROSCOPY (CARS)

Coherent anti-Stokes Raman spectroscopy (CARS) is capable of the diagnostic probing of high interference environments due to its high signal conversion efficiency and coherent signal behavior. CARS signal levels are often orders of magnitude stronger than those produced by spontaneous Raman scattering. Its coherent character means that all of the generated signal can be collected, and over such a small solid angle that collection of interferences is greatly minimized. CARS thus offers signal to interference ratio improvements of many orders of magnitude over spontaneous Raman scattering and appears capable of probing practical combustion environments over a broad operational range. In experiments at our laboratory and elsewhere, CARS has been successfully demonstrated in

practical combustion situations. With such "real world" demonstrations, one might anticipate CARS to see widespread practical utilization in the coming years

The theory and application of CARS are well explained in several reviews which have appeared recently (Refs. 1,11-14). Briefly, as illustrated in Fig. 1, incident laser beams at frequencies ω_1 and ω_2 (often termed the pump and Stokes beams respectively) interact through the third order nonlinear susceptibility of the medium, $\chi^{(3)}_{ijkl}(-\omega_3,\omega_1,\omega_1,-\omega_2)$, to generate a polarization field which produces coherent radiation at frequency $\omega_3 = 2\omega_1-\omega_2$. It is for this reason that CARS is often referred to as "three wave mixing". When the frequency difference $(\omega_1-\omega_2)$ is close to the frequency of a Raman active resonance, ω_v, the magnitude of the radiation at ω_3, then at the anti-Stokes frequency relative to ω_1, i.e. at $\omega_1+\omega_v$, can become very large. Large enough, for example, that with the experimental arrangement described herein, the CARS signals from room air N_2 or O_2 are readily visible. By third order is meant that the polarization exhibits a cubic dependence on the optical electric field strength. In isotropic media such as gases, the third order susceptibility is actually the lowest order nonlinearity exhibited, i.e due to symmetry considerations, second order effects are nonexistent. The third order nonlinear susceptibility tensor is of fourth rank. The subscripts denote the polarization orientation of the four fields in the order listed parenthetically. In isotropic media, the tensor must be invariant to all spatial symmetry transformations and the 81 tensor elements reduce to just three independent components, χ_{xyyx}, χ_{xyxy} and χ_{xxyy} where $\chi_{xxxx} = \chi_{xyyx} + \chi_{xyxy} + \chi_{xxyy}$. In CARS, which is frequency degenerate, $\chi_{xyxy} = \chi_{xxyy}$ and there are only two independent elements.

The susceptibility consists of resonant components from transitions in the species of interest and, unfortunately, a nonresonant, electronic contribution from all of the molecular constituents present. For very low concentrations, the "signal", i.e. the resonant terms, merges into essentially a baseline level derived from the nonresonant background susceptibility. When the modulation of this background becomes undetectable, the trace species is nominally no longer measurable. At one time, this was perceived to be a major limitation to CARS diagnostics. However, the resonant and nonresonant terms contribute differently to the susceptibility components. By proper orientation of the laser field and CARS detection polarizations, the nonresonant electronic contributions can be cancelled permitting measurements to lower concentrations providing the signal level is adequate. In certain concentration ranges, the presence of the nonresonant susceptibility can actually be used to advantage. As long as the background modulation is detectable, concentration measurements can actually be made from the shape of the CARS spectrum, a unique feature of CARS spectroscopy. Both of these aspects will be subsequently demonstrated in CO and O_2.

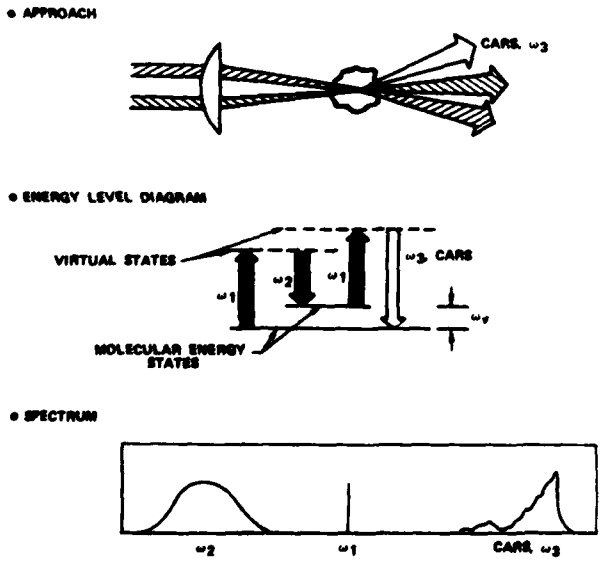

Fig. 1 CARS - Coherent anti-Stokes Raman spectroscopy.

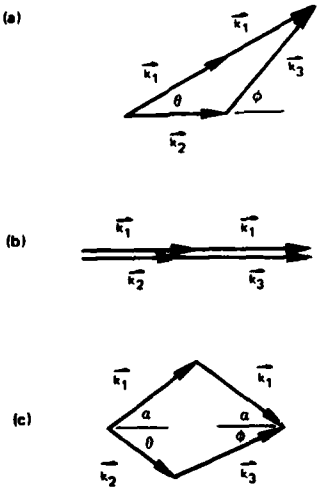

Fig. 2 CARS phase-matching approaches: (a) general. (b) collinear. (c) crossed-beam or BOXCARS.

Reprinted with permission

(Ref. 16)

Measurements of medium properties are performed from the shape of the spectral signature and/or intensity of the CARS radiation. The CARS spectrum can be generated in either one of two ways. The conventional approach is to employ a narrowband Stokes source which is scanned to generate the CARS spectrum piecewise. This approach provides high spectral resolution and strong signals and eliminates the need for a spectrometer. However, for nonstationary and turbulent combustion diagnostics, it is not appropriate due to the nonlinear behavior of CARS on temperature and density. Generating the spectrum piecewise in the presence of large density and temperature fluctuations leads to distorted signatures weighted toward the high density, low temperature excursions from which true medium averages cannot be obtained. The alternate approach (Ref.15) used here is to employ a broadband Stokes source as depicted in Fig. 1. This leads to weaker signals but generates the entire CARS spectrum with each pulse permitting, in principle, instantaneous measurements of medium properties. Repeating these measurements a statistically significant number of times will permit determination of the probability density function (pdf) from which true medium averages and the magnitude of turbulent fluctuations can be ascertained.

For efficient signal generation, the incident beams must be so aligned that the three wave mixing process is properly phased. The general phase-matching diagram for three wave mixing as seen in Fig. 2 requires that $2\bar{k}_1=\bar{k}_2+\bar{k}_3$. $\bar{k}_i$ is the wave vector at frequency ν_i with absolute magnitude equal to $\nu_i\, n_i/c$, where c is the speed of light, and n_i, the refractive index at frequency ν_i. Since gases are virtually dispersionless, i.e., the refractive index is nearly invariant with frequency, the photon energy conservation condition $\nu_3=2\nu_1-\nu_2$ indicates that phase matching occurs when the input laser beams are aligned parallel or collinear to each other. In many diagnostic circumstances, collinear phase matching leads to poor and ambiguous spatial resolution because the CARS radiation undergoes an integrative growth process. This difficulty is circumvented by employing crossed-beam phase matching, such as BOXCARS (Ref.16), or a variation thereof (Refs.17-19). In these approaches, the pump beam is split into two components which, together with the Stokes beam, are crossed at a point to generate the CARS signal. CARS generation occurs only where all three beams intersect and very high spatial precision is possible.

CARS spectra are more complicated than spontaneous Raman spectra which are an incoherent addition of a multiplicity of transitions. CARS spectra can exhibit constructive and destructive interference effects. Constructive interferences occur from contributions made from neighboring resonances, the strength of the coupling being dependent on the energy separation of the adjacent resonances and on the Raman linewidth which together determine the degree of overlap. Destructive interferences occur when resonant transitions interfere with each other or with the nonresonant background signal contributions of electrons and remote resonances. For most molecules of combustion interest, these effects can be readily handled numerically since the physics describing CARS generation is fairly well understood. At UTRC, CARS computer codes have been developed and validated experimentally for the diatomic molecules, N_2, H_2, CO and O_2 (Ref. 20) and one triatomic H_2O (Ref. 21). Computer codes are extremely useful for studying the parametric behavior of CARS spectra and, when validated, for actual data reduction.

Although CARS has no threshold per se and can be generated with cw laser sources, high intensity pulsed laser sources are required for most gas phase and flame diagnostics to generate CARS signals well in excess of the various sources of interference and with good photon statistics, particularly with broadband generation and detection (Ref.1). In the CARS work to be reported, a frequency-doubled neodymium laser provides the pump beam and drives the broadband Stokes dye laser as well as seen in Fig. 3. The laser actually emits two beams at the neodymium second harmonic by sequentially doubling the primary and residual 1.06μ from the first frequency doubler. The primary beam, 2ω, is typically about 2W, i.e. 200 mJ pulses, 10^{-8} sec pulse duration, at 10Hz, and the secondary, $2\omega'$, about an order of magnitude lower. Various dyes and concentrations flowing through spectrophotometer cells are employed to generate Stokes wavelengths appropriate to the molecule being probed. Crossed-beam phase matching (BOXCARS) is used to ensure good spatial precision. The CARS signatures are dispersed in a 0.6 or 1-m spectrograph and detected with an optical multichannel analyzer (OMA) which permits capture of the entire CARS spectrum in a single pulse. In laminar flames and situations where fluctuation magnitudes are small, the CARS spectrum can be averaged on the OMA or scanned with the monochromator using a boxcar averager. Greater detail about the apparatus and procedures employed may be found in (Refs. 22,23).

3. THERMOMETRY

Temperature measurements derive from the spectral shape of the CARS signature. Because of this, thermometry is more easily performed than concentration measurements, which generally, but not always, require determination of absolute signal intensity

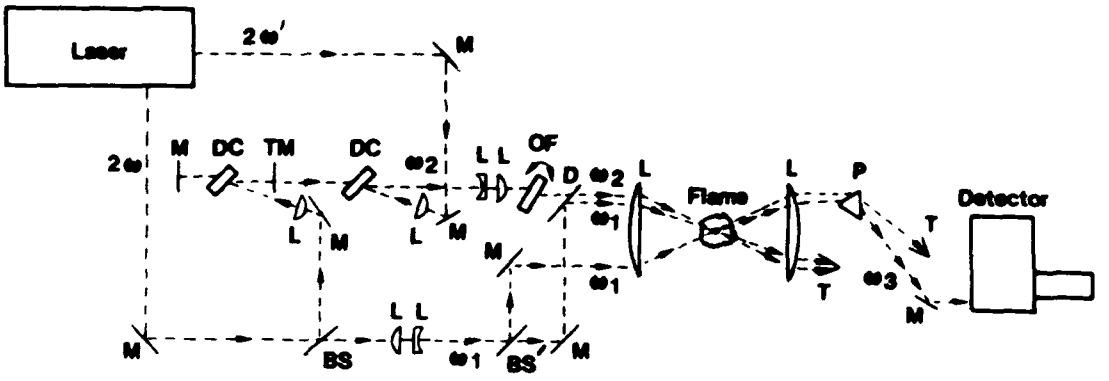

Fig. 3 Schematic of UTRC BOXCARS experimental arrangement. Code: BS, beamsplitter; L, lens; D, dichroic; OF, optical flat; P, prism; F, filter; DC, dye cell; T, trap; TM, partially transmitting mirror; M, mirror.

Reprinted with permission (Ref. 25)

levels. Temperature information can be extracted from any of a number of molecular constituents. In this section CARS thermometry from several molecules in a number of different measurement situations will be illustrated.

Nitrogen - Nitrogen is the dominant constituent in airfed combustion processes and is present in large concentrations despite the extent of chemical reaction. Performing temperature measurements from N_2 provides information on the location of the combustion heat release and, to some degree, the extent of chemical reaction. In Fig. 4 is displayed the calculated temperature dependence of the N_2 CARS spectrum computed for parameters corresponding to the experimental approach employed here, i.e, $\Delta\omega_1$ = 0.8 cm^{-1}, $\Delta\omega_2$ = 130 cm^{-1}, 1.00 cm^{-1} spectral resolution. In the calculations, a constant Raman linewidth of 0.1 cm^{-1} was employed. A description of the computer code employed is summarized in Ref. 20. At low temperatures, one sees the v=0→1 band containing low J value Q branch transitions, i.e. $\Delta J=0$, where J is the rotational quantum number. As is apparent the low J Q branches are unresolved. As the temperature increases, the band broadens as the rotational population distribution spreads out due to the vibration-rotation interaction, $\alpha_e J(J+1)$. At very high temperatures, the spreading of the band is sufficiently large to permit the resolution of the individual even J Q branches, ranging from Q(20) to Q(40). The odd Q branches, which have a nuclear spin weighting equal to half of the even numbered branches, are reduced in intensity by about a factor of four and do not stand out. At intermediate temperatures, fewer Q branch transitions are resolvable. For Q branches beyond Q(40), overlap with the v=1→2 band transitions occurs giving rise to two prominent peaks in the "hot" band. At lower spectral resolution, e.g. ∿ 3 cm^{-1}, the fine structure shown in Fig. 4 is lost, but the spectra still exhibit fine temperature sensitivity. Ref.22 contains calculated N_2 CARS spectra at 2.7 cm^{-1} spectral resolution in 100 K increments from 1500 to 2600°K.

The accuracy of CARS N_2 thermometry has been examined in premixed flat flames by comparison with radiation-corrected, coated, fine wire thermocouples (Ref.20,22). The radiation corrections were experimentally calibrated at different flame temperatures by sodium line reversal. In Fig. 5, the CARS spectrum scanned at a resolution of 1 cm^{-1} in a 2110°K flame is displayed. The dotted curve shown in the computer synthesized spectrum at 2150°K which yielded the best agreement with the experimental scan. As seen, fairly good agreement with the experimental trace was obtained. Similar agreement, i.e. ∿ 40 K, was also obtained at lower flame temperatures.

In Refs. 22-24, the capability of CARS for use in highly sooting flames was demonstrated. Although incoherent and coherent interferences from C_2 were encountered in the N_2 CARS bands from a 5320 Å pump laser (Ref. 23), they were for the most part suppressible by appropriate Stokes laser bandwidth selection and use of a polarization filter. The C_2 is produced by the laser vaporization of soot which occurs even for 0 (10^{-8} sec) duration

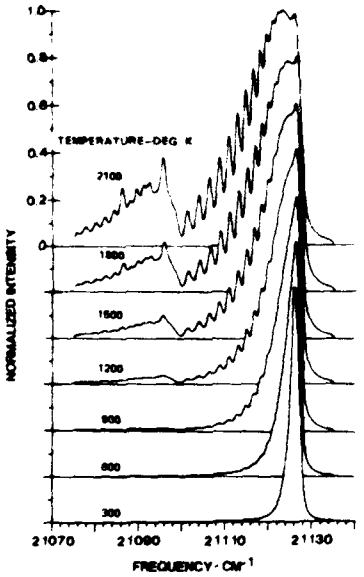

Fig. 4 Computed temperature variation of N_2 CARS spectra in 300K steps from 300°K to 2100°K for 1.0 cm^{-1} slit width and 0.8 cm^{-1} pump linewidth.
Reprinted with permission (Ref. 25)

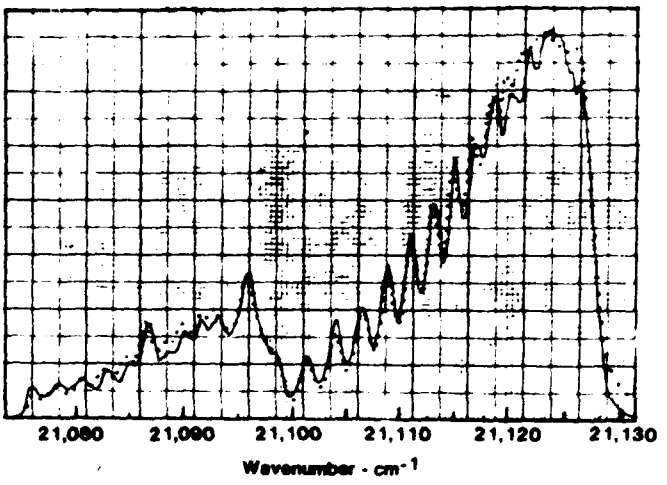

Fig. 5 BOXCARS spectrum of N_2 over 2.5-cm dia. hexagonal flat flame burner operating on CH_4/air at 2110°K and nominal 1 cm^{-1} spectral resolution. Dotted curve is the best computer fit at 2150°K, 0.8 cm^{-1} slit, and 0.1 cm^{-1} Raman linewidths.

Reprinted with permission (Ref. 20)

laser pulses. In Fig. 6 both a single pulse (10^{-8}sec) and an averaged N_2 CARS spectrum from a highly sooting, laminar propane diffusion flame are displayed for a spatial resolution of 0.3 x 1 mm. The spectra are interference free and of high quality. The single pulse CARS spectrum is possible at laser energies an order of magnitude lower than those typically employed for single pulse spontaneous Raman scattering. Furthermore, in this sooting flame situation, laser modulated particulate incandescence (Ref.5) would exceed the Raman signal by several orders of magnitude precluding successful measurements. In a turbulent flame, such single pulse temperature measurements, for a statistically significant sample, would lead to determination of the temperature probability distribution function (pdf) from which fluctuation magnitudes and true time averaged temperatures could be obtained. Data such as those displayed in Fig. 6 have been employed to perform detailed axial and radial temperature surveys in laminar propane diffusion flames (Ref.25). Figure 7 displays the axial variation of temperature in the sooting flame with height above the burner.

Recently, as mentioned earlier, the feasibility of CARS for measurements in practical combustion systems has been demonstrated. In tests at our laboratory (Ref. 9), BOXCARS thermometry was performed in two different, liquid-fueled combustors housed in a 50-cm dia. combustion tunnel. Delicate instrumentation was housed in a control room adjacent to the burner test cell and the CARS signals were piped out employing 20m long, 600 dia. fiber optic guides (Ref.26). In Fig. 8 are shown CARS signatures of N_2 averaged for 10 sec. at two different axial locations in the primary zone of a Jet A fueled swirl burner. At the upstream, x=6cm, location, CARS measurements were made through the fuel spray and the temperature was found to be about 900°K for an overall equivalence ratio of 0.8. At the downstream location, where the flame was visually very luminous, the temperature increased to 1500°K. In Fig. 9 is shown a comparison of a single pulse (10^{-8}sec) and averaged CARS spectrum (10 sec) in the Jet A fueled swirl burner fitted with a refractory back wall to simulate a furnace more closely. The single pulse, although of slightly lower quality, is fairly good and would permit creditable measurements. Measurements were also successfully performed in the exhaust of a JT-12 combustor burning Jet A. In Fig. 10, CARS signatures display the operational temperature variation in the exhaust 13 cm from the can exit plane. These spectra were actually attenuated by an order of magnitude to maintain detector linearity. Single pulse spectra were virtually undiscernable from the averaged data shown in Fig. 10 (Refs.9,10). CARS measurements further downstream in the exhaust were in very good agreement, i.e. 10-50°K, with temperatures determined by aspirating thermocouple probes.

Hydrogen H_2, when abundant enough, is ideal for combustion thermometry because of the simplicity of its spectrum as seen in the computer calculations of Fig. 11 (Ref. 27). The line spectra, labelled Q(J) are components of the vibrational Q branch, v=0→1, ΔJ=0. The

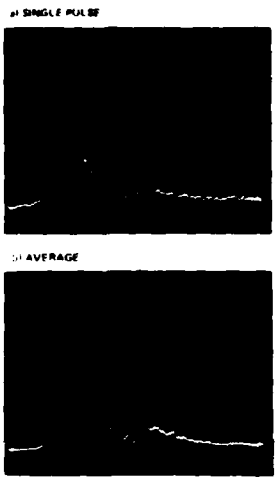

Fig. 6 Comparison of single-pulse (10^{-8} sec) and averaged CARS spectra of flame N_2 recorded on an optical multichannel analyzer. Reprinted with permission (Ref. 25)

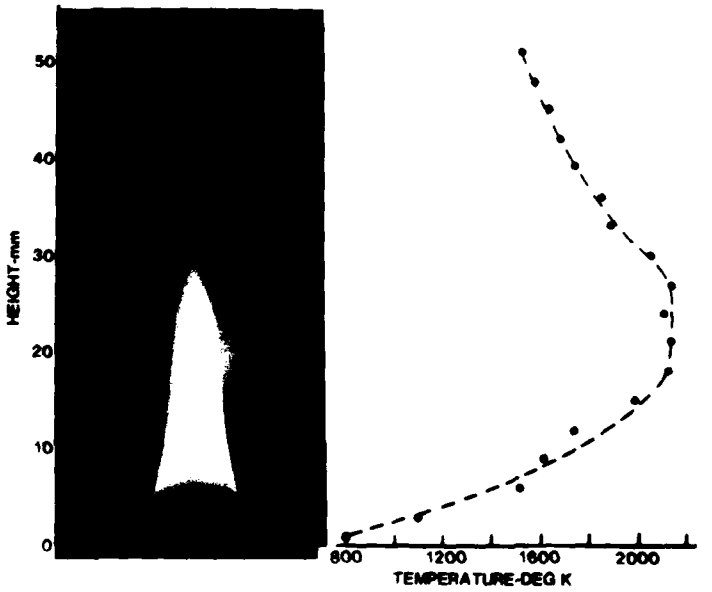

Fig. 7 Axial variation of CARS temperature in a laminar propane diffusion flame. Reprinted with permission (Ref. 25)

Fig. 8 Spatial variation of temperature from averaged CARS spectra of N_2 in swirl burner with Jet A fuel and an air flow of 0.15 lb/sec. The overall equivalence ratio was 0.8. CARS from $\chi_{1212} + \chi_{1122}$.

Reprinted with permission (Ref. 9)

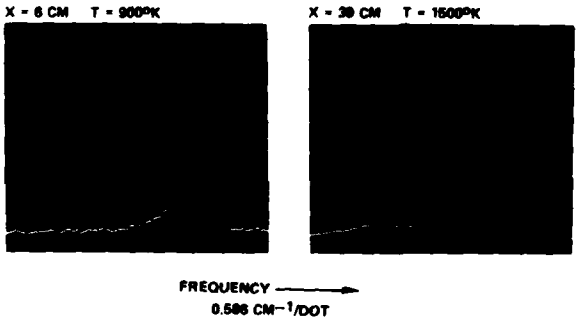

Fig. 9 Comparison of averaged and single (10^{-8} sec) pulse N_2 CARS spectra in swirl burner with refractory back wall fueled with Jet A at an overall equivalence ratio of 0.8. Measurement made on centerline 39 cm downstream of burner exit. Air flow, 0.15 lb/sec. CARS from χ_{1111}.

Reprinted with permission (Ref. 9)

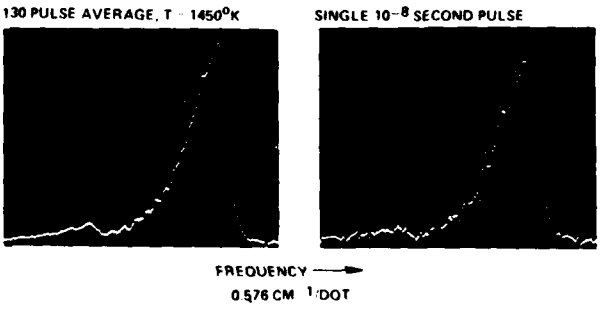

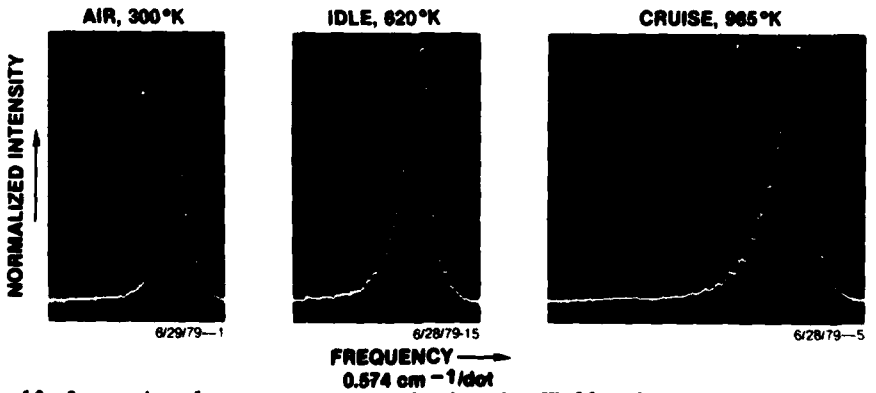

Fig. 10 Operational temperature variation in JT-12 exhaust. Measurement made 13.2 cm downstream of can exit plane. Jet A fuel. Air flow, ~1 lb/sec.

adjacent rotational components are well separated due to the strong vibration-rotation interaction in H_2 making the spectrum particularly simple to calculate. The intensity alteration between even and odd J lines stems from the nuclear spin degeneracy in H_2 in which the odd lines have three times the weighting of the even numbered transitions. In Fig. 12, experimental H_2 BOXCARS signatures are displayed at various locations through a flat H_2-air diffusion flame (Ref. 28). Approximate temperatures are indicated which were deduced from the ratios of the CARS intensities among the Q(1), Q(3) and Q(5) transitions. Agreement among the temperatures deduced from the three intensity ratios was good, i.e. the standard deviation varied from 2 to 8 percent over the range of 900°K to 2100°K. In this regard, better accuracy would probably result from using ratios of integrated line strengths instead of just the peak intensities. The results of temperature profiling the flat diffusion flame are shown in Fig. 13 where temperatures deduced from H_2 and O_2 CARS spectra are compared to measurements with a radiation corrected thermocouple. The CARS spectrum of O_2, omitting spectroscopic details, is qualitatively quite similar to that of N_2. The temperatures agree quite well in cooler regions of the flame. Larger discrepancies occur at the higher temperatures where the concentrations are low and signal to noise ratio is poorer. By spectrally integrating the H_2 spectra and comparing the integrated intensity to that generated simulataneously from a high pressure gas cell in a parallel reference leg, density measurements have been made in the flat diffusion flame. These compare fairly well, i.e. ~ 50%, with H_2 concentrations measured by spontaneous Raman scattering.

Water Vapor Water vapor is the major product of airfed hydrogen combustion and often the dominant product species of hydrocarbon-fueled combustion. Its measurement is an important gauge of the extent of chemical reaction and of overall combustion efficiency. Figure 14a displays the scanned CARS spectrum at $1cm^{-1}$ resolution of H_2O vapor in the post-flame region of an atmospheric pressure, premixed CH_4/air flame at 1675°K (Ref.21). Of particular note is the breadth of the spectrum at flame temperatures. In Fig. 14b is shown the CARS computer code prediction for the experimental conditions. While only the ν_1 symmetrical mode of H_2O is Raman active, the involved rotational energy level structure of this asymmetric rotor gives rise to a complex CARS signature. Each rotational quantum state J possesses 2J + 1 sublevels corresponding to values of the pseudo quantum number τ in the range $-J<\tau<J$. If all possible transitions obeying the Raman selection rules are considered, approximately $(5/4)\ (J+1)^2$ transitions would have to be taken into account for each value of J possessing significant population. Fortunately, only isotropic Q-branch transitions turn out to be important due to the very small depolarization (< 0.06) of the ν_1 mode. Isotropic Q-branch scattering obeys the simplified selection rules $\Delta J=0$, $\Delta\tau=0$. The peaks in the H_2O spectrum arise from spectral overlaps of the τ states belonging to neighboring J states. In particular, the dominant peak at 22433 cm^{-1} results from the near coincidence of the J transitions 9_{-5}, 10_{-10} and 10_{-9} of the fundamental (000-100) with a small contribution from the 4_{-3} of the 010-110 band. The agreement between the experimental and theoretical spectra is fairly good, although the theory does not account for the strength of the strongest peak. This and a few other quantitative discrepancies concerning peak heights may be due to insufficient knowlege of the Raman linewidths. It is also interesting to note that because of the relatively large spontaneous Raman cross section for H_2O, there is little interference from the background nonresonant susceptibility at the 10 percent H_2O concentration level. For a background susceptibility approximately equal to that of N_2, the H_2O CARS spectrum should be relatively interference-free down to the few percent level.

In Fig. 15 the computed temperature sensitivity of the H_2O CARS spectrum is displayed. As seen the predicted spectra exhibit a pronounced sensitivity to temperature as the rotational population distributions shifts and broadens. The possibility of performing temperature measurements from the CARS spectrum of water vapor thus appears very promising. Due to the many rotational transitions involved at flame temperatures, thermometry would most likely be quite accurate.

Carbon Dioxide The other major product of hydrocarbon combustion besides water vapor is of course carbon dioxide. In Fig. 16 is shown the CARS spectrum of CO_2 in the postflame zone of a CO/O_2 flame at 1360°K. The spectrum was recorded in the 1200-1460 cm^{-1} Fermi resonance region and bands arising from vibrational transitions between energy levels v_1, v_2, l, v_3, r are labelled. In this notation v_1, v_2, and v_3 are the quantum numbers respectively of the symmetric, bending and asymmetric stretching modes; l is the angular momentum quantum number associated with the bending mode; r is a number that identifies the level within the group of v_1 + 1 levels which are in Fermi resonance. Also shown as the inset is the region of larger frequency shift in a flame at 1274°K. Unlike the other spectra presented earlier, there is little rotational smearing of the vibrational transitions, even at flame temperatures, due to the extremely small vibration-rotational interaction in CO_2. Some of the levels labelled have been previously identified in spontaneous Raman studies (Ref.29), however, other transitions corresponding to these frequency shifts also should be Raman active. These transitions are indicated by interogatories. In all cases, the contributions of these levels, although smaller than the major transitions, could be significant particularly at flame temperatures. At present, we have not yet modelled the CARS spectrum of CO_2, although it too should be attractive for thermometry.

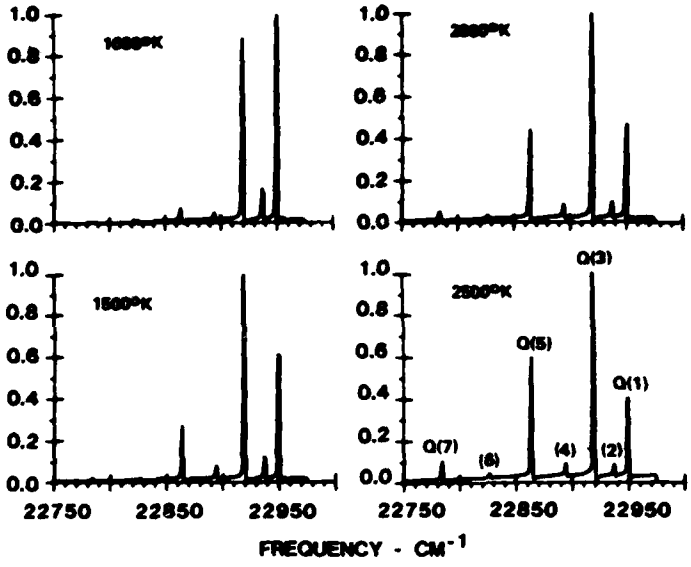

Fig. 11 Computed CARS spectra of hydrogen at 1% concentration. Q branch transitions identified. 1 cm^{-1} slitwidth.

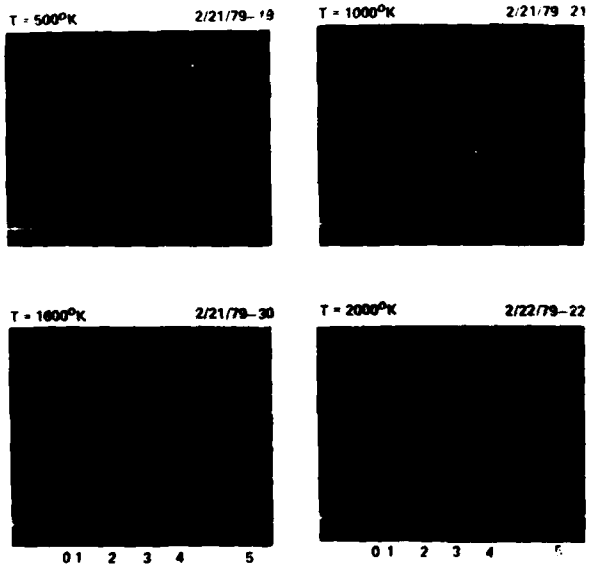

Fig. 12 CARS spectra of H_2 in flat H_2-air diffusion flame at several temperatures determined from Q branch transition ratios. Frequency scale, 0.6 cm^{-1}/dot.

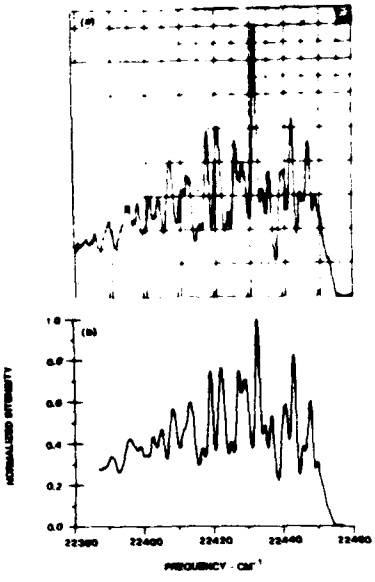

Fig. 14 (a) Experimental CARS spectrum of H_2O in a premixed, methane-air flame at atmospheric pressure. Temperature determined by a radiation-corrected 10% Pt-Pt-Rh thermocouple was 1675K. (b) Computed CARS spectrum of H_2O at 1675K for a pump-laser bandwidth of 0.8 cm^{-1} and a triangular slit function of 1 cm^{-1} FWHM. The gas mixture is assumed to be 10% H_2O and 90% N_2, and the homogeneous linewidths for all transitions are taken to be 0.1 cm^{-1}.

Reprinted with permission (Ref. 21)

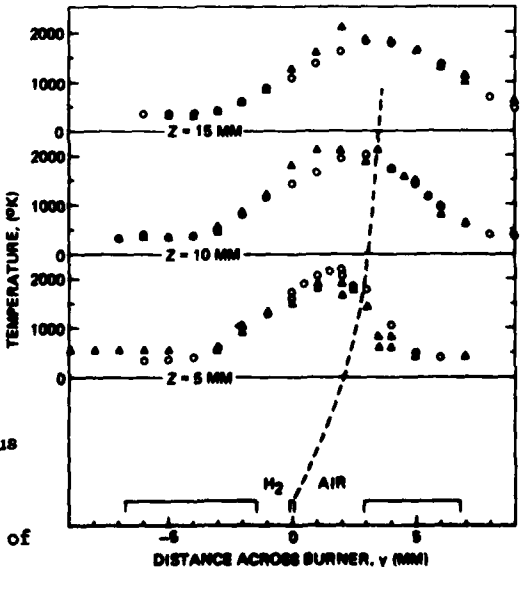

Fig. 13 Temperature measurements in flat H_2-air diffusion flame at various heights above burner exit. Symbols: circles, Pt-Pt 10% Rh thermocouple; open triangles, H_2 CARS; solid triangles, O_2 CARS. Dotted curve locus of maximum temperature.

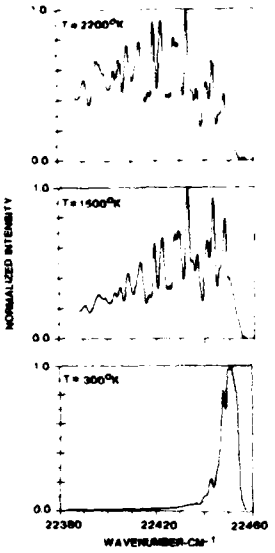

Fig. 15 Calculated effect of temperature on CARS H_2O spectrum.
Reprinted with permission (Ref. 21)

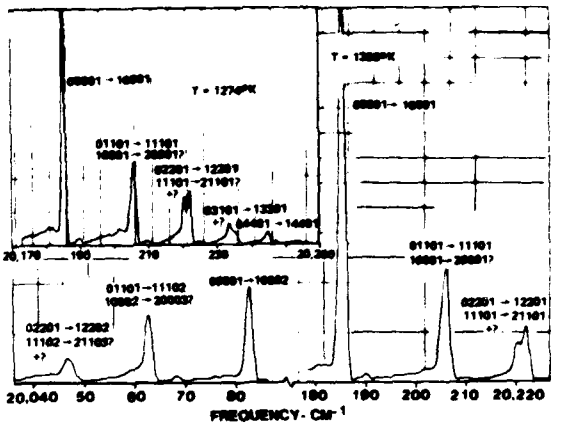

Fig. 16 Experimentally scanned CARS spectra of CO_2 in postflame region of a CO/O_2 flame.

Reprinted with permission (Ref. 35)

4. CONCENTRATION MEASUREMENTS

In general, concentration information derives from the intensity of the spectrally integrated CARS signal (Ref. 30). As alluded to earlier, species detection sensitivity is limited for conventional CARS approaches, i.e. aligned polarizations, due to the presence of the background nonresonant susceptibility. This situation is quite evident in the computer calculations for O_2 at 2000°K shown in Fig. 17. Similar calculations for CO my be found in Refs. 20, 23. The CARS spectrum at 20% concentration rises well out of the nonresonant background, only slightly evident, and the hot band, v=1→2 transitions, is quite prominent. As the concentration decreases, significant modulation of the nonresonant background occurs; however, the depth of the modulation becomes less with decreasing O_2 concentrations. At 1% concentration, the modulation depth is only 10%. To the extent that the nonresonant susceptibility is known or can be approximated, the concentration of a particular species can be obtained from the shape of the CARS spectrum obviating the requirement for absolute intensity measurements. The concentration range appropriate to spectral curve fitting for concentration measurements will vary from molecule to molecule and upon gas composition and temperature. For molecules with closely spaced rotational transitions such as CO, O_2 and N_2 and at flame temperatures, the range is approximately between 0.1 and 20 percent. This approach has been quantitatively verified in the case of CO (Ref. 23). Figure 18 displays examples of low concentration O_2 spectra from a flat H_2-air diffusion flame, which have been employed to map O_2 decay through the flame (Ref.27).

For concentration measurements at lower levels or for measurements over a wide density range, the background nonresonant susceptibility can be cancelled by appropriately orienting the laser field and CARS detection polarizations (Refs.31-33). Unfortunately, this approach leads to a loss in signal intensity by, at least, a factor of sixteen. Number densities are then obtained from the strength of the spectrally integrated signal after appropriate calibration. In Fig. 19, background susceptibility cancellation is demonstrated for CO in a flat CO-air diffusion flame. Folded, i.e. nonplanar, BOXCARS was employed as well as broadband generation and detection. With aligned polarizations, the typically observed modulated type of CARS spectrum was obtained. By orienting the ω_1 pump fields at 60° and the CARS analyzer at 120° to the horizontally polarized ω_2 Stokes field, the nonresonant susceptibility was reduced by over two orders of magnitude and the background free CARS spectrum of CO was observed as seen.

Since virtually all hydrocarbon fuels are Raman active (Ref.34) and often with large cross sections, CARS can in principle be used to monitor fuel mixing and pyrolysis processes. Other than observing CARS spectra of hydrocarbons in flames (Refs. 7,35), little work of a quantitative nature has been reported although this should be a fruitful area for future investigations.

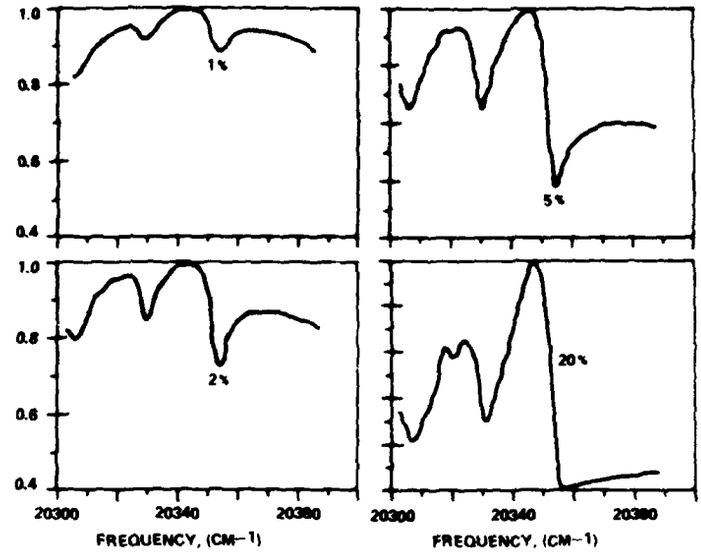

Fig. 17 Computed CARS spectra of oxygen at various concentrations and 2000°K. Slit-width, 2.7 cm^{-1}. χ^{nr} = 1.5(10-8) cm^3/erg.

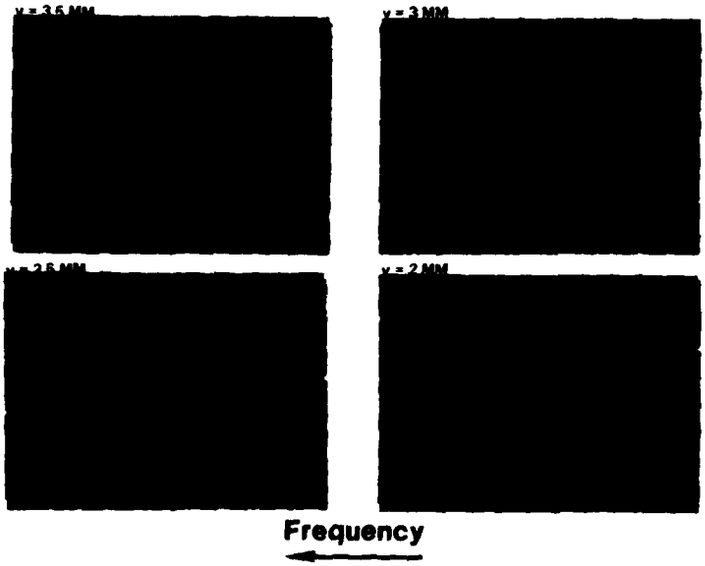

Fig. 18 CARS spectra of O_2 in flat H_2-air diffusion flame at various locations across the flame 5 mm above burner exit. Frequency scale, 0.44 cm^{-1}/dot.

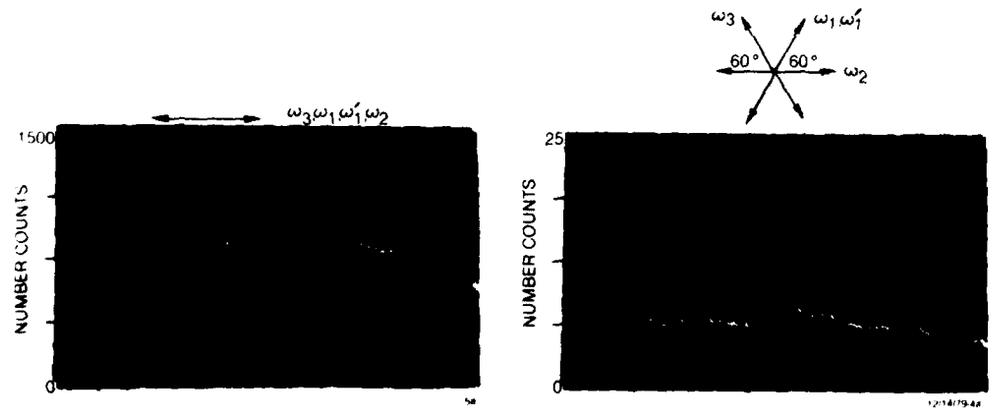

Fig. 19 Nonresonant susceptibility cancellation in CARS by polarization rotation. Folded BOXCARS in a flat CO-air diffusion flame. Polarizations oriented as shown.

5. REFERENCES

1. A. C. Eckbreth, P. A. Bonczyk and J. F. Verdieck: Laser Raman and Fluorescence Techniques for Practical Combustion Diagnostics. Appl Spect Rev., Vol 13, pp 15-164, 1978.

2. M. Lapp and C. M. Penney: Laser Raman Gas Diangostics. Plenum Press, New York, 1974

3. S. Lederman: The Use of Laser Raman Diagnostics in Flow Fields and Combustion Prog Energy Comb. Sci., Vol. 3, pp. 1-34, 1977.

4. D. P. Aeschliman and R. E. Setchell: Fluorescence Limitations to Combustion Studies Using Raman Spectroscopy. Appl. Spect., Vol. 29, pp. 426-429, 1975.

5. A. C. Eckbreth: Effects of Laser-Modulated Particulate Incandescence on Raman Scattering Diagnostics. J. Appl. Phys., Vol. 48, pp. 4473-4479, 1977.

6. G. L. Switzer, W. M. Roquemore, R. P. Bradley, P. W. Schreiber, and W. B. Roh: CARS Measurements in a Bluff-Body Stabilized Diffusion Flame. Appl. Opt., Vol. 18, pp. 2343-2345, 1979.

7. I. A. Stenhouse, D. R. Williams, J. B. Cole and M. D. Swords: CARS in an Internal Combustion Engine. Appl. Opt., Vol.18, pp. 3819-3825, 1979.

8. B. Attal, M. Pealat and J. P. Taran: CARS Diagnostics of Combustion. AIAA Paper No. 80-0282, presented at the 18th Aerospace Sciences Meeting, Pasadena, CA., 1980.

9. A. C. Eckbreth: CARS Thermometry in Practical Combustors. Combust. Flame, accepted for publication, 1980. Also see Laser Focus, Vol. 15, pp. 32-36, 1979.

10. A. C. Eckbreth: Spatially Precise Laser Diagnostics for Practical Combustor Probing. in D. R. Crosley, Ed.: Laser Probes of Combustion Chemistry, ACS Symposium Series, 1980.

11. J. W. Nibler, W. M. Shaub, J. R. McDonald, and A. B. Harvey: Coherent Anti-Stokes Raman Spectroscopy.in J. R. Durig, Ed.: Vibrational Spectra and Structure. Vol. 6, Elsevier, Amsterdam, 1977.

12. S. Druet and J. P. Taran: Coherent Anti-Stokes Raman Spectroscopy.in C. B. Moore, Ed: Chemical and Biological Applications of Lasers. Academic Press, New York, 1979.

13. J. W. Nibler and G. V. Knighten: Coherent Anti-Stokes Raman Spectroscopy. in A. Weber, Ed: Raman Spectroscopy of Gases and Liquids. Springer-Verlag, Berlin, 1979.

14. A. C. Eckbreth and P. W. Schreiber: Coherent Anti-Stokes Raman Spectroscopy - Application to Combustion and Gas Phase Diagnostics. in A. B. Harvey, Ed.: Chemical Applications of Nonlinear Raman Spectroscopy. Academic Press, New York, 1980.

15. W. B. Roh, P. W. Schreiber and J.P.E. Taran: Single-Pulse Coherent Anti-Stokes Raman Scattering. Appl. Phys. Letts., Vol. 29, pp. 174-176, 1976.

16. A. C. Eckbreth: BOXCARS: Cross-Beam Phase-Matched CARS Generation in Gases. Appl. Phys. Lett., Vol. 32, pp. 421-423, 1978.

17. G. Laufer and R. B. Miles: Angularly Resolved Coherent Raman Scattering. Opt. Comm., Vol. 28, pp. 250-254, 1979.

18. A. Compaan and S. Chandra: Coherent Anti-Stokes Raman Scattering with Counterpropagating Laser Beams. Opt. Lett., Vol. 4, pp. 170-172, 1979.

19. K. A. Marko and L. Rimai: Space-and Time-Resolved Coherent Anti-Stokes Raman Spectroscopy for Combustion Diagnostics. Opt. Lett., Vol. 4, pp. 211-213, 1979.

20. R. J. Hall: CARS Spectra of Combustion Gases. Combust. Flame, Vol. 35, pp. 47-60, 1979.

21. R. J. Hall, J. A. Shirley and A. C. Eckbreth: Coherent Anti-Stokes Raman Spectroscopy, Spectra of Water Vapor in Flames. Opt. Lett., Vol. 4, pp. 87-89, 1979.

22. A. C. Eckbreth and R. J. Hall: CARS Diagnostic Investigations of Flames. pp. 943-972 in Vol. 2 of Proceedings of the 10th Materials Research Symposium, NBS Special Publication 561, 1979.

23. A. C. Eckbreth: CARS Investigations in Flames. pp. 975-983 in Proceedings of the XVIIth (International) Symposium on Combustion, The Combustion Institute, Pittsburgh, PA., 1979.

24. I. R. Beattie, J. D. Black and T. R. Gilson: An Approach to Rotational Temperatures of Nitrogen in Diffusion Flames Using Coherent Anti-Stokes Raman Scattering. Combust Flame, Vol. 33, pp. 101-102, 1978.

25. A. C. Eckbreth and R. J. Hall: CARS Thermometry in a Sooting Flame. Combust Flame, Vol. 36, pp. 87-98, 1979.

26. A. C. Eckbreth: Remote Detection of CARS Employing Fiber Optic Guides. Appl. Opt., Vol. 18, pp. 3215-3216, 1979.

27. J. A. Shirley, A. C. Eckbreth and R J. Hall: Investigation of the Feasibility of CARS Measurements in Scramjet Combustion. Proceedings of the 16th JANNAF Combustion Meeting, Moneterey, CA., 1979.

28. H. G. Wolfhard and W. G. Parker: A New Technique for the Spectroscopic Examination of Flames at Normal Pressures. Proc. Phys. Soc. A, Vol. 62, pp.722-730, 1949.

29. M. Lapp and C. M. Penney: Raman Measurements on Flames. in R.J.H. Clark and R. E. Hester, Eds.: Advances in Infrared and Raman Spectroscopy, Vol. 3, Heyden, London, 1977.

30. W. B. Roh and P. W. Schreiber: Pressure Dependence of Integrated CARS Power. Appl Opt., Vol. 17, pp. 1418-1424, 1978.

31. J. J. Song, G. L. Eesley and M. D. Levenson: Background Suppression in Coherent Raman Spectroscopy. Appl. Phys. Letts., Vol. 29, pp. 567-569, 1976.

32. L. A. Rahn, L. J. Zych and P. L. Mattern: Background-Free CARS Studies of Carbon Monoxide in a Flame. Opt. Comm., Vol. 30, pp. 249-253,1979.

33. J. L. Oudar, R. W. Smith and Y. R. Shen: Polarization-Sensitive Coherent Anti-Stokes Raman Spectroscopy. Appl. Phys. Letts., Vol. 34, pp.758-760, 1979.

34. D. A. Stephenson: Raman Cross Sections of Selected Hydrocarbons and Freons. J. Quant. Spect. Rad. Trans., Vol. 14, pp. 1291-1301, 1974.

35. A. C. Eckbreth, R. J. Hall and J. A. Shirley: Investigation of Coherent Anti-Stokes Raman Spectroscopy (CARS) for Combustion Diagnostics. AIAA Paper No. 79-0083, 1979.

6. ACKNOWLEDGEMENTS

Separate portions of the research described herein were sponsored in part by the EPA, NASA Langley and Project SQUID. The authors wish to express their appreciation to Drs. C. J. Ultee and J. F. Verdieck for many stimulating discussions and to Mr. Edward Dzwonkowski for his very capable technical assistance.

DISCUSSION

V.Wittmer, Ge

Are you able to measure with the presented technique (CARS) fluctuating quantities (for example, temperature, concentration)?

Author's Reply

For most combustion applications at moderate pressures, for example, one to forty atmospheres, high intensity laser sources are required which operate typically at ten to twenty pulses per second. Thus we are restricted to statistically sampling the turbulence, that is, measuring probability density functions. At very high pressures, greater than 10^3 atmospheres typical of some ballistic propellant applications, it may be possible to use sources with pulse repetition rates of the order of 10^4 Hz permitting near real time resolution of some events.

M.Pealat, Fr

Has the H_2 spectrum been recorded by multiplex CARS and, in this case, how can you obtain a dye laser spectrum broad enough to extend from the Q (0) and the Q (4) lines of H_2?

Author's Reply

Yes, the H_2 spectrum was obtained using a broad-band dye laser. To obtain efficient laser operation at about 6800 Å required to excite H_2, we use a binary dye mixture to increase the absorption of the frequency-doubled neodymium laser. In general, binary mixtures lead to broader Stokes bandwidths. In the H_2 spectrum, we take into account the shape of the Stokes laser in the computer calculations. Experimentally, the Q (1) to Q (5) lines reside within the full width at half height of the dye spectrum.

M.Lapp, US

The agreement of your CARS experimental spectra with theory appears to be quite good. Concerning the strong peak seen in the H_2O vapour contour, R.L. St. Peters (G.E.C. Research and Development, Schenectady) has completed a theoretical study recently which shows agreement with that peak strength. This work was completed under an AFAPL contract and will be published soon.

Author's Reply

We intend to pursue a more thorough experimental validation of our H_2O computer code from 400 K to 2000 K later this year. We would clearly be interested in receiving a copy of your report when it is available.

K.Kohse-Hoinghaus, Ge

I should like to ask two questions.

(1) Can you say something about the chance of measuring hydrocarbons with CARS?

(2) Could you please comment on the feasibility of other non-linear optical techniques for temperature and concentration measurements in combustion processes?

Author's Reply

(1) Most hydrocarbons have fairly strong Raman cross sections and potentially appear amenable to diagnostics by CARS. Furthermore, the characteristic C-H vibrational frequencies are well enough separated for various hydrocarbons for them to be separately monitored. Hence one may be able to study fuel pyrolysis using CARS. CARS may also be useful as a total hydrocarbon monitor by spectrally integrating over the entire C-H region. However, considerable work is required in this area before these potentialities can be realised.

(2) Besides CARS I think stimulated Raman gain spectroscopy (SRG) is the only other viable alternative for combustion diagnostics. At low pressures, about one to twenty atmospheres, the technique is restricted to laminar flames primarily because the gains are too low for the technique to be multiplexed, that is, single shot data capture. At high pressures, the technique looks quite attractive because the gains are large enough for "instantaneous" measurements. In fact it may be preferable to CARS at high pressures where pump laser intensities are limited, not because of optical breakdown considerations but to avoid Raman gain perturbation of the Stokes field. In any event, one uses the same laser and detection equipment for multiplex CARS or SRG and hence, can use whichever technique is preferable in a given pressure regime.

D.A.Greenhalgh, UK

(1) What level of intensification do you use on your multi-channel detector?

(2) How do you see photon statistics affecting the accuracy of a 'single shot' measurement in a practical combustor?

Comment: Raman gain spectroscopy (RGS) has marginally better performance in terms of window attenuation and may be better for concentration measurements because RGS has a linear dependence and not a squared dependence on concentration.

Author's Reply

(1) We have always used an SIT tube, a vidicon with a single intensifier stage. One advantage of performing CARS with a frequency-doubled ND:YAG laser (5320 Å) is that there is virtually no difference in sensitivity between a singly (SIT) and doubly intensified (ISIT) vidicon.

(2) Yes, in the single shot spectrum form the swirl burner that I showed there were about fifty counts in the hot band peak, in a narrow spectral interval. This leads to a peak height ratio uncertainty of about ± 14% or a temperature uncertainty of about ± 100 K. In a situation like this it would be preferable to contour fit the entire spectrum instead of using simple algorithms to extract temperature. In essence, then one is spectrally averaging to some degree and this would improve the accuracy of a single shot measurement. The goal of single shot measurements is of course to repeat the measurement a statistically significant number of times to assemble the probability distribution function. In assembling the PDF, photon statistics are in effect averaged out and hence I believe the PDF can be obtained with an accuracy better than that of the individual temperature measurements.

Comment response: Raman gain spectroscopy (SRG) may have a different density dependence than CARS, but the problem with density measurements in a single shot is the pulse to pulse power fluctuations together with shot to shot laser steering instabilities. CARS of course scales as $I_1^2 I_2^2$ and depends quite sensitively on alignment. The gain in SRG varies as the exponential of the pump intensity, I_1, and, for high spatial resolution crossed beam approaches, would also depend sensitively on alignment. Experimentally I don't think it would be much simpler. The density dependencies of the various approaches I believe is primarily a data reduction problem.

W.Stricker, Ge

Why do you pump your dye laser slightly off axis and not transversely which is more common? Has it any influence on the performance of a CARS experiment?

Author's Reply

I prefer to pump the dye laser slightly off axis whenever possible because I believe we obtain better mode (beam) quality from the laser and hence higher Stokes laser intensities in the wave mixing zone. Off-axis pumping is able to provide high oscillation efficiencies in most dyes in the 6000 to 7000 Å region.

G.Winterfeld, Ge

Would it be possible to develop the CARS technique into a single ended apparatus, so that temperature measurements in turbomachines would be possible?

Author's Reply

We've given a great deal of thought to that problem. We really do not think that in terms of the physics there is really any way you can generate a signal in the backward direction. The one point I should make is that in the practical tunnel work that I did, when the signal emerged from the combustor we focused it into a fibre optic and we transmitted it to our spectrograph which was remotely located. We foresee, for example, in annular combustor cans where you might go through air bleed holes in the combustor, to have a very small receiver placed inside the annular can, with fibre optic transmission of the CARS signal to remotely located instrumentation. In the near term that would certainly be the approach we would look at.

THE STUDY OF TURBULENT DIFFUSION FLAMES:
MODELING NEEDS AND EXPERIMENTAL LIGHT SCATTERING CAPABILITIES

M. Lapp and R.M.C. So

General Electric Company
Corporate Research & Development
P.O. Box 8
Schenectady, New York 12301 U.S.A.

SUMMARY

A comparison is given here of the capabilities of advanced light-scattering measurement techniques with the needs of new combustion modeling approaches. Such comparisons are useful in working toward the coupled goals of developing and verifying new flame models and providing guidance for the development of experimental probe methods along the most productive paths. The types of experimental data available a e compared with those often required in combustion modeling, permitting one to asses the present and potential contributions of the techniques. This assessment is illustrated by consideration of some current analytical results based upon Pratt's coalescence/dispersion model, and by some recent experimental results from Raman scattering diagnostics of turbulent diffusion flames. The experimental data shown include simultaneously-determined values of temperature and major species densities, and are presented in the form of pdf's and density-temperature correlations.

1. INTRODUCTION

The need to better utilize our limited fossil fuel resources has renewed tremendous interest in the study of combustion phenomena [1]. Such interest centers on both the experimental understanding of the combustion processes and the development of predictive methods to calculate the key flow field and thermodynamic variables. The driving force for this interest arises from the necessity to cope with diverse ("alternate") fuels possessing variable ("wide spec") properties, requirements for increased efficiency and greater operational safety along with improved compatibility with engineering materials and with the environment, and improved cost- and time-saving features in the design, construction, and testing of new combustion devices.

In order to address the technological goals faced by combustor designers, models must be developed which provide not only design and testing aids, but which also are directed toward producing new insight into the basic behavior of high temperature chemically reacting flows that can be turbulent and out of chemical or thermal equilibrium. Turbulence models have been successfully devised for flows with constant fluid properties [2,3,4]; these have provided the foundation for extension to flows with variable density and combustion. However, the ability to measure and calculate accurately the fields of velocity, major species concentration, temperature, and pollutant concentration in practical systems, such as gas turbine combustors, internal combustion engines, industrial furnaces, etc., remains limited.

On the experimental side, new data of importance are being generated by advanced optical techniques only recently developed for flame diagnostics [5]. These techniques allow, for the first time, the simultaneous measurement of instantaneous values of the flow and thermodynamic variables in a combustion environment without either perturbing the environment or giving rise to discomforting questions concerning probe survivability. In many cases, several different optical methods can be coupled together with the same general optical access, to provide a more nearly complete picture of the flame system, and, of course, these can be coupled with other probes (such as sampling devices, optical imaging techniques, plasma probes, etc.) to provide even more information. These optical methods have, however, clear limitations. The most important of these relate to the requirements imposed for optical access and the difficulty of obtaining high quality data from an environment which can be strongly luminous and particle-laden. That these problems have been overcome in some circumstances is encouraging for the future application of optical measurement methods to practical test-bed combustors [6]. Of equal importance is the fact that, in bench-scale combustors carefully chosen to provide tests of important flame properties (such as pollutant formation) under well-controlled laboratory conditions, data of high quality can be obtained by these new techniques that have the promise to provide basic information needed by theoreticians in order to make fundamental improvements in variable density, chemically-reacting flow models [5].

On the theoretical side, development of calculation procedures that can handle time-dependent flows and three-dimensional geometries is a significant complication, but does not present insurmountable problems. The major obstacle for combustion modeling, however, is the difficulty of treating finite rate chemistry, i.e., the problem of evaluating mean formation rates for important species [7]. In the next section, we will outline the needs and capabilities of turbulent diffusion flame modeling, omitting time-dependent and three-dimensional effects, but focusing on the key problem of evaluating mean formation rates. Following this, we will mention various new optical probes suitable for flame diagnostics, and then specialize the discussion to a consideration of vibrational Raman scattering methods which, combined with laser velocimetry, have been developed as an integrated probe system for determining instantaneous values of flame temperature, major species density, and flow velocity. Finally, we will compare the

species density, and flow velocity. Finally, we will compare the needs of modelers with recently-developed capabilities in optical measurement techniques, and assess the present state-of-the-art.

2. MODELING CAPABILITIES AND NEEDS

In turbulent reactive flow modeling, the mean species conservation equations must be solved simultaneously with the mean flow equations. Since the mean species conservation equations have an additional term associated with the mean formation rates of the species due to chemical reactions, their solutions require a knowledge of the mean formation rates. The evaluation of these rates represents the main problem in combustion modeling. This can be seen easily by considering a simple irreversible reaction such as

$$A + B \xrightarrow{k_f} C. \tag{1}$$

The instantaneous formation rate of C (combustion product) may be represented by an equation of the form

$$R_C = k_f \rho^2 m_A m_B, \tag{2}$$

where m_i is the instantaneous mass fraction of species i, ρ is the instantaneous mixture mass density expressed by the perfect gas law, and k_f is the modified Arrhenius forward rate constant defined as

$$k_f = \text{const} \times T^N \exp(-T_a/T). \tag{3}$$

In Eq. (3), T is the instantaneous temperature, T_a is the activation temperature, and N is a constant. If the reaction occurs in a constant mean pressure environment and the density fluctuation caused by turbulent pressure fluctuations is negligible compared to density variation due to the temperature change caused by chemical reaction, then with the help of the perfect gas law, R_C can be written as

$$R_C = \text{const} \times T^{N-2} m_A m_B \exp(-T_a/T). \tag{4}$$

Thus, R_C is a strongly nonlinear function of T, and can, in general, be nonlinear in mass fractions as well. It follows that the mean value of R_C, denoted by $\bar{R}_C$, is therefore not equal to the value of R_C that would be evaluated based on the mean values of T, m_A, and m_B [8,9]. In more detail, if $\bar{R}_C$ is calculated by expanding Eq. (4) according to Reynolds decomposition of an instantaneous variable (where a prime will be used to denote the fluctuating part of that variable) and by taking the time-average of the expansion [8,9], an infinite series results for large activation energies (as would be the case for the major flame reactions), the leading term of which is given by Eq. (4) with the instantaneous variables replaced by their time-averaged counterparts. The remaining infinite series of terms contains products of the form of $\overline{T'm_A'}$, $\overline{m_A'm_B'}$, $\overline{T'^2}$, etc. For $\bar{R}_C$ to be evaluated correctly, an infinite number of these moments containing the variables T, m_A, and m_B would have to be determined.

The practice in the past is to determine $\bar{R}_C$ by considering either the first or first two terms of the expansion. However, this approach can lead to erroneous mean formation rates for some reactions [8,9]. Borghi [8] estimated that, for a wide variety of reactions and chemical species, $\bar{R}_C$ can be approximated by considering a finite number of terms in the expansion (typically, seven terms involving eight third-order and lower moments of T, m_A, and m_B). The various terms in the expansion, other than the first, can be determined by solving simultaneously their governing mean transport equations, which can be derived through turbulence modeling. As a result, combustion modeling, even of simple flow systems, is a much more formidable task and much less accurate than the modeling of nonreactive turbulent flows.

2.1 Current Approach to Combustion Modeling. The evaluation of mean formation rates is so complex that current models are applicable only to systems which can be described either with the assumption of chemical equilibrium (very fast reaction rates) or in terms of one or two global finite rate reactions. Since most of the reactions associated with the high temperature oxidation of hydrocarbon and hydrogen fuels have very short time scales compared with those characteristic of the turbulence field, the assumption of fast chemistry is suitable for the study of these reactions. (Reaction time scales for these fuels are perhaps of the order of 0.1 ms, while the turbulent time scale is given by the Kolmogorov microscale which, through dimensional arguments, is found to be proportional to the square root of the kinematic viscosity divided by the dissipation rate [10]. For thin shear flows, the Kolmogorov microscale is estimated to be of the order of 10 ms.) On the other hand, the estimation of unburnt fuel, formation of pollutants such as NO_x and CO, and the study of such phenomena as ignition and blowout require consideration of finite rate reactions.

First, the current approach will be briefly examined for its capabilities and limitations. This approach can only be applied to combustion systems where fuel and oxidant are injected separately. Under the assumption of fast chemistry, the equilibrium composition, temperature, and mixture density can be determined once the elemental mass fractions, enthalpy, and pressure of the system are known. In this case, there is no need to evaluate the mean formation rates of species and the major difficulty in combustion modeling is removed. Further assumptions of negligible heat loss to the surroundings and of species and heat diffusion proceeding at the same rate (i.e., unity Lewis number) allow the thermodynamic state of the gas to be expressed as a function of a single conserved scalar variable. A typical choice for the conserved scalar is the mixture fraction, f, defined here as the mass fraction of fuel atoms in the fuel/oxidant mixture. This parameter can be related to the equivalence ratio, ϕ, by

$$f = \frac{\dot{}}{\dot{}+r} \,, \qquad (5)$$

where r is the stoichiometric mass ratio of oxidant to fuel. The species conservation equations are then reduced to an equation for f and the additional source term vanishes because f is a conserved scalar.

The current approach involves solving the mean flow equations with the mean conservation equation for f. Closure of the mean governing equations is usually accomplished through the use of the two-equation turbulence model of Jones and Launder [11] and the assumption of a turbulent Schmidt number (ratio of momentum to mass diffusivities) [12,13]. This model requires the simultaneous solution of two additional equations that govern the transport of mean kinetic energy and its dissipation rate. Through dimensional arguments, the eddy diffusivity of momentum that appears in the mean flow equations can be related to the mean turbulent kinetic energy and its dissipation rate. Hence, the equation set is closed. In order to account for the fluctuations (with time) of f, a two-parameter probability density function (pdf) for f is often assumed. The two parameters in the pdf are then determined in terms of $\bar{f}$ and its variance $\overline{f'^2}$. An equation for $\overline{f'^2}$ can be derived from the conservation equation for f and suitable closure assumptions [14]. Once the pdf is determined, the mean value and variance of other scalars, $\phi(f)$, can be determined from

$$\bar{\phi} = \int_0^1 \phi(f)\, P(f)\, df \qquad (6)$$

and

$$\overline{\phi'^2} = \int_0^1 \phi^2(f)\, P(f)\, df - \bar{\phi}^2, \qquad (7)$$

where the pdf, P(f), must satisfy the conditions

$$\left.\begin{aligned} P(f) &> 0 \qquad 0 \le f \le 1, \\ P(f) &= 0 \qquad f < 0,\ f > 1. \end{aligned}\right\} \qquad (8)$$

Various shapes for P(f) (such as rectangular waves, clipped Gaussians, and the β - pdf) have been proposed and tried by a number of investigators [12-16] and the calculated results compared with the measurements of an H_2/air jet diffusion flame [17]. Jones [16] found that the β - pdf gave the best overall comparison.

The extent to which the current approach can calculate the aerodynamic flow field depends on the turbulent closure assumptions. If the well-known "two-equation" model [11] is used, the flow properties that can be calculated include the mean velocity field, the mean turbulent kinetic energy, and its dissipation rate. By adopting more advanced concepts, such as a Reynolds stress model [2], the mean Reynolds stress field can be determined. However, none of these models can assess the importance of such mean quantities as the one-point correlations between the velocity and mixture density field. These quantities are of great significance if the question of extending the constant density turbulence models to reactive flow modeling is to be answered. Assumptions about modeling these quantities can be avoided if, instead of using Reynolds averaging, the density-weighted values (i.e., Favre averaging [18]) are used to derive the governing equations. However, since some optical techniques (such as Raman scattering) that are capable of providing detailed information for these flames produce data in the form of unweighted quantities, a comparison of measured and calculated values requires a knowledge of the density and velocity correlations. Therefore, if these latter quantities can be measured, some basic questions concerning the extension of the constant density turbulence models to reactive flow modeling [7,8,12,13,16] can be answered.

Besides the drawbacks discussed above, the main weakness of the current approach lies in the assumptions used to model the chemical reactions. The model cannot account for the effects of complex finite rate chemistry. Its ability to handle more than one reaction is limited and it cannot be used to model reactive flows with fuel and oxidant premixed.

In practical combustion systems, reactions usually occur at what may be considered finite rates and in multiple steps; this is likely the case for such combustion phenomena as formation of NO_x [19] and CO, unburnt hydrocarbons, ignition, and blowout. Since a prime reason for developing the ability to calculate the properties of flames is to help in the design of practical combustion systems, a model is required in which the chemical reactions are evaluated realistically. Furthermore, it is highly desirable that the model be able to treat premixed as well as non-premixed fuel/oxidant flows in order to be applicable to new combustor designs.

2.2 Alternative Approach to Combustion Modeling. An advanced approach to model combustion correctly can be formulated by applying the coalescence/dispersion model of Pratt [9] for continuous combustion in jet-stirred reactors to the calculation of turbulent reactive flows. The idea behind this approach is to use a "hybrid" scheme to calculate these flows. First, the aerodynamic flow field is determined by solving the mean flow equations closed by an appropriate turbulence model (such as the well-known "two-equation" [11] or Reynolds stress [2] model). Then the coalescence/dispersion model of Pratt is used to determine the thermodynamic properties of the reactive flow field. The solution of the mean flow equations is well documented [11-16]; therefore, we proceed to a brief description of Pratt's model.

The coalescence/dispersion model is based on Curl's equation [20] for binary mixing. The solution of Curl's equation for one-dimensional flow is accomplished through the use of a "Monte Carlo" simulation technique. With suitable assumptions for the flow and the coalescence/dispersion (or mixing) frequency, β_t, the simulation is carried out as follows. The reactor is divided into K cells. If there are N discrete fluid particles in

the reactor, then the number of fluid particles in each cell is N/K. The fluid particle feed rate into each cell is $\dot{m}$ N/m where $\dot{m}$ is the mass flow rate through the reactor and m is the total mass in the reactor at any moment. For each cell j (j=1, K), a discrete number of particle pairs are selected randomly for mixing so that all conserved properties of the pair, such as enthalpy, mass concentration of the species, etc., are averaged. After mixing, each particle pair assumes the averaged properties thus obtained. The particle residence time in each cell is $\Delta t = t_s/K$, where t_s is the mean residence time in the reactor. This, together with τ_t, determines the number of binary encounters in each cell; namely, $\tau_t/\Delta t(N/K)$. Finally, the particles in the cell are allowed to undergo adiabatic batch reaction, using either a chemical equilibrium assumption or finite rate reaction, as desired. The whole procedure is repeated until the entire process has become time-stationary. Mean values, as well as the second and higher moments of fluctuations of the thermodynamic state of the gas can be obtained from instantaneous ensemble-averaging over the reactor population.

This concept of simulating mixing and thereby allowing chemical reactions to be evaluated numerically can be extended to calculate reactive flows provided a correct ensemble of scalar elements (such as mixture fraction, elemental mass fractions, enthalpy, etc.) can be created at every spatial location in the flow field. By an "ensemble of scalar elements" is meant an ensemble, the elements of which have only scalar properties. This means that, if a finite difference scheme is used to solve the mean flow equations, a correct ensemble of scalar elements has to be created for each finite difference cell. Since the mean transport equation for the scalar is not solved simultaneously with the mean flow equations, the creation of a correct ensemble in any finite difference cell should take into account the effects of the various transport processes; namely, entrainment, convection, diffusion, and local mixing. Once the correct ensemble has been created, Pratt's coalescence/dispersion model can be used to calculate the scalar properties within the ensemble. Since there are no added complexities in the formulation when finite rate reactions and multiple reaction sets are considered, the ability of the present approach to handle complex reactive flows is limited only by the availability and reliability of kinetic mechanism and rate data. The question of mean formation rates is bypassed, because the instantaneous formation rate is calculated and the mean formation rate can be evaluated by simply ensemble-averaging over the cell population. The pdf's of the various thermodynamic properties are also available. Therefore, the moments and cross-moments of the scalars can be calculated and compared with measurements.

From this discussion, it is clear that the "hydrid" scheme can be made to work if a scalar transport model is formulated to create an ensemble in a finite difference cell such that the transport processes are fully accounted for. Such a model for two-dimensional/axisymmetric turbulent flows has been formulated and validated with measurements from non-reactive two-dimensional mixing layers and round jets [21,22]. Good agreement with measured data was obtained. The extension of the approach to reactive flow calculation is not difficult if fast chemistry is assumed. If finite rate chemistry is assumed, the chemical rate equations have to be solved also. Therefore, use of this approach is not formidable if the reaction mechanisms and rates are known and if an efficient computational algorithm capable of solving these highly non-linear rate equations is available.

The approach outlined above is similar to an approach in which a transport equation for the pdf, P(f), is solved together with the mean flow equations. The advantage of solving an equation for P(f) rather than assuming a shape for P(f) is obvious. Besides greatly simplifying the calculations, it also eliminates the unpleasant necessity of having to determine the shape of the pdf by only a finite number of moments of f (usually two, or at most three). The derivation and closure of the transport equation for P(f) are given by Janicka et al. [23] and Borghi [24]. Solutions of this equation together with the mean flow equations have been obtained by Janicka et al. [25], Janicka and Kollmann [26], and Pope [27]. Results obtained by Janicka et al. [24] with the assumption of chemical equilibrium for an H_2/air flame compared favorably with the measurements of Kent and Bilger [13], as did results for heated jets [26]. Since Janicka and his coworkers solved the equation for P(f) using a finite difference scheme, its extension to finite rate reactions is not immediately obvious. Pope [27] proposed to solve the equation for P(f) using a "Monte Carlo" simulation scheme and obtained results for the pdf comparable to those obtained by So et al. [22]. Since then, Pope has also demonstrated that his approach can be used to calculate reactive flows with finite rate reactions exactly.

From the above discussion, it follows that the thermodynamic properties can be calculated without approximation in a combustion flow (to within the limit of the input chemistry information), as well as the single and joint pdf's of these properties. Therefore, a combustion experiment with the thermodynamic properties correctly measured will provide the right data for the verification of these calculation models.

Although the advanced approaches are very powerful in calculating the thermodynamic properties, the accuracy of these results depend to a large extent on the accuracy with which the turbulence models can help to resolve the velocity and turbulence field properties [22,27]. In this sense, these new approaches suffer the same basic weakness as the current approach, i.e., the key to correct combustion modeling lies in the turbulence models for variable density flow and not in the chemistry models. It is precisely in this area that experimental measurements, especially innovative measurements of the velocity and thermodynamic properties of the combustion flow, can help, both in the understanding of the physics of combustion and in developing correct modeling procedures for the combustion flow field. Further discussion is given in Section 4.

3. LIGHT SCATTERING MEASUREMENT TECHNIQUES

We have just discussed the need for improved temperature, concentration, and velocity fluctuation data in order to help unravel key questions in turbulent flame modeling; we discuss now the use of new light scattering probes to provide these data.

Laser light-scattering measurement techniques are now at the stage where they can be employed to determine many of the important properties of combustion flows. In particular, the use of Raman scattering methods can provide data leading to temperature and major species densities for many flames with excellent space and time resolution -- and can, in some instances, provide these data in correlations that include needed results from other optical probes (such as Rayleigh scattering, laser velocimetry, etc.). The general compatibility of geometrical access with these other probes leads one to the conclusion that the possibility for integration of several non-intrusive techniques is a valuable attribute of light scattering diagnostics, as is their general compatability with other forms of optical and solid probe apparatus.

In order to put the major capabilities and limitations of light scattering probes into perspective, we consider the organization shown in Table I, in which the various methods are grouped into those based upon elastic and inelastic processes. (The elastic processes are actually slightly inelastic, and, in fact, depend upon this inelasticity for some of the measurement methods. Thus, direct temperature determinations for Rayleigh line shapes depend upon the line broadening mechanism, but the overall character of these processes is dominated by the scattered signal being very close in frequency to the source laser frequency.)

3.1 Elastic Scattering Methods. Elastic scattering has been focused, to date, upon the acquisition of velocity data from light scattered from particles either seeded into the flow or naturally present, and upon the study of particles that are formed in flames [28]. Among all the probes mentioned in Table I, in fact, only laser velocimeters are available as commercially-packaged devices. More recently, Rayleigh scattering has been utilized by Rambach, et al. [29] for temperature measurements in a turbulent diffusion flame for which the reactant and product gases had Rayleigh scattering cross-sections sufficiently close in value that valid total density data could be obtained directly from the scattering intensities. The ideal gas law was then used to relate density to temperature. In those cases where Rayleigh scattering can produce the desired data (i.e., under conditions where total density can be obtained and is sufficient for the required analyses), its greater signal strength compared with Raman scattering clearly mitigates in its favor. (See, for example, analyses by Storm [30] and Robben [31].)

3.2 Inelastic Scattering Methods: Raman Scattering. Inelastic scattering processes, that is, scattering which is shifted to a greater or lesser degree from the source laser line, are tabulated in the second part of Table I. These shifts are characteristic of the particular molecular species undergoing the scattering process, in its initial state of excitation. Therefore, these signals correspond to species densities (with, in principle, information available about the "population" temperatures corresponding to the initial internal mode distribution).

The characteristic difference between Raman and Rayleigh scattering can be seen by examination of the classical explanation for these processes. The electric field of the exciting laser beam distorts the electron clouds of the probed molecules, causing induced oscillating dipoles, which behave such that the induced dipole moments in the molecules under study are proportional to the oscillating electric field vector $\vec{E}$ of the incident laser beam, with the molecular polarizability α as the proportionality factor. These induced dipoles radiate, therefore, according to the product of the internal mode molecular frequencies (from α) with the frequency of the incident laser beam; thus, scattered signals result which are unshifted from the laser beam frequency (Rayleigh scattering) together with signals both up- and down-shifted from this central frequency by amounts corresponding to the various molecular internal mode frequencies (rotational and vibrational Raman scattering, where shifts to lower frequency are termed Stokes lines or bands, and shifts to higher frequency, anti-Stokes lines or bands). (See Figure 1. The vibrational Stokes Q-branch band, shown enlarged in the inset portions of this figure at ambient and elevated temperatures for the N_2 molecule, is often used for combustion measurements. The Q-branch is the strongest part of the vibrational Raman scattering signature, and corresponds to the sum of those lines for which the vibrational quantum number changes by +1, while the rotational quantum number remains unchanged.)

In addition to specific responses for different species, RS possesses a response linear with the test molecule number density and independent of other species present. The response is effectively instantaneous, and useful data can be obtained for source wide range of species that can be probed includes homonuclear molecules, such as N_2 and O_2, which do not possess infrared spectra. Remote in situ probing can be accomplished with good three-dimensional spatial resolution, often to less than 0.1 mm^3.

The overriding limitation for RS diagnostics is the weakness of the scattered signal. (See Table I.) However, a wide variety of combustion flow measurements are possible with modern high-sensitivity detection apparatus and energetic pulsed laser sources (as well as with cw laser sources with suitable time domain analysis) [32]. In applying RS techniques to flames, however, it is necessary to be aware of some specific limitations.

Discrimination of the various types of molecules present by RS techniques cannot always be easily accomplished; spectral interferences can exist and make less definitive the study of chemical composition, but these are the exception rather than the rule. For example, detection of CO from its Stokes vibrational Raman Q-branch scattering signal is difficult in lean hydrocarbon/air flames because of the presence of excess N_2, which possesses an overlapping spectral signature [33]. (In rich hydrocarbon flames, however, Setchell [34] has shown that sufficient CO is present to permit utilizing these techniques.)

Background radiation, either induced by the incident laser beam (such as particle scattering or incandescence, gas-phase or particulate fluorescense, scattering from test

cell optical interfaces, etc.) or independent of the beam (such as detector noise, flame luminosity, etc.) can cause limitations to the experimental accuracy, and can, in severe circumstances, prevent useful data from being acquired [6,33].

Spatial resolution can be limited by its trade-off with RS signal accuracy, which is related to the number of detected photons, and therefore, to the incident laser beam pulse energy. This pulse energy Q has an upper bound imposed by causing gas breakdown perturbations [35]; this occurs for $Q = Q^* s^2$, where Q^* is the energy density threshold for breakdown and s is the incident beam diameter. Thus, for a given value of Q^*, Q and s^2 are proportional. The value of Q is related to the number of detected photons, and thus to the experimental accuracy, while s^2 is a measure of the spatial resolution [33].

3.3 Inelastic Scattering Methods: CARS and Fluorescence. CARS (coherent anti-Stokes Raman spectroscopy) is a nonlinear scattering process possessing great signal strength compared with spontaneous vibrational and rotational Raman scattering [6,36], and has developed into a valuable combustion probe since its introduction by Regnier and Taran [37] in 1973. This technique also possesses species specificity, as can be seen from Figure 2. The incident beams (pump, ω_P, and Stokes ω_S) are focused, in this configuration, nearly colinearly within the probed volume. When one beam is tuned so that the frequency difference between the beams is equal to a Raman shift ($v = 0 \rightarrow v = 1$) for the test molecules, a third beam at the anti-Stokes frequency, ω_A, of intense strength is produced along the same line. This CARS beam is shifted to the blue from the pump beam by the Raman shift frequency, producing a method for detecting specific molecules.

Other configurations of CARS have been developed that free the CARS process from being essentially colinear; this relaxation of geometric access can be of great importance for utilization in combustion experiments that possess limited optical viewing. Phase matching takes place in these modifications with the incident beams being brought together from different directions. Thus, Eckbreth [38] has developed a two-frequency approach termed BOXCARS, in which the beams are brought together from three directions (one for the Stokes beam and two for the pump) in such a fashion that the wave-vectors of the incident and scattered (anti-Stokes) beams form a boxlike geometry. Compaan and Chandra [39] have devised a counterpropagating laser beam method involving three incident frequencies which also shows good promise.

Another innovation of importance for CARS combustion studies is the utilization of a tunable laser pump beam [40], so that temperature can be determined from single pulsed laser shots (i.e., from the CARS contours resulting from the interaction of a fixed frequency Stokes beam interacting with the continuous spectrum pump beam).

Since fluorescence is based upon optical absorption by the test molecules, followed by re-emission (with possible redistribution of the excited state population), molecular species are distinguishable, once again, from the unique energy level structure of each molecular species. This technique has been undergoing a period of intense development in recent years, particularly with regard to application for low density species measurements. A case in point, of considerable interest for combustion research, is the detection of the OH radical. No Raman scattering measurements have appeared, although a calculation of Raman line intensities for OH has been given [41]. (In Figure 3, we show a calculated vibrational RS Spectrum for OH as a function of temperature. The strongest part of OH RS scattering occurs at a shift of 3500 to 3600 cm^{-1}, in which range H_2O vapor RS possesses sufficient spectral intensity to cause detection problems for OH in the excess H_2O concentrations found in flames). However, a large number of investigations of OH laser-induced fluorescence in flames have been undertaken [42-51] which promise to provide a basis for developing important flame radical diagnostics. Included in this work is the study of saturation effects in which intense laser sources are used to populate the excited states sufficiently that freedom (or partial freedom) from collisional quenching effects results.

3.4 Application of Vibrational Raman Scattering Techniques to Flame Measurements. A wide variety of applications of RS diagnostics to flame research now exists; these are described in a number of publications. (See, for example, Refs. 5, 6, 32, 33, 52-55.) In Table I, we have detailed the major approaches taken for vibrational RS efforts according to the type of data which can be retrieved (and which has a direct correspondence to the type of laser source chosen) [32]. These data are divided into major categories according to their ability to provide characteristic information concerning basic turbulent combustion properties, viz., probability density functions (pdf's), frequency spectra, and spatial gradient data. In each case, we consider spatially and temporally well-resolved data, which results in fluid mechanic and/or flame chemistry information of useful accuracy for comparison with analyses.

The first category (short, energetic, low rep rate laser pulses) corresponds to the work performed in this laboratory [5,32,56-58] for which pdf's of temperature and major composition have been obtained, as well as velocity-temperature correlations; these data will be described in more detail in Sections 3.5 and 3.6. Lederman has also obtained pdf's and correlations for flames [55,59]. Sochet, et al. [60] have found spatial gradients in a flame using optical multiple-spectral-channel techniques, which promise to open a new era in combustion diagnostics. This type of detection is illustrated in Figure 4, in which a two-dimensional array of very small detectors is used for both wavelength and spatial discrimination. Black and Chang [61] have used similar methods and have presented time-averaged results which demonstrated the feasibility of data acquisition for fluctuation gradients in a jet.

The second category in the inset portion of Table I (long strongly energetic laser pulses) has been used by Pealat, et al. [62] to produce the time history of turbulence over a duration of roughly 300 μs in an $H_2/O_2/N_2$ flame produced on a flat flame burner. The flame was made turbulent by a cross flow of cold gas from a small horizontal nozzle.

The third category (cw laser), in which pdf's are produced from a finite sequence of photon count moments, is generally restricted to low luminosity flows. In this area, spectral density data have been obtained by Chabay, et al. [63], autocorrelation functions and pdf's by Birch, et al. [64], and pdf's by Penney, et al. [65].

We have discussed, so far, point or spatial gradient measurements in categorizing vibrational RS data. Another area of importance for flame diagnostics is that of two-dimensional optical imaging. This was accomplished by Hartley [66] before the era of diode detector arrays through use of a thin sheet of frequency-doubled ruby laser light, interference filters, an image intensifier, and a photographic plate. Hartley termed this species concentration mapping procedure "Ramanography." This method has been extended by Chang and co-workers [67], who performed two-dimensional digitized Raman imaging of jet flows with spectral filters and a multiple-spectral-channel detector. Their work produced average concentration maps for an 8 mm x 8 mm x 100 cm plane using an argon ion laser source and multipass cell to create an approximate sheet of source light. These results have enabled them to predict that a frequency-doubled ruby laser source should be able to produce time-resolved data, and thus take "snapshots" of flame zones in species-specific light.

3.5 Measurements of Temperature and Concentration Probability Density Functions from Vibrational Raman Scattering Data. As an example of the application of vibrational RS techniques to flame diagnostics, we discuss here some recent results, reported by Drake, et al. [58], Warshaw, et al. [57], and Lapp [5], of an experimental program to measure the thermodynamic and flow field properties of an H_2-air co-flowing jet turbulent diffusion flame. The most recent data have been obtained in the fan-induced combustion tunnel shown in Figure 5; for scale, the test section is 15 cm x 15 cm square pipe, and the length of the test section window is 0.9m. The tunnel is movable in three dimensions in order to permit the use of fixed-bed optics -- a highly desirable feature for locking together and fixing the test zone configurations of the optical probes utilized.

Raman scattering was used (in the fashion indicated in first category of the inset portion of Table I) to determine the temperature from the Stokes/anti-Stokes intensity ratio for N_2, and the concentrations of N_2, H_2, and H_2O from their Stokes signal intensities calibrated against standards. A pulsed dye laser source capable of producing 1J pulses at rep rates up to 1 pulse/s was used at 488 nm. For velocity data, cw real fringe laser velocimetry was used together with nominal 1-μm-diameter alumina seed [57].

The RS data [58] have been presented in the form of pdf's, and are shown in Figure 6 at various radial positions for an axial station 50 fuel-tip-diameters (x/d-value) downstream of the fuel tip for a 50 m/s stream of H_2 flowing into a 10 m/s air stream, to produce a cold flow Reynolds number Re of 1500.[2] For the data shown in Figure 7, these velocities were each increased by 50% to produce a flow corresponding to Re ≈2200. We note that no evidence of flow intermittency or bimodal temperature pdf is seen in Figure 6; in Figure 7, however, clear evidence of intermittent mixing is seen in the pdf's.

In order to evaluate these data, comparisons were made of simultaneously-acquired species/temperature concentration data pairs with predictions from adiabatic isobaric equilibrium calculations of species concentration and temperature as a function of fuel/air equivalence ratio. (See Figure 8.) This calculation is made on the basis that a turbulent diffusion flame arises from burning at a distribution of equivalence ratios, and that it can be considered therefore as the resultant distribution of product-gas equilibrium mixtures. Fast chemistry is assumed, radiative cooling is neglected, and the Lewis number Le is set equal to 1. Reasons for deviating from these theoretical comparison plots include statistical data scatter and possible non-isothermal test zones (since RS signals have a nonlinear response with temperature for large temperature excursions), in addition to possible violations of the assumptions just given.

Results for N_2 [58] for x/d = 75 and 150 are shown in Figure 9. Here we see that the N_2 data agree reasonably well with this simple theory for the lean portions of the flame, while consistent deviations of slope appear in the rich legs, to an increasing degree with increasing values of x/d. Additional data for N_2 at other axial positions, as well as similar data taken for H_2, show this behavior trend. Experimental data acquired across the entire flame diameter confirm analyses according to the simple adiabatic theory that buoyancy is not responsible for these results. We have not been able to explain these deviations by other considerations involving heat transfer, nor have we been able to determine systematic errors leading to this behavior. One possible suggestion currently under investigation is that such departures may be caused by the relative effects of heat and mass transfer (Le ≠ 1).

3.6 Conditioned Sampling Approaches: Near-Simultaneous RS and LV Data, and Intermittent Data in a Hostile Environment. To our knowledge, the earliest near-simultaneous RS and LV data were obtained by Hillard et al. [68] for a high speed free jet, in which mean values (1 min. averages) of temperature and nitrogen density were found from rotational RS in an experiment coordinated with LV measurements. In order to obtain coordinated fluctuation data, additional experimental control is required.

As an example, a "velocity-preferred" trigger system can be used to acquire RS and LV data in close time proximity. This method is basically a conditioned sampling technique. In Figure 10, we show a timing diagram which illustrates how the RS source laser is triggered by a validation pulse from the LV processor. Thus, after a valid LV signal is accepted, the RS signal is produced at a desired later time, nearly simultaneous from a fluid mechanic point of view, but with a long enough delay for the particle producing the LV burst signal to move out of the test zone before the energetic RS source laser pulse hits it. Utilizing such a technique, Warshaw et al. [57] obtained temperature-velocity correlation data.

In another conditioned sampling experiment, Drake et al. [58] made a preliminary assessment of the possibility of probing hydrocarbon flames with pulsed RS methods. Premixed laminar propane-air flames with equivalence ratios ϕ of 1 to 3 were investigated on a porous plug burner. In one set of experiments, a spectrometer slit function was obtained by using the relatively broad high temperature N_2 RS signal induced by the pulsed laser as the light source while the spectrometer wavelength drive was swept slowly. (See Figure 11). For a stoichiometric flame (which was non-luminous), a well-determined slit function was obtained. For a fuel-rich flame (ϕ = 3), much of the data obtained corresponded to saturation of the optical/electronic detection chain (caused by strong laser-induced optical signals), but was obtained over an apparent envelope. By setting the electronic detection apparatus to omit all signals greater than an amount determined to be larger than any possible RS signal, the cluttered trace shown in the central part of Figure 11 was transformed to that shown in the lower trace (i.e., an approximation of the upper trace). This result of conditioned sampling suggests that RS data was observed from a non-luminous flame zone under conditions for which a laser-induced luminous zone can oscillate in and out of the optical detection area. The result of the sampling procedure applied to the central part of this figure is obvious; the important point is the demonstration that this technique can be applied to obtain valid RS data in hostile environments.

4. DISCUSSION

In the preceding section, we have outlined some of the capabilities of new light-scattering diagnostic methods for flame research, with some emphasis on vibrational Raman scattering methods applied to turbulent diffusion flames. Although still in its infancy, these techniques are clearly past the basic proof-of-principle status. They are now in the process of being applied to significant combustion/fluid mechanic problems designed both to bring new fundamental knowledge to this field by means of well-designed investigations into specific critical points of interest, and more focused experimental investigations into questions of importance to engineering studies.

In this contribution, we have concentrated upon the more basic part of the spectrum, and summarize in Table II an ordering of turbulent flame point property measurement and prediction capabilities. The table is formulated to illustrate the close interaction required of modelers and experimentalists in order to achieve the technological goals faced by combustion researchers and combustor designers. With this in mind, we separate the physical quantities of interest into three categories and outline in the table the measurement and modeling capabilities and needs.

The first category is for those variables that can be classified as flow field properties. Here, we used the term "flow field" loosely so that flux quantities such as $\overline{\rho' u_i'}$, $\overline{m_i' u_i'}$, $\overline{T' u_i'}$ can be included in this category. The second grouping contains thermodynamic properties of the flow field only, while the third category includes any trace species found in the combustion flow and all pollutants found in the burning of hydrocarbon and H_2 fuels.

The table is divided into five columns, the first two of which list the types of measurements and the physical quantities of interest that can be measured. Under the second column, the physical quantities to be measured in each category are listed in increasing order of difficulty. Some quantities listed do not represent direct measurements but are inferred from other measurements. A good example of this is the mixture density. These quantities are normally put at the bottom of the list. The third column deals with measurement capabilities and is subdivided into three different columns under the heading of "Proven Technology," "Developing Technology," and "Difficult?" Modeling capabilities are grouped under the fourth column with subcolumns for the "Current Approach" and "Alternate Approach." It should be pointed out that the difference between these two approaches is mainly in the model used to tackle the chemistry part of the problem. As for the fluid mechanical part of the problem, the two approaches share the same basic model. A detailed discussion concerning the fluid mechanical model and the need for more advanced measurements is given below. Finally, column five is reserved for comments which are directed to both experimental and modeling capabilities and needs.

Although the first four items under the first category can be measured using proven techniques such as impact probes and LV, their accurate measurement does present some difficulty. (For example, LV data of good quality for quantities such as $\overline{v'^2}$, $\overline{w'^2}$, $\overline{u'v'}$, $\overline{v'w'}$, etc., are difficult to obtain. Additionally, these data can be biased by seeding considerations; as a result, such velocity data may be close to Favre-averaged instead of Reynolds-averaged.)

For simple flows, the impact probe provides a way to measure the momentum flux $\overline{\rho u^2}$; therefore, an independent check on the indirect measurement of $\overline{\rho' u'}$ can be made provided the term $\overline{\rho' u'^2}$ can be considered small compared to $\bar{\rho}\,\overline{u'^2}$ or $\bar{u}\,\overline{\rho' u'}$. These four items also provide basic flame data for the validation of the turbulence model used in the two approaches discussed. The measurements of $\overline{T' u'}$, $\overline{m_i' u'}$,..., not only add new insights into the understanding of the combustion processes in diffusion flames but also provide data, for the first time, to assess the applicability of the gradient transport model for reactive flow study (again see below for detailed discussion).

In category two, the various moments and joint moments of T and major species m_i are direct measurements. However, the pdf of these quantities are inferred measurements in that the discrete data points must be interpreted in the form of a histogram. These measurements, besides providing data for model validation, can also be used to help improve existing models. Finally, the trace species and pollutants are difficult to measure. Therefore, their use as validation data for overall flame modeling is limited.

Having discussed the experimental and modeling capabilities and needs as summarized in Table II, we would like to make an attempt to point out some of the more difficult questions faced by both modelers and experimentalists. To do this, the main weakness of the two approaches outlined in Section 2 is examined in more detail. Through this examination, the benefits of close interaction between experimentalists and modelers are revealed.

It was pointed out in Section 2 that the main weakness of the two approaches lies in the turbulence models used to close the set of mean transport equations. The reason is that the turbulence models used are similar to those formulated for constant density flows. Although these models work very well for a wide variety of constant density shear flows, their direct application to reactive shear flows is in doubt [69]. Some basic deficiencies of these models were pointed out recently by Williams and Libby [70]. Among the basic questions raised is the applicability of the gradient transport assumption for reactive flows. In turbulent flows, flux terms such as $\bar{\rho}\,\overline{u_i'u_j'}$, $\bar{\rho}\,\overline{m_i'u_j'}$, etc. appear in the mean transport equations as a result of the turbulent fluctuations and the non-linearity of the convection terms. Conventional wisdom in nonreactive flow modeling is to postulate a relation between these fluxes and the mean rates of strain for the Reynolds stresses and the gradient of the mean scalars for scalar fluxes. The turbulent exchange coefficients in these relations are usually assumed to be scalar quantities whose magnitudes can be determined from a knowledge of the turbulent kinetic energy and its dissipation rate [2,11]. This assumption gives fairly accurate results [2-4] in nonreactive flow modeling for a wide range of engineering problems because in most constant density turbulent flows the fluxes and the mean rates of strain behave similarly. However, this is not necessarily true for reactive flows. In a study made by Clavin and Williams [71], they found that the fluxes change sign in a region where the sign of the mean gradient remains the same. Further experimental evidence of this countergradient diffusion phenomenon can be found in the helium-air mixing experiment of Stanford and Libby [72] and LaRue and Libby [73]. In view of this, measurements of the turbulent fluxes and mean velocities in a reactive flow would be most helpful in the pursuit of a better turbulence model for such flows.

As indicated in Table II, the fluxes $\bar{\rho}\,\overline{u_i'u_j'}$, $\bar{\rho}\,\overline{m_i'u_j'}$, etc. can be measured in a simple flame using a combination of LV and RS optical techniques. In the process, the mean velocity profiles are also obtained. Therefore, the present experimental technique provides, for the first time, an opportunity to assess the applicability of the gradient transport model for turbulent reactive flows.

The unity turbulent Lewis number assumption is usually made in the current approach to combustion modeling. Although this assumption is not explicitly stated in the alternate approach, it is implied in the formulation of the model [21,27]. In some flows, such as in gas turbine combustors, reactions and significant heat release are confined in a small region, thereby producing very large spatial gradients for the thermodynamic variables. Under such circumstances, the turbulent Lewis number cannot be expected to be one. The understanding of the effects of a non-unity turbulent Lewis number on combustion modeling, therefore, becomes important. Ability to measure the various turbulent fluxes, $\bar{\rho}\,\overline{u_i'u_j'}$, $\bar{\rho}\,\overline{m_i'u_j'}$, in a diffusion flame affords the opportunity to assess the validity and extent of the unity turbulent Lewis number assumption in a simple reactive shear flow. It is hoped that based on this understanding, a more general combustion model can be formulated.

In principle, the alternate approach can calculate the thermodynamic variables in a combustion system with improved accuracy. However, in practice, its ability to do that depends on the availability and reliability of rate data, kinetic mechanisms and an efficient computational algorithm for the solution of the strongly nonlinear rate equations. The exact calculation of thermodynamic variables is not always possible because of the lack of reliable rate data and kinetic mechanisms for a wide range of fuels. Here again, the ability to measure the single and joint pdf of temperature and major species in a simple reactive flow would provide guidance for understanding the significant flame chemistry to be considered in the calculations.

Another point raised by Williams and Libby [70] concerns the modeling of the dissipation terms in the Reynolds transport equations. Firstly, the off-diagonal component of the dissipation function is not necessarily negligible in reactive flow. Secondly, the proposed model for $\varepsilon = \text{const.} \times \bar{\rho}\, k^{3/2}/\ell$, where ε is the dissipation and ℓ is the length scale characteristic of the large eddies, is not always appropriate for reactive flows.

The dissipation terms, even in non-reactive turbulent flows, are very difficult to measure [10]. Although advances in hot wire anemometry and optical probe techniques have made the measurement of the spatial gradients (in the macro sense) of velocity, temperature, and concentration a reality [60,74], the measurement of the spatial gradient terms in a region where dissipation is important is still a very difficult (but, we hope, not an impossible) task. As a result, experimental work directed to overcome this difficulty would be most helpful to modelers.

From the above discussion, it is evident that a strong and continued interaction between modelers and experimentalists is necessary, as has begun in various workshops (for example, Ref. 75), conference series (for example, Ref. 76), and special publications (for example, Ref. 77), to further our understanding of combustion phenomena and to improve the capabilities of existing combustion models.

REFERENCES

1. National Research Council, Committee on High Temperature Science and Technology, "High Temperature Science: Future Needs and Anticipated Developments", 1979, Chapter 3.

2. Launder, B.E., Reece, G.J. and Rodi, W., "Progress in the Development of a Reynolds-Stress Turbulence Closure," J. Fluid Mech., Vol. 68, 1975, pp. 537-566.

3. Lumley, J.L., "Prediction Methods for Turbulent Flows," Lecture Series No. 26, von Karman Inst., Belgium, 1975.

4. Reynolds, W.C., "Computation of Turbulent Flows," Annual Review Fluid Mech., Vol 8, 1976, pp. 183-207.

5. Lapp, M., "Raman Scattering Measurements of Combustion Properties," to appear in Laser Probes for Combustion Chemistry, ed. by D.R. Crosley, Amer. Chem. Soc. Symp. Series, Vol. 134, Washington, D.C., 1980.

6. Eckbreth, A.C., Bonczyk, P.A., and Verdieck, J.F., "Laser Raman and Fluorescence Techniques for Practical Combustion Diagnostics," Appl. Spectrosc. Rev., Vol. 13, No. 1, 1978, pp. 15-164.

7. Pope, S.B., "The Statistical Theory of Turbulent Flames," Phil. Trans. Roy. Soc., Vol. 291, 1979, pp. 529-568.

8. Borghi, R., "Chemical Reactions Calculations on Turbulent Flows: Application to CO-Containing Turbojet Plume," Adv. Geophysics, Vol. 18B, 1974, pp. 349-365.

9. Pratt, D.T., "Mixing and Chemical Reaction in Continuous Combustion," Prog. Energy Combust. Sci., Vol. 1, 1976, pp. 73-86.

10. Bradshaw, P., An Introduction to Turbulence and Its Measurement, Oxford, Pergamon Press, 1971, p. 38.

11. Jones, W.P. and Launder, B.E., "The Prediction of Laminarization with a Two-Equation Model of Turbulence," Int. J. Heat Mass Transfer, Vol. 15, 1972, pp. 301-314.

12. Kent, J.H. and Bilger, R.W., "The Prediction of Turbulent Diffusion Flame Fields and Nitric Oxide Formation," 16th Symp. (International) on Combustion, 1976, pp. 1643-1656.

13. Bilger, R.W., "Turbulent Flows with Nonpremixed Reactants," to appear in Turbulent Reacting Flows, ed. by P.A. Libby and F.A. Williams, Heidelberg, Springer-Verlag, Topics in Applied Physics Series, Chapt. 3.

14. Spalding, D.B., "Concentration Fluctuations in a Round, Turbulent Free Jet," J. Chem. Eng. Sci., Vol. 26, 1971, pp. 95-109.

15. Khalil, E.E., Spalding, D.B. and Whitelaw, J.H., "The Calculation of Local Flow Properties in Two-Dimensional Furnaces," Int. J. Heat Mass Transfer, Vol. 18, 1975, pp. 775-791.

16. Jones, W.P., Workshop on pdf Methods for Turbulent Flows, Technische Hochschule, Aachen, 1977.

17. Kent, J.H. and Bilger, R.W., "Turbulent Diffusion Flames," 14th Symp. (International) on Combustion, 1973, pp. 615-625.

18. Favre, A., "Statistical Equations of Turbulent Gases," in Problems of Hydrodynamics and Continuum Mechanics, SIAM, 1969, pp. 231-266.

19. Gouldin, F.C., "Role of Turbulent Fluctuations in NO Formations," Comb. Sci. Tech., Vol. 9, 1974, pp. 17-23.

20. Curl, R.L., "Dispersed Phase Mixing, I. Theory and Effects on Simple Reactors," AIChE J., Vol. 9, 1963, pp. 175-181.

21. Hooven, M.D., Pratt, D.T., and So, R.M.C., "Coalescence/Dispersion Modeling of a Reacting Shear Layer," Spring Meeting, Western States Section/The Combustion Institute, Los Angeles, 21-22 April, 1980.

22. So, R.M.C., Pratt, D.T., and Hooven, M.D., "Modeling of Scalar Transport in Turbulent Shear Flows," submitted for publication.

23. Janicka, J., Kolbe, W., and Kollmann, W., "Closure of the Transport Equation for the Probability Density Function of Turbulent Scalar Fields," J. Non-Equib. Thermodyn., Vol. 4, 1979, pp. 47-66.

24. Borghi, R., Office National D'etudes et de Recherches Aerospatiales, Chatillon, France, "Models of Turbulent Combustion for Numerical Predictions," 1979, Rept. No. 1979-1.

25. Janicka, J., Kolbe, W., and Kollmann, W., "The Solution of a pdf Transport Equation for Turbulent Diffusion Flames," 26th Fluid Mech. Heat Transfer Inst., 1978, pp. 296-312.

26. Janicka, J. and Kollmann, W., "Prediction Model for the pdf of Turbulent Temperature Fluctuations in a Heated Round Jet," 2nd Symp. Turbulent Shear Flows, Imperial College, London, 1979.

27. Pope, S.B., "A Monte Carlo Method for the pdf Equations of Turbulent Flow," submitted for publication.

28. Experimental Diagnostics in Gas Phase Combustion Systems, ed. by B.T. Zinn, Vol. 53, Progress in Astronautics and Aeronautics, New York, AIAA, 1977, Chapt. III (Laser Anemometry and Related Particle Scattering Measurements).

29. Rambach, G.D., Dibble, R.W., and Hollenbach, R.E., Sandia Laboratories, Livermore, CA, "Velocity and Temperature Measurements in Turbulent Diffusion Flames," 1980, SAND79-8775.

30. Storm, E., "The Possible Application of Raman Scattering Measurements to Turbulent Mixing Layers," in Laser Raman Gas Diagnostics, ed. by M. Lapp and C.M. Penney, New York, Plenum Press, 1974, pp. 369-377.

31. Robben, F., "Comparison of Density and Temperature Measurement Using Raman Scattering and Rayleigh Scattering," in Combustion Measurements, ed. by R. Goulard, New York, Academic Press, 1976, pp. 180-196.

32. Lapp, M. and Penney, C.M., "Instantaneous Measurements of Flame Temperature and Density by Laser Raman Scattering," in Proceedings of the Dynamic Flow Conference 1978 on Dynamic Measurements in Unsteady Flows, P.O. Box 121, DK-2740 Skovlunde, Denmark, 1979, pp. 665-683.

33. Lapp, M. and Penney, C.M., "Raman Measurements on Flames," in Advances in Infrared and Raman Spectroscopy, Vol. 3, ed. by R.J.H. Clark and R.E. Hester, London, Heyden, Chapt. 6.

34. Setchell, R.E., "Analysis of Flame Emissions by Laser Raman Spectroscopy," 1974, Western States Section/The Combustion Institute, Paper No. WSS/CI 74-6.

35. Switzer, G.L., Meyers, C.G., Roh, W.B., and Schreiber, P.W., "Gas Breakdown Thresholds in Flame Induced by Ruby Laser," AIAA J., Vol. 16, 1978, pp. 766-768.

36. Nibler, J.W., Shaub, W.M., McDonald, J.R., and Harvey, A.B., "Coherent Anti-Stokes Raman Spectroscopy," in Vibrational Spectra and Structure: A Series of Advances, Vol. 6, ed. by J.R. Durig, Amsterdam, Elsevier, 1977, Chapt. 3.

37. Regnier, P.R. and Taran, J.P.E., "Gas Concentration Measurement by Coherent Raman Anti-Stokes Scattering," in Laser Raman Gas Diagnostics, ed. by M. Lapp and C.M. Penney, New York, Plenum, 1974, pp. 87-103.

38. Eckbreth, A.C., "BOXCARS: Crossed-Beam Phase-Matched CARS Generation in Gases," Appl. Phys. Lett., Vol. 32, 1978, pp. 421-423.

39. Compaan, A. and Chandra, S., "Coherent Anti-Stokes Raman Scattering with Counterpropagating Laser Beams," Opt. Lett., Vol. 4, 1979, pp. 170-172.

40. Roh, W.B., Schreiber, P.W., and Taran, J.P.E., "Single-Pulse Coherent Anti-Stokes Raman Scattering," Appl. Phys. Lett., Vol. 20, 1976, pp. 174-176.

41. Miller, J.A., Coll, C.F., and Melius, C.F., "Theoretical Computations of Spontaneous Vibration-Rotation Raman Scattering from OH ($X\ ^2\pi$) and NO ($X\ ^2\pi$), J. Quant. Spectrosc. Radiat. Transfer, Vol. 21, 1979, pp. 193-211.

42. Anderson, W.R., "Laser Excited Fluorescence Measurement of OH Rotational Temperatures in a CH_4/N_2O Flame," 1979, Eastern States Section/The Combustion Institute, Paper No. 3.

43. Chan, C. and Daily, J.W., "Laser Excitation Dynamics of OH in Flames," to appear in Appl. Optics.

44. Crosley, D.R. and Smith, G.P., "Vibrational Energy Transfer in Laser-Excited $A^2\ ^+OH$ as a Flame Thermometer," Appl. Optics, Vol. 19, 1980, pp. 517-520.

45. Stepowski, D. and Cottereau, M.J., "Direct Measurement of OH Local Concentration in a Flame from the Fluroescence Induced by a Single Laser Pulse," Appl. Optics, Vol. 18, 1979, pp. 354-359.

46. Muller, C.H., Schofield, K., Steinberg, M., and Broida, H.P., "Sulfur Chemistry in Flames," 17th Symp. (International) on Combustion, 1978, pp. 867-879.

47. Cattolica, R.J., "OH Rotational Temperature from Laser Induced Fluorescence," 1978, Western States Section/The Combustion Institute Spring Meeting.

48. Fujiwara, J.D., Omenetto, N., Bradshaw, J.B., Bower, J.N., Nikdel, S., and Winefordner, J.D., "Laser Induced Molecular Background Fluorescence in Flames," Spect. Acta, Vol. 34B, 1979, pp. 317-329.

49. Lucht, R.P., Mayer, J., Sweeney, D.W., and Laurendeau, N.M., "Saturated Fluorescence Measurement of OH," submitted for publication.

50. Bechtel, J.H., and Teets, R.E., "Hydroxyl and Its Concentration Profile in Methane-Air Flames," Appl. Optics, Vol. 18, 1979. pp. 4138-4144.

51. Wang, C.C. and Davis, L.I., "Ground-State Population Distribution of OH Determined with a Tunable uv Laser," Appl. Phys. Lett., Vol. 25, 1974, pp. 34-35.

52. Lapp, M. and Penney, C.M., ed., Laser Raman Gas Diagnostics, New York, Plenum Press, 1974.

53. Goulard, R., ed., Combustion Measurements, New York, Academic Press, 1976.

54. Hastie, J.W., ed., Characterization of High Temperature Vapors and Gases, Vol. 2, Washington, D.C., NBS Special Publication 561/2, 1979.

55. Lederman, S., "Developments in Laser Based Diagnostic Techniques," to appear in Proceedings of the 12th International Symposium on Shock Tubes and Waves, Jerusalem, 1979.

56. Lapp, M., "The Study of Flames by Raman Spectroscopy," in Proceedings of the Sixth International Conference on Raman Spectroscopy, Vol. 1, ed. by E.D. Schmid, R.S. Krishnan, W. Kiefer, and H.W. Schrotter, London, Heyden, 1978, pp. 219-232.

57. Warshaw, S., Lapp, M., Penney, C.M., and Drake, M., "Temperature-Velocity Correlation Measurement for Turbulent Diffusion Flames from Vibrational Raman Scattering Data," to appear in Laser Probes for Combustion Chemistry, ed. by D.R. Crosley, Amer. Chem. Soc. Symp. Series, Vol. No. 134, Washington, D.C., 1980.

58. Drake, M., Lapp, M., Penney, C.M., and Warshaw, S., "Measurements of Temperature and Concentration Fluctuations in Turbulent Diffusion Flames Using Pulsed Raman Spectroscopy," to appear in Proceedings of the 19th Symp. (International) on Combustion.

59. Lederman, S., Celentano, A., and Glaser, J., "Temperature, Concentration, and Velocity in Jets, Flames, and Shock Tubes," Phys. Fluids, Vol. 22, 1979, pp. 1065-1072.

60. Sochet, L.R., Lucquin, M., Bridoux, M., Crunelle-Cras, M., Grase, F., and Delhaye, M., "Use of Multichannel Pulsed Raman Spectroscopy as a Diagnostic Technique in Flames," Comb. and Flame, Vol. 36, 1979, pp. 109-116.

61. Black, P.C. and Chang, R.K., "Laser-Raman Optical Multi-Channel Analyzer for Transient Gas Concentration Profile and Temperature Determinations," AIAA J., Vol. 16, 1978, pp. 295-296.

62. Pealat, M., Bailly, R., and Taran, J.P.E., "Real Time Study of Turbulence in Flames by Raman Scattering," Opt. Comm., Vol. 22, 1977, pp. 91-94.

63. Chabay, I., Rosasco, G.J., and Kashiwagi, T., "Species-Specific Raman Spectroscopic Measurements of Concentration Fluctuations in Unsteady Flow," J. Chem. Phys., Vol. 70, 1979, pp. 4149-4154.

64. Birch, A.D., Brown, D.R., Dodson, M.G., and Thomas, J.R., "The Determination of Gaseous Turbulent Concentration Fluctuations Using Raman Photon Correlation Spectroscopy," J. Phys. D: Appl. Phys., Vol. 8, 1975, pp. L167-L170.

65. Penney, C.M., Warshaw, S., Lapp, M., and Drake, M., "Observations of Fast Turbulent Mixing in Gases Using a cw Laser," to appear in Laser Probes for Combustion Chemistry, ed. by D.R. Crosley, American Chem. Soc. Symp. Series, Vol. 134, Washington, D.C., 1980.

66. Hartley, D.L., "Raman Gas Mixing Measurements and Ramanography," in Laser Raman Gas Diagnostics, ed. by M. Lapp and C.M. Penney, New York, Plenum Press, 1974, pp. 311-314.

67. Webber, B.F., Long, M.B., and Chang, R.K., "Two-dimensional Average Concentration Measurements in a Jet Flow by Raman Scattering," Appl. Phys. Lett., Vol. 35, 1979, pp. 119-121.

68. Hillard, M.E., Hunter, W.W., Meyers, J.F., and Feller, W.V., "Simultaneous Raman and Laser Velocimeter Measurements," AIAA J., Vol. 12, 1974, pp. 1445-1446.

69. Libby, P.A. and Bray, K.N.C., "Counter-Gradient Diffusion in Premixed Turbulent Flames," AIAA Paper No. 80-0013, 1980.

70. Williams, F.A. and Libby, P.A., "Some Implications of Recent Theoretical Studies on Turbulent Combustion," AIAA Paper No. 80-0012, 1980.

71. Clavin, P. and Williams, F.A., "Effects of Lewis Number on Propagation of Wrinkled Flames in Turbulent Flow," to appear in AIAA Progress in Aeronautics and Astronautics Series, 1980.

72. Stanford, R.A. and Libby, P.A., "Further Applications of Hot Wire Anemometry to Turbulence Measurements in Helium-Air Mixtures," Phys. Fluids, Vol. 17, 1974, pp. 1353-1361.

73. LaRue, J.C. and Libby, P.A., "Measurements in the Turbulent Boundary Layer with Slot Injection of Helium," Phys. Fluids, Vol. 20, 1977, pp. 1192-1202.

74. Van Atta, C.W., "Multi-channel Measurements and High-order Statistics," in Proceedings of the Dynamic Flow Conference 1978 on Dynamic Measurements in Unsteady Flows, P.O. Box 121, DK-2740 Skovlunde, Denmark, 1979, pp. 919-942.

75. Project SQUID (Office of Naval Research) Workshop on Combustion Measurements in Jet Propulsion Systems, Purdue, 1975; reported in Ref. 53.

76. AGARD Conferences and Lecture Series, such as those reported in Conference Proceedings No. 193 on Applications of Non-Intrusive Instrumentation in Fluid Flow Research, 1976; Conference Preprint No. 275 on Combustor Modelling, 1979; and Lecture Series 90 on Laser Optical Measurement Methods for Aero Engine Research and Development.

77. Comb. Sci. Tech. Special Issue on Turbulent Reactive Flows, ed. by F.V. Bracco, Vol. 11, Numbers 1-6, 1976.

ACKNOWLEDGMENTS

The authors are grateful to their colleagues, M. Drake, B. Gerhold, C.M. Penney, and S. Warshaw for their collaboration, and to F. Gouldin (Cornell University) and D. Pratt (Univ. of Michigan) for valuable discussions. The authors also acknowledge with pleasure partial support of this research by the U.S. Department of Energy, the Air Force Office of Scientific Research, and the Office of Naval Research (Project SQUID).

Table I: Information Available from Elastic and Inelastic Molecular Light Scattering Processes Concerning Fluctuation Properties of Flames, with Additional Detail Shown for Data Obtained from Vibrational Raman Scattering.

Observation	Scatterer	Scattering Process	Characteristic Differential Cross Section (cm^2/sr)	Information	Comments
Elastic (unshifted) scattering	Particles	Tyndall (Mie)	10^{-7} (10 μm diam.) 10^{-13} (0.1 μm diam.)	Characterization of particle distribution	Information can be difficult to interpret for non-ideal particle systems.
				Velocimetry	Particles must be small enough to follow flow fluctuations.
	Gas	Rayleigh	10^{-27} (N_2, 488 nm)	Total density, temperature	Require low particle loading & knowledge of major composition; difficult to instrument for direct temp. meas.
Inelastic (shifted) scattering	Gas	Raman (Vibrational)	5×10^{-31} (N_2, Stokes Q-branch, 488 nm)	Temperature, Major Species Densities	Too weak for luminous systems; temp. data independent of composition, but density data requires temp. for high temps.
	Gas	Raman (Rotational)	10^{-29} (N_2, all lines, 488 nm)	Temperature, Major Species Densities	Difficult to separate effects of different species for spectroscopically-similar molecules.
	Gas	Coherent Anti-Stokes Raman Spectroscopy (CARS)	Strong nonlinear process	Temperature, Major and Intermediate Species Densities	Strong signal; tolerates particle loading & intense luminosity; more difficult to instrument and interpret than vib. or rot. Raman scattering; density data more difficult to obtain than temp. data.
	Gas	Fluorescence	10^{-19}-10^{-24} (simple molecules)	Minor Species Densities	Strong signal; saturated fluorescence can reduce dependence upon collisional quenching for some species; analysis can be difficult.

Fluctuation Data Obtained From Vibrational Raman Scattering

pdf	Frequency Spectra	Spatial Gradients	Character of Experimental Laser Source
Yes	No	Yes	Short, energetic, low rep rate laser pulses (dye, Nd:YAG, Q-switched ruby,...)
Yes	kHz - 50 kHz	Difficult	Long, strongly energetic laser pulses (free-running ruby, intracavity experiments,...)
Yes	Hz - kHz	Difficult	cw laser (either cw or chopped) with time domain analysis (argon ion, krypton ion,...)

Table II: Comparison of Representative Turbulent Flame Point Measurement and Prediction Capabilities in Increasing Difficulty. Here, Instantaneous Value x = Mean Value $\bar{x}$ + Fluctuation Value x'; LV Denotes Laser Velocimetry; RS, Raman Scattering; RayS, Rayleigh Scattering; and pdf, Probability Density Function.

Type of Measurement	Physical Quantities	Measurement Capabilities			Modeling Capabilities		Comments
		Proven Technology	Developing Technology	Difficult ?	Current Approach	Alternate Approach	
Flow Field Properties	$\overline{\rho u^2}$,...	X			X	X	Impact probe
	$\bar{u}$,...	X			X	X	LV
	$\overline{u'^2}$,...	X		X	X	X	LV; difficult for v, w << u; needed to improve models.
	$\overline{u'v'}$,...	X		X	X	X	LV; difficult for v, w << u; needed to improve models.
	$\overline{m_i'u'}$,... & $\overline{T'u'}$,...		X	X			LV + RS or RayS (see comments for T); difficult for v, w << u; needed to improve models - related to enthalpy terms.
	$\overline{\rho'u'}$,...		X	X			LV + RayS or RS (see comments for ρ); difficult for v, w << u; needed to improve models - can include new terms.
Thermodynamic Properties	Mean and Variance of T, m	X	X		X	X	RS for major species; RayS for T; thermocouples (mean values), gas sampling (mean values); absorption/emission spectroscopy (not 3-dimensional); needed to improve models.
	Single and Joint pdf for T, m		X			X	RS for major species; RayS for T (with ideal gas law, composition, and cross sections); needed to improve models.
	ρ		X		X	X	RayS (knowing composition and cross sections); RS (using ΣM_i), or T (with fast chem. and ideal gas law).
Pollutant Emissions	$\overline{m_{O_2}'m_{N_2}'}$		X	X		X	RS; difficult in rich zones; needed for NO_x prediction model; accomplished for similar species.
	$\overline{m_{O_2}'T'}$, $\overline{m_{N_2}'T'}$		X	X		X	RS; difficult in rich zones; needed for NO_x prediction model; accomplished for N_2.
	$\overline{m_{O_2}'m_{N_2}'T'}$, etc.		X	X		X	RS; difficult in rich zones; needed for NO_x prediction model.

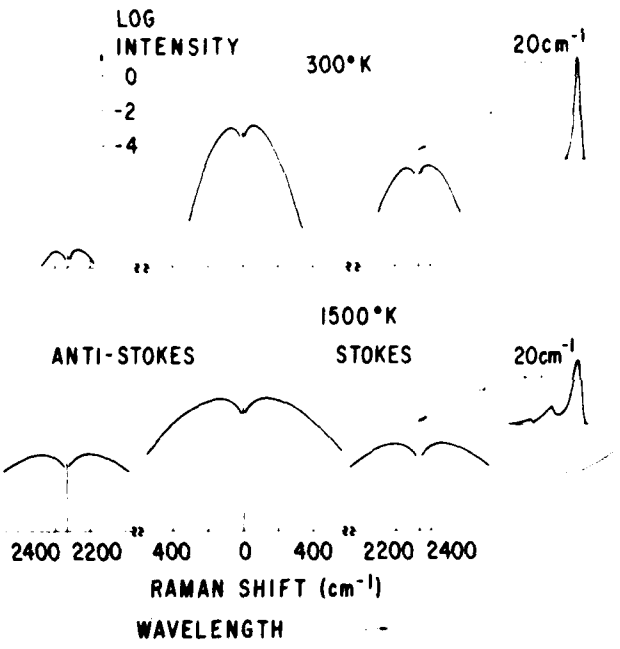

Figure 1. Schematic of Rayleigh and N_2 Raman Scattering Spectra at Ambient and Elevated Temperatures. The N_2 vibrational Q-branch bands, shown in the inset diagrams on a linear scale, were convoluted with a typical experimental spectrometer triangular-shape spectral slit function used for contour scans with laser excitation in the mid-visible, namely, $6cm^{-1}$ (0.18nm) full width at half-maximum.

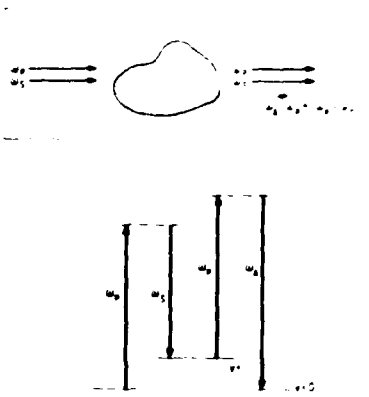

Figure 2. Schematic of Coherent Anti-Stokes Raman Spectroscopy (CARS) Process, Shown Here in Nearly-Colinear Optical Configuration.

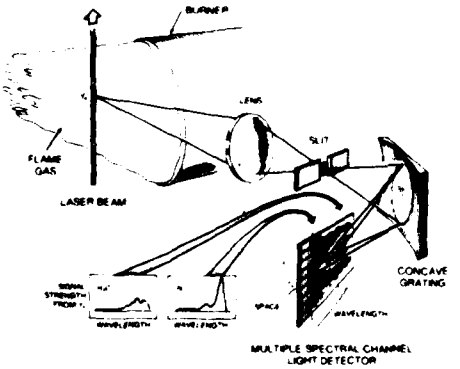

Figure 4. Schematic of Multiple-Spectral-Channel Detection of Raman Data from a Flame Source. Used in this fashion, wavelength information is obtained along the detector horizontal axis, and spatial information along the vertical axis. Thus, flame temperature and major species concentration data can be obtained along the trajectory of the incident laser beam.

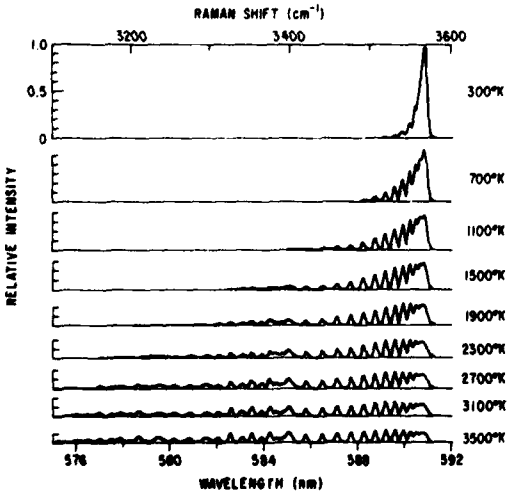

Figure 3. Calculated Vibrational Raman Scattering Spectral Contours for OH Radical, for 488 nm Laser Source.

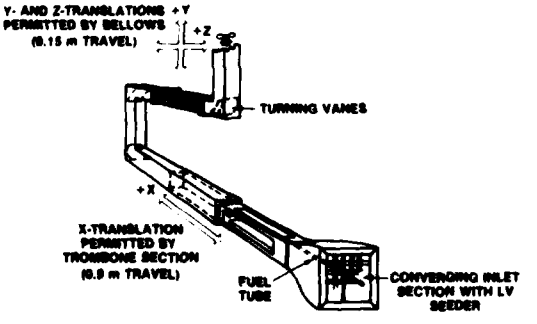

Figure 5. Schematic of Fan-Induced Movable Combustion Tunnel, Shown Here with the Test Section (0.15m x 0.15m Square Pipe with 0.9m Viewing Length) Fully Inserted in the x-Direction [57,58]. Turbulent diffusion flames are produced on a central 3-mm-diameter fuel tube.

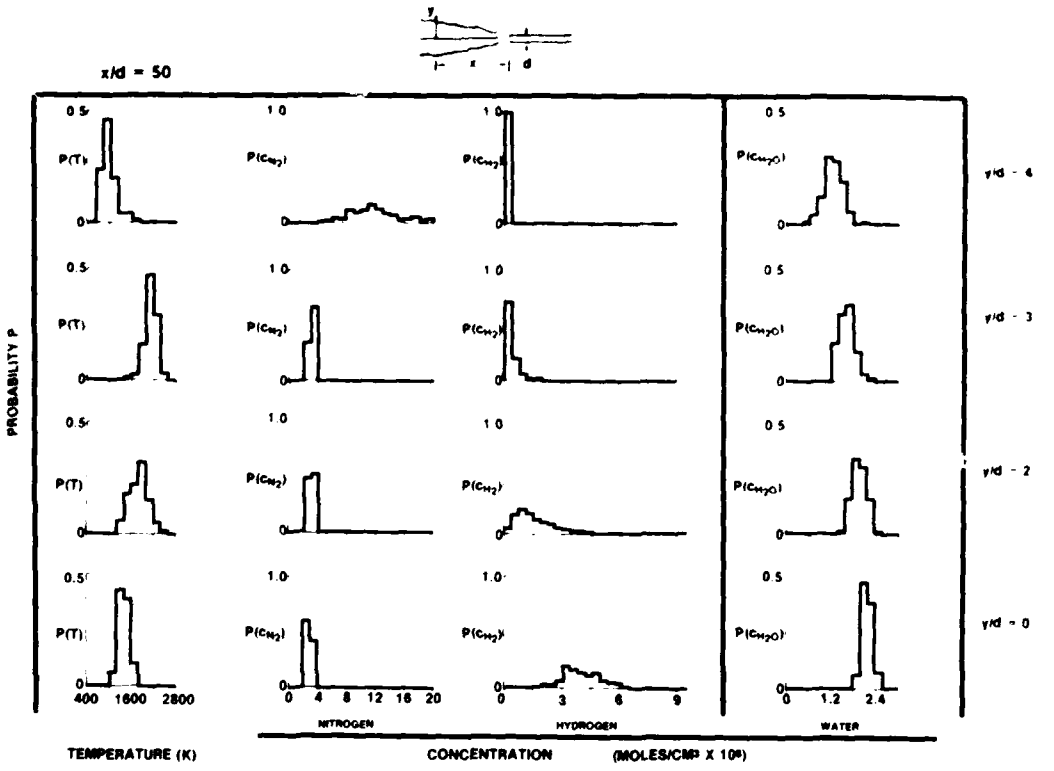

Figure 6. Probability Density Functions (Histograms) for Temperature and $\overline{N_2}$, $\overline{H_2}$, and $\overline{H_2O}$ Concentrations for H_2-Air Turbulent Diffusion Flame, for $\overline{Re} \simeq 1500$ [58]. These data were taken 50 fuel-tip-diameters downstream, at the centerline and at various off-axis positions. A smooth progression of the character of the histograms was observed as y/d was increased; i.e., flame boundary effects were not prominent.

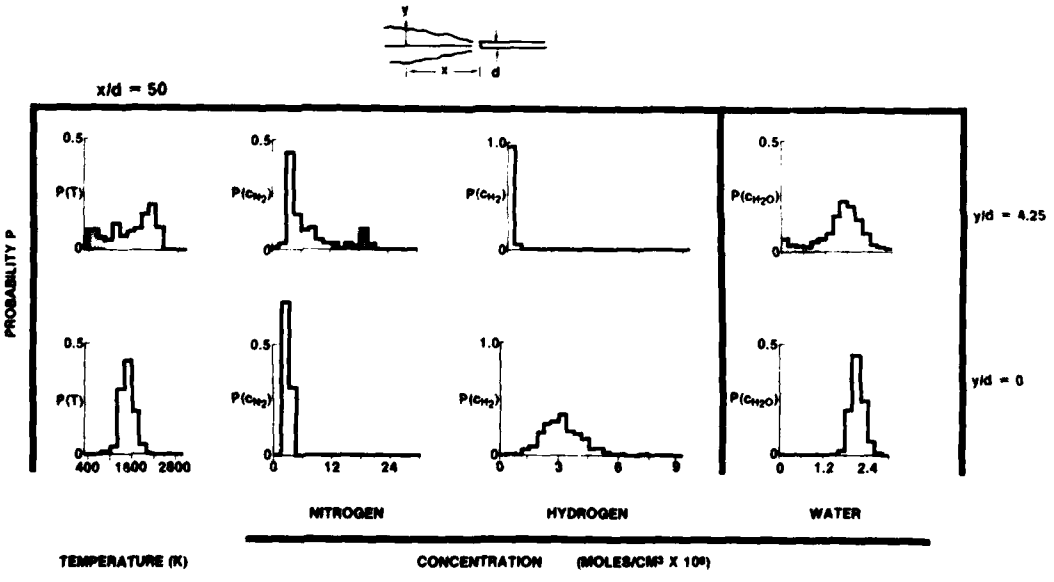

Figure 7. Probability Density Functions (Histograms) for Temperature and $\overline{N_2}$, $\overline{H_2}$, and $\overline{H_2O}$ Concentrations for H_2-Air Turbulent Diffusion Flame, for $\overline{Re} \simeq 2200$ [58]. The shaded zones in the temperature, nitrogen concentration, and water concentration histograms for y/d = 4.25 correspond to the same simultaneously-acquired data sets, and illustrate intermittent effects at the flame boundary. The increase in turbulence over that corresponding to the flame considered in Fig. 6 caused a significant decrease in flame length and a greatly broadened temperature histogram at the flame boundary.

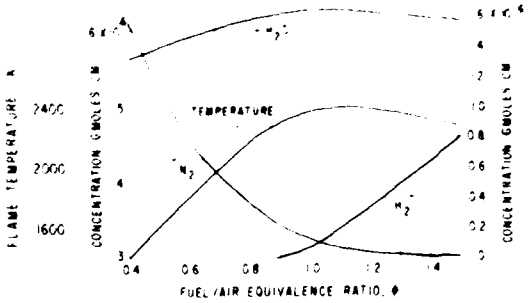

Figure 8. Value of H_2/Air Flame Temperature and Major Species Concentration, Calculated for Adiabatic Equilibrium Conditions, as a Function of Fuel/Air Equivalence Ratio Φ.

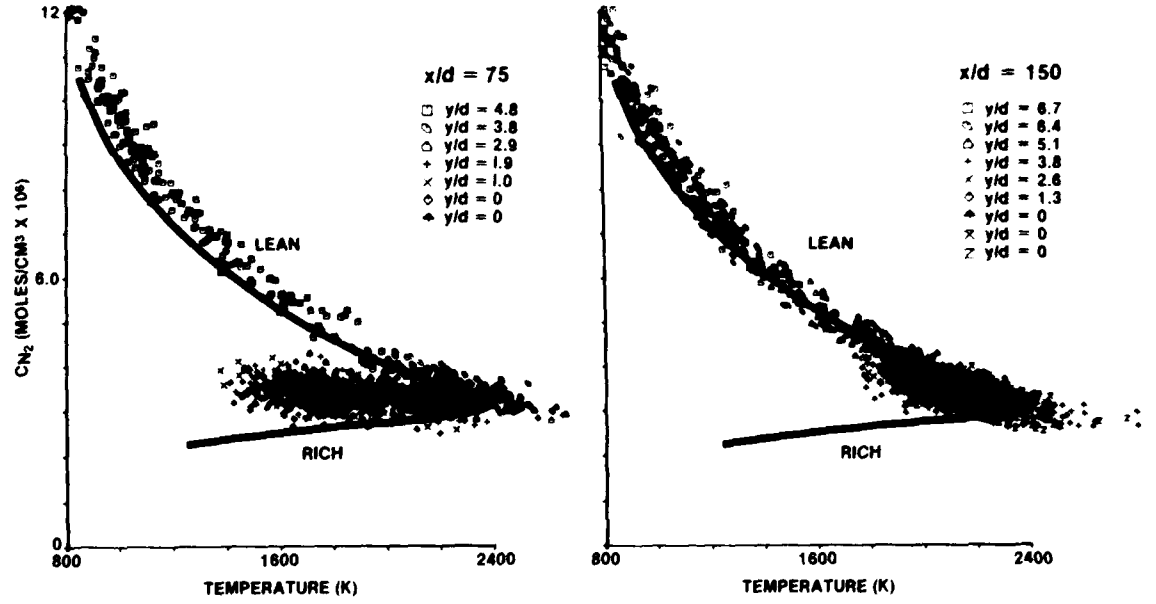

Figure 9. Comparison of Simultaneously-Acquired N_2 Concentration and Temperature Data with Theoretical Curve Calculated for Adiabatic Equilibrium Flame Conditions [58]. These are data sets similar to those contained in the histograms shown in Figures 6 and 7, but, in this case, for x/d = 75 and 150. The stoichiometric point for the theoretical curves, near 2400 K, is obscured by the density of data in this region. Flame buoyancy affects the experimental data by causing them to be translated along the theoretical curve to another locus of fuel/air equivalence ratio points, corresponding to the true flame position. This expectation has been confirmed by observations of data for both positive and negative values of y/d.

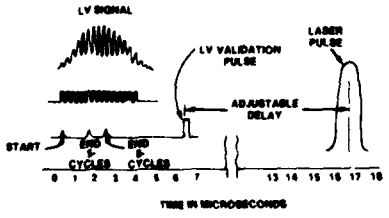

Figure 10. Timing Diagram for Near-Simultaneous Laser Velocimetry and Raman Scattering Data Acquisition [57]. The LV signal is shown both raw and with conditioning. The laser pulse used for Raman scattering occurs after an adjustable delay following validation of the velocity data in the LV processor. This delay can be set to allow slow seed particles to escape from the test volume.

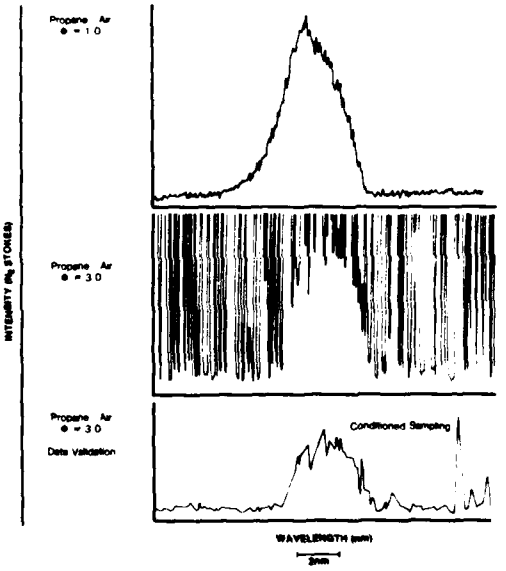

Figure 11. Measurement of Spectrometer Slit Function, for Propane-Air Flames Corresponding to Fuel/Air Equivalence Ratios Φ of 1 and 3. For the middle curve, the spikes resulted from strong laser-induced optical signals. The bottom curve has been treated by conditioned sampling. The spike at the right-hand edge is a laser-induced signal that was not suppressed by the sampling threshold. [58]

DISCUSSION

D.A.Greenhalgh, UK

Does not your conditioned sampling technique unfairly weight PDF's towards lean areas of the flame passing through your control volume because the rich portions will contain higher soot densities?

Author's Reply

Yes, but that is the point of the procedure. We are attempting, by means of the conditoned sampling, to probe a relatively 'clean' part of the flame (that is, lean) under circumstances for which a laser induced luminous portion (that is, rich) can oscillate in and out of the control volume.

G.Alessandretti, It

(1) Do you need the inforamtion on temperature to obtain your measurements of water and hydrogen concentrations?

(2) Could you please comment on your choice of the Stokes/anti-Stokes ratio for thermometry, instead of looking at the different bands in the Stokes spectrum.

Author's Reply

(1) Yes. Temperature information is required because the fractions of the Raman spectral contours for the molecule under question that are contained within their respective spectral band passes of the polychromator, are dependent upon temperature. This is an especially important consideration for molecules such as H_2 and H_2O, which possess very broad Raman contours. Additionally, the total vibrational Raman signal (that is, integrated contour area) is also sensitive to the temperature at flame temperatures, via the vibrational partition function.

(2) We utilised the Stokes/anti-Stokes (SAS) technique for temperature measurement because it produced stronger signals than methods based on analysis of the Stokes profile alone, and because it was well suited for implementation with an available polychromator system. However, analysis of the Stokes contour by means of a multiple spectral channel detector possesses some advantages, even though it does not utilise some of the scattered light (namely the anti-Stokes scattering). Calibrations dependent upon the temperature sensitivity of the contours, which are required because of the fixed slit widths employed in the SAS method, are not necessary with the multiple spectral channel detector. Furthermore, the Stokes and anti-Stokes channels of the SAS method are widely separated spectrally, which can produce additional calibration problems; this type of difficulty does not exist over the relatively narrow spectral extent utilised by the multiple spectral channel detector. Also, analysis of light scattered from gases not in thermal equilibrium is made possible with this scheme.

A.Eckbreth, US

An advantage of the Stokes/anti-Stokes approach is that you spectrally integrate over the Raman band and thus maximise your photon count and minimise errors due to photon statistics. One problem with using an optical multichannel detector for a spontaneous Raman band is that the photon count per spectral interval would be quite low and hence the spectrum quite noisy. Would you comment on that?

Author's Reply

I agree that the Stokes/anti-Stokes (SAS) vibrational Raman scattering method for temperature measurement utilises to the fullest extent the available number of scattered photons and therefore minimises statistical errors. For this reason, as well as others relating to experimental convenience, it has been our choice for our turbulent diffusion flame measurements. That is not to say that multiple spectral channel detectors do not possess some strong advantages for such use. Most importantly, the SAS method depends upon spectral calibrations of the two channels, which can be difficult to make because of the interaction between the test gas temperature sensitive Raman spectral contours and the fixed exit slit widths of the polychromator channels. The accuracy limitations due to lower photon counts with use of the multiple spectral channel detector are certainly present, but are not so severe as to prevent its application. Note that we do not require a full contour analysis to determine temperature in this way. Instead, sections of the contour (N_2 ground state band peak region, peak region for the first upper state band, etc.) can be integrated to give temperature sensitive signals of useful strength.

FLAME TEMPERATURE PROFILES OBTAINED BY THE TWO-LINE ATOMIC FLUORESCENCE METHOD

by
G. Zizak, F. Cignoli and S. Benecchi
CNPM, CNR-Politecnico
via F. Baracca, 69
20068-Peschiera Borromeo,Milano
Italy

SUMMARY

In this work several flame temperature measurements are described, performed by using the two-line atomic fluorescence method (TLAF).
Many kinds of flames were investigated, someone of that were completely mapped. This was made in order to point out that, also with a thermal light source, extensive temperature investigations can be carried out.
Even if it seems that low power sources allow only measurements in laboratory steady flames, the low cost of the system and the simplicity of the data processing confirm the validity of this method.

PREFACE

Several techniques were recently proposed and developed for local temperature measurements by means of fluorescence and Raman signal analysis [1], [2], [3].
High spatial resolution and short time of operation may be generally obtained in this way.
Laser sources are normally employed, because of the low cross sections exhibited by the involved phenomena.
On the other hand, the great available powers allow the investigation of a great part of the interesting combustion systems and, besides, the attainment of other information, like species concentration.
Other techniques exist, which use spectral lamps as light source; the line-reversal method is a well known example of those. In this case only averaged measurements are possible, from which, under particular conditions of symmetry and homogeneity, local temperature can be drawn by means of complex mathematical procedures. Furthermore a thermal equilibrium is requested over the whole flame.
The two-line atomic fluorescence method (TLAF), proposed some years ago by Omenetto et al.[4], may combine the different characteristics of the two branches, being possible to use a lamp and to obtain a local measurement.
Successful applications were made [5] by using the lock-in amplifier, in hydrogen and acetylene laboratory flames.
Being a general result the weakness of the fluorescence signal in comparison of the background noise, the photon-counting technique with synchronous background subtraction was also used [6].
As it will be shown further, this kind of signal processing allows to improve the SNR by increasing the measuring times.

In the present work several flames are investigated and a general conclusion may be drawn: when a lamp is used, the measuring times are, for many important flames, too much long. Hence, in actual combustion systems, difficulties arise, which may not be easily solved. Otherwise if a source with higher energy (i.e. a laser) becomes necessary, other techniques are preferable , being, for istance, not suffering of quenching effects.

GENERAL

The theoretical basis of TLAF are well known and diffusely explained in several works [7], [8] , [9] , hence only a brief description is here reported.
The flame is seeded with atoms of convenient material having a three level atomic scheme in which the transition 01, in radiative way, is inhibited (fig. 1). A light beam of wavelenght corresponding to the transition 02 is sent on the flame and the outcoming radiation, caused by the 2→1 fluorescence decay, is detected (Stokes line). The same procedure is repeated in the opposite direction (anti-Stokes line).
It is obvious that, when the exciting source and the fluorescence intensities are measured, we have an information on the electronic population of the levels and hence, through the Boltzmann law, on the electronic temperature.

The foundamental formula, giving the flame temperature as a function of the measured fluorescence intensities, is:

$$T_f = \frac{V_1/k}{\ln\left(\frac{E_{12}}{E_{02}}\right)+5\cdot\ln\left(\frac{\lambda_{21}}{\lambda_{20}}\right)+\ln\left(\frac{F_{21}}{F_{20}}\right)} \qquad (1)$$

where: E_{12} = spectral irradiance of the exciting source at λ_{12}
E_{02} = spectral irradiance of the exciting source at λ_{02}
F_{21} = spectral irradiance of the Stokes fluorescence
F_{20} = spectral irradiance of the anti-Stokes fluorescence
V_1 = excitation energy of the level 1
k = Boltzmann constant.

The relationship (1) may be assumed valid in thermal equilibrium and without self-absorption, when F_{21} , F_{20} are measured in digital way, while E_{12} , E_{02} are measured in analog way.

A great importance has, of course, the choice of the seeding atoms. Thallium and Indium show good performances [9] in concentration of 100 - 500 ppm.

From the above formula we can see that the error of the flame temperature is depending from two quantities, that is the error related to the measure of the incident radiations and that related to the fluorescence measure. Either these two are, in their turn, influenced by the calibration function of the system, which has to be evaluated very carefully. As far as the measure of the fluorescence signal is concerned, which is in practice the only random error, some further considerations may be done [10]. When the fluorescence signal is detected, we have the superimposition of different kinds of radiations at the same wavelength corresponding to: a) the Stokes (or anti-Stokes) transition, b) the background luminosity of the flame, c) the spontaneous decay of the seeding atoms. Only the first term is the useful signal, the others resulting only in a background noise. A parameter is defined when the photon counting method is used:

$$K = N_s / (N_s+N_b) \tag{2}$$

where N_s is the signal counting rate, N_s+N_b the total counting rate.

When a photon counting technique with synchronous backround subtraction is used, a light chopper drives the up-down scaler. As a consequence, during the up phase N_s+N_b is measured, while during the down phase only N_b is measured. The resulting SNR may be written:

$$S/N = C \cdot \sqrt{\tau} \tag{3}$$

where:
$$C = \left(\frac{K}{2-K}\right)^{1/2} \cdot N_s^{1/2}$$

and τ is the counting time.

Obviously, all the given quantities are valid for either the Stokes and anti-Stokes measurements, and the total SNR is given by

$$\left(\frac{1}{(S/N)}\right)^2_{Tot} = \left(\frac{1}{(S/N_{20})}\right)^2 + \left(\frac{1}{(S/N_{21})}\right)^2 \tag{4}$$

Practical relationships were found which may be used to establish the more convenient counting time for a prefixed temperature precision. In particular, when the SNR is deduced from the following equation, plotted in Fig.2,

$$\frac{\Delta T_f}{T_f} = \frac{T_f \cdot K}{V_1} \cdot \frac{1}{(S/N)_{Tot}} \tag{5}$$

the corresponding counting times are given by

$$\tau_{21} = \frac{R+1}{R} \cdot \frac{(S/N)^2_{Tot}}{C^2_{21}} \qquad \tau_{20} = \frac{(R+1)\cdot(S/N)^2_{Tot}}{C^2_{20}} \tag{6}$$

where $R = C_{20}/C_{21}$.

In this way, under favourable experimental conditions (long term flame stability), it is possible to reach noticeable precision, of the order of less then 1% .
Otherwise at first glance we see that a high precision in the flame temperature requires long counting times, being the anti-Stokes signal generally very low. In effect, in flames with a strong background noise, the involved times are of the order of some minutes.
As a consequence, the TLAF applications may give good results in laboratory flames, owing to their simple structure and stability.

EXPERIMENTAL

The system under test was the flames produced by a 30 mm. multi-hole circular burner, of the type developed at the Fysisch Laboratorium Rijksuniversiteit, Utrecht, The Netherlands (fig. 3) . The burner structure allows to have an inner flame (Φ=20 mm.) and a shield flame, supplied by two separated lines.
The flame had high characteristics in stability, uniformity and reproducibility. The optical set-up consisted in an usual 90° arrangement (fig. 4) . The light source (OSRAM high pressure Xenon lamp 250 W, supplied by a IREM E2X20P electronic power supply), was placed in a home-made housing, furnishing a good position control and high collection efficiency. The trasmitting optics was set in order to have narrow beam in the chopper zone, to minimize the loss of energy and to easily correct the probe volume position. A heat absorbing glass was used to avoid a superheating of the color filter, wich select the useful wavelengths. At the end of the trasmitting line, a spherical mirror was placed to increase the luminous energy in the measuring zone.
The receiving optics furnished a 1:1 magnification on the entrance of MONO 1.
The resulting probe volume was 1x1.5x3 mm.
The fluorescence signal was detected by means of the MONO 1 monochromator (HILGER & WATTS D330) and an EMI photomultiplier (EMI 9863 QB/140), housed in a suitable Peltier-effect cooler (EMI-GENCOM mod. ZD-50). This detection device was characterized by a very low dark pulses rate (100-150 pulses/sec).
A continous test of the lamp emission was made by drawing a portion of the emitted light with the monochromator MONO 2 (JOBEN YVON H20) and the associated PM 2 (RCA 1P28).

The corrisponding signal was recorded on a strip chart (YOKOGAWA F TYPE 3052). This was made because a previous check showed that, in long times experiments, the intensities of the two lines of interest (5350 Å, 3776 Å) changed in different ways, giving a considerable drift in the ratio E_{as}/E_{es} .

The signal processing (fig. 5) was performed by amplification and shaping of the photomultiplier pulses. The d.c. off-set of the amplifier is often controlled to avoid dangerous oscillations around the discriminator threshold. The squared pulses are at last sent to the up-down scaler (LABEN 6318, with display expanded to 8 digits).

All the flames were seeded by Thallium solutions injected in the flame by means of pneumatic nebulization. The Tl concentration was mantained at 500 ppm for each kind of flame.

RESULTS

Several kinds of flames were investigated, with different flow rates and, in some cases, in the shielded and unshielded configurations. In the shielded flames, only the inner part was seeded; these particularly convenient conditions suggested to perform line-reversal testing comparisons.

Four different $H_2/O_2/Ar$ flames were completely mapped, being the features of these very favourable for TLAF applications. The maps consist in six radial profiles at different heights (step 5 mm), starting 5 mm above the head of the burner.

In fig. 6 is reported the map of the flame obtained with flow rates H_2=1/O_2=1/Ar=6 lt/min (nominal flows). An expected increasing of the temperature is present in the external part of the flame; in effect, being the flame rich, a secondary reaction is produced with the surrounding air.
A significant flattening of the profiles is caused by the shield flame (fig. 7) (same flow rates of the inner flame), where the dotted line is referred to the mixing zone and to the shield flame, in which the seeding atoms concentration is due only to the diffusion from the inner. In both these cases the factor K (see eq. 2) was very high (.9 and .3 for Stokes and anti-Stokes respectively), as a consequence the measuring times, for each point, were of the order of a few seconds. The temperatures were in good agreement with the values furnished by the line reversal test.

In fig. 8 and 9 are shown the profiles associated to the same flames, but with flow rates of H_2=1/O_2=2/Ar=6 lt/min. Now the temperatures are increased and the maximum occours on the axis of the burner; this is a consequence of the quasi-stoichiometric ratio between O_2 and H_2 The effect of the shield flame is the same than in the previous case.

The fig. 10 and 11 are referred to air-acetylene flames (air=7.5/C_2H_2=0.5 lt/min). For these the background radiation is very high, especially for the anti-Stokes line. Hence, to obtain a reasonable SNR, counting times of minutes were requested (about 1 and 4 minutes for Stokes and anti-Stokes lines). Also in this case, a comparison with line-reversal temperature gave good results.

A slight enhancement is obtained in a similar flame (fig. 12), produced by an O_2/Ar mixture (flow rates C_2H_2=0.4/O_2=1/Ar=7 lt/min) . A reduction of the quenching effect may explain the different behaviour of the two flames, concerning to the fluorescence emission.

At last an air-propane flame (air=6/C_2H_2=0.2 lt/min) was investigated (fig. 13). In practice no significant differences were noticed with respect to the air-acetylene flames, having in both cases a general deterioration of the signal and long measuring times.

CONCLUSIONS

The investigations described in this work, show that the TLAF applications may give reliable results in a great number of laboratory flame.
Even when a thermal source is used, and the available signals are very low, the photon-counting allows satisfactory precision measurements. On the other hand long measuring times are involved, so that only long term stability flames may be successfully investigated.
Hence, applications on industrial burner cannot be reasonably proposable, and if, to increase the signals, a laser source is adopted, other techniques exist, showing attractive performances.
Finally, special applications like calibration in laboratory flames of other thermometric techniques and basic combustion researches seems to be the only possible fields in which the TLAF method can be conveniently used.

REFERENCES

[1] M. Lapp and C. M. Penney, Laser Raman Gas Diagnostics, Plenum, New York,(1974)
[2] A. C. Eckbreth, P.A.Bonczyk,and J.F.Verdieck, Appl. Spectrosc. Reviews, 13(1), 15-164(1978)
[3] J.D.Bradshaw, N.Omenetto, G.Zizak, J.N.Bower, and J.D.Winefordner, Five Laser Excited Fluorescence Methods to Measure Spatial Flame Temperatures. Part I. Therotical Basis, To be published on Appl. Spectrosc.
[4] N.Omenetto, P.Benetti, G.Rossi, Spectrochim. Acta, 27B, 453-461(1972)
[5] H.Haraguchi, and J.D.Winefordner, Appl. Spectrosc.,31, 195-200(1977)
[6] U.Ghezzi, G.Zizak, A.Coghe, F.Cignoli,and S.Benecchi, AGARD CP-229 (1977)
[7] C.T.J.Alkemade, Pure Appl. Chem., 23, 73-98 (1970)

[8] N.Omenetto, R.Browner, J.Winefordner, G.Rossi, and P.Benetti, Anal. Chem., 44, 1683-1686 (1972)
[9] H.Haraguchi, B.Smith, S.Weeks, D.J.Johnson, and J.D.Winefordner, Appl. Spectrosc., 31 156-163 (1977)
[10] G.Zizak, F.Cignoli, and S.Benecchi, Appl. Spectrosc., 33, 179-182 (1979)

ACKNOWLEDGMENT

Particular thanks are addressed to Aldo Coghe for the precious advice prodigally furnished. (thank to zaif of ek).

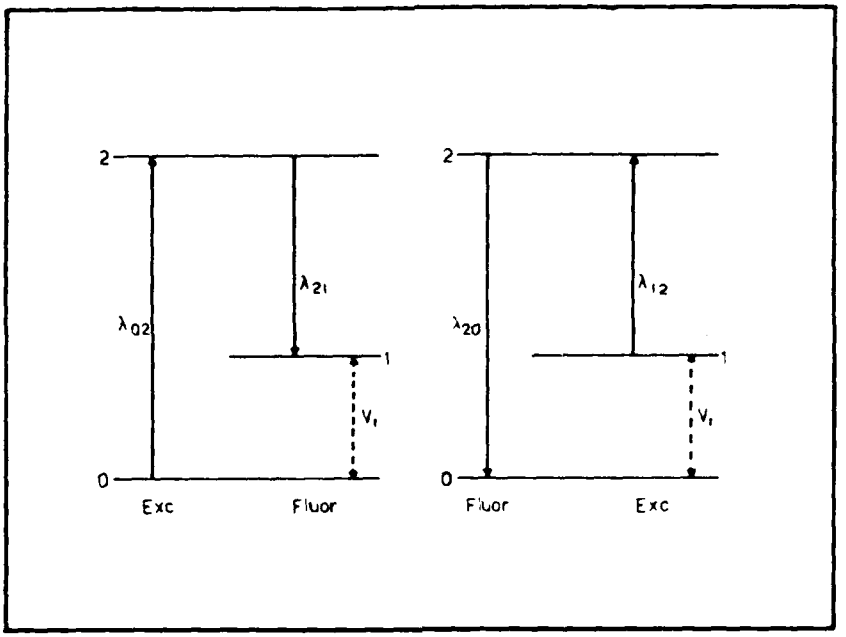

Fig. 1 - Schematic representation of a three level atomic system. For the TLAF method Stokes and anti-Stokes direct line fluorescences are detected.

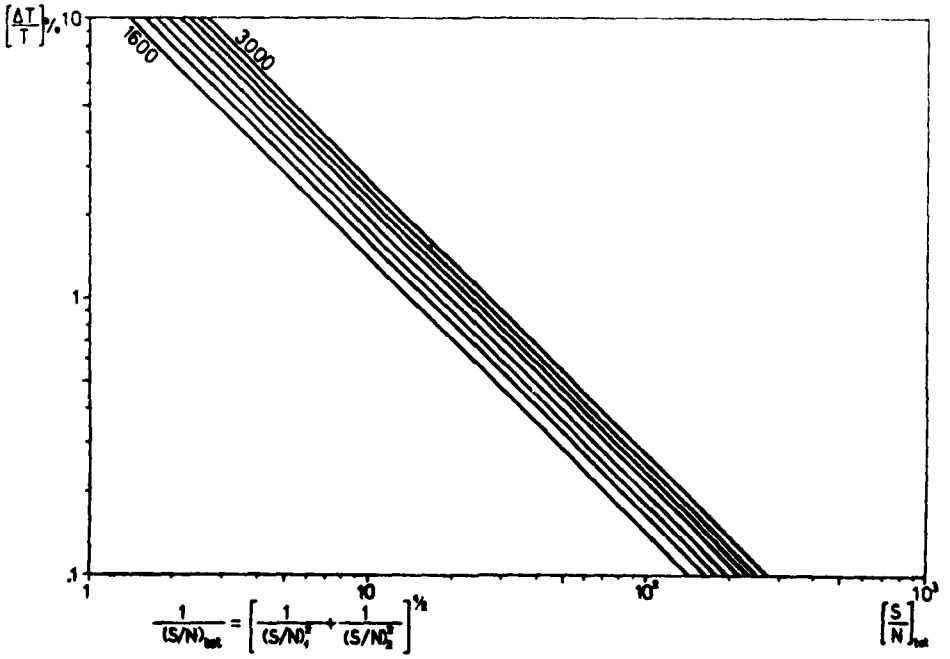

Fig. 2 - Relative error in the flame temperature vs. SNR_{Tot}.

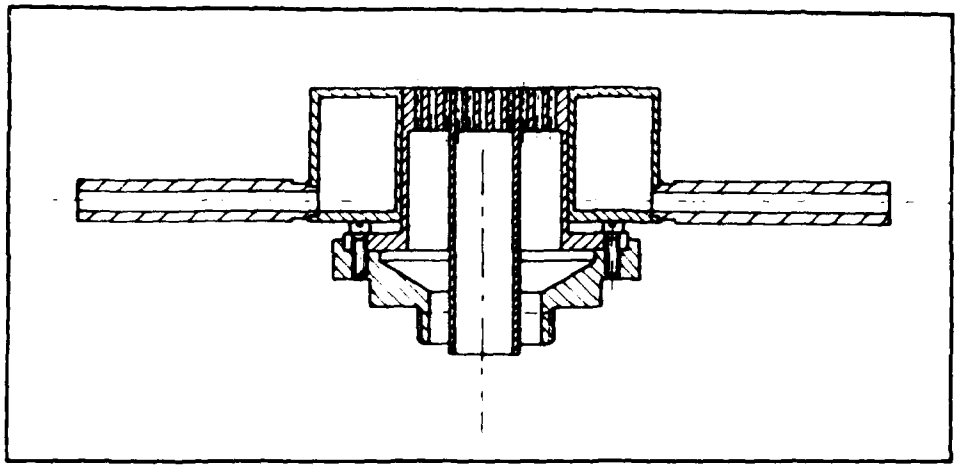

Fig. 3 - Design of the multi-hole circular head of the burner.

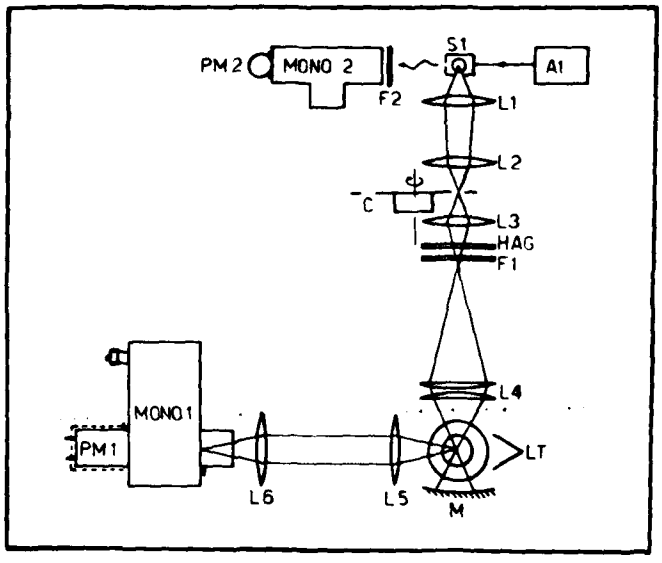

Fig. 4 - The optical arrangement used for fluorescence measurements.

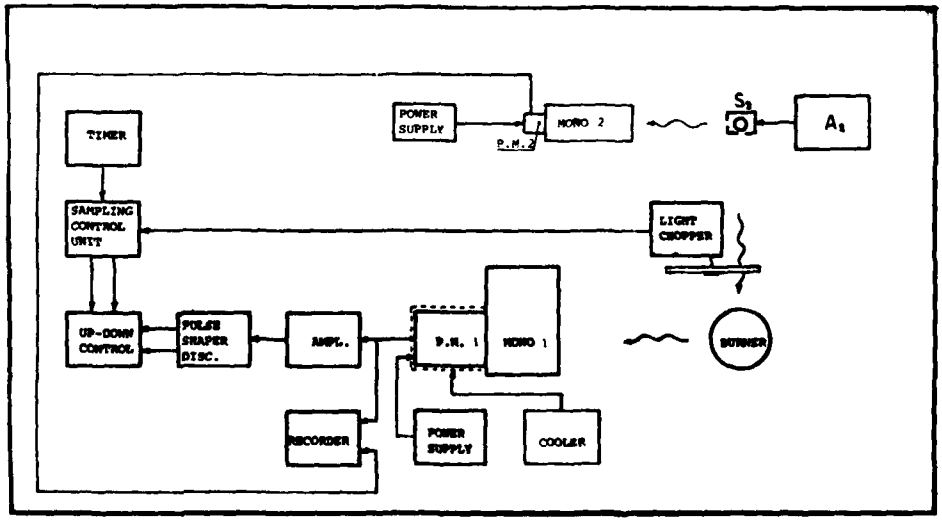

Fig. 5 - The electronic equipment used to perform the experiments.

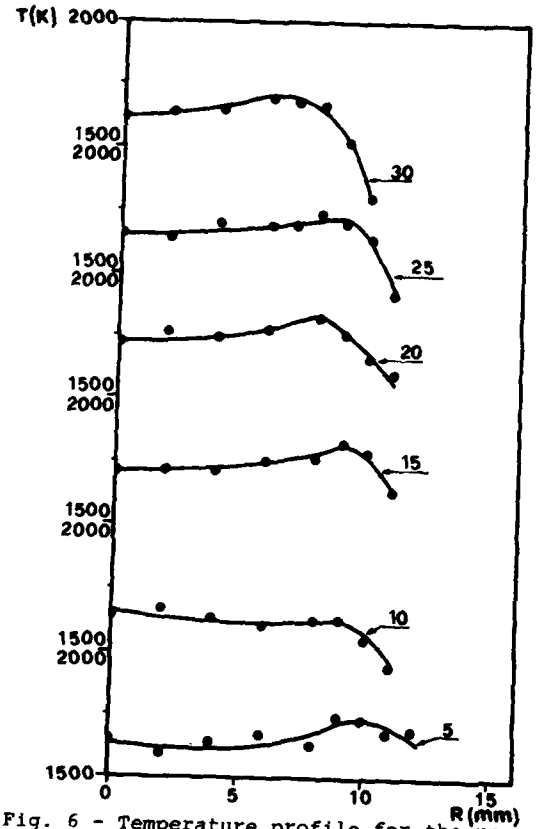

Fig. 6 - Temperature profile for the unshielded flame:
H_2= 1 O_2= 1 Ar= 6 lt/min

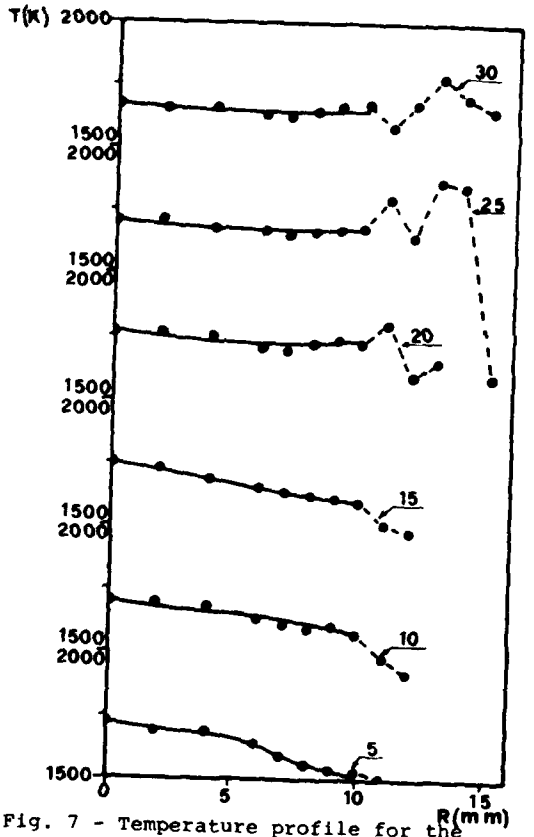

Fig. 7 - Temperature profile for the shielded flame:
H_2= 1 O_2= 1 Ar= 6 lt/min

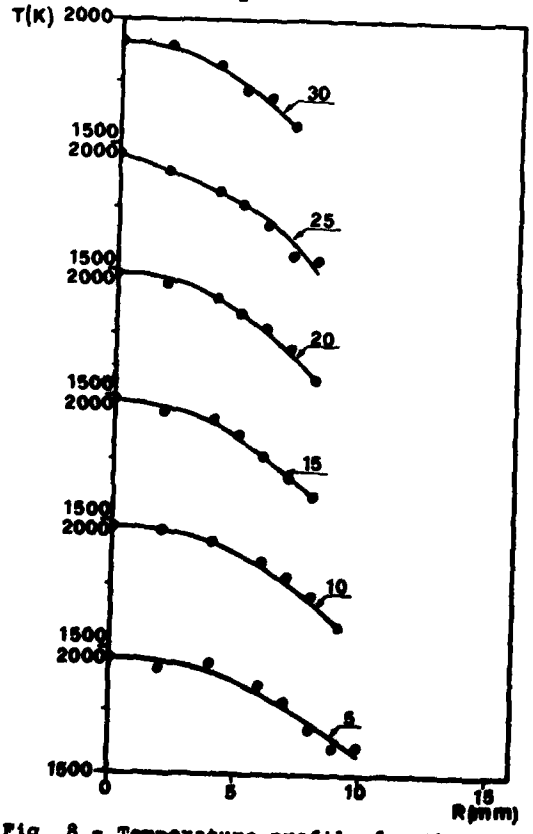

Fig. 8 - Temperature profile for the unshielded flame:
H_2= 1 O_2= 2 Ar= 6 lt/min

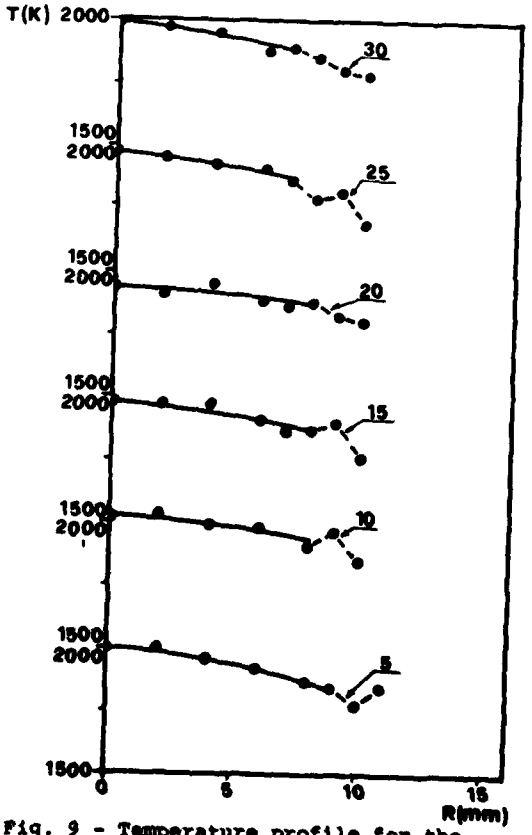

Fig. 9 - Temperature profile for the shielded flame:
H_2= 1 O_2= 2 Ar= 6 lt/min

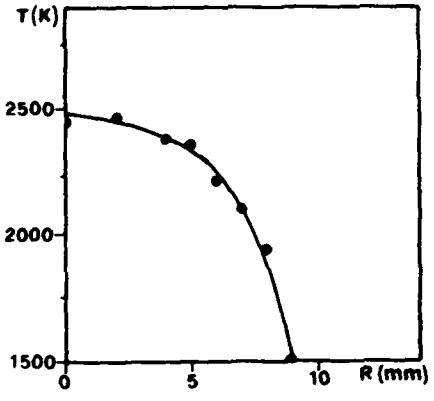

Fig. 10 - Temperature profile for the unshielded flame: air= 7.5 C_2H_2= 0.5 lt/min

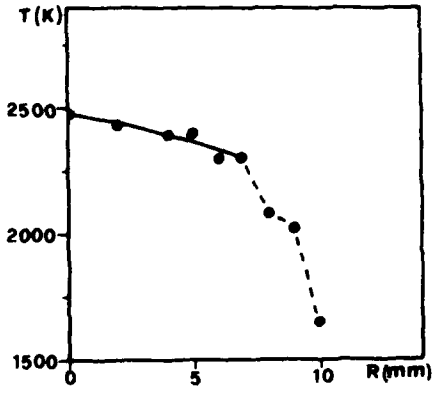

Fig. 11 - Temperature profile for the shielded flame: air= 7.5 C_2H_2= 0.5 lt/min

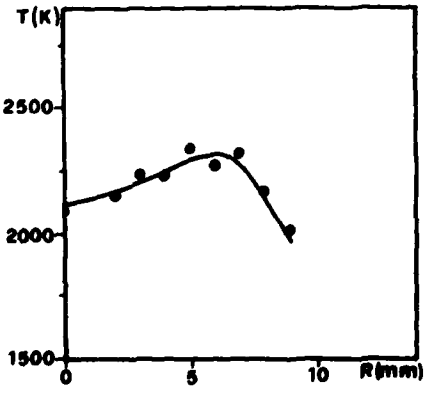

Fig. 12 - Temperature profile for the unshielded flame: C_2H_2= 0.4 O_2= 1 Ar= 7 lt/min

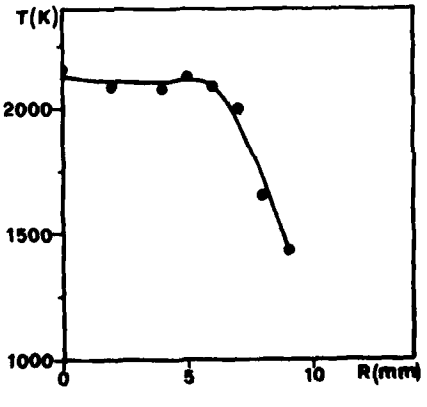

Fig. 13 - Temperature profile for the unshielded flame: air= 6 C_3H_8= 0.2 lt/min

APPLICATIONS OF OPTICAL DIAGNOSTIC TECHNIQUES IN COMBUSTION RESEARCH*

D. L. Hartley
M. A. Gusinow
Sandia Laboratories
Livermore, CA 94550
USA

Summary

This paper presents a summary of the application of laser based optical techniques to the diagnostics of combustion problems. The emphasis of this work has been on the determination of temperature and species concentrations in a combusting environment. The application of these techniques has centered on laminar flames, turbulent flames, particulate-laden flows, and internal combustion engines. In all of this work the constraints of spatial and temporal resolution have been achieved as well as the detection of intermediate species in certain laboratory experiments.

Introduction

The challenge of providing the detailed information necessary to understand combustion devices requires experimental capabilities across a broad spectrum of environments. Prior to the clean air act of the 1960's and the Arab oil crisis of the 1970's, the only information required by designers of combustion systems was an overall measure of gross performance and very little sophistication in experimental methods was required. Today, however, with acceptable performance depending intimately on the many subprocesses involved in the combustion device, the experimental methods must be capable of resolving (with space and time resolution) details which have not previously been attainable with standard methods. Fortunately, some entirely new, sensitive methods have been developed and certain older techniques have been improved to the point that they can now be applied to some of these critical problems.

At the Department of Energy's Sandia Laboratories in Livermore, California, a major new program has been developed to provide the experimental methods necessary for these severe combustion problems. To provide a focus for such a development, the Combustion Research Facility has been established at Sandia Laboratories and will be operational in late 1980. The primary mission of the Combustion Research Facility is to develop advanced diagnostic techniques, improve existing ones, and apply them to critical problems in combustion science over a broad spectrum of applications.

To accomplish the breadth of research goals dictated by design problems in combustion science requires a spectrum of research capabilities with an emphasis on the more sophisticated diagnostic techniques. To this end, in this paper, we will address the required diagnostic capabilities for laminar flames, turbulent flames, particle laden flames, and ultimately for the more severe environments characteristic of actual combustion devices. As shown on Table I, research activities are underway at Sandia Laboratories to develop, apply, and evaluate measurement techniques for velocity, number density, temperature, and species concentrations in a variety of systems. This paper, however, will concentrate primarily on those techniques which have been developed to measure temperature and species concentration and will limit those to laser-based diagnostics.

Application to Laminar Flames

A number of programs are being pursued in fundamental flame research. These studies provide a basis for understanding the isolated fluid mechanic and chemical kinetic processes that are important to combustion. These simple flames also provide test beds for developing diagnostic tools. Temperature measurements in our laminar flame studies have been carried out primarily by the application of spontaneous Raman scattering. Recently Mitchell and Schoenung[1] at Sandia made a careful comparison of the measurements of temperature obtained by thermocouples and by spontaneous Raman scattering using the Q-branch spectrum of nitrogen. Their results demonstrate that the degree of accuracy that can be provided with these laser-based scattering methods is excellent. Even more recently Stephenson[2] has measured temperature in this type of flame by using the complex spectrum of CO_2. The calculated and measured CO_2 spectrum is shown in Fig. 1 and in some cases can provide an even more accurate measure of temperature than the simple nitrogen vibrational Q-branch spectrum. Figure 1 also illustrates the degree to which one can match computed spectra to measured spectra for complex molecules like CO_2. Stephenson has done similar calculations and measurements for the nonlinear water molecule as shown in Fig. 2. Smith[3] has used Rayleigh scattering in an atmospheric pressure diffusion flame to deduce temperature profiles with high temporal resolution. The significantly larger cross-section for Rayleigh scattering allowed sufficiently fast measurement to resolve fluctuating elements of the laminar diffusion flame under study. Yet another method of obtaining temperatures in these flames has been pursued by Cattolica[4] who has used two-line molecular fluorescence to obtain the temperature of OH in reacting flows.

*This work supported by U.S. Department of Energy under Contract DE-AC04-76DP00789.

Finally, Mattern, Rahn, and Farrow[5] have demonstrated an improved method of applying CARS to reacting flows for temperature measurements.

In a chemically reacting environment, measurements of the gas temperature and the concentrations of various species cannot always be accomplished independent of each other. Invoking the assumption of local thermodynamic equilibrium (LTE) allows the measurement of temperatures without an explicit measurement of species concentrations. The temperature can then be determined from the shape of the spectrum and does not require absolute measurements. Concentration measurements, on the other hand, typically require absolute measurement unless only relative concentrations are desired. In many cases the measurement of concentration may also require independent determination of the temperature since temperature does effect the spectral shape and, depending on which portion of the spectrum is being detected for concentration measurement, this temperature effect must be considered. By carefully choosing the detection bandpass and spectral location, however, this temperature effect can often be reduced to negligible values.

Several examples of optical concentration measurement have been performed in our program. As discussed above, Stephenson has been using Raman scattering to measure the temperature and relative concentration of complex combustion molecules such as CO_2 and water vapor. Similarly Miller and Setchell[6] have demonstrated that spontaneous Raman scattering can be used to measure concentrations of nitric oxide in ammonia-oxygen flames where the NO concentration varied from 0.1 to 1% of the ambient atmospheric mixture. Figure 3 shows typical relative concentrations of nitric oxide plotted as a function of local temperature for the ammonia oxygen flame. The results clearly demonstrated a super-equilibrium concentration of nitric oxide existed in the system.

A method of obtaining total atomic abundances in a reacting flow has been pursued by Schmieder[7] who showed that by using laser pulses of sufficiently high power it is possible to cause a complete avalanche breakdown of combusting gases, dissociating all the molecules and producing a small volume of very hot plasma. Spectroscopic analysis of the emission from this spark shows characteristic atomic and ionic lines whose intensities are related to the atomic abundances. Figure 4 shows the results of applying this technique to the measurement of the constituents of the fuel-air distribution in a methane-air flame. The abundances of nitrogen and oxygen from the air and carbon from the methane fuel are clearly resolved as a function of position in the flame.

Most of the techniques discussed above have clearly been shown to be useful for the measurements of major species in reacting flows. A more challenging problem, and one which is of critical importance to the combustion scientist, is the measurement of minor and intermediate species (such as radicals) in these flows while still maintaining the sub-millimeter spatial resolution that will permit measurements within the flame front.

To achieve these measurements, laser fluorescence, laser absorption, and background subtraction CARS has been successfully applied to simple flames. Using the frequency-doubled radiation from a tunable dye laser Cattolica has explored the spatial variation of the intermediate, OH, in methane-air flat flames.[8] Figure 5 shows typical results of the OH concentration in the post-flame region obtained by laser absorption. Cattolica has also used laser induced fluorescence of OH as an alternate diagnostic for the measurement of its concentration.

Because of the spatial resolution constraints imposed by a flame at atmospheric pressure (a very narrow reaction zone), Green[9] has pursued detailed studies of flame structure in a low pressure flat flame utilizing laser absorption. Figure 6 shows typical absorption spectra of the NH_2 radical as measured in a low-pressure ammonia flame using a cw tunable dye laser. Finally, Rahn has extended the CARS technique to the precise measurement of flame species by developing a polarization technique[8] which eliminates the nonresonant background and greatly increases the detection capability (signal/noise) of conventional CARS. Recently, Farrow[10] has made a crossed-beam version of polarization CARS which results in high spatial resolution and detection sensitivity. Figure 7 shows a spatially resolved spectra of CO from the highly luminous region of a premixed methane-air flame. The ability to detect and precisely measure this species in such a hostile environment is a major step forward in the application of nonlinear optical spectroscopy to combustion studies.

Application to Turbulent Diffusion Flames

An important project which has been pursued at Sandia Laboratories is the measurement fluctuating parameters in a well-characterized turbulent reacting flow field. To this end, the turbulent diffusion flame facility, shown in Fig. 8, has been developed, and diagnostic techniques for measuring fluid velocity, temperature, and species concentration within the flame have been demonstrated. The present goal of the investigation is to obtain the cross-correlation of fluctuations of velocity and density and the cross-correlations of velocity and temperature within a confined round turbulent reacting jet. Figure 9 shows results obtained by Rambach[11] et. al. utilizing laser Doppler velocimetry to measure the flow-field velocity characteristics of that flame. Both the mean and fluctuating values of the velocity are plotted on the figure. Rambach is now using a two-dimensional LDV system to measure auto-correlations of velocity fluctuations in two directions. In a parallel effort, Dibble[12] et. al. have utilized Rayleigh scattering to measure temperature fluctuations in a round turbulent diffusion jet. Figure 10 shows measured probability distribution functions (pdf) of temperature in the flame and also show the mean and fluctuating values of temperature as a function of radial position in the flame. The application of Rayleigh scattering to measure temperature profiles

in this combustion system required a special fuel mixture of methane and hydrogen which produced a constant value of Rayleigh scattering cross-sections for the fuel, the oxidizer, and the combustion products. This allows the Rayleigh scattering signal to be related directly to density without any concern for variations in the Rayleigh cross-section for different combustion species. Dibble is currently using a high powered dye laser to obtain time-resolved Raman measurements of both temperature and species concentration in the turbulent diffusion flame.

Applications to Particle-Laden Flows

In a separate but intimately related project, Wang and Flower[13] are developing techniques which can be utilized in particle-laden flow fields. These studies are directed toward the measurement of temperature, species concentration, and particulate number density in flow fields characteristic of gases existing in coal-fired combustors and gas turbine systems. The bulk of this activity to date has dealt with particle sizing methods. Recent results by Flower, utilizing background subtraction techniques with spontaneous Raman scattering, have successfully demonstrated that spontaneous Raman scattering can be applied in some cases to measure species concentrations in the presence of relatively high densities of particulates. Some of the nonlinear optical techniques being investigated and developed by Rahn and Farrow also look very promising for application to these particulate-laden flowfields.

Two important facilities are being constructed at our laboratory to aid in the further development of these diagnostic techniques in particulate-laden flows. The first, the atmospheric pressure combustor exhaust simulator facility (ACES) has been built and is operational. The particulate sizing methods of Wang and the background subtraction Raman scattering system of Flower are presently being adapted to this facility. A new facility is the pressurized atmosphere combustor exhaust simulator (PACES), which is capable of providing 2 lbs/sec of air flow at 10 atmospheres of pressure and will be installed in the new Combustion Research Facility. Both of these facilities will be utilized for further development of diagnostics pertinent to "dirty" flows.

Application to Internal Combustion Engines

The role of Sandia Laboratories in the DOE engine combustion technology program has been to apply laser-based diagnostic techniques to the study of critical problems in advanced i.c. engine concepts. Specifically, the studies have been directed toward investigating the problems which arise in DISC, direct-injected stratified charge; DHC, dilute homogeneous charge; and diesel engines. A simplified version of these systems is the high pressure combustion bomb which has been used by Dyer to study a variety of diagnostic methods for application to the combustion processes within i.c. engines. Flow visualization techniques have been used to investigate sprays and mixing patterns as well as flame spread patterns in i.c. engine-like environments. Laser velocimetry has been utilized to measure the velocity field with and without combustion. Rayleigh scattering has been applied to the measurement of density, temperature, flame speed, and flame structure in the combustion bomb. More recently Mie scattering and extinction techniques have been used to measure particulate size and number density for highly sooting situations in the combustion bomb.[14]

Laser Doppler velocimetry (LDV) has been used[15] to map velocity fields, including mean values and turbulent fluctuating values within homogeneous and direct-injected stratified charge engines. Witze[16] has compared LDV and hot-wire anemometry. The results provide the first step in model validation for two-dimensional computational techniques which are being used for the prediction of combustion processes inside this class of engine. In order to understand the more intimate details of fuel injection and mixing, Johnston[17] has applied cw spontaneous Raman scattering to measure the fuel-air distribution inside an operating version of this engine. The first series of measurements were directed toward mapping the space and time resolved values of the fuel-air distribution during and after the injection process in the highly swirling environment that had been mapped by Witze. Typical results of the fuel-air distributions compared to flow visualization results are shown in Figure 12. Regions of lean mixture were observed which would not ignite and this was further verified by dynamometer tests using the same engine. More recently this technique has been applied to the measurement of the fuel-air distribution in the gap of a spark plug inserted in these engines.[18] The goal of this experiment was to determine the inflammability limits of fuel-air mixtures inside engines and to deduce any time-dependent or transient effects which might influence that inflammability limit. Figure 13 shows a typical plot of the ignition probabilities compared to measurements of local equivalence ratio by Raman scattering in that engine.

In a parallel experiment, Smith[19] has used a high powered laser pulse to obtain temperature measurements with spontaneous Raman scattering from another operating version of the engine studied by Johnston and Witze. Spatial and temporal temperature measurements were obtained along with the probability distribution function. Currently, Johnston and Rahn are attempting to apply the cross-beam polarization background subtraction CARS technique to measure species concentrations in these stratified-charge engines.

Conclusions

The major experimental emphasis of the Sandia Laboratories combustion program has been on the continued development of new diagnostic techniques, primarily those utilizing laser-based spectroscopy, where many of the constraints of time and space resolution can be achieved and the demands for intermediate species detection in particulate-laden flows can be satisfied. This technology is clearly no longer in the infant state as existed in the early 1970's. Major advances in laser technology, optical detection and processing, computer availability, and the application of these elements to combustion-oriented problems has created a unique opportunity for scientific-engineering studies. We believe it is timely to tackle the complicated problems facing combustion system designers. It is also our intention that the techniques and research capabilities pursued and developed at the Combustion Research Facility be made available to outside users from government, university, and industrial laboratories.

References

1. S. M. Schoenung, R. E. Mitchell, "Comparison of Raman and Thermocouple Temperature Measurements in Flames," Combustion and Flame 35, 207 (1979).

2. D. A. Stephenson, R. J. Blint, "Theoretical Fitting of Computer Processed Laser Raman Spectra from Methane- and Propane-Air Flames," Appl. Spect. 33, 41 (1979). R. J. Blint, J. H. Bechtel, and D. A. Stephenson, "Carbon Dioxide Concentration and Temperature in Flames by Raman Spectroscopy," JQSRT 23, 89 (1980).

3. J. R. Smith, Rayleigh Temperature Profiles in a Hydrogen Diffusion Flame, Sandia Report, SAND78-8726 (1978).

4. R. J. Cattolica, OH Rotational Temperature from Two-Line Laser Excited Fluorescence, Sandia Report, SAND80-8209 (1980).

5. R. L. Farrow and P. L. Mattern, Background Subtraction CARS with Improved Spatial Resolution, Sandia Report, SAND80-8209 (1980).

6. R. E. Setchell and J. A. Miller, "Raman Scattering Measurements of Nitric-Oxide in Ammonia-Oxygen Flames," Combustion and Flame 32, 23 (1978).

7. R. W. Schmieder, Laser Spark Ignition and Extinction of a Methane-Air Diffusion Flame, Sandia Report SAND79-7288 (1979).

8. R. J. Cattolica, Laser Absorption Measurements of OH in a Methane-Air Flame, Sandia Report SAND79-8717 (1979).

9. R. M. Green, "Laser Absorption Measurements of NH_2 in a NH_3/Air Flame at Low Pressure," Sandia Combustion Research - Annual Report, 1979 (1980).

10. L. A. Rahn, L. J. Zych and P. L. Mattern, "Background-Free CARS Studies of Carbon Monoxide in a Flame," Opt. Comm. 30 (2), 249 (1979).

11. G. D. Rambach, R. W. Dibble and R. E. Hollenbach, Velocity and Temperature Measurements in Turbulent Diffusion Flames, Sandia Report SAND79-8775 (1979).

12. R. W. Dibble, G. D. Rambach and R. E.Hollenbach, "Temperature Measurement in Turbulent Flows via Rayleigh Scattering," Lasers in Combustion, ACS Symposium Series, (1979).

13. J. C. F. Wang, W. L. Flower and D. R. Hardesty, "Diagnostic Development for Advanced Power Systems," ASME Paper 80-GT-128, New Orleans, LA, March 1980.

14. T. M. Dyer and W. L. Flower, "Time- and Space-Resolved Measurements of Particulate Formation During Premixed Constant Volume Combustion," Central States Meeting, The Combustion Institute, Baton Rouge, LA, March 1980.

15. S. C. Johnston, C. W. Robinson, W. S. Rorke, J. R. Smith and P. O. Witze, "Applications of Laser Diagnostics to an Injected Engine," SAE Paper 7900092, SAE Congress (1979).

16. P. O. Witze, A Critical Comparison of Hot-Wire Anemometry and Laser Doppler Velocimetry for I.C. Engine Applications," Sandia Report SAND79-8685 (1979).

17. S. C. Johnston, "Precombustion Fuel/Air Distribution in a Stratified Charge Engine Using Laser Raman Spectroscopy," SAE Paper 790443 (1979).

18. S. C. Johnston, "Raman Spectroscopy and Flow Visualization Study of Stratified Charge Engine Combustion," SAE Paper 800136 (1980).

19. J. R. Smith, "Temperature and Density Measurements in an Engine by Pulsed Raman Spectroscopy," SAE Paper 800137 (1980).

Table I

OPTICAL TECHNIQUES FOR COMBUSTION ANALYSIS AT SANDIA

Parameter / Environment	Macroscopic Features	Particle Velocity	Particle Size	Species Concentration	Temperature
clean flames	V/E	LDV	Mie	sparks fluorescence absorption spon. Raman stim. Raman CARS	Rayleigh fluorescence absorption spon. Raman stim. Raman CARS
"dirty" flames	V/E	LDV	Mie	spon. Raman *stim. Raman CARS	spon. Raman *stim. Raman CARS
turbulent flames	V/E	LDV	--	*spon. Raman	Rayleigh
combustion bomb	V/E	LDV	Mie	---	Rayleigh
engines	V/E	LDV	--	spon. Raman *CARS	spon. Raman *CARS

V/E - visualization-extinction

*experiments presently being implemented

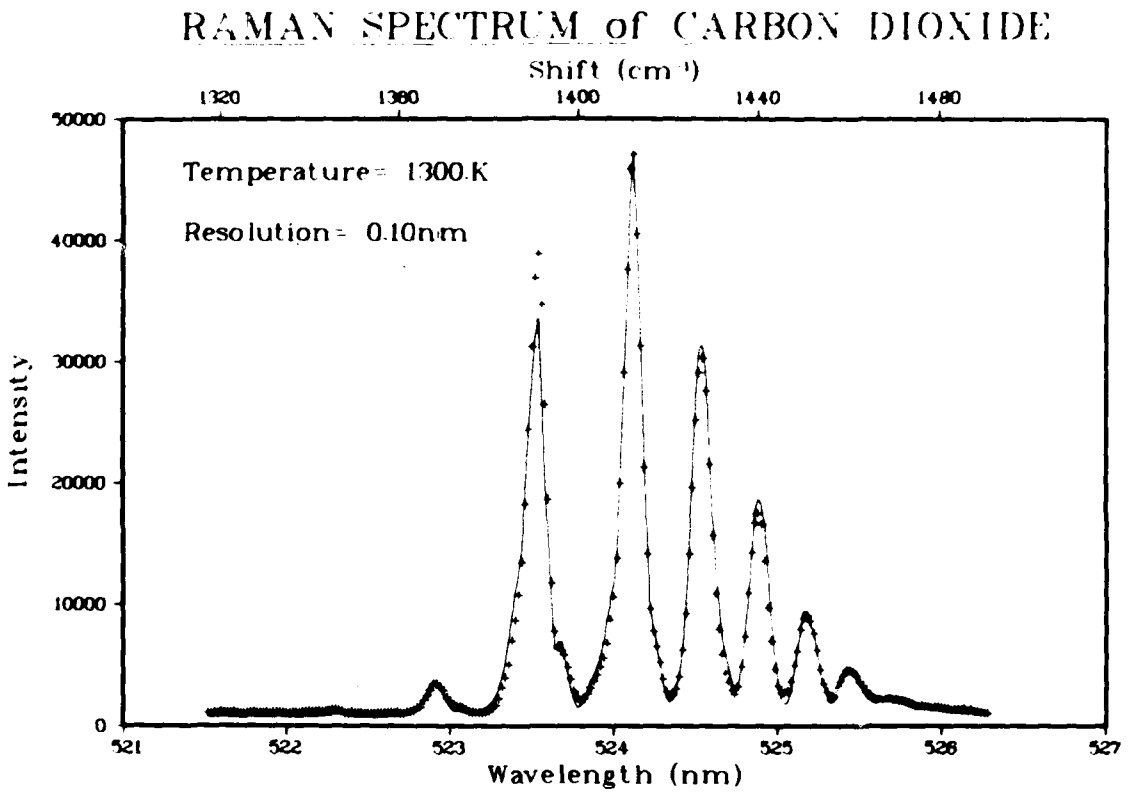

Figure 1: The Raman spectra of CO_2 in a CO/air atmospheric pressure flame.

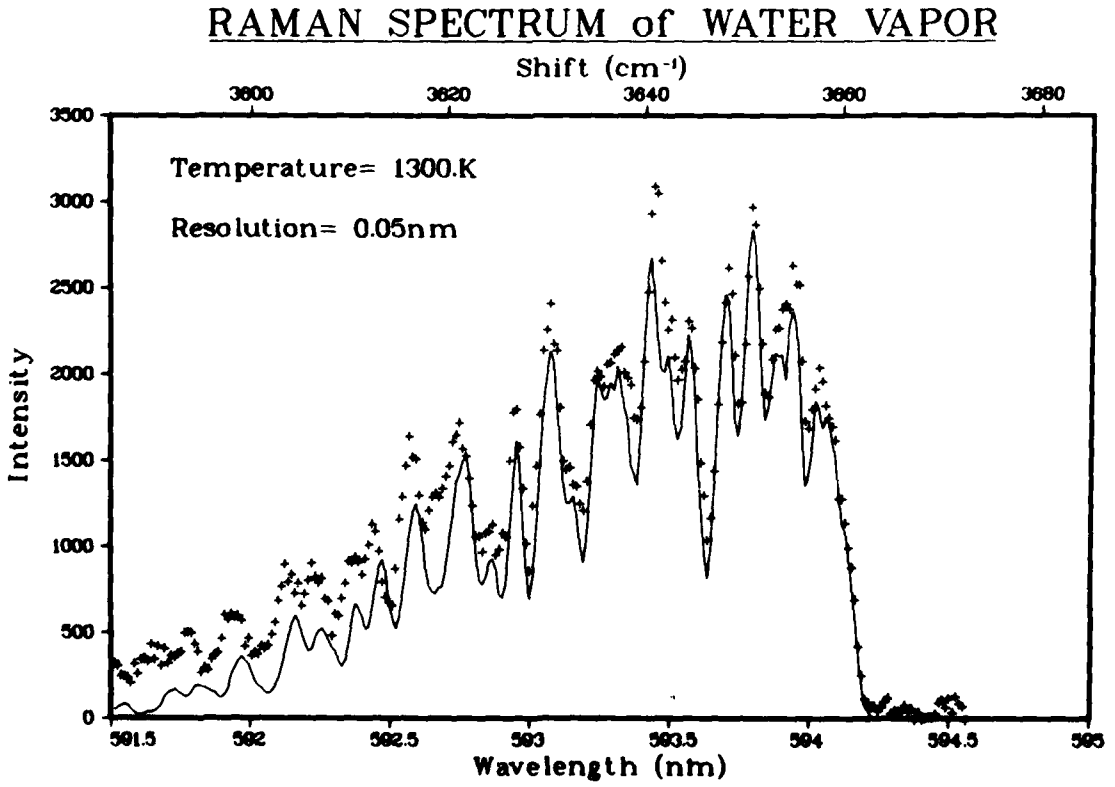

Figure 2: The Raman spectrum of H_2O in a H_2/air atmospheric pressure flame.

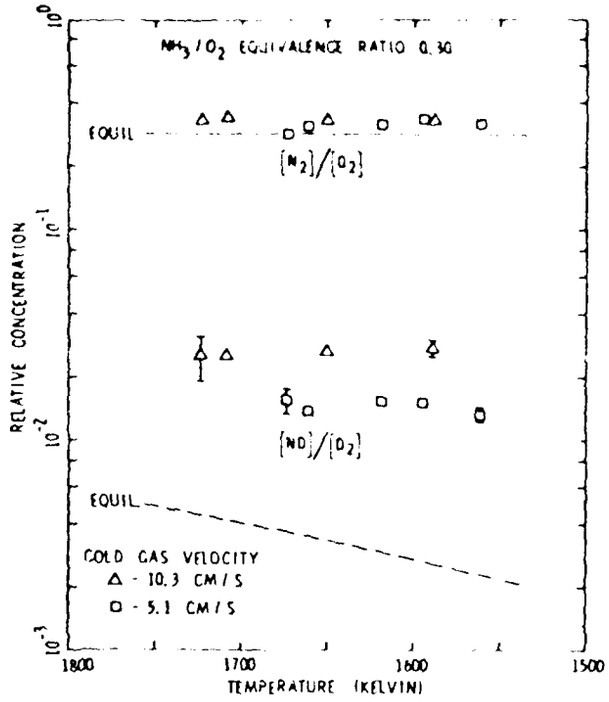

Figure 3: Raman measurements relative concentration of N_2 and NO in an ammonia-oxygen flame plotted as a function of local temperature.

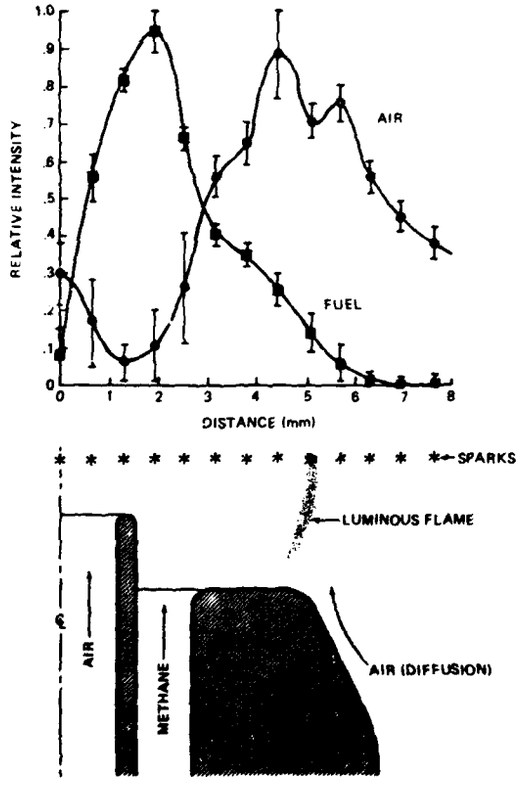

Figure 4: Fuel/air measurements in a methane flame inferred from atomic abundances obtained from spark spectrographs created with a focused CO_2 laser.

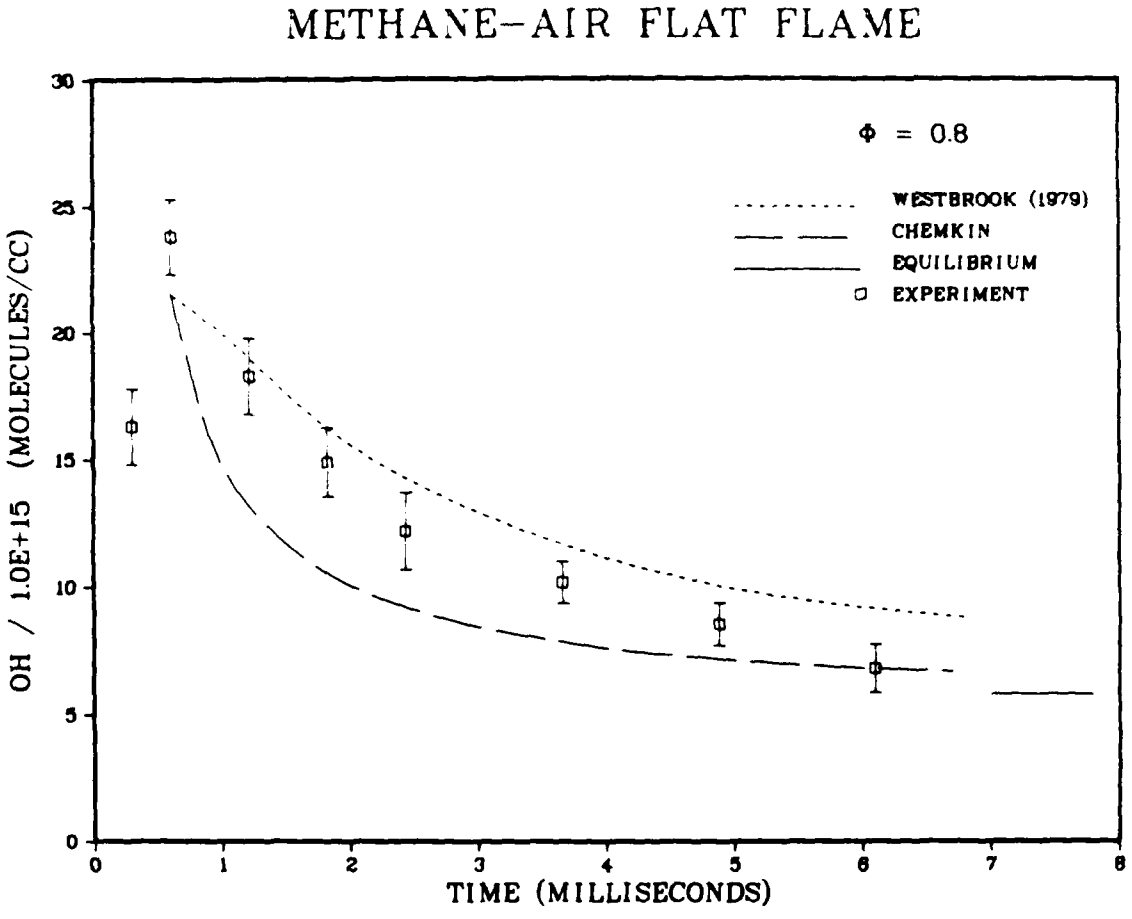

Figure 5: Laser absorption measurements of hydroxyl radical concentrations in the post-flame region of an atmospheric pressure methane/air flame.

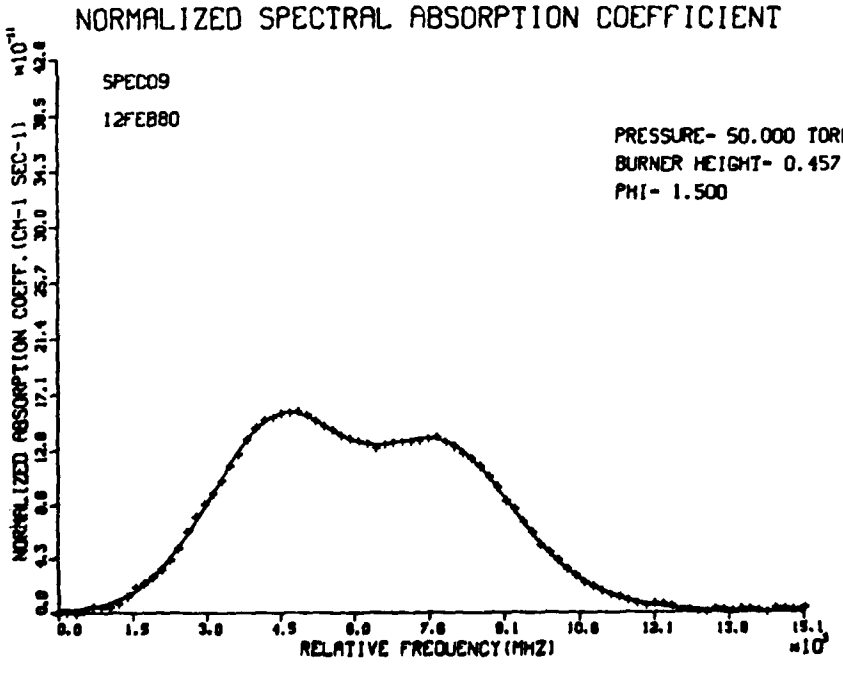

Figure 6: The normalized spectral absorption coefficient for NH_2 in a NH_3/O_2 flame.

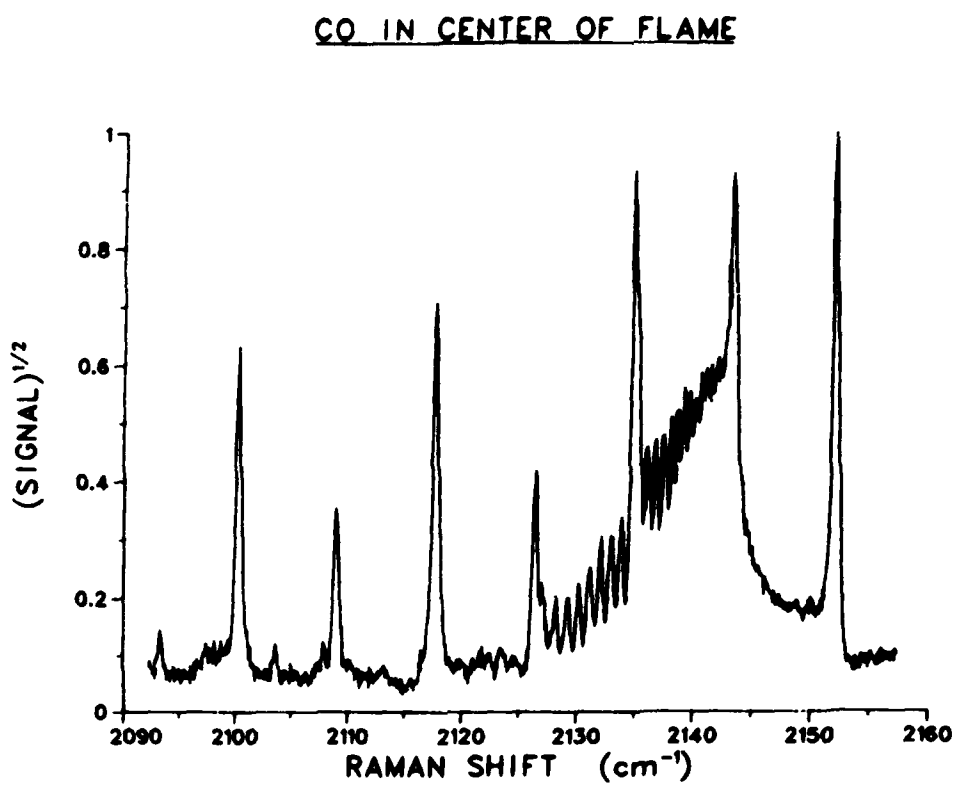

Figure 7: CARS spectrum of CO and N_2 in a rich methane-air flame. A crossed-beam configuration and background subtraction were used.

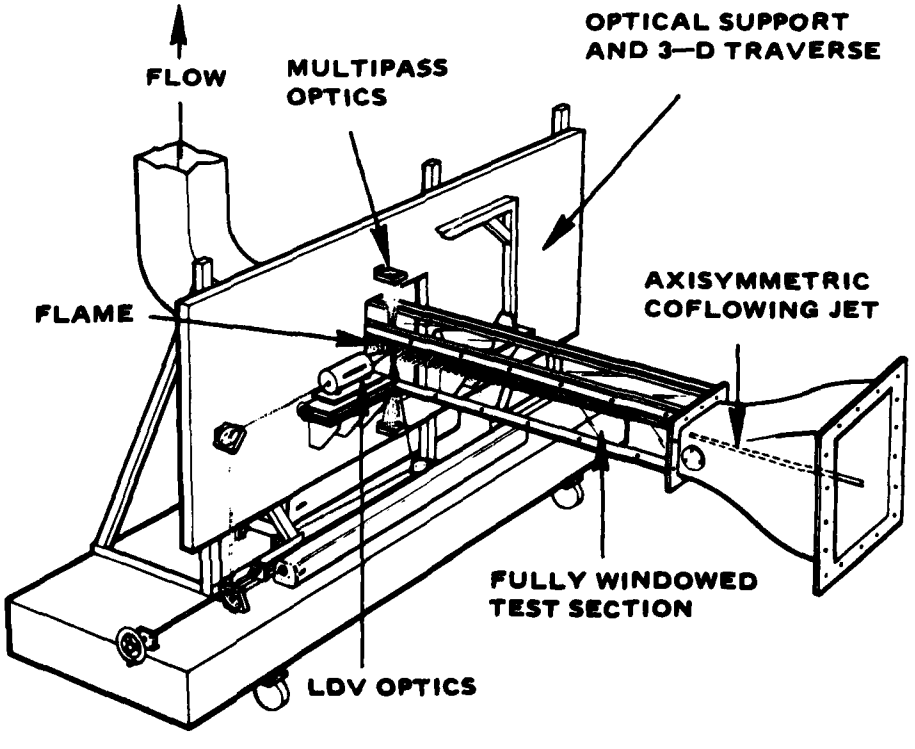

Figure 8: The Sandia Turbulent Diffusion Flame Facility.

Figure 9: Successive frames of high speed shadowgraph movies of reacting, turbulent, hydrogen-air diffusion flame. Velocity ratio = 4.02, Re = 1850, Jet dia. = 4.6 mm, each frame has superimposed visible flame boundary. (a) radial profiles of RMS velocity, (b) pdf's and radial profiles of turbulence intensity, (c) radial profiles of mean velocity.

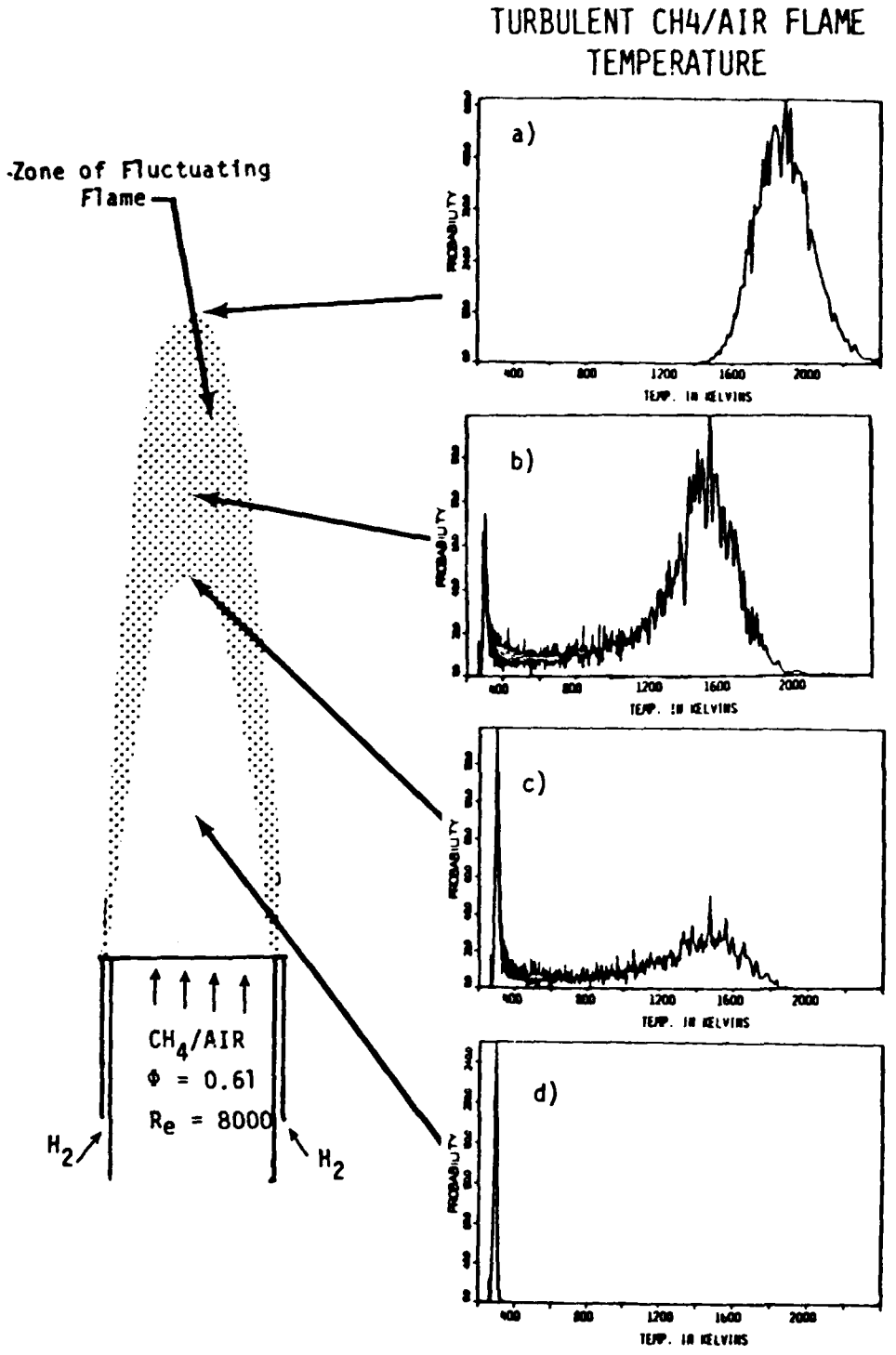

Figure 10: Rayleigh scattering measurements of temperature probability at various centerline locations in the premixed turbulent flame.

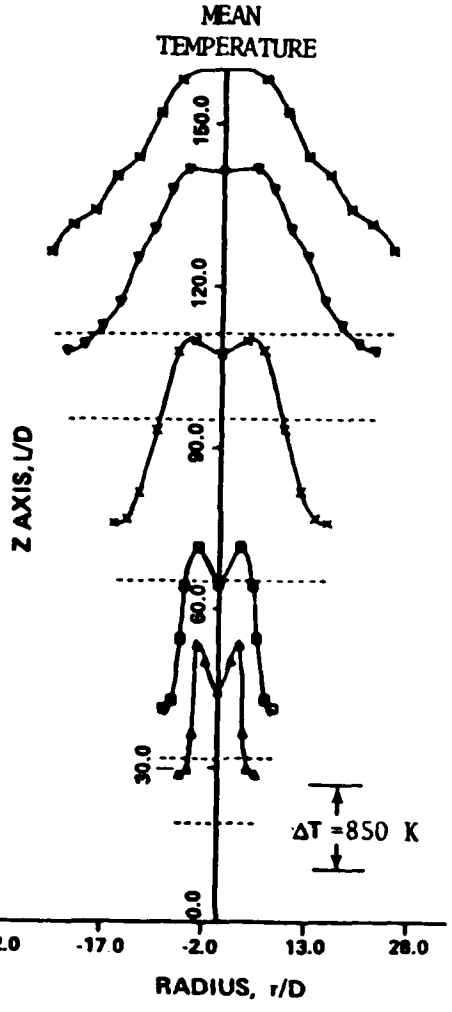

Figure 11a: Temperature profile in turbulent jet diffusion flame. Dotted lines are position of radial traverse.

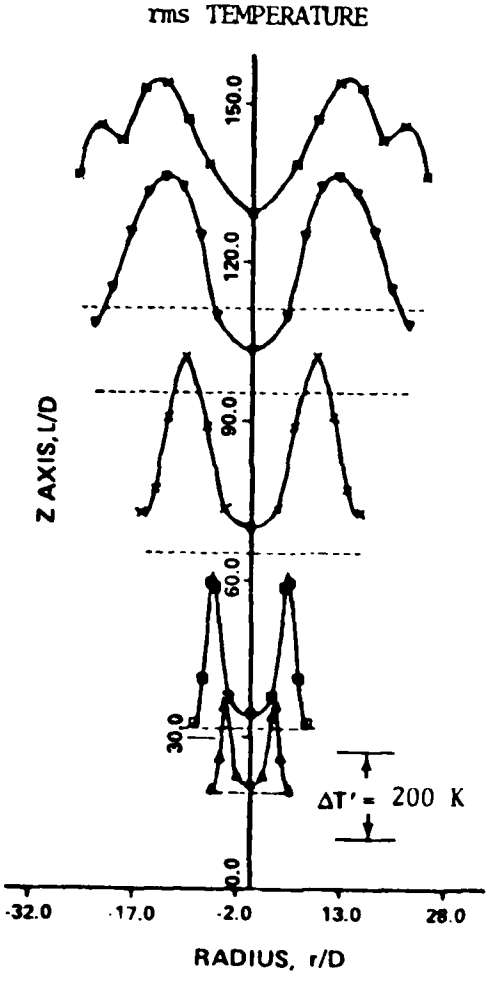

Figure 11b: RMS temperature profile in turbulent jet diffusion flame. Dotted lines are position of radial traverse.

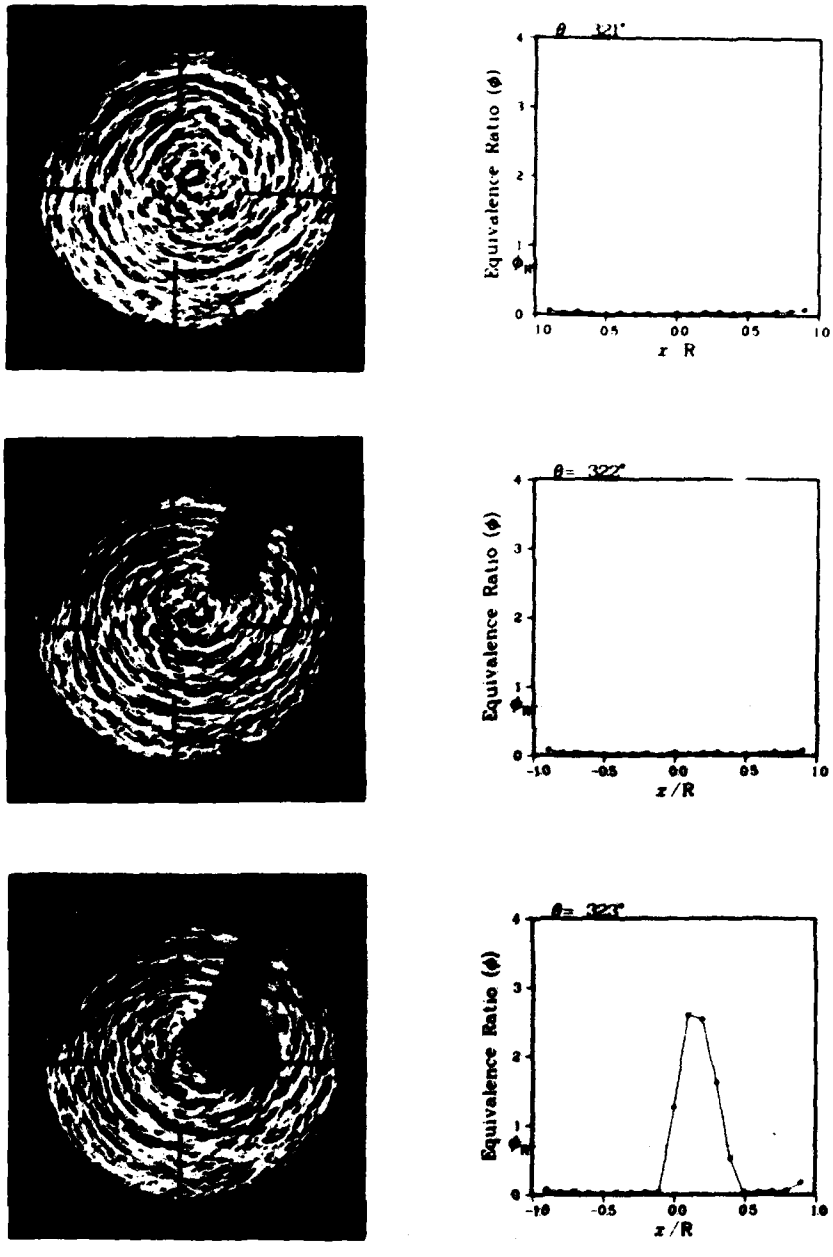

Figure 12: Raman measurements of equivalence ratio distribution compared to flow visualization photographs (shadowgraphs) at different crank angles. Raman data are taken across major horizontal diameter.

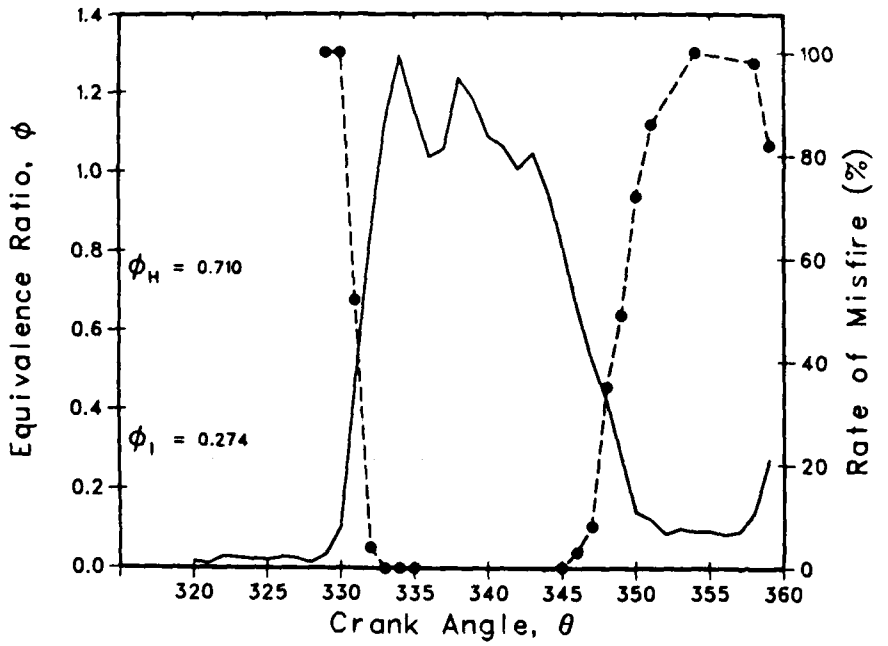

Figure 13: Raman measurement of fuel-air equivalence ratio in the gap of the spark-plug in a Sandia research engine. The equivalence ratio and misfire rate are measured as a function of crank-angle. ϕ_H is the equivalence ratio approached in the limit of complete mixing. ϕ_I represents the ideal inflammability limit obtained under quiescent conditions.

DISCUSSION

G.Winterfeld, Ge

What measuring technique has been used for the determination of the equivalence ratio in the fuel jet injected into the swirling flow inside the reciprocating engine cylinder?

Author's Reply

The way that is done is with the Raman scattering. With spontaneous Raman scattering one can look at the propane and the oxygen, and from that one can establish the equivalence ratio.

G.Winterfeld, Ge

In the investigation of the methane-air diffusion flame, sparks are used to trigger the measuring events. Do these sparks produce disturbances of the processes to be investigated?

Author's Reply

In that particular instance they didn't, but in fact one can contrive an experiment where they do. In fact, if one is not careful, by making a spark one can blow out the whole flame. So yes, it is not a technique we wish to advertise very strongly, it's just to show the variety of things that one can think of.

J.S.Lewis, UK

The measurement of equivalence ratio using Raman scattering was carried out with propane fuel which was fully vaporised. What would be the influence of liquid droplets on such a measurement?

Author's Reply

I can't answer that for you.

DROPLET SIZE MEASUREMENTS IN COMBUSTION BY THE VISIBILITY METHOD.

A. COGHE, C. BRIOSCHI, F. GAMMA CNPM
Via F. Baracca 69
20068 Peschiera Borromeo
Milano Italy

and

U. GHEZZI
Politecnico di Milano
Piazza L. da Vinci 32
20133 Milano, Italy

SUMMARY.

The possibility of droplet size measurements in a flame of liquid fuel sprays by means of the visibility method was already proved by some authors. This method, based on the classical LDV optical system, makes it is possible to extract size information from the visibility of the scattered signal generated by a single droplet crossing the probe volume.

The purposes of this paper are: 1) to present basic principles and numerical results of the theoretical model based on Mie scattering; 2) to present results obtained by experimental tests performed on liquid fuel sprays under burning conditions; 3) to discuss the reliability and the limits of this method, its sensitivity and an impreved data processing prodedure.

1. INTRODUCTION.

It has been shown by many authors (1) (2) (3) (4) that, by means of laser interferometry it is possible, among the other things, to obtain sizing of moving particles, some conditions being satisfied (f.e. spherical particles, refractive index constant and known, particle concentration not too high, etc.).

More specifically these tecniques are mainly based on the introduction of a nondimensional parameter called visibility, wich can be defined starting from the intensity modulation of the radiation scattered by a particle moving in the crossing region.(probe volume) of two laser beams.

Referring to fig. 1 it is well known that visibility can be defined as:

$$V = \frac{I_{max} - I_{min}}{I_{max} + I_{min}} = \frac{D}{P} \qquad (1)$$

The ability of visibility V to be employed in particle sizing comes from the fact that it depends on the particle diameter D, that is:

$$V = V(D, \text{other parameters}) \qquad (2)$$

The relation of eq. 2 between visibility and diameter can be obtained in general by means of Mie scattering theory as in the present case.

As a principle, it is then possible to associate a visibility (or a visibility distribution) to a diameter (or to a diameter distribution).

Beside the diameter, the other parameters in the visibility function of eq. 2 are(fig. 1):

- the wavelenght λ of incident light
- the refractive index m of the particle
- the position of the collecting system (defined by means of γ and φ fig. 1)
- the angle between beams β
- the aperture angle of the collecting system, Ω.

Visibility tecnique seems to be very actractive for particle sizing expecially because it is not intrusive and allowing in situ measurements; moreover no calibration is required.

Also from an experimental point of view it is easier to measure nondimensional signals rather than absolute values (for example intensity of radiation) as required by other tecniques (5) (6).

Moreover there are many problems, both theoretical and experimental, to be solved if relyable results must be obtained.

First of all it is necessary to detect the experimental arrangements most suitable for the spray characteristics (in connection f. e. with the range of diameters, refractive index of the particle, accessibility of the system).

Moreover the relation between visibility and diameter is not an univocal one and it is necessary to arrange tecniques able to solve the ambiguity.

In the experiments it is very important to find procedures able to minimize errors (coming for example from very high concentration of particles, strong background noise as in the case of combustion, etc.).

Moreover tecniques able to control the results should be introduced.

In the case of cold sprays, expecially in small diameter range, a good experience has been gained (7) (8); with sprays in combustion, moreover, very few and only preliminary results have been obtained (9) (10).

This work is intended to contribute with some experimental results to the improvement

of visibility tecnique for particle sizing in not isothermal sprays.

2. AMBIGUITY RESOLUTION.

Fig. 2 shows the characteristic behaviour of a visibility VS. diameter (V - D) diagram.

It can be observed that the V - D relation is not of the one to onetype, that is the same value of visibility can lead to different values of the diameter.

From the point of view of the interpretatcon of the experimental results this represents a rather troublesome problem, also if it is possible to overcome it, at least in principle, by changing the V - D curve, to obtain other informations able to solve the ambiguity.

In many cases what is of interest is not the diameter of a single particle, but a diameter distribution function f(D); this means that with an assigned V - D curve experimentally a visibility distribution function g(V) of the type of fig. 3 is obtained.

The g(V) function is of course the starting point to obtain the required diameter distribution function f(D).

An iterative procedure can be used to find f(D) from g(V), if some information about f(D) are known (mainly the type of function as a rosin-rammler distribution f.e.).

The followed procedure is:

- a temptative diameter distribution function $f_t(\Delta)$ is assigned
- on the basis of the V - D function used a visibility distribution function $q_t(V)$ is calculated
- the experimental g(v) is compared with the calculated one $q_t(V)$
- if the agreement between g(V) and $q_t(V)$ is not good enough, another temptative $f_t(V)$ is assigned
- the interative procedure ends when the agreement between g(V) and $q_t(V)$ is conside.ed adequate.

A lot of numerical tests have been performed to control the ability of the method to give an univolcal answer to the problem (11).

To compare g(V) and $q_t(V)$ some acceptability criteria have been assigned.

The following parameters are here analyzed:

- the absolute value Δ of the difference between the mean visibilities $\bar{V}$ and $\bar{V}_t$, defined as:

$$\Delta = \left|\bar{V} - \bar{V}_t\right| = \left| \int_0^1 V q(V)\, dV - \int_0^1 V q_t(V)\, dV \right| \qquad (3)$$

- the absolute value δ_i (i = 1...N) of the difference of the visibility distribution functions g(V) and $q_t(V)$ that is:

$$\delta_i = \left| q(V_i) - q_t(V_i) \right| \qquad (i = 1,\dots N) \qquad (4)$$

in correspondence of N chosen values V_i of the visibility.

- the mean value of these differencies δ_M defined as:

$$\delta_M = \frac{\Sigma\, \delta_i}{N} \qquad (5)$$

The calculated visibility distribution function $q_t(V)$ is accepted if Δ, the maximum δ_i and δ_M are less than some prefixed values.

Here a rosin rammler type distribution function has been employed for $f_t(\Delta)$ in the iterative procedure.

Extensive numerical tests have been performed to control the stability of the method by changing the $f_t(\Delta)$ function (that is to analyze ff a small change in the shape of $f_t(\Delta)$ function can lead to large changes in the results) (11).

Numerical analysis has shown that a good stability can be achieved and the ambiguity problem overcome.

In particular very good results have been obtained in the determination of the mean diameter of the distribution.

As an example of numerical test it is represented in fig. 4 a distribution function obtained by using this procedure.

Curve A represents the real distribution function f(D) while curve B represents the obtained one $f_t(\Delta)$.

The real distribution f(D) is a parabola and the tenmptative function $f_t(\Delta)$ a rosin-rammler one.

In fig. 5 the visibility distribution function of curves A and B of fig. 4 are shown, while fig. 6 represents the behaviour of the parameter δ_M as a function of the mean diameter Δ_m of $f_t(\Delta)$ distribution.

3. RESULTS IN COMBUSTION.

The experimental tests have been performed in an industrial furnace (mass flow rate of fuel 40 kg/hr) to control the possibility of a practical use of the method.

The experimental set up is shown in fig. 7.

The combustion chamber is whithout heat exchange at the walls has an inner diameter of .8 m, an inner lenght of 1.0 m, and it is equipped with optical windows to allow optical measurements.

A forward scattering configuration has been employed to allow accessibility and also to obtain an optical configuration suitable in the case of large particles.

The visibility VS. diameter curve related to this configuration is represented in fig. 2.

An argon ion laser with 488 Nm wavelenght and at 200 mw power has been used.

The crossing angle of the beams can be changed by means of a continuos beam splitter without modification of the geometry of the system; also the iris aperture of the collecting lens can be changed to modify the collecting solid angle.

The output signal of the multiplier has been amplified and divided in two lines.

The band pass filtered signal has been sended to the burst counter for velocity measurements, while the non filtered one is connected with the oscilloscope.

The filtered signal has also been used to trigger the scope.

In this way only the D.C signals with non zero modulation have been visualized and stored.

Diameter distribution measurements have been made in correspondence of points A, C, E of fig. 7; also mean velocities have been measured here mainly to control the signals.

Diameter distribution functions were calculated by means of the iterative tecnique previously shown, starting from the experimental visibility distribution functions.

The tenmptative distribution function $f_t(D)$ adopted is:

$$f_t(D-D_o) = n\left\{\frac{D-D_o}{\bar{D}}\right\}^{n-1}\frac{1}{\bar{D}}\exp-\left\{\frac{D-D_o}{\bar{D}}\right\}^n \qquad (6)$$

where:

n = characteristic exponent

D_o = initial value

$$\bar{D} = \sqrt[n]{\frac{n}{n-1}}\left(D_{max} - D_o\right) = \text{mean value}$$

D_{max} = max value

As an exapple the experimental visibility distribution function obtained in point A 6f fig. 7 is reported in fig. 8.

The deduced diameter distribution is reported in fig. 9; here also the distributions corresponding to point C and E are represented.

In conditions of combustion a reliability control has been performed by seeding the flame with alumina particles.

The visibility of the seeding particles in the optical configuration here employed was ranging between .8 and 1.

The visibility distribution function in the case od the flame seeded with alumina was measured; f. e. fig. 10 shows the results in the case of point A of fig. 7.

Distribution of fig. 10 should be compared with that of fig. 8; it is possible to observe that the addition of alumina changes the distribution function introducing values of V different from zero also in the .8-1 interval.

This seems to mean that the visibility measurement system is basically correct also in the case of combustion.

Table I summarize the experimental conditions of the tests.

It results from table I that the probe volume is of the order of about 10 mm^3; it is mainly determined by accessibility reasons connected with the geometry of the optical windows.

In the case of a probe volume of such a dimension it is easy to obtain a single Particle scattering signal with particle concentrations till to $10^8 m^{-3}$.

In any case, single particle signals were obtained whitout problems here.

It is note worthy that with more suitable orptical configurations it is possible to work with higher particle concentrations (of the order of $10^{10} m^{-3}$).

From an experimental point of view, to obtain a precise measurement of the visibility it is necessary to be able to select the signals, to accept only those coming from the central region of the probe volume, as required from the theoretical model.

In the case of large probe volumes, as here, the probability of receiving signals not coming from the center of the probe volume increases and also from this point of view some validation criteria should be introduced.

For the acceptability of the signal the following criteria have been here adopted:

- Gaussian shape
- definite number of fringes
- limited range of doppler frequency
- continuos high frequency modulation whitout change of phase
- not ambiguous resolution of the signal from the background D.C. level.

In a luminous flame the background radiation masksthe lower signals increasing the difficulties of correctly evaluating the pedestal amplitude, and then preventing an accurate evaluation of the visibility.

In the present case, to eliminate as much as possible this disturbance, an interferential optical filter centered at the laser wavelenght was placed in front of the P.M..

In large flame it is also necessary to take into account the large gradients of refractive index, caused by temperature gradients, which lead to a deflection of the laser beams.

As a consequence large drop-out in the photo detector signals are observed.

In connexion with this, it could be observed that the reliability test performed with alumina seeding have shown that refractive index gradients do not cause large distorsions in the doppler signal.

4. COMMENTS AND CONCLUSION.

Visibility tecnique for particle sizing seems to be able to be applied in the field of combustion, also if the bad environmental conditions make a reliable data acquisition difficult.

From the theoretical point of view, numerical analysis based on Mie scattering allows to choose the most suitable experimental configurations; also the ambiguity in the correspondence between visibility and diameter can be overcome by means of the iterative tecnique of sec .2.

To obtain this results it is necessary to have some sort of an "a priori" knowledge of the diameter distribution function, f.e. the number of mawima of f(D) to be able to choose an suitable for the iteration.

This does not seem to be a strong limitation at least in the case of conventional nozzle generated sprays, because in this case the main features of the distribution are in general known.

The main advantages of visibility are connected with the fact that this tecnique is not intrusive, it allows in situ measurements and does not require a calibration.

The refractive index of the particle must be known, but it is note worthy that it is possible to find optical configurations in wich visibility is very weakly dependent on the refractive index. (5) (6)

Moreover, a very high spatial resolution can be obtained and, at the same time of particle size, also velocity and concentration can be obtained if necessary.

On the other hand many problems arise in the practical use of the tecnique, wich can limit rather strongly the applicability of the method in some circumstances.

Firsto of all, in an hostile environment as an industrial flame, the signal to noise ratio is reduced and reliability and accuracy of the method deteriorate.

Moreover, the necessity of a single particle scattered signal on the P.M. requires a not too high particle concentration or the use of rather sophisticated experimental arrangements, difficult to be applied f.e. in the case of combustion.

In many cases the application of the validation criteria to control that the doppler signal can be used in connection with the theoretical model is rather intricate and the accumulation of enough data to have a good statistics is time consuming, because of the very large number of measurements necessary to obtain a reliable visibility distribution.

The application of validation criteria is also difficult to be automatized, and a visual control is in many cases required to avoid very complicated data acquisition systems.

From the point of view of diameters to be measured, it is possible to extend the range till to about 100 μm.

The upper limit depends on the geometrical configuration of the system and mainly on the dimension of the probe volume.

Also at the side of small diamters problems can arise because of the low amplitude of the scattered signal when compared to background radiation, expecially in the case of combustion.

Concerning the precision of the tecnique it is mainly connected with accuracy both in visibility measurements and in passage from visibility to diameter.

Accuracy of measurements can be critical in the case of small particles because of the background radiation masking the low amplitude signals.

The visibility-diamter passage take place through the visibility VS.diameter curve.

In the regions were the V-D diagram is flat small errors in V lead to rather large errors in D.

Also if the V-D curve is very irregular (with a lot of oscillations f.e.), problems in accuracy can arise.

Another source of imprecision comes from the fact that in general the temptative diameter distribution functions $f_t(D)$ are only approximations of the real one f(D).

In conclusion, however, also if a lot of problems can be found in its application, visibility tecnique for particle sizing in combustion seems to be a promising one, taking also into account the great difficulties of all the available experimental tecniques in such a bad environment.

5. REFERENCES

1. Farmer,W.M., Applied Optics, 11, 11, pp.2603-2612 (1972).
2. Robinson,D.M., and Chu,W.P., Applied Optics, 14, 9, pp.2177-2183 (1975).
3. Adrian,R.J., and Orloff,K.L., Applied Optics, 16, 3, pp.677-684 (1977).
4. Coghe,A., and Ghezzi,U., Proceedings of the Dynamic Flow Conference 78 (Skovlunde: DISA), pp.825-849 (1978).
5. Yule,A.J., Chigier,N.A., Atakan,S., and Ungut,A., J.Energy, 1, 4, pp.220-228 (1977).
6. Swithenbank,J., Beer,J.M., Taylor,D.S., Abbot,D., and McCreath,G.C., Paper 76-69 of the AIAA 14th Aerospace Sciences Meeting, (1976).
7. Anglesio,P., Coghe,A., and Ghezzi,U., Meeting of the Aerodynamics and Oil Panel of the Intern. Flame Research Foundation, Lyon, France, (1978).
8. Ghezzi,U., Coghe,A., and Miot,F., 4th Intern. Symposium on Air Breathing Engines, Florida, USA, (1978).
9. Coghe,A., and Ghezzi,U., Annual Meeting of the American Chemical Society's, Washington, USA, (1979).
10. Farmer,W.M., Morris,R.D., Schwartz,F.A., and Doherty,R.H., University of Tennessee Space Institute, GDTP-79-102, (1979).
11. Brioschi,C., Coghe,A., and Ghezzi,U., CNPM-Politecnico di Milano, RI n.20, (1980).

TABLE 1: parameters of the optical geometry.

Laser power	200 mW
Laser wavelength	488 nm
Beam cross angle	1.16°
Fringe spacing	24.16 μm
Collection angle	0.50°
Probe volume dimensions(1/e)+	x=0.47 mm
	y=46.7 mm
	z=0.47 mm
Fringe number	20
Magnification of the collecting optics	1/2

+Probe volume dimensions are evaluated from the geometrical optics formula.

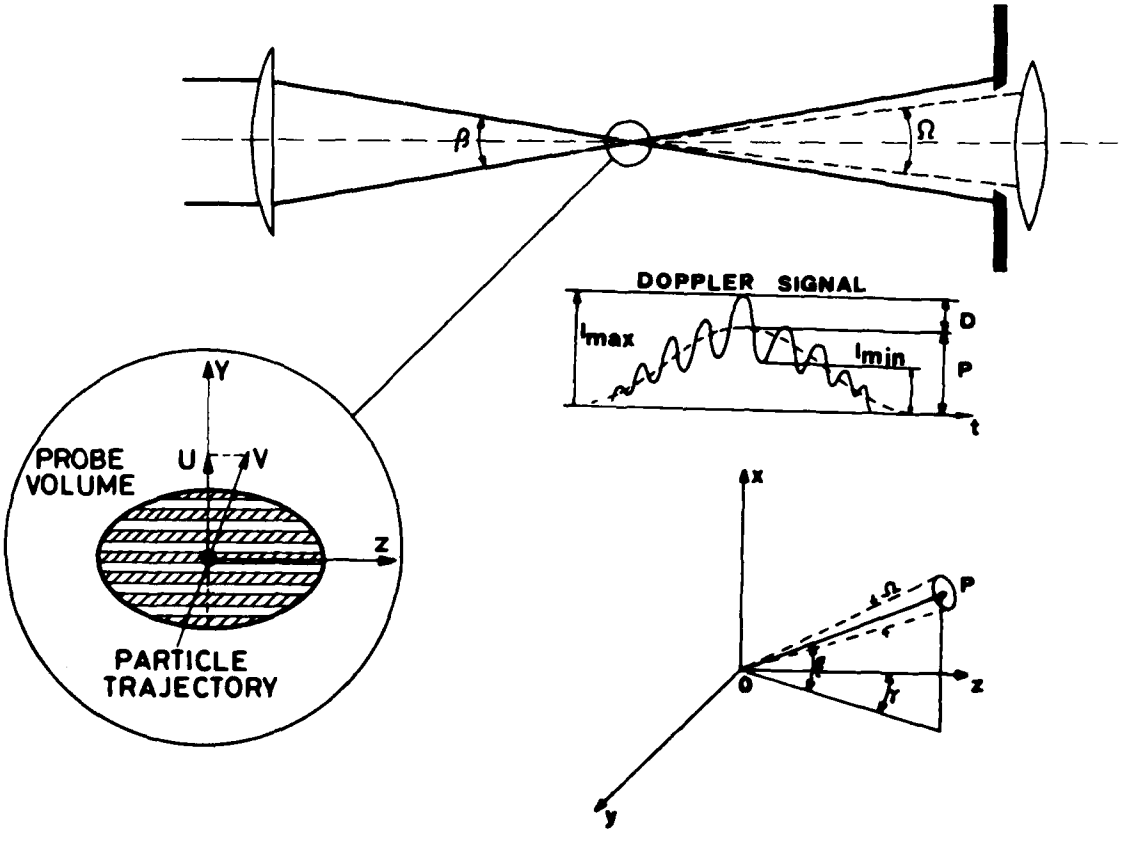

Fig.1 Schematic of the dual-beam interferometer. The probe volume is enlarged to show the fringe system and a typical single particle Doppler signal is drawn. Also the coordinate system used in the theoretical model is shown

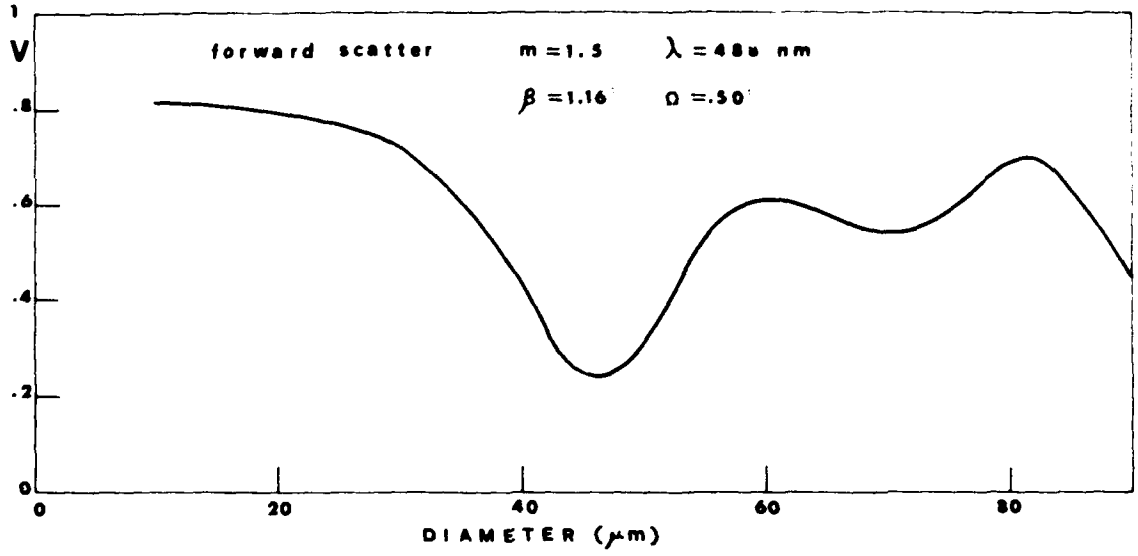

Fig.2 The visibility curve vs particle diameter, corresponding to the experimental set-up used for measurements

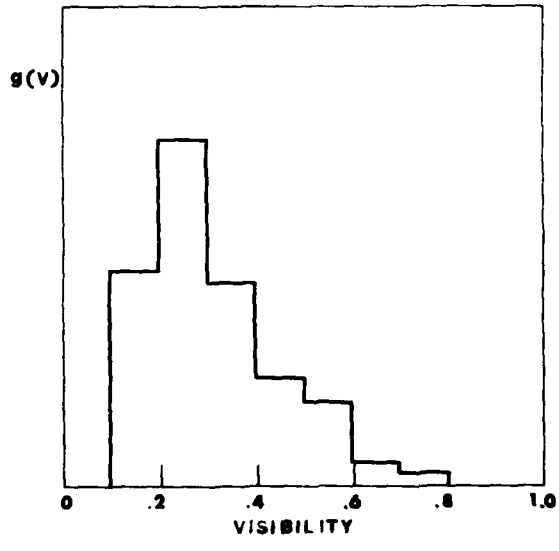

Fig.3 A typical measured visibility distribution

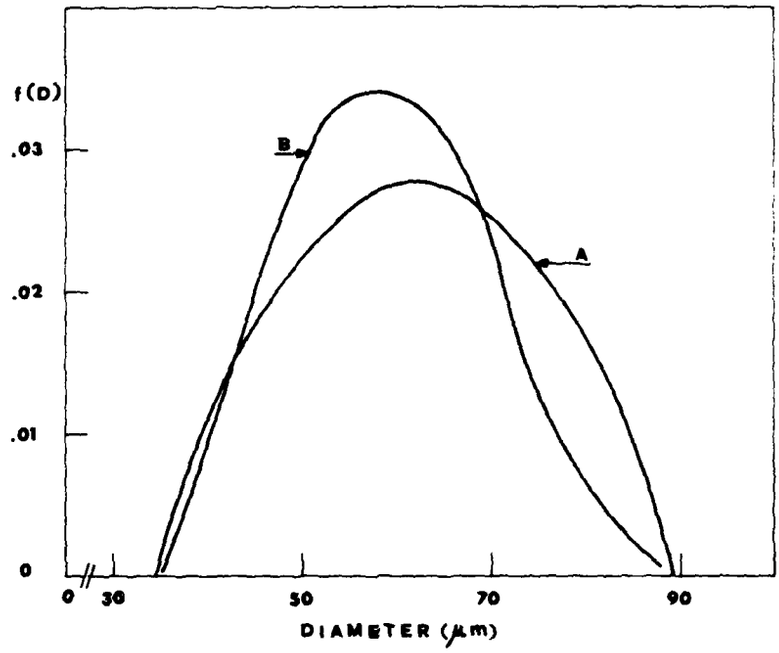

Fig.4 Example of numerical tests: curve A represents the real distribution; curve B represents the obtained one, starting from a Rosin-Rammler type distribution

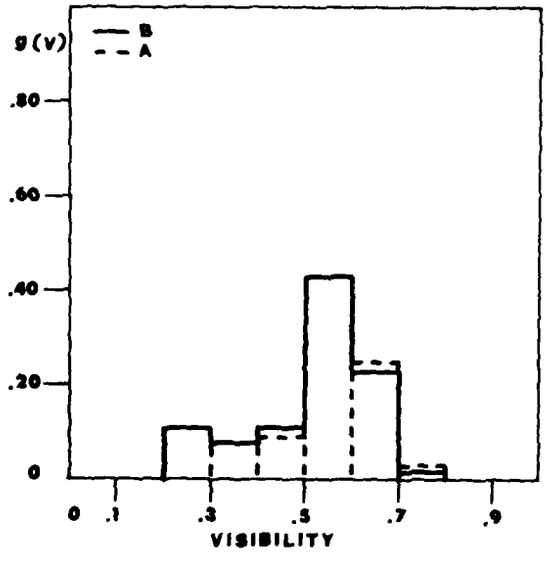

Fig.5 Visibility distribution functions corresponding to curves A and B of Figure 4

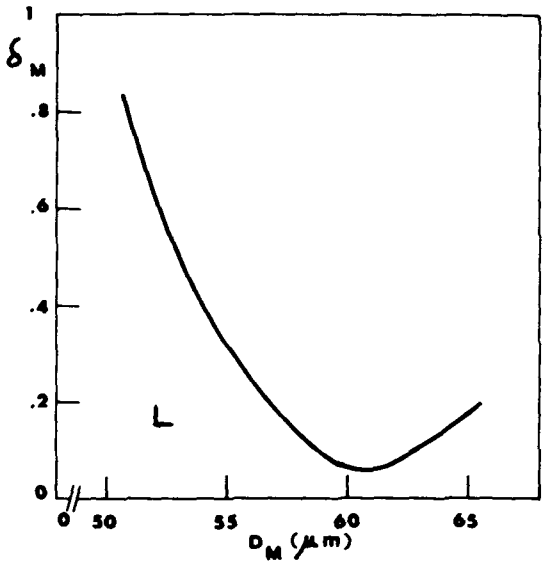

Fig.6 Behaviour of the parameter δ_M vs mean diameter D_M

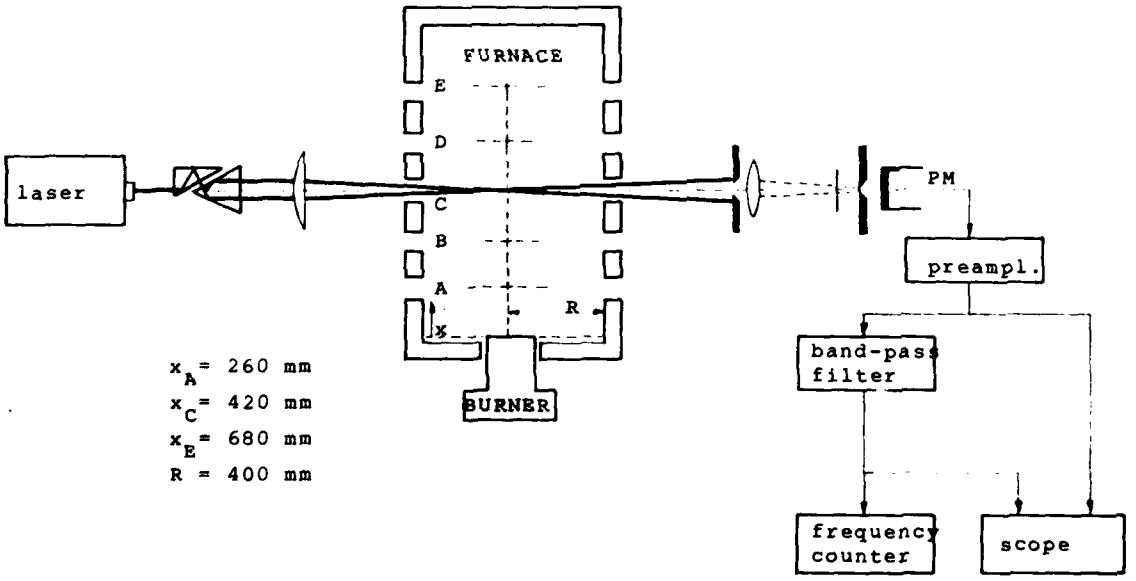

Fig.7 The experimental set-up for the visibility measurements in the furnace

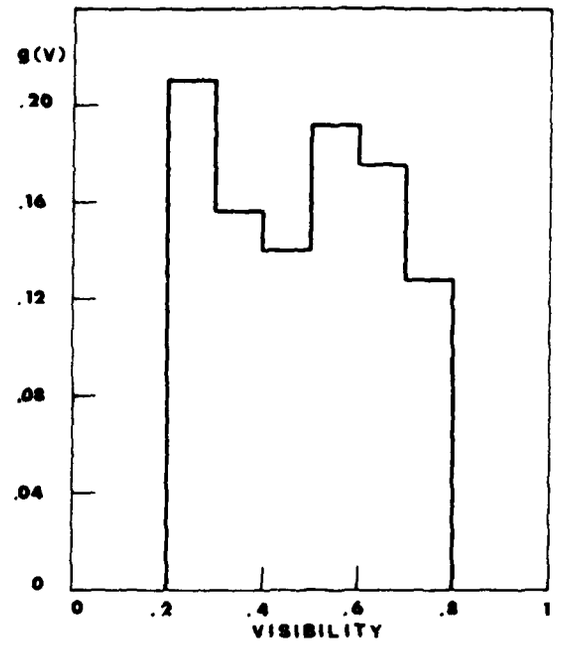

Fig.8 The experimental visibility distributions measured in the point A on the axis of the furnace, shown in Figure 7

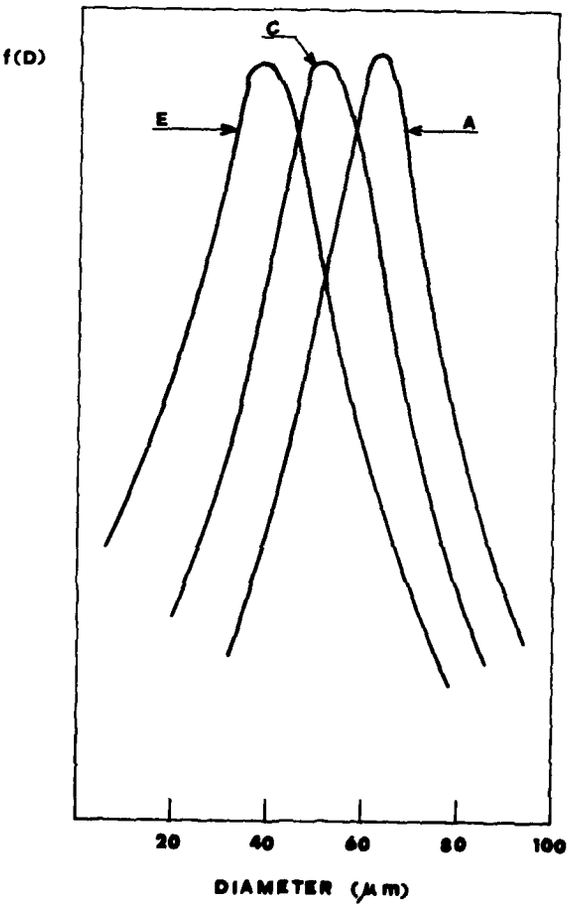

Fig.9 The particle distribution functions deduced for points A, C and E in the furnace

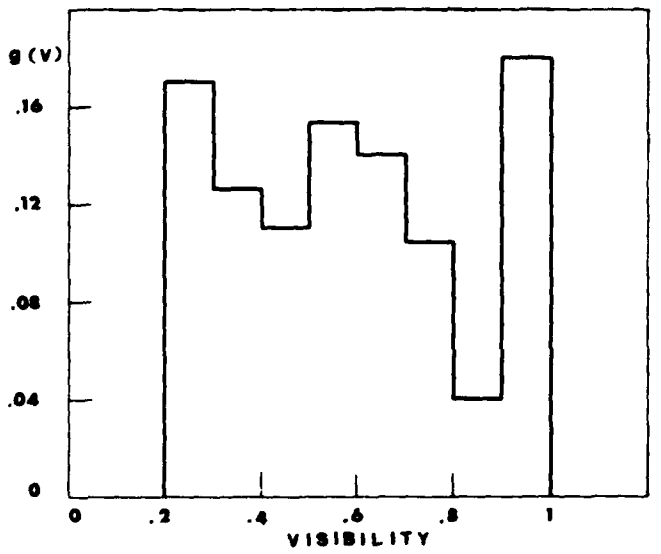

Fig.10 The experimental visibility distribution measured in the point A of the flame seeded by alumina

DISCUSSION

A.M.Mellor, US

Have you directly calibrated the instrument? How large were the alumina seed particles?

Author's Reply

The system has been calibrated by means of alumina particles injected into the flame. In fact, what we have calibrated is the visibility distribution function, to confirm that the data acquisition system is reliable.

Concerning the diameter of the alumina particles, it is in the range 0 to 10 μm. This diameter was chosen because it is able to give a visibility not present in the spray.

A METHOD FOR THE MEASUREMENTS OF MIXING PROPERTIES IN A FLOW

C. Borrego
and
D. Olivari
von Karman Institute for Fluid Dynamics
Chaussée de Waterloo, 72,
B - 1640 Rhode Saint Genèse, Belgium

ABSTRACT

A laser doppler velocimeter (LDV) and a laser-scatter meter (LSM) were used to measure flow velocity and tracer concentration.

To evaluate this new system, tests were carried out on a turbulent air jet of circular cross section exhausting into still air.

The method for measuring certain parameters relevant to the mixing process has been tested involving laser equipment in combination with the introduction of a tracer in the jet in the form of oil smoke.

The flow field was examined at locations varying from two to twenty diameters downstream of the nozzle. Main parameters recorded at each downstream station were : mean axial velocity, mean concentration, fluctuating velocity and concentration and velocity-concentration correlation.

Taking advantage of the laser scatter meter and as a confirmation of their possibilities, this technique was also tested in a much more complicated flow : a model experiment on a release of a heavy gas into the atmospheric boundary layer. A comparison with more conventional methods did allow the validation of both techniques.

1. INTRODUCTION

The detailed knowledge of the mechanisms of diffusion and passive contaminants in turbulent shear flows is essential for the description of many physical processes of practical interest such as dispersion of pollutants and rate at which chemical reactions may take place. Little experimental research has been done in this field due to difficulties in measuring concentration on a real time basis, remotely and with high spatial resolution In the present work, it is demonstrated the feasibility of measuring simultaneously not only the concentration and velocities, but also the correlation between their fluctuating components, an interesting development which may lead to better understanding of the dynamics of the turbulent transport of contaminants and particles (Ref. 1).

The experimental technique used is based mainly on non-intrusive optical detection methods. The technique of light scatter is long-established for the analysis of samples of liquid or gases contaminated by particle suspensions, but its application to the determination of concentration fields is more recent. One of these techniques (Ref. 2) uses fiber optics to generate the measuring volume through which the fluid is allowed to pass. Then the concentration value is obtained measuring either the absorption or the scattering of the light. This technique has two major drawbacks : first it introduces a probe into the flow and hence is a source of distortion; secondly, it does not allow simultaneous measurement of the local velocity. Another technique (Ref. 3) measures light scattered from a sheet or beam of light using a high intensity vapor or arc light as its source. Borrego (Ref. 4) and Borrego & Olivari (Ref. 5) carried the light scattering method a step forward by using a focalized helium-neon laser as light source. In this way, they improved spatial resolution and signal-to-noise ratio.

To evaluate the proposed new system, tests were carried out on a circular turbulent jet, discharging in still air, a simple "reference" configuration for which a considerable amount of results are available. The results obtained are discussed in detail in the next section.

The excellent performances of the system with respect to the expected behaviour and the good agreement with the results obtained by other techniques (when available) suggested that it could be applied to more complex flow situations with a high degree of confidence. As an example of such an application, some results are reported here of measurements made during a model test of the release of a heavy gas in simulated atmospheric boundary layer at ground level. The detailed structure of this flow, three dimensional plume spreading on a rough surface under a turbulent flow field and high negative buoyancy, has up to now not been widely investigated due to inherent difficulties in the measurements required.

2. MEASUREMENT TECHNIQUE

The instrumentation consisted mainly of a laser doppler velocimeter (LDV) and a light scatter meter (LSM). Both systems share a laser light source and associated optics of suitable characteristics and two different detector systems consisting of two photomultipliers and optics which respond to light scattered by particles in a precisely defined region of the flow field. As usual with optical techniques, it is necessary to seed the flow with particles, but for this application care has to be taken to ensure that they will behave in a manner which is representative of the transport properties.

2.1 Velocity measurement

The laser doppler method is based on the measurement of the doppler shift of laser light scattered from the small particles carried along with the fluid. Because of the motion of the particles, the frequency of the scattered light will be shifted by an amount (doppler frequency shift) :

$$f_D = f_s - f_i = \frac{\vec{U}}{\lambda_i} (\vec{k}_s - \vec{k}_i) \qquad (1)$$

where $\vec{U}$ represents the particle velocity in the measuring volume, $\vec{k}_i$ is the wave vector of the incident light which has a wave length λ_i and $\vec{k}_s$ is the wave vector of the scattered light. It should be noted that the relation between doppler frequency and the velocity U is linear; thus, calibration is limited to the determination of the coefficient of proportionality given by the laser wavelength λ_i and the beam intersection angle. A detailed description of the LDV technique and associated bibliography can be found in references 6 and 7.

The operation of the burst-signal processor (single particle measurement or individual realization) used in the present work assume one particle present in the measuring volume at most time.

2.2 Concentration measurement

The technique is based on the measurement of the amount of light scattered by particles present in the flow. When the concentration of particles is sufficiently small, but with many particles simultaneously occupying the measuring volume, the photocurrent contributions from the individual particles add incoherently at the detector surface :

$$I(t) = \Sigma\ I_n(t) \tag{2}$$

where $I_n(t)$ is the detector current caused by each individual particle independent of the others, i.e., the intensity of the scattered light is proportional to the number of particles in the control volume :

$$I(t) \alpha \frac{n(t)}{V_c} \tag{3}$$

where n(t) is the time dependent number of particles, and V_c the measuring volume. With a suitable optical system this volume can be made small enough to be considered as a "point".

It can be shown that the proportionality between the number of particles in the measuring volume and the amount of scattered light becomes a linear relation only for uniformly sized particles under conditions of independent scattering. The criterion for effectively independent scatter by monodisperse spheres is that the center-to-center distance between particles must be larger than 3 radii (Ref. 9), which corresponds to the rather high volume fraction of particles of about 30%. Therefore, this condition of independent scattering can be met using reasonable operating conditions. However, it is quite difficult to achieve uniformly sized particles (Ref. 10).

In order to control the characteristics of the particle motion it is desirable to work only with monodisperse scattering particles uniformly distributed in the fluid. When this is not possible, which is the most usual case, the validity of the previous approximation depends on the average number of particles $\bar{N}$ in the measuring volume at any instant. When $\bar{N}$ becomes too small, the sample may not be sufficient to be typical of the distribution. This is precisely the condition for which ambiguity noise becomes larger; this noise, also called "marker" shot noise, arises from the random arrival of the particles in the control volume (Refs. 3, 8, 11).

Thus, the applicability of the technique depends on the existence of an average number density small enough for independent scattering to occur and large enough for the particle size distribution in the measuring volume to be the same everywhere at any time.

In summary, the difficulty of measuring absolute concentrations should be pointed out because of the difficulty of generating and measuring uniformly sized smoke particles. However, it is much easier to measure relative concentrations and, for the purpose of studying diffusion, only relative concentrations are of interest, provided the absolute concentrations are small and the value at some reference point is known.

3. INSTRUMENTATION AND TEST FACILITIES

3.1 Optical system

A helium-neon laser was used as the light source for all the measurements (λ=0 6328μm and maximum power of 15 mW). To determine the flow velocity field, the forward scatter arrangement was adopted. The optical system consisted of a beam splitter which produced two parallel beams of light, separated by 50 mm; focusing was accomplished with a single lens with a focal length of 180 mm. The measuring volume was roughly 0.12×0.13×1.0 mm^3. The fringe spacing was 2.3 μm which suggests a pin-hole diameter of about 50 μm (Ref. 6).

If the probability that two or more particles are present simultaneously in the measuring volume is negligible, the best signal-to-noise ratio of the doppler signal is obtained collecting a maximum of scattered light from a single particle (Ref. 12). The detector optics is fully able to resolve the interference fringe pattern existing in the measuring volume (this mode of operation is often referred to as the fringe mode). For concentration measurements, many particles simultaneously present on the measuring volume are needed to reduce the fluctuations in light intensity due to non-uniform seeding and therefore, to make ambiguity noise negligible. This precludes the use of the same receiver optics for velocity and concentration measurements. Since the pin-hole of the PM and the incident beams together define the measuring volume, a larger scattering volume for the concentration system was obtained by using a second PM having a larger aperture (500 μm) and smaller magnification. The PM high voltage supply was varied to yield maximum signal-to-noise ratio.

The signal processing system handled simultaneously the outputs from the photomultipliers for the velocity and concentration signals. The doppler signal was first band-pass filtered and processed through a counter type data processor. The output of the counter was connected to a true averager for $\bar{U}$; to an rms voltmeter for $\sqrt{u^2}$ and to one channel of an analogue correlator. The output from the concentration PM was low-pass filtered at 1 kHz and then divided to obtain voltages proportional to $\bar{C}$ and $\sqrt{c^2}$ and to provide a second input to the correlator.

3.2 Test facility

The test facility (Fig. 1) simply consisted of a circular duct supplied with compressed air and discharging to atmospheric conditions through a nozzle of 6 mm diameter. The Reynolds number of the tests was 5×10^4 approximately, based on the nozzle diameter.

3.3 Calibration

If the concentration of particles is sufficiently small, so that both secondary scattering and absorption are insignificant, the output voltage of the PM should be linear with concentration. Under the assumption of independent scattering, it is possible to show (Ref. 3) that the response E of the PM to light scattered by particles inside the measuring volume is a linear measure of the particle concentration.

To check the validity of these assumptions, a calibration was carried out in a wind tunnel having a test section of 120×120 mm² and 1 m long. The velocity could be adjusted to any speed within the range of 0.3 to 1.. m/s. Particles were injected into the flow before the settling chamber, care being taken to ensure a uniform mixing. Since the rate of particles injected was held constant :

$$\dot{N} = \overline{C}_m \, \overline{U}_m \, A \quad \rightarrow \quad \overline{C}_m = \frac{\dot{N}}{A} \frac{1}{\overline{U}_m} \qquad (4)$$

where $\dot{N}$ is the average number of particles injected per unit time, $\overline{U}_m$ is the mean velocity at the center of the wind tunnel test section and $\overline{C}_m$ is the mean particle concentration. The velocity was measured with the LDV.

Figure 2 shows the values of the PM output plotted as a function of the inverse of the velocity for two different injection rates. The results confirm the assumption of linearity indicated above. Care was taken to avoid saturation of the PM and be in the linear region of the calibration curve (Ref. 5). The results show that an accuracy of the order of 2.5% can be obtained in the concentration measurements.

4. TEST RESULTS

4.1 Jet flow

4.1.1 Mean velocity and concentration measurements

The LDV was used to measure mean axial velocity from approximately two to twenty diameters downstream. The mean velocity at nozzle exit was measured with a total head tube. The results are shown in figure 3 plotted in function of r/δ_u, δ_u being the half width of velocity profile : $\overline{U}(\delta_u) = \frac{1}{2} \overline{U}_{max}$.

The mean velocity profiles are found to be similar. A comparison is made in the same figure with two theoretical models for predicting the shape of the mean velocity profiles (Refs. 13 and 14).

The decay of the center line velocity is presented in figure 4 and agrees well with other experimental results. The virtual origin of the flow is located at about 2 diameters downstream of the nozzle. The difference observed with Tollmien's theory (Ref. 13) can be attributed to the predominant effect of turbulence at nozzle exit on the location of the virtual origin (Ref. 15).

The transverse distributions of mean concentration (Fig. 5) show distinct similarity of the profiles after a distance of 8 nozzle diameters fromthe nozzle exit.

The data obtained agree with those measured by Catalano et al. (Ref. 16) and Shaughnessy et al. (Ref. 8), shown in figure 6 with the theoretical model of Prandtl-Görtler-Richardt. This figure also includes the mean temperature profile reported by Abramovich (Ref. 13) for the heated free jet. The fact that the temperature and concentration profiles are substantially similar supports the suggestion made by Hinze (Ref. 17) that there is little difference between the transport of heat and matter in turbulent jet and confirms the experimental results of Timm (Ref. 26).

The variation of the mean concentration along the jet center line is given in figure 7. The virtual origin of the flow, considering the decay of concentration, is located at about 0.8 nozzle diameter downstream. This agrees well with the theoretical model of Prandtl-Görtler-Richardt and with the experimental data of reference 19.

Available results in the literature indicate that the spread of heat and matter is greater than of momentum. Table 1 shows the ratio δ_c/δ_u at various locations. For comparison purpose, this ratio was also computed from data of Corrsin (Ref. 20) and Corrsin et al. (Ref. 21). The present measurements indicate that the value of the ratio δ_c/δ_u remains constant with the distance from the nozzle exit. This would show that matter spreads at the same rate as momentum. Such a hypothesis is supported by the equations governing the two phenomena.

4.1.2 Turbulent intensities

The axial distribution of the turbulent intensity is shown in figure 8 and the concentration fluctuations are presented in figure 9.

Measurements in the outer region of the jet are complicated by the fact that the mean concentration rapidly falls to levels of the order of instrument noise while the fluctuations remain large. The occurrence of fluctuation intensities in the 100% range is evidence of the highly intermittent nature of the flow field in the outer region.

4.1.3 Concentration-velocity correlation

The concentration-velocity correlation coefficient is defined as

$$R_{uc} = \frac{\overline{uc}}{\sqrt{\overline{u^2}}\ \sqrt{\overline{c^2}}} \qquad (5)$$

where u and c are measured at the same point and time. R_{uc} is plotted in figure 10 against the non dimensional radius $r/r_{\frac{1}{2}}$, since the half width of the velocity and concentration profiles, $r_{\frac{1}{2}u}$ and $r_{\frac{1}{2}c}$, have not the same value.

The value of the concentration-velocity correlation is an indication of how closely related the concentration field is with the velocity field. A zero correlation would indicate that the fluctuations of the concentration are totally independent of the turbulent velocity fluctuations (or the absence of fluctuations). This is the case for the profile taken at $x/2r_j = 2$, for $r/r_{\frac{1}{2}} \leq 0.2$.

Considering such a profile, inside the potential core $R_{uc} = 0$ near the center, then it it becomes negative and finally positive near the edge. It reaches a maximum at $r/r_{\frac{1}{2}}$ equal to approximately one, where also both $\sqrt{\overline{u^2}}$ and $\sqrt{\overline{c^2}}$ attain their maximum value. The three conditions correspond to :

- $R_{uc} = 0$: absence of fluctuations near the center. The very small values measured of both $\sqrt{\overline{u^2}}$ and $\sqrt{\overline{c^2}}$ are probably due to imperfect seeding;
- $R_{uc} < 0$: within the region of the jet which has not been contaminated by external air, the consideration developed in equation (4) on the relationship between concentration and velocity would apply leading therefore to a negative correlation between the fluctuations of velocity and concentration;
- $R_{uc} > 0$: the mixing of the entrained air from the unseeded atmosphere surrounding the jet leads to local variations of jet velocity and concentration, which are expected to be correlated. An input, in the mixing process, from air entrained from the ambient atmosphere would influence local velocity and concentration in the same way (decrease) as would, but in the opposite sense (increase), an input from seeded air from the high velocity, high concentration side of the jet.

The measurement of velocity fluctuations at the edge of the jet by means of the LDV needs to be discussed in more detail. The jet is uniformly seeded at the nozzle exit, then downstream the seeded material will correspond exactly with the turbulent fluid, and there will be no seeding in the nonturbulent part exterior to the turbulent/nonturbulent interface. Since the processor holds the last value of the signal each time the signal drops out, the probability density of the velocity will be exactly that measured in the turbulent part of the fluid only, which is observed to differ considerably from that measured in both turbulent and nonturbulent parts (Ref. 27). Since in most flows, intermittency extends deep into the flow, this is not a useful way to measure overall properties. It is, however, an ideal way to measure properties in the turbulent fluid only, which is of considerable interest. Such an application would eliminate the necessity of establishing threshold criteria for the velocity field, always more or less unsatisfactory. The results obtained should be essentially comparable with those obtainable with the hot wire by conditional sampling on a temperature signal, if the turbulent fluid is heated.

This does not mean that the drop out time increases and is so large near the edges as to make the correlation measurements impossible with the equipment used, since it is making analog averages over a long time and $c = 0$ when u is in error.

4.2 Diffusion of a heavy gas in turbulent boundary layer

4.2.1 Experimental arrangement

In this section are reported measurements from a model experiment on a release of a heavy gas into the atmosphere, at ground level. In the case of such an escape, one would expect the dense has to flow down to the ground close to the source and then be carried downwind in the form of a plume with gas concentration decreasing with the distance from the source. The negative buoyancy produced by the high density of the gas would tend to reduce the amount of vertical mixing associated with a ground plume because the vertical density gradient caused by the plume would tend to suppress the turbulence which is responsible for the mixing process which dilutes the gas as it travels downstream. As a result, one would expect the dense plume of gas to mix much less than a normal ground plume and retain high gas concentrations for much greater downstream distances.

Figure 11 shows the experimental arrangement. The characteristics of the background flow, i.e., the turbulent boundary layer, were determined following the usual practice for atmospheric modeling work : the Reynolds number similarity was allowed to lapse. The simulation of the lower third of the atmospheric boundary layer in the wind tunnel (working section : 180 mm width × 350 mm high × 2000 mm long) was achieved from the accelerated growth of an adiabatic boundary layer over a rough surface by the artificially induced mixing of an initial velocity deficit at ground level; the high intensity, large scale turbulence typical of the atmospheric boundary layer was provided using vortex generators.

The diameter of the heavy gas-smoke releasing jet is 4.2 mm placed at 7 mm height and 1000 mm downstream, laid along the center line of the tunnel. Practical considerations necessitates a large release velocity (≈ 18 m/s) compared to the tunnel free stream speed of 7 m/s; then the behaviour of the three dimensional source in the present experiment is expected to be similar to a wall jet.

The measurement chain was identical to that described in § 3.1. The mean values of concentration measured on the plane of symmetry were compared with those obtained with a heat transfer type gas concentration probe (Ref. 28).

Profiles were taken 20-60 jet diameters downstream of the heavy gas-smoke source. The main quantities to be measured in this preliminary experiment to document the velocity and concentration fields are the mean velocity and concentration, the rms velocity and concentration and concentration spectra. Spectra were obtained by the FFT method on a PDP 11/34 computer.

4.2.2 Experimental results

The characteristics of the turbulent boundary layer were determined and found to compare well with full scale data. All these measurements were made with a hot wire anemometer. The turbulence intensity profiles are shown in figure 12 and the power spectral density (at 7 m height) in figure 13, compared with the proposed curve by Davenport (Ref. 29).

Figures 14, 15 and 16 show the means and fluctuating profiles of concentration and velocity at, respectively, x = 20D, x = 44D and x = 60D. The mean concentration profiles normalized with the maximum value in each position, measured with the light-scatter meter (LSM) agrees very well with those measured using the gas concentration probe. The shape of the curves is that expected by the use of a heavy gas in the jet : the gravity plays an important role and the gas flows down to the ground. At a certain height, the jet velocity is essentially equal to the local boundary layer velocity as expected.

Figure 17 shows the spectra of the concentration signal at three different positions. Differences between the different spectra are small indeed, however, they indicate that the energy of the concentration fluctuations increases from x = 20D up to x = 44D, decreasing up to x = 60D. Correlation coefficients R_{uc} at these positions have been computed giving, respectively, 0.18, 0.33 and 0.006, which is in agreement with the expected behaviour of the plume coming downstream. The concentration spectra exhibit a region of -5/3 slope; however, this does not necessarily indicate the existence of an inertial subrange for the moderate turbulence Reynolds number encountered in this experiment.

5. DISCUSSION OF THE RESULTS AND CONCLUSIONS

Several comments might be made following the present experiments. The combined laser-doppler velocimeter and laser-scatter meter have shown to permit an accurate description of the nozzle fluid concentration and velocity fields for a round turbulent free jet. The concentration measurement technique has proven to be reliable and practical. The comparison between the two different concentration measurement techniques is also a validation of the gas sampling one. Since the two techniques are based on completely different principles, it is not likely that systematic errors appear in both.

The technique demonstrated in the present paper can only be used properly if a correct seeding of the source is possible, in which no coupling exists between flow of gas and tracer.

The existence of regions where high correlation exists between gas concentration and velocity puts forward the pending question of possible bias of velocity measurement using a LDV when the seeding method is likely to produce nonuniformities of particle concentration that can influence velocity statistics. Buchhave et al. (Ref. 30) have examined this problem and their conclusions agree with the present results. They showed that sufficiently far downstream of a releasing point of particles one can get

$$\frac{\tau_L \bar{U}}{2L} \ll 1 \qquad (6)$$

where τ_L is the Lagrangian integral time scale, $\bar{U}$ is the mean velocity and L is the x-distance from the source, from where the spurious mean and rms velocity introduced by the nonuniform seeding is negligible. Roughly speaking, $\tau_L \approx \ell/3\bar{u}^2$ (Ref. 31), then

$$\frac{\tau_L \bar{U}}{2L} \approx \frac{1}{6}\,\frac{\bar{U}}{\bar{u}^2}\,\frac{\ell}{L} \ll 1 \qquad (7)$$

a situation which is reached, in the present case, at x = 60D, giving a value of about 0.013. Hence, at least in a large region of the flow considered, it can be expected that conditions are reached to allow to neglect the effects of nonuniformities of particle concentration.

The equipment and technique which has been described and tested, may be used to collect much needed experimental data in studies concerning turbulent mass diffusion and provide new data to assist in the modeling and closure of the diffusion equations. Also, some (heuristic) mixing length models for the diffusion process could be developed using the present data.While models of this kind have little theoretical basis, they have proven to be useful in many engineering applications.

REFERENCES

1. LUMLEY, J.L.: Turbulent transport of passive contaminants and particles : fundamentals and advanced methods of numerical modeling. in "Pollutant Dispersal". VKI LS 1978-7, May 1978.
2. YANG, B.T. & MERONEY, R.N.: A portable laser light scattering probe for turbulent diffusion studies. Review of Scientific Instruments, Vol. 45, No 2, 1974, pp 210-215
3. BECKER, H.A.; HOTTEL, H.C.; WILLIAMS, G.C.: On the light scatter technique for the study of turbulence and mixing. J. Fluid Mechanics, Vol. 30, Part 2, 1967, pp 259-284
4. BORREGO, C.: Local measurements of velocity and concentration. VKI PR 1978-17, June 1978.
5. BORREGO, C. & OLIVARI, D.: A method for the measurement of mixing properties in a turbulent jet flow. VKI TN 130, June 1979.
6. TROLINGER, J.D.: Laser instrumentation for flow field diagnostics. AGARDograph 186, 1974.

7. DURST, F.; MELLING, A.; WHITELAW, J.H.: Principles and practice of laser doppler anemometer.
London, Academic Press, 1976.
8. SHAUGHNESSY, E. & MORTON, J.B.: Laser light scattering measurements of particle concentration in a turbulent jet.
J. Fluid Mechanics, Vol. 80, Part 1, 1977, pp 129-148
9. VAN DER HULST, C.H.: Light scattering by small particles.
New York, J. Wiley & Sons, 1957.
10. MELLING, A. & WHITELAW, J.H.: Optical and flow aspects of particles.
Proc. LDA-75 symposium "The accuracy of flow measurements by laser doppler methods", Copenhagen, 1975, pp 382-402.
11. LUMLEY, J.L., GEORGE, W.K.; KOBASHI, Y.: The influence of ambiguity and noise on the measurements of turbulent spectra by doppler scattering.
Proc. Symposium Turbulence Measurements in Liquids, U. Missouri-Rolla, 1969.
12. MELLING, A.: A technique for simultaneous velocity and concentration measurements.
Proc. LDA-75 Symposium "The accuracy of flow measurements by laser doppler methods", Copenhagen, 1975, pp 505-509.
13. ABRAMOVICH, H.: The theory of turbulent jets.
Cambridge, MIT Press, 1963.
14. SCHLICHTING, H.: Boundary layer theory.
New York, McGraw-Hill, 1968.
15. FLORA, J.J. & GOLDSCHMIDT, V.W.: Virtual origin of a free plane turbulent jet.
AIAA J. Vol. 7, No 12, 1969, pp. 2344-2346.
16. CATALANO, G.D.; MORTON, J.B.; HUMPHRIS, R.R.: An experimental investigation of an axisymmetric jet in a coflowing airstream.
AIAA J., Vol. 14, No 9, 1976, pp. 1157-1158.
17. HINZE, J.O.: Turbulence.
New York, McGraw-Hill, 1975.
18. WYGNANSKI, I. & FIEDLER, H.J.: Some measurements in the self preserving jet.
J. Fluid Mechanics, Vol. 38, Part 3, 1969, pp. 577-612.
19. BECKER, H.A.; HOTTEL, H.C.; WILLIAMS, G.C.: The nozzle fluid concentration field of the round, turbulent free jet.
J. Fluid Mechanics, Vol. 30, Part 2, 1967, pp 285-303.
20. CORRSIN, S.: Investigation of flow in an axially symmetrical heated jet of air.
NACA Wartime Report 94, 1943.
21. CORRSIN, S. & UBEROI, M.S.: Further experiments on the flow and heat transfer in a heated turbulent air air.
NACA TN 1865, 1949.
22. ABBISS, J.B.;BRADBURY, L.J.S.; WRIGHT, M.P.: Measurements on an axisymmetric jet using a photon correlator.
Proc. LDA-75 Symposium "The accuracy of flow measurements by laser doppler methods", Copenhagen, 1975, pp 319-335.
23. DURST, F.: Laser doppler measurements in jet and wake flows.
10 LDA Application Notes, DISA Information, 1975.
24. SAMI, S.: Balance of turbulence energy in the region of jet flow establishment.
J. Fluid Mechanics, Vol. 29, Part 1, 1967, pp. 81-92.
25. FORSTAL, W. & SHAPIRO; A.: Momentum and mass transfer in coaxial jets.
J. Applied Mechanics, Vol. 17, 1950.
26. TIMM, G.K.: Heated and simulated heated jet exhausting into still air at ambient temperature.
VKI PR 1969-240, June 1969.
27. HEDLEY, T.B. & KEFFER, J.F.: Some turbulent/nonturbulent properties of the outer intermittent region of a boundary layer.
J. Fluid Mechanics, Vol. 64, Part 4, 1974, pp. 645-665.
28. OLIVARI, D.: VKI gas concentration meter C-probe series 5.
VKI ID-1, 1979.
29. DAVENPORT, A.G. & ISYUMOV, N.: The application of the boundary layer wind tunnel to the prediction of wind loading. in "Wind effects on buildings and structures", Ottawa, Paper 7, 1967.
30. BUCHHAVE, P.; GEORGE, W.K.; LUMLEY, J.L.: The measurement of turbulence with a laser doppler anemometer.
in "Annual Review of Fluid Mechanics", Vol. 11, 1979, pp. 443-503.
31. TENNEKES, H. & LUMLEY, J.L.: A first course in turbulence.
Cambridge, MIT Press, 1972.

$\frac{x}{2r_0}$	$\frac{\delta_T}{\delta_u}$ or $\frac{\delta_c}{\delta_u}$	Reference
2	1.00	Present work
4	1.11	
8	1.03	
12	1.03	
20	1.03	
2	1.00	Reference 16
4	1.19	
8	1.09	
5	1.24	Reference 20
10	1.42	
20	1.38	
15	1.25	Reference 21
20	1.35	

TABLE 1

Velocity and admixture profiles half-width ratios

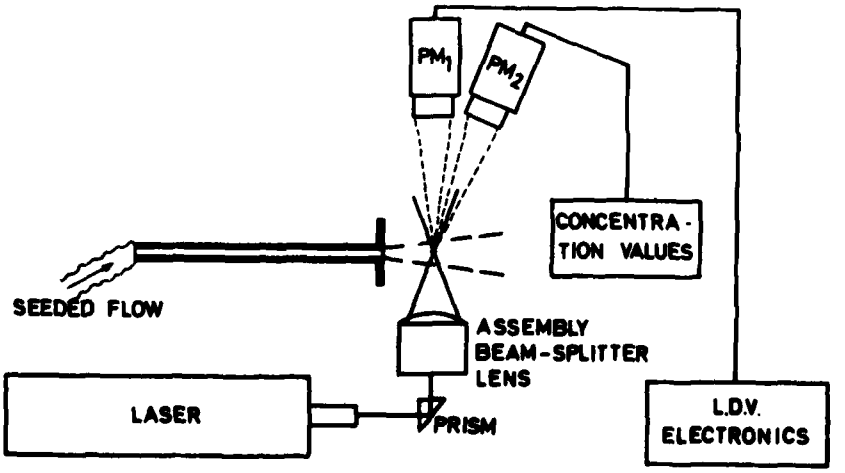

FIG. 1 - DIAGRAM OF EXPERIMENTAL ARRANGEMENT.

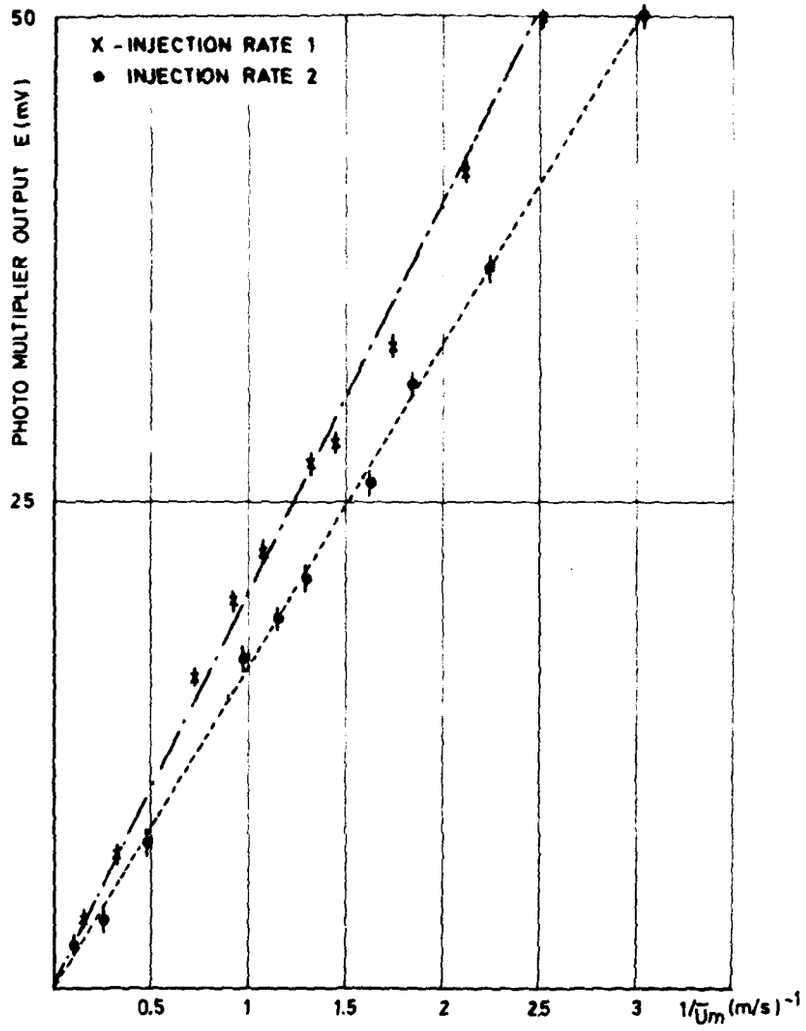

FIG. 2 - CONCENTRATION CALIBRATION CURVES

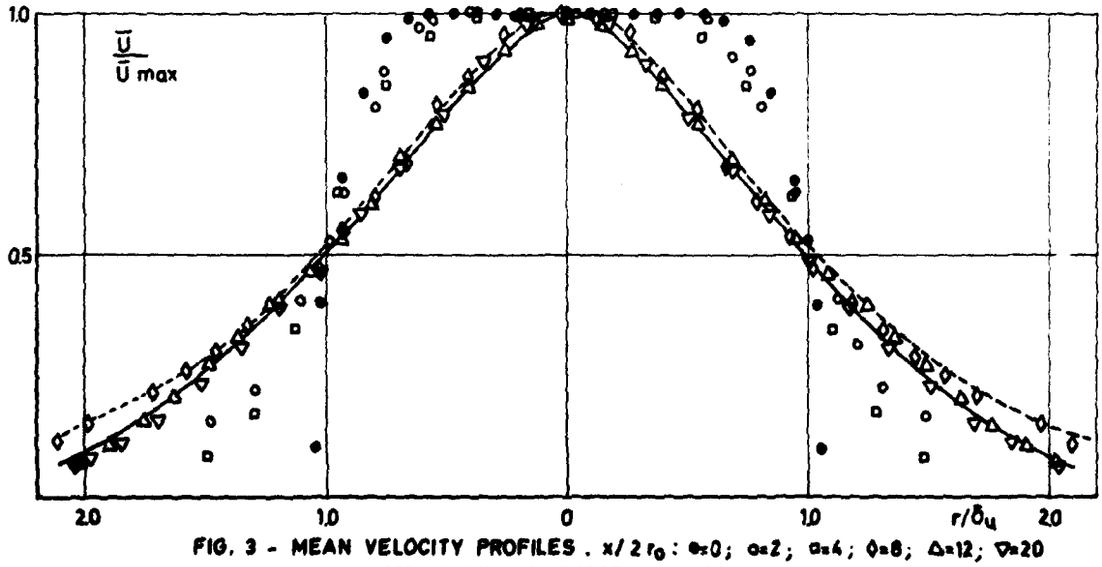

FIG. 3 - MEAN VELOCITY PROFILES . $x/2r_0$: ●=0; □=2; ○=4; ◇=8; △=12; ▽=20
------ SCHLICHTING'S THEORY (ref. 14)
——— TOLLMIEN'S THEORY (ref. 13)

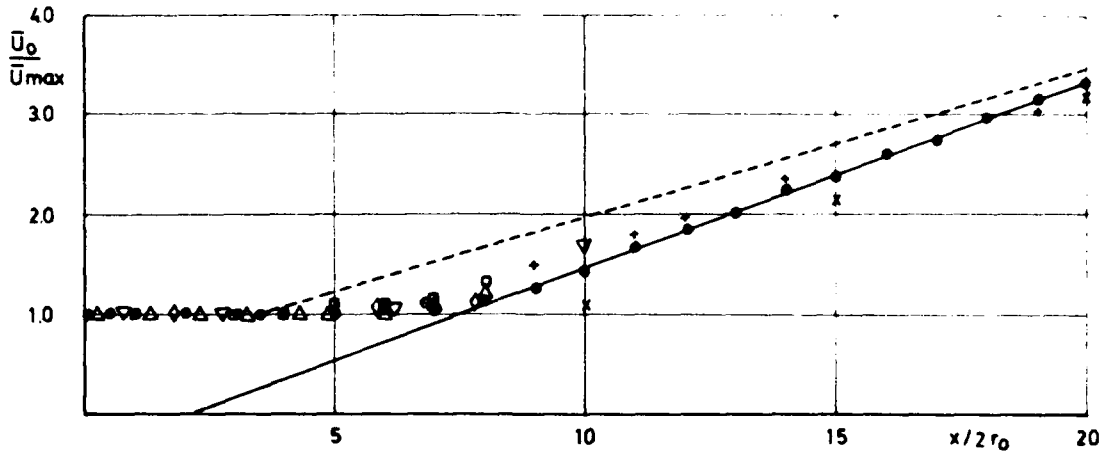

FIG. 4 - DECAY OF CENTRE LINE VELOCITY:
● = PRES.WORK; □ =REF.16; ● = PABST (CITED REF. 16); x = REF. 18;
+ = REF. 22; △ = REF. 23; ▽ =REF. 24; ◇ = REF. 25;
-----TOLLMIEN'S THEORY (REF 13).

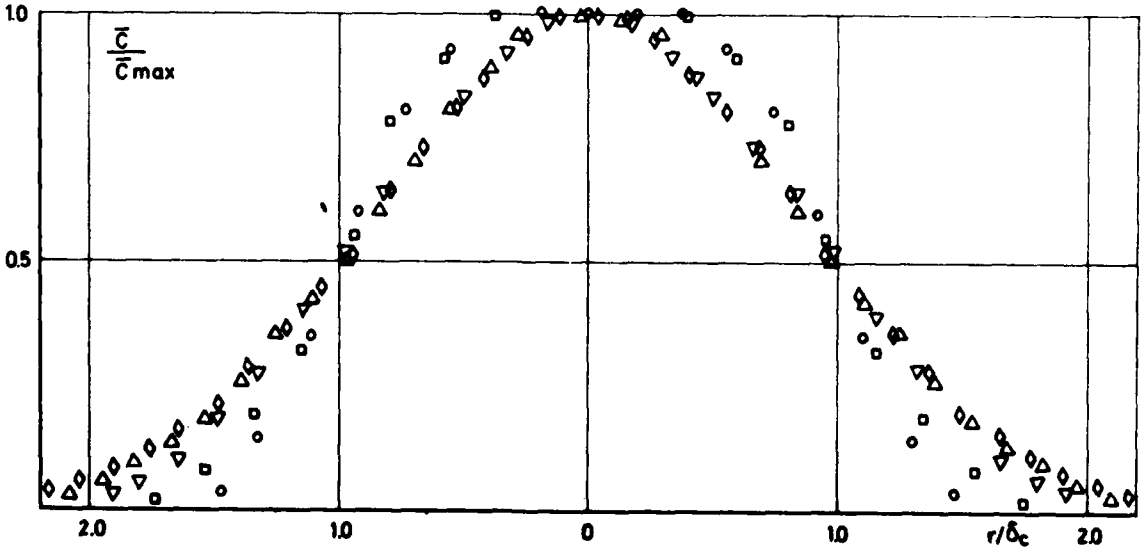

FIG. 5 - MEAN CONCENTRATION PROFILES. $x/2r_o$: ○ = 2; □ = 4; ◇ = 8; △ = 12; ▽ = 20

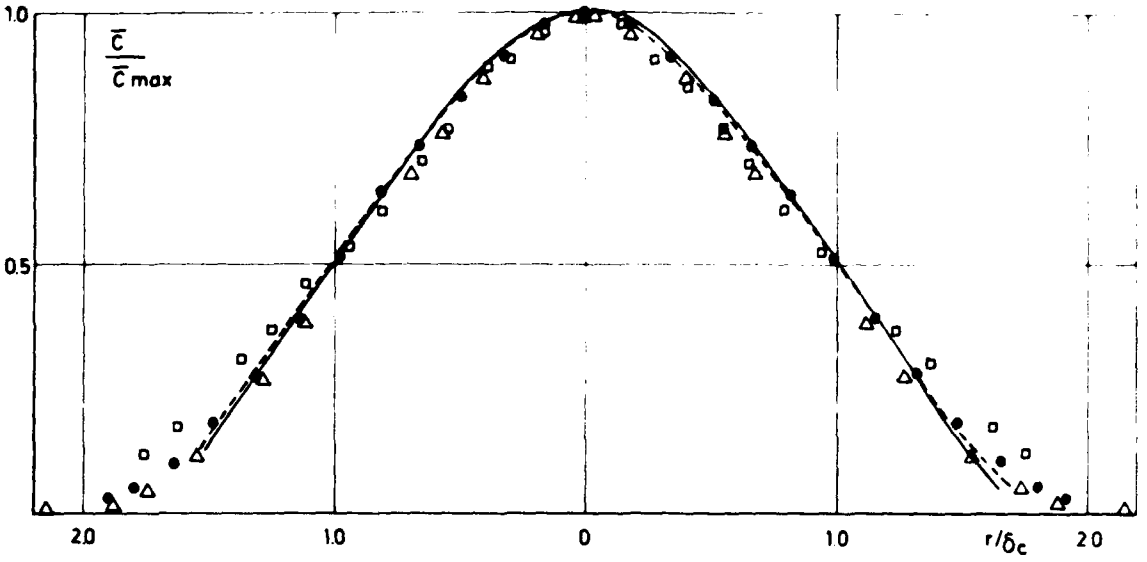

FIG. 6 - MEAN ADMIXTURE PROFILES AT $x/2r_0 = 20$: ● = PRES. WORK; △ = REF. 8
□ = REF. 16
-----TEMPERATURE PROFILE (REF. 13)
—— PRANDTL - GÖPTLER - REICHARDT'S THEORY (REF. 13)

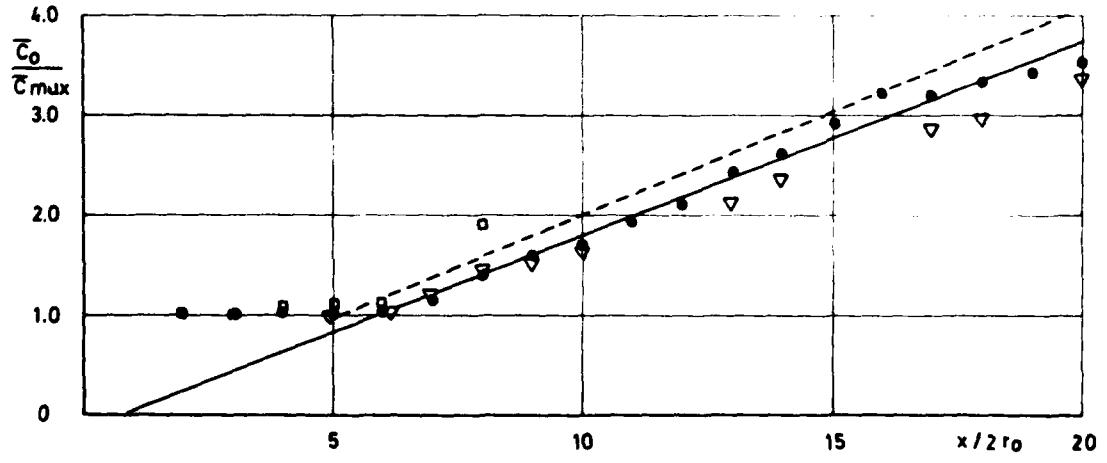

FIG. 7 - DECAY OF CENTRE LINE CONCENTRATION:
● = PRES. WORK; □ = REF. 16; ▽ = REF. 19
---- PRANDTL - GÖRTLER - REICHARDT'S THEORY (REF. 13)

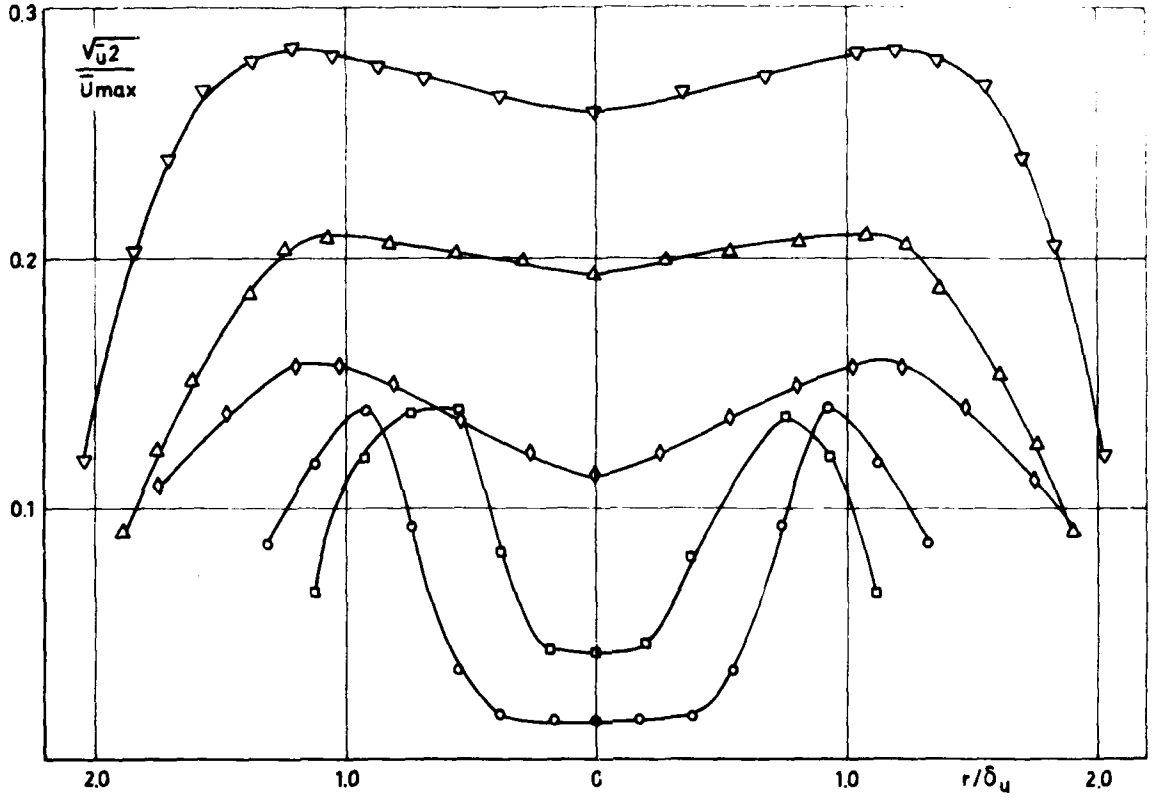

FIG. 8 - TURBULENT INTENSITY PROFILES :
$x/2r_o$: o = 2 ; □ = 4 ; ◇ = 8 ; △ = 12 ; ▽ = 20

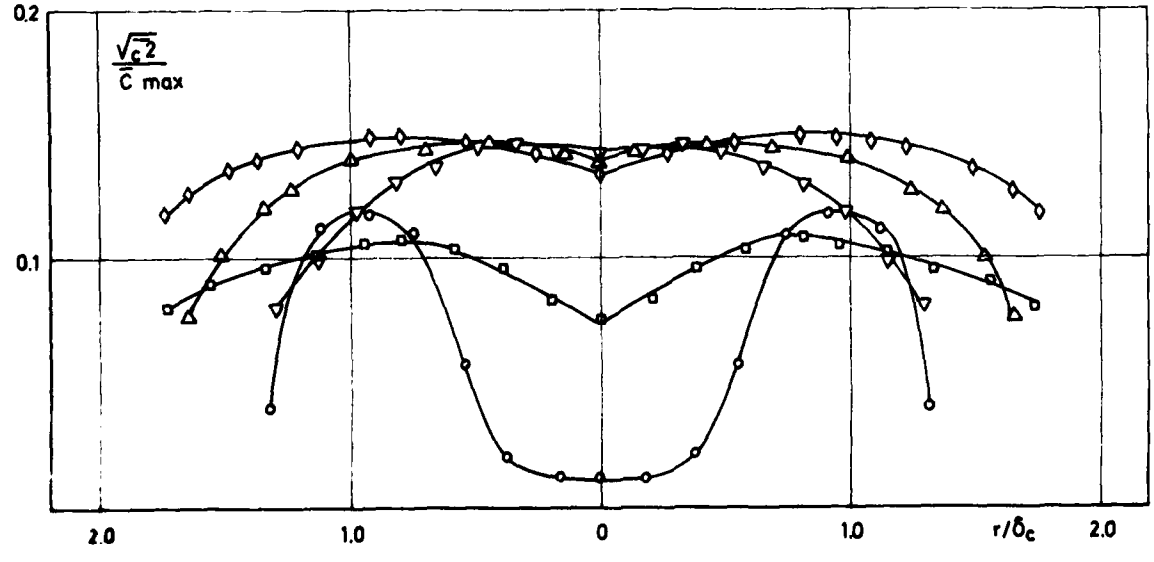

FIG 9 - CONCENTRATION FLUCTUATION PROFILES :
$x/2r_o$: o = 2 ; □ = 4 ; ◇ = 8 ; △ = 12 ; ▽ = 20

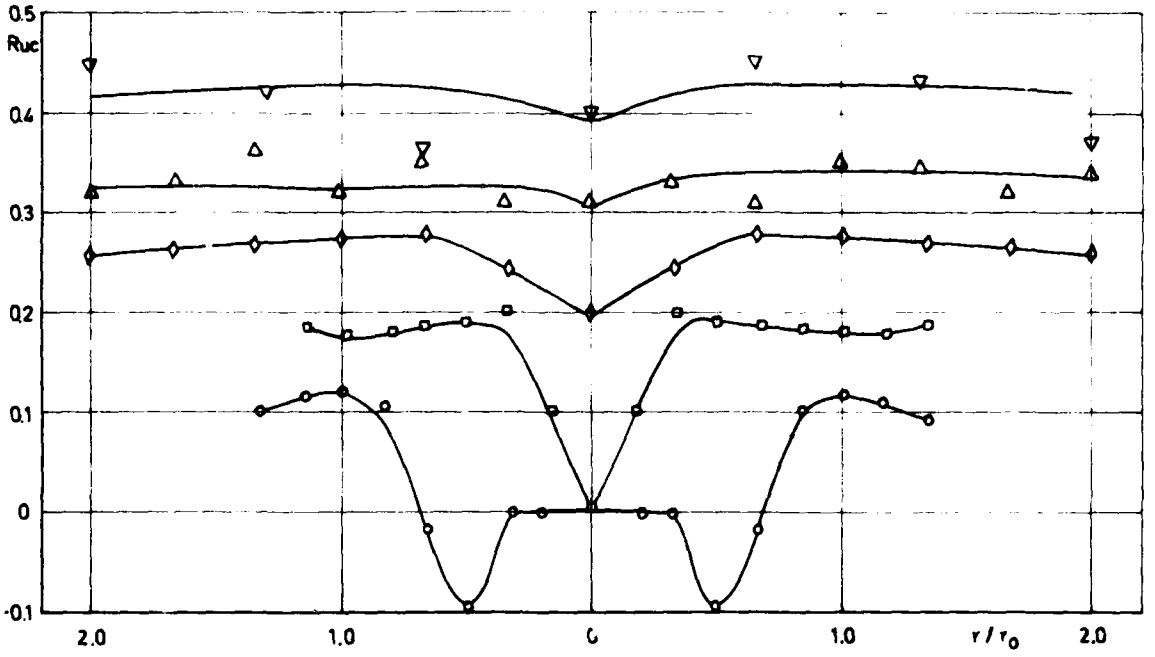

FIG. 10 - CONCENTRATION - VELOCITY CORRELATIONS:
$x/2r_0$: o = 2 ; □ = 4 ; ◊ = 8 ; Δ = 12 ; ▽ = 20

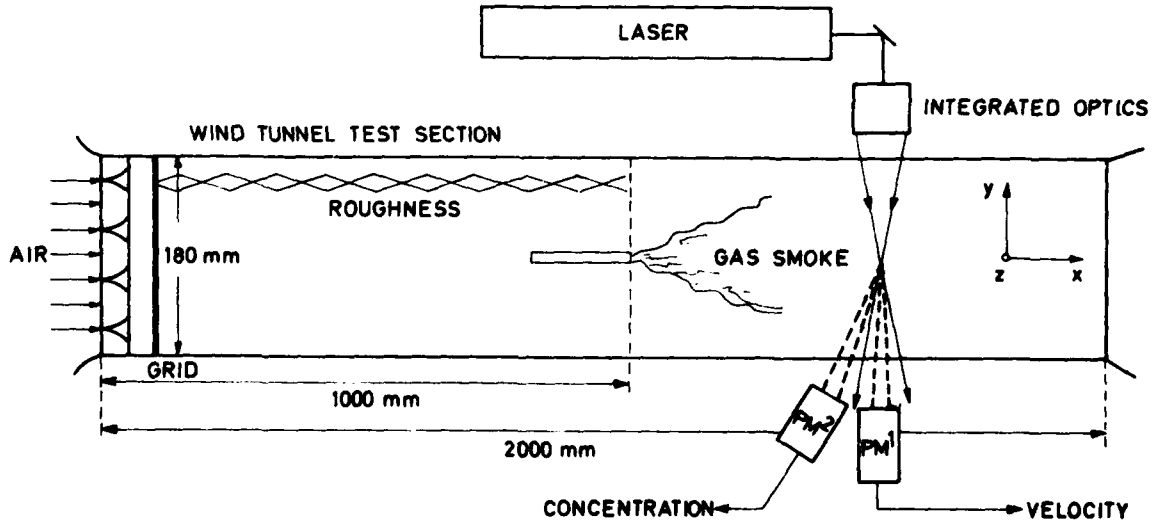

FIG. 11- SCHEMATIC OF WIND-TUNNEL AND OPTICAL ARRANGEMENT

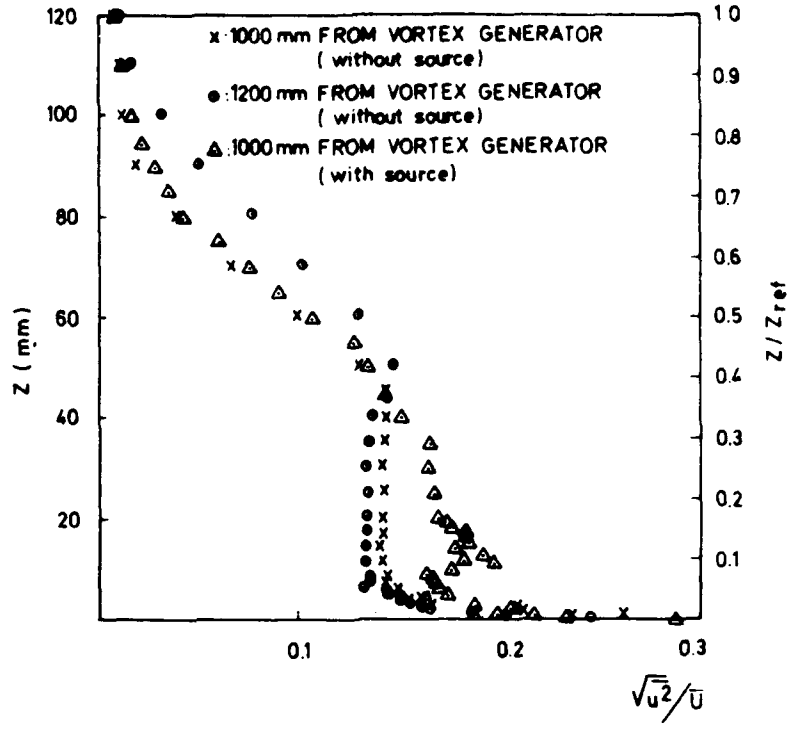

FIG. 12 - PROFILES OF TURBULENCE INTENSITY

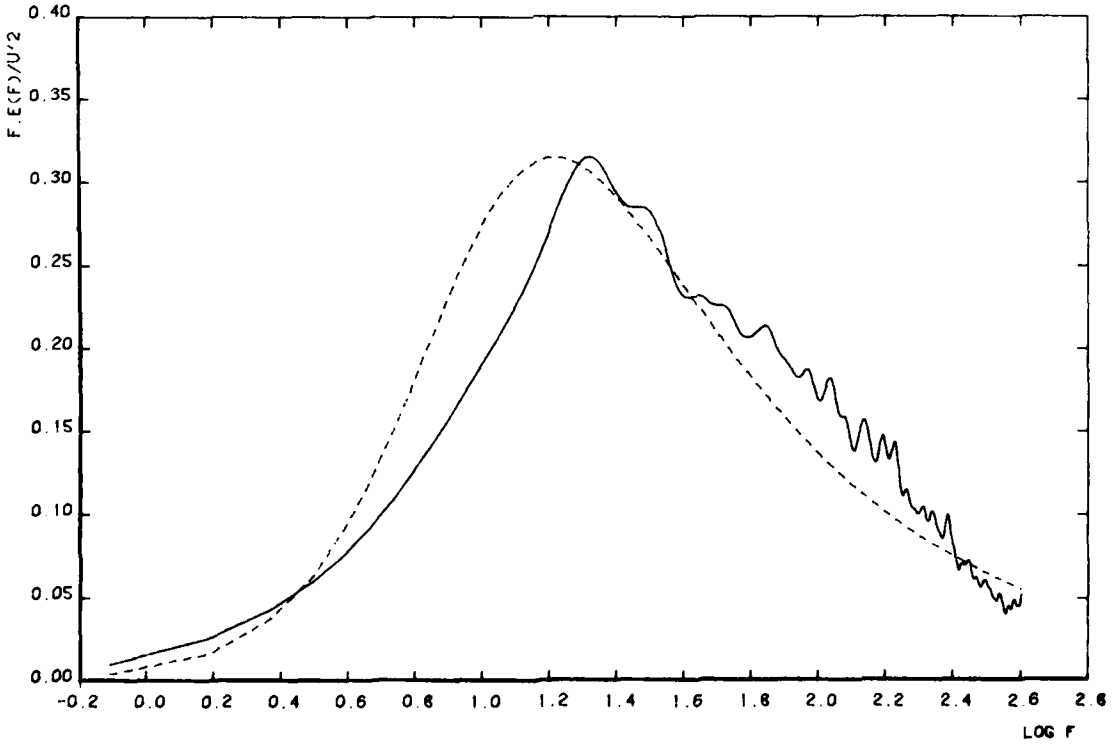

FIG. 13 : BOUNDARY LAYER SPECTRUM (SF=800 HZ) AT X=1.0 M, Z=7 MM.
----- SPECTRUM FROM "DAVENPORT"

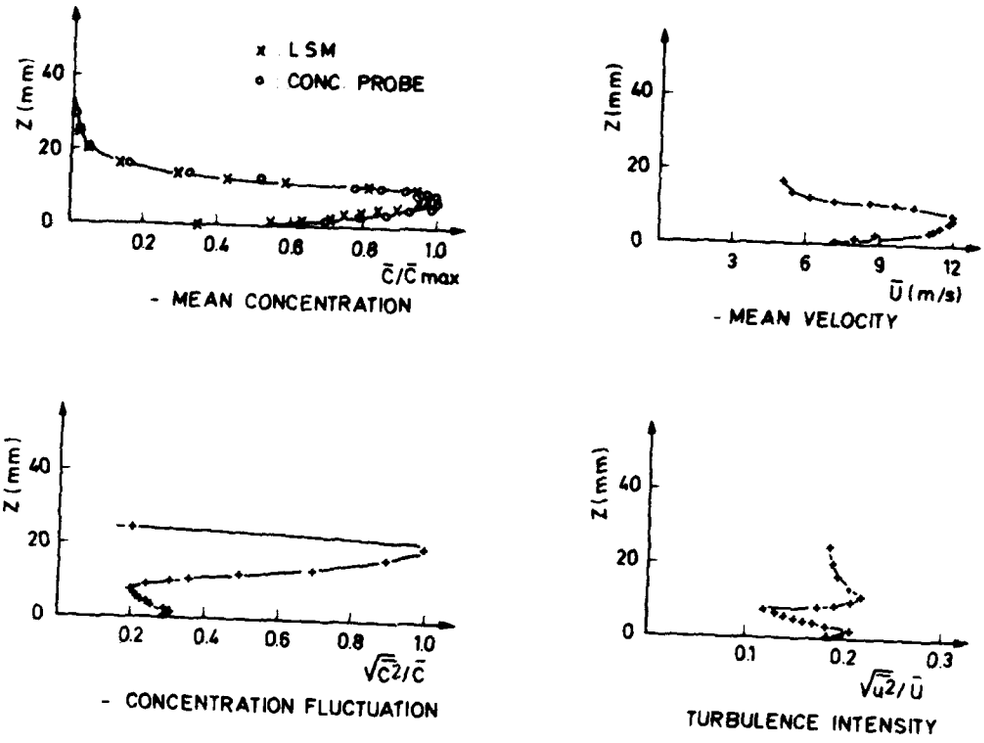

FIG. 14. X = 20 DIAMETERS DOWNSTREAM OF THE SOURCE

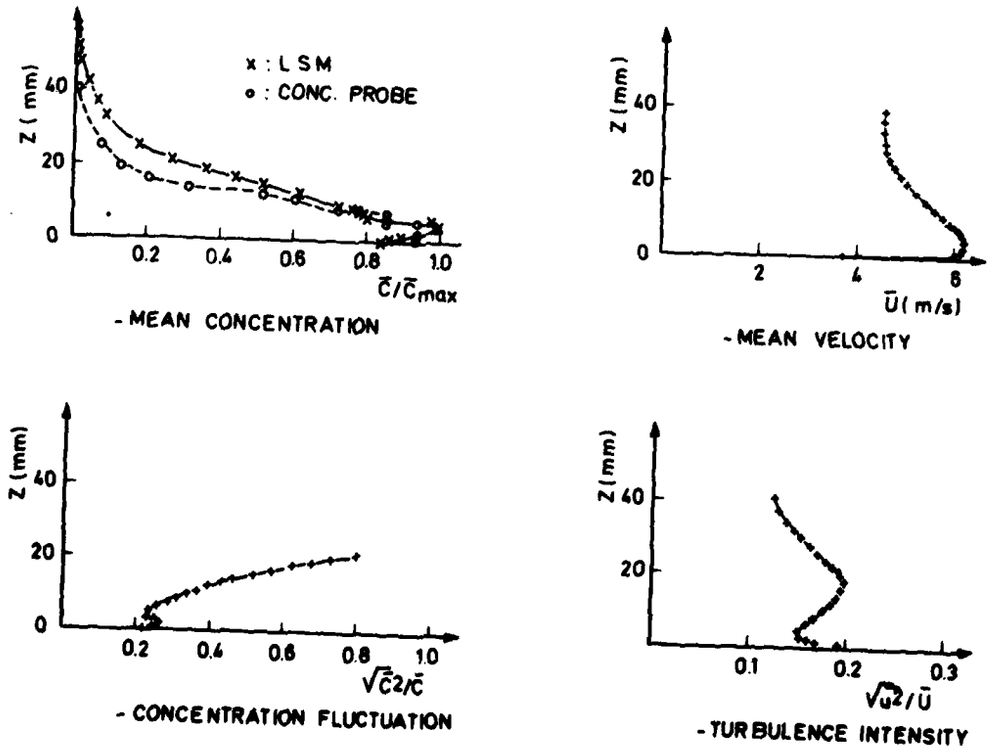

FIG. 15 - X = 44 DIAMETERS DOWNSTREAM OF THE SOURCE

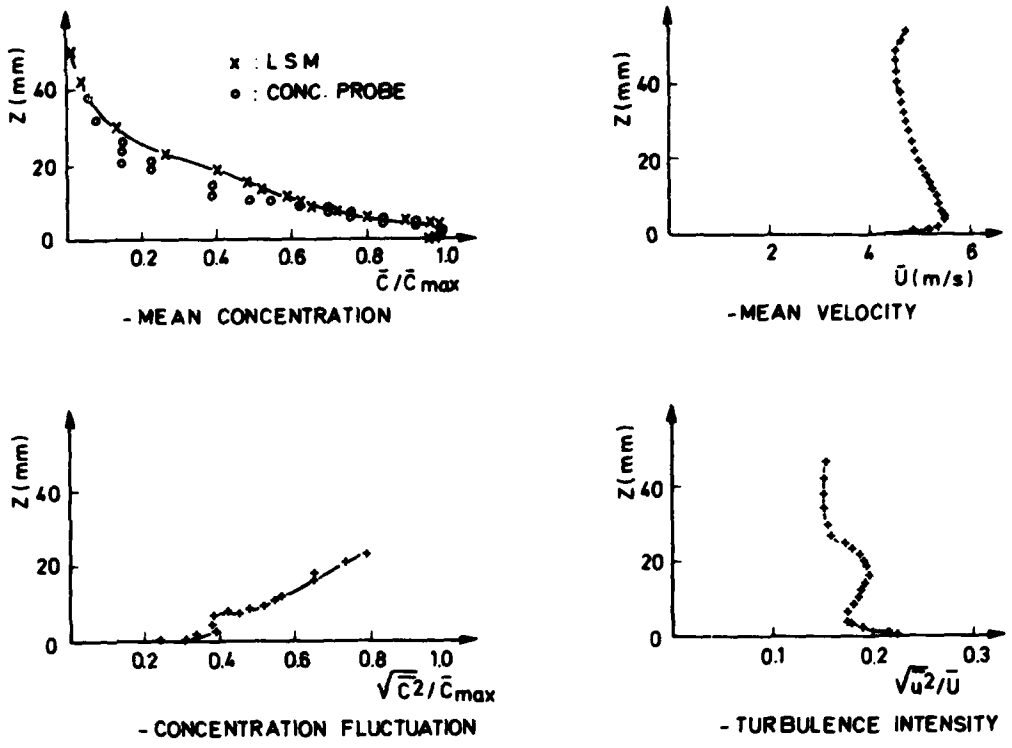

FIG. 16- X = 60 DIAMETERS DOWNSTREAM OF THE SOURCE.

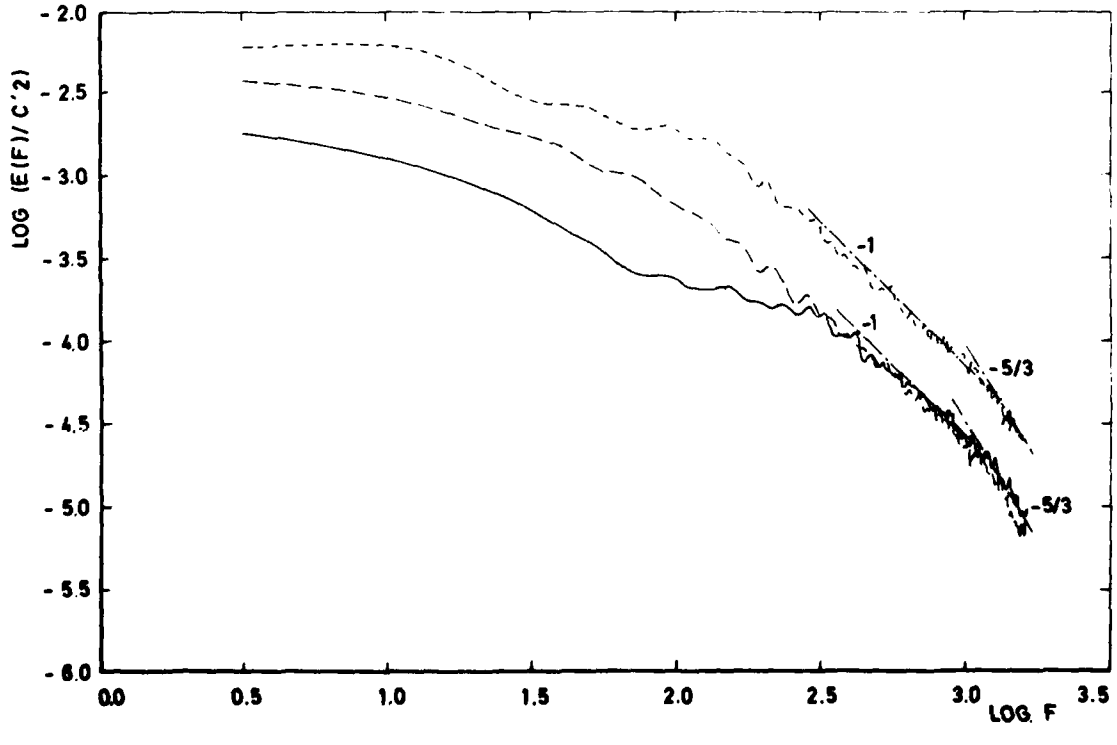

FIG. 17 - CONCENTRATION SPECTRUM (SF = 3200 HZ) AT Z = 7 mm

——— X = 20 D, ------- X = 44 D, — — — X = 60 D

DISCUSSION

W.G.Alwang, US

Did you conclude that a large correlation between velocity and concentration is a problem in reducing the velocimeter data for mean velocity and turbulence?

Author's Reply

Not yet. We are now preparing for this kind of reduction using the corrections for non-uniformities in the concentration field. Furthermore, we are making a comparison with hot-wire data from the same flow, to form a conclusion as to what could be the influence of the velocity-concentration correlations.

V.Wittmer, Ge

You used a 1 kHz low pass filter. The result is that you only measure concentration fluctuations up to 1 kHz. Why did you use such a filter, which will lead to errors in your measurements?

Author's Reply

This imposes a low limit on the frequency spectra and is a necessary limitation because of the type of photomultiplier used for the present measurements.

G.Winterfeld, Ge

One of the critical points of the method seems to be particle loading of the stream which is truly constant with time space. How is this achieved and checked?

Author's Reply

We have checked this, and one of the main problems of these experiments was to get constant concentration with our smoke generator. We achieved this by very fine regulation of our injector, and oil and air injector, keeping constant always the temperature of the hot plate using a variac and with a very steady, high injector pressure. In this way the fluctuations were around 3% as seen during calibration tests and measuremens with the light scattering meter were ± 3% of the constant value.

REPORT DOCUMENTATION PAGE

1. Recipient's Reference	2. Originator's Reference	3. Further Reference	4. Security Classification of Document
	AGARD-CP-281	ISBN 92-835-0272-8	UNCLASSIFIED

5. Originator Advisory Group for Aerospace Research and Development
North Atlantic Treaty Organization
7 rue Ancelle, 92200 Neuilly sur Seine, France

6. Title TESTING AND MEASUREMENT TECHNIQUES IN HEAT TRANSFER AND COMBUSTION

7. Presented at the 55th(A) Specialists' Meeting of the AGARD Propulsion and Energetics Panel, held at the Royal Library, Brussels, Belgium, on 5–7 May 1980.

8. Author(s)/Editor(s)	9. Date
Various	September 1980
10. Author's/Editor's Address	**11. Pages**
Various	292

12. Distribution Statement This document is distributed in accordance with AGARD policies and regulations, which are outlined on the Outside Back Covers of all AGARD publications.

13. Keywords/Descriptors

Heat transfer	Temperature measurement
Combustion	Flow measurement
Measurement	Chemical composition

14. Abstract

These Conference Proceedings contain the 22 papers presented at the AGARD Propulsion and Energetics 55th(A) Specialists' Meeting on Testing and Measurement Techniques in Heat Transfer and Combustion, which was held in Brussels, Belgium, on 5–7 May 1980. The questions and answers after the presentation of each paper are included.

The Technical Evaluation Report in included at the beginning of the Conference Proceedings.

The meeting consisted of five sessions: Engine Related Measuring Techniques; Heat Transfer for Measurement Techniques; Optical Velocity Measurement Techniques in Flames; Optical Techniques for Temperature and Composition Measurements (Parts I and II).

The meeting was intended to be a complement to the recent PEP meetings on 'High Temperature Problems in Gas Turbine Engines', and on 'Combustor Modelling'. Emphasis was placed on experimental techniques relevant to both of these areas. Recent advances in temperature measurements, flow measurements, composition and chemical measurements, and in general techniques, were discussed.

The aim of the meeting was to furnish a comprehensive survey of modern test rigs and measurement techniques to development engineers for combustors and other high temperature components; to provide research scientists in these areas with new techniques developed during recent years; and to provide a platform for discussing and comparing the different techniques.

Agard Conference Proceedings No. 281 Advisory Group for Aerospace Research and Development, NATO TESTING AND MEASUREMENT TECHNIQUES IN HEAT TRANSFER AND COMBUSTION Published September 1980 292 pages These Conference Proceedings contain the 22 papers presented at the AGARD Propulsion and Energetics 55th(A) Specialists' Meeting on Testing and Measurement Techniques in Heat Transfer and Combustion, which was held in Brussels, Belgium, on 5–7 May 1980. The questions and answers after the presentation of each paper are included. P.T.O.	AGARD-CP-281 Heat transfer Combustion Measurement Temperature measurement Flow measurement Chemical composition	Agard Conference Proceedings No. 281 Advisory Group for Aerospace Research and Development, NATO TESTING AND MEASUREMENT TECHNIQUES IN HEAT TRANSFER AND COMBUSTION Published September 1980 292 pages These Conference Proceedings contain the 22 papers presented at the AGARD Propulsion and Energetics 55th(A) Specialists' Meeting on Testing and Measurement Techniques in Heat Transfer and Combustion, which was held in Brussels, Belgium, on 5 7 May 1980. The questions and answers after the presentation of each paper are included. P.T.O.	AGARD-CP-281 Heat transfer Combustion Measurement Temperature measurement Flow measurement Chemical composition
Agard Conference Proceedings No. 281 Advisory Group for Aerospace Research and Development, NATO TESTING AND MEASUREMENT TECHNIQUES IN HEAT TRANSFER AND COMBUSTION Published September 1980 292 pages These Conference Proceedings contain the 22 papers presented at the AGARD Propulsion and Energetics 55th(A) Specialists' Meeting on Testing and Measurement Techniques in Heat Transfer and Combustion, which was held in Brussels, Belgium, on 5–7 May 1980. The questions and answers after the presentation of each paper are included. P.T.O.	AGARD-CP-281 Heat transfer Combustion Measurement Temperature measurement Flow measurement Chemical composition	Agard Conference Proceedings No. 281 Advisory Group for Aerospace Research and Development, NATO TESTING AND MEASUREMENT TECHNIQUES IN HEAT TRANSFER AND COMBUSTION Published September 1980 292 pages These Conference Proceedings contain the 22 papers presented at the AGARD Propulsion and Energetics 55th(A) Specialists' Meeting on Testing and Measurement Techniques in Heat Transfer and Combustion, which was held in Brussels, Belgium, on 5 7 May 1980. The questions and answers after the presentation of each paper are included. P.T.O.	AGARD-CP-281 Heat transfer Combustion Measurement Temperature measurement Flow measurement Chemical composition

The Technical Evaluation Report is included at the beginning of the Conference Proceedings. The meeting consisted of five sessions: Engine Related Measuring Techniques; Heat Transfer for Measurement Techniques; Optical Velocity Measurement Techniques in Flames; Optical Techniques for Temperature and Composition Measurements (Parts I and II). The meeting was intended to be a complement to the recent PEP meetings on 'High Temperature Problems in Gas Turbine Engines', and on 'Combustor Modelling'. Emphasis was placed on experimental techniques relevant to both of these areas. Recent advances in temperature measurements, flow measurements, composition and chemical measurements, and in general techniques, were discussed. The aim of the meeting was to furnish a comprehensive survey of modern test rigs and measurement techniques to development engineers for combustors and other high temperature components; to provide research scientists in these areas with new techniques developed during recent years; and to provide a platform for discussing and comparing the different techniques. ISBN 92-835-0272-8	The Technical Evaluation Report is included at the beginning of the Conference Proceedings. The meeting consisted of five sessions: Engine Related Measuring Techniques; Heat Transfer for Measurement Techniques; Optical Velocity Measurement Techniques in Flames; Optical Techniques for Temperature and Composition Measurements (Parts I and II). The meeting was intended to be a complement to the recent PEP meetings on 'High Temperature Problems in Gas Turbine Engines', and on 'Combustor Modelling'. Emphasis was placed on experimental techniques relevant to both of these areas. Recent advances in temperature measurements, flow measurements, composition and chemical measurements, and in general techniques, were discussed. The aim of the meeting was to furnish a comprehensive survey of modern test rigs and measurement techniques to development engineers for combustors and other high temperature components; to provide research scientists in these areas with new techniques developed during recent years; and to provide a platform for discussing and comparing the different techniques. ISBN 92-835-0272-8
The Technical Evaluation Report is included at the beginning of the Conference Proceedings. The meeting consisted of five sessions: Engine Related Measuring Techniques; Heat Transfer for Measurement Techniques; Optical Velocity Measurement Techniques in Flames; Optical Techniques for Temperature and Composition Measurements (Parts I and II). The meeting was intended to be a complement to the recent PEP meetings on 'High Temperature Problems in Gas Turbine Engines', and on 'Combustor Modelling'. Emphasis was placed on experimental techniques relevant to both of these areas. Recent advances in temperature measurements, flow measurements, composition and chemical measurements, and in general techniques, were discussed. The aim of the meeting was to furnish a comprehensive survey of modern test rigs and measurement techniques to development engineers for combustors and other high temperature components; to provide research scientists in these areas with new techniques developed during recent years; and to provide a platform for discussing and comparing the different techniques. ISBN 92-835-0272-8	The Technical Evaluation Report is included at the beginning of the Conference Proceedings. The meeting consisted of five sessions: Engine Related Measuring Techniques; Heat Transfer for Measurement Techniques; Optical Velocity Measurement Techniques in Flames; Optical Techniques for Temperature and Composition Measurements (Parts I and II). The meeting was intended to be a complement to the recent PEP meetings on 'High Temperature Problems in Gas Turbine Engines', and on 'Combustor Modelling'. Emphasis was placed on experimental techniques relevant to both of these areas. Recent advances in temperature measurements, flow measurements, composition and chemical measurements, and in general techniques, were discussed. The aim of the meeting was to furnish a comprehensive survey of modern test rigs and measurement techniques to development engineers for combustors and other high temperature components; to provide research scientists in these areas with new techniques developed during recent years; and to provide a platform for discussing and comparing the different techniques. ISBN 92-835-0272-8

END

DATE
FILMED

2-81

DTIC